Multicomponent Polymer Materials

Published on December 9, 1985 on http://pubs.acs.org | doi: 10.1021/ba-1986-0211.fw001

ADVANCES IN CHEMISTRY SERIES 211

Multicomponent Polymer Materials

D. R. Paul, EDITOR
University of Texas—Austin

L. H. Sperling, EDITOR
Lehigh University

Developed from a symposium sponsored by
the Division of Polymeric Materials Science and Engineering
at the 188th Meeting
of the American Chemical Society,
Philadelphia, Pennsylvania,
August 26–31, 1984

American Chemical Society, Washington, DC 1986

Library of Congress Cataloging in Publication Data

Multicomponent polymer materials.
(Advances in chemistry series, ISSN 0065-2393; 211)

Includes bibliographies and index.

1. Polymers and polymerization—Congresses.
2. Plastics—Congresses.

I. Paul, Donald R. II. Sperling, L. H. (Leslie Howard), 1932- . III. American Chemical Society. Division of Polymeric Materials: Science and Engineering. IV. Series.

QD1.A355 no. 211 [TP1105]
540 s [668.9] 85-20475
ISBN 0-8412-0899-9

Advances in Chemistry Series

M. Joan Comstock, *Series Editor*

Advisory Board

FOREWORD

The ADVANCES IN CHEMISTRY SERIES was founded in 1949 by the American Chemical Society as an outlet for symposia and collections of data in special areas of topical interest that could not be accommodated in the Society's journals. It provides a medium for symposia that would otherwise be fragmented because their papers would be distributed among several journals or not published at all. Papers are reviewed critically according to ACS editorial standards and receive the careful attention and processing characteristic of ACS publications. Volumes in the ADVANCES IN CHEMISTRY SERIES maintain the integrity of the symposia on which they are based; however, verbatim reproductions of previously published papers are not accepted. Papers may include reports of research as well as reviews, because symposia may embrace both types of presentation.

ABOUT THE EDITORS

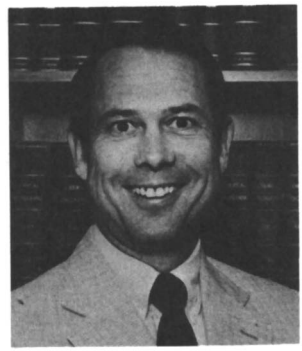

D. R. PAUL received a B.S. degree in chemical engineering from North Carolina State University and M.S. and Ph.D. degrees in chemical engineering from the University of Wisconsin. He now holds the Melvin H. Gertz Regents Chair in Chemical Engineering at the University of Texas at Austin where he teaches courses and does research in various areas of polymers including polymer blends and transport behavior.

He is director of the Center for Polymer Research and recently ended an eight-year term as chairman of the Chemical Engineering Department at the University of Texas. Paul has received many awards for teaching and research including the 1985 Materials Engineering and Sciences Division Award of the American Institute of Chemical Engineers, the 1984 American Chemical Society Phillips Award for Applied Polymer Science, the 1982 Society of Plastics Engineers Research Award, the Engineering New-Record Award in 1976, and the 1973 American Chemical Society Arthur K. Doolittle Award. He serves on the editorial boards of the *Journal of Applied Polymer Science, Polymer Engineering and Science,* and the *Journal of Membrane Science.*

He and S. Newman edited the two-volume book entitled "Polymer Blends", which appeared in 1978 and has subsequently been translated into Russian. He has participated in numerous short courses, has organized various symposia, and is an active consultant to industry. Current research programs include thermodynamics of polymer blends, compatibilization of polymer blends, transport behavior in multicomponent polymer systems, and the use of polymeric membranes for gas separations.

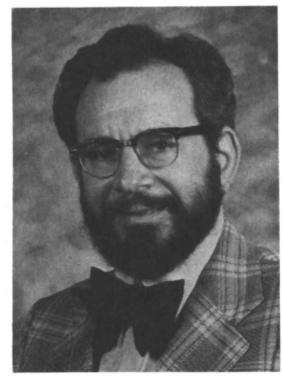

L. H. SPERLING received a B.S. in chemistry from the University of Florida in 1954 and M.S. and Ph.D. degrees in chemistry from Duke University in 1957 and 1959, respectively. He joined the staff of Lehigh University in June 1967 as an assistant professor of chemical engineering and as a senior staff member of the Materials Research Center. He is now a full professor. From 1958 to 1965, he was employed by the Buckeye Cellulose Corporation, Memphis, Tennessee. He performed research on gels in cellulosic solutions, on optical properties of cellulose acetate plastics, and on the relationship between mechanical and structural properties of rayon yarns. During this period, he was also a night instructor at Christian Brothers College in Memphis, teaching freshman chemistry and polymer chemistry. From July 1965 to May 1967, he was a postdoctoral research associate at Princeton University studying under A. V. Tobolsky. His research was in the physical and mechanical properties of high polymers, thermoelasticity, and the thermal stability of elastomeric networks.

His present research interests include morphological and mechanical behavior of polymers, synthesis and properties of interpenetrating polymer networks (IPNs), polymer miscibility, crystalline block copolymer materials, and polymer properties via small-angle neutron scattering. He has written four books in the areas of polymer blends and composites, IPNs, and polymers from renewable resources. He has written more than 100 papers, about 50 of which are about IPNs, and he has chaired several symposia in the areas of multicomponent polymer materials and polymers from renewable resources.

PREFACE

THE SCIENCE OF MULTICOMPONENT POLYMER MATERIALS arose because of the continued need to make and to understand improved engineering polymers and because of the reduced probability of discovering new, inexpensive, broad utility homopolymers. Through the developing science of mixing known polymers, advantageous property relationships can be found.

Polymers may be mixed with many materials. They may be plasticized with small molecules, colored, reinforced with particulate or fibrous fillers, or cross-linked through a variety of mechanisms. This work emphasizes the results of recent research on the mixing of two or more polymers.

Polymer mixtures have been called by many names. The term *polymer blends* is widely used not only to describe mechanical mixtures of two polymers, but also to provide a generic description of graft and block copolymers, AB-cross-linked polymers, and interpenetrating polymer networks. Another name for polymer mixtures is *polymer alloys*, a term which reminds us of the metallic counterparts of polymer mixtures. Incidentally, many metallic alloys, including steel, exhibit phase separation, an important aspect of most polymer mixtures. An older term not in wide use today is *interpolymers*. The title of this book, "Multicomponent Polymer Materials", presents a new and broader way to name collectively all the methods to combine two or more polymers.

Kato's discovery of osmium tetroxide staining in 1964 provided an important new tool for the study of certain polymer blends. With properly stained samples, electron microscopy revealed a wealth of morphological detail down to a level of about 100 Å. For example, solution graft copolymers of polybutadiene and polystyrene could easily be distinguished from mechanical blends. The reasons for the former's greater impact strength became clearer in terms of the domain size and complexity of domain structure. The probable locus of grafting sites was identified, and the interrelationships among synthetic detail, morphology, and mechanical properties were established. However, polymer blend science of that day was largely qualitative and depended on interpretation of such information as modulus–temperature curves, stress–strain data, and impact resistance in the light of their morphologies.

Starting with research in the early 1970s, polymer scientists learned that by choosing complementary polymer pairs that attracted one

another, rather than similar pairs that merely repelled one another to lesser degrees, miscible polymer pairs could be systematically identified. The resulting phase diagrams often show lower critical solution temperatures, and these results have led to a more sophisticated science for polymer blend thermodynamics.

The editors wish to thank many people for their part in making this book possible. First are the many secretaries who typed each of the manuscripts, perhaps many times. Susan Robinson of the American Chemical Society did an outstanding job in handling the mechanics of refereeing and editing. We also wish to thank our respective universities for providing the many professional services that ease the path to the preparation of books.

D. R. PAUL
University of Texas—Austin

L. H. SPERLING
Lehigh University

August 1985

1

Polymer Blends: Phase Behavior and Property Relationships

D. R. PAUL

Department of Chemical Engineering and Center for Polymer Research, The University of Texas, Austin, TX 78712

The phase behavior of multicomponent polymeric materials is a crucial factor in determining their physical properties and subsequently their utility. For systems forming separate phases, the important issues are phase morphology (size and shape) and the nature of the interface (wetting and adhesion) between phases. For decades nearly all polymer–polymer mixtures were believed to form immiscible mixtures or to be incompatible. However, research and development within the last decade has substantially revised this view. The result is a strong commercial and fundamental interest in polymer blends exhibiting all types of phase behavior. The various types of phase behavior commonly encountered among polymer blend systems and the relationship to properties are reviewed here including basic thermodynamic issues. For most systems, the central factor is the interaction between the polymer–polymer segments; this interaction also has a large influence on property relationships.

RUBBER-TOUGHENED AMORPHOUS GLASSES have been important forms of polymer blends since the 1940s; however, only in the last decade or so has physical blending of polymers for other purposes become of greater general interest. Today, activity has increased in this area of research because this physical approach is believed to be a more rapid and a less expensive route to meeting the demands of the marketplace than the development of new polymers. The successful implementation of physical blends requires sophisticated knowledge and technology, albeit of a different nature than the more well-known, chemistry-oriented technology required for the introduction of new polymers. Blending of preexisting polymers offers a means of engineering into one material certain combinations of desired properties exhibited individually by the component polymers. Often the driving force to formulate blends is to achieve cost dilution or an optimum cost-to-benefit ratio. A central issue in this technology, of course, is the nature of the

0065–2393/86/0211/0003$06.00/0

property relationships generated by blending. These properties are strongly influenced by the phase behavior of the blend or the interactions between the components. The purpose of this chapter is to give a brief review of the current state of knowledge in this area and some of its applications.

Background and Historical Perspective

Prior to 1975, the scientific literature on polymer blends was dominated by three key papers (*1–3*), which are still frequently referenced and quoted. The subject of these papers was "compatibility," and each stressed "incompatibility" as the rule and "compatibility" as the exception. The term *compatibility*, in their usage, referred to the formation of a single-phase mixture on blending of two polymers. *Incompatibility* referred to the formation of more than one phase on mixing. Today, some authors (*4–8*) prefer to use the term *miscibility* because of its more precise scientific meaning with regard to an equilibrium state of mixing or solubility and to avoid the confusion associated with the less precise technological usage of the term compatibility.

The pessimistic forecast for polymer–polymer miscibility made originally by Dobry and Boyer-Kawenoki (*1*) was rapidly given a scientific basis by Scott (*9*). Scott used the liquid lattice theory for estimating the combinatorial entropy of mixing published simultaneously in 1942 by Flory (*10*) and by Huggins (*11*). The rudiments of the effect of component molecular size on the entropy of mixing are pictorially represented in Figure 1. This figure clearly indicates that the combinatorial entropy change is very small when high molecular weight polymers are mixed—in contrast to mixing two low molecular weight solvents or even a polymer and a solvent. This fact, combined with an expectation that the heat of mixing (often assumed to be parabolic in composition as expressed by van Laar

$$\Delta H_m = B\phi_1\phi_2 = RT\chi_1 n_1\phi_2 \tag{1}$$

or in the "chi" notation of the Flory–Huggins formulation) is usually endothermic or positive, makes it unlikely to realize the necessary negative free energy of mixing

$$\Delta G_m = \Delta H_m - T\Delta S_m \tag{2}$$

required for miscibility or the more stringent sufficient conditions for phase stability. The notion that *like-dissolves-like*, quantified by the solubility parameter approach (*3*), fails to identify many miscible polymer pairs. Bohn (*2*) made the situation seem even more hopeless by noting that "... all known compatible systems involve noncrystalline polymers." For some time afterwards, any form of phase separation was regarded as the incom-

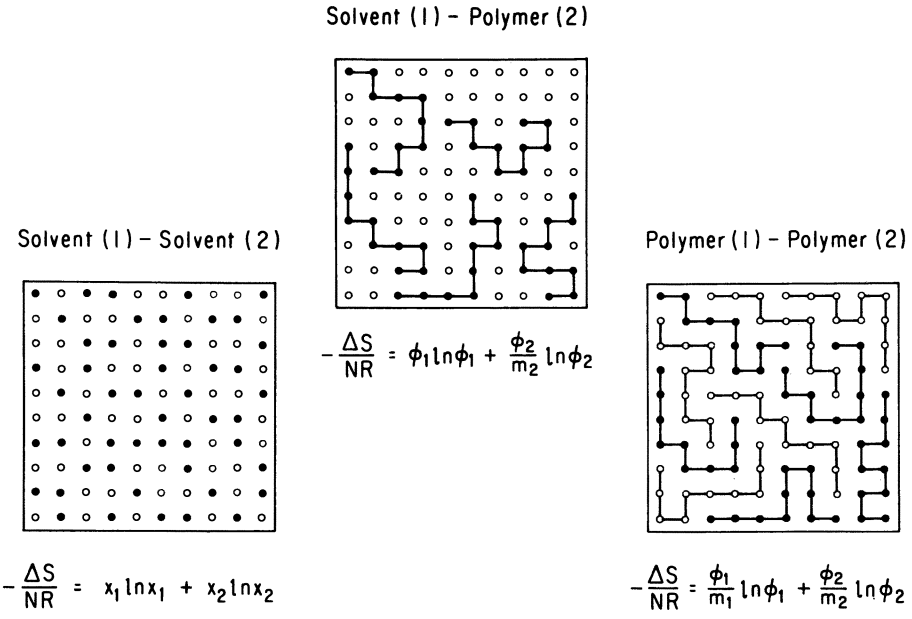

Figure 1. Lattice model for combinatorial entropy of mixing. N *equals total lattice sites,* m_1 *and* m_2 *are sites occupied by species 1 and 2,* x_i *equals the mole fraction of* i, *and* ϕ_i *equals the volume fraction of* i.

patibility of the component polymers. No distinction was made between liquid–solid and liquid–liquid phase behavior (*4*, *12*).

This early literature may have inadvertently impeded progress in the development of polymer blending as a technique for creating "new" materials or for problem solving by associating a negative connotation with phase-separated mixtures. In fact, the use of the term incompatibility to describe such situations may itself have been a psychological barrier to exploring their potential applications because the term means "not capable of being combined." Developments in the past decade have proved that *some* phase-separated or immiscible blends do offer definite advantages or opportunities for commercial application. Incompatibility does remain an apt description for many polymer–polymer mixtures, but techniques of overcoming the associated poor property relationships by using agents to improve compatibility and phase morphology control are emerging.

A great deal of progress has been made during the past decade in commercial exploitation of polymer blending and in giving this technology a sound scientific basis. New products based on this approach have emerged rapidly, and intense research efforts have been established in both industrial and academic laboratories. An indication of this activity may be seen

from some recent reviews, symposia, and monographs (*4–8*, *13–29*). Since the review in 1972 by Krause, many new miscible blends have been identified. In fact, the lists given in References 5 and 6 are now quite out of date, but updating them is beyond the scope of this review. From the current rate at which new miscible systems are being reported, one must conclude that categorizing them as exceptions to a rule is an overstatement of the "rule" and that miscible blends must be considered as an important source of new products. This progress has been primarily the result of some rethinking of two tenets implied by the early literature.

The first change was a shift in emphasis from entropy to heat of mixing as a driving force for miscibility. In most of the early literature, the heat of mixing was assumed to be positive. However, it is now more widely appreciated that negative or exothermic heats of mixing circumvent the problem of a very small or even zero combinatorial entropy of mixing and that this circumvention is the basis for blend miscibility in most systems (*see*, for example, References 30 and 31). Exothermic mixing is quite common for polar molecules, whereas nonpolar molecules generally mix endothermically. This point of view redirects the search for miscibility from seeking structural similarity to finding appropriate complementing dissimilarities.

The second change was the realization that the investigation of miscibility or phase homogeneity in blends involving crystalline polymers should be focused on the amorphous phase of the semicrystalline mixture. It is now well known that a completely homogeneous mixture may be formed above the melting points of its components. However, on cooling a pure crystalline phase may develop in coexistence with an amorphous phase that is a homogeneous or completely miscible mixture of the two polymers (*12*). That is, a distinction is made between phase separation caused by crystallization of one of the components from the melt solution and phase separation resulting from liquid–liquid immiscibility. This point is extremely important because many of the newly discovered "miscible" blends do involve a crystallizable component; several of the recently commercialized blend products are of this type. From a technological viewpoint, crystallinity in polymers is often a highly desirable feature (e.g., to achieve high heat distortion temperatures or chemical resistance). Clearly, incompatibility is a misnomer when the only source of phase heterogeneity is crystallization.

A Contemporary View of Blend Phase Behavior

Blends with a homogeneous amorphous phase exhibit a single glass transition. This transition occurs at a temperature (T_g) intermediate between the values for the two pure component polymers. This intermediate temperature reflects the mixed environment in which the two types of chain segments coexist. This transition is similar to what occurs in a random copolymer. When this homogeneity exists for all blend proportions, the T_g relationship will be something like that shown in Figure 2; and, if this sys-

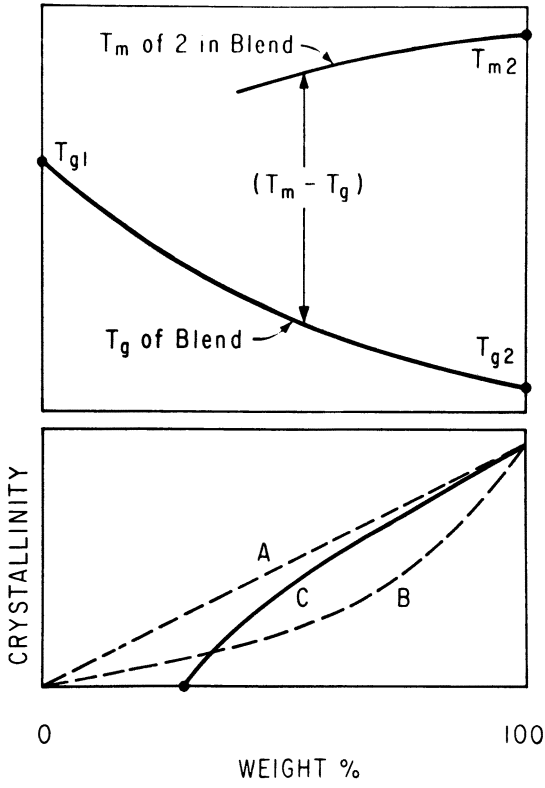

Figure 2. Schematic of transitional and crystallization behavior of miscible blends with one crystallizable component. (Reproduced with permission from Ref. 45. Copyright 1978 Society of Plastics Engineers.)

tem is an equilibrium state, complete liquid–liquid miscibility exists. If one of the components is crystallizable (e.g., species 2), a separate crystalline phase of pure 2 can form at temperatures sufficiently below the melting point, T_m, of pure 2. The crystals of 2 will coexist with a mixed amorphous phase made up of components 1 and 2 in the manner pictorially represented in Figure 3. As a result of the depletion of component 2 from the amorphous phase, the shape of the T_g–composition relationship will be affected because the amorphous phase will be richer in species 1 than the overall composition of the blend. Because polymers do not crystallize completely, the amorphous phase will always contain some of the crystallizable species. The fraction of the crystalline phase, based on total blend mass, may be similar to one of the curves shown in the lower part of Figure 2. Formation of miscible blends will affect the temperature interval available for crystallization, $T_m - T_g$ as shown in Figure 2, and, thus, influence the kinetics of this process. Curve A is believed to be the limiting situation for

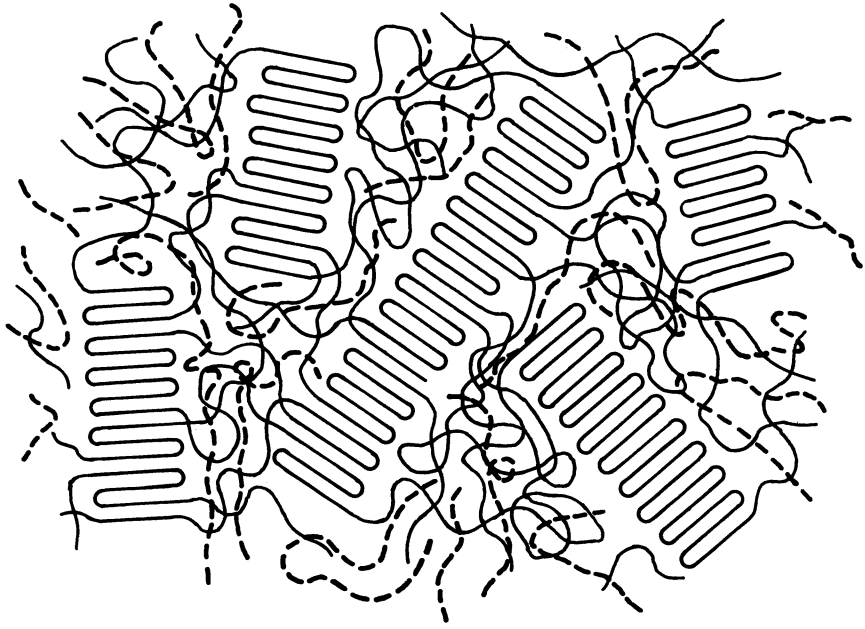

Figure 3. Idealized representation of a blend with a mixed amorphous phase and with one component partially crystallized.

long crystallization times and corresponds to a fixed level of crystallinity that is based on the mass of species 2 in the blend and equal to the crystallinity existing in the unblended polymer. Curves B and C are representative of the crystallinity when finite crystallization conditions are imposed. Total suppression of crystallinity may occur for some composition regions, depending on the time allowed for the process to occur and on the value of the glass transition of polymer 1. Except near T_m, the suppression of crystallization is kinetic in origin because, as shown in Figure 4, the relative magnitudes of the heats of mixing and crystallization in the typical system (*12*) are such that thermodynamics cannot preclude the formation of crystals of polymer 2 at equilibrium. The melting point of these crystals at equilibrium will be depressed by a few degrees (as suggested in Figure 2) because of the lowered activity or chemical potential of this species in the amorphous phase.

Mixtures that are homogeneous at one temperature may undergo a liquid–liquid type phase separation at other temperatures. The common experience is for phase separation to occur on cooling, in which case an upper critical solution temperature, UCST, exists. UCST behavior is characteristic of endothermic mixing and a positive entropy of mixing and is well known in mixtures of low molecular weight species and for polymer

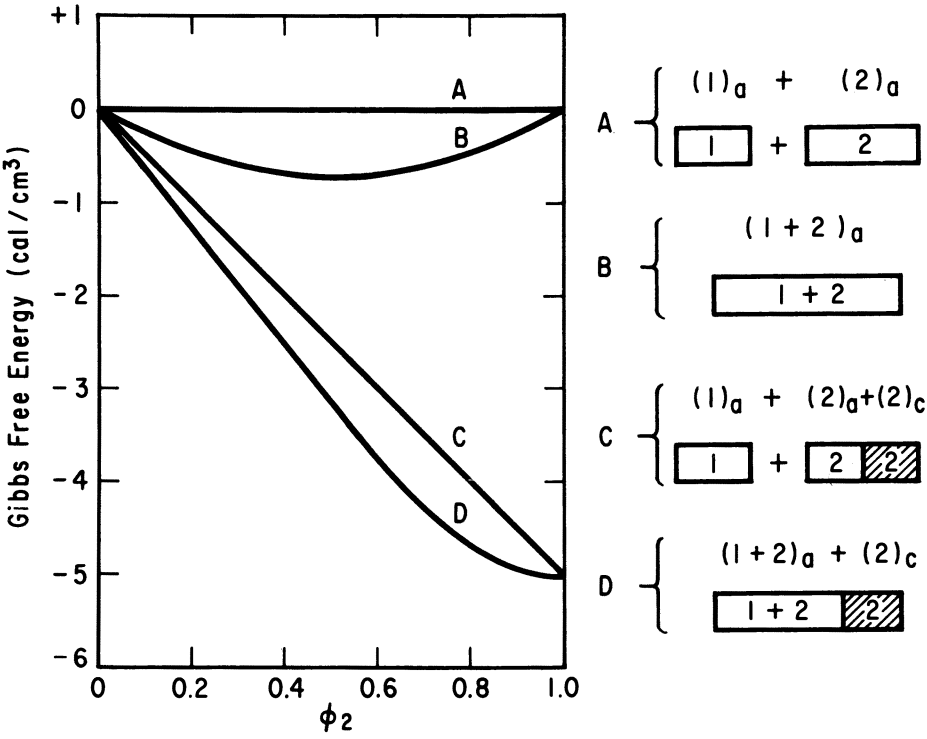

Figure 4. Free energy for miscible blends with and without crystallinity for typical energy parameters. Notation on right pictorially defines state considered: subscript c and shading denote crystalline phase, and subscript a and lack of shading denote amorphous phase. (Reproduced with permission from Ref 21. Copyright 1979 Plenum.)

solutions. However, for blends of high molecular weight polymers, UCST behavior does not seem to occur and generally should not be expected. On the other hand, phase separation on heating (*see* Figure 5) caused by a lower critical solution temperature, LCST, is rather prevalent in all blends (*6*, *33*). LCST behavior is characteristic of exothermic mixing and a negative excess entropy (*32*). It is not explained by the simple Flory–Huggins theory; however, the newer "equation of state" theories for mixtures (*8*, *25*) do predict such behavior. The common belief now is that "free-volume" effects are responsible for this mode of phase separation. The LCST is strongly influenced by the strength of the segmental interactions, in addition to free-volume effects. Mixtures with a large negative interaction parameter, B, will not phase separate except at very high temperatures that may exceed the thermal stability of the components (*8*).

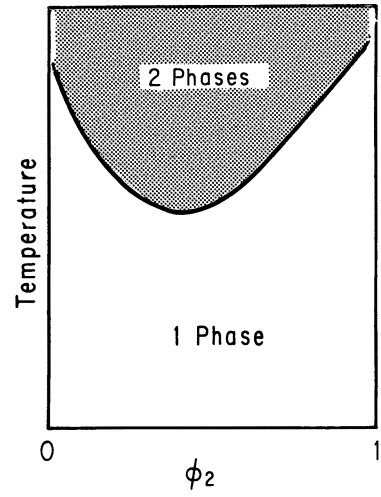

Figure 5. Liquid–liquid phase diagram showing LCST behavior.

Of course, liquid–liquid phase separation temperatures may occur in the vicinity of solid–liquid transitions, T_m or T_g, and make the blend phase diagram quite complex. In such systems, a homogeneous amorphous phase may be observed only over a portion of the composition spectrum.

Intense research efforts are in progress at several laboratories to quantify the interactions for polymer–polymer systems and to understand their origin. Only through such knowledge can equilibrium phase behavior be explained and related to component molecular structures so that technologically important multicomponent polymers can be precisely engineered. Through the use of a variety of techniques, progress is being made to understand the nature of the specific intermolecular and the intramolecular interactions involved. Interestingly, random copolymers often form miscible blends with other polymers, whereas the respective homopolymers do not [e.g., poly(methyl methacrylate) (PMMA)–poly(styrene-*co*-acrylonitrile), poly(vinyl chloride) (PVC)–poly(ethylene-*co*-vinyl acetate), or PVC–poly(butadiene-*co*-acrylonitrile)]. Intramolecular interactions are believed to be a factor in such behavior (*34*).

In spite of the intense activity and progress in the area of miscible blends, most polymer–polymer pairs are not miscible to any substantial degree, as the early literature suggested. However, such systems may nevertheless be of great technological value; hence, there is a strong incentive to develop a better scientific understanding of the important issues in such mixtures. Progress has been made in this area, but generally the subject has not yet generated the same fervor as miscibility. The main factors important to immiscible blends are the spatial arrangements of the phases (morphology) and the nature of the interface between them.

The most commonly expected phase morphology for immiscible blends is for one of the components to form a continuous matrix within which the other component is dispersed. The dispersed phase may be nearly spherical particles or highly elongated fibrils depending on the conditions used to fabricate the blend (e.g., elongational flows associated with orientation of sheet or film or with injection molding favor fibrillar morphologies). Generally, the major component is expected to form the continuous phase. However, as suggested in Figure 6, phase continuity is also influenced rather substantially by the relative rheological characteristics, viscosity to a first approximation, of the components (*6*). Under certain conditions cocontinuity of both components may exist. Interpenetrating networks, or IPNs, of phases formed from thermoplastic components are to be contrasted from molecular networks formed from two thermosetting polymers described by the same terminology (*19*). An IPN morphology is especially useful when the two phases do not adhere well to each other.

Phase morphology is not an inherent characteristic for a blend. It is substantially influenced by the method and conditions used to form the mixture. Technological advances are being made in the control of the nature and scale of phase dispersion in many blend products through the judicious use of sophisticated intensive mixing equipment, such as the various types of twin screw devices. Similarly, proper balancing of the rheological

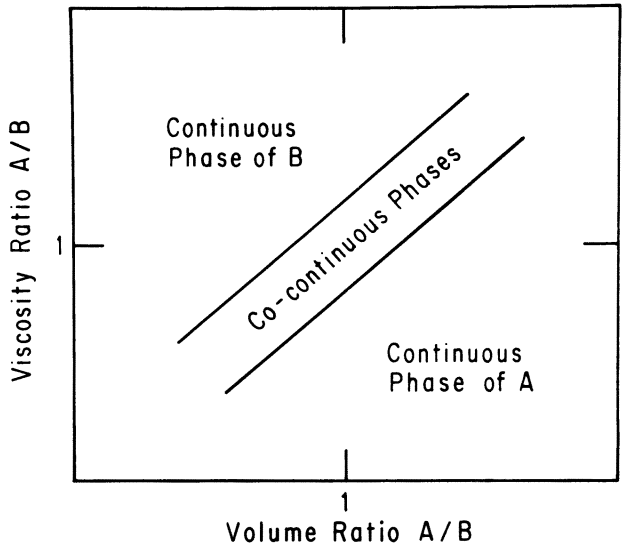

Figure 6. Effect of relative component proportions and viscosity on phase morphology. (Reproduced with permission from Ref 6. Copyright 1980 Marcel Dekker.)

properties of the components in the melt state by selection of appropriate molecular weight distribution grades is another important means for successfully tailoring morphology to meet product needs. In view of these considerations, Figure 6 is clearly a highly oversimplified picture and fundamental research on mixing and flow behavior of multiphase polymer systems (*35*) is needed to guide technological advances in blend compounding.

Another key factor is the nature of the interface between the phases. In the fluid state, the issue is the magnitude of the interfacial tension because it affects the extent of dispersion during mixing (*36*). In the solid state, the related issue is interfacial adhesion (*36*), which governs transfer of mechanical stresses between phases and how they share in supporting external loads. For components with low affinity for each other, the melt interfacial tension will be high and a fine dispersion of phases will be difficult to achieve. In the solid state, adhesion will be low and poor mechanical properties result. On the other hand, components with a stronger affinity for each other, but not so great as to cause miscibility, will have a low interfacial tension and high interfacial adhesion, both of which favor good property relationships. Recent work (*37*) has shown, as might be expected, that systems with significant partial miscibility also exhibit strong interfacial adhesion and good mechanical properties. Selection of systems on the "edge of miscibility" appears to be a means of reaping the benefits of phase separation without incurring the disadvantages. Knowing how to molecularly design for this type of system would provide an important technological advance.

Unfortunately, interactions between polymers that otherwise might be blended advantageously are weak, and the nature of the interface poses problems in both the melt and the solid state. One way to resolve this problem is to add suitably chosen block or graft copolymers that can function as coupling agents between the phases (*see* Figure 7). This concept is widely used in the technology of rubber toughening of plastics (*22*). It may be used in a more general way to make grossly immiscible components more compatible to form functionally useful blends (*see* Chapter 12 of Reference 4). This terminology does not imply that such additives render the system miscible, only that the interfacial problem is solved.

The most obvious choice for an interfacial agent or agent to effect compatibility is one where the segments of the polymers forming phases A and B are identical, respectively, with the segments C and D forming the block or graft copolymer. Recent work (*38*) has focused on the optimal molecular design of such additives. However, choosing systems where A is identical with C and B is identical with D is often rather restrictive. Frequently, the chemistry required to create such blocks or grafts is not known or is too expensive for practical use. Considerable relaxation of these restrictions occurs when one realizes that similar, or perhaps better, results

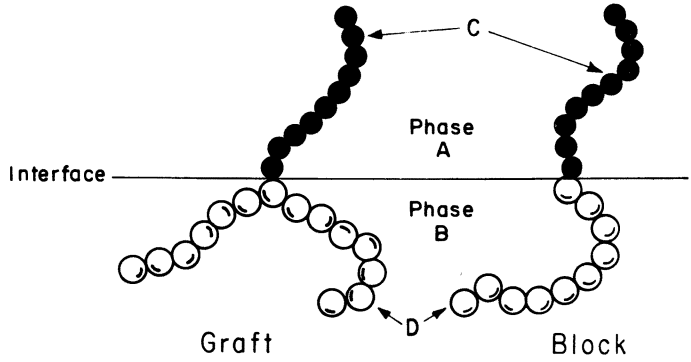

Figure 7. Idealized conformation of a block or graft copolymer at interface between phases. (Reproduced with permission from Ref. 4. Copyright 1978 Academic.)

may be had if A is miscible with C and B is miscible with D. In fact, design of coupling agents may be one of the most important uses of the growing knowledge about miscible blends. In the final analysis, it may be sufficient that A adheres to C and that B adheres to D. In reports of the beneficial use of block copolymers in blends (*39*, *40*), the simplistic interfacial configuration shown in Figure 7 is not possible. Apparently, the benefits stem from the ability of the block copolymer to adhere to both components and its propensity to promote an IPN morphology.

Property Relationships and Applications

The central motive for polymer blending is to create, in an economical fashion, products with desirable properties. Usually, the objective is not to achieve a certain value of a single property but a combination of characteristics (e.g., a critical balance between maximum use temperature, toughness, ease of fabrication, and perhaps resistance to chemicals or burning). A methodical approach to formulation requires experience about how blends behave or, even better, quantitative "mixing rules" for the various individual properties of interest. Parameters of these relationships are blend phase behavior and the interactions between components. To illustrate these points, some selected properties and examples of important blends systems are discussed (*6*, *41*).

Figure 8 contrasts the behavior of modulus, or stiffness, for miscible and immiscible blends of simple amorphous polymers. Miscible blends behave most nearly like random copolymers in that stiffness decreases precipitously at a single temperature that depends on composition. Thus, miscible blends of poly(phenylene oxide) (PPO) and polystyrene (PS) may be formulated to have any softening temperature between that of the more heat-resistant PPO and that of PS. Of course, the price varies accordingly

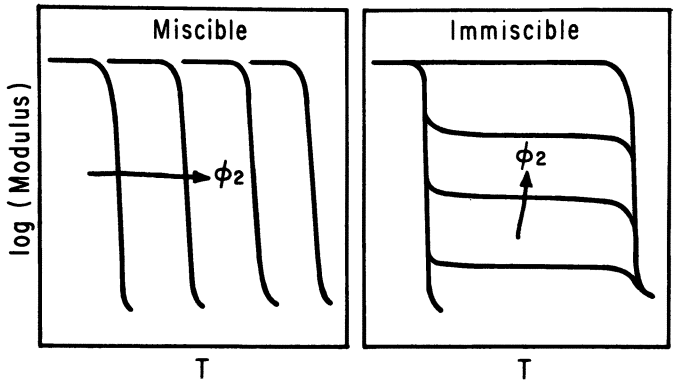

Figure 8. Effect of composition on temperature dependence of the modulus or stiffness of miscible and immiscible blends.

because PPO is more expensive, but overdesign for a given application can be minimized. Commercial success for this system derives partly from the improved processibility resulting from adding PS to PPO. Immiscible blends behave more like composites. In general, properties are dominated by the continuous phase. Commercial blends of acrylonitrile–butadiene–styrene (ABS) and polycarbonate (PC), which are not fully miscible, may have, at low stresses, a softening temperature near that of PC when this component is the continuous phase. The cost reduction and improved processibility that results from adding ABS to PC has made this system a successful product. When both phases are cocontinuous, stiffness is a nearly additive function of composition. Several products based on this concept made of crystalline polyolefins and ethylene–propylene elastomers have been introduced.

Failure characteristics, such as strength or toughness, are more complex than stiffness and may show more extreme behavior depending on the blend parameters. Figure 9 illustrates this concept in a schematic way for tensile strength. Curve A shows an interesting synergism that has been observed for both strength and modulus in some miscible blends (*42*, *43*). This response is believed to be the result of the contraction of free volume, or densification, on mixing that is an expected consequence of the energetic interactions responsible for miscibility in systems like PPO–PS. Curve C illustrates the opposite extreme where grossly immiscible blends fail at low stresses because of poor interfacial adhesion between components (*44*). Curve B shows a range of nearly additive responses that might be expected for miscible blends with little densification or for immiscible mixtures with good adhesion (*37*).

Figure 10 shows an example (*44*) where poor mechanical performance of an immiscible blend has been greatly improved by adding an agent to

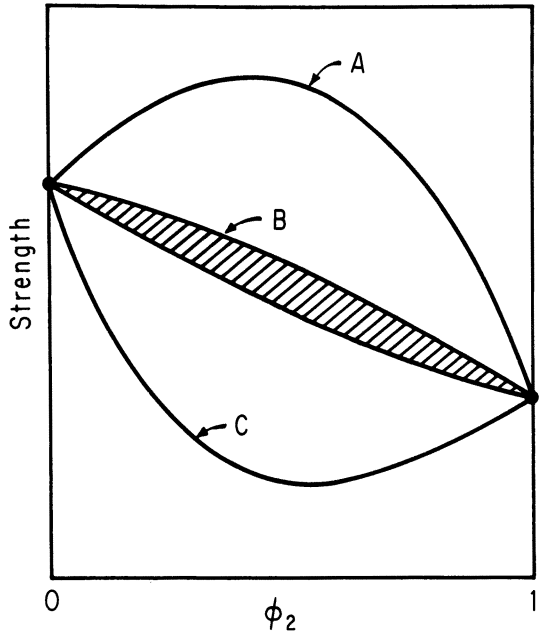

Figure 9. Possible strength–composition relationships for blends.

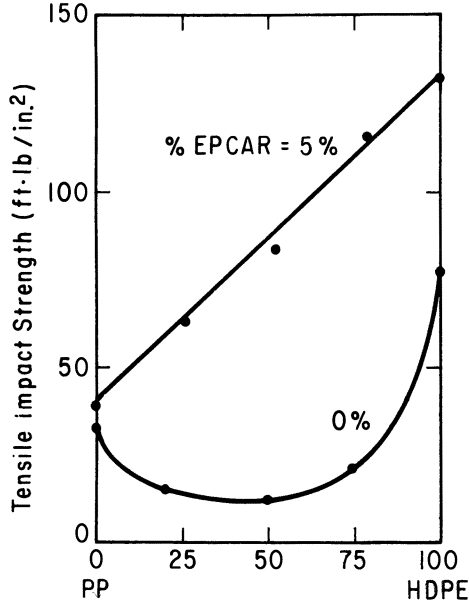

Figure 10. Effect of adding an ethylene–propylene copolymer (Epcar) on the mechanical behavior of polypropylene–high density polyethylene blends. (Reproduced with permission from Ref. 44. Copyright 1982 John Wiley and Sons.)

increase compatibility. A property relationship of type C in Figure 9 has been essentially converted to the more desirable type B.

Interest is growing in the use of polymers as barrier materials and as membranes for separation processes. Blending may provide a new dimension in product development for these applications. Figure 11 shows an example of gas permeation through miscible PPO–PS blends. The experimental data fall well below that predicted by a recently derived mixing rule for this property (*42*) that assumes additivity of free volume. The discrepancy between the data and the prediction may be a result of the segmental inter-

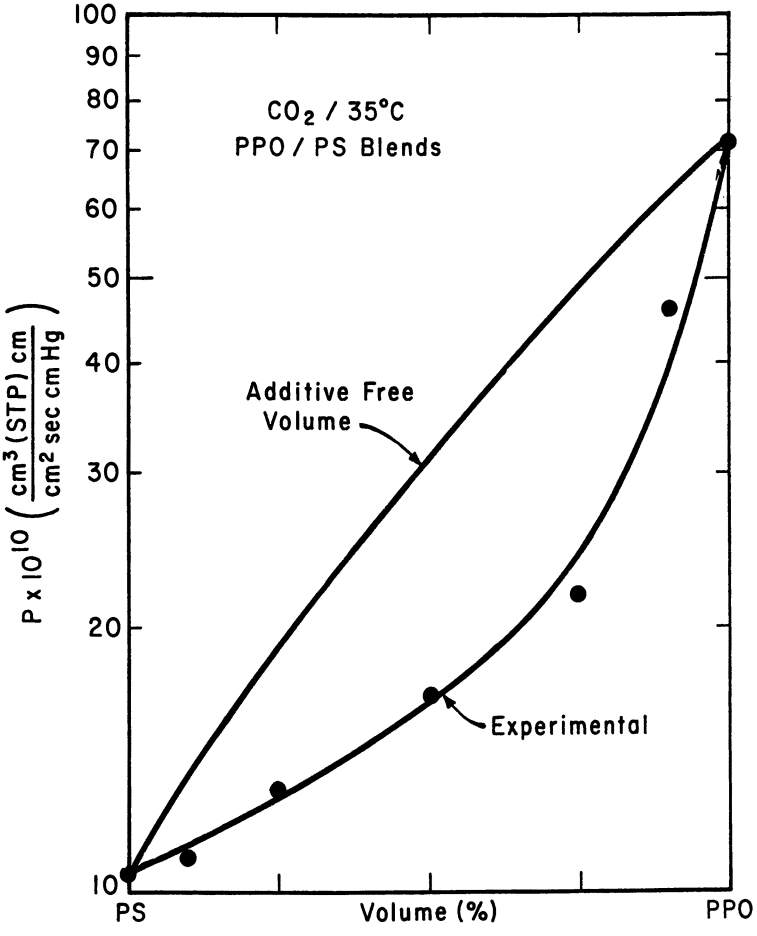

Figure 11. Gas permeation through PS–PPO blends.

actions between these two components. Interestingly, addition of small amounts of PS significantly improves the barrier characteristics of PPO. Transport of small molecules in phase-separated blends may be modeled by using composite theory (*see* Chapter 10 of Reference 4). Phase morphology is an important parameter governing the rate of permeation.

Crystallization of one or both components from a miscible blend is an extremely important factor in the resulting property relationship, but space does not permit full elaboration. A good example of the benefits of crystallization is the resistance to chemicals it imparts. For example, blends of semicrystalline poly(vinylidene fluoride) (PVF_2) with amorphous polymethacrylates (PMA) have recently been introduced partly because of the improved chemical resistance PVF_2 brings to the marriage. The same benefits may be imparted by crystallinity in blends with partial or limited miscibility. Recent commercial examples of this type include blends of amorphous PC with either poly(ethylene terephthalate) (PET) or poly(butylene terephthalate) (PBT) (General Electric's Xenoy series) (*41*).

Basic research on factors affecting the property relationships for polymer blends is expected to become more intense in the near future. The role of the various factors discussed should then become clearer.

Nomenclature

B	Interaction energy density, cal/cm^3
χ_1	Flory–Huggins interaction parameter
ΔG_m	Gibbs free energy of mixing, cal
ΔH_m	Enthalpy of mixing, cal
ΔS_m	Entropy of mixing, cal/K
n_i	Moles of species i
ϕ_i	Volume fraction of species i
R	Gas constant, cal/mole K
T	Absolute temperature, K

Acknowledgment

Acknowledgment is made to the donors of the Petroleum Research Fund, administered by the American Chemical Society, and to the Army Research Office for their support of this research.

Literature Cited

1. Dobry, A.; Boyer-Kawenoki, F. *J. Polym. Sci.* **1947**, *2*, 90.
2. Bohn, L. *Rubber Chem. Technol.* **1968**, *41*, 495.
3. Krause, S. *J. Macromol. Sci. Rev. Macromol. Chem.* **1972**, *C7*, 251.
4. Paul, D. R.; Newman, S., Eds. "Polymer Blends"; Academic: New York, 1978; Vols. 1 and 2.
5. Olabisi, O.; Robeson, L. M.; Shaw, M. T. "Polymer–Polymer Miscibility"; Academic: New York, 1979.

6. Paul, D. R.; Barlow, J. W. *J. Macromol. Sci. Rev. Macromol. Chem.* **1980**, *C18*, 109.
7. Barlow, J. W.; Paul, D. R. *Annu. Rev. Mater. Sci.* **1981**, *11*, 299.
8. Paul, D. R.; Barlow, J. W. In "Polymer Compatibility and Incompatibility: Principles and Practices"; MMI Press Symposium Series; Harwood Academic: New York, 1982; Vol. 2; Chap. 1.
9. Scott, R. L. *J. Chem. Phys.* **1949**, *17*, 279.
10. Flory, P. J. *J. Chem. Phys.* **1942**, *10*, 51.
11. Huggins, M. L. *J. Phys. Chem.* **1942**, *46*, 151.
12. Paul, D. R.; Barlow, J. W. *Polym. Sci. Technol.* **1979**, *11*, 239.
13. Platzer, N. A. J., Ed. "Multicomponent Polymer Systems"; ADVANCES IN CHEMISTRY SERIES No. 99; ACS: Washington, D.C., 1971.
14. Platzer, N. A. J., Ed. "Copolymers, Polyblends, and Composites"; ADVANCES IN CHEMISTRY SERIES No. 142; ACS: Washington, D.C., 1975.
15. Cooper, S. L.; Estes, G. M., Eds. "Multiphase Polymers"; ADVANCES IN CHEMISTRY SERIES No. 176, ACS: Washington, D.C., 1979.
16. Manson, J. A.; Sperling, L. H. "Polymer Blends and Composites"; Plenum: New York, 1976.
17. Solc, K., Ed. "Polymer Compatibility and Incompatibility: Principles and Practices"; MMI Press Symposium Series; Harwood Academic: New York, 1982; Vol. 2.
18. Sperling, L. H., Ed. "Recent Advances in Polymer Blends, Grafts, and Blocks"; Plenum: New York, 1974.
19. Sperling, L. H. "Interpenetrating Polymer Networks and Related Materials"; Plenum: New York, 1981.
20. Klempner, D.; Frisch, K. C., Eds. "Polymer Alloys: Blends, Blocks, Grafts and Interpenetrating Networks"; Plenum: New York, 1977.
21. Klempner, D.; Frisch, K. C., Eds. "Polymer Alloys II: Blends, Blocks, Grafts and Interpenetrating Networks"; Plenum: New York, 1979.
22. Bucknall, C. B. "Toughened Plastics"; Appl. Sci.: London, 1977.
23. Martuscelli, E.; Palumbo, R.; Kryszewski, M., Eds. "Polymer Blends: Processing, Morphology, and Properties"; Plenum: New York, 1979.
24. Olabisi, O. In "Kirk-Othmer: Encyclopedia of Chemical Technology," 3d ed.; Wiley: New York, 1982; Vol. 18, p. 443.
25. Sanchez, I. C. *Annu. Rev. Mater. Sci.* **1983**, *13*, 387.
26. "Polymer Blends: 1981" *Polym. Eng. Sci.* **1982**, *22*, No. 2.
27. "Polymer Blends: 1982" *Polym. Eng. Sci.* **1982**, *22*, No. 17.
28. "Rheology and Processing of Polymer Blends" *Polym. Eng. Sci.* **1983**, *23*, No. 11.
29. "Specific Interactions in Polymer Blends" *Polym. Eng. Sci.* **1983**, *23*, No. 12.
30. Cruz, C. A.; Barlow, J. W.; Paul, D. R. *Macromolecules* **1979**, *12*, 726.
31. Harris, J. E.; Paul, D. R.; Barlow, J. W. *Polym. Eng. Sci.* **1983**, *23*, 676.
32. Taylor, L. D.; Cerankowski, L. D. *J. Polym. Sci. Polym. Chem. Ed.* **1975**, *13*, 2551.
33. Bernstein, R. E.; Cruz, C. A.; Paul, D. R.; Barlow, J. W. *Macromolecules* **1977**, *10*, 681.
34. Paul, D. R.; Barlow, J. W. *Polymer* **1984**, *25*, 487.
35. Han, C. D. "Multiphase Flow in Polymer Processing"; Academic: New York, 1981.
36. Wu, S. "Polymer Interface and Adhesion"; Dekker: New York, 1982.
37. Barlow, J. W.; Paul, D. R. *Polym. Eng. Sci.* **1984**, *24*, 525.
38. Foyt, R.; Jerome, R.; Teyssie, P. *J. Polym. Sci. Polym. Phys. Ed.* **1982**, *20*, 2209.

39. Gergen, W. P.; Davison, S. U.S. Patent 4 107 130, 1978.
40. Traugott, T. D.; Barlow, J. W.; Paul, D. R. *J. Appl. Polym. Sci.* **1983**, *28*, 2947.
41. *Chem. Week* **1983**, *Mar. 2*, 72.
42. Paul, D. R. *J. Membr. Sci.* **1984**, *18*, 75.
43. Kleiner, L.; Karasz, F. E.; MacKnight, W. J. *Polym. Eng. Sci.* **1979**, *19*, 519.
44. Bartlett, D. W.; Barlow, J. W.; Paul, D. R. *J. Appl. Polym. Sci.* **1982**, *27*, 2351.
45. Paul, D. R.; Barlow, J. W.; Bernstein, R. E.; Wahrmund, D. C. *Polym. Eng. Sci.* **1978**, *18*, 1225.

RECEIVED for review November 15, 1984. ACCEPTED February 11, 1985.

2

Recent Developments in Interpenetrating Polymer Networks and Related Materials

L. .I. SPERLING

Polymer Science and Engineering Program, Department of Chemical Engineering, Materials Research Center No. 32, Lehigh University, Bethlehem, PA 18015

An interpenetrating polymer network, IPN, is defined as a combination of two polymers in network form, at least one of which is synthesized and/or cross-linked in the immediate presence of the other. In this chapter, the literature and patents on IPNs are reviewed from 1979 to the present. Many compositions contain two continuous phases, which contribute to their toughness. A new area of IPN interest is the thermoplastic IPN concept, where the IPNs have physical rather than chemical cross-links.

AN INTERPENETRATING POLYMER NETWORK, IPN, previously was defined as a combination of two polymers in network form, at least one of which is synthesized and/or cross-linked in the immediate presence of the other (*1*). Although this definition still fits most materials called IPNs, now some hybrid compositions, such as the thermoplastic IPNs, call for a broader view. This chapter will review the IPN literature from 1979 to the present. The choice of year 1979 is dictated by the advent of several reviews covering the literature up to that time (*1–4*).

During the 1960s and 1970s, several synthetic methods were developed to prepare IPNs. These methods include materials now called sequential IPNs, where the networks are made sequentially, and simultaneous interpenetrating networks, SINs, where both monomers are mixed together and polymerized by independent and noninterfering routes. Surprisingly, most workers find it is better to polymerize one of the two networks in an SIN faster than the other, as will be explored further. Other methods of synthesis include latex IPNs, where both networks are on each latex particle, and interpenetrating elastomeric networks, IENs, where two latexes are mixed and subsequently cross-linked.

0065-2393/86/0211/0021$9.75/0

The two-phased nature of these materials was established by a series of experiments involving transmission electron microscopy (TEM), dynamic mechanical spectroscopy (DMS), and a host of other instrumental methods. Dual phase continuity was established for several of these materials. The effect of fillers was examined. A number of mechanical properties were studied; these studies showed synergistic effects for IPNs based on rubber–plastic compositions. In particular, plastic and leathery compositions based on a glassy network and a rubbery network were found to be surprisingly tough. Other IPNs were shown to have superior high temperature stability. Anionic–cationic IPNs were found to have excellent ion-exchange capabilities. The beginnings of a systematic nomenclature scheme were developed.

In all, about 125 papers and 75 patents had appeared by 1979. This review will examine new papers and patents; the discussion will have to be incomplete because of space limitations. Several IPN-based products were identified by 1979, and new ones will be mentioned in this review.

Nomenclature

The nomenclature of polymer blends, blocks, grafts, and IPNs is advancing rapidly. Two new nomenclature documents are now before their various committees at the International Union of Pure and Applied Chemistry (IUPAC) (*5*) and the Polymer Chemistry Division of the American Chemical Society (*6*). The first of these (*5*) updates and develops the nomenclature of random and alternating copolymers, graft copolymers, and block copolymers. The second (*6*) presents a nomenclature scheme for polymer blends, networks, and IPNs.

A few of the most important points relating to multicomponent polymeric materials from both of these documents will now be described.

Block Copolymers. A block copolymer is defined as a polymer comprising molecules in which there is a linear arrangement of blocks; a block is defined as a portion of a polymer molecule in which the monomeric units have at least one constitutional or configurational feature absent from the adjacent portions. In the sequence arrangements

–AAAAAAAAAA–BBBBBBBBBB–

and

–AAAAAAAAAA–BBBBBBBBBB–AAAAAAAAAA–

the corresponding polymers are named polyA-*block*-polyB and polyA-*block*-polyB-*block*-polyA, respectively. The triblock copolymer of polystyrene–polybutadiene–polystyrene is thus named polystyrene-*block*-polybu-

tadiene-*block*-polystyrene. The older way of naming this composition was poly(styrene-*b*-butadiene-*b*-styrene).

Graft Copolymers. A graft copolymer is a polymer comprising molecules with one or more species of block connected to the main chain as side chains. These side chains have constitutional or configurational features that differ from those in the main chain. The simplest case of a graft copolymer can be represented by

```
-AAAAAAAAAAAAXAAAAAAAAAAAA-
                |
                BBBBBBBBBBBBB-
```

The corresponding name is polyA-*graft*-polyB.

If more than one graft chain is attached to the backbone, semicolons are used to separate the names of the grafts or their symbolic representations. For example, where polystyrene (PS) and poly(methyl methacrylate) (PMMA) chains are grafted to a polybutadiene (PB) backbone, the polymer is named polybutadiene-*graft*-[polystyrene:poly(methyl methacrylate)].

Cross-linked Polymers. This material is a three-dimensional polymer structure, where (ideally) all of the chains are connected through cross-links. Cross-linked polybutadiene is named poly(*cross*-butadiene). A conterminously linked copolymer is a polymer chain that is linked at both ends or along its chain to the same or constitutionally or configurationally different chain or chains: a polymer cross-linked by a second species of polymer. The conterminously linked copolymers used to be called AB-cross-linked copolymers. For poly(vinyl trichloroacetate) cross-linked with PS, the polymer is named poly(vinyl trichloroacetate)-*cross*-polystyrene.

Interpenetrating Polymer Networks. An IPN is a combination of two cross-linked polymers that (ideally) are not bonded to each other. Usually, they are an intimate mixture of two polymers that are both in network form; at least one is synthesized and/or cross-linked in the immediate presence of the other. An IPN of poly(ethyl acrylate) and PMMA synthesized in that order is named poly[*cross*-(ethyl acrylate)]-*inter*-poly[*cross*-(methyl methacrylate)]. Previously, this composition was written as poly(ethyl acrylate)/poly(methyl methacrylate). The present nomenclature allows for the two semi-IPNs in a natural way, by leaving out the first or second *cross*.

SINs, which are simultaneously polymerized pairs of networks, are indicated by placing square brackets around "-[*inter*]-".

The term *-stat-* stands for statistical copolymer and replaces the term *-co-*, which now represents unknown combinations (5).

Polymer Blends. A polymer blend is an intimate combination of two or more polymer chains of constitutionally or configurationally different

features that are not bonded to each other. A polymer blend of polyisoprene and PS is named polyisoprene-*blend*-polystyrene.

The power of the improved nomenclature schemes lies both in the scientist's ability to name complex combinations of polymers clearly and precisely and as an aid to the imagination of new combinations, not yet made, but easily arrived at through permutations of the several linking symbols now available.

Sequential IPN Morphology

The main problems in sequential IPN morphology have centered around the shapes and sizes of the phases and aspects of dual phase continuity. During the 1970s, detailed studies of sequential IPN morphology were carried out by Huelck et al. (*7*, *8*) and Donatelli et al. (*9*, *10*). Modulus studies between the lower and higher glass transition temperatures, T_g, suggested dual phase continuity for many of the compositions studied, whereas transmission electron microscopy suggested the presence of spheres. However, most of the so-called "spheres" were really somewhat ellipsoidal, as illustrated in Figure 1 (*7*).

In spite of the slightly contradictory experimental picture, Donatelli et al. (*11*), Michel et al. (*12*) and Yeo et al. (*13*) derived equations showing how the phase domain diameters of the sphere diameters of polymer II, D_2, varied with the cross-link density (concentration of network chains) of net-

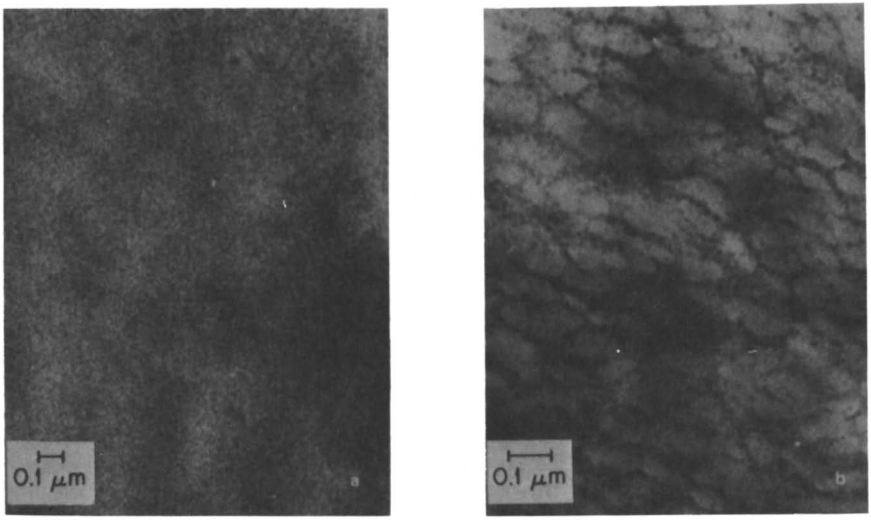

Figure 1. Morphology of sequential IPNs. (a) Poly(ethyl acrylate)–poly(methyl methacrylate), showing significant miscibility. (b) Poly(ethyl acrylate)–polystyrene, immiscible, showing a typical cellular structure. (Reproduced from Ref. 7. Copyright 1972 American Chemical Society.)

works I and II (polymerized in that order), ν_1 and ν_2; the interfacial tension, γ; each phase, ϕ_1 and ϕ_2; and temperature, T. The final equation for a full sequential IPN may be written (*13*)

$$D_2 = \frac{4\gamma}{RT(A\nu_1 + B\nu_2)} \tag{1}$$

$$A = \tfrac{1}{2}\left(\frac{1}{\phi_2}\right)(3\phi_1^{1/3} - 3\phi_1^{4/3} - \phi_1 \ln \phi_1) \tag{2}$$

$$B = \tfrac{1}{2}(\ln \phi_2 - 3\phi_2^{2/3} + 3) \tag{3}$$

Thus, the domain diameters of the second polymerized polymer may be predicted solely on the knowledge of the networks and their interaction.

Theoretical results are compared to experimental data for the IPN system poly[*cross*-(*n*-butyl acrylate)]-*inter*-poly(*cross*-styrene) (PnBA–PS) in Table I (*13–16*). The agreement between theory and experiment for this system as well as others is excellent, in fact, better than could be expected, noting the approximations. Yeo et al. (*13*) realized that spheres were a poor approximation for many sequential IPNs.

Widmaier and Sperling (*17–19*) approached the question of dual phase continuity through use of a de-cross-linking and extraction route and by using scanning electron microscopic (SEM) techniques developed by Kresge (*20*). In brief, samples of PnBA were cross-linked with acrylic acid anhydride, AAA. Then, sequential IPNs were made with PS. On soaking in warm ammonia water, the AAA was hydrolyzed, and the polymer de-cross-linked. The PnBA was then extracted, and the sample was examined by SEM. The porous structure shown in Figure 2 was found (*17*). The spherical-type structures of about 0.1 μm in diameter correspond to the spheres previously mentioned. However, clearly they are bound together to make a continuous structure. One such possibility is modeled in Figure 3.

Table I. Domain Diameters of P(nBA)–PS IPNs

P(nBA)–PS Volume Ratio	*Diameter (Å)*	
	D_2, *Experiment*	D_2, *Theory*
25:75	800	845
40:60	650	644
50:50	550	572

NOTE: Molecular characteristics: ν_1 is 3.7×10^{-5} mol/cm^3, ν_2 is 21.8×10^{-5} mol/cm^3, and γ is 3.65 dyne/cm.

SOURCE: Reproduced with permission from Ref 13. Copyright 1983 *Polymer*.

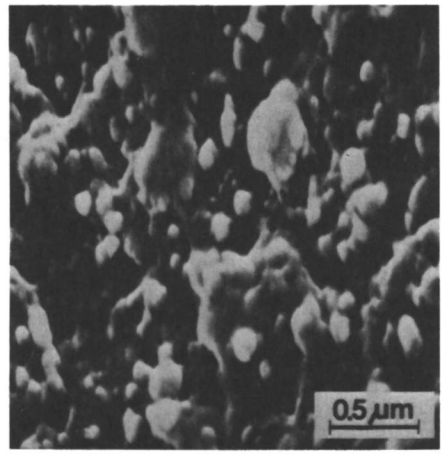

*Figure 2. De-cross-linked and extracted PnBA(AAA)–PS(DVB) 50:50, viewed by SEM. The polystyrene phase remains, and the poly(*n*-butyl acrylate) was removed. (Reproduced from Ref. 17. Copyright 1982 American Chemical Society.)*

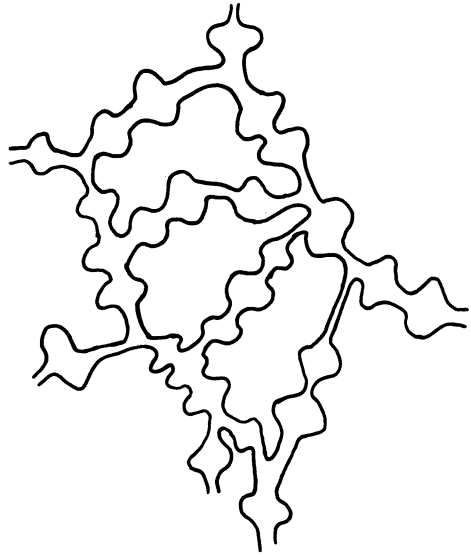

Figure 3. Model of sequential IPN morphology.

Very recently, the morphology of poly(*cross*-butadiene)-*inter*-poly(*cross*-styrene), PB–PS, sequential IPNs and semi-I IPNs was examined via small-angle neutron scattering (SANS) (*21*). In this study, the PS was deuterated to provide contrast. The information obtained is summarized in Table II. By using the Debye plot, the correlation distance, *a*, was obtained. From that quantity, chord lengths, equivalent sphere diameters, and surface areas may be estimated. Except for the equivalent sphere diameters, no particular model of phase domain shape is required. In fact, the Debye model works best for completely random phase structures.

The results are compared to TEM studies on osmium tetroxide stained samples in Table II. The chord lengths and equivalent sphere diameters are in rough agreement with electron microscopy, especially the lower end of the size range reported. Surface areas in the range of 150–200 m^2/g indicate true colloidal dimensions for the phase domains[1].

The nomenclature for IPNs has been discussed. Broadly defined, a sequential IPN is a material in which network I is fully formed before monomer II is introduced. Thus, the chains are extended by the swelling action of monomer II, and the phase domain size is greatly reduced. In SINs, both monomers (or prepolymers) are introduced together. Ideally, both monomers are reacted simultaneously, but independently. In fact, this reaction is rarely done exactly. It seems much more convenient, and better materials result, if the reactions are carried out more or less sequentially after the monomers are introduced simultaneously. In an SIN, ideally, the chains of neither polymer should be perturbed or extended. By varying the reaction scheme, many materials may be made that do not fit clearly into one category or the other.

Table II. PB-PS(D_8) IPNs and Semi-I IPN Dimensions by SANS and TEM Techniques

Sample Code	*Volume Fraction*		*Correlation Length*	*Intercept Length (Å)*			*Diameter (Å)*	
	ϕ_1	ϕ_2	a (Å)	L_1[a]	L_2[a]	S_{sp}[b] (m^2/g)	D[c]	D[d] *Range*
A	0.193	0.807	106	131	549	58.8	D_1 197	300–2000
							D_2 824	700–1500
B	0.270	0.730	53	73	194	149	D_1 109	150–1200
							D_2 294	350–600
C	0.230	0.770	58	75	252	122	D_1 113	150–1200
							D_2 378	500–1100
D	0.240	0.760	37.5	49	154	196	D_1 74	300–600
							D_2 234	400–800

NOTE: Subscript 1 is polybutadiene, and subscript 2 is polystyrene.
[a] L = length. [b] S_{sp} = specific surface area. [c] From SANS, $D_1 = (3/2)[a/(1 - \phi_1)]$; $D_2 = (3/2)[a/(1 - \phi_2)]$. [d] From TEM measurements.
SOURCE: Reproduced from Ref 21. Copyright 1983, *Polymer Preprints*.

[1] Further studies of IPNs with SANS can be found in Chapter 10 of this volume.

Interfacial Characterization

Lipatov and coworkers have continued their characterization of sequential IPNs (*22*) and SINs (*23*) via small-angle X-ray scattering (SAXS) and diffraction. Several quantities were determined that characterize the two-phased nature of these materials: specific surface area, S/V; distance of heterogeneity, l_c; reduced inhomogeneity length, l_p; average radius of the largest heterogeneous regions, R; and interlayer thickness, B.

The sequential IPN (*22*) was based on a polyurethane (PU) and polystyrene–divinylbenzene (DVB) (3%). The SIN was based on a PU and polyurethane acrylate (PUA). The values reported by Lipatov et al. (*22*, *23*) are summarized in Table III.

Of special interest are the values of B reported for the poly(*cross*-urethane)-*inter*-poly(*cross*-styrene) (PU–PS) IPN. As more PS was added, B got smaller; this result indicated that mixing between the phases was relatively greater at low PS levels than in midrange compositions. The specific surface areas reported for the poly(*cross*-urethane)-[*inter*]-poly[*cross*-(urethane acrylate)] (PU–PUA) SIN are of the same order of magnitude as reported by Sperling et al. (*21*) using SANS (*see* Table II).

Truly Miscible IPNs

The entropy of mixing two polymeric species is very small because of the very long chains involved. Coupled with the usually positive heat of mixing, the resulting free energy of mixing is positive and causes these materials to phase separate. This tendency to phase separate is true for polymer blends, grafts, blocks, and IPNs alike. The one known way to achieve truly miscible polymer blends is to have negative heats of mixing (i.e., the two polymers attract one another).

All of the IPN systems described are thought to have positive heats of mixing because they phase separate. The blend of poly(2,6-dimethyl-1,4-

Table III. Domain Characterization of IPNs and SINs via SAXS Techniques (*22*, *23*)

Composition	*Percent Second Polymer*	l_p (Å)	B (Å)	l_c (Å)	R (Å)	S/V (m^2/g)
PU–PS	3.6	20	37	320	—	—
IPN	8.6	24	30	120	—	—
	31.4	72	23	180	—	—
	35.4	80	21	190	—	—
PU–PUA	0	—	—	550	—	—
SIN	5	—	—	440	360	10
	10	—	—	475	480	40
	40	—	—	454	450	290
	50	—	—	533	730	120
	75	—	—	123	430	320
	90	—	—	134	540	100
	100	—	—	280	—	—

phenylene oxide) (PPO) with PS is known to have a negative heat of mixing. Indeed, these two polymers are miscible in all proportions (*24*). Frisch and coworkers (*25*, *26*) made SINs out of this polymer pair to achieve better interpenetration of the two networks.

Frisch and coworkers (*25*, *26*) cross-linked the PPO by brominating the polymer, followed by reaction with a tertiary amine. The PS was cross-linked with DVB. The PPO with ethylene diamine was dissolved in styrene monomer containing DVB and azobisisobutyronitrile (AIBN) and heated to 70 °C for 24 h. Semi-SINs and linear blends were also synthesized. As perhaps expected, all of these materials exhibited a single T_g, which varied systematically with composition, and no phase separation was observed via electron microscopy. These observations lead to the conclusion that truly interpenetrating polymer networks were produced.

The study of homo-IPNs can be related to maximizing molecular interpenetration. A homo-IPN is one in which both networks are identical in composition. Several teams have studied homo-IPNs of PS–PS, and this work was recently reviewed (*27*). Although molecular interpenetration was extensive, a slight degree of segregation was found. The segregation, of the order of 50–100 Å, may be caused by random fluctuations in network I. By and large, little evidence was seen for added cross-links in the system, probably because both networks dilute each other. However, evidence was found for domination of the physical properties by network I, which behaves as if it is more continuous in space.

Two-Phased IPNs

Because of the low entropy of mixing and the positive heats of mixing, most polymer blends phase separate. IPNs are no exception.

Adachi and coworkers made a detailed study of the synthesis and properties of three sequential IPN systems:

1. poly[*cross*-(ethyl acrylate)]-*inter*-poly[*cross*-(methyl methacrylate)], PEA–PMMA (*28*);
2. poly(*cross*-oxyethylene)-*inter*-poly[*cross*-(acrylic acid)] (*29*); and
3. poly[*cross*-(acrylonitrile-*stat*-butadiene)]-*inter*-poly[*cross*-(methyl methacrylate)] (*30*).

In each system, semi-IPNs were compared with full IPNs.

In the PEA–PMMA IPNs, two synthetic routes were taken. In the first, the cross-linked PEA (polymer I) was swelled with methyl methacrylate (MMA) monomer plus ethylene dimethacrylate (EDMA) and AIBN for various periods of time, and the MMA polymerized. This series is the SW-series. This synthetic method was very similar to that employed by Huelck et al. (*7*, *8*). In the second synthetic route, the PEA was fully swollen with monomer, by about a factor of 3. In each system, the polymerization was

permitted to proceed for short periods of time, and the remaining monomer was removed by evaporation. This series is called the CV-series.

Amazingly, the two series were not alike. The SW-series, like the studies of Huelck et al. (*7*, *8*) were transparent materials that exhibited one broad glass transition. The CV-series, however, exhibit opaque optical behavior and have two peaks in the tan δ–temperature plots.

Adachi and Totaka (*28*) concluded that PMMA microgels of various sizes were presumably formed within the PEA network. The PMMA microgels eventually interconnect and develop into a fully interpenetrating network with a microheterogeneous nodular structure. (*See* Figure 3 for a model of such a structure.) Adachi and Totaka (*28*) were able to isolate this structure at an early stage of development by interrupting the reaction.

Most interestingly, this study applies to theories of network formation. Although important theories suggest that a network polymerization from a vinyl and divinyl reaction is random, at least three theories have suggested an early microgel formation (*31*–*33*). In each theory, a mixture of monomer and linear polymer is formed, and the microgel is floating around in the mixture. As the polymerization proceeds, the gels eventually aggregate and connect together. In polymerizing monomer II in the presence of network I, the viscosity of the polymerizing mixture is very high. Perhaps this high viscosity causes the microgel aspects to be emphasized.

Sperling and Widmaier (*34*) point out that even though a polymer blend becomes more immiscible as the molecular weight is raised, an IPN becomes more miscible as the cross-link level is raised. In fact, the major force in making an IPN more miscible is the cross-linking itself. (Grafting obviously contributes as well, if the concentration of graft sites is significant.) Sperling and Widmaier carried out a preliminary thermodynamic analysis of the effects of cross-links and calculated the expected miscibility in sequential IPNs based on PnBA and PS.

Simultaneous Interpenetrating Networks

SINs refer to that subclass of IPNs in which both monomer or prepolymer mixes are blended or mutually dissolved before network formation of either component. Although this scheme has many variations, one possible test of the difference between an SIN and a sequential IPN (not foolproof) is to ask if either network is strained. In most of the sequential IPNs, network I is swollen and strained at points in the synthesis, whereas in most of the SINs, both networks are relaxed throughout.

The major exception is the system in which there is an exchange of components. For example, network I is formed in the presence of a solvent. The solvent is evaporated and replaced with a monomer II mix. The monomer II mix is then polymerized; the mix volume just equals the volume of the removed solvent. The result is better classified as a sequential IPN, but intermediate systems can and have been made.

Park et al. (*35*) outlined several factors controlling the extent of miscibility in SINs:

1. Compatibility of each of the component polymers
2. Relative rates of reaction and network formation
3. Average molecular weight per cross-link
4. Weight fraction of each polymer network component
5. Degree of polymerization at the time of gelation
6. Mobility of the polymer chains, especially to phase separate.

Park et al. (*35*) investigated SINs based on PU and poly(styrene-*stat*-acrylonitrile). The glass transition behavior determined by DMS showed relatively large T_g shifts with similar gel times and smaller M_c (the molecular weight between cross-links). A simultaneously gelled SIN may have dual phase continuity and is likely to have the greatest extent of interpenetration.

Dubuisson et al. (*36*, *37*) studied a modified type of homo-SIN. Both polymers possessed the bisphenol A group, but one network had an acrylic function that led to a chain reaction, and the other network had an epoxy function that led to polycondensation. These homo-SINs were miscible and had one T_g. The T_g had a minimum, and the density was slightly less than expected from the simple average. This result suggests that the SINs were barely miscible and perhaps close to the point of phase separation.

Lim et al. (*38*) prepared three-component IPNs made from polyurethane–poly(*n*-butyl methacrylate)–poly(methyl methacrylate), PU–PBMA–PMMA. In various combinations, either the PU–PMMA or the PU–PBMA blends were made in SIN form, and the third polymer network was added by sequential polymerization modes. The glass transition behavior of the three component IPNs showed three separate but broad T_g values for the (PU–PMMA)–PBMA IPNs, one broad T_g for the PU transition, and the other at an intermediate temperature between the PMMA transition and the PBMA transition. Both three-component IPNs showed high damping characteristics; tan δ was in the range of 0.2–0.4 in the temperature range of -30 to $+90$ °C.

Lee and Kim (*39*) prepared PU–PMMA SINs under high pressure, up to 20,000 kg/cm^2. The PU phase domain sizes decreased from ~ 300 to ~ 30 Å as the pressure was increased up to 20,000 kg/cm^2. The phase continuity also changed with pressure. The PU phase was continuous at low pressure, whereas the PMMA phase became continuous at higher pressures. The SINs prepared at 20,000 kg/cm^2 exhibited a very broad glass transition ranging from ~ 0 °C to ~ 100 °C, and the materials were optically transparent.

Meyer and coworkers (*40–45*) reported a very detailed study of an SIN system based on poly(*cross*-urethane)-[*inter*]-poly[*cross*-(methyl methacry-

late)], PU–PMMA. The synthesis, in general, was as follows. The PU network was formed by an aromatic triisocyanate and a polyether glycol, catalyzed by stannous octanoate. The PMMA network resulted from an AIBN-initiated free radical polymerization of MMA with a trimethacrylate. All of the monomer components were mixed together. The PU network was formed first at room temperature, and then the PMMA network was formed by raising the temperature. Light had to be excluded at early stages in the reaction or the PMMA began polymerization prematurely, and nontransparent or otherwise undesirable products resulted. Grafting was found to be negligible.

The mechanical behavior of these PU–PMMA SINs was investigated by Morin et al. (*40*). The PU–PMMA SINs exhibited two loss peaks, in tan δ versus temperature studies, but the transitions were shifted inward significantly, with broadening. These researchers concluded that these materials exhibited phase separation, but that it was quite incomplete.

Morin et al. (*40*) studied a range of mechanical behavior of these SINs. Table IV (*40*) shows the ultimate elongation of some of these materials as a function of the cross-linker concentration in each network. Lower cross-linking in the PMMA phase and/or higher cross-linking in the PU phase seems to increase elongation. Only above the T_g does cross-linking appear to reinforce a polymeric material.

Phase-separated IPNs and SINs have outstanding mechanical properties. For example, the PB–PS 20–80 IPN has an impact resistance of approximately 5 ft–lb/in. of notch (*9*, *10*), or within the range of important ABS plastics. Space did not permit a detailed treatment of the many papers on mechanical behavior.

Yet, some of the highest potentials of IPNs and SINs lie not in the realm of rubber-toughened plastics, but in the leathery and rubbery compositions. Here, compositions must be cross-linked to prevent flow or adhesive behavior. The cross-links in an IPN or SIN serve two purposes: (1) They control and reduce domain sizes, and (2) where two continuous

Table IV. Ultimate Elongation of PU–PMMA SINs with Cross-linker Content

	Percent TRIM[b]		
K[a]	*5*	*1*	*0*
0.77	46	—	70
0.89	99	—	56
1.01	99	—	223
1.07	184	264	336
1.13	191	—	220

NOTE: PUR content is 34%.
[a]NCO to OH ratio.
[b]Trimethylol-1,1,1-propane trimethacrylate.

phases exist, they mechanically keep the two phases in close juxtaposition. These unique features provide not only mechanical toughness, but also a range of other possibilities.

Thus, reinforced elastomers in which submicroscopic plastic domains play some of the role of carbon blacks or silicas are of interest. Medical applications such as denture bases require tough, leathery compositions. Transport phenomena such as variable and controllable diffusion rates are also of interest.

Noise and Vibration Damping Materials

Both the loss modulus, E'', and the loss tangent, tan δ, are measures of noise and vibration damping, which requires a transformation of mechanical energy into heat. Somewhat similar to the absorption of IR electromagnetic radiation to increase molecular motion, damping might be called mechanical spectroscopy. The noise emitted by a brass band is only sufficient to warm a cup of tea.

Immiscible IPNs exhibit two glass transitions and two tan δ–temperature peaks. Compositions that are nearly (but not quite) miscible and in which the phases are very small exhibit one very broad peak that sometimes spans 100 °C or more. Temperature and frequency are equivalent according to the Williams–Landel–Ferry (WLF) equation, and so this peak is equivalent to about 13 decades of frequency.

Although the molecular basis of damping is not yet completely understood, features such as flexible chains rubbing over stiffer ones are thought to be important (*1*).

In one study on acoustical damping, Hourston and McCluskey (*46*) swelled a cross-linked poly(vinyl isobutyl ether) polymer with methyl acrylate and DVB to make a sequential IPN. The IPNs exhibited high damping over a broad temperature range and had relatively constant E'' peaks over the temperature range of -20 to $+20$ °C.

Hourston and Zia (*47*) made what can best be described as a semi-II SIN. They mixed PU precursors with unsaturated polyesters, styrene, and methyl acrylate. The linear PU was formed at 20 °C. Then the temperature was raised to 70 °C and the polyester–styrene–methyl acrylate network was formed. Although these materials were not specifically examined for noise and vibration damping, they seemed semicompatible, or in the newer terminology, semimiscible (*see* Figure 4) (*47*).

Hourston and Zia (*48*) also made both semi-I and semi-II versions of SIN compositions of PU and PMA. By using the Davies equation, they found that both phases exhibited some degree of phase continuity. Hourston et al. (*49*) are also studying the behavior of latex IPNs made from acrylics. These materials have a core and a shell and are synthesized sequentially from two different monomers and their respective cross-linkers in latex form.

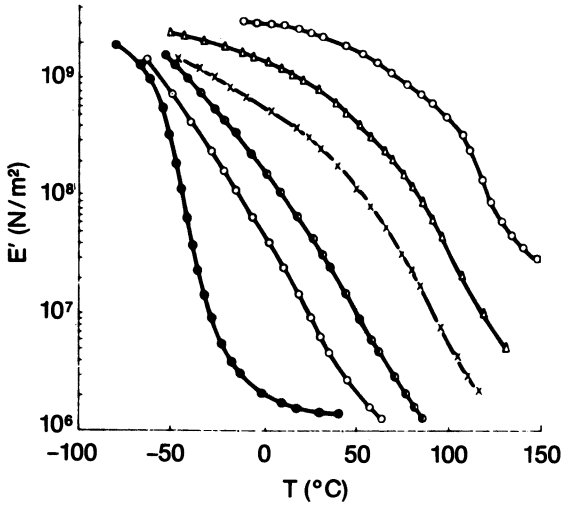

Figure 4. The dynamic storage modulus, E', of polyurethane (linear) and poly(ester-styrene-methyl methacrylate) (cross-linked) semi-II SINs. The midrange compositions have very broad glass transitions. (Reproduced with permission from Ref. 47. Copyright 1979 Polymer.*)*

Different Synthetic Routes for Making SINs

In the previous discussion, sequential IPNs were distinguished from SINs. However, three different routes are available for making an SIN after mixing the two monomers or prepolymers: Monomer I may be polymerized first, monomer II may be polymerized first, or the two might be truly simultaneously polymerized. Suzuki and coworkers (*50*) made a systematic study of the effects of each of these three ways using an acrylate and an epoxy system. UV light and heat were used to control the two reaction rates. The three products were, as might be expected, significantly different. The normal SIN, with the acrylic polymerized first, was heterogeneous, whereas the other two behaved much more homogeneously. In all three systems, significant deviation of the densities from the additivity rule was observed, and all three, again, were different.

IPN-Based Ion-Exchange Resins

Ion-Exchange Resins. Effective ion-exchange resins have their cation- and anion-exchange portions in close proximity. However, although the two charges should be close together in space, they need to be phase separated or the two charges may react with one another and cause coacervation.

IPNs can be made into ion-exchange resins in several ways. In one system, one of the networks has the anionic ion-exchange capacity, and the

other has the cationic ion-exchange capacity. Alternately, only one of the networks is charged; the other holds the network in place and prevents excess swelling. One particularly effective mode was developed by Kolarz (*51*, 52), who used poly(styrene-*stat*-DVB) for network I, and poly(methacrylic acid-*stat*-DVB) for network II. The interesting feature of these IPNs is that the PS network is formed by suspension polymerization chemistry in the presence of aliphatic solvents. These aliphatic solvents dissolve the monomer mix, but, on polymerization, the PS precipitates. A high concentration of DVB is required, because the PS must form a network before precipitation ensues. After polymerization of network I is complete, the structure is a highly porous bead. Monomer mix II is then swollen in and most of it goes in the pores; on polymerization, an IPN is formed. In this system, only the methacrylic acid portion serves as an ion-exchange resin. Kolarz (52) determined the concentration of elastically active chains and found 0.06 to 0.17 volume fraction of interpenetration.

Alternatively, the ionic IPN can be made into a membrane that possesses good transport properties toward strong mineral acids. Such a system was developed by Pozniak and Trochimczuk (*53*, *54*). They employed a membrane of PE, into which were swollen mixtures of styrene and DVB. After polymerization, the PS portions were reacted via a chloromethylation procedure and subsequent amination with diethylamine to form a weak base type of membrane.

Donnan Dialysis Membranes. Cox et al. (*55*) studied anion-exchange membranes based on PE and cross-linked poly(4-vinylpyridine) and cation-exchange membranes based on PE and cross-linked PS. The latter was sulfonated via a chlorosulfonation process for activation.

Cox et al. (*55*) suggested a model for the optimum ion-exchange membranes for Donnan dialysis. The most important factor, they stated, is the presence of a continuous network of ion-exchange sites through the width of the membrane. Then, site-to-site diffusion can occur continuously from the sample to the receiver. Thus, as long as the chain of exchange sites is not broken, dual phase continuity must be present in the system. Pore size and tortuosity are not critical when site-to-site mechanisms prevail.

The anion-exchange membranes prepared from 4-vinylpyridine and PE yielded site-to-site diffusion control mechanisms, whereas the cation-exchange membranes that contained poly(styrene sulfonate) and PE did not.

Metamorphosis of an IPN

Exactly how do the domains form and grow during IPN formation? As discussed, Adachi and coworkers (*28–30*) concluded that network II microgels of various sizes form, grow, and eventually interconnect to develop into a fully interpenetrating microheterogeneous nodular structure. The actual

development of the second phase impinges upon important parts of network theory and the theory of gelation.

Kolarz (*51*) summarized much of the thinking towards understanding the actual mechanics and kinetics of gelation in real systems. An important point relates to the fact that some cross-linkers, especially DVB, exhibit different and perhaps higher reactivities than the monomer that they are cross-linking (*56*). If the reactivity of the cross-linker is higher than the monomer, the early formed polymer will be rich in pendent double bonds and more highly cross-linked (*31–33*). This result leads to microgel formation. The microgels are linked together through long entangled polymer chains.

More recently, percolation theory has been applied to the kinetics of formation of these microgels (*57*). Computer analysis of various systems using percolation theory indicates regions of polymer gel formation, surrounded by regions of lesser polymer formation. These developments model network I and suggest an inhomogeneous network formation. Interestingly, they also model the nascent state of network II, which develops with fresh monomer and fresh cross-linker.

Lipatov et al. (*58*) pointed out that the degree of phase separation in an IPN depends on the rate of three-dimensional network formation and the rate of interdiffusion of the components. Studying semi-II IPNs based on PnBA and cross-linked PS, they showed the intensity of light scattered in polymerizing systems as a function of time. The light intensity remains unchanged for a period of time, then increases rather linearly, followed by no substantial increase. An increase in the linear polymer concentration (from low values) leads to a lowering of the time for the onset of turbidity. The percent of DVB in the styrene seems to make little difference in the time for beginning of turbidity. This last observation suggests that linear polymer I is doing most of the diffusing in the critical range.

Fernandez and Sperling (*59*) studied the development of phase domains in poly(*cross*-butadiene)-*inter*-poly(*cross*-styrene), PB–PS, sequential IPNs by SANS. For partial PS polymerization, they found a peak in the scattering intensity that moved to smaller angles during the early portions of monomer II polymerization. This peak movement might indicate the development of growing spherical structures. About 1.5×10^{16} domains/cm^3 were estimated in one composition; this estimation was supported by an examination of the appropriate electron micrograph. After ~ 40% conversion of monomer II, however, domain size via the SANS maximum remained substantially constant. This result was interpreted as an indication of the development of cylindrical structures.

Rosovizky et al. (*60*), quoting a thesis by Karbanova (*61*) on poly(*cross*-urethane)-[*inter*]-poly[*cross*-(urethane acrylate)] (PU–PUA) SINs, reported on electron microscopy and SAXS. According to the thesis, the number of the PUA regions in the SIN increases with the volume fraction of

PUA up to 0.4. Beyond 0.5, the size of the PUA regions increases, and the volume fraction of the interfacial layer (with a thickness of 20–40 Å) decreases.

Fernandez and Sperling (59) thought that although the domain diameters (cylinders?) remained substantially constant, a reorganization of the structure part way through polymerization of monomer II was occurring. In particular, the electron micrographs showed a fine structure in the PS phase on the order of 100 Å. These structures apparently become fused into larger domains as the polymerization proceeds.

SINs from Special Functional Triglyceride Oils

Most triglyceride oils, such as corn oil or soy bean oil, have only double-bond functionality. A few oils, however, have other functional groups. For example, castor oil has one hydroxyl group per acid residue and will allow the synthesis of polyesters and of polyurethanes, which are commercial. These oils are also fine candidates for making SINs. A special reason for research in this area is that these oils are renewable resources.

SINs made from castor oil and PS (*62*, *63*) made a series of tough plastics or reinforced elastomers; the material formed depends on the relative quantities of each product.

Research in this area then shifted to vernonia oil, which comes from a wild plant growing in Kenya, Africa. Vernonia oil is especially interesting because each acid residue has an epoxy group (*64*).

New research in this area involves the study of oils coming from *Lesquerella palmeri*, a desert wildflower growing in western Arizona and northern Mexico (*65*). *Lesquerella palmeri* is known to the people of the area as "popweeds" or "bladderpods," because of the structure of the seed pod. Lesquerella oil has hydroxyl groups, like castor oil, but not quite so many. However, the acid residue is a little longer, so the T_g from lesquerella–sebacic (decanedioic) acid rubber networks is lower than castor, about -50 to -60 °C (*see* Table V). The epoxidized oils yield higher T_g values, but the reaction is controllable.

Lesquerella oils make tough sequential IPNs and SINs with PS. The energy to break in elongation ranged from about 2 to about 11 MJ/m^3, which compares with about 1 MJ/m^3 for PS. Like many of these materials, the more interesting compositions are in the leathery or stiff rubbery range.

Recycling of Plastics Wastes

As more and more plastics are consumed, the problem of plastics wastes gets worse. To recover or recycle the plastics wastes by converting them into new useful products is now becoming both ecologically and financially desirable. Plastics wastes are usually mixtures of incompatible materials, and straight blending and molding produces poor materials.

Table V. *Lesquerella palmeri* Compositions and Glass Transition Temperatures (T_g)

Composition	T_{g1}[a]	T_{g2}[b]
Elastomer		
Poly[LP(SULF(1%)),SA(1.0)]	−65	—
Poly[LP,SA(0.75),TDI(0.25)]	−55	—
Poly[ELP,SA(0.70)]	−28	—
SIN 50/50		
Poly[(LP(TBHP(1%)),SA(1.0)SIN-(S,DVB(5%))]	−52	114
Poly[(LP,SA(0.40),TDI(0.60))-SIN-(S,DVB(5%))]	−55	113
Poly[(LP(SULF(1%)),SA(1.0),TDI(0.40)-SIN-(S,DVB(5%))]	−55	120
Poly[(ELP,SA(0.40),TDI(0.60)SIN-(S,DVB(5%))]	−13	110
Poly[(ELP,SA(0.70))-SIN-(S,DVB(5%))]	−8	112
IPN 50/50		
Poly[(ELP,SA(0.70))-IPN-(S,DVB(5%))]	44	—

NOTE: Key to abbreviations: LP, crude *Lesquerella palmeri* oil; ELP, epoxidized *L. palmeri* oil; SA, sebacic acid; TBHP, *tert*-butyl hydroperoxide; S, styrene; and SULF, sulfur. Polystyrene T_{g2} = 92 °C.

[a] Temperature (°C), elastomer phase.

[b] Temperature (°C), plastic phase.

SOURCE: Reproduced with permission from Ref. 65. Copyright 1984 *Journal of Polymer Materials.*

Djomo et al. (*66*) studied the effects of combining blends of PS and poly(vinyl chloride) (PVC) through the use of either a PS network based on styrene and DVB or an elastomeric network based on poly(ethyl acrylate) (PEA) and hexanediol diacrylate.

These materials are technically semi-II IPNs because two polymer I components are blended. According to the nomenclature described, the second of these two semi-II materials can be named [polystyrene-*blend*-poly(vinyl chloride)]-*inter*-poly[*cross*-(ethyl acrylate)].

Djomo et al. (*66*) found that the semi-II IPN with PS gave marginal improvements in tensile strength and impact resistance. However, the elastomer network did make a significant improvement in these properties, especially with cross-linker contents of about 2%.

SIN-Based Reaction Injection Molded Systems

The spectacular rise of reaction injection molding, RIM, in the automotive and other industries was caused by the high speed of the process and the high energy efficiency. Current RIM materials are based on PU technology because hydroxyl groups and isocyanate groups react rapidly and completely. In addition, the finished urethanes can be made with high moduli and strength. However, the industry would like RIM plastics with still higher moduli. Although reinforced RIM, RRIM, containing glass fibers or other materials has become important, the high viscosities and abrasiveness of the filled systems presents some disadvantages.

A novel solution to the problem is the use of SIN-based RIM systems being developed by Frisch and coworkers (*67–69*). For example, an elastomeric PU can be used in combination with a plastic epoxy resin to produce a rapid-reaction SIN (*67*, *68*). Depending on the composition, Pernice et al. (*67*, *68*) made their IPN-based RIM materials by curing in the mold at 100 °C for 5 min, followed by postcuring at 121 °C for 1 h.

RIM materials made in this way developed good phase separation, as indicated by their T_g values (*see* Table VI) (*68*). Three T_g peaks are observed via DSC: two for the soft and hard segments of the PU, and one for the epoxy. The inward shifting of the T_g values provides some indication of the extent of actual phase mixing. The Frisch IPN–RIM system is visualized as an alternative to RRIM (*69*).

Manson and Sperling (*70*) suggested making RIM systems from castor oil based SINs. As a natural triglyceride, castor oil is unusual because it has three hydroxyl groups per molecule, one for each acid residue. Castor oil is already used to make commercial urethane elastomers, especially foam rubber. Castor oil can be combined with toluene 2,4-diisocyanate (TDI), styrene, DVB, and initiators and reacted to make tough plastics and elastomers by the SIN route. Other oils that can be used include vernonia (epoxy bearing) and lesquerella (hydroxyl bearing) (*62–64*, *71*). What is required is the development of catalytic systems to react these materials with the required speed.

Thermoplastic IPNS

Thermoplastic IPNs are defined as IPNs in which the chemical cross-links have been replaced by physical cross-links. Three principal types of physical cross-links include the hard blocks in block copolymers, the ionic portions of ionomers, and the crystalline portions of semicrystalline polymers. In all of these materials, the cross-links make the material behave as a thermoset at service temperature but soften and permit the material to flow at some elevated temperature. A thermoplastic IPN is formed by combining

Table VI. Glass Transition Temperatures of Urethane–Epoxy SIN-RIM Materials

Composition PU–Epon 828	T_{g1}	T_{g2}	T_{g3}
100–0	−99	+95	—
90–10	−91	+82	—
80–20	−89	+96	+114
70–30	−93	+85	+119
60–40	−92	+86	+118
0–100	—	—	+119

NOTE: Temperatures are in degrees Celsius.
SOURCE: Reproduced with permission from Ref. 68. Copyright 1982 Technomic Publishing Co.

two polymers each with some type of physical cross-links. These materials are really hybrids, or crosses between blends and IPNs. Like many hybrids, some will resemble one parent more than another. For nomenclature purposes, they will be considered blends. However, many of these materials have special synergistic properties, resulting from very special mixing and/or reaction conditions.

The earliest thermoplastic IPNs were based on polypropylene and ethylene–propylene–diene (EPDM) rubber, and were invented in the early 1970s. Siegfried et al. (*72–74*) described a series of thermoplastic IPNs based on Kraton rubber, polystyrene-*block*-poly(ethylene-*co*-butylene)-*block*-polystyrene (SEBS), and poly(styrene-*stat*-sodium methacrylate).

The materials made by Siegfried et al. (*72–74*) were called chemically blended thermoplastic IPNs because the styrene–methacrylic acid mix was swollen into the block copolymer and polymerized in situ. The mechanically blended system was made by separately synthesizing the two polymers and mechanically blending the two later. The chemically blended thermoplastic IPNs had tensile strengths of about 5000 psi, and were somewhat better generally than their mechanically blended counterparts.

Davison and Gergen (*75*, *76*) prepared mechanically blended thermoplastic IPNs from SEBS; Kraton; and nylon, PE, or PC. These and other thermoplastic IPNs seem to have the very special property of dual phase continuity.

Dual phase continuity is not a new concept; however it is sometimes difficult to understand and even more difficult to prove in the laboratory. A simple example of dual phase continuity is an air filter and the air that flows through it. A Maxwell "demon" can traverse the entire material space within either the air phase or the filter phase, for both are continuous throughout the occupied space.

A concept important to understanding how dual phase continuity can be brought about in polymer blends and thermoplastic IPNs is that of phase inversion. If one phase is continuous and the other discontinuous and if conditions are changed such that the second becomes continuous and the first phase becomes discontinuous, it is said that a phase inversion has taken place. At some time during the inversion, however, both phases were continuous. Frequently the polymer scientist then wants to stop the phase inversion process somewhere near its midpoint and, thus, attain the special, desired features.

Requirements for Dual Phase Continuity. A quantitative model for predicting phase continuity and inversion in stirred, two-phased systems is shown in Figure 5 (*77*). The quantities η_1 and η_2 represent the viscosity of phases 1 and 2, and ϕ_1 and ϕ_2 represent the volume fraction of phases 1 and 2, respectively. Thus, the phase with the lower viscosity or higher volume fraction will tend to be the continuous phase and vice versa (*78*). If phase inversion occurs during the reaction, mixing, or heating path, the idealized

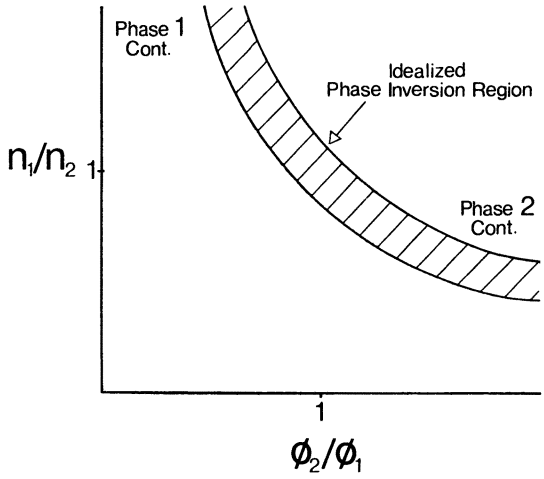

Figure 5. Theoretical phase continuity diagram (77). The hatched area indicates the approximate range of dual phase continuity. A phase I (oil-rich) continuous material can be made into a phase II (PS-rich) continuous material by crossing this boundary.

line or region should be crossed. The phase inversion is probably not instantaneous, but more likely a slower transition in which a region of dual phase continuity exists. By assuming symmetrical behavior, an equation expressing the midpoint of the phase inversion region may be written

$$\frac{\eta_1}{\eta_2} \cdot \frac{\phi_2}{\phi_1} \cong 1 \tag{4}$$

Of course, the viscosities vary with temperature, perhaps following the WLF equation, and can be made to vary with slight degrees of cross-linking. Polymerization of the remaining monomer or evaporation of the solvent will also obviously affect Equation 4. Sudden gelation, however, may cause interference with the phase inversion phenomenon (77).

The model illustrated in Figure 5 and Equation 4 requires that the system be stirred to undergo phase inversion. Yet, because the shear rate is not part of this simplified model, the shear rate is assumed to be small, and hence, by extrapolation, should work best in the limit of zero shear rate.

SEBS-Based Thermoplastic IPNs. Gergen (79) described the synthesis and properties of some thermoplastic IPNs based on SEBS and poly(ether sulfone), nylon 11, or polypropylene. Gergen stresses the importance of the primary morphological characteristics in classifying these types of thermoplastic IPNs.

In this synthesis, the SEBS polymer phase is penetrated by a molten resin and forms an IPN structure. The SEBS does not dissolve or disperse, because its cross-links hold it together. The material retains its structure after the resin has been solidified. Further, this structure is retained even during melt processing without loss of the interpenetrating cocontinuous structure. Even though strong forces attempt to reverse the intimate mixing, the viscoelastic characteristics brought about by the PS end blocks stabilize the structure indefinitely, even in the melt.

The morphology of the two interlocking phases is modeled in Figure 6 (*79*). Here, the left and right portions illustrate the spatial arrangements of the two phases in the interlocking form. Gergen (*79*) emphasizes that each phase is distinct and of a size much larger than molecular dimensions. Individual specimens can be prepared for examination by extracting one phase or the other with an appropriate solvent for one phase but not for the other. The remaining component can then be studied via SEM. For example, the thermoplastic IPN of SEBS and poly(ether sulfone) has phase sizes on the order of 15–20 μm, and resembles a magnified view of a sponge (i.e., a very open-celled structure). Phase sizes as small as 0.1 μm can be obtained, however, by controlling such features and the solubility parameter differences, or the volume fractions of each phase. The SEBS polymer provides both the template within which the IPN structure is formed as well as the resistance to retraction of these phases into discrete particle morphology.

Modeled Systems. Widmaier et al. (*80*, *81*) prepared thermoplastic IPN model systems based on polystyrene-*block*-polyisoprene-*block*-polystyrene, SIS, and cross-linked PS. The styrene component was swollen into the triblock copolymer along with a solvent and polymerized via anionic polymerization in place. Then, the living PS was cross-linked through the addition of a controlled quantity of DVB, and the reaction was terminated. Various series of samples were made up where the M_c value of the PS was varied. TEM showed that smaller M_c for the PS resulted in coarser morphologies, especially when M_c was smaller than the primary molecular

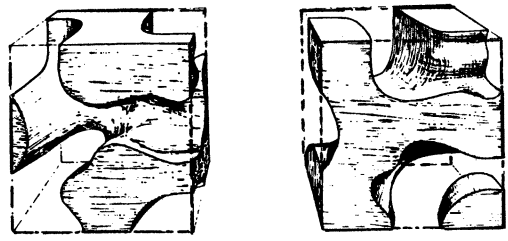

Figure 6. Gergen's model of an IPN morphology illustrating dual phase continuity. (Reproduced with permission from Ref. 79. Copyright 1984 Kautschuk & Gummi Kunststoffe.)

weight of the triblock copolymer. As M_c became greater than M_{SIS} (molecular weight of the block copolymer), more SIS could be extracted.

Interpenetrating Polymer Networks and Cocontinuous Phases

Recently, a point of confusion has arisen in IPN terminology; two groups of definitions have been presented for the term IPN. To clarify the situation, the terms of interest are defined in Table VII. In one definition, the term IPN has been used to describe two polymer networks that are polymerized and/or cross-linked in the immediate presence of one another, the meaning that will be used throughout this review. This term was coined before the implications of phase separation were fully realized and does not necessarily imply molecular interpenetration, although molecular interpenetration is often present.

On the other hand, the term IPN, sometimes shortened to interpenetrating networks, has been used to describe the phase structure of polymers. This definition refers to one of three nearly identical terms: interpenetrating phases, interlocking phases, or cocontinuous phases. The first two terms more clearly indicate that portions of each phase meet each other on different sides of the juxtaposing phase. The last term merely indicates that in some way a Maxwell's demon could traverse all macroscopic space within either phase. If an anisotropic condition is permitted (for relaxed samples), alternating lamellae might also satisfy the requirements for dual phase continuity. Therefore, macroscopic isotropy is implicit in all of the terms as used in this discussion. To minimize confusion arising through

Table VII. Interpenetrating Polymer Network Terminology

Term	*Definition*
Chemical cross-links	Covalent bonds linking two or more chains.
Physical cross-links	Noncovalent bonds linking two or more chains arising from crystallinity, block copolymer domains, or ionomer domains.
Polymer network	A three-dimensional structure of chains linked by chemical or physical cross-links.
Interpenetrating polymer networks (IPNs)	Two polymer networks that are polymerized and/or cross-linked in the immediate presence of one another (by chemical bonds).
Thermoplastic IPN	An interpenetrating polymer network cross-linked with physical rather than chemical bonds.
Intertwining polymer networks	A term sometimes used to mean interpenetrating polymer networks.
Phase	A definite part of a system, homogeneous throughout, and physically separated from other phases by distinct boundaries.
Interpenetrating phases, interlocking phases, cocontinuous phases, dual phase continuity	Two phases that are each continuous in space, such that each contacts all portions of the sample space. Terms nearly synonymous in meaning.

similarity, the term *cocontinuous phases* will be used in this chapter. Adding to the confusion, the materials that make up IPNs frequently have cocontinuous phases. Also, cocontinuous phase materials often possess crosslinks and may be IPNs; however, the two groups are not synonymous. A few examples are in order. If a polymer blend of two linear, amorphous polymers is prepared so that the phases interpenetrate or are cocontinuous, the material is not an IPN. If the polymers are chemically cross-linked by covalent bonds, the material simultaneously fulfills both definitions.

For the intermediate case, where the cocontinuous phase material consists of physical cross-links arising from crystallinity, block copolymer domains, or ionomeric attractions, the term thermoplastic IPN is used. As previously discussed, thermoplastic IPNs are hybrid materials possessing some of the properties of both thermoplastic blends and IPNs.

Likewise, an IPN need not possess cocontinuous phases or even significant molecular interpenetration. Swelling in a small proportion of monomer II (plus cross-linker) into network I and polymerizing II may result in network II being discontinuous in space and forming a cellular structure. If the two polymers are totally immiscible, a minimum of molecular interpenetration will occur, even at the interface.

Nevertheless, an IPN will more frequently exhibit synergistic behavior if the phases do interlock. Further improvements frequently arise when significant molecular mixing or network interpenetration occurs, especially at the phase interface. In addition, cocontinuous phase materials containing physical cross-links (thermoplastic IPNs) are often most desired. In fact, the whole area of thermoplastic IPNs and cocontinuous phase materials is one of the *hottest* areas of current research.

Gradient IPNs and Microencapsulation

Controlled Drug Delivery Systems. Whereas most of the applications described relate to mechanical behavior, IPNs find several other uses. Anionic–cationic ion-exchange resins have already been mentioned. A new application involves controlled drug delivery.

Conventional oral dosage forms of water-soluble drugs consist of coated tablets. After dissolution of the coating in the stomach, they disintegrate more or less rapidly. As a result, drug concentrations in the blood quickly reach a sharp peak, followed by a decrease at a rate determined by the metabolic half-life in the body. For many purposes, a controlled, steady drug delivery is desirable.

One solution to the problem of controlled drug delivery makes use of insoluble hydrogel beads that are loaded with the drug. Then, delivery depends on the hydrophilicity of the polymer, the diameter of the bead, and the diffusion rate. This last parameter can be controlled by using coatings or shell structures that form multilayered beads with different diffusion

rates. Because retardation of the delivery rate is generally desired, the outer layer(s) should have a low permeability toward the drug.

A simple method of preparing a multilayered bead involves gradient IPN technology (*82–86*). A gradient IPN can be made in two ways. For chain polymerization, network I is briefly swollen with monomer II mix and polymerized before diffusion creates a uniform solution. For step polymerizations, one of the component monomers is swollen into the bead first, and the second component is added to the outside later.

Mueller and Heiber (*87–88*) prepared a gradient IPN based on hydrogel beads with substrates of 2-hydroxyethyl methacrylate (HEMA) and *N*-vinylpyrrolidone (NVP). Polymer I was cross-linked with poly(*n*-butylene oxide) capped with isophorone diisocyanate, which reacts with the hydroxyl groups on the HEMA. The beads were swelled with a diol or triol and a PU-gradient IPN was formed by reaction with 2,4,4(2,2,4)-trimethylhexane 1,6-diisocyanate, TMDI, by diffusion-controlled reaction.

An important feature of gradient IPNs is the concentration of network II as a function of distance from the surface. Mueller and Heiber (*87*) noted that the boundary between IPN-modified surface regions and the unmodified core was sharpest when polymer network I was more polar and, therefore, had a lower affinity for TMDI. The nonuniform polyurethane distribution was studied by SEM X-ray microprobe methods using brominated diols (*see* Figure 7) (*87*).

Oxprenolol HCl, highly water and ethanol soluble, was used as a model compound. Mueller and Heiber found that the hydrophilicity rate of swelling and the permeability of the IPN was highest for the most hydrophilic polymer matrice. Thin network II layers synthesized on the surface of network I act as membranes and retard the release of isoprenolol HCl.

In another system, Raghunathan et al. (*89*) used a gel-type DVB–sulfonic acid cation-exchange resin, which held phenylpropanolamine in an acid–base complex. Ethylcellulose was used as the diffusion barrier material. There are several advantages of adsorbing basic nitrogen-containing drugs onto sulfonic acid ion-exchange resins for dosage forms: (a) prolonged drug release from the complex, (b) reduced toxicity by slowing drug absorption, (c) protection of the drug from hydrolysis or other degradation, (d) improved palatability, and (e) ease of formulation (*90*). Ion-exchange resin beads have also been microencapsulated acacia and gelatin (*91*).

Microencapsulation also serves to improve the gritty and astringent taste of finely divided PS–DVB copolymer anion-exchange resins for swallowing. One method is to coat the particles with an acrylic polymer cross-linked with allyl sucrose to make a surface-modified sequential IPN (*92*).

Miscellaneous Applications. In addition to interfacial polymerization, which produces a core-shell structure, multiwalled structures have been made. For example, a three-layer structure composed of epoxy resin, polyurea, and polyamide can be prepared by emulsifying an aqueous pol-

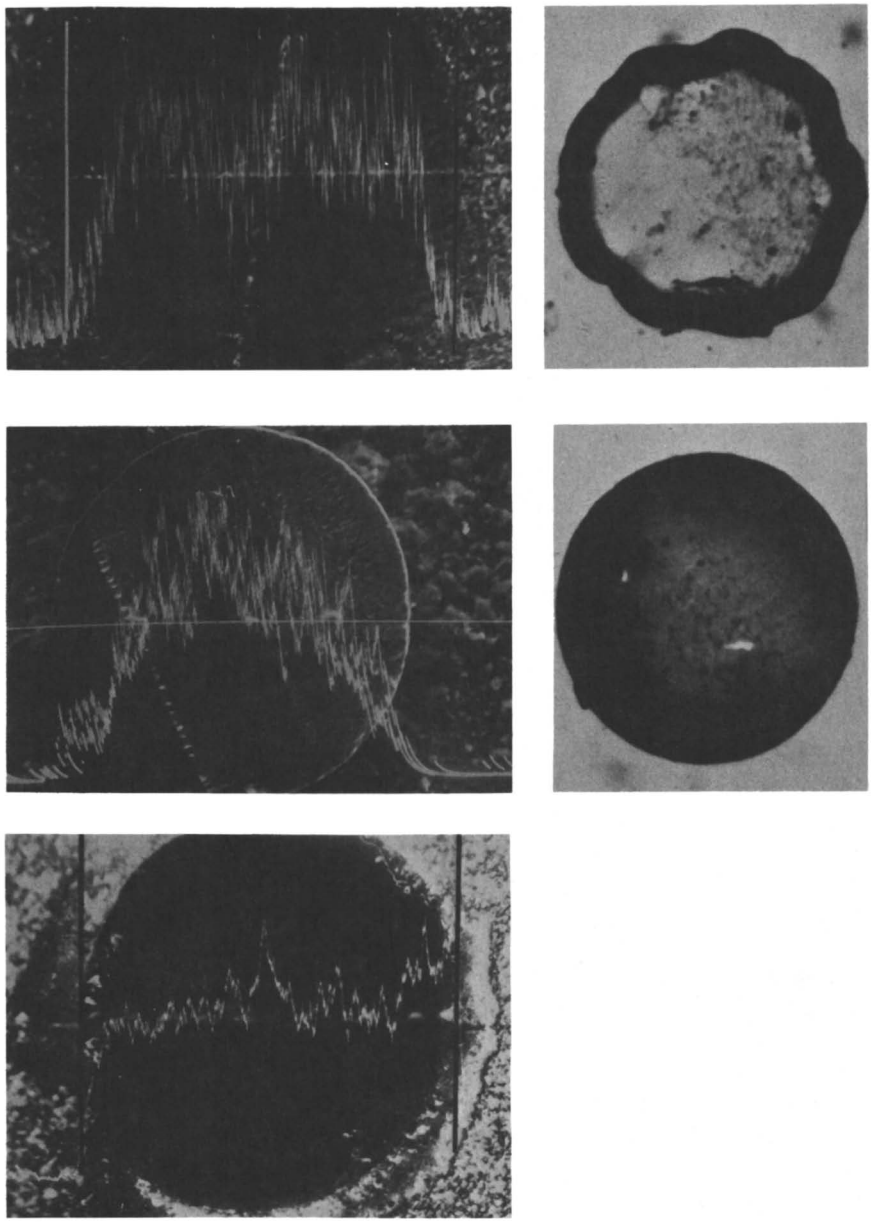

*Figure 7. SEM X-ray linescan for bromine in a suspension IPN of poly(2-hydroxyethyl methacrylate-co-*N*-vinylpyrrolidone)–dibromoneopentylglycol–TMDI polyurethane, 75:25. Note the morphology of the system. (Reproduced with permission from Ref. 87. Copyright 1982 John Wiley & Sons.)*

yamine in toluene and adding the epoxy, isocyanate, and acyl chloride components sequentially (*93*). The final microcapsule has an aqueous droplet in the center.

An IPN-related process involves gelatin–gum arabic coacervates, which are finally cross-linked with formaldehyde. This product serves as a wall and has an oily core (*93*).

Other applications of microcapsules include carbonless copy paper, containment of perfumes, food flavorings, decongestants, marine feeding, artificial blood cells, and augmenting artificial kidney function (*94*). Although it is not obvious that all of these applications make use of IPNs or semi-IPNs, the potential is clear.

The first group of applications depends on breakage of the shell for release of contents.

Artificial blood cells, containing sheep hemolysate, require diffusion in both directions. For augmenting artificial kidney function, microcapsules containing activated carbon are ingested. Intestinal adsorption of creatinine and uric acid are also of interest.

Dental Applications of IPNs

Possible applications of IPNs in the field of dentistry include denture bases, false teeth, and fillings. Fillings based on acrylic semi-II IPNs that can be cured by UV via fiber optics are of special interest. Compositions vary (*95*, *96*), but the general idea is the use of cross-linked PMMA that may originate from suspension polymerization and/or may be ground after polymerization. This material is mixed with silica filler and MMA monomer plus cross-linker to make up the restorative.

The Patent Literature

A number of IPN patents have been issued. Skinner et al. (*97*) made SIN coatings (some grafted) of vinyl and urethane compositions that are, respectively, radiationally and thermally polymerized. Frisch et al. (*98*) obtained a patent on their IENs. Sperling et al. (*99*) patented tough plastic compositions based on polymerized castor oil and very recently, they patented their thermoplastic IPNs (*73b*).

Foscante et al. (*100*, *101*) have a patent on a semi-SIN composition of epoxy–siloxane in which the epoxy is cross-linked and the siloxane is linear. The Foscante et al. IPN material is intended for use as a coating material. It is supplied as a two-package system and applied to a surface by conventional techniques such as spraying or brushing. Acid and solvent resistance are mentioned. Possible applications cited include the steel structures of chemical processing plants and oil refineries and the internal surfaces of tanks of petroleum tankers.

Sebastiano (*102*) invented a transparent polyurethane–polyacrylate SIN coating for safety glass. The monomer–polymer or prepolymer solu-

tions can be applied on the inside glass of automobiles by spraying; thicknesses of 100 to 190 μm yield good optical properties and tear resistance.

Prosthetic teeth and other dental appliances made from a sequential acrylic IPN composition were invented by Tateosian and Roemer (*103*). In one example, cross-linked PMMA in suspension-sized particles, linear PMMA, and methyl methacrylate monomer and cross-linker were mixed with initiator and pigment, molded, and polymerized to an impact- and wear-resistant tooth structure.

A thermoplastic semi-IPN consisting of a rubbery ionomer and poly(dimethyl siloxane) was invented by Lundberg et al. (*104*). Improved melt flow and a lower coefficient of friction are cited.

De La Mare and Brownscombe (*105*) describe an epoxy–stryene–cross-linker RIM SIN material. Cure times of 1–10 min are described. Catalysts are selected from Group I or Group II salts for the epoxy component.

Polypropylene or Polyethylene–EPDM Thermoplastic IPNS

A new class of IPN was invented by Fischer (*106*) in the period 1973–74. His materials were primarily blends of isotactic polypropylene and EPDM. During the blending operation, while the mix was subjected to a shearing action, the EPDM component was partly cross-linked. The resultant materials, dynamically partly cured, retained a thermoplastic nature. On cooling, the polypropylene component crystallizes and forms a type of physical cross-link. These materials are called thermoplastic IPNs (*see* Table VIII, No. 2).

Also, dynamically shearing a polymer in blend form during cross-linking (as in the case of the EPDM) results in a two-dimensional structure of cylindrical shape (i.e., elongated droplets). The cylindrical structure interpenetrates the other polymer to form a material with two continuous phases. These materials are actually hybrids between polymer blends and IPNs and exhibit some of the properties of both.

These ideas naturally led to further developments. Coran and Patel (*107–10*) learned how to prepare thermoplastic vulcanizates with the rub-

Table VIII. Polypropylene–EPDM or Polyethylene Thermoplastic IPN Patents

No.	*Major Feature*	*Company*	*Patent No.*
Dynamically partly cured			
1.	EPDM precured then blended	Uniroyal	U.S. 3 758 643
2.	EPDM blended then cured	Uniroyal	U.S. 3 806 558
3.	EPDM of high molecular weight	Uniroyal	U.S. 3 835 201
4.	Dynamically fully cured	Monsanto	U.S. 4 130 535
5.	High ethylene length index (with PE)	Goodrich	U.S. 4 046 840
6.	High ethylene sequence index (with PP)	Goodrich	U.S. 4 036 912
7.	70–85% (by weight) of ethylene EPDM with dicyclopentadiene	Uniroyal	U.S. 4 031 169
8.	Dual phase continuity	Exxon	U.S. 4 132 698

ber completely cured (*see* Table VIII, No. 4). If the EPDM was prepared with high ethylene sequence lengths so that it crystallized slightly, no crosslinking was required at all [*see* Table VIII, Nos. 5 (*111*) and 6 (*112*)]. Having a high ethylene content in the EPDM also allows partial crystallization [*see* Table VIII, No. 7 (*113*)]. Of course, the EPDM can be precured then blended (No. 1), or of high molecular weight (No. 3). Dual phase continuity is important in No. 8 (Table VIII). Thus, there are several different ways of preparing thermoplastic IPNs of this type. The subject was recently reviewed (*114*).

New Products

During the last several years, companies have taken a significant interest in IPNs and related materials. Table IX illustrates some commercial products.

Table IX. IPN Commercial Materials

Manufacturer	*Trade Name*	*Composition*	*Application*
Shell Chemical Co.	Kraton IPN	SEBS–polyester	Automotive parts
Petrarch Systems, Inc.	Rimplast	Silicone rubber–nylon or PU	Gears or medical
ICI Americas Inc.	ITP	PU–Polyester–styrene	Sheet molding compounds
DSM N.V.	Kelburon	PP–EP rubber–PE	Automotive parts
Shell Research B.V.	—	Rubber–PP	Tough plastic
Uniroyal (Reichhold Chemical Co.)	TPR	EPDM–PP	Auto bumper parts
Sun Marketing & Refining Co.	—	PE–PP	Low temperature plastics
Exxon Corp.	—	PE–PP	Low temperature plastics
Rohm & Haas	—	Anionic–cationic	Ion-exchange resins
Monsanto	Santoprene	EPDM–PP	Tires, hoses, belts, and gaskets
Du Pont	Somel	EPDM–PP	Outdoor weathering
BF Goodrich	Telcar	EPDM–PP or PE	Tubing, liners, and wire and cable insulation
Allied Chemical	ET polymer	Butylrubber–PE	—
Hercules	Profax	EPDM–PP	Ultrahigh impact resistance
Exxon	Vistalon	EPDM–PP	Paintable automotive parts
Freeman Chemical	Acpol	Acrylic-urethane-polystyrene	Sheet molding compounds
Dentsply International	Trubyte Bioform IPN De Trey Biostabil	Acrylic-based	Artificial teeth

The first of these is Shell's new Kraton G-based thermoplastic elastomer (TPE) system, which blends Kraton G with other materials such as polyester[poly(ethylene terephthalate)] or nylon (*115*, *116*). This material is a type of thermoplastic IPN in which two types of physical cross-linking exist: one network is cross-linked by glassy block copolymer segments, and the other polymer is cross-linked by crystalline regions. Because both phases exhibit some degree of dual continuity, the polymer remains flexible down to the T_g of the elastomer center block and remains serviceable up to the melting temperature of the crystalline polymer. These materials are formulated by mechanical blending, rather than the chemical blending techniques employed by Siegfried et al. (*73–75*).

The second IPN product was announced by Petrarch Systems (*117–19*). Rimplast is based on silicone rubber and polyurethanes. The silicone rubber is cross-linked via a functional silicone that is reacted with a silicone carrying a reactive hydrogen atom. The reaction results in a silicone network evenly distributed throughout the polyurethane. Applications include the medical market.

The chemical basis for Rimplast technology uses a separation of the hydride and vinylsilicone components in separate solid pellets of polyurethane in the second polymer. Upon entering the melt state during conventional injection molding or extrusion, the confinement of the reactive silicones to separate pellets collapses, and they begin to react with one another (*120*, *121*).

Several second polymers have been used in Rimplast formulations to make semi-IPNs (polyurethanes), thermoplastic IPNs (polyester elastomer, SBS and SEBS Kraton block copolymers, and polyamides), and full IPNs (EPDM). The most important of these materials for biomedical applications are the polyurethane semi-IPNs. Depending on the extent of cross-linking in the silicone rubber, these materials become thermoset with a content between 10 and 60% of silicone, indicating the onset of dual phase continuity. The commercial products, all slightly cross-linked and containing below about 25% silicone, remain thermoplastic.

In addition to those materials shown in Table IX, Allied Corporation has a semi-IPN that they are considering for commercial production (*122–25*). This material is based on cross-linking dicyanates and a linear second polymer.

Dicyanates of bisphenol A trimerize to form a network (*see* Figure 8) (*123*). The resultant network in the semi-IPN tends to cluster and has a large number of internal cycles. Dual phase continuity is achieved when a concentration of more than 30% of dicyanate is present, as indicated by the material becoming thermoset.

Thermoplastic second polymers have included copolyester–carbonate, polycarbonate, polysulfone, poly(ethylene terephthalate), and polyether sulfone.

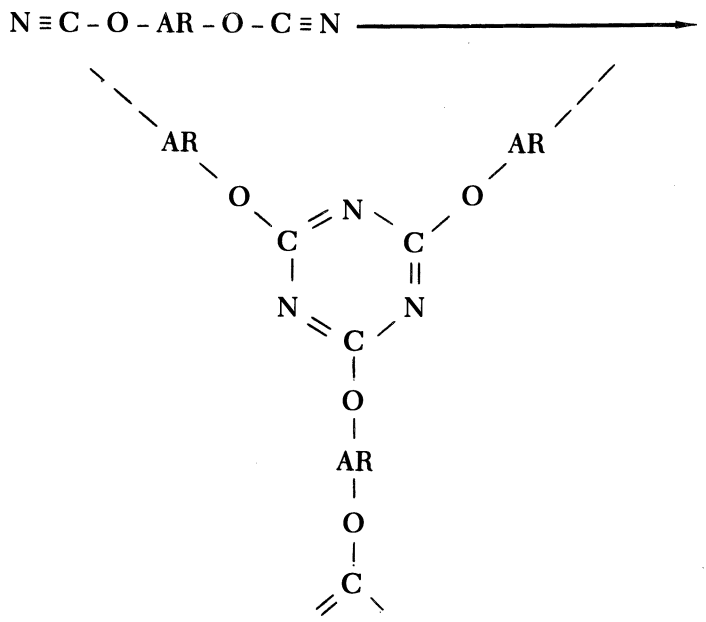

Figure 8. Dicyanates are trimerized to form a highly cross-linked network. (Reproduced with permission from Ref. 123. Copyright 1984 Plastics Engineering.)

Compositions containing 50–50 dicyanate and a thermoplastic were shown to have tensile strengths in the 10,000- to 12,000-psi range, with elongations of 10–17%. Thus, the materials are very tough. High temperature properties are also cited.

Concluding Remarks

The field of IPNs is very much alive and growing rapidly. Only a decade ago, only three major academic laboratories were devoted to IPN investigations. Now there are at least eight (*see* Table X). In addition, many industrial organizations are interested in IPNs, as delineated in this chapter and the approximately 14 identifiable IPN products listed in Table IX.

Interest has been renewed in multicomponent polymer nomenclature. At one point, I realized that there were at least 150 different, distinguishable, and interesting ways to put two polymer chains together to make what really constitute different molecules. A proper nomenclature would go far to making it easy to distinguish these compositions for research and application purposes and to describe them in the literature.

With the advent of the thermoplastic IPNs, the line between an IPN and a polymer blend became blurred. Whereas in a very restricted sense one might say it is nice to keep the materials apart, I strongly encourage the

Table X. Major Academic IPN Laboratories

Director(s)	*Location*	*Emphasis*
Y. S. Lipatov	Kiev, U.S.S.R.	Small-angle X-ray scattering
G. C. Meyer and J. M. Widmaier	Strasbourg, France	Thermoplastic IPNs
D. J. Hourston	Lancaster, England	Vibration damping
H. Adachi	Osaka, Japan	Structure–property relationships
K. C. Frisch and D. Klempner	Detroit, Mich.	RIM-IPNs
H. Frisch	Albany, N.Y.	RIM-IPNs
S. C. Kim	Seoul, Korea	High pressure syntheses
L. H. Sperling and D. A. Thomas	Bethlehem, Pa.	Morphology, SANS
W. Trochimczuk and B. N. Kolarz	Wroclaw, Poland	Ion-exchange membranes

development of all sorts of new materials. If the polymer community has to write yet new nomenclature schemes, that will only be a sign of continued growth.

Acknowledgment

The author thanks the National Science Foundation for support under Grant No. DMR-8405053, Polymers Program.

Literature Cited

1. Sperling, L. H. "Interpenetrating Polymer Networks and Related Materials"; Plenum: New York, 1981.
2. Lipatov, Y. S.; Sergeeva, L. M. "Interpenetrating Polymeric Networks"; Naukova Dumka: Kiev, 1979.
3. Lipatov, Y. S.; Sergeeva, L. M. *Russ. Chem. Rev.* **1976**, *45(1)*, 63; translated from *Usp. Khim.* **1976**, *45*, 138.
4. Klempner, D. *J. Angew. Chem.* **1978**, *90*, 104.
5. Ring, W.; Mita, I.; Jenkins, A. D.; Bikales, N. M. "Source-Based Nomenclature for Copolymers"; IUPAC Commission on Macromolecular Nomenclature, Recommendations, 1983. Available through Dr. N. M. Bikales, National Science Foundation, Washington, D.C. 20550.
6. Donaruma, L. G.; Elias, H. G.; Meier, D. J.; Sperling, L. H. "Source-Based Nomenclature for Polymer Blends, Interpenetrating Polymer Networks, and Related Materials"; Polymer Chemistry Division Nomenclature Committee, American Society, 1984. Available through Dr. L. H. Sperling, Lehigh University, Bethlehem, PA 18015.
7. Huelck, V.; Thomas, D. A.; Sperling, L. H. *Macromolecules* **1972**, *5*, 340.
8. Huelck, V.; Thomas, D. A.; Sperling, L. H. *Macromolecules* **1972**, *5*, 348.
9. Donatelli, A. A.; Sperling, L. H.; Thomas, D. A. *Macromolecules* **1976**, *9*, 671.
10. Donatelli, A. A.; Sperling, L. H.; Thomas, D. A. *Macromolecules* **1976**, *9*, 676.

11. Donatelli, A. A.; Sperling, L. H.; Thomas, D. A. *J. Appl. Polym. Sci.* **1977**, *21*, 1189.
12. Michel, J.; Hargest, S. C.; Sperling, L. H. *J. Appl. Polym. Sci.* **1981**, *26*, 743.
13. Yeo, J. K.; Sperling, L. H.; Thomas, D. A. *Polymer* **1983**, *24*, 307.
14. Yeo, J. K.; Sperling, L. H.; Thomas, D. A. *Polym. Eng. Sci.* **1981**, *21*, 696.
15. Yeo, J. K.; Sperling, L. H.; Thomas, D. A. *J. Appl. Polym. Sci.* **1981**, *26*, 3283.
16. Yeo, J. K.; Sperling, L. H.; Thomas, D. A. *Polym. Eng. Sci.* **1982**, *22*, 190.
17. Widmaier, J. M.; Sperling, L. H. *Macromolecules* **1982**, *15*, 625.
18. Widmaier, J. M.; Sperling, L. H. *J. Appl. Polym. Sci.* **1982**, *27*, 3513.
19. Widmaier, J. M.; Yeo, J. K.; Sperling, L. H. *Colloid Polym. Sci.* **1982**, *260*, 678.
20. Kresge, E. N. In "Polymer Blends"; Paul, D. R.; Newman, S., Eds.; Academic: New York, 1978; Vol. 2.
21. Sperling, L. H.; Klein, A.; Fernandez, A. M.; Linne, M. A. *Polym. Prepr.* **1983**, *24(2)*, 386.
22. Lipatov, Y. S.; Shilov, V. V.; Bogdanovitch, V. A.; Karbanova, L. V.; Sergeeva, L. M. *Vysokomol. Soedin.* **1980**, *A22(6)*, 1359; *Polym. Sci. USSR* **1980**, *22*, 1492.
23. Shilov, V. V.; Lipatov, Y. S., Karbanova, L. V.; Sergeeva, L. M. *J. Polym. Sci. Polym. Chem. Ed.* **1979**, *17*, 3083.
24. MacKnight, W. J.; Karasz, F. E.; Fried, J. R. In "Polymer Blends"; Paul, D. R.; Newman, S., Eds.; Academic: New York, 1978; Vol. 1.
25. Frisch, H. L.; Klempner, D.; Yoon, H. K.; Frisch, K. C. In "Polymer Alloys II"; Klempner, D.; Frisch, K. C., Eds.; Plenum: New York, 1980.
26. Frisch, H. L.; Klempner, D.; Yoon, H. K.; Frisch, K. C. *Macromolecules* **1980**, *13(4)*, 1016.
27. Siegfried, D. L.; Thomas, D. A.; Sperling, L. H. In "Polymer Alloys II"; Klempner, D.; Frisch, K. C., Eds.; Plenum: New York, 1980.
28. Adachi, H.; Kotaka, T. *Polym. J.* **1982**, *14(5)*, 3791.
29. Adachi, H.; Nishi, S.; Kotaka, T. *Polym. J.* **1983**, *15*, 985.
30. Adachi, H.; Kotaka, T. *Polym. J.* **1983**, *15(4)*, 285.
31. Bobalek, E. G.; Moore, E. R.; Levy, S. S.; Lee, C. C. *J. Appl. Polym. Sci.* **1964**, *8*, 625.
32. Labana, S. S.; Newman, S.; Chompff, A. J. In "Polymer Networks"; Champff, A. J.; Newman, S., Eds.; Plenum: New York, 1971.
33. Dusek, K. In "Developments in Polymerization-3"; Haward, R. N., Ed.; Appl. Sci.: London, 1982.
34. Sperling, L. H.; Widmaier, J. M. *Polym. Eng. Sci.* **1983**, *23*, 693.
35. Park, I. H.; Lee, J. H.; Kim, S. C. *Polym. Bull.* **1983**, *10*, 126.
36. Dubuisson, A.; Ades, D.; Fantanille, M. *Polym. Bull.* **1980**, *3*, 391.
37. Dubuisson, A.; Fontanille, M.; Zaoui, A. *Rheol. Acta* **1981**, *20*, 463.
38. Lim, D. S.; Lee, D. S.; Kim, S. C. *IUPAC Proc.* **1982**, 223.
39. Lee, D. S.; Kim, S. C. *Macromolecules* **1984**, *17*, 268.
40. Morin, A.; Djomo, H.; Meyer, G. C. *Polym. Eng. Sci.* **1983**, *23*, 394.
41. Djomo, H.; Morin, A.; Danyanidu, M.; Meyer, G. *Polymer* **1983**, *24*, 65.
42. Djomo, H.; Widmaier, J. M.; Meyer, G. C. *Polymer* **1983**, *24*, 1415.
43. Hermant, I.; Damyanidu, M.; Meyer, G. C. *Polymer* **1983**, *24*, 1419.
44. Hermant, I.; Meyer, G. C. *Eur. Polym. J.* **1984**, *20*, 85.
45. Jehl, D.; Widmaier, J. M.; Meyer, G. C. *Eur. Polym. J.* **1983**, *19*, 597.
46. Hourston, D. J.; McCluskey, J. A.; *Polymer* **1979**, *20*, 1573.
47. Hourston, D. J.; Zia, Y. *Polymer* **1979**, *20*, 1497.

48. Hourston, D. J.; Zia, Y. *J. Appl. Polym. Sci.* **1983**, *28*, 2139, 2745, 3849; **1984**, *29*, 629.
49. Hourston, D. J., presented at the *R. Soc. Chem. Meet.*, Lancaster, England, April 1983.
50. Suzuki, Y.; Frijimoto, T.; Tsunoda, S.; Shibayama, K. *J. Macromol. Sci. Phys.* **1980**, *B17(4)*, 787.
51. Kolarz, B. M. *Angew. Makromol. Chem.* **1980**, *90*, 167.
52. Kolarz, B. M. *Angew. Makromol. Chem.* **1980**, *90*, 183.
53. Pozniak, G.; Trochimczuk, W. *Agnew. Makromol. Chem.* **1980**, *92*, 155.
54. Pozniak, G.; Trochimczuk, W. *Angew. Makromol. Chem.* **1982**, *104*.
55. Cox, J. A.; Gajek, R.; Litwinski, G. R.; Carnaham, J.; Trochimczuk, W. *Anal. Chem.* **1982**, *54*, 1153.
56. Kwant, P. W. *J. Polym. Sci. Polym. Chem. Ed.* **1979**, *17*, 1331.
57. Boots, H. M. J.; Pandy, R. B. *Polym. Bull.* **1984**, *11*, 415.
58. Lipatov, Y. S.; Shilov, V. V.; Gomza, Y. P.; Kovernik, G. P.; Grigor'eva, O. P.; Sergeyeva, L. M. *Makromol. Chem.* **1984**, *185*, 347.
59. Fernandez, A. M.; Sperling, L. H. unpublished data.
60. Rosovizky, V. F.; Ilavsky, M.; Hrouz, J.; Dusek, K.; Lipatov, Y. S. *J. Appl. Polym. Sci.* **1979**, *24*, 1007.
61. Karabanova, L. V. Thesis, Institut Chimii Vysokomomolekuljarnyck Sojedinenij, Akad, Nauk. U.S.S.R. Kijev, 1977.
62. Sperling, L. H.; Manson, J. A. *J. Am. Chem. Soc.* **1983**, *60(11)*, 1887.
63. Sperling, L. H.; Manson, J. A.; Qureshi, S.; Fernandez, A. M. *I&EC Prod. Res. Dev.* **1981**, *20*, 163.
64. Linne, M. A.; Sperling, L. H.; Fernandez, A. M.; Qureshi, S.; Manson, J. A. *Polym. Mater. Sci. Eng. Prepr.* **1983**, *49*, 513.
65. Sperling, L. H.; Manson, J. A.; Linne, M. A. *J. Polym. Mater.* **1984**, *1*, 54.
66. Djomo, H.; Colmenares, R.; Meyer, G. C. *Eur. Polym. J.* **1981**, *17*, 521.
67. Pernice, R.; Frisch, K. C.; Navare, R. In "Polymer Alloys III"; Klempner, D.; Frisch, K. C., Eds.; Plenum, New York, 1983.
68. Pernice, R.; Frisch, K. C.; Navare, R. J. *Cell. Plast.* **1982**, *Mar.–Apr.* 121.
69. *Plastics Technol.* **1983**, *Jan.*, 76.
70. Manson, J. A.; Sperling, L. H.; Qureshi, S.; Fernandez, A. M. *Prepr. 13th Nat. SAMPE Tech. Conf.* **1981**, *13*, 81.
71. Devia, N.; Manson, J. A.; Sperling, L. H.; Conde, A. *Macromolecules* **1979**, *12*, 360.
72. Siegfried, D. L.; Thomas, D. A.; Sperling, L. H. *J. Appl. Polym. Sci.* **1981**, *26*, 117.
73. Siegfried, D. L.; Thomas, D. A.; Sperling, L. H. *Polym. Eng. Sci.* **1981**, *21*, 39; U.S. Patent 4 468 499, 1984.
74. Siegfried, D. L.; Thomas, D. A.; Sperling, L. H. *J. Appl. Polym. Sci.* **1981**, *26*, 141.
75. Davison, S.; Gergen, W. P. U.S. Patent 4 041 103, 1977.
76. Gergen, W. P.; Davison, S. U.S. Patent 4 101 605, 1978.
77. Sperling, L. H.; Manson, J. A.; Jordhamo, G. M. In "Reactive Oligomers"; Harris, F. W.; Spinelli, H. J., Eds.; ACS SYMPOSIUM SERIES No. 282, ACS: Washington, D.C., 1985.
78. Paul, D. R.; Barlow, J. W. *J. Macromol. Sci. Rev. Macromol. Chem.* **1980**, *C18*, 109.
79. Gergen, W. P. *Kautsch. Gummi* **1984**, *37(4)*, 284.
80. Widmaier, J. M.; Hubert, J.; Meyer, G. C. *J. Polym. Sci. Polym. Lett. Ed.* **1981**, *19*, 463.

81. Widmaier, J. M.; Hubert, J.; Meyer, G. *Macromol. Chem.* **1982**, *183*, 249.
82. Akovali, G.; Biliyar, K.; Shen, M. *J. Appl. Polym. Sci.* **1976**, *20*, 2419.
83. Shen, M.; Bever, M. B. *J. Mater. Sci.* **1972**, *7*, 741.
84. Berry G. C.; Dvor, M. *Prepr. Am. Chem. Soc. Div. Org. Coat. Plast. Chem.* **1978**, *28*, 465.
85. Jasso, C. F.; Hong, S. D.; Shen, M. In "Multiphase Polymers"; Cooper, S. L.; Estes, G. M., Eds.; ADVANCES IN CHEMISTRY SERIES No. 176; ACS: Washington, D.C., 1979; p. 444.
86. Martin, G. C.; Enssani, E.; Shen, M. *J. Appl. Polym. Sci.* **1981**, *26*, 1465.
87. Mueller, K. F.; Heiber, S. J. *J. Appl. Polym. Sci.* **1982**, *27*, 4043.
88. Mueller, K. F.; Heiber, S. J. European Patent Application 0 046 136, 1982; U.S. Patent 4 423 099, 1983.
89. Raghunathan, Y.; Amsel, L.; Hinsvark, O.; Bryant, W. *J. Pharm. Sci.* **1981**, *70(4)*, 379.
90. Keating, J. W. U.S. Patent 2 990 332, 1961.
91. Motycka, S.; Nairn, J. G. *J. Pharm. Sci.* **1979**, *68(2)*, 211.
92. Macek, T. J.; Sloop, C. E.; Stauffer, D. R. U.S. Patent 3 499 960, 1970.
93. Watanabe, A.; Hayashi, T. In "Microencapsulation"; Nixon, J. R., Ed.; Dekker: New York, 1976.
94. "Microencapsulation"; Nixon, J. R., Ed.; Dekker: New York, 1976.
95. Kusy, R. P.; Lytwyn, B. J.; Turner, D. T. *J. Dent. Res.* **1976**, *55(3)*, 452.
96. Phillips, R. W. "Skinner's Science of Dental Materials"; Saunders: Philadelphia, 1982; p. 233–34.
97. Skinner, E.; Emeott, M.; Jevne, A. U.S. Patent 4 247 578, 1981.
98. Frisch, H. L.; Frisch, K. C.; Klempner, D. U.S. Patent 4 302 553, 1981.
99. Sperling, L. H.; Manson, J. A.; Devia-Manjarres, N. U.S. Patent 4 254 002, 1981.
100. Foscante, R. E.; Gysegem, A. P.; Martinich, P. J.; Law, G. H. U.S. Patent 4 250 074, 1981.
101. Foscante, R. E.; Gysem, A. P.; Martonich, P. J.; Law, G. H. Intl. Patent PCT-US79-00833.
102. Sebastiano, F. Intl. Patent 0 035 130, 1981.
103. Roemer, F. D.; Tateosian, L. H. European Patent 0 014 515, 1984.
104. Lundberg, R. D.; Phillips, R. R.; Duvdevani, I. U.S. Patent 4 330 447, 1982.
105. De La Mare, H. E.; Brownscombe, T. F. U.S. Patent 4 389 515, 1983.
106. Fischer, W. K. U.S. Patent 3 806 558, 1974.
107. Coran, A. Y.; Das, B.; Patel, R. P. U.S. Patent 4 130 535, 1978.
108. Coran, A. Y.; Patel, R. *Rubber Chem. Technol.* **1980**, *53*, 141.
109. Coran, A. Y.; Patel, R. *Rubber Chem. Technol.* **1981**, *54*, 91.
110. Coran, A. Y.; Patel, R. *Rubber Chem. Technol.* **1982**, *55*, 1063.
111. Carman, C. J.; Batuik, M.; Herman, R. M. U.S. Patent 4 046 840, 1977.
112. Stricharczuk, P. T. U.S. Patent 4 036 912, 1977.
113. Morris, H. L. U.S. Patent 4 031 169, 1977.
114. O'Connor, G. E.; Fath, M. A. *Rubber World* **1981**, *185(3)*, 25; **1982**, *185(4)*, 26.
115. School, R. *Rubber Plast. News* **1982**, *Mar. 15*, 20.
116. *Mod. Plast.* **1982**, *Apr.*, 55.
117. *High Technol.* **1983**, *Sept.*, 79.
118. *Mod. Plast.* **1983**, *Feb.*, 12.
119. *Chem. Mark. Rep.* **1983**, *Jan. 31*, 7.
120. Arkles, B. *Prepr. Polym. Mater. Sci. Eng.* **1983**, *49*, 6; *Chemtech* **1983**, *13*, 542.

121. Arkles, B.; Carreno, C. *ANTEC '84* **1984**, 486.
122. *Polym. News* **1983**, *9(No. 6)*, 188.
123. Wertz, D. H.; Prevorsek, D. C. *Plast. Eng.* **1984**, *Apr.*, 31.
124. Wertz, D. H.; Prevorsek, D. C. *ANTEC '84* **1984**, 483.
125. Prevorsek, D. C.; Chung, D. C. U.S. Patent 4 157 360, 1979.

RECEIVED for review November 15, 1984. ACCEPTED February 22, 1985.

3

Poly(2,6-dimethyl-1,4-phenylene Oxide) Blends Studied by Inverse Gas Chromatography

A. C. SU and J. R. FRIED

Department of Chemical and Nuclear Engineering and the Polymer Research Center, University of Cincinnati, Cincinnati, OH 45221

Miscibility of blends of poly(2,6-dimethyl-1,4-phenylene oxide) (PMMPO) with polystyrene (PS) and poly(4-methylstyrene) (P4MS) has been investigated by inverse gas chromatography (IGC). The Flory interaction parameter determined for the PMMPO–PS blend at 270 °C was 0.21 ± 0.3. The lower portion of this range coincides with values reported from melting point depression measurements and recent small-angle neutron scattering (SANS) studies of this blend. In comparison, the value determined for PMMPO–P4MS was −1.21 ± 0.3; this value suggests a more favorable free energy of mixing for this blend. Conclusions drawn from earlier glassy state property measurements or consideration of the lattice fluid theory of Sanchez and Lacombe in the present work supports the conclusion of miscibility of this blend, but shows little distinction between the two. Critique of the IGC results is given in terms of the limitations inherent with this technique.

Miscibility of polystyrene (PS) and poly(2,6-dimethyl-1,4-phenylene oxide) (PMMPO) has been well documented by a variety of experimental techniques including thermal analysis (*1*, *2*), magic-angle spinning NMR (*3*), and small-angle neutron scattering (SANS) (*4–6*). Recently, we reported evidence from differential scanning calorimetry (DSC), density, and mechanical property measurements for the compatibility of PMMPO with poly(4-methylstyrene) (P4MS) (*7*). In this chapter, we report results of the measurement of the Flory interaction parameter (χ) of both PMMPO–PS and PMMPO–P4MS blends by use of inverse gas chromatography (IGC) (*8*). Estimates of χ for PMMPO–PS blends were reported previously from melting point (T_m) depression measurements of PMMPO, which can undergo solvent-induced crystallization in solution or when cast from certain solvents. Shultz and McCullough (*9*) concluded that a value of

0065-2393/86/0211/0059$06.00/0

approximately zero was consistent with the observed T_m depression of PMMPO in a ternary mixture with PS and toluene. In support of a near zero value for χ, Kwei and Frisch (*10*) later demonstrated that morphological effects alone may account for the small T_m depression observed for high molecular weight PMMPO–PS blends. These conclusions are consistent with the small exothermic heat of mixing reported for this blend from solution calorimetric measurements (*11–13*) and from recent CO_2 sorption studies (*14*). In a recent SANS study, Maconnachie et al. (*6*) reported values of χ for deuterated PMMPO in a PS matrix that varied from -0.033 to -0.021 over a temperature range of 104 to 273 °C. The dependence of the second virial coefficient on temperature was used to predict a θ temperature in the region of 345 ± 55 °C.

Experimental

Materials. PMMPO was obtained as an additive-free powder from General Electric. Samples of PS and P4MS were obtained as pellets stabilized with butylated hydroxytoluene [BHT, 2,6-bis(1,1-dimethylethyl)-4-methylphenol] through the courtesy of B. Z. Gunesin of Mobil Chemical Company. Molecular weights determined by gel permeation chromatography (GPC) were reported previously (*7*). Weight-average molecular weights obtained by low-angle laser scattering measurements (Chromatix KMX-6 photometer) are in good agreement with the GPC results. These values are 35,900, 226,000, and 308,000 for PMMPO, PS, and P4MS, respectively. Polymers used for IGC studies were purified by precipitation from dilute chloroform solution into a large volume ratio of methanol.

Chromatography. Packings for IGC measurements were prepared by making a slurry of Chromosorb P (60:40 mesh, acid washed, and dimethyldichlorosilane (DMCS) treated calcinated diatomaceous earth) with dilute chloroform solutions of each of the three polymers and 50.1:49.9 weight ratios of PMMPO–PS and PMMPO–P4MS blends. Packings were dried at 70 °C in a vacuum for approximately 1 week. These packings were then loaded into sections of 0.25-in. O.D. stainless steel tubing about 3 ft in length and conditioned overnight at about 285 °C in a Perkin-Elmer model 990 gas chromatograph equipped with a thermal conductivity (TC) detector. The weight of polymer stationary phase on the support was determined for each column by Soxhlet extraction in chloroform over 4 days. For the five columns used in this study, the weight ratios of polymer to support ranged from 0.0424 to 0.0729. The carrier gas used in the IGC measurements was helium at a flow rate of approximately 5 mL/min as determined by a soap bubble flowmeter. Solute probes were reagent (or better) grade benzene, toluene, ethylbenzene, and *ortho*-, *meta*-, and *para*-xylenes. Typical sample sizes were 5 μL for air and <0.04 μL for solute probes. Injector and detector temperatures were approximately 200 and 300 °C, respectively. Column temperatures were determined to within 0.5 °C by means of a calibrated platinum resistance thermometer.

Data Analysis. Probe–polymer (χ_{1i}) and polymer–polymer (χ_{23}) interaction parameters were determined from measurement of specific retention volumes, V_g^0, and application of classical Flory thermodynamic treatment. For a multicomponent stationary phase, by assuming moderate pressure and that the mixture of solute probe and inert carrier gas does not deviate significantly from ideal gas behav-

ior, the volume fraction activity coefficient of the probe 1 at infinite dilution may be given by the expression (*15*, *16*) (*see* Nomenclature list on page 64)

$$\ln(a_1/\phi_1)^\infty = \lim_{\phi_1 \to 0} \ln(a_1/\phi_1) = \ln[(237.16R \sum_{i \neq 1} w_i v_i)/V_g^0 P_1^0 V_1] - (P_1^0/RT)(B_{11} - V_1) \quad (1)$$

where

$$V_g^0 = t_N FJ/W \quad (2)$$

Values of P_1^0, V_1, and B_{11} were determined by Antoine's equation, the Gunn and Yamada method, and Tsonopoula's correlation, respectively, as given by Reid et al. (*17*). Values of specific volume for PS and PMMPO were obtained from *PVT* data given by Zoller and Hoehn (*18*); specific volume for P4MS was obtained from dilatometric data (*19*).

For a binary mixture of a low molecular weight probe, 1, and polymer, 2, in the stationary phase, the Gibbs free energy of mixing is given as (*20*)

$$\Delta G_M/RT = n_1 \ln \phi_1 + n_2 \ln \phi_2 + \chi_{12} n_1 \phi_2 \quad (3)$$

Differentiation with respect to n_1 yields the volume fraction activity coefficient

$$\ln(a_1/\phi_1) = (1 - \phi_1)[1 - (1/m_2)] + \chi_{12}(1 - \phi_1)^2 \quad (4)$$

At infinite dilution and for a high molecular weight polymer,

$$\ln(a_1/\phi_1)^\infty \approx \chi_{12} + 1 \quad (5)$$

By equating Equations 1 and 5, the probe–polymer interaction parameter from IGC measurements may be obtained as

$$\chi_{12} = \ln[(273.16Rw_2v_2)/V_g^0 P_1^0 V_1] - 1 - (P_1^0/RT)(B_{11} - V_1) \quad (6)$$

Extension of the Flory theory to the ternary system of probe and binary polymer blend (*21*) yields the probe volume fraction activity coefficient at infinite dilution and for high molecular weight polymers as

$$\ln(a_1/\phi_1)^\infty = 1 + \chi_{12}\phi_2 + \chi_{13}\phi_3 - \chi'_{23}\phi_2\phi_3 \quad (7)$$

The binary polymer interaction parameter, χ'_{23}, may be obtained by equating Equations 1 and 7 once χ_{12} and χ_{13} have been determined from separate experiments. To avoid cumulative errors associated with uncertainties in the values of P_1^0, B_{11}, and V_1, Al-Saigh and Munk (*22*) suggested an alternative form using only experimental values of V_g^0 obtained for the blend (V_{g23}^0) and two unblended polymers (V_{g2}^0 and V_{g3}^0)

$$\chi'_{23} = \chi_{23} V_1/V_2 = \{\ln[V_{g23}^0/(w_2v_2 + w_3v_3)] - \phi_2 \ln(V_{g2}^0/v_2) - \phi_3 \ln(V_{g3}^0/v_3)\}/\phi_2\phi_3 \quad (8)$$

Results and Discussion

To evaluate the consistency of the experimental procedures and the method of data analysis, IGC results for PS at 150 and 175 °C were compared with those reported in the literature (*23–25*). Agreement was satisfactory as shown by comparison of weight fraction activity coefficients (a_1/w_1) at infinite dilution in Table I.

Values of V_g^0 and corresponding values of χ_{1i} (Equation 6) representing the interaction of the six probes used in the present study with PS, P4MS, and PMMPO are given in Table II. Values of V_g^0 for each probe and χ'_{23} (Equation 8) calculated for the two blends, PMMPO–PS and PMMPO–P4MS, at 270 °C are given in Table III. For PMMPO–PS, the mean value of χ'_{23} averaged over the six probes was 0.21. Error bounds are estimated to be ±0.3 and arise principally from probe variation, uncertainties in loading determination, and inaccuracies associated with measurement of the relatively small retention volumes obtained at the high temperature used in this study. This result is consistent with the *PVT* measurements of PMMPO–PS blends by Zoller and Hoehn (*18*) at comparable temperatures at which a near zero excess free volume of mixing was reported.

By comparison, the value of χ'_{23} of −1.21 determined for PMMPO–P4MS suggests a more favorable free energy of mixing at this temperature.

Table I. Weight Fraction Activity Coefficients in Polystyrene

	Ω_∞ at 150 °C				Ω_∞ at 175 °C		
Probe	*This Study*	*Ref. 23*	*Ref. 24*	*Ref. 25*	*This Study*	*Ref. 23*	*Ref. 25*[a]
Benzene	4.82	5.44	—	4.85	4.87	5.67	4.88
Ethylbenzene	4.98	4.96	—	5.01	5.05	5.47	5.04
Toluene	4.80	5.22	5.3	4.90	4.88	5.29	4.98

Note: $\Omega_\infty = \lim_{w_i \to 0} (a_1/w_1)$.

[a] Average of values reported at 170 °C and 180 °C.

Table II. Specific Retention Volumes and Interaction Parameters for Unblended Polymers

	V_g^0 (mL/g)			χ_{1i}		
Probe	*PS*	*P4MS*	*PMMPO*	*PS*	*P4MS*	*PMMPO*
Benzene	2.25	3.90	5.09	0.01	−0.50	−0.83
Ethylbenzene	3.85	6.67	8.65	0.19	−0.33	−0.66
Toluene	3.09	5.09	6.77	0.10	−0.37	−0.72
o-Xylene	4.42	7.70	9.87	0.23	−0.29	−0.61
m-Xylene	3.87	6.81	8.61	0.24	−0.29	−0.59
p-Xylene	3.82	6.58	8.58	0.24	−0.27	−0.60

Table III. Specific Retention Volumes and Interaction Parameters for Blends

	V_g^0 (mL/g)		χ'_{23}	
Probe	*PMMPO–PS*	*PMMPO–P4MS*	*PMMPO–PS*	*PMMPO–P4MS*
Benzene	3.43	3.04	0.07	−1.51
Ethylbenzene	6.00	5.56	0.18	−1.23
Toluene	4.81	4.36	0.22	−1.17
o-Xylene	7.10	6.40	0.31	−1.22
m-Xylene	6.11	5.77	0.25	−1.12
p-Xylene	6.02	5.78	0.23	−1.03

This result was unexpected because of our earlier study of the glassy state properties of these blends (*7*). These studies suggested a slightly more marginal compatibility state for PMMPO–P4MS when compared to PMMPO–PS. Conclusions in that study were drawn primarily from density measurements at ambient temperature and the associated mechanical property behavior of the two blends.

Significant differences in miscibility between these two blends also would not be expected from consideration of the lattice fluid (LF) theory of Sanchez and Lacombe (*26*). The LF equation of state parameters for PS and PMMPO have been determined at 267 °C from the *PVT* data of Zoller and Hoehn (*18*). For P4MS, for which *PVT* is not yet available, the equation of state parameters was obtained from the thermal expansion coefficient (α) determined from dilatometry measurements (*19*) and from the isothermal compressibility (β) estimated by the parachor method of McGowan (*27*). Solubility parameters (δ) at 267 °C also can be determined by use of the relationship

$$\delta = (T\alpha/\beta)^{1/2} \tag{9}$$

Values of the close-packed mer volume (v^*), characteristic temperature (T^*), characteristic pressure (P^*), and solubility parameters are given in Table IV. As shown, the values for PS and P4MS are not greatly different.

As discussed by Sanchez (*26*), miscibility is favored when the ratios of characteristic temperature ($\tau = T_1^*/T_2^*$) and characteristic mer volumes ($v = v_1^*/v_2^*$) are both greater than unity. As shown by values given in Table

Table IV. LF and Solubility Parameters

Polymer	T^* *(K)*	P^* *(bar)*	v^* *(cc/mol)*	δ *(cal/cc)*
PS	835	4196	16.6	8.72
P4MS	853	4144	17.2	8.73
PMMPO	763	4632	13.7	8.86

Table V. Miscibility Criteria

Blend	$\lvert\Delta T^*\rvert$	τ	ν	$\lvert\Delta\delta\rvert$
PMMPO–PS	72	1.094	1.21	0.14
PMMPO–P4MS	90	1.118	1.26	0.13

V, both PMMPO–PS and PMMPO–P4MS fulfill these conditions, and only small differences appear between the two. In addition, the difference in solubility parameters between PMMPO and PS and between PMMPO and P4MS is within typical critical bounds often cited as a criterion for miscibility of high molecular weight blends. That the solubility parameter theory may be a useful indicator of miscibility in these blends may not be totally unexpected because miscibility may be associated only with the dispersive interactions between the phenyl ring of PS and the phenylene ring of PMMPO (*28*).

Specific reasons for the apparent difference between the interaction parameters determined for the PMMPO–PS and PMMPO–P4MS blends cannot be definitely identified at present. It should be noted that intrinsic limitations of the IGC technique make a strict quantitative evaluation of results questionable (*29*, *30*). The most severe limitation may be the use of the original Flory expression for ΔG_m. If an alternative phenomenological form is used to include the dependence of χ_{ij} on composition (*22*, *31*), the apparent χ'_{23} obtained from IGC measurements can be shown to be a function of χ'_{23}, χ_{1i}, and the derivative of χ'_{23} with respect to ϕ_2 from which χ'_{23} cannot be easily resolved (*32*). This result would explain the usually significant variation of χ'_{23} with the choice of probe that is often attributed to specific interactions of the probe with one blend component or the occurrence of nonrandom mixing (*29*). This variation is typically handled by averaging values as was done in this study. In this study, probes were selected with chemical structures comparable to that of the PS component, and, therefore, probe variation of χ'_{23} values was minimized. Further comparison of the miscibility state of these two blends by alternate and less ambiguous techniques that eliminate the need of a solute probe, such as heat of mixing measurements of low molecular blends (*29*) or measurement of χ'_{23} by neutron scattering (*33*), would be desirable.

Nomenclature

- a Activity
- B_{11} Second virial coefficient of probe at T
- F Flow rate (Q) of carrier gas standardized to atmospheric pressure and corrected for P_w; $F = Q\ (760/P_o)\ [(P_o - P_w)/P_o]$
- J Correction factor for gas compressibility; $J = (3/2)\ [(P_i/P_o)^2 - 1]/[(P_i/P_o)^3 - 1]$

m_i Number of polymer chain segments expressed as the ratio of molar volumes of polymer to solute, V_i/V_1
n Number of molecules
P_i Inlet pressure to gas chromatograph
P_o Outlet pressure of gas chromatograph
P_w Vapor pressure of water at T_a
P_1^0 Vapor pressure of pure probe at T
R Ideal gas constant
t_N Net retention time; the time between the appearance of the noninteracting (air) and solute probe peaks as measured at peak maxima
T Column temperature
T_a Ambient temperature
v_i Specific volume of polymer at T
v_1 Liquid state molar volume of solute at T
V_g^0 Specific retention volume as normalized to 0 °C
w_i Weight fraction of polymer in the stationary phase
W Total polymer weight of column
ϕ Volume fraction
χ_{ij} Flory interaction parameter
χ'_{23} Normalized interaction parameter for polymer–polymer blend; $\chi'_{23} = (V_1/V_2)\chi_{23}$

Literature Cited

1. MacKnight, W. J.; Karasz, F. E.; Fried, J. R. in "Polymer Blends"; Paul, D. R.; Newman, S., Eds.; Academic: New York, 1978; Vol. 1, p. 185.
2. Fried, J. R. In "Developments in Polymer Characterization"; Dawkins, J. V., Ed.; Appl. Sci.: London, 1983; Vol. 4, p. 39.
3. Stejskal, E. O.; Schaefer, J.; Sefcik, M. D.; McKay, R. A.; *Macromolecules* **1981**, *14*, 276.
4. Wignall, C. D.; Child, H. R.; Li-Aravena, F. *Polymer* **1980**, *17*, 640.
5. Kambour, R. P.; Bopp, R. C.; Maconnachie, A.; MacKnight, W. J. *Polymer* **1980**, *21*, 133.
6. Maconnachie, A.; Kambour, R. P.; White, D. M.; Rostami, S.; Walsh, D. J. *Macromolecules* **1984**, *17*, 2645.
7. Fried, J. R.; Lorenz, T.; Ramdas, A. *Polym. Eng. Sci.*, in press.
8. Lipson, J. E. G.; Guillet, J. E. In "Developments in Polymer Characterization"; Dawkins, J. V., Ed.; Appl. Sci.: London, 1982; Vol. 3, p. 33.
9. Shultz, A. R.; McCullough, C. R. *J. Polym. Sci. Polym. Phys. Ed.* **1972**, *10*, 307.
10. Kwei, T. K.; Frisch, H. L. *Macromolecules* **1978**, *11*, 1267.
11. Weeks, F. E.; Karasz, F. E.; MacKnight, W. J. *J. Appl. Phys.* **1977**, *48*, 4068.
12. Karasz, F. E.; MacKnight, W. J. *Pure Appl. Chem.* **1980**, *52*, 409.
13. Ryan, C. L., Ph.D. Thesis, Univ. of Massachusetts, Amherst, 1980.
14. Morel, G.; Paul, D. R. *J. Membr. Sci.* **1982**, *10*, 273.
15. Everett, D. H. *Trans. Faraday Soc.* **1965**, *61*, 1637.
16. Deshpande, D. D.; Patterson, D.; Schreiber, H. P.; Su, C. S. *Macromolecules* **1974**, *7*, 530.

17. Reid, R. C.; Prausnitz, J. M.; Sherwood, T. K. "The Properties of Gases and Liquids"; 3d ed.; McGraw-Hill: New York, 1977.
18. Zoller, P.; Hoehn, H. H. *J. Polym. Sci. Polym. Phys. Ed.* **1981**, *20*, 1385.
19. Gunesin, B. Z. Mobil Chemical Company, personal communication.
20. Flory, P. J. "Principles of Polymer Chemistry"; Cornell Univ. Press: Ithaca, New York, 1971.
21. Scott, R. L. *J. Chem. Phys.* **1949**, *17*, 279.
22. Al-Saigh, Z. Y.; Munk, P. *Macromolecules* **1984**, *17*, 803.
23. Newman, R. H.; Prausnitz, J. M. *J. Phys. Chem.* **1972**, *76*, 1492.
24. Olabisi, O. *Macromolecules* **1975**, *8*, 316.
25. Schuster, R. H.; Grater, H.; Cantow, H.-J. *Macromolecules* **1984**, *17*, 619.
26. Sanchez, I. C. In "Polymer Blends"; Paul, D. R.; Newman, S., Eds.; Academic: New York, 1978; Vol. 2, p. 115.
27. McGowan, J. C. *Polymer* **1967**, *8*, 58.
28. Wellinghoff, S. T.; Koenig, J. L.; Baer, E. *J. Polym. Sci. Polym. Phys. Ed.* **1977**, *15*, 1913.
29. Walsh, D. J.; Higgins, J. S.; Rostami, S.; Weeraperuma, K. *Macromolecules* **1983**, *16*, 391.
30. Doube, C. P.; Walsh, D. J. *Eur. Polym. J.* **1981**, *17*, 63.
31. Narasimhan, V.; Burns, C. M.; Huang, R. Y. M. In "Polymer Blends and Composites in Multiphase Systems"; Han, C. D., Ed.; ADVANCES IN CHEMISTRY SERIES No. 206, ACS: Washington, D.C., 1984; p. 3.
32. Su, A. C.; Fried, J. R. *J. Polym. Sci., Polym. Lett. Ed.*, in press.
33. Hadziioannou, G.; Stein, R. S. *Macromolecules* **1984**, *17*, 567.

RECEIVED for review January 7, 1985. ACCEPTED March 11, 1985.

4

Miscibility in Random Copolymer Blends

F. E. KARASZ and W. J. MacKNIGHT

Polymer Science and Engineering Department, University of Massachusetts, Amherst, MA 01003

Compatibility in homopolymer–copolymer and copolymer–copolymer mixtures may be enhanced by the repulsion of dissimilar segments in the random copolymer chain. A mean field approach for this phenomenon is presented that gives a quantitative description of this phenomenon and that accounts for many of the phenomena observed. It can also be used to derive segmental interaction parameters from miscibility measurements. The treatment is generalized to cover other situations: (a) homopolymers with copolymers containing a common segment, (b) copolymer–copolymer blends in which the blend constituents contain the same two segments but in differing ratios, and (c) copolymer–copolymer blends containing one common segment. Graphical representatives of model calculations for several of these systems are shown.

THE GENERAL IMMISCIBILITY OF POLYMERS has been established experimentally and accounted for in thermodynamic terms. Exceptions have often been explained by invoking "specific interactions," which are associated with either an extremely small positive or, indeed, a negative nonconfigurational free energy of mixing. This thermodynamic requirement is necessitated by the negligible configurational entropy associated with binary high molecular weight polymer mixtures.

In random copolymers blended either with a homopolymer or a second random copolymer, an alternative mechanism can lead to miscibility. Miscibility may occur if the mutual repulsion between the dissimilar segments in the copolymer is sufficient to, in effect, overcome the repulsion between these segments and those in the second component of the mixture. In thermodynamic terms, this effect can lead to the negative net interaction energy necessary to induce miscibilization.

Such effects have been recognized on an empirical basis. An example is the well-known miscibility of polyvinyl chloride with random copolymers of ethylene and vinyl acetate for certain composition ranges of the latter system (*1*). These and similar findings recently were explained in a quantitative manner in a mean field theory for miscibility in copolymer blends

0065–2393/86/0211/0067$06.00/0

(2). This theory has permitted substantial insights into the effect of chemical structure and composition, of temperature, and of molecular weight on phase behavior in such systems. The theory parallels the well-established mean field approach for concentrated polymer solutions in that it divides the free energy of mixing, ΔG_m, into purely configurational and nonconfigurational terms. The nonconfigurational terms are described in terms of a dimensionless interaction parameter, χ_{blend}. Thus

$$\frac{\Delta G_m}{RT} = (\Phi_1/n_1) \ln \Phi_1 + (\Phi_2/n_2) \ln \Phi_2 + \Phi_1\Phi_2\chi_{\text{blend}} \quad (1)$$

where Φ_1 and Φ_2 are the volume fractions of components 1 and 2, and n_1 and n_2 are their respective degrees of polymerization.

The overall interaction parameter, χ_{blend}, in a blend containing copolymers is a linear combination of individual interaction parameters of the form

$$\chi_{\text{blend}} = \sum_{i,j} c_{ij}\chi_{ij} \quad (2)$$

where $\chi_{ij} (i \neq j)$ corresponds to each possible segmental interaction in a given system. The coefficients c_{ij} are functions of the copolymer composition(s) with $0 \leq c_{ij} \leq 1$.

The homopolymer–copolymer blend $A_n/(B_xC_{1-x})_{n'}$ (with degrees of polymerization n and n', respectively) has three segmental interaction terms χ_{AB}, χ_{AC}, and χ_{BC}; Equation 2 becomes

$$\chi_{\text{blend}} = x\chi_{AB} + (1 - x)\chi_{AC} - x(1 - x)\chi_{AB} \quad (3)$$

The general system of two random copolymers $(A_xB_{1-x})_n$ and $(C_yD_{1-y})_{n'}$ has six χ_{ij} values corresponding to each nonidentical segment interaction:

$$\chi_{\text{blend}} = xy\chi_{AC} + (1 - x)y\chi_{BC} + x(1 - y)\chi_{AD} + (1 - x)(1 - y)\chi_{BD} - x(1 - x)\chi_{AB} - y(1 - y)\chi_{CD} \quad (4)$$

This first-order treatment neglects many of the corrections found in modern polymer–solvent theories. These corrections can be introduced in principle at the expense of additional complications. For example, the temperature, composition, and concentration dependences of individual χ_{ij} values could be introduced at the outset with semiempirical methods that parallel methods used by Koningsveld and coworkers for polymer solutions (3). Our treatment is sufficient, however, to account in a self-consistent

manner for most of the phenomena experimentally observed. These phenomena include the existence of "windows of miscibility" in homopolymer–copolymer blends and the sensitivity of many blend phenomena to small changes in chemical composition, temperature, and molecular weight (*4*). (Windows of miscibility are seen when compatibility behavior is shown for a homopolymer–copolymer blend as a function of temperature and copolymer composition; miscibility windows have been designated "*T–c* plots." (*See* Figure 1.) Furthermore, in a recent test the theory was found to have predictive value. Thus, values of χ_{ij} obtained from data for miscibility in poly(2,6-dimethylphenylene oxide) (PPO) and polyhalostyrene binary combinations were used to predict behavior in the polystyrene (PS)–poly(*o*-chlorostyrene-*co*-*p*-chlorostyrene) system with reasonable success (*5*).

The quantitative determination of χ_{ij} values from our theory requires the experimental observation of miscibility–immiscibility boundaries as a function of copolymer composition. The number of such boundaries at a given temperature must be equivalent to, or greater than, the number of independent χ_{ij} values that are to be determined (*6*). In principle, the copolymer compositions can be permuted until the required number of boundaries is obtained. For example, a system $A_n/(B_xC_{1-x})_{n'}$ may yield zero, one, or two boundaries at a given temperature and can be combined with the boundaries from the system $B_{n''}/(A_xC_{1-x})_{n'''}$ and/or the third homopolymer–copolymer permutation to independently determine the desired χ_{ij} values.

The same mean field treatment may also be used to account for miscibility in blends of other copolymeric combinations of the given segments.

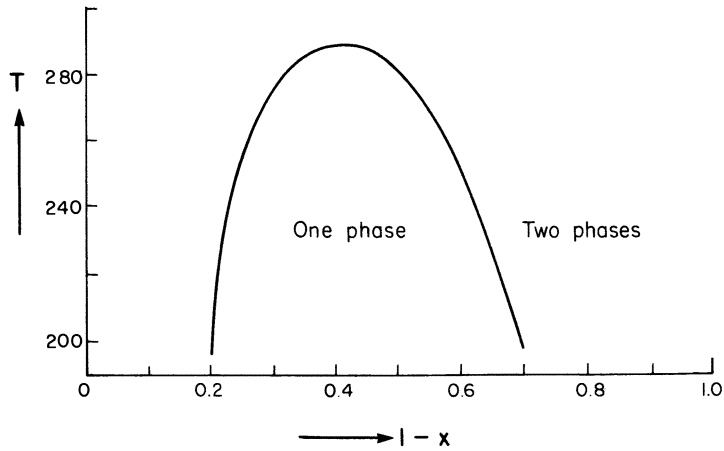

*Figure 1. Miscibility window for PPO–poly(*o*-chlorostyrene-co-*p*-chlorostyrene) blends: P (oClS$_x$-co-pClS$_{1-x}$)/PPO. (See Reference 4.)*

For example, in blends of the type $A_n/(A_xB_{1-x})_{n'}$ miscibility behavior is a function of the single interaction parameter, χ_{AB} and, by determining the miscibility–immiscibility boundary in this type of system for finite n,n' (*see* the next section), this parameter can be measured. An alternative approach would be to determine behavior in the copolymer–copolymer blend $(A_xB_{1-x})_n/(A_yB_{1-y})_{n'}$, which again is a function of a single interaction parameter χ_{AB}. This simple strategy is predicated, of course, on the validity of the approximation of a composition-independent χ_{ij}. However, this concept could be investigated and, if necessary, taken into account by measuring miscibility for different ranges of x and y (7).

Some Applications

$A_n/(B_xC_{1-x})_{n'}$. The most extensively studied systems in terms of the mean field theory are those consisting of a homopolymer and copolymer blend. This system involves three independent interaction parameters that can be evaluated from appropriate miscibility boundary data. Systems containing the homopolymer PPO with copolymers containing a combination of styrene and halostyrene monomers have been studied in this context (2). Miscibility windows are observed because all $\chi_{ij} > 0$, and χ_{BC} is sufficiently positive to render $\chi_{\text{blend}} < 0$ for certain ranges of x. For copolymers containing styrene homopolymer, a single boundary in the T–c plot is observed; this observation is consistent with the fact that PPO and PS are miscible. More recently, mixtures of PS with copolymers of *o*- and *p*-chlorostyrenes have been studied (5). These data have permitted us to refine values of χ_{ij} not only for this system but also to calculate a self-consistent set of values for a wider range of χ_{ij}. All the systems studied to date have displayed lower critical solution temperature (LCST) behavior; however, upper critical solution temperature (UCST) behavior may also be found. The predicted T–c behavior for this system is shown in Figure 2. The extremum in this plot corresponds to the instance in which the two consolute points just merge.

Systems containing PS and copolymers of *o*- and *p*-styrene exhibit extreme sensitivity to the degree of polymerization of either or both components. This effect is partially a result of the very low positive value of the interaction parameter representing styrene and *o*-chlorostyrene interactions. A recent extension of our investigations to lower molecular weight systems has shown that the temperature maxima of the miscibility windows increase substantially as the degree of polymerization is lowered and can readily be selected to cover the entire accessible experimental temperature range. The resulting data have enabled us to calculate the temperature dependence of the respective χ_{ij} values with some accuracy (8).

$(A_xB_{1-x})_n/(A_yB_{1-y})_{n'}$. Blends of random copolymers containing identical segments but of different overall compositions are predicted to be

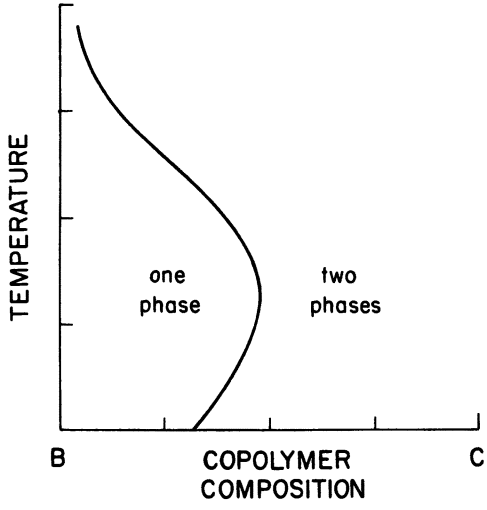

Figure 2. Predicted miscibility boundary for $A_n/(B_xC_{1-x})_{n'}$ *blend* ($\chi_{AB} < 0$ *and the two other* χ *values are positive) displaying both upper and lower critical solution temperatures. The boundary is the locus of UCSTs and LCSTs for positive and negative slope temperature regimes, respectively.*

incompatible when the respective polymers are of infinite molecular weight. The limiting miscibility condition $|x - y| = 0$ is relaxed, however, for $n,n' < \infty$. This behavior has been verified (*9*) for chlorinated polyethylenes (which may conveniently be treated as random copolymers of CH_2 and CHCl segments). In our work on this system, an extensive series of UCST values has been observed for chlorinated polyethylene blends whose glass transition temperature (T_g) values are sufficiently low (*10*).

$(A_xB_{1-x})_n/(C_yD_{1-y})_{n'}$. No systematic blend study of miscibility in two random copolymers has yet been reported. As already mentioned, behavior in this system is a function of six independent χ_{ij} values. A convenient representation of the predictions for this system is in the form of isothermal composition–composition plots ("*c–c* plots") displaying the miscibility–immiscibility boundary as a function of x and y ($0 \leq x, y \leq 1$). The boundary condition (for infinite molecular weight polymers) $\chi_{blend} = 0$ is a generalized quadratic function of x and y whose coefficients are functions of the respective individual χ_{ij} values. This function implies that the miscibility (or, in certain systems, immiscibility) domains will be conic sections. Whether these sections are ellipses or parabolas and whether these sections in fact lie wholly or partly in the regime of physical relevance ($0 \leq x, y \leq 1$) will depend on the numerical values of the χ_{ij} values.

In analogy to the homopolymer–copolymer system, even if all $\chi_{ij} > 0$ (and $n,n' \rightarrow \infty$), domains of miscibility can still be found (Figure 3) in the c–c representation. The ellipse shown cannot extend to the corners of the diagram because these areas correspond to immiscible blends of homopolymers of A and C and A and D, for example. However, for certain χ_{ij} the ellipse will intersect one or more of the boundaries of the diagram (e.g., the line $x = 0$, $0 \leq y \leq 1$ in Figure 4 corresponding to the instance of homopolymer–copolymer miscibility that displays the "window of miscibility") shown in Figure 1. A different type of miscibility domain is predicted if one or more χ_{ij} are negative. *See* Figure 5.

The special blend of copolymers containing a common segment [e.g., $(A_xB_{1-x})_n/(A_yC_{1-y})_{n'}$] may also be conveniently represented in this manner. In this system, again only three χ_{ij} values are required to describe the system, and the regimes of miscibility are bound by straight lines intersecting at the origin, $x,y = 0$. *See* Figure 6.

Conclusions

The theory provides explanations for a range of phenomena involving random copolymer containing blends. The interaction parameters that may be derived are sufficiently quantitative to be of predictive value in at least one system. Experimental determination of miscibility boundaries for copoly-

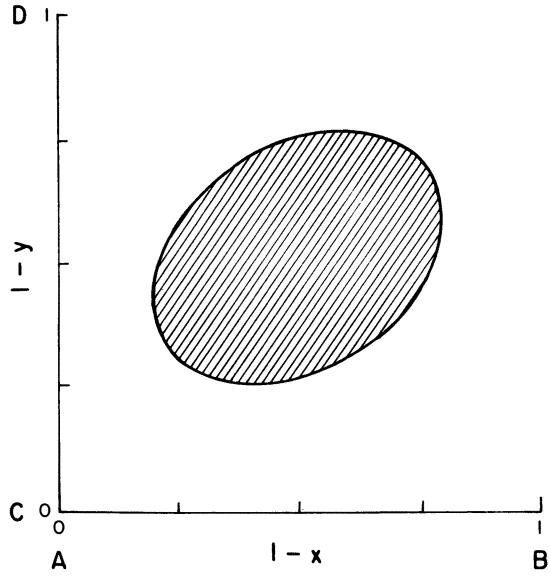

Figure 3. Calculated miscibility domain (shaded region) in copolymer blends. The degree of polymerization of the two copolymers is infinite. The interaction parameters χ_{AB}, χ_{AC}, χ_{AD}, χ_{BC}, χ_{BD}, *and* χ_{CD} *are 0.3, 0.1, 0.2, 9.2, 0.1, and 0.4, respectively.*

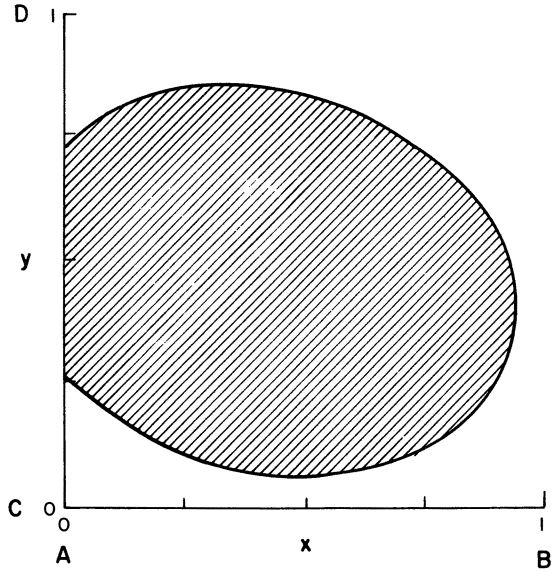

Figure 4. Calculated miscibility domain for a copolymer blend (infinite molecular weights) with χ_{ij} values of 0.3, 0.2, 0.1, 0.1, 0.1, and 0.5 (same order as in Figure 3).

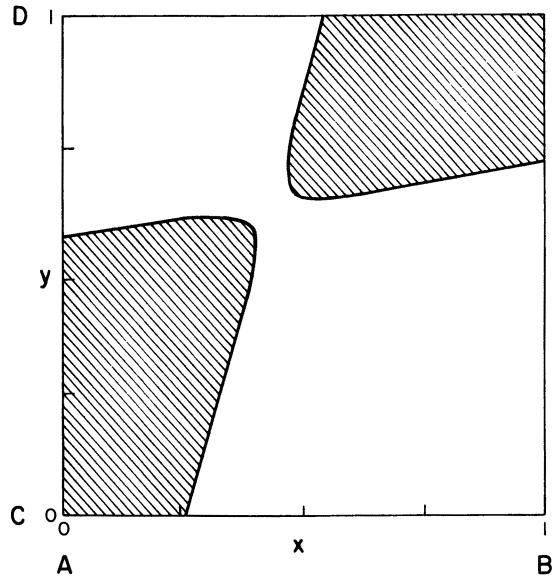

Figure 5. Calculated miscibility domains for a copolymer blend (infinite molecular weights) with χ_{ij} values of 0.1, −0.1, 0.17, 0.37, −0.1, and 0.2 (same order as in Figure 3).

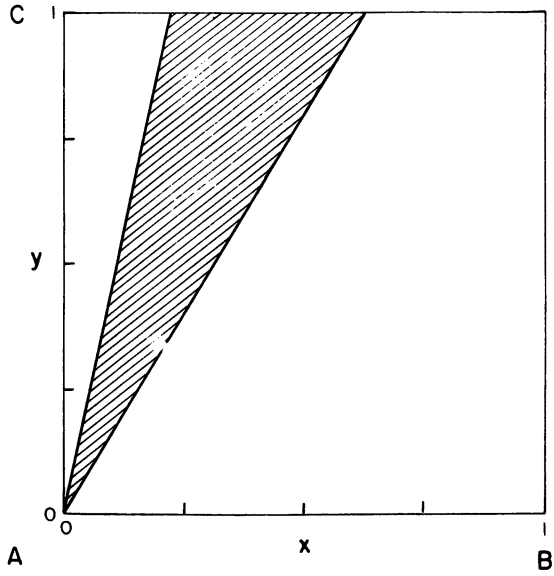

Figure 6. Calculated miscibility domain for a copolymer blend (infinite molecular weights) containing the common segment A. *The interaction parameters* χ_{AB}, χ_{AC}, *and* χ_{BC} *are 0.7, 0.1, and 0.2, respectively.*

mer–copolymer systems provides the means for further verification of the treatment.

An important aspect is the possibility for a rational design of copolymers to yield miscible systems. For example, miscibility that occurs in the *AB–AC* system may be viewed as a miscibilization of homopolymers of *B* and *C* by the respective copolymerization with the common segment *A*. Special requirements, such as conditions for minimizing the total consumption of *A*, for example, may be readily evaluated.

Extensions of the theory to take into account composition and concentration dependencies of the interaction parameters are formally possible. In addition the effect of chain microstructure (i.e., a relaxation of the requirement of random monomer placement in the copolymer) is feasible and is being incorporated in extensions of this work.

Acknowledgment

We acknowledge with thanks support from AFOSR Grant 84–0100 for this research.

Nomenclature

$\Delta G_m/RT$	Reduced free energy of mixing per monomer mole
Φ_i	Volume fraction of component i

n_i Degree of polymerization of component i

χ_{ij} Thermodynamic interaction parameter (dimensionless) between segment i and j

χ_{blend} Net thermodynamic interaction parameter for blend (dimensionless)

Literature Cited

1. Hammer, C. F. *Macromolecules* **1971**, *4*, 69.
2. ten Brinke, G.; Karasz, F. E.; MacKnight, W. J. *Macromolecules* **1983**, *16*, 1827. *See also* Paul, D. R.; Barlow, J. W.; *Polymer* **1984**, *25*, 487.
3. Koningsveld, R.; Kleintjens, L. A. *J. Polym. Sci. Polym. Symp.* **1977**, *61*, 221.
4. Alexandrovich, P.; Karasz, F. E.; MacKnight, W. J. *Polymer* **1977**, *17*, 1023.
5. ten Brinke, G.; Rubinstein, E.; Karasz, F. E.; MacKnight, W. J.; Vukovic, R. *J. Appl. Phys.* **1984**, *56*, 2440.
6. Karasz, F. E.; MacKnight, W. J. *Polym. Mater. Sci. Eng. Prepr.* **1984**, *51*, 280.
7. Karasz, F. E. "Polymer Blends and Mixtures"; Walsh, D. J., Ed.; Nijhoff: The Hague, Neth., 1985; p. 25–36.
8. Cimmino, S.; Karasz, F. E.; MacKnight, W. J., unpublished data.
9. Chai, Z.; Sun, R. *Polymer* **1983**, *24*, 1279.
10. Ueda, H.; Karasz, F. E. *Macromolecules*, in press.

RECEIVED for review November 15, 1984. ACCEPTED February 12, 1985.

5

Poly(vinylphenol) Blends with Poly(vinyl Acetate) and Ethylene–Vinyl Acetate Copolymers

E. J. MOSKALA, J. P. RUNT, and M. M. COLEMAN

Materials Science and Engineering Department, The Pennsylvania State University, University Park, PA 16802

Fourier transform IR and differential scanning calorimetric studies of poly(4-vinylphenol) (PVPh) blends with poly(vinyl acetate) (PVAc) and three ethylene–vinyl acetate copolymers (EVA[70], EVA[45] and EVA[25] containing 70, 45, and 25 wt% vinyl acetate, respectively) are presented. The results indicate that PVPh–PVAc and PVPh–EVA[70] blends are miscible (single phase) over the whole composition range, and the PVPh–EVA[25] blend system is immiscible. In contrast, the PVPh–EVA[45] appears to be an intermediate multiphased system in which there is, nonetheless, a significant degree of mixing. In addition, preliminary results are presented that demonstrate that the fraction of hydrogen-bonded carbonyl groups present in blends of PVPh and EVA[45] is dependent upon the molecular weight of the PVPh component.

FOURIER TRANSFORM IR (FTIR) STUDIES of a series of polymer blends based on poly(4-vinylphenol) (PVPh) were reported in two of our publications (*1*, *2*). Included were blends of PVPh with poly(vinyl acetate) (PVAc), three ethylene–vinyl acetate (EVA) copolymers, the polyesters poly(ϵ-caprolactone) and poly(β-propiolactone), poly(vinylpyrrolidone), poly(ethylene oxide), and three poly(alkyl vinyl ethers). IR bands attributable to intermolecular interactions involving the phenolic hydroxyl group with either carbonyl or ether groups of the second component in the blends were identified. An indication of the relative strengths of the different intermolecular interactions was also gained from the frequency shifts observed in the hydroxyl stretching region of the spectrum. But perhaps the most significant aspect of this previous work concerns the ability to quantitatively measure the fraction of hydrogen-bonded carbonyl groups in PVPh–PVAc and PVPh–EVA blends, as a function of temperature. From this information, we were able to obtain an estimation of the strength of the intermolec-

0065-2393/86/0211/0077$06.00/0

ular interaction (ΔH) from a Van't Hoff plot by assuming a simple equilibrium scheme. In addition, the effects of solvents and glass transition temperature (T_g) of the polymer blends were discussed in terms of the fraction of hydrogen-bonded carbonyl groups. In this chapter we present some further observations on the PVPh blends with PVAc and EVA copolymers.

Experimental

The two samples of poly(4-vinylphenol), PVPh and HMWPVPh (Polysciences Inc.) have reported weight average molecular weights of 1,500–7,000 and 30,000, respectively. The PVAc (Polysciences, Inc.) has a molecular weight (undefined) of 30,000. The ethylene–vinyl acetate copolymers (Mobay Chemical Company) have molecular weights (undefined) of 100–120 $\times$ 10^3.

Thin films of the PVPh blends prepared for FTIR studies were cast from 1% tetraohydrofuran (THF) solutions (weight per volume) onto potassium bromide windows at room temperature. Films prepared for thermal analysis were cast in aluminum pans. After a majority of the solvent had evaporated, the films were transferred to a vacuum desiccator to remove residual solvent and stored under vacuum.

IR spectra were obtained on a Digilab FTS/15E FTIR spectrometer. A minimum of 32 scans at a resolution of 2 cm^{-1} were signal averaged and stored on a magnetic disc system. The frequency scale is internally calibrated with a reference helium–neon laser to an accuracy of 0.2 cm^{-1}. A SPECAC high-temperature cell mounted in the spectrometer was used to obtain elevated temperature spectra to an accuracy of ± 2 K. All of the films were sufficiently thin to be within a range where the Beer–Lambert law is obeyed.

Thermal analysis was conducted on a Perkin-Elmer differential scanning calorimeter (DSC-2) coupled to a thermal analysis data station. A heating rate of 20 K/min was used in all experiments and the T_g was taken as the midpoint of the heat capacity change.

Results and Discussion

Figure 1 (*1*) shows the fraction of hydrogen-bonded carbonyl groups as a function of temperature for 80:20 PVPh blends by weight with PVAc and three EVA copolymers (EVA[70], EVA[45], and EVA[25], which contain 70, 45, and 25 wt% of vinyl acetate, respectively). The polymer blend samples were cast from THF solution and heated to 463 K to remove solvent effects (*1*). The FTIR spectra were recorded at intervals as the sample was cooled to room temperature. Major differences are immediately apparent in the fraction of hydrogen-bonded carbonyl groups at any given temperature for the PVPh blends with EVA[25], EVA[45], and EVA[70] or PVAc. For example, in these blends at room temperature, approximately 7, 50, and 75% of the carbonyl groups are hydrogen bonded, respectively. We have direct evidence from thermal analysis that the PVPh–PVAc and PVPh–EVA[70] blends are miscible. On the other hand, the PVPh–EVA[25] blend is, to all intents and purposes, immiscible. The question arises, "is the PVPh–EVA[45] blend miscible (single phase) or in some intermediate state?" Certainly the IR results indicate a significant degree of mixing.

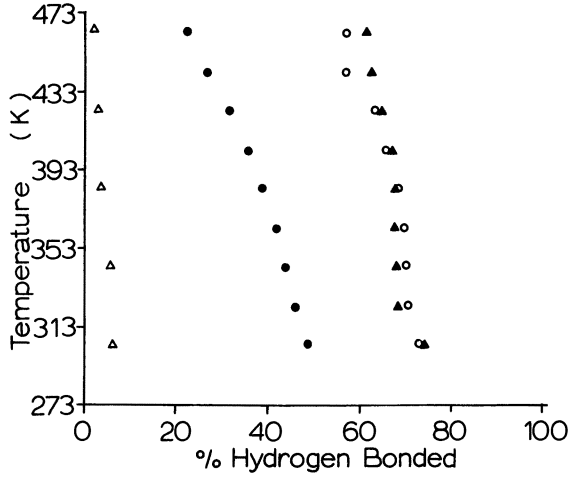

Figure 1. Graph of temperature vs. fraction of hydrogen-bonded carbonyls for samples of 80:20 wt % blends heated to 463 K and measured as a function of decreasing temperature. Key: △, PVPh–EVA[25]; ●, PVPh–EVA[45]; ○, PVPh–EVA[70]; and ▲, PVPh–PVAc.

Figure 2 shows differential scanning calorimetric (DSC) thermograms of PVPh–PVAc blends of varying composition. A single T_g is observed for all blend compositions that occur between the T_g values of pure PVAc and PVPh. This T_g increases systematically as the concentration of PVPh increases. These results are entirely consistent with the generally accepted definition of a single-phase system. The PVPh–EVA[70] blend samples exhibit similar DSC results. Figure 3 shows the DSC thermograms of pure EVA[70], PVPh, and a 50:50 PVPh–EVA[70] blend. Again, evidence is presented for a single phase.

Naturally, the DSC thermograms obtained for the PVPh–EVA[45] blends are not so simple! Figure 4 shows the thermograms obtained for pure PVPh, pure EVA[45], and blends of the two containing 50:50 and 80:20 wt%. The thermogram of pure EVA[45] is complicated. In general, one might expect a random copolymer of ethylene and vinyl acetate containing 45 wt% (21 mol%) of vinyl acetate to be essentially amorphous. The thermogram of EVA[45], however, shows a poorly resolved T_g at about 250 K that is superimposed on a broad peak that spans a temperature range from about 260 to 320 K. This thermogram is essentially identical to a previously reported thermogram (*3*) of EVA[45]. A reasonable interpretation of the broad endotherm might be that it is associated with the melting of short sequences of ethylene-type crystallinity. Another complication could be the existence of an endothermic response at T_g, which is seen in the thermograms of many glassy polymers (*4*). The thermogram of the

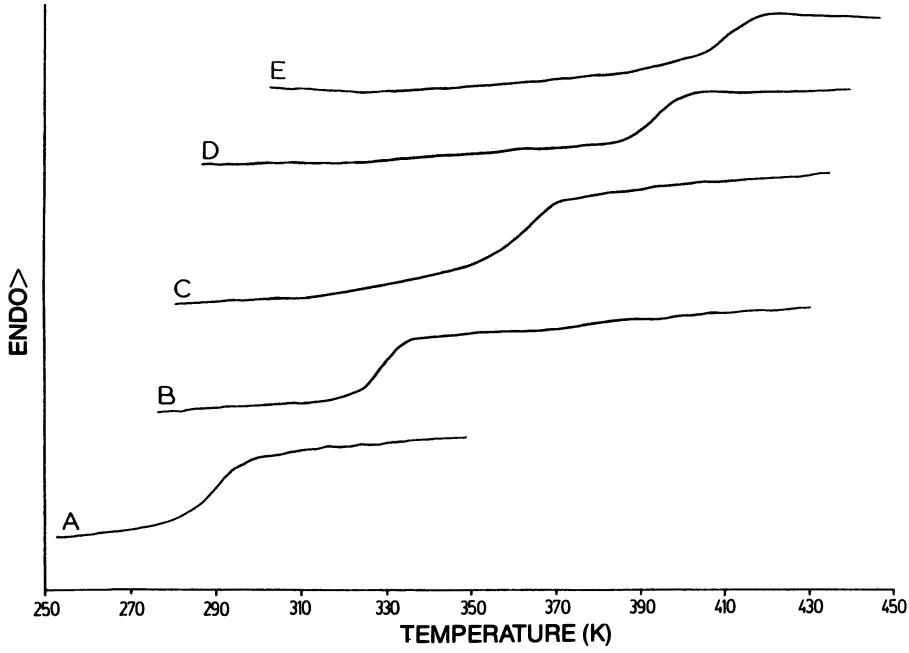

Figure 2. DSC thermograms for PVPh–PVAc blends containing A, 100; B, 80; C, 50; D, 20; and E, 0 wt % PVAc.

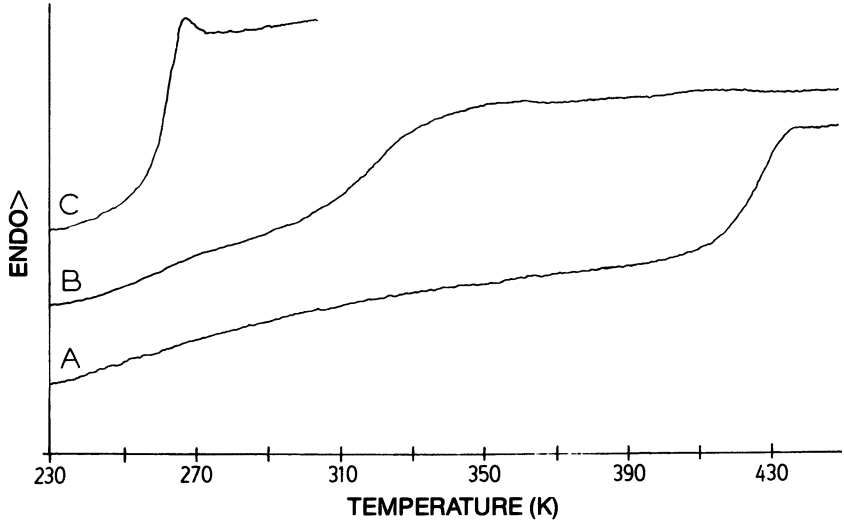

Figure 3. DSC thermograms for A, PVPh; B, EVA[70]; and C, a 50:50 wt % PVPh–EVA[70] blend.

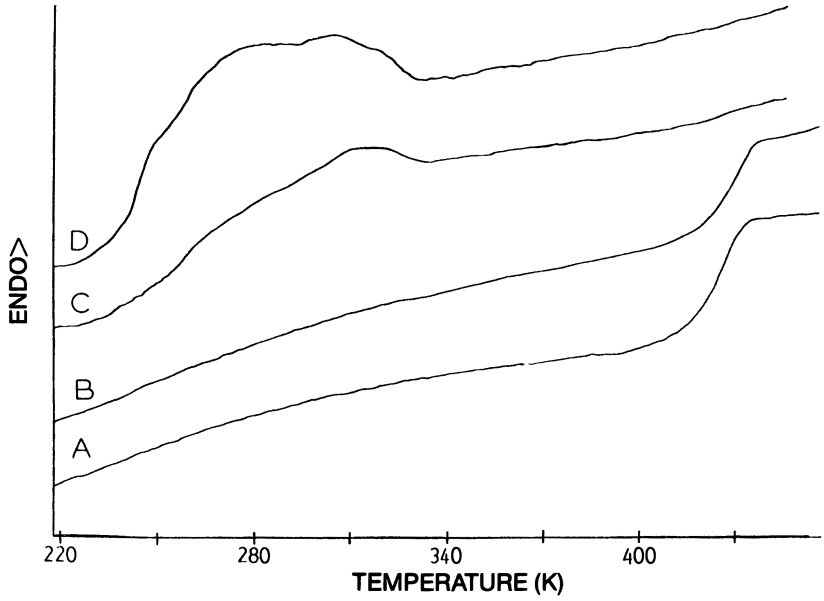

Figure 4. DSC thermograms for PVPh–EVA[45] blends containing A, 100; B, 80; C, 50; and D, 0 wt% PVPh.

50:50 PVPh–EVA[45] blend shows similar characteristics. One cannot confidently assign a T_g to either the pure EVA[45] or a miscible mixture of the two polymers. In addition, we could not detect the T_g of a pure PVPh component. If we now consider the thermogram of the 80:20 PVPh–EVA[45] blend, the picture becomes even more complicated. In this system, a T_g attributable to essentially pure PVPh is observed, but (perhaps not too surprising because of the concentration of EVA[45] in the blend) no obvious T_g attributable to pure EVA[45] or a miscible mixture is observed. How then are we to explain these thermograms from the IR results?

The IR data indicate a significant degree of mixing. For this system, approximately 50% of the EVA[45] carbonyl groups are hydrogen bonded to PVPh hydroxyl groups in the 80:20 PVPh–EVA[45] blend at room temperature. The thermogram of the 80:20 blend, on the other hand, shows a definitive T_g corresponding to the T_g of pure PVPh. Taken in isolation, the DSC results might lead to the conclusion that the PVPh–EVA[45] blend was immiscible. We believe, however, that the IR and DSC results suggest that the blend is a multiphased system consisting of essentially pure PVPh and a mixture of PVPh and EVA[45] phase.

IR spectroscopy is sensitive to the environment of individual chemical groups in the blend. Thermal analysis (and other methods that measure T_g values), however, yields information at the level of segmental motion, a

level that is at a much larger scale and involves many chain repeating units. One cannot definitively prove that a particular blend exists in a single phase from IR spectroscopy alone, but, in specific systems, one can determine that the polymer blend is significantly mixed. On the other hand, the existence of a single intermediate T_g is commonly accepted to be evidence of a single phase, and the detection of two T_g values at the same temperatures of the pure components is considered to be evidence of a completely immiscible blend system. These examples represent two extremes. However, the interpretation of DSC thermograms obtained from blends that are multiphased, but that have a significant degree of mixing at the molecular level, is often quite difficult. A combination of IR spectroscopy and thermal analysis appears to offer considerable potential for the study of these intermediate polymer blend systems.

The Effect of Molecular Weight

The PVPh used in our previous studies (*1*, *2*) is of modest molecular weight ($\overline{M_w}$ equals 1500–7000). It could be argued that we were not truly studying a polymer–polymer blend, but rather a polymer–oligomer mixture. Because miscibility decreases with increasing molecular weight, we repeated some of our earlier experiments using a recently acquired PVPh of considerably higher molecular weight (HMWPVPh, $\overline{M_w}$ equals 30,000). Further, this study also allows us to see if any differences occur in the degree of mixing of the polymers as we increase the molecular weight of the PVPh.

Figure 5 shows IR spectra in the carbonyl stretching region (1650–1800 cm^{-1}) of a series of HMWPVPh–PVAc blends cast from THF solution. The results are very similar to those published previously for the lower molecular weight PVPh blends with PVAc (*1*). The band at 1739 cm^{-1} is attributed to "free" (nonhydrogen bonded) PVAc carbonyl groups, whereas the 1714-cm^{-1} band is assigned to PVAc carbonyl groups hydrogen bonded to HMWPVPh hydroxyl groups. The insert in Figure 5 shows the corresponding hydroxyl stretching region (3500–3800 cm^{-1}). The spectrum of pure HMWPVPh (E) is characterized by a relatively narrow band at 3525 cm^{-1}, attributed to "free" hydroxyl groups, and a broad band centered at 3360 cm^{-1}, attributed to a wide distribution of intermolecularly hydrogen bonded hydroxyl groups (self-association). Upon mixing with PVAc, the hydroxyl stretching region is composed of three main contributions: free hydroxyl groups (3525 cm^{-1}), hydroxyl–hydroxyl interactions (3360 cm^{-1}), and hydroxyl groups hydrogen bonded to PVAc carbonyl groups (3430 cm^{-1}). Thus, as previously discussed in detail (*1*), the relative strength of the OH–O=C interaction is weaker than the self-association of PVPh. The only difference between the PVAc blends containing the two PVPh samples of different molecular weight is a slight increase in the concentration of hydrogen-bonded PVAc carbonyl groups in the lower molecular weight PVPh. This effect is much more dramatic in the EVA[45] blend systems.

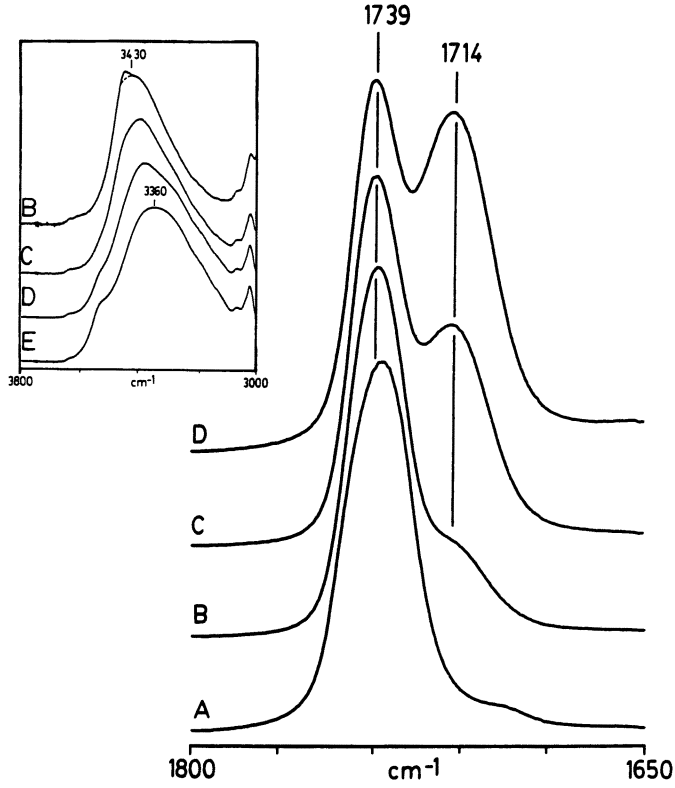

Figure 5. FTIR spectra in the regions from 3800–3000 and 1800–1650 cm^{-1} recorded at room temperature of HMWPVPh–PVAc blends cast from THF containing A, 100; B, 80; C, 50; D, 20; and E, 0 wt% PVAc.

In a previous publication (*1*), we presented a discussion of the quantitative method for determining the fraction of hydrogen-bonded carbonyl groups in PVPh–EVA[45] blends and the effects of solvent and T_g. Figure 6 shows the carbonyl stretching region of an 80:20 HMWPVPh–EVA[45] blend that was cast from THF and heated to 463 K to eliminate solvent effects. Spectra were then recorded as a function of decreasing temperature in a manner consistent with our previous studies on the lower molecular weight PVPh. The results given in Figure 6 show a trend similar to the previous studies. The concentration of hydrogen-bonded EVA[45] carbonyl groups increases with decreasing temperature. However, the fraction of hydrogen-bonded carbonyls at any temperature is considerably less than the fraction obtained for the analogous lower molecular weight PVPh blend (*compare* Figure 6 with the corresponding Figure 5 of Reference 1). This fact is more readily visualized in Figure 7, which is a plot of the fraction of hydrogen-bonded carbonyl groups as a function of temperature for

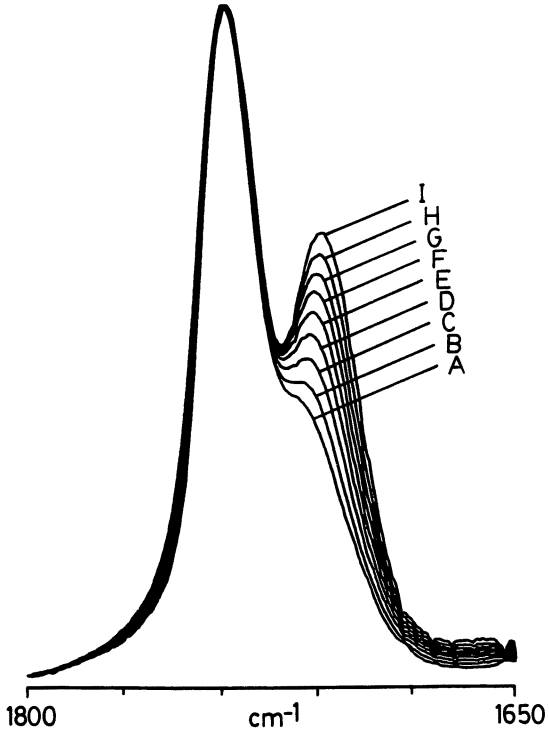

Figure 6. FTIR spectra in the 1800–1650 cm^{-1} region of an 80:20 HMWPVPh–EVA[45] blend cast from THF, heated to 463 K and recorded as a function of decreasing temperature A, 463 K; B, 443 K; C, 423 K; D, 403 K; E, 383 K; F, 363 K; G, 343 K; H, 323 K; and I, room temperature.

the two different molecular weight PVPh blends with EVA[45]. The degree of mixing is significantly less for the higher molecular weight PVPh blend. Incidentally, the thermograms of the EVA[45] blends containing the two different molecular weight PVPh materials are almost identical.

In this chapter, we have presented evidence that indicates that the PVPh–EVA[45] blends are not single-phased systems. Rather, they are complicated multiphased systems that have a significant degree of mixing. The results displayed in Figure 7 suggest that the degree of mixing is considerably less for the system containing the higher molecular weight PVPh. For example, at room temperature there is a difference of 14% in the fraction of EVA[45] carbonyl groups that are hydrogen bonded.

Generalizations concerning the effect of molecular weight on the degree of mixing are difficult to make from these two PVPh blends. One of the major difficulties is the polydispersity of the PVPh samples. We are currently studying blends of the high molecular weight PVPh with essen-

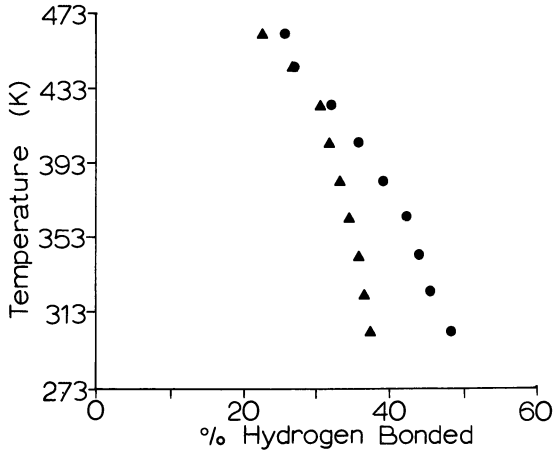

Figure 7. Graph of temperature vs. fraction of hydrogen-bonded carbonyls for samples of 80:20 wt % blends heated to 463 K and measured as a function of decreasing temperature. Key: ●, HMWPVPh–EVA[45]; and ▲, PVPh–EVA[45].

tially monodispersed samples of poly(methyl methacrylate) and will report our results in a future publication.

Acknowledgments

The financial support of the donors of the Petroleum Research Fund Grant PRF 14822-AC7, administered by the American Chemical Society, is gratefully acknowledged.

Nomenclature

EVA[x]	Ethylene–vinyl acetate copolymers containing x wt % vinyl acetate
T_g	Glass transition temperature
cm^{-1}	Wave number
$\overline{M_w}$	Weight average molecular weight

Literature Cited

1. Moskala, E. J.; Howe, S. E.; Painter, P. C.; Coleman, M. M. *Macromolecules* 1984, *17*, 1671.
2. Moskala, E. J.; Varnell, D. F.; Coleman, M. M. *Polymer* 1985, *26*, 228.
3. Elmquist, C.; Svanson, S. E. *Eur. Polym. J.* 1976, *12*, 559.
4. Flick, J. R.; Petrie, S. E. B. *Stud. Phys. Theor. Chem.* 1978, *10*, 145.

RECEIVED for review November 15, 1984. ACCEPTED April 18, 1985.

6

Specific Interactions in Polyester–Poly(vinyl Halide) Blends

Fourier Transform IR and Carbon-13 NMR Studies

PATRICE COUSIN and ROBERT E. PRUD'HOMME

Groupe de Recherche sur les Macromolécules, Département de Chimie, Université Laval, Québec, Canada G1K 7P4

Calorimetric measurements indicate that poly(vinyl chloride) (PVC) is miscible with a large number of polyesters, whereas poly(vinyl bromide) (PVB) is miscible with a smaller number of polyesters, and poly(vinyl fluoride) (PVF) is immiscible with all the polyesters investigated. This chapter demonstrates that the miscible blends exhibit a frequency shift of the carbonyl vibration band, and an increase of its width at half-height, in their high-temperature Fourier transform IR spectra. In contrast, the carbonyl vibration band of the polyester is not perturbed in immiscible blends. No significant difference could be detected between the carbonyl vibration band of miscible polyester–PVC and miscible polyester–PVB blends, at a given molar composition. Carbon-13 NMR spectroscopy was also used to study specific interactions between model compounds in binary solvents: methyl acetate was used as a model compound for polyesters, and halogenated molecules were used as model compounds for halogenated polymers. A comparison of the constants of association measured for several chlorinated and brominated model compounds shows that the chlorinated groups are more associated with the esters than the brominated groups, in agreement with the calorimetric measurements which indicate a higher degree of miscibility of PVC than of PVB with polyesters.

SEVERAL POLYESTERS ARE MISCIBLE with poly(vinyl chloride) (PVC) and other chlorinated polymers (1–12). The miscibility of polyester–poly(vinyl bromide) (PVB) blends also was studied by differential scanning calorimetry (*13*). PVB, like PVC, is miscible in the solid state with poly(caprolactone) (PCL) and poly(hexamethylene sebacate) (PHMS). However, it is immiscible with poly(valerolactone) (PVL), poly(butylene adipate) (PBA), poly(α-methyl α-propyl β-propiolactone) (PMPPL), and poly(α-methyl α-ethyl β-propiolactone) (PMEPL), whereas PVC is miscible with these four

0065–2393/86/0211/0087$06.75/0

polyesters. These results are summarized in Table I and compared with those obtained by mixing poly(vinyl fluoride) (PVF) with the same polyesters (*10*). PVF is immiscible with all the polyesters listed in Table I.

The difference in miscibility between PVF and PVC with polyesters has been explained by the high electronegativity of the fluorine atom, which leads to intramolecular interactions between PVF segments instead of intermolecular interactions with polyesters as found with PVC. However, the difference in miscibility between PVC and PVB with polyesters is more difficult to understand in view of the very similar properties of the chlorine and bromine atoms. Nevertheless, other examples of the higher miscibility of a chlorinated polymer compared to a brominated polymer have been reported. For example, ten Brinke et al. (*14*) observed that poly(*o*-chlorostyrene-*co*-*p*-chlorostyrene) is miscible with poly(2,6-dimethyl-1,4-phenylene oxide) (PPO), whereas poly(*o*-bromostyrene-*co*-*p*-bromostyrene) is immiscible with PPO.

In this chapter we present two different techniques used to investigate further the miscibility behavior of polyester–PVC, polyester–PVB, and polyester–PVF blends. Fourier transform IR (FTIR) spectra of miscible and immiscible blends will be analyzed as a function of the composition of the blends. The FTIR method has been shown to give useful information concerning the specific interactions occurring between polymer segments in polyester–PVC blends (*3*, *4*, *15*). It was also proposed (*16*, *17*) that the shift of the carbonyl absorption band of a polyester, in a miscible blend, can be related to the strength of the interaction between polymer segments. In that context, it seems interesting to compare the FTIR spectra of miscible polyester–PVC and polyester–PVB blends, for which different strengths of interaction have been suggested from the calorimetric measurements (*18*).

In the second part of this chapter we present ^{13}C-NMR spectroscopic studies on the interactions between model compounds for polyesters (i.e.,

Table I. Comparison of the Miscibility Behavior of Polyester–Poly(vinyl Halide) Blends

Polyester	*Polyester–PVC*	*Polyester–PVB*[a]	*Polyester–PVF*
PCL	Miscible	Miscible	Immiscible
PHMS	Miscible	Miscible	Immiscible
PVL	Miscible	Immiscible	Immiscible
PBA	Miscible	Immiscible	Immiscible
PMPPL	Miscible	Immiscible	Immiscible
PMEPL	Miscible	Immiscible	Immiscible
PEA	Immiscible	Immiscible	Immiscible

[a] In earlier work (*13*), the PVL–PVB and PBA–PVB blends were given as miscible. Additional measurements (*18*) showed that two glass transition temperatures can be found at certain concentrations: these blends are, therefore, immiscible according to the miscibility criterion defined in Reference 13.

methyl acetate) and several chlorinated and brominated molecules that are model compounds for PVC and PVB. More specifically, we pursued earlier work (*19*) and compared the association behavior of several chlorinated molecules ($CHCl_3$, CH_2Cl_2, and 1,3-dichlorobutane) with methyl acetate. In addition, we compared the association behavior of brominated and chlorinated model compounds and have studied the behavior of (1) brominated molecules ($CHBr_3$, CH_2Br_2, 1,3-dibromobutane) in a methyl acetate–heptane binary solvent, (2) chlorobrominated molecules (1-bromo-2-chloroethane and 1-bromo-3-chloropropane) in the same binary solvent, (3) methyl acetate in a 1,1,2,2-tetrachloroethane–heptane binary solvent and a 1,1,2,2-tetrabromoethane–heptane binary solvent, and (4) PCL in three binary solvents: $CHCl_3$–CCl_4, $CHBr_3$–CCl_4, and $CHCl_2CCl_3$–CCl_4. Differences in interactions between the chlorinated and brominated model compounds with esters and polyesters can be associated with differences of miscibility between PVB–polyester and PVC–polyester blends.

Indeed, FTIR and NMR measurements on model compounds can provide useful information concerning the interactions between polymer segments, as shown previously (*19*). For example, PCL dissolved in a binary solvent composed of 1,1,2,2-tetrachloroethane and carbon tetrachloride exhibited a double IR absorption peak for the carbonyl group. In NMR, a single chemical shift, which is a weighted average of the chemical shifts of the solute in its two association states, was observed for each carbon atom of PCL owing to the rapid exchange of the solute between the two components of the solvent. An association constant between PCL, or a model ester, and the two components of the solvent could therefore be calculated. The association constants indicated the existence of a specific interaction between the carbonyl group of the polyester, or ester, and the –CHCl– group of the chlorinated solvent. The presence of other sorts of interactions was not necessarily excluded, but they were much weaker than the interaction between C=O and CHCl.

These two series of studies should give a better understanding of the nature and strength of the specific interactions that are responsible for the miscibility behavior of polyester–PVC and polyester–PVB blends.

Experimental

The PVB sample (Polysciences) was purified by dissolution in tetrahydrofuran and precipitation in methanol. It has a weight-average molecular weight ($\bar{M}_w$) of 26 kg/mol. PVC (Shawinigan Chemical) had a $\bar{M}_w$ of 80 kg/mol. Finally, PVF (Aldrich Chemical) had an intrinsic viscosity of 1.7 dL/g in *N*-methyl-2-pyrrolidone at 298 K.

Three polyesters [PCL, PBA, and poly(ethylene adipate) (PEA)] were purchased from Aldrich, and one (PHMS) from Scientific Polymer Products; the others were synthesized in our laboratory (*9*, *20*, *21*). Values of 20, 30, 33, 9, 88, 10, and 2.6 kg/mol were found for the $\bar{M}_w$ of PCL, PHMS, PVL, PBA, PMPPL, PMEPL,

and PEA, respectively. All other chemicals were supplied by Aldrich and used without purification, unless the manufacturer suggested purification.

FTIR results were obtained with a BOMEM DA3.02 spectrometer. Thin polymer films were cast onto a KBr window from 3% (w/v) solutions in tetrahydrofuran (polyester–PVB and polyester–PVC blends) or dimethylformamide (PCL–PVF blends). To remove all traces of solvent, the films were dried in a vacuum, at room temperature, for more than 12 h. The KBr windows were then transferred into a high-temperature cell connected to an Omega D-921 thermoregulator and mounted in the spectrometer. After a temperature of 80 °C was reached, 100 scans were made at a resolution of 2 cm^{-1} and the spectra were stored on a magnetic disk.

Carbon-13 NMR results were obtained with a Brucker WP-80 spectrometer at 20 °C, by using a pulse width of 1.9 μs and a pulse delay of 679 ms. The number of scans was close to 2000. The solute concentration was 9%. To eliminate any interaction between the solution and the reference compound, a coaxial NMR tube was used. The external standard was a solution of tetramethylsilane (TMS) in deuterated chloroform (20% by volume). Chemical shifts were corrected to account for differences in magnetic susceptibility between the two solutions in the field (*22*, *23*). This correction is well described (*24–26*).

In the NMR technique, a solute dissolved in a binary solvent composed of an associated component and a less associated component can be expected to exhibit two different chemical shifts for every carbon atom. However, only one peak is normally observed because of the high rate of exchange between the solute and the two components of the solvent. The position of this peak is a weighted average of the position observed with each of the two associated species. Therefore, one can write

$$[X_A] = \frac{\delta - \delta_B}{\delta_A - \delta_B} \tag{1}$$

where $[X_A]$ is the molar fraction of solute associated with component A, and δ, δ_A, and δ_B are the chemical shifts of one particular carbon atom of the solute in the binary solvent, in pure solvent A, and in pure solvent B, respectively. When the solute contains more than one carbon, X_A refers only to the association of the carbon under investigation and not to the entire solute molecule.

A constant of association K can now be defined (*19*) by

$$K = \frac{[X_A]}{[X_B]} \frac{[B]}{[A]} \tag{2}$$

where [B] and [A] are the molar fractions of the two components of the solvent, and $[X_A]$ and $[X_B]$ are the molar fractions of the associated and less associated solute. Constant K is then a measure of the interaction between the solute and the associative solvent (*19*, *27*).

Results

FTIR Spectroscopy. The FTIR spectra of PCL–PVC, PCL–PVB, and PCL–PVF blends were recorded, at 80 °C, as a function of the composition of the blends. At this temperature, PCL is completely melted and the spectra are, therefore, independent of the degree of crystallinity of the sample.

The analysis of the FTIR spectra showed that the only vibration band which is significantly perturbed as a function of the composition of the mixture is the carbonyl stretching vibration band at about 1735 cm^{-1}. A similar observation was made in previous studies of this sort (*3*, *4*, *15*, *28*), and it was postulated that the shift of the carbonyl vibration band is due to a hydrogen bonding interaction occurring between the carbonyl group of the polyester and the methine proton of the halogenated polymer. The occurrence of a hydrogen bonding interaction perturbs the carbonyl group by changing its electronic environment. In this sort of analysis, it is assumed that the carbonyl stretching vibration does not couple significantly with the backbone vibrations of the polymer. In other words, it is assumed that the carbonyl stretching vibration band is conformationally insensitive.

However, it was expected that a hydrogen bonding interaction could lead not only to a perturbation of the carbonyl vibration band of the polyester but also to a perturbation of the methine stretching vibration bands of the halogenated polymer. This phenomenon was not observed because the methine vibration bands occur in the same frequency range as the methylene stretching modes; the methylene groups are numerous and the intensity of their vibration buries that of the methine groups, whatever the composition of the blend (*28*). A perturbation of the methine stretching vibration band has, however, been observed in a mixture of PCL with an α-deuterated PVC (*29*). On the other hand, the C–X (X = Cl, Br, or F) stretching modes of PVC, PVB, and PVF are highly coupled and conformationally sensitive (*28*). Therefore, the C–X vibration bands cannot be used to study specific interactions in polymer blends.

Figure 1 gives a comparison of the frequency shift of the carbonyl vibration band of PCL in PCL–PVC, PCL–PVB, and PCL–PVF blends, as a function of the poly(vinyl halide) (PVX) weight percent in the mixture. Within experimental error, there is no shift for the PCL–PVF mixture, but the carbonyl vibration band of PCL shifts to lower frequencies for PCL–PVC and PCL–PVB blends. The magnitude of the shift increases with increasing PVX concentrations. The PCL–PVC values reported in Figure 1 are comparable with those published (*3*).

These results indicate that the PCL–PVF mixture is immiscible because the carbonyl group of the PCL is not perturbed by the presence of PVF. This blend probably forms a two-phase structure, with domains composed uniquely (or almost uniquely) of PCL and domains composed uniquely (or almost uniquely) of PVF. This conclusion is in agreement with the calorimetric measurements reported in Table I and in References 10 and 13.

These results also indicate that the PCL–PVC and PCL–PVB mixtures are miscible at all compositions, again in agreement with the calorimetric measurements (Table I and Reference 13), because the carbonyl group of PCL is perturbed by the presence of PVC and PVB. These blends probably

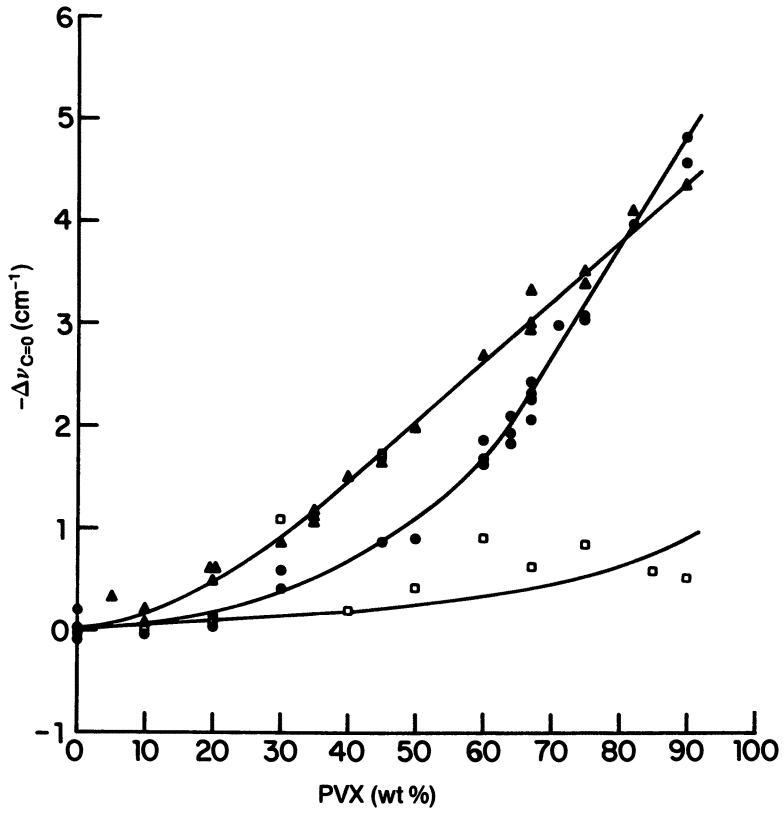

Figure 1. Frequency shift of the carbonyl group of PCL as a function of the PVX weight percent in the mixture. Measurements made at 80 °C. Key: □, PVF; ●, PVB; and ▲, PVC.

form a one-phase structure with an intimate mixture of PCL and PVC or PVB molecules.

Figure 1 shows a small difference between the frequency shifts of the carbonyl vibration band of PCL, at intermediate compositions, for PCL–PVC and PCL–PVB blends. Figure 2 shows that this difference disappears if the frequency shift is plotted as a function of the molar composition of PVX in the mixture. Most likely, PCL–PVX interactions occur on a mole-to-mole basis. When this fact is taken into account, as is done in Figure 2, no difference is seen between the frequency shift data taken for PCL–PVC and PCL–PVB blends.

In addition, Figure 3 shows that the width at half-height of the carbonyl vibration band of PCL increases with increasing PVC content in PCL–PVC miscible blends, whereas it remains almost constant with increasing PVF content in PCL–PVF immiscible blends. This increase of the

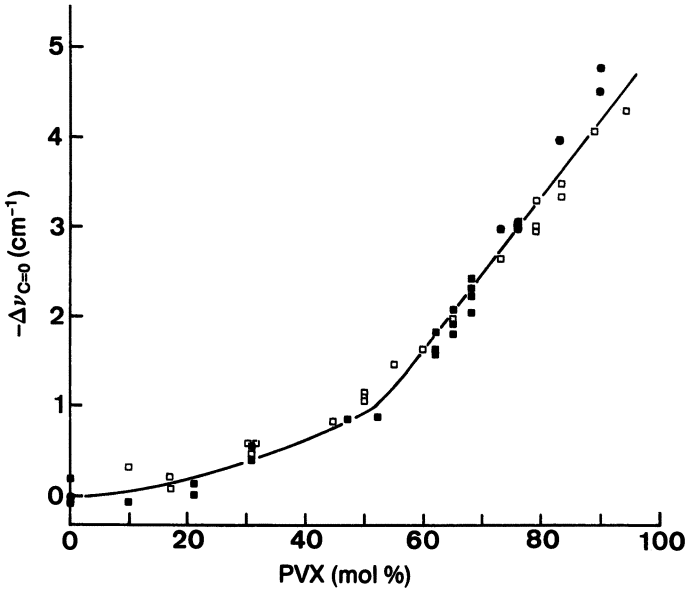

Figure 2. Frequency shift of the carbonyl group of PCL as a function of the PVX mole percent in the mixture. Measurements made at 80 °C. Key: □, PVC; and ■, PVB.

width at half-height of the carbonyl band of the polyester is also a characteristic feature of miscible polyester–PVC blends (*3*, *4*, *15*); values similar to those shown in Figure 3 were reported by Coleman and Zarian for PCL–PVC blends (*3*). The PCL–PVB blends also give increases in the width at half-height of the carbonyl band of PCL; these increases are similar to those reported in Figure 3.

Figure 4 shows the frequency shifts of the carbonyl vibration band of PHMS, in PHMS–PVC and PHMS–PVB blends, as a function of the molar composition of PVX in the mixtures. In both cases, a regular increase of the frequency shift occurs with increasing PVX content. This increase indicates the miscibility of these mixtures over the whole range of concentration, in agreement with calorimetric results. A small difference is observed between the two sets of results at intermediate concentrations, the frequency shift being larger in PHMS–PVC blends than in PHMS–PVB blends, but we do not believe that this difference is really significant because it is of the order of 0.5 cm^{-1} in the best cases. The PHMS–PVC and PHMS–PVB blends also exhibit an increase of the width at half-height of the carbonyl vibration band of PHMS with increasing PVX content.

Figure 5 shows the frequency shifts of the carbonyl vibration band of PVL, in PVL–PVC and PVL–PVB blends, as a function of the molar composition of PVX in the mixtures. In both cases, a regular increase of the

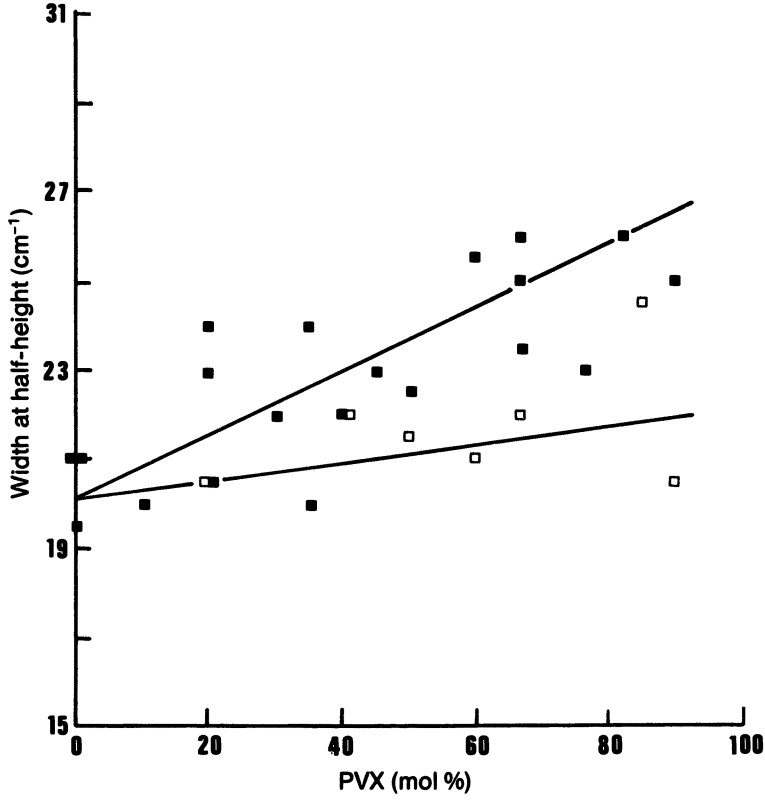

Figure 3. Width at half-height of the carbonyl vibration band of PCL as a function of the PVX mole percent in the mixture. Measurements made at 80 °C. Key: □, PCL–PVF; and ■, PCL–PVC.

frequency shift occurs with increasing PVX content, and this increase indicates the miscibility of these mixtures. However, the frequency shifts reported in Figure 5 are small, smaller than those observed in PCL–PVX and PHMS–PVX blends, particularly at low PVX concentrations.

The PVL–PVC results of Figure 5 are in general agreement with those reported by Varnell and Coleman (*4*), and with the calorimetric results (*10*). However, the thermodynamic interaction parameter between PVL and PVC is close to zero, and this value was taken as an indication of the low degree of miscibility between these two polymers (*10*), in agreement with the small frequency shifts reported in Figure 5 at low PVX concentrations.

The PVL–PVB data of Figure 5 appear to be in disagreement with the calorimetric results, which indicate the immiscibility of this mixture (Table I and Reference 18). However, the FTIR and the calorimetric measure-

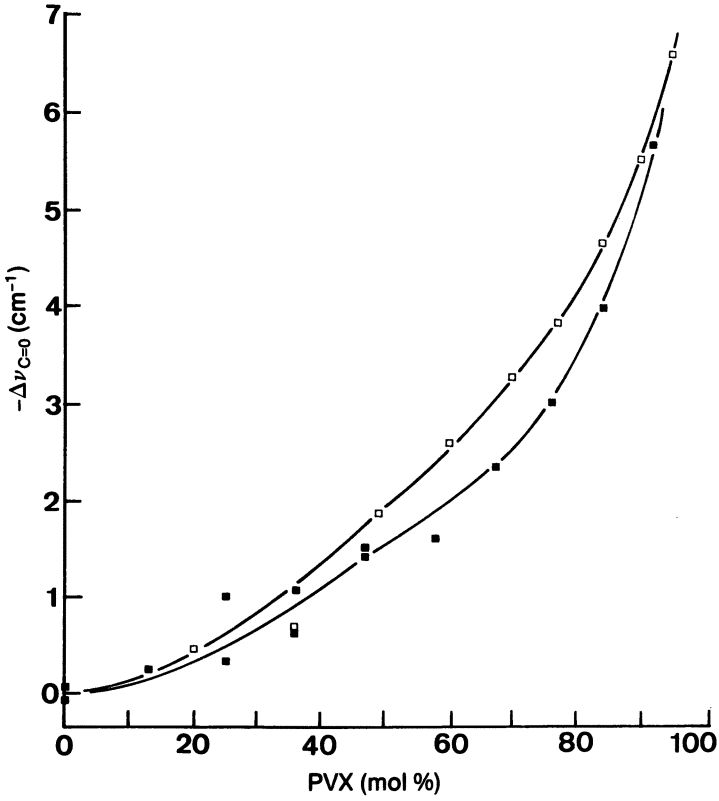

Figure 4. Frequency shift of the carbonyl group of PHMS as a function of the PVX mole percent in the mixture. Measurements made at 80 °C. Key: □, *PVC; and* ■, *PVB.*

ments were carried out under different temperature conditions: the FTIR data were obtained at 80 °C, whereas the calorimetric measurements were made at the glass transition temperature (T_g) of the mixture, which is much lower. In addition, the FTIR measurements were made on systems at equilibrium, because at 80 °C, the mixture is in the melt and has a relatively low viscosity. On the other hand, calorimetric measurements were most probably made on systems that are not at equilibrium, because they are made in the glassy region where the long-range motions of the chains are forbidden.

Finally, a careful examination of the calorimetric results reveals that the PVL–PVB mixtures exhibit partial miscibility (partial miscibility is called immiscibility, according to the definitions of References 10 and 13). More precisely, in the so-called immiscible PVL–PVB blends, a single T_g was observed at a 75 wt% PVB concentration, but two T_g values were re-

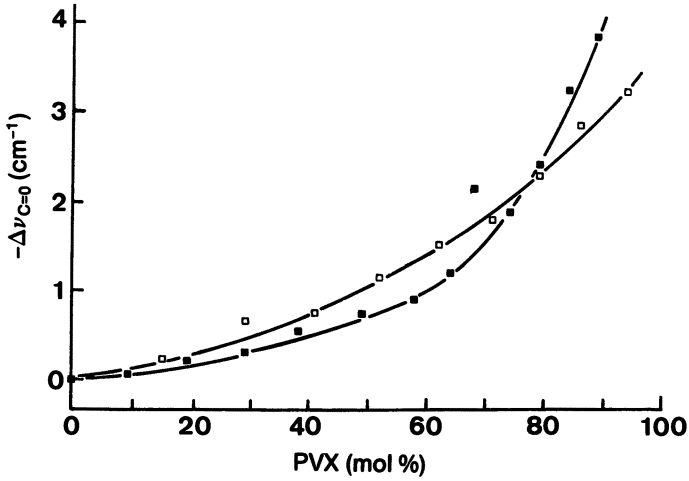

Figure 5. Frequency shift of the carbonyl group of PVL as a function of the PVX mole percent in the mixture. Measurements made at 80 °C. Key: □, PVC; and ■, PVB.

corded at 25 and 50 wt% PVB concentrations. These observations are not very far from those reported in Figure 5, where a significant shift of the carbonyl vibration band is observed at a 75% PVB concentration and a very small shift of this band is seen at 25 and 50% concentrations.

Figure 6 shows the frequency shifts of the carbonyl vibration band of PBA, in PBA–PVC and PBA–PVB blends, as a function of the molar composition of PVX in the mixtures. With PBA–PVC mixtures, regular increase of the frequency shift occurs with increasing PVC content, and indicates the miscibility of this mixture, in agreement with calorimetric measurements (*1*). However, the magnitude of the shift is small, particularly at low PVC concentrations.

With PBA–PVB mixtures, two regions can be distinguished easily. At low PVB concentrations, no frequency shift occurs, and this result agrees with the observation of immiscibility by calorimetry (*18*). At high PVB concentrations, a shift does occur, in agreement with the calorimetric measurements in which a single T_g was observed (*18*). Thus, the FTIR and the calorimetric data are in general agreement since both indicate partial miscibility of PBA–PVB blends.

With PVL–PVX and PBA–PVX blends, we could not establish a relationship between the frequency shift and the width at half-height of the carbonyl vibration band due to the dispersion of the latter data. In general, a change of the width at half-height seems to occur at high PVX concentrations, but no conclusion could be drawn with the results obtained at low PVX concentrations.

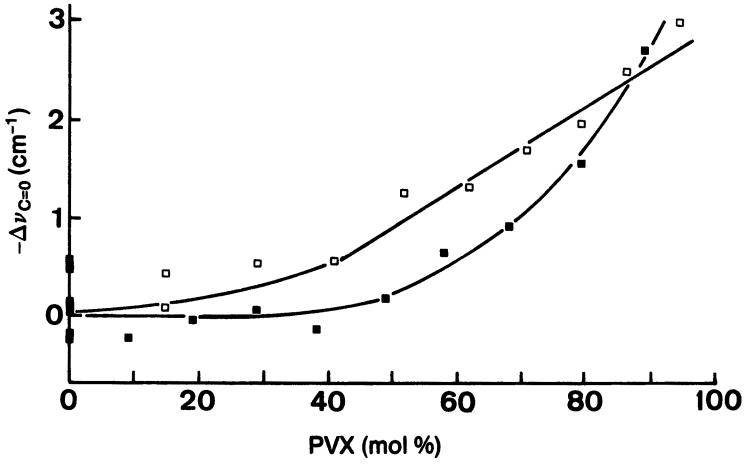

Figure 6. Frequency shift of the carbonyl group of PBA as a function of the PVX mole percent in the mixture. Measurements made at 80 °C. Key: □, PVC; and ■, PVB.

NMR Spectroscopy. The calorimetric measurements presented in Table I and in Reference 18 suggest that the strength of interaction of miscible polyester–PVC blends is higher than that of the corresponding miscible polyester–PVB blends of similar composition. However, this suggestion is not supported by the FTIR spectroscopy measurements reported earlier. In this section, the association behavior of several chlorinated and brominated model compounds will be analyzed to detect a difference in the strength of interaction between these two series of halogenated compounds with esters.

CHLORINATED SOLUTES IN A METHYL ACETATE–HEPTANE SOLVENT. Figure 7 shows a plot of the $[X_A]/[X_B]$ ratio as a function of [B]/[A], where X represents the solute ($CHCl_3$ and CH_2Cl_2), and A and B are the two components of the binary solvent. X_A was determined from NMR measurements and Equation 1, X_B from the $X_A + X_B = 1$ condition, and [A] and [B] were calculated from the volume composition of the binary solvent.

When $[X_A]/[X_B]$ is plotted as a function of [A]/[B], Equation 2 predicts a linear relationship with a slope equal to K. This behavior is verified in the two examples of Figure 7. In addition, both series of data show a deviation from the dashed reference line, which corresponds to the ideal case where $K = 1$. This deviation indicates a preferential association of the solute with methyl acetate rather than with heptane. If the interaction of the solute with methyl acetate and with heptane was similar, then K would equal unity.

Figure 7 also shows that $CHCl_3$ is more associated with methyl acetate than CH_2Cl_2. The respective association constants are 6.0 and 2.4 (Table

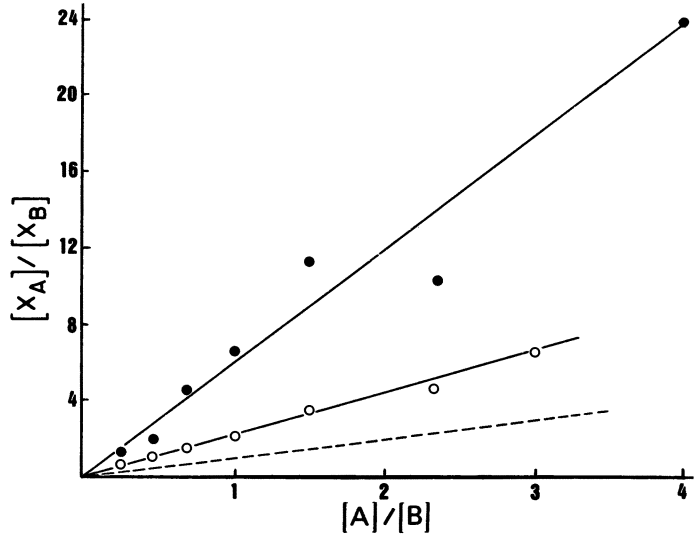

Figure 7. Ratio of the concentration of solute associated with component A to the concentration of solute associated with component B of the binary solvent, as a function of the ratio of the concentration of A to the concentration of B. In this example, the solute is $CHCl_3$ (●) or CH_2Cl_2 (○), and the solvent is composed of methyl acetate (A) and heptane (B).

II). The larger number of chlorine atoms of $CHCl_3$ compared to CH_2Cl_2 increases the polarity of the C–H bond and promotes the creation of stronger hydrogen bonds with the carbonyl group of the ester, leading to a larger value of K.

It may be argued at this point that $CHCl_3$ and CH_2Cl_2 are unsatisfactory models for PVC since they do not bear atoms in positions 1, 3, 5, etc. From this point of view, 1,3-dichlorobutane can be considered a better choice. However, the results obtained with $CHCl_3$ and CH_2Cl_2 are truly significant because the type of association found between methyl acetate and these two model compounds is the same as the intermolecular bonding involved in polyester–poly(vinyl halide) blends. However, $CHCl_3$ and CH_2Cl_2 probably give stronger hydrogen bonds than PVC due to the larger polarization of their C–H group.

Table II gives a comparison of the constants of association of the carbons in positions 1 and 3 (or position α) of 1,3-dichlorobutane (13DCB) in the methyl acetate–heptane binary solvent. Values of 1.3 and 1.5 have been observed for C-3 and C-1, respectively, indicating a stronger association of 13DCB with methyl acetate than with heptane. The two other carbons of 13DCB at positions 2 and 4 (C-2 and C-4 or position β) show variations of chemical shifts that are too weak to be truly significant. Nevertheless, they certainly have, despite a larger error, constants of asso-

Table II. Values of the Association Constant *K* for the Mixtures Investigated

Solute	*Binary Solvent*	K
$CHCl_3$	Methyl acetate–heptane	6.0 ± 1.0[a]
CH_2Cl_2	Methyl acetate–heptane	2.4 ± 0.2
13DCB	Methyl acetate–heptane	1.5 ± 0.2 (C-1)
		1.3 ± 0.2 (C-3)
$CHBr_3$	Methyl acetate–heptane	4.1 ± 0.2
CH_2Br_2	Methyl acetate–heptane	2.1 ± 0.2
13DBB	Methyl acetate–heptane	1.2 ± 0.2 (C-1)
		1.2 ± 0.2 (C-3)
1B2CE	Methyl acetate–heptane	1.9 ± 0.1 (C-2)
		1.8 ± 0.1 (C-1)
1B3CP	Methyl acetate–heptane	1.7 ± 0.4 (C-3)
		1.4 ± 0.4 (C-1)
Methyl acetate	1122TCE–heptane	2.0 ± 0.2
Methyl acetate	1122TBE–heptane	1.6 ± 0.2
Methyl acetate	$CHCl_3$–heptane	2.1 ± 0.2
PCL	$CHCl_3$–CCl_4	1.5 ± 0.1
PCL	$CHBr_3$–CCl_4	1.4 ± 0.1
PCL	PCE–CCl_4	1.8 ± 0.1

[a] Standard deviation measured using the least-squares method.

ciation that are close to unity. Finally, the signals of the carbons bearing chlorine atoms (C-1 and C-3) always shift towards low fields in the methyl acetate–heptane binary solvent compared to the chemical shifts found in heptane, whereas the signals of the nonchlorinated carbons (C-2 and C-4) shift towards high fields (Table III).

BROMINATED SOLUTES IN A METHYL ACETATE–HEPTANE SOLVENT. Figure 8 shows the association behavior of $CHBr_3$ and CH_2Br_2 in the methyl acetate–heptane binary mixture. A linear relationship is obtained in both cases, with a slope larger than unity, indicating a preferred association of $CHBr_3$ and CH_2Br_2 with methyl acetate. However, $CHBr_3$ is more associated with methyl acetate than is CH_2Br_2, with respective *K* values of 4.1 and 2.1 (Table II), resulting from the larger polarity of the C—H bond in $CHBr_3$.

The analysis in a similar fashion of the four carbon atoms of 1,3-dibromobutane (13DBB) leads to the same general conclusions as the analysis of 13DCB (Tables II and III), except that all values of *K* are slightly smaller than in the previous case.

The behavior of the brominated model compounds in a binary solvent mixture is then qualitatively similar to that of the chlorinated model compounds reported in the last section. However, the values of the constants of association *K* of the brominated solutes are smaller than those of their chlo-

Published on December 9, 1985 on http://pubs.acs.org | doi: 10.1021/ba-1986-0211.ch006

Table III. Analysis of NMR Results by *t* Test

Solute	*Solvent*	K ± σ		*Probability*[a] (%)
		X = Br	*X = Cl*	
CHX_3	Methyl acetate–heptane	4.1 ± 0.2	6.0 ± 1.0	≃100
CH_2X_2	Methyl acetate–heptane	2.1 ± 0.2	2.4 ± 0.2	98
13DXB	Methyl acetate–heptane	1.2 ± 0.2 (C-1)	1.5 ± 0.2 (C-1)	99
		1.2 ± 0.2 (C-3)	1.3 ± 0.2 (C-3)	66
1B2CE	Methyl acetate–heptane	1.8 ± 0.1	1.9 ± 0.1	83
1B3CP	Methyl acetate–heptane	1.4 ± 0.4	1.7 ± 0.4	95
Methyl acetate	1122TXE–heptane	1.6 ± 0.2	2.0 ± 0.2	≃100
PCL	CHX_3/CCl_4	1.4 ± 0.1	1.5 ± 0.1	83

[a] Probability that K_{Br} is smaller than K_{Cl}.

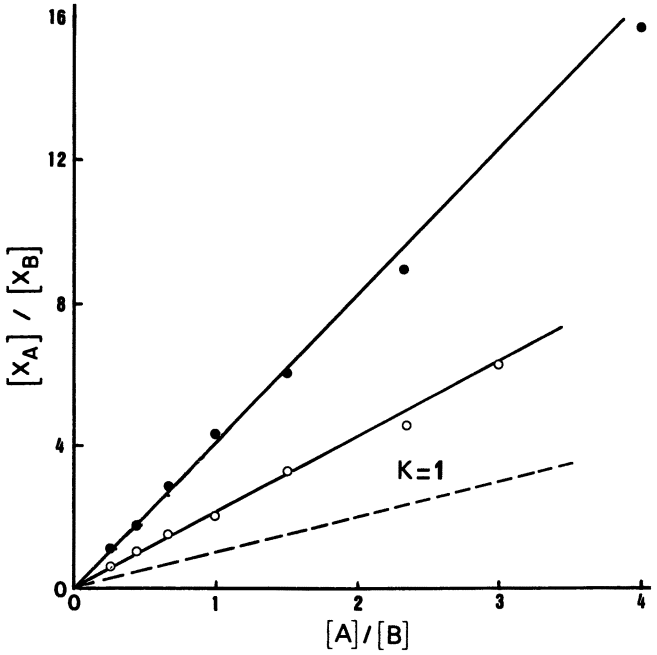

Figure 8. Ratio of the concentration of solute associated with component A to the concentration of solute associated with component B of the binary solvent, as a function of the ratio of the concentration of A to the concentration of B. In this example, the solute is $CHBr_3$ (●) or CH_2Br_2 (○), and the solvent is composed of methyl acetate (A) and heptane (B).

rinated homologues. Therefore, it can be concluded that the brominated model compounds investigated are less associated with methyl acetate than are the corresponding chlorinated compounds.

CHLOROBROMINATED SOLUTES IN A METHYL ACETATE–HEPTANE SOLVENT. Two molecules containing chlorine and bromine atoms simultaneously, i.e., 1-bromo-2-chloroethane (1B2CE) and 1-bromo-3-chloropropane (1B3CP), were dissolved in the binary solvent. Both exhibited an interaction with the carbonyl group of the ester (Table II) through their brominated and chlorinated carbons because constants of association larger than unity were observed. Moreover, the chlorinated groups have a slightly stronger affinity for the ester than the brominated groups because the K values of the chlorinated carbons are slightly larger than the association constants of the corresponding brominated carbons.

METHYL ACETATE IN A HALOGENATED MOLECULE–HEPTANE SOLVENT. The difference between the association behavior of chlorinated and brominated molecules with an ester can be followed not only by dissolving the halogenated molecule in a binary solvent having an ester as one

of its components, but also by dissolving an ester in a binary solvent having the halogenated molecule as one of its components.

In the latter situation, illustrated in Figure 9, methyl acetate is dissolved in 1,1,2,2-tetrachloroethane–heptane and 1,1,2,2-tetrabromoethane–heptane solvents. Both systems have a constant of association larger than unity, indicating preferential association of methyl acetate with 1,1,2,2-tetrachloroethane (1122TCE) and 1,1,2,2-tetrabromoethane (1122TBE). Figure 9 and Table II also show that methyl acetate is more strongly associated with 1122TCE (K = 2.0) than with 1122TBE (K = 1.6), relative to heptane. This result leads to the conclusion that the carbonyl group forms a stronger interaction with chlorinated groups than with brominated groups.

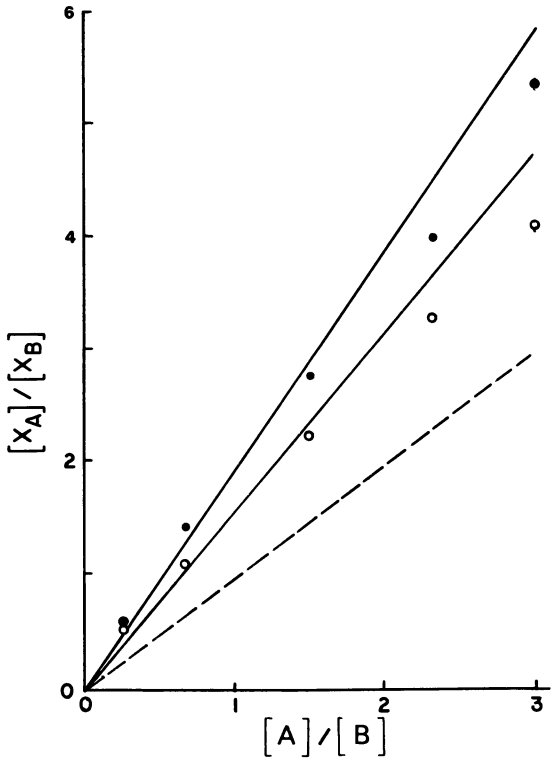

Figure 9. Ratio of the concentration of solute associated with component A to the concentration of solute associated with component B of the binary solvent, as a function of the ratio of the concentration of A to the concentration of B. In this example, the solute is methyl acetate, and the solvent is composed of 1,1,2,2-tetrachloroethane (1122TCE) or 1,1,2,2-tetrabromoethane (1122TBE) (A) and heptane (B). Key: ●, 1122TCE; and ○, 1122TBE.

PCL IN A HALOGENATED MOLECULE–CCl_4 SOLVENT. Like methyl acetate, its model compound in this work, poly(caprolactone) (PCL) is associated with halogenated molecules. Table II and Figure 10 show that its constant of association is slightly larger with $CHCl_3$ (K = 1.5) than with $CHBr_3$ (K = 1.4). Moreover, the value of K increases when PCL is dissolved in a solvent containing a larger chlorine concentration. For example, a constant equal to 1.8 is obtained with pentachloroethane (PCE), compared to a value of 1.5 with $CHCl_3$ and 1.4 with CH_2Cl_2. This behavior is due to the greater polarity of the proton of PCE, compared to that of $CHCl_3$, because of the electronic drainage provided by its five chlorine atoms. Therefore, hydrogen bonding is stronger between PCL and PCE than between PCL and $CHCl_3$.

Discussion

A main objective of this work was to determine differences in the strength of interaction between polyesters and halogenated polymers. FTIR spec-

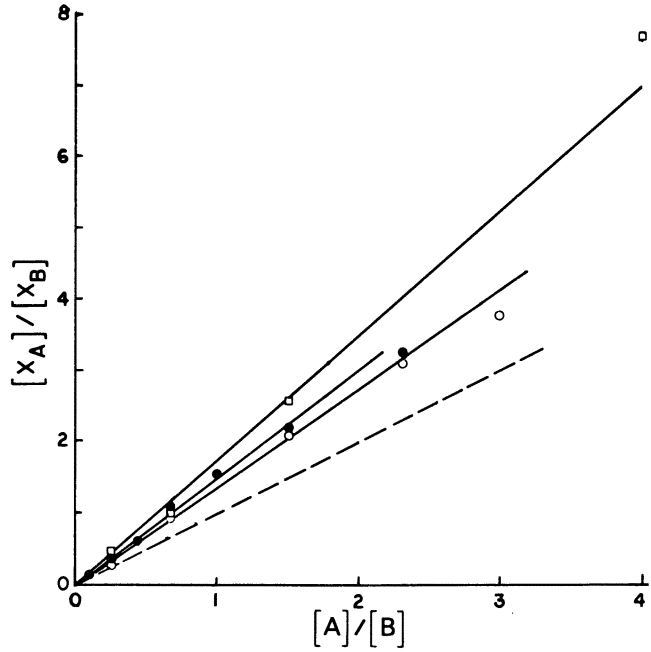

Figure 10. Ratio of the concentration of solute associated with component A to the concentration of solute associated with component B of the binary solvent, as a function of the ratio of the concentration of A to the concentration of B. In this example, the solute is poly(caprolactone), and the solvent is composed of pentachloroethane (PCE), $CHCl_3$, or $CHBr_3$ (A) and CCl_4 (B). Key: □, PCE; ●, $CHCl_3$; and ○, $CHBr_3$.

troscopic studies showed that small frequency shifts and increases of the width at half-height of the carbonyl vibration band of polyesters are seen in miscible polyester–PVX blends, whereas no shift and no increase of the width of this band are observed in immiscible polyester–PVF blends. Moreover, in partially miscible blends (i.e., in the PBA–PVB mixtures) no shift was detected in a concentration range of 0 to 50 mol% PVB, but a shift was observed at higher PVB concentrations. This result is in agreement with the calorimetric data.

In all miscible blends, the shift of the carbonyl vibration band is small at low PVX concentrations, but it increased with increasing PVX. This general behavior is related to the relative concentration of carbonyl groups interacting with PVX segments. At low PVX concentrations, a small number of PVX molecules is dispersed in a polyester matrix. The number of carbonyl groups interacting with PVX is, therefore, small. This situation leads to a small perturbation of the position of the carbonyl band. However, at high PVX concentrations, a small number of polyester molecules is dispersed in a PVX matrix. Then, a large number of carbonyl groups, but not necessarily all of them, can interact with PVX segments. This situation gives a larger shift of the carbonyl vibration band.

However, even at high PVX concentrations, a fair number of carbonyl groups can remain unperturbed by the presence of the PVX segments because of the conformation of the polyester chain. In other words, the relative rigidity of the polyester chain and its random coil conformation signify that certain carbonyl groups are in volume elements that are poor in PVX segments and others are in positions unfavorable to interactions with PVX segments. In both cases, these carbonyl groups will vibrate at the same frequency position as they do in a pure polyester matrix. If all carbonyl groups interacted with PVX segments, a shift in the position of the carbonyl vibration band would be seen. The band broadening observed experimentally is believed to be due to a distribution of interactions, ranging from no interaction at all to relatively strong hydrogen bonds, with all intermediate situations.

The shifts observed at large PVX concentrations decrease in this order: PHMS > PCL > PVL > PBA. This is a decreasing order of carbonyl concentration on the repeat unit of the polyester and, at the same time, an increasing order of rigidity of the polyester chain. The more rigid the chain, the larger is the number of carbonyl groups that do not interact with PVX groups and the smaller is the shift of the carbonyl vibration band.

In this work, no significant difference could be detected between the FTIR frequency shifts and the widths at half-height shown by miscible polyester–PVC and miscible polyester–PVB blends. To determine a difference in the strength of interaction between a polyester and different halogenated polymers, we studied model compounds by NMR spectroscopy.

The association constant of a solute in a binary solvent can be calculated if the fraction of the solute that is more strongly associated is mea-

sured, the remaining fraction being less associated (or nonassociated). Previously (*19*), we showed that two carbonyl bands corresponding to these two species are recorded in FTIR spectroscopy. In NMR spectroscopy, only one peak is observed owing to the rapid rate of exchange between the two species. However, its frequency is located between that of the more strongly associated solute fraction and that of the less associated solute fraction. NMR spectroscopy then gives the same kind of information as FTIR spectroscopy, but it also permits one to study selectively the different carbons of the molecule and especially the C–Cl groups.

The credibility of the conclusions drawn depends upon the validity of Equations 1 and 2. These equations are based upon several assumptions concerning the type of association existing between the solute and each component of the solvent, the concentration of the solute, and the composition of the binary solvent.

First, it is assumed that the carbons of the solute can be associated with solvents A and B in only one manner and, therefore, can only produce two signals corresponding to the X_A and X_B species. The observed NMR signal of each carbon of the solute dissolved in a binary solvent represents an average of these two signals. The hypothesis of the occurrence of only one X_A species and one X_B species was tested satisfactorily by Laszlo (*27*), who used a computational technique for the study of hydrogen bonding phenomena in solution.

Second, NMR measurements should ideally be done at infinite dilution to eliminate the concentration dependence of K. Unfortunately, obvious experimental problems exclude this possibility. The effect of concentration of the solute was studied, however, in earlier work (*19*). A decrease of the solute concentration from 9 to 1% was shown to have a limited influence on the value of the constant of association K.

Third, in Equation 2 it is assumed that the relative proportion of the two components of the solvent does not modify the value of K. However, a decrease in the value of K, corresonding to a curvature of the ideal straight line predicted by Equation 2, is generally observed at high concentrations of the associative solvent. This curvature is usually small.

From Table II, one can draw the following conclusions: Low molecular weight chlorinated molecules bearing protons in the α position are associated with the carbonyl group of methyl acetate. The intensity of this interaction depends, however, upon the number of chlorine atoms in the molecule and decreases in the following order: 1,1,2,2-tetrachloroethane > $CHCl_3$ > CH_2Cl_2 > 1,3-dichlorobutane > heptane. This ranking is in agreement with that published previously (*19*), where the ester was taken as the solute and the chlorinated molecule as one component of the solvent.

Low molecular weight brominated molecules also interact with esters and can be ranked in the same order as their chlorinated homologues.

The differences found between the values of K for the brominated and chlorinated molecules are generally small and often within the limits of

accuracy of the method. However, all the data given in Table II point in the same direction and support the same conclusion: The values of the constants of association K are slightly larger with chlorinated molecules than with brominated molecules. For example, the value of K for $CHCl_3$ (K = 6.0) dissolved in the methyl acetate–heptane binary solvent is larger than the value of K for bromoform (K = 4.1). This difference is smaller between molecules containing two halogen atoms (i.e., CH_2Cl_2 and CH_2Br_2), but it always favors the chlorinated molecule ($K_{CH_2Cl_2}$ = 2.4 versus $K_{CH_2Br_2}$ = 2.1).

We can then evaluate the probability of the chlorine atom being more strongly associated than the bromine atom with the carbonyl group of the ester. We studied eight groups or systems containing bromine or chlorine atoms, and we always found that the constants of association of the chlorine atoms are larger than those of the bromine atoms. If there were no difference between the strength of specific interactions of the chlorine and bromine atoms, the probability that $K_{Br} < K_{Cl}$ or $K_{Br} > K_{Cl}$ would be the same and equal to ½. In other words, the probability that $K_{Br} < K_{Cl}$ is ½ and the probability of getting this result in eight independent experiments is $(½)^8$ = 0.04%. This calculation leads to the conclusion that the experimental probability of the chlorine atom interacting more strongly than the bromine atom with a carbonyl group is equal to 99.96%.

We also used a t test for the same purpose (*30*). The results obtained for all the systems or groups analyzed are given in Table III. The probability that $K_{Br} < K_{Cl}$ is usually larger than 80%.

These two calculations demonstrate on a statistical basis that the differences in association constants observed in this study are really due to a stronger intermolecular interaction of esters (and polyesters) with chlorinated molecules than with brominated molecules.

The interaction between esters and halogenated molecules involves the carbonyl group of the ester and the hydrogen linked to the halogenated carbon (*5*). Therefore, this interaction is likely a hydrogen bonding interaction. The weak shift of the signals of the nonchlorinated carbons of 1,3-dichlorobutane (carbons 2 and 4) and the small values of K associated with them ($K \simeq 1$) show that the >C=O---H bond in the β position is much weaker than the >C=O---H bond in the α position (Table IV).

PCL exhibits the same kind of behavior as methyl acetate. However, the intensity of its interaction with chlorinated species is weaker than that of methyl acetate because of the relative inaccessibility of the interacting groups of the polyester compared to those of low molecular weight esters. PCL is also more weakly associated with the brominated molecules than it is with the chlorinated model compounds. Moreover, PCL interacts more strongly with pentachloroethane then with $CHCl_3$, because of the higher polarity of the C–H bond of the former.

However, the values of K calculated with halogenated solutes are larger than those calculated with ester solutes. The most striking example

Table IV. Carbon-13 NMR Shifts of the Signals of the Carbons of 1,3-Dichlorobutane and 1,3-Dibromobutane and Corresponding Values of *K*

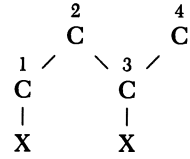

Compound	*Carbon Number*	*Shifts (ppm)*[a]	K ± σ
13DCB	1	1.589	1.3 ± 0.2
	2	−0.679	0.9 ± 0.2
	3	0.858	1.5 ± 0.2
	4	−0.533	0.8 ± 0.2
13DBB	1	2.174	1.2 ± 0.1
	2	−0.533	0.9 ± 0.2
	3	1.369	1.2 ± 0.2
	4	−0.460	1.0 ± 0.2

[a] Difference between the chemical shifts observed in pure heptane and those observed in pure methyl acetate.

of Table II concerns the $CHCl_3$–(methyl acetate–heptane) and methyl acetate–($CHCl_3$–heptane) mixtures for which the association constants K are equal to 6.0 and 2.1, respectively. The ratio of the two values is 2.9. The same ratio is obtained with the corresponding brominated compounds, because the values of K are then equal to 4.1 and 1.5, respectively, indicating the same kind of association. No clear explanation of this phenomenon has been found so far.

Finally, calorimetric measurements indicate that PVB is less miscible with linear polyesters than PVC (*13*, *18*). It is less miscible because it exhibits miscibility with a smaller number of polyesters (Table I). It is also less miscible because the comparison of blends of a given polyester with PVB and PVC, in which both mixtures are miscible, gives a larger value of the Gordon–Taylor parameter with PVC (*18*). The Gordon–Taylor parameter was shown to be proportional to the strength of the interaction between two polymers in a series of polyester–poly(vinyl halide) blends (*1*).

The weaker association of brominated model compounds with esters, or polyesters, compared to their corresponding chlorinated homologues explains the difference in miscibility of PVC and PVB. The difference between the two series of association constants is, however, small, in agreement with the small differences found between the properties of the chlorine and bromine atoms. These differences are large enough to induce important differences in the miscibility behavior of PVC and PVB. This observation emphasizes that the miscibility–immiscibility boundary in

polymer blends is often due to subtle factors that cannot be predicted easily.

In conclusion, the enthalpy of mixing of $CHCl_3$ with ethyl propionate is equal to -2.5 kcal/mol (*31*). This value is very small and is of the same order of magnitude as the dipolar forces acting between these two molecules. Because the enthalpy of mixing between a polyester and a PVX chain is still lower than that between the corresponding model compounds, polymer blends are often located close to the miscibility–immiscibility boundary, some of them being above and others below, but in all cases small changes in the nature of the polymers suffice to shift a given blend to the other side of the boundary.

Nomenclature

[A]	Molar fraction of solvent A
[B]	Molar fraction of solvent B
1B2CE	1-Bromo-2-chloroethane
1B3CP	1-Bromo-3-chloropropane
13DBB	1,3-Dibromobutane
13DCB	1,3-Dichlorobutane
13DXB	1,3-Dihalobutane
K	Constant of association
$\overline{M}_w$	Weight-average molecular weight
PBA	Poly(butylene adipate)
PCL	Poly(caprolactone)
PEA	Poly(ethylene adipate)
PHMS	Poly(hexamethylene sebacate)
PMEPL	Poly(α-methyl α-ethyl β-propiolactone)
PMPPL	Poly(α-methyl α-propyl β-propiolactone)
PPO	Poly(2,6-dimethyl 1,4-phenylene oxide)
PVB	Poly(vinyl bromide)
PVC	Poly(vinyl chloride)
PVF	Poly(vinyl fluoride)
PVL	Poly(valerolactone)
PVX	Poly(vinyl halide)
1122TBE	1,1,2,2-Tetrabromoethane
1122TCE	1,1,2,2-Tetrachloroethane
1122TXE	1,1,2,2-Tetrahaloethane
T_g	Glass transition temperature
TMS	Tetramethylsilane
[X]	Molar fraction of solute
$[X_i]$	Molar fraction of solute associated with solvent i
δ	Chemical shift in binary solvent
δ_i	Chemical shift in solvent i

Acknowledgments

The authors thank the National Sciences and Engineering Research Council of Canada and the Department of Education of the Province of Quebec (FCAC program) for the research grants that supported this work.

Literature Cited

1. Prud'homme, R. E. *Polym. Eng. Sci.* **1982**, *22*, 90.
2. Ziska, J. J.; Barlow, J. W.; Paul, D. R. *Polymer* **1981**, *21*, 918.
3. Coleman, M. M.; Zarian J. *J. Polym. Sci. Polym. Phys. Ed.* **1979**, *17*, 837.
4. Varnell, D. F.; Coleman, M. M. *Polymer* **1981**, *22*, 1324.
5. Paul, D. R. In "Polymer Blends"; Paul, D. R.; Newman, S., Eds.; Academic: New York, 1978; Chap. 1.
6. Garton, A.; Aubin, M.; Prud'homme, R. E. *J. Polym. Sci. Polym. Lett. Ed.* **1983**, *21*, 45.
7. Aubin, M. Bédard, Y.; Morissette, M. F.; Prud'homme, R. E. *J. Polym. Sci. Polym. Phys. Ed.* **1983**, *21*, 233.
8. Olabisi, O.; Robeson, L. M.; Shaw, T. M. "Polymer–Polymer Miscibility"; Academic: New York, 1979.
9. Aubin, M.; Prud'homme, R. E. *Polymer* **1981**, *22*, 1223.
10. Aubin, M.; Prud'homme, R. E. *J. Polym. Sci. Polym. Phys. Ed.* **1981**, *19*, 1245.
11. Aubin, M.; Prud'homme, R. E. *Macromolecules* **1980**, *13*, 365.
12. Aubin, M.; Bussières, D.; Duchesne, D.; Prud'homme, R. E. In "Polymer Compatibility and Incompatibility"; Solc, K., Ed.; MMI: Midland, 1982; p. 223.
13. Cousin, P.; Prud'homme, R. E. *Eur. Polym. J.* **1982**, *18*, 957.
14. ten Brinke, G.; Karasz, F. E.; MacKnight, W. J. *Macromolecules* **1983**, *16*, 1827.
15. Varnell, D. F.; Coleman, M. M. *J. Polym. Sci. Polym. Phys. Ed.* **1980**, *18*, 1403.
16. Cangelosi, F.; Shaw, M. T. *Polym. Eng. Sci.* **1983**, *23*, 669.
17. Iskandar, M.; Tran, C.; Robeson, L. M.; McGrath, J. E. *Polym. Eng. Sci.* **1983**, *23*, 682.
18. Cousin, P., Ph.D. Thesis, Université Laval, Quebec, Canada, 1984.
19. Garton, A.; Cousin, P.; Prud'homme, R. E. *J. Polym. Sci. Polym. Phys. Ed.* **1983**, *21*, 2275.
20. Spassky, N., Leborgne, A.; Reix, M.; Prud'homme, R. E.; Bigdeli, E.; Lenz, R. W. *Macromolecules* **1978**, *11*, 716.
21. Duchesne, D.; Prud'homme, R. E. *Polymer* **1979**, *20*, 1199.
22. Landolt, H. H.; Bornstein, R. "Zahlenwerte und Funktionen"; Springer: Berlin, 1967; Vol. 10.
23. Weast, R. C., Ed. "Handbook of Chemistry and Physics," 49th ed.; CRC: Cleveland, 1969.
24. Lussan, C. *J. Chim. Phys. Phys. Chim. Biol.* **1968**, *60*, 1100.
25. Lumbroso, N.; Wu, T. K.; Dailey, B. P. *J. Chem. Phys.* **1963**, *67*, 2469.
26. Tiffon, B.; Dubois, J. E. *Org. Magn. Reson.* **1978**, *11*, 295.
27. Laszlo, P. In "Progress in NMR Spectroscopy"; Emsley, J. W.; Feeney, F.; Sutcliffe, L. H., Eds; Pergamon: New York, 1967; Vol. 3.
28. Coleman, M. M.; Moskala, E. J.; Painter, P. C.; Walsh, D. J.; Rostami, S. *Polymer* **1983**, *24*, 1410.

29. Varnell, D. F.; Moskala, E. J., Painter, P. C.; Coleman, M. M. *Polym. Eng. Sci.* **1983**, *23*, 658.
30. Montgomery, D. C. "Design and Analysis of Experiments"; Wiley: New York, 1976.
31. Joesten, M. D.; Schaad, L. J. "Hydrogen Bonding;" Dekker: New York, 1974; p. 366.

RECEIVED for review November 15, 1984. ACCEPTED May 7, 1985.

7

Crystallization and Melting in Compatible Polymer Blends

J. P. RUNT and LYNN M. MARTYNOWICZ

Department of Materials Science and Engineering, Polymer Science Program, The Pennsylvania State University, University Park, PA 16802

Some of the important aspects concerning crystallization and melting in semicrystalline, compatible polymer blends are reviewed. Crystallization in these systems is governed by a variety of factors, and crystallization rates both decrease and increase upon diluting the crystallizable species. Spherulitic growth rates are frequently analyzed via a modified Turnbull and Fisher approach, and the good correlation of experimental data indicates that the dependence of growth rate on temperature is quite similar to pure crystalline polymers. Analysis of the equilibrium melting point depression in these blends provides an estimate of the magnitude of the polymer–polymer interactions (χ). Direct use of experimental melting points in the expression describing melting point depression can potentially result in a serious underestimation of χ.

MISCIBLE POLYMER BLENDS in which one or more of the components are crystallizable have been studied with considerable interest recently. Determination of the factors that control crystallization rate and the overall degree of crystallinity in these systems is of obvious practical importance. A review of current knowledge of the crystallization process constitutes the first portion of this chapter. The second part deals with a review of melting behavior and how equilibrium melting points can be used to estimate interaction parameters. Some of the problems inherent in using experimental data rather than equilibrium melting points in such an analysis are also discussed.

Crystallization

As in pure polymers, crystallization in miscible blends is restricted to temperatures between the glass transition temperature (T_g) and the equilibrium melting point (T_m^0), and crystallization or spherulitic growth rates reflect the competition between nucleation rate and the rate of transport or diffusion in the melt. Nucleation rate decreases with increasing tempera-

0065-2393/86/0211/0111$06.00/0

ture and dominates the overall growth rate at temperatures approaching T_m^0. Rates of transport in the melt increase with temperature and dominate near T_g. Between these extremes, the crystallization rate passes through a maximum, as illustrated in Figure 1 for pure isotactic polystyrene (i-PS) and several i-PS blends with atactic polystyrene (a-PS).

We will restrict our discussion to binary blends of crystallizable polymer 1 with miscible, noncrystalline polymer 2. Clearly, crystallization rates in such blends will be different from pure polymer 1 because of dilution of the crystallizable species. The result of this diluent effect is expected to be a decrease in crystallization rate in proportion to the concentration of component 2 (*1*, *2*). However, a miscible diluent will also alter T_g and the equilibrium melting point. Therefore, the range of available crystallization temperatures (T_c) will be expanded or contracted, depending on the T_g of the diluent (Figure 2). Crystallization rates will also be influenced by the

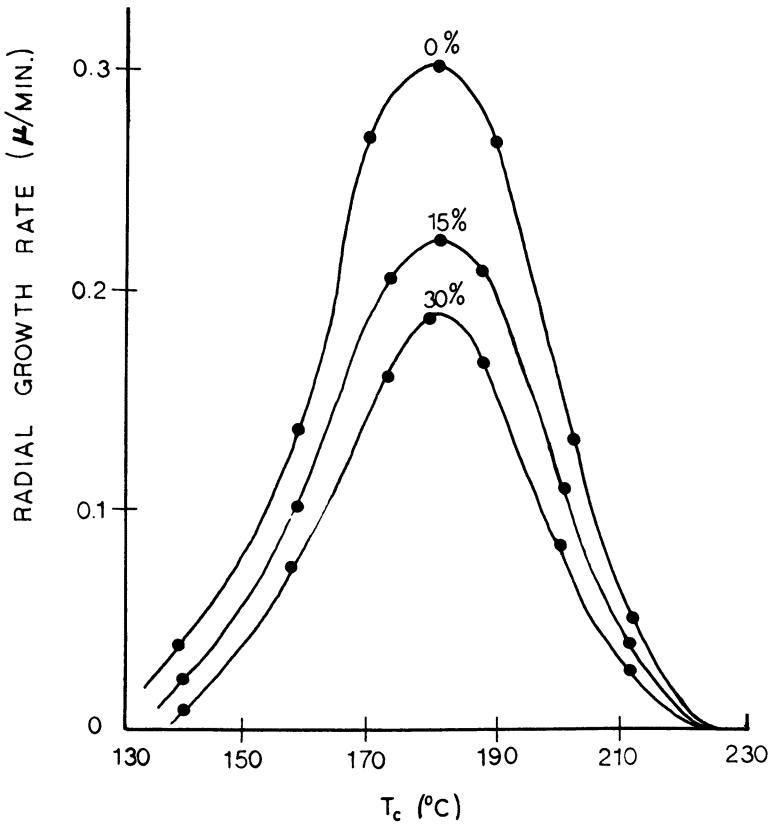

Figure 1. The radial growth rates of spherulites in i-PS and in blends containing 15% and 30% of a-PS. (Reproduced with permission from Ref. 14. Copyright 1964 Journal of Applied Physics.*)*

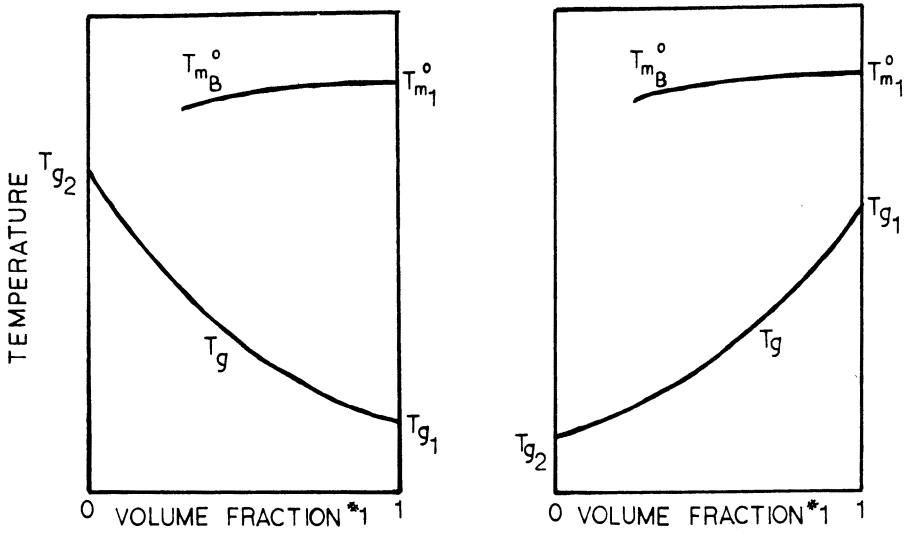

Figure 2. Possible relationships between T_g *and equilibrium melting point with respect to blend composition for miscible systems.*

variation in T_g and $T^0_{m_B}$ (T^0_m of polymer 1 in the blend). A decrease in crystallization rate (reflecting a decrease in the rate of nucleation) would be expected to follow a decrease in $T^0_{m_B}$. This effect is expected to be more important at low supercoolings. Simplistically, the transport term, which is more important at lower T_c values, can be evaluated by considering the difference between T_g and T_c. For instance, in a miscible blend in which the addition of polymer 2 causes a decrease in the amorphous phase T_g (right side of Figure 2), chain mobility (at a constant T_c) will increase with an increase in polymer 2. Therefore, the crystallization rate will increase. The overall crystallization rate is a result of competition between several different factors, and increasing (*3*) and decreasing (*4–8*) rates have been observed experimentally.

For blends of low T_g polymer 1 with relatively high T_g polymer 2, a series of compositions are frequently observed (at high concentrations of polymer 2) in which no crystallization occurs. This gap is associated with the blend T_g exceeding T_c and inhibiting crystallization (*9*, *10*). Crystallizing in the presence of a solvent during solution casting will decrease the effective T_g (and $T^0_{m_B}$) and can induce crystallization in blends that normally show no evidence of crystallization from the melt (*11*).

When T_g does not approach T_c prior to or during crystallization, polymer 1 in the blend should develop, given sufficient time, a level of crystallinity similar to pure 1. For example, the degree of crystallinity of the poly(ϵ-caprolactone) (PCL, $T_g \approx -60$ °C) portion of a 10:90 PCL–poly-

epichlorohydrin ($T_g \approx -15$ °C) blend crystallized at room temperature is the same as that for pure PCL, that is, approximately 70% (*12*).

If component 2 is of sufficiently high molecular weight, the spherulite radius varies linearly with time (constant radial growth rate, G). The implication is that molecules of polymer 2 become trapped within the superstructure of the growing crystals and that the mixture composition at the crystal growth front does not vary during the crystallization process. The crystallization rate of polymer 1 apparently outstrips the rate at which polymer 2 can diffuse away from the growth front. Keith and Padden, in their pioneering work (*13*, *14*) on mixtures of atactic and isotactic polypropylene (a-PP–i-PP) and polystyrene (PS), showed that nonlinear growth may be expected if component 2 is of sufficiently low molecular weight (Figure 3). If polymer 2 diffuses radially more rapidly than the spherulite fibers grow, the concentration of component 2 in the as yet uncrystallized

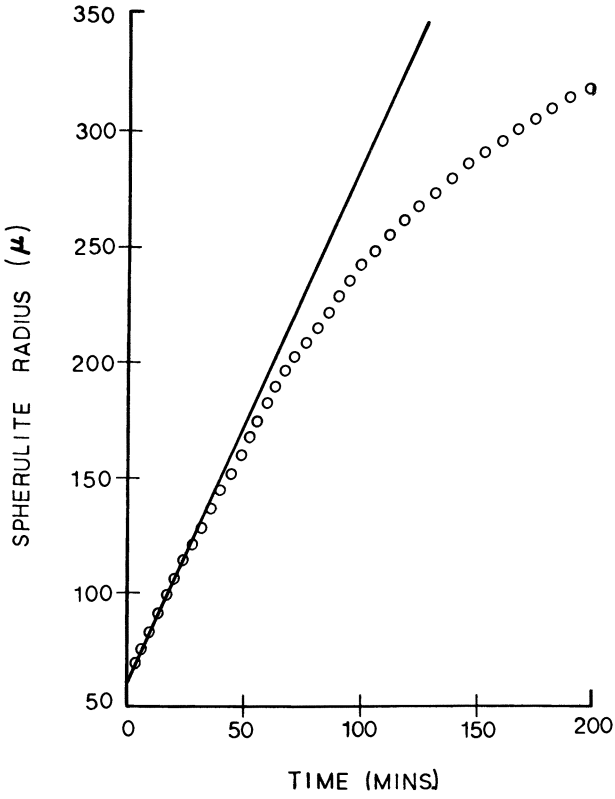

Figure 3. Nonlinear growth behavior for a spherulite grown isothermally (at 135 °C) in a blend of isotactic and low molecular weight atactic polypropylene. (Reproduced with permission from Ref. 14. Copyright 1964 Journal of Applied Physics.)

melt will increase as the spherulite grows. Thus, the growth rate should correspondingly decrease with time. For a melt of given composition, nonlinear growth is favored by decreasing the molecular weight of polymer 2 or by increasing T_c so as to cause slower growth yet to increase molecular diffusion (*14*). Consequently, nonlinear growth might be expected in relatively high molecular weight polymer blends under the proper crystallization conditions. This behavior has in fact been observed (*15*) in a 50:50 i-PS–poly(2,6-dimethylphenylene oxide) (PPO) blend. The i-PS lateral lamellar growth rate was found to conform to a time law characteristic of growth controlled by diffusion of the PPO away from the growth front.

When a single G can be associated with crystallization at a given T_c and composition, growth rates can be analyzed in more detail by using the modified Turnbull–Fisher expression or the treatment of Lauritzen and Hoffman (*16*, *17*). The former approach will be highlighted because this method is followed most frequently in the literature (*1*, *2*, *8*, *18*). The spherulitic growth rate has been described as:

$$G = G_o \exp\left[\frac{-\Delta E}{kT_c}\right]\exp\left[\frac{-\Delta F^*}{kT_c}\right] \tag{1}$$

where ΔE is the activation energy for transport of the crystallizing units across the melt-crystal interface, ΔF^* is the free energy required to form a nucleus of critical size from the melt, k is Boltzmann's constant, and G_o is a constant. Boon and Azcue (*1*) showed that ΔF^* can be expressed as

$$\Delta F^* = \frac{4b_o\sigma\sigma_e}{\Delta F'} - \frac{2\sigma kT_c(\ln V_1)}{b_o\Delta F'} \tag{2}$$

for a crystalline polymer–diluent mixture. In this equation, b_o is the thickness of a monomolecular layer; σ_e and σ are the fold and side surface free energies, respectively; V_1 is the volume fraction of crystallizable polymer; and $\Delta F'$ is the free energy difference between the supercooled liquid and the crystal of the blend. The value of $\Delta F'$ can be approximated by (*19*)

$$\Delta F' = \frac{\Delta H_f^0(T_{m_B}^0 - T_c)}{T_{m_B}^0} \tag{3}$$

where ΔH_f^0 is the perfect crystal heat of fusion of polymer 1.

The second term on the right side of Equation 2 has been included to account for the probability of selecting the required number of crystalline polymer sequences from the mixture. The first term on the right side of Equation 1 can be replaced by a term based on the Williams, Landel, and Ferry (WLF) relation for viscous flow (*20*). The growth rate for polymer–diluent mixtures can then be written as

$$G = V_1 G_o \exp\left[\frac{-C_1}{R(C_2 + T_c - T_g)}\right] \exp\left[\frac{-4b_o\sigma\sigma_e T^0_{m_B}}{k\Delta H^0_f T_c(T^0_{m_B} - T_c)} + \frac{2\sigma T^0_{m_B} \ln V_1}{b_o \Delta H^0_f (T^0_{m_B} - T_c)}\right] \quad (4)$$

where T_g is the glass transition temperature of the blend and C_1 and C_2 are constants. The preexponential factor G_o is multiplied by V_1 because the rate of nucleation is proportional to the concentration of crystallizable units (*21*).

Equation 4 can be expressed as

$$\alpha = \ln G_o - C_3 \frac{T^0_{m_B}}{T_c(T^0_{m_B} - T_c)} \quad (5)$$

where

$$\alpha = \ln G - \ln V_1 + \frac{C_1}{R(C_2 + T_c - T_g)} - \frac{0.2\, T^0_{m_B}(\log V_1)}{T^0_{m_B} - T_c}$$

and

$$C_3 = \frac{4b_o\sigma_e\sigma}{k\Delta H^0_f}$$

From knowledge of G, $T^0_{m_B}$, and T_g, a plot of α versus $T^0_{m_B}/[T_c(T^0_{m_B} - T_c)]$ can be constructed. This plot should be linear, and the slope is equal to C_3. From knowledge of b_o and ΔH^0_f and by using the empirical relationship σ equals $0.1\, b_o \Delta H^0_f$ (*22*), σ_e values can be derived from the slope. Although equilibrium blend melting points should be used in these expressions, experimental T_m values are generally used in their place.

The use of Equation 5 is illustrated in Figure 4 by the data of Calahorra et al. (*18*) for the blend of poly(ethylene oxide) (PEO) and poly(methyl methacrylate) (PMMA). The straight line in Figure 4 represents the fit of Equation 5 to their experimental data by taking C_1 equal to 4120 cal/mol and C_2 equal to 51.6 deg (these values are based on the "universal" WLF constants). The good fit of Equation 5 to the data of Calahorra et al. and others indicates that the dependence of growth rate on temperature is quite similar to that of homopolymers. Over the limited composition range examined, σ_e appears to be independent of PMMA concentration, an observation similar to the findings of other authors (*2*, *19*).

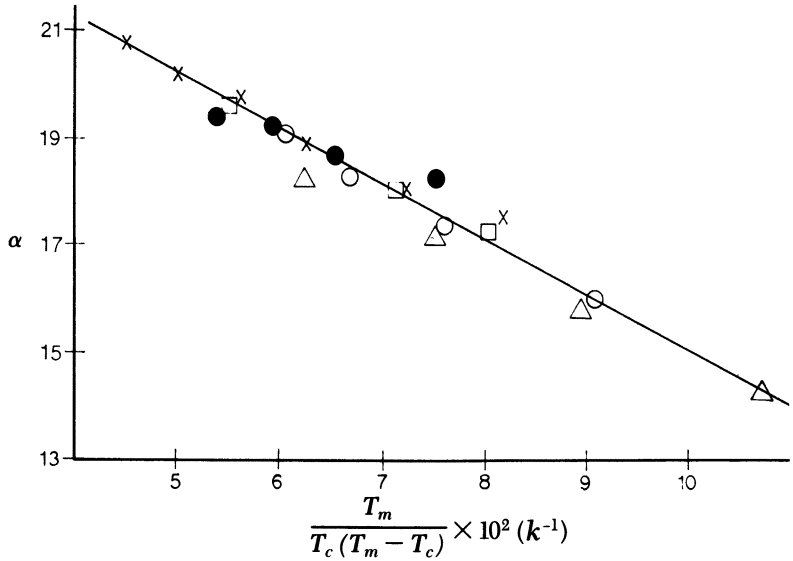

Figure 4. Plot of α against $T_m/T_c(T_m - T_c)$ *for various compositions. Key:* △, *100:0;* ○, *90:10;* □, *80:20;* ×, *70:30; and* ●, *60:40. (Reproduced with permission from Ref. 18. Copyright 1982* Polymer.*)*

Melting

Besides the obvious practical significance of determining melting behavior, blend melting points are frequently used to estimate the magnitude of the polymer–polymer interactions at $T^0_{m_B}$. Using the thermodynamic considerations of Scott (*23*), Nishi and Wang (*24*) derived a relationship describing the equilibrium melting point depression of a crystalline polymer as a result of the presence of a miscible diluent. When the entropy of mixing is negligible,

$$\frac{1}{T^0_{m_B}} - \frac{1}{T^0_m} = \frac{-R\bar{V}_1}{\Delta H^0_f \bar{V}_2}(\chi V_2^2) \tag{6}$$

where T^0_m is the equilibrium melting point of the pure crystallizable component, R is the gas constant, $\bar{V}$ is the molar volume of the polymer repeat unit, and χ is the interaction parameter. From Equation 6, a plot of $(1/T^0_{m_B}) - (1/T^0_m)$ versus V_2^2 should be linear and have a slope proportional to χ.

The practical difficulty in using this expression is that, strictly speaking, equilibrium melting points are required. Thus, $T^0_{m_B}$ values for individual blends must be determined by the methods of Hoffman and Weeks (*17*). Probably the most reliable way of determining $T^0_{m_B}$ (or T^0_m) is from experimentally determined melting points on specimens of known crystalline thickness (L). The Hoffman–Weeks expression can be written as

$$T_{m_B} = T^0_{m_B}\left(1 - \frac{2\sigma_e}{\Delta H^0_f L_B}\right) \tag{7}$$

where T_{m_B} and L_B are the experimentally observed melting point and crystal thickness of the crystalline polymer in the blend, respectively. A plot of T_{m_B} versus $1/L_B$ should be linear and have a y-intercept (at infinite crystal thickness) of $T^0_{m_B}$. Values of $T^0_{m_B}$ for blends of various compositions determined in this way can then be plotted via Equation 6 to obtain χ. However, this approach has never been used to estimate blend equilibrium melting points because of the difficulties encountered in determining L values. Measurement of L is usually conducted by using small-angle X-ray scattering. Experimentally, the long-period thickness (crystalline + amorphous thickness) rather than L is obtained directly from the scattering curve. In a number of semicrystalline miscible blends, the rejected, noncrystallizing species resides in interlamellar regions (*25–27*). The measured long-period and amorphous phase thicknesses vary appreciably with blend composition, but these variations are not simply related to L. Procedures for extracting L from the scattering data have proven to be quite complex and somewhat model dependent (*28*).

Alternatively, if the crystals initially formed at T_c (of initial thickness, l^*) thicken with time at T_c by some factor, β, T_{m_B} can be expressed as

$$T_{m_B} = T^0_{m_B}\left[1 - \frac{2\sigma_e}{\Delta H^0_f(\beta l^*)}\right] \tag{8}$$

where βl^* equals L_B, the final crystal thickness. From the kinetic theory of crystallization, l^* can be written as (*17*)

$$l^* = \frac{2\sigma_e}{\Delta F'} + \delta \tag{9}$$

where $\Delta F'$ is the free energy difference between the supercooled liquid phase and the bulk crystal phase and can be approximated by Equation 3. The term δ is defined as the thickness that gives the crystals the necessary stability to form by creating a situation where the free energy of crystal formation is negative. By substituting the relationship for l^* into Equation

8 and by assuming δ to be small and β to be independent of T_c, T_{m_B} can be expressed as a linear function of T_c (*17*):

$$T_{m_B} = T^0_{m_B}\left(1 - \frac{1}{\beta}\right) + \frac{T_c}{\beta} \tag{10}$$

The value of $T^0_{m_B}$ (or T^0_m) can be determined from a plot of T_{m_B} versus T_c where $T^0_{m_B}$ is the intercept of the extrapolated T_m values and the line defined by T_m equal to T_c.

Because only T_{m_B} values need to be determined, this technique has been the method of choice for estimating blend equilibrium melting points (*4*, *6*, *19*, *24*, *29–31*). For illustrative purposes, the data of Eshuis et al. (*29*) on blends of poly(vinylidene fluoride) (PVF_2) and isotactic poly(ethyl methacrylate) (i-PEMA) are shown in Figure 5. For these blends, the experimental melting points of the various compositions extrapolate to ap-

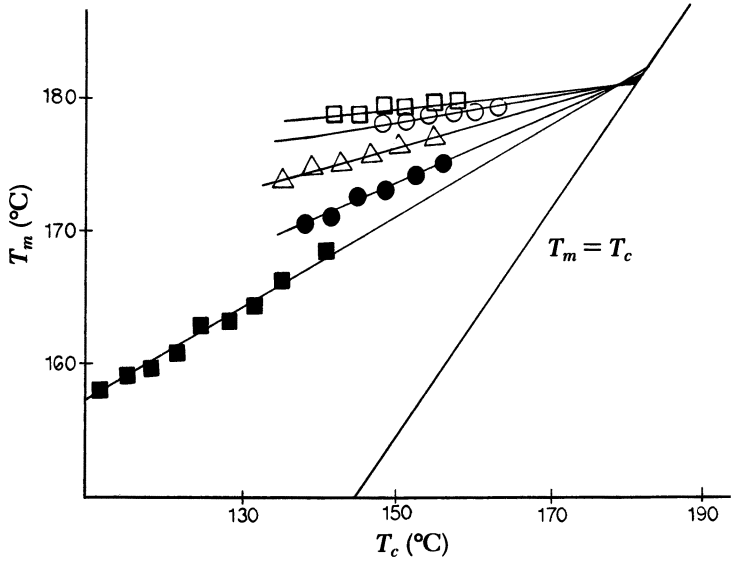

Figure 5. Hoffman–Weeks plots of melting temperatures of pure PVF_2 and PVF_2 in blends with i-PEMA as a function of crystallization temperature for various PVF_2–i-PEMA compositions. Key: ○, *100:0;* □, *95:5;* △, *75:25;* ●, *50:50; and* ■, *40:60. (Reproduced with permission from Ref. 29. Copyright 1982* Polymer.*)*

proximately the same equilibrium melting point as pure PVF_2, a result that implies that χ is approximately equal to zero.

More frequently, however, investigators use experimental (nonequilibrium) T_m values in place of $T^0_{m_B}$ and T^0_m in Equation 6 to estimate χ. The assumption is usually made that no changes in crystalline thickness accompany blending, but direct verification is rarely undertaken. Clearly, if the two polymers interact in the melt and χ is negative, Equation 6 shows that an equilibrium melting point depression should be observed. If pure polymer 1 and polymer 1 in a miscible blend are crystallized at the same T_c, then L for polymer 1 in the blend should be larger than that in the pure state as a consequence of the decreased supercooling. Therefore, in any semicrystalline miscible blend, changes in L would be anticipated. Changes in crystallite size (lateral crystalline order) and perfection upon blending are also possible, but little is known about these factors.

If only crystal thickness and thermodynamic effects are considered (*32*, *33*), then

$$\Delta T_m = \Delta T^0_m + \frac{2\sigma_e}{\Delta H^0_f}\left(\frac{T^0_{m_B}}{L_B} - \frac{T^0_m}{L}\right) \tag{11}$$

assuming that σ_e remains constant upon blending (*2*, *18*, *19*). In this expression, the term $\Delta T_m = T_m - T_{m_B}$ is the difference in experimentally observed melting points between the pure crystalline polymer and the crystalline polymer in the blend, and the term $\Delta T^0_m = T^0_m - T^0_{m_B}$ is the difference in equilibrium melting points. The value of ΔT_m is, therefore, a reflection of the competition between the tendency for a melting point depression because of polymer–polymer interactions and a melting point elevation as a result of the increased crystal thickness of polymer 1 in the blend. Substitution for L and L_B from the kinetic theory of crystallization (*17*) and subsequent rearrangement results in

$$\Delta T_m = \Delta T^0_m\left(1 - \frac{1}{\beta}\right) \tag{12}$$

for relatively large β values. Equations 11 and 12 illustrate two points: Under the constraints of the model, the thermodynamic effect always offsets the crystal thickness term. Thus, despite the increase in crystal thickness, the experimental melting point should always decrease with decreasing concentration of the crystallizable species. However, this decrease can be much less than the equilibrium depression, and, if experimental melting points are used in Equation 6, the magnitude of the intermolecular interactions can be seriously underestimated.

Another complication is the difficulty in determination of the "true" experimental melting point of the crystals that were actually formed at a

given T_c. Semicrystalline polymers are frequently believed to undergo lamellar thickening (annealing) upon heating during a thermal analysis experiment. Consequently, the observed melting behavior will be a reflection of the melting of the crystals formed at T_c along with a recrystallization exotherm and the melting of the reorganized material. Experimentally, multiple or single melting endotherms may be observed. Single peaks do not necessarily imply an absence of lamellar reorganization because resolution of the various processes may not be possible. In general, extreme care must be taken in choosing a T_m that is indicative of the melting of crystals formed at T_c. Very often, the experimental melting points are strongly dependent on heating rate. By performing the thermal analysis at high rates, reorganization should be minimized and "true" T_m values should be obtainable. However, in practice, problems arise as a consequence of low polymer thermal conductivity especially when relatively large sample sizes are used. Loss of peak resolution and spuriously high T_m values are frequently associated with high heating rates, an observation reflecting the difficulty in rapid heat transfer through the specimen.

Nomenclature

χ	Polymer–polymer interaction parameter
T_g	Glass transition temperature
T_m^0	Equilibrium melting point
T_c	Crystallization temperature
T_{mB}^0	Equilibrium melting point of polymer 1 in the blend
ΔH_f^0	Perfect crystal heat of fusion
G	Spherulitic growth rate
$\Delta F'$	Free energy difference between the supercooled liquid and the crystal of the blend
G_o	A preexponential constant
k	Boltzmann's constant
ΔE	Activation energy for transport of the crystallizing units across the melt–crystal interface
V	Volume fraction
ΔF^*	Free energy required to form a nucleus of critical size from the melt
σ	Side surface free energy
b_o	Thickness of a monomolecular layer
σ_e	Fold surface free energy
C_1	WLF constant
C_2	WLF constant
α	A constant
C_3	A constant
R	Gas constant
$\bar{V}$	Molar volume of the polymer repeat unit
L	Crystalline thickness

L_B Crystal thickness of the crystalline polymer in the blend
T_{mB} Experimental melting point of the crystalline polymer in the blend
β Lamellar thickening factor
l^* Initial crystal thickness
δ Thickness that gives the crystals the necessary stability to form by creating a situation where the free energy of crystal formation is negative

Literature Cited

1. Boon, J.; Azcue, J. M. *J. Polym. Sci. Part A-2* **1968**, *6*, 885.
2. Ong, C. J.; Price, F. P. *J. Polym. Sci. Polym. Symp.* **1978**, *63*, 59.
3. Escala, A.; Stein, R. S. In "Multiphase Polymers"; Cooper, S. L.; Estes, G. M., Eds.; ADVANCES IN CHEMISTRY SERIES No. 176; ACS: Washington, D.C., 1979.
4. Martuscelli, E.; Demma, G.; Drioli, E.; Nicolais, L.; Spina, S.; Hopfenberg, H. B.; Stannett, V. T. *Polymer* **1979**, *20*, 571.
5. Berghmans, H.; Overbergh, N. *J. Polym. Sci. Polym. Phys. Ed.* **1977**, *15*, 1757.
6. Yeh, G. S. Y.; Lambert, S. L. *J. Polym. Sci. Part A-2* **1972**, *10*, 1183.
7. Robeson, L. M. *J. Appl. Polym. Sci.* **1973**, *17*, 3607.
8. Martuscelli, E.; Demma, G. B. In "Polymer Blends: Processing, Morphology and Properties"; Martuscelli, E.; Palumbo, R.; Kryszewski, M., Eds.; Plenum: New York, 1980; p. 101.
9. Paul, D. R.; Barlow, J. W.; Bernstein, R. E.; Wahrmund, D. C. *Polym. Eng. Sci.* **1978**, *18*, 1225.
10. Rim, P. B.; Runt, J. *Macromolecules* **1983**, *16*, 762.
11. Runt, J.; Rim, P. B. *Macromolecules* **1982**, *15*, 1018.
12. Runt, J.; Butera, R.; Rim, P. B.; Martynowicz, L., unpublished data.
13. Keith, H. D.; Padden, F. J. *J. Appl. Phys.* **1964**, *35*, 1270.
14. Keith, H. D.; Padden, F. J. *J. Appl. Phys.* **1964**, *35*, 1286.
15. Hachmann, U.; Petermann, J. *J. Polym. Sci. Polym. Phys. Ed.* **1982**, *20*, 1633.
16. Lauritzen, J. I.; Hoffman, J. D. *J. Appl. Phys.* **1973**, *44*, 4340.
17. Hoffman, J. D.; Davis, G. T.; Lauritzen, J. I. In "Treatise on Solid State Chemistry"; Hanay, N. B., Ed.; Plenum: New York, 1976; Vol. 3, Chap. 6.
18. Calahorra, E.; Cortazar, M.; Guzman, G. M. *Polymer* **1982**, *23*, 1322.
19. Wang, T. T.; Nishi, T. *Macromolecules* **1977**, *10*, 421.
20. Hoffman, J. D.; Weeks, J. J. *J. Chem. Phys.* **1962**, *37*, 1723.
21. Mandelkern, L. "Crystallization of Polymers"; McGraw-Hill: New York, 1964.
22. Thomas, D. G.; Staveley, L. A. K. *J. Chem. Soc.* **1952**, 4569.
23. Scott, R. L. *J. Chem. Phys.* **1949**, *8*, 909.
24. Nishi, T.; Wang, T. T. *Macromolecules* **1975**, *8*, 909.
25. Khambatta, F. B.; Warner, F.; Russell, T.; Stein, R. S. *J. Polym. Sci. Polym. Phys. Ed.* **1976**, *14*, 1391.
26. Wenig, W.; Karasz, F.; MacKnight, W. J. *J. Appl. Phys.* **1975**, *46*, 4194.
27. Russell, T. P.; Stein, R. S. *J. Polym. Sci. Polym. Phys. Ed.* **1982**, *20*, 2243.
28. Warner, F. P.; MacKnight, W. J.; Stein, R. S. *J. Polym. Sci. Polym. Phys. Ed.* **1977**, *15*, 2113.
29. Eshuis, A.; Roerdink, E.; Challa, G. *Polymer* **1982**, *23*, 735.

30. Morra, B. S.; Stein, R. S. *J. Polym. Sci. Polym. Phys. Ed.* **1982**, *20*, 2243.
31. Plans, J.; MacKnight, W. J.; Karasz, F. E. *Macromolecules* **1984**, *17*, 810.
32. Rim, P. B.; Runt, J. *Macromolecules* **1984**, *17*, 1520.
33. Runt, J.; Rim, P. B.; Howe, S. E. *Polym. Bull.* **1984**, *11*, 517.

RECEIVED for review November 15, 1984. ACCEPTED April 19, 1985.

Glass Transitions of Both Blocks of Styrene–Butadiene Block Copolymers

ALICE T. GRANGER[1], BAOYU WANG[1], SONJA KRAUSE[1], and LEWIS J. FETTERS[2]

[1]Department of Chemistry, Rensselaer Polytechnic Institute, Troy, NY 12180
[2]Corporate Research Laboratories, Exxon Research and Engineering Company, Annandale, NJ 08801

The glass transition temperatures (T_g) of both blocks of styrene–butadiene (S–B) block copolymers were found by using volume–temperature (V–T) measurements for the S microphase and differential scanning calorimetry (DSC) for both microphases. Ideal diblock and triblock copolymers, tapered block copolymers, and an 18-arm starblock copolymer were studied. Trends of T_g and the width of the glass transition (ΔT_g) with molecular weight, composition, and microstructure are discussed. The T_g of the S microphase is lower than that of homopolystyrene (PS) of the same molecular weight up to an S-block molecular weight (M_n^S) of 12.1 × 10^4. No variance of S microphase T_g with composition was observed. The B microphase T_g was little affected by B-block molecular weight (M_n^B) but varied appreciably with microstructure and composition of the B block. A sample with a low B content (26% B) had a lowered T_g, probably because of thermal stress effects.

GLASS TRANSITION TEMPERATURE (T_g) studies of the microphases in phase-separated block copolymers of styrene (S) with dimethylsiloxane (DMS) (*1*, *2*) or with butadiene (B) from this laboratory were published (*3*). The T_g values of the S microphases in these block copolymers depended both on the molecular weight of the S block (M_n^S) and the chemical nature of the rubbery block. In the S–DMS system, the S microphase T_g was lower than that of homopolystyrene (PS) of similar molecular weight up to M_n^S of 1.5 × 10^4. Above this S-block molecular weight, the T_g of the S microphase was equal to that of PS with comparable molecular weight (*1*, *2*). In the S–B block copolymers, on the other hand, the T_g of the S microphase was lower than that of PS of comparable molecular weight up to the highest S-block molecular weight studied, 2.2 × 10^4 (*3*). Therefore, the T_g values of S microphases in S-B block copolymers with M_n^S greater than 2.2 × 10^4 were studied.

0065–2393/86/0211/0127$06.00/0

Past studies in this laboratory (*1–3*) have included only "ideal" block copolymers. Others (*4–6*) have done studies on tapered block copolymers. These polymers consist of a B block containing a small amount of S that changes gradually to an almost pure S block. Tapered block copolymers were studied to see if mixing occurred in an interphase region between microphases or by mixing of whole block copolymer chains into the microdomains. Hashimoto et al. (*6*) called the first effect a *domain-boundary* effect and the second a *mixing-in-domain* effect. Their results from small-angle X-ray scattering (SAXS) showed a narrow interphase and, therefore, little domain-boundary effect. Rather, the SAXS peaks indicating the long-range order of the microphases decreased in intensity with increasing temperature and showed a loss of this order. This observation, they concluded, indicated the mixing-in-domain effect. Similar results were observed in SAXS measurements by Roe et al. (*7*) on ideal block copolymers.

Other workers (*8*, *9*) studied "ideal" styrene–isoprene triblock copolymers of varying block size and composition by using differential scanning calorimetry (DSC). In samples with a total molecular weight of less than or equal to 3×10^4 and an isoprene content of 30% or less, either a third, intermediate glass transition was observed, or a single T_g value intermediate between the component T_g values expected for the pure microphase was observed. The microphases apparently became more compatible as the molecular weight and isoprene content decreased. This increased compatibility resulted first in an interphase of mixed chains between the styrene and isoprene microdomains. This microphase was presumably incompatible enough with the styrene and isoprene microphases to show an intermediate T_g. At very low total molecular weight and isoprene content, only the intermediate T_g was visible. This observation was attributed to an expansion of the "interphase" to include both of the microdomains. Therefore, S–B tapered block copolymers were studied to determine if an interphase effect could be observed.

The T_g values of both the B and DMS microphases are lower than that of the S microphase. Thermal stress effects, as described in work on filled rubbers (*10*) and diblock copolymers (*11*), should affect the glass transitions of the B and DMS microphases. Thermal stresses arise in these samples because the S microphase and the B or DMS microphase have different thermal expansion coefficients. At temperatures below the S microphase glass transition, the lower thermal expansion coefficient of the S microphase results in a dilatational stress on the B or DMS microphase. The B or DMS microphase is constrained to occupy a larger than "equilibrium" volume, and, if the B or DMS microphase is the inclusion, the T_g is expected to be lowered (*10*, *11*). Conversely, if the B or DMS microphase is the matrix, the T_g would be expected to be higher. In some S–DMS samples in which the DMS microphase was fully amorphous and DMS was the majority component and expected to be the matrix, the DMS microphase T_g was slightly

higher than that of homopoly(dimethylsiloxane) (PDMS) (*1*). Also, in one sample in which the DMS was the minority, the DMS block T_g was lower than that of PDMS.

No effects of composition were observed in S–B block copolymers. However, only a limited range of compositions was studied, and many of the samples were quite polydisperse (*3*). In this work, two S–B block copolymers were studied in which the B microphases were expected to be inclusions in an S matrix. One was an S–B diblock copolymer, and the other was an 18-arm starblock copolymer with styrene as the outer part of the arms. A similar 18-arm starblock copolymer, but with isoprene as the rubbery blocks, has (*12*) a morphology of isoprene inclusions in an S matrix.

Experimental

Samples. HOMOPOLYMERS. Properties of the homopolystyrene standards (ARRO Company) are presented in the literature (*1*, *13*). They have a M_w/M_n of less than 1.1 and M_n from 600 to 1.8×10^6. Characterization data for the homopolybutadiene standards (Scientific Polymer Products, Inc. and Goodyear Chemicals) are presented in Reference 3.

BLOCK COPOLYMERS. Four types of block copolymers were studied. All block copolymers (ideal diblocks and triblocks) were synthesized for this work and were used as received. Their synthesis is described in the literature (*3*, *5*, *6*, *12*).

Gel Permeation Chromatography (GPC). The Knauer GPC (Utopia Instruments) was calibrated by using 1% solutions of PS and PB standards in both distilled toluene and HPLC grade tetrahydrofuran (Fisher Scientific) at 44 °C and at a flow rate of 1 mL/min. The elution times of PB and PS for each molecular weight were quite different. However, for both PB and PS, the elution times were within 5% in the two solvents. Calibration curves in toluene are shown in Reference 3. All block copolymer samples were analyzed in both solvents. Their molecular weights were found by logarithmically interpolating between the S and B calibration curves by using the weight percent of S found by nuclear magnetic resonance (NMR).

Nuclear Magnetic Resonance (NMR). Proton and carbon-13 spectra were collected on 10% solutions of polymers in a 50:50 mixture of $CDCl_3$ and CCl_4 on a Varian XL–200 NMR spectrometer. The electronic integration on the XL–200 was used to evaluate peak areas and intensities. The method of Senn (*14*) was used to evaluate the weight percent of styrene, butadiene, 1,2-added butadiene, and 1,4-added butadiene. Carbon-13 NMR signal intensities at 130.3, 130.2, 129.8, and 129.6 ppm were used to determine *cis* and *trans* addition, because these signals had similar nuclear Overhauser enhancement (NOE) effects (*15*). Two spectra, with and without gated NOE decoupling, were run on the same sample, and the calculated *cis* and *trans* contents agreed within 3%.

Oxidative Degradation. The amount of pure block S in the tapered block copolymers was determined by using osmium tetroxide catalyzed, *tert*-butyl hydroperoxide degradation of the B block as described by Kolthoff et al. (*16*). Triplicate reactions were run on the tapered block copolymers and on an ideal block copolymer. The ideal block copolymer block S content found by this method was within 3% of that found by NMR.

Volume–Temperature Measurements. Samples were pressed into films ~1–2 mm thick at 425 K. Pieces of these films, ~0.5 g total, were sealed into a glass bulb that had been sealed onto the end of a precision-bore capillary tube. The bore diameter was determined by measuring with a traveling microscope the length of a weighed amount of mercury inside the tube. The sealed dilatometer was then degassed under vacuum ($\sim 10^{-6}$ Torr) at room temperature for at least 30 h, then at 390 K for another 4 h before mercury was added. Each sample was equilibrated in the mercury for 1 h at 390 K before any measurements were taken. The dilatometers were placed in a silicone oil bath, temperature controlled to an accuracy of 0.2 K, at 400 K and allowed to equilibrate for 1 h. Measurements of the column height were made by using a cathetometer, to an accuracy of 0.03 mm. Measurements were then taken while cooling stepwise in 5–8 K intervals. The first measurement was taken after 20 min at a temperature. Measurements were then taken every 10 min until two readings agreed within 1%. The data were evaluated according to the method of Bekkedahl (*17*).

DSC Measurements. All measurements were obtained with a Perkin-Elmer DSC-4, interfaced with an Ithaca Intersystems minicomputer. Samples of 12–20 mg were packed as received into flat aluminum DSC pans. Two empty pans for the reference and baseline were also prepared, as well as a pan packed with alumina powder as a heat capacity standard. The alumina powder was calibrated against a sapphire pellet and had the same heat capacity (within 3%) of that of the sapphire for the temperature range used (153–423 K). The sample was first cooled in the instrument from 423 K to 153 K at a rate of 10 K/min. Data were collected on the subsequent heating at 10 K/min. A baseline and alumina scan were also made to evaluate heat capacity. In some measurements, simple baseline subtraction from the sample heat flow curve gave a less noisy curve than the heat capacity curve for better evaluation of the glass transition. The T_g was the temperature of half the heat capacity change between the extrapolated glassy and rubbery baselines. The width of the glass transition (ΔT_g) was the difference in the temperatures of the intersections of the tangent to the heat capacity curve at T_g with the extrapolated baselines. These parameters are shown in Figure 1 of Reference 1. Examples of some typical DSC data are shown in Figure 1.

Results

Table I shows the molecular weight, molecular-weight distribution, styrene composition, and B-block microstructure for the polymers studied. The first of the two weight percent S values for the Solprenes denotes the total S content determined by NMR. The second value is the block S content determined by oxidative degradation. The GPC results show that most samples have a M_w/M_n of less than 1.2. The molecular weights of some of these samples are slightly different than those cited previously (*3*) because logarithmic rather than linear interpolation was used to evaluate the "as block" molecular weight. The logarithmic method was used because it gave slightly better agreement with other methods used for determining molecular weight, for example, those methods giving the "nominal" values shown in Reference 3.

Table II shows the dilatometric data for the S microphase and of some PS samples. These data are from one run on each sample. Tables III and IV

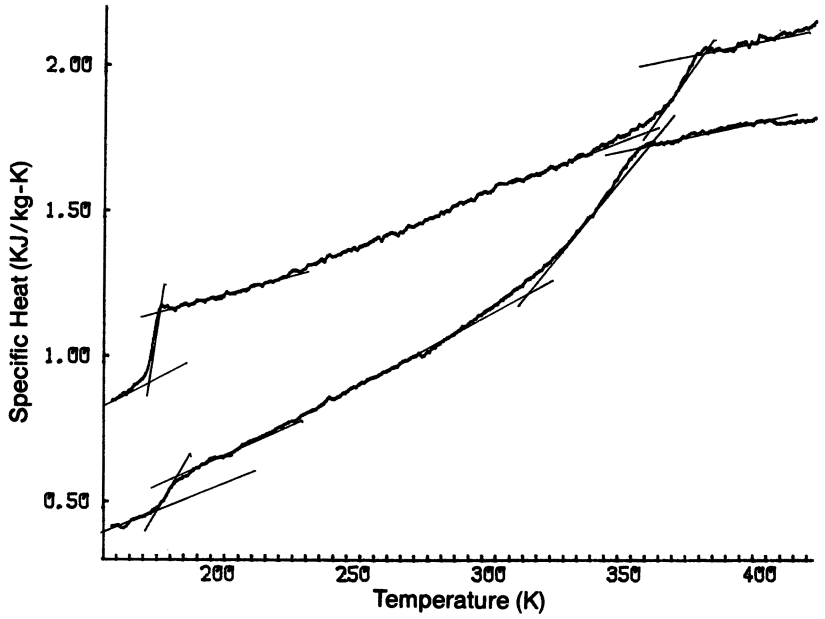

Figure 1. DSC curves for samples 55592 (top) and 52112 (bottom), showing effects of block size and composition. Curves are offset by 20% of full scale for clarity.

show the DSC data for the S microphase and B microphase, respectively. The designations M_n^S and M_n^B in the tables are the number-average molecular weights of the S and B blocks, respectively. The two values for the Solprene samples under weight percent S have the same meaning as in Table I. In Table IV, the microstructure of the B block is given again to show the general trend of glass transition with microstructure. The two homopolymer standards are shown to indicate the small dependence of T_g on molecular weight of PBs of similar microstructure.

Discussion

The S Microphase. Figure 2 shows a plot of T_g versus M_n^S using both the volume–temperature (V–T) data obtained in the present work and the n–T data obtained previously (*3*). The curve is drawn through the PS points. This plot shows that, even at the highest M_n^S studied (12.1×10^4), the T_g is still substantially lower than that of PS of the same molecular weight. This result is probably an effect of the greater compatibility present in the S–B system than in the S–DMS system, as may be seen from the measured interaction parameters of the two systems. Roe and Zin (*18*) found the S–B interaction parameter (χ_{S-B}) to be 0.08 by using cloud point

Table I. Molecular Weight and Structure Characterization of Block Copolymers

Sample	Type	S[a] (wt %)	1,2[a,b] (%)	cis 1,4[b,c] (%)	trans 1,4[b,c] (%)	M_n ($\times 10^{-4}$)[d]	$\bar{M}_w/\bar{M}_n$[d]
52110	ideal SB	28	29	30	41	3.01	1.03
52111	ideal SB	52	23	34	43	2.94	1.55
52112	ideal SB	74	24	35	41	2.67	1.13
55591	ideal SB	50	21	37	42	8.75	1.05
55592	ideal SB	49	16	41	43	12.4	1.14
55593	ideal SB	52	9	44	47	22.4	1.20
55594	ideal SB	50	17	40	43	16.4	1.27
Solprene 308	tapered SB	30, 19[e]	11	43	46	12.3	1.18
Solprene 1205	tapered SB	28, 17[e]	9	43	48	8.3	1.10
Starblock	18-arm starblock	27	9	46	45	66.7[f]	
TR-41-2443	ideal SBS	31	12	40	48	13.5	1.14
TR-41-2445	ideal SBS	28	12	42	46	6.7	1.10
TR-41-2446	ideal SBS	35	41	22	37	12.9	1.09
TRW-6-1086	ideal SBS	30	6	44	50	9.5	1.06
TRW-6-1087	ideal SBS	35	18	41	41	12.1	1.20
Kraton 1101	ideal SBS	32	7	44	49	12.4	1.16
PP-629B	ideal SB	34	14	44	42	11.8	1.18
PX-1000-2	ideal SB	9	12	44	44	6.9	1.09
D-1101	ideal SBS	32	9	43	48	7.1	1.10

[a] From ^{1}HMR.
[b] Percent of total B that is this isomer.
[c] From ^{13}C NMR.
[d] From GPC.
[e] From oxidative degradation.
[f] 18 arms, 3.7×10^4 each, from synthesis data.

Table II. Dilatometry on S Microphases

Sample	$\bar{M}_n^s$ ($\times 10^{-3}$)	S (%)	T_g (K)
Starblock	10	27	341
Solprene 308	19	30, 19[a]	352
Kraton 1101	21	32	344.5
TR-41-2443	23	31	343.5
55591	42	50	348.5
55592	55	48	359.5
55593	121	52	361.5
PS 1	10.3	100	361
PS 2	20.4	100	363.5
PS 3	860	100	373

[a] Block S from oxidative degradation.

Table III. Styrene Microphase Glass Transitions from DSC

Sample	$\bar{M}_n^S$ ($\times 10^{-4}$)	*S* (*wt%*)	T_g (K^a)	ΔT_g (K^a)
52110	0.78	28	312 ± 3	37 ± 5
Starblock	1.0	27	349 ± 4	50 ± 5
Solprene 1205	1.0	28, 17[b]	334 ± 3	49 ± 6
TR-41-2445	1.0	28	339 ± 5	47 ± 10
52111	1.35	52	345 ± 2	19 ± 2
TRW-6-1086	1.4	30	346 ± 1	20 ± 1
52112	1.7	76	344 ± 3	20 ± 4
Solprene 308	1.9	30, 19[b]	361 ± 7	49 ± 9
Kraton 1101	2.1	32	357 ± 4	32 ± 6
TRW-6-1087	2.3	35	357 ± 3	29 ± 7
TR-41-2443	2.3	31	351 ± 1	28 ± 6
TR-41-2446	2.3	35	360 ± 5	46 ± 7
55591	4.2	50	367 ± 4	25 ± 3
55592	5.5	49	372 ± 3	25 ± 5
55594	8.5	50	367 ± 7	21 ± 8
55593	12.1	52	369 ± 5	18 ± 6

[a] Error limits are average deviations, 3–4 runs each.
[b] Block styrene from oxidative degradation.

Table IV. Butadiene Microphase Glass Transitions from DSC

Sample	$\bar{M}_n^B$ ($\times 10^{-4}$)	*B* (*wt%*)	*1,2* (*%*)	trans (*%*)	cis (*%*)	T_g (K^a)	ΔT_g (K^a)
Kraton 1101	8.1	68	7	49	44	179	6
Starblock	2.7	73	9	45	46	180	7
55593	11.1	48	9	47	44	180	7
Solprene 1205	5.2	72	9	48	43	182	8
D 1101	4.8	68	9	48	43	179	7
Solprene 308	8.5	70	11	46	43	184	7
DX-1000-2	6.3	91	12	44	44	177	5
TR-41-2445	5.1	72	12	46	42	179	8
TR-41-2443	10.0	69	12	48	40	179	6
PP-629B	7.8	66	14	42	44	176	6
55592	5.7	51	16	43	41	178	7
55594	8.5	50	17	43	40	179	7
TRW-6-1087	8.6	65	18	41	41	177	6
55591	4.2	50	21	42	37	179	7
52111	1.25	48	23	43	34	194	11
52112	0.6	26	24	41	35	183	14
52110	2.0	72	28	41	30	193	6
TR-41-2446	8.5	65	41	37	22	203	7
PB 1	0.235	100	6	53	41	173	5
PB 2	20.6	100	6.7	43.5	49.8	177	5

[a] One or two runs; for more than one run T_g and ΔT_g, the results are identical.

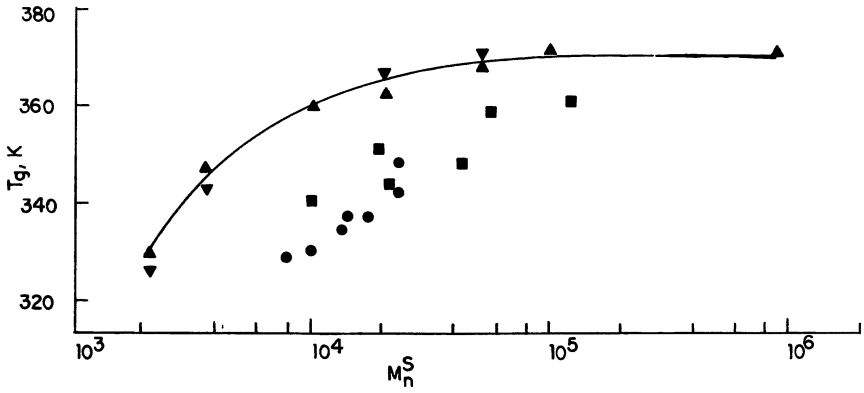

Figure 2. Glass transition vs M_n^S *from dilatometry and refractive index–temperature measurements. Key: (block copolymers)* ●, *n–T;* ■, *V–T; (PS)* ▼, *n–T; and* ▲, *V–T.*

measurements. Galin and Rupprecht (*20*) found the S–DMS interaction parameter ($\chi_{S\text{-}DMS}$) to be 0.5 by using reversed-phase chromatography. The T_g values were sharply defined in the *V–T* curves, as sharply defined as T_g values of the S blocks in the S–DMS block copolymers found by *n–T* measurements.

Figure 3 is a plot of the S-microphase T_g versus M_n^S from the DSC data. The crosses (PS) and circles (S microphases) indicate the average T_g values of the samples. The vertical bars are ΔT_g of the samples. As in the *n–T* and *V–T* plot, the S-block T_g values are all lower than those of PS of the same molecular weight, although the values of T_g are somewhat higher in the DSC measurements. The trend of T_g with molecular weight in both figures seems to indicate that block and homopolymer T_g values will finally converge at a higher S block molecular weight than 12.1×10^4.

Figure 3 also shows that the width of the glass transition decreases with increasing molecular weight. This effect was also observed in the S–DMS system, but in that system, even at the highest molecular weights, ΔT_g was still about twice that of PS (*2*). The width of the glass transition may be attributable to domain-boundary effects (*6*), and the actual depression may be attributable to mixing-in-domain effects (*6*). Although many DSC glass transition regions of the S microphases were broad and diffuse, all *V–T* samples had sharp glass transition regions. This difference is probably due to the different time scale of the experiments. In the very slow *n–T* and *V–T* experiments, the domain-boundary effects in the domains may be closer to "equilibrium," and the domains may have more perfect morphologies. On the other hand, the DSC data were collected after rapid cooling (10 K/min), and high-temperature chain conformations and morphologies may be already set.

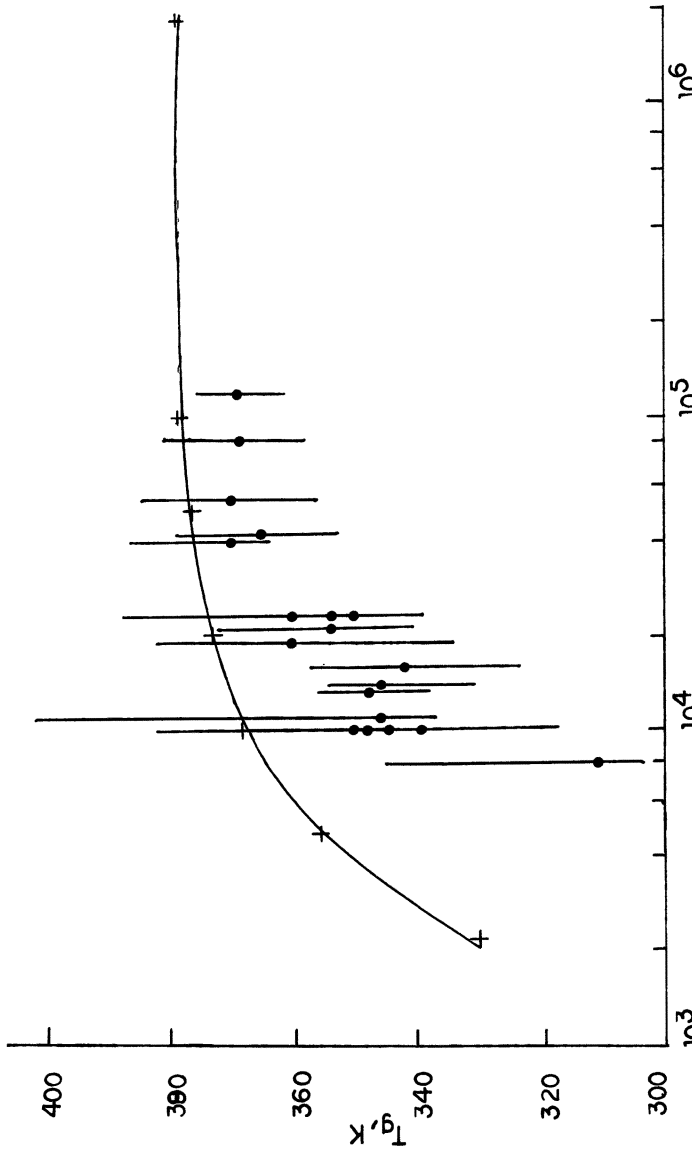

Figure 3. Glass transition vs. M_n^S from DSC measurements. Key: +, PS; and ●, microphases.

Only two T_g values were observed in the Solprene (graded diblock) samples. No third T_g between the S microphase and B microphase was observed. Thus the existence of an appreciable intermediate incompatible microphase is precluded in these samples.

The B Microphase. In previous work (*3*), no clear-cut trends of the B microphase T_g with molecular weight, microstructure, or composition were observed. However, these samples had a limited variety of composition and many were quite polydisperse.

The possible effect of molecular weight on the PB T_g was studied by using two PB standards with similar microstructure but with molecular weights of 2350 and 2.06×10^5 (*see* Table IV). Their T_g values were 173 K and 177 K; these values show a very small molecular-weight effect. The M_n^B values in the block copolymers are between 6×10^3 and 1.11×10^5, well within this range.

The influence of microstructure was much greater than the influence of molecular weight on the B microphase T_g, as expected from previous work on PB (*19*). The T_g values of 100% *cis*-1,4-butadiene, 100% *trans*-1,4-butadiene, and atactic 1,2-butadiene are estimated (*19*) to be 159, 171, and 266 K, respectively. Sample TR-41-2446, for example, is 41% 1,2-butadiene, the highest 1,2-butadiene content of the samples, and has a T_g of 203 K.

There are some breaks in the smooth increase of T_g of the B microphases with microstructure as shown in Table IV. The two Solprene samples have slightly elevated B-block T_g values. This deviation shows that the B microphase is not pure B; it is B with some S monomer copolymerized into it. This result is consistent with the increase of the loss modulus maximum temperature in similar block copolymers observed by Hashimoto et al. (*6*).

The other difference from the trend of increasing T_g with increasing vinyl content was observed for sample 52112. This sample is the only one studied in which B is the minority component, and it is also the sample with the lowest M_n^B (6×10^3). The B block T_g was lower, and the width of the glass transition was about twice that of all the other B-microphase glass transitions. The lowered T_g is probably evidence of thermal stress effects and is expected in samples of this type. The larger ΔT_g may be a result of a molecular-weight effect because the sample (52111) with the second smallest M_n^B (1.25×10^4) also has a larger ΔT_g than the other samples. Figure 1 shows the difference in the glass transition region of both microphases, but especially of the B microphase, between 52112 and 55592. Sample 55592 is representative of the other block copolymers studied.

The starblock copolymer was assumed to have a S matrix with B inclusions (*12*); therefore, a lowered T_g would be expected, as in sample 52112. This lower value was not observed. Annealed styrene–isoprene starblock

copolymers with 30 wt% S, containing six or more arms, were reported (*21*) to have an ordered bicontinuous structure consisting of short S rods connecting with each other through a matrix of isoprene. If our 18-arm S–B starblock has a similar morphology, the effects of thermal stresses expected for rubbery inclusions in a glassy matrix should not be observed. A study of the morphology of our 18-arm starblock sample would be interesting. In addition, studies of samples of starblocks with higher proportions of styrene in the arms and linear block copolymers with large B blocks but low B percent composition would be interesting to examine further the thermal stress problem.

Nomenclature

T	Absolute temperature
T_g	Glass transition temperature
ΔT_g	Width of the glass transition region
$\chi_{S\text{-}B}$, $\chi_{S\text{-}DMS}$	Flory–Huggins interaction parameters
M_n^S	Molecular weight of styrene block
M_n^B	Molecular weight of butadiene block

Acknowledgments

We thank C. I. Chung for the use of his DSC equipment and for providing us with some samples. Also, we thank R.-J. Roe, R. L. Smith, and E. B. Nauman for providing polymer samples. We thank the Goodyear Tire and Rubber Company for its support in the form of the Goodyear Tire and Rubber Foundation Fellowship. This work was also supported by the National Science Foundation Polymers Program under Grant No. DMR81-06107.

Literature Cited

1. Krause, S.; Iskandar, M.; Iqbal, M. *Macromolecules* **1982**, *15*, 105–11.
2. Lu, Z-h.; Krause, S. *Macromolecules* **1982**, *15*, 112–14.
3. Krause, S.; Lu, Z–h.; Iskandar, M. *Macromolecules* **1982**, *15*, 1076–82.
4. Hashimoto, T.; Tsukahara, Y.; Kawai, H. *Polym. J.* **1983**, *15*, 699–711.
5. Tsukahara, Y.; Nakamura, N.; Hashimoto, T.; Kawai, H.; Nagaya, T.; Sugimura, Y.; Tsuge, S. *Polym. J.* **1980**, *12*, 455.
6. Hashimoto, T.; Tsukahara, Y.; Tachi, K.; Kawai, H. *Macromolecules* **1983**, *16*, 648–57.
7. Roe, R.–J.; Fishkis, M.; Shang, J. *Macromolecules* **1981**, *14*, 1091–1103.
8. Meyer, G. C.; Widmaier, J. M. *J. Polym. Sci Polym. Phys. Ed.* **1982**, *20*, 389–98.
9. Widmaier, J. M.; Meyer, G. C. *J. Therm. Anal.* **1982**, *23*, 193–99.
10. Wang, T. T.; Sharpe, L. J. *J. Adhes.* **1969**, *1*, 69–75.
11. Paterno, J. J., Ph.D. Thesis, Rensselaer Polytechnic Institute, Troy, N.Y., 1970.
12. Handlin, D. L., Jr.; Kinning, D. J.; Fetters, L. J.; Thomas, E. L. *Bull. Am. Phys. Soc.* **1983**, *28*, 310.

13. Krause, S.; Lu, Z-h. *J. Polym. Sci.* **1981**, *19*, 1925–28.
14. Senn, W. L., Jr. *Anal. Chim. Acta* **1963**, *29*, 505–9.
15. Walckiers, E.; Julemont, M. *Makromol. Chem.* **1981**, *182*, 1541–52.
16. Kolthoff, I. M.; Lee,. T. S.; Carr, C. W. *J. Polym. Sci.* **1946**, *1*, 429–33.
17. Bekkedahl, N. *J. Res. Natl. Bur. Stand.* **1949**, *42*, 145–56.
18. Roe, R.-J.; Zin, W.-C. *Macromolecules* **1980**, *13*, 1221–28.
19. Kraus, G.; Childers, C. W.; Gruver, J. T. *J. Appl. Polym. Sci.* **1967**, *11*, 1581–91.
20. Galin, M.; Rupprecht, M. C. *Macromolecules* **1979**, *12*, 506–11.
21. Alward, D.; Thomas, E. L.; Fetters, L. J., unpublished data.

RECEIVED for review November 11, 1984. ACCEPTED March 12, 1985.

9

Three Types of Poly(styrene–Ethylene Oxide) Block Copolymers

Synthesis and Study of Their Emulsifying and Crystalline Properties

HONGQUAN XIE and PEIGUANG ZHOU
Hubei Research Institute of Chemistry, Wuhan, China

The polystyrene (PS)–polyoxyethylene (PEO) diblock copolymer was synthesized in toluene with α-phenylethylpotassium as an initiator. The PS–PEO–PS triblock copolymer was prepared by coupling 2 mol of the PS–PEO diblock copolymer containing one hydroxyl end group and by using toluene 2,4-diisocyanate as coupling agent. The PEO–PS–PEO triblock copolymer was made by polymerizing styrene in toluene with naphthalenylpotassium as the bifunctional initiator; the polystyrene was then copolymerized with ethylene oxide. The copolymers were purified by extractions and characterized by gel permeation chromatography, proton NMR, IR, UV, and differential scanning calorimetry. The emulsifying ability of the block copolymers increased with increasing PEO content, decreasing molecular weight, and increasing concentration of the block copolymers. It decreased in the following order: graft copolymer > PEO–PS–PEO > PEO–PS. X-ray diffraction experiments showed that the degree of crystallinity increases with PEO content and decreases in the following order: PEO–PS–PEO > PS–PEO > PS–PEO–PS.

BLOCK COPOLYMERS OF STYRENE (S) AND ETHYLENE OXIDE (EO) are amphiphilic because of the hydrophilic and crystalline polyoxyethylene (PEO) blocks and the hydrophobic and amorphous polystyrene (PS) blocks. These copolymers have many uses including polymeric surfactants, electrostatic charge reducers, compatibility enhancers in polymer blending, or phase transfer catalysts.

Szwarc (*1*) first reported the synthesis of a PEO–PS–PEO block copolymer (BAB type). He used a successive anionic polymerization of S and EO in tetrahydrofuran that was initiated by naphthalenylsodium. Finaz et al. (*2*) described the preparation of a BAB block copolymer with a disodium compound of α-methylstyrene tetramer as the initiator. Zgonnik (*3*) used

0065–2393/86/0211/0139$06.00/0

biphenylpotassium as the initiator and tetrahydrofuran as the solvent in a successive polymerization of S and EO to also form a BAB block copolymer. A dipotassium compound of α-methylstyrene tetramer was used by Marti (*4*) for the the preparation of the same type block polymer.

A PS–PEO block copolymer (AB type) was synthesized (*2*, *4*, *5*) by a successive anionic polymerization of S and EO with cumylpotassium as the initiator. Minoura (*6*) reported the preparation of an AB block copolymer by first dissolving PEO in S and then stirring the mixture with very high speed to produce free radicals and initiate the polymerization of styrene. The product obtained was not well characterized, however, and a large amount of homopolymers might be produced.

The PS–PEO–PS block copolymer (ABA type) cannot be obtained directly by anionic polymerization because of the weak alkalinity of the PEO anion, which cannot initiate the polymerization of styrene. Therefore, Finaz (*2*) reported the synthesis of an ABA block copolymer by treating the PS anion with an excess of $COCl_2$ in toluene. This mixture was then reacted with polyethylene glycol in the presence of pyridine. This type of copolymer was also prepared by Orhan (*7*) via a reaction of polyethylene glycol with diisocyanate to form the isocyanate-capped prepolymer. The NCO group was then reacted with dihydroperoxide to peroxycarbamate, which then initiated with radical polymerization of styrene. Obviously, the product obtained by radical polymerization had wide molecular-weight distribution and contained an amount of homopolymer from chain transfer.

Seiler (*8*) obtained the same type of copolymer by coupling an AB block copolymer with one hydroxyl end group and using butadiene diepoxide as the coupling agent. Lundberg (*9*) combined a PS containing one OH group with polyethylene glycol by using toluene 2,4-diisocyanate as the coupling agent in the synthesis of a PS–PEO–PS copolymer.

The emulsifying properties of the block copolymer were studied by Riess and his coworkers (*10*), who demonstrated that the PS–PEO block copolymer could act as a nonionic surfactant in the emulsification of a water–toluene mixture and the preparation of a microemulsion with the addition of a cosurfactant. They also correlated the molecular characteristics of the block copolymer to the emulsifying properties (i.e., phase inversion, particle size, and stability of emulsion).

Gervais and Gallot (*11*, *12*) reported the liquid crystalline behavior of a PS–PEO block copolymer in diethyl phthalate or nitromethane. They found by differential scanning calorimetry (DSC) that a first endothermic peak was due to melting of the PEO block and a second exothermic peak was due to transition of the liquid crystal.

In this chapter, we discuss the synthesis and characterization of three types of these block copolymers (i.e., PEO–PS, PEO–PS–PEO, and PS–PEO–PS block copolymers) using a new catalyst and a new method. We also study their emulsifying and solid crystalline properties.

Experimental

Materials. Styrene (A.R.) was purified by distillation in a nitrogen atmosphere over CaH_2 under reduced pressure and stored in a refrigerator. Toluene (C.P.), used as solvent, was purified by standing over a 4A molecular sieve overnight, then treated with CaH_2. Ethylene oxide was treated first with KOH, then with CaH_2, and then distilled into purified toluene. Ethylbenzene, 1-chlorobutane, and *n*-heptane were dried by storing over a 4A molecular sieve overnight. Toluene 2,4-diisocyanate (C.P.) was used as received.

Preparation of Initiators. α-Phenylethylpotassium was prepared as follows: 1-Chlorobutane (7.8 mL) was added dropwise over a 3-h period to potassium sand (6.5 g) in *n*-heptane at 0°C in a nitrogen atmosphere. Ethylbenzene (40 mL) was then added at room temperature, and the reaction was continued for a week. The active concentration was determined by double titrations with chloromethyl benzene as the coupling agent. The preparation of naphthalenylpotassium was similar to that of naphthalenylsodium (*1*).

Polymerization. All polymerizations were carried out under nitrogen atmosphere in serum bottles capped, baked, and rinsed with dried toluene.

SYNTHESIS OF THE PS-PEO DIBLOCK COPOLYMER. Purified S was injected by syringe into a dried bottle containing an amount of purified toluene. The α-phenylethylpotassium initiator was then added by microsyringe. After several minutes of induction period (from 0.5 to 30 min), which depended on temperature, polymerization began. The whole system changed from bluish white to dark red, and heat was evolved. No color change occurred after standing for a week. If more S was added, the system evolved heat again and the viscosity increased. A purified toluene solution of EO was added to the living PS. The whole system changed from dark red to light green, and its viscosity increased significantly with polymerization time. After polymerization for 2 days at 40 °C, several drops of acetic acid were added to terminate the polymerization. The solvent was then evaporated, and the product was vacuum dried at 50 °C for 2 days.

SYNTHESIS OF THE PS-PEO-PS TRIBLOCK COPOLYMER. The dried PS-PEO diblock copolymer was dissolved in purified toluene after stirring. Toluene 2,4-diisocyanate was introduced by syringe to an NCO:OH ratio of 1.2. With a small amount of dibutyltin dilaurate as catalyst, the reaction was carried out at 40 °C for 6 h. A small amount of ethylene glycol was then added, and the reaction was continued for 2 h (with stirring) to completely couple the NCO group probably remaining at the end of the PS-PEO block copolymer.

SYNTHESIS OF THE PEO-PS-PEO TRIBLOCK COPOLYMER. A dried serum bottle was charged with toluene and S and purged with purified nitrogen. To remove impurities, the tetrahydrofuran solution of naphthalenylpotassium was then added via a microsyringe until the characteristic color of PS anion persisted for 5 min. An amount of naphthalenylpotassium initiator was then added, and polymerization took place quickly. Naphthalenylpotassium was added to the purified toluene solution of EO to which several drops of S had been added as an indicator. When the toluene-EO solution changed from colorless to reddish yellow, it was added to the living PS. The color of the PS then changed from dark red to light yellow.

The polymerization bottle was then stored at 60 °C for several days. When polymerization was nearly completed, a few drops of acetic acid were added to stop the polymerization. The solution was evaporated after the addition of a small

amount of antioxidant, and the product was dried in a vacuum oven at 50 °C for 2 days.

Characterization. Gel permeation chromatography (GPC) was carried out in an SN-01 type apparatus with tetrahydrofuran as the eluant. The number-average molecular weight was determined by a membrane osmometer (Knauer) with toluene as the solvent. IR spectra were measured (Perkin-Elmer 580B) by using a KBr crystal coated with a $CHCl_3$ solution of the copolymer. The phenyl content was measured by UV spectrophotometry (λ = 262 nm). Proton NMR spectra were obtained with a 100-MHz spectrometer by using CCl_4 as the solvent and $Si(CH_3)_4$ as the internal standard. Dynamic mechanical properties of the block copolymer were studied by using torsional braid analysis (TBA) (NB-1) with a heating rate of 2 °C/min. Transition temperatures and decomposition temperature were determined with a CDR-1 type DSC with a heating rate of 10 °C/min under nitrogen atmosphere.

Properties of the Block Copolymers. EMULSIFYING TEST. The emulsifying properties of the copolymer were examined by using a conductometer (DDS-11A). The change in conductivity was measured of an emulsion formed by dropping water slowly into a toluene solution of the block copolymer during stirring.

MEASUREMENT OF CRYSTALLINITY (X_c) AND MELTING TEMPERATURE (T_m). Crystallinity of the block copolymers was measured by X-ray diffraction (Rigaku 3015). The melting temperature of the crystals was examined by DSC.

Results and Discussion

Purification and Characterization of the Block Copolymers. PEO-PS-PEO TRIBLOCK COPOLYMER. Water and cyclohexane were used separately for extracting the homopolymers of EO and S from the block copolymer. The efficiency of the extractions was evaluated. Two extractions for each solvent efficiently separated the homopolymers from the copolymer. According to GPC results, the elution count (V_e) of PS was 46, and its molecular weight distribution was narrow. The V_e shifted to 43, however, after block copolymerization with EO; this shift indicates a molecular weight increase and the disappearance of PS after the extractions. The proton NMR spectrum of the copolymer indicated that the two peaks at 6.2 and 6.8δ are due to the phenyl ring protons, the single peak at 3.2δ is from the methylene group in the $-OCH_2CH_2-$, and the peak at 1.1δ is due to the $Ar-CHCH_2-$ group. Thus, the purified polymer contains both S units and oxyethylene units. The T_m and T_g of the triblock copolymer were determined by TBA as shown in Figure 1. Mechanical damping showed two maxima at 56 and 93 °C, corresponding to the T_m of PEO and T_g of PS. All these results indicate that the purified polymer is really a block copolymer.

PEO-PS DIBLOCK COPOLYMER. Water and cyclohexane were also used separately for extracting homopolymers from the diblock copolymer. The IR spectrum in Figure 2 shows a characteristic peak at 1120 cm^{-1} for the ether linkage, a multipeak at 1610 and 3040 cm^{-1} for the benzene ring, and a single peak at 2930 cm^{-1} for the methylene group. However, the

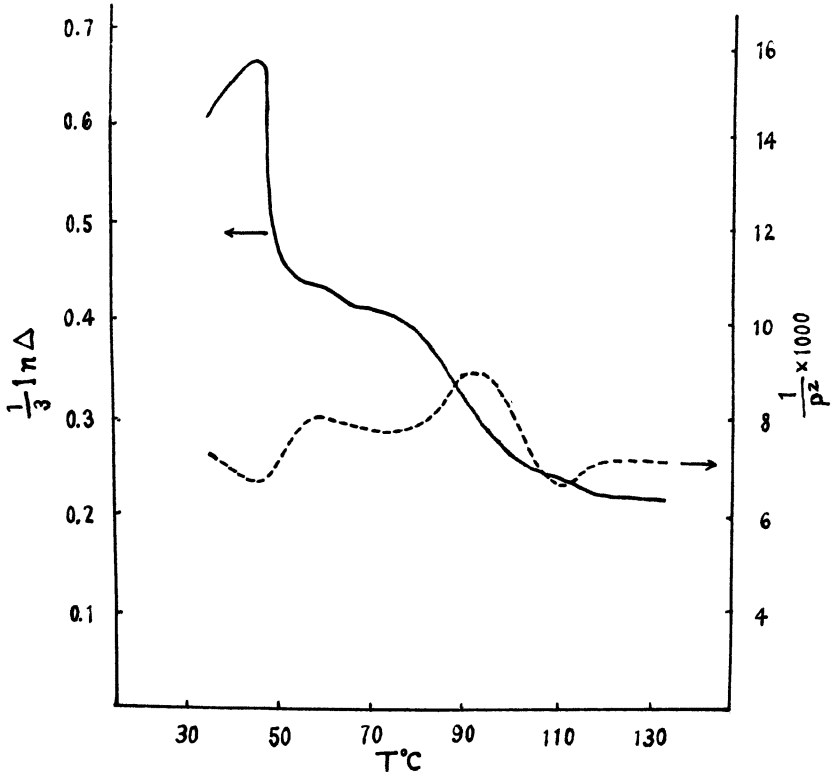

Figure 1. TBA curve of the PEO–PS–PEO triblock copolymer.

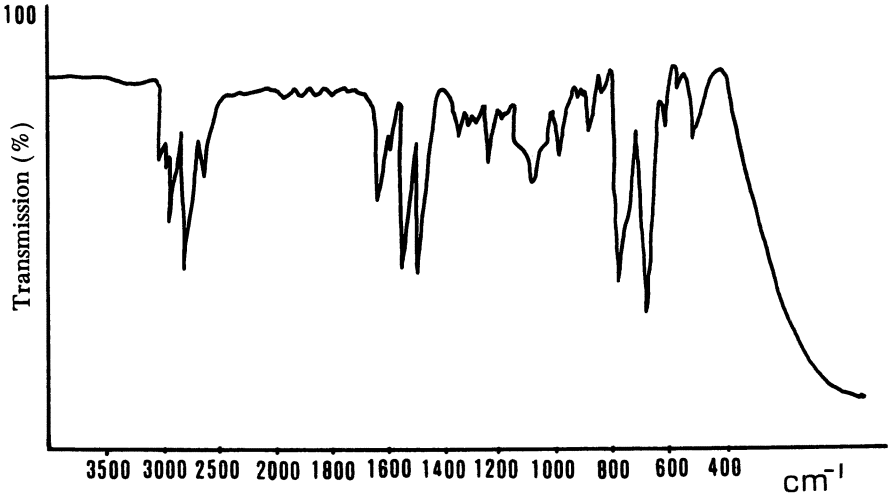

Figure 2. IR spectrum of the PEO–PS diblock copolymer.

peak in the GPC curve appears somewhat wider than that of the PEO–PS–PEO triblock copolymer. This increase in peak width is probably due to the poor solubility of α-phenylethylpotassium in toluene. Figure 3 presents the DSC curves of the diblock copolymer and the blend of homopolymers. It shows the T_m of the PEO block, the T_g of the PS block, an exothermic transition of liquid crystals at about 180 °C, and a single decomposition temperature (T_d) of the copolymer. However, two T_d values are shown for the blend of homopolymers.

PS–PEO–PS Triblock Copolymer. Purification of the PS–PEO–PS block copolymer can be successfully done by fractional precipitation with toluene as the solvent and petroleum ether as the precipitating agent. First, the point at which the diblock polymer just begins to precipitate from its toluene solution is determined. Fractional precipitation of the corresponding coupled copolymer is then carried out at this predetermined condition. Thus, most of the product remaining in solution should be the PS–PEO diblock copolymer, and most of the precipitate should be the ABA block copolymer. For example, the M_n of the precipitate was 5.8×10^4, whereas the M_n of the diblock copolymer was 2.75×10^4. The ratio of the former to the latter is equal to 2.12.

Properties of the Three Types of Block Copolymers. Emulsifying Property. The emulsifying property of the block copolymers in the water–toluene system was measured by a conductometric method. The conductivity of the toluene solution of the block copolymer at constant temperature and concentration is a constant. An emulsion was formed by

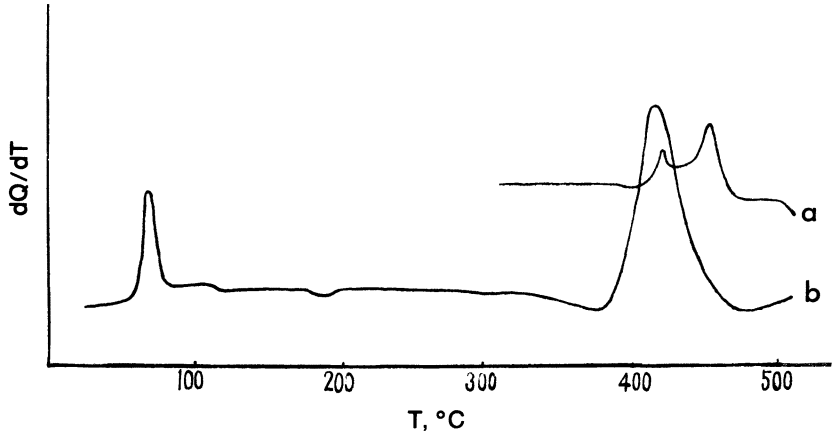

Figure 3. DSC curves of the PEO–PS diblock copolymer (b) and a blend of PS and PEO (a).

adding water to the toluene solution. When the emulsion changed from the oily continuous phase to the aqueous continuous phase, an abrupt rise in conductivity was detected. The conductivity increased gradually as water was added. The conductivity began to fall, however, when the amount of water reached a critical value (Figure 4). Upon further addition of water, the emulsion was destroyed, and phase separation into two layers resulted. The critical amount of water added per weight of copolymer was defined as the emulsifying ability of the block copolymer, and the amount of water added per weight of copolymer corresponding to the abrupt rise in conductivity was defined as the phase-inversion point.

In Figure 5, the phase-inversion point of the PEO–PS diblock copolymer is less than that of the graft copolymer, which was obtained by copolymerization of an epoxy ether terminated PS macromer with EO (*13*). The conductivity of the block copolymer in the water–toluene emulsion increased abruptly with the increasing amount of water added, whereas that of the graft copolymer increased gradually.

As seen in Figure 6, the emulsifying ability of the block copolymers increased with PEO content. At a similar PEO content, M_n, and concentration, the emulsifying ability decreases in the following order: graft copolymer > PEO–PS–PEO > PS–PEO.

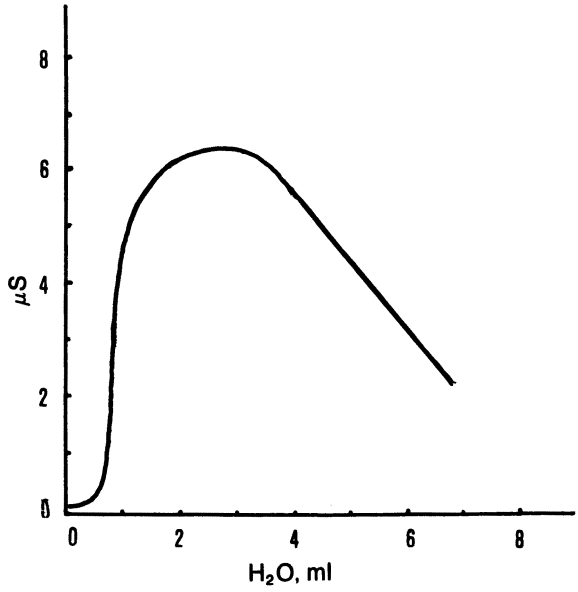

Figure 4. Relationship between the conductivity of the toluene solution of PEO–PS and the quantity of water added.

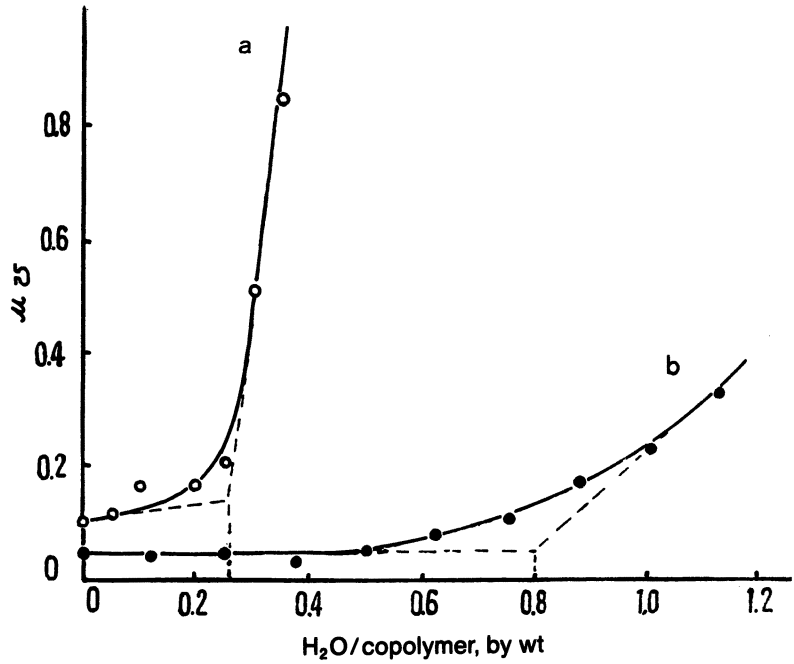

Figure 5. Phase-inversion points of a PEO–PS diblock copolymer (a) and a graft copolymer (b).

This difference is probably due to the following reasons: In the PEO–PS–PEO block copolymer, the PEO blocks are at both ends of the chain and easily interact with water. In the PS–PEO block copolymer, the PEO block is shielded by the PS block at one end of the chain, and the emulsifying ability is less. In the graft copolymer, hydrophobic PS grafts of equal length are distributed along the hydrophilic PEO chain. When water is added to this toluene solution, the PEO chain is probably in a ring-like structure in the toluene solution. Therefore, the hydrophobic grafts are arranged outside the ring, and water is included within the ring. Hence, the emulsifying ability is enhanced.

Figure 6 also shows the effect of diblock copolymer concentration on emulsifying ability. When the concentration is less than 6% of PS–PEO in toluene, the emulsifying ability increases with concentration. At the same concentration and nearly the same PEO content, however, the emulsifying ability seems to decrease with increasing molecular weight (Table I).

Crystalline Properties. *Crystallinity* (X_c). According to X-ray analysis, the homopolystyrene is amorphous. The crystallinity of the block

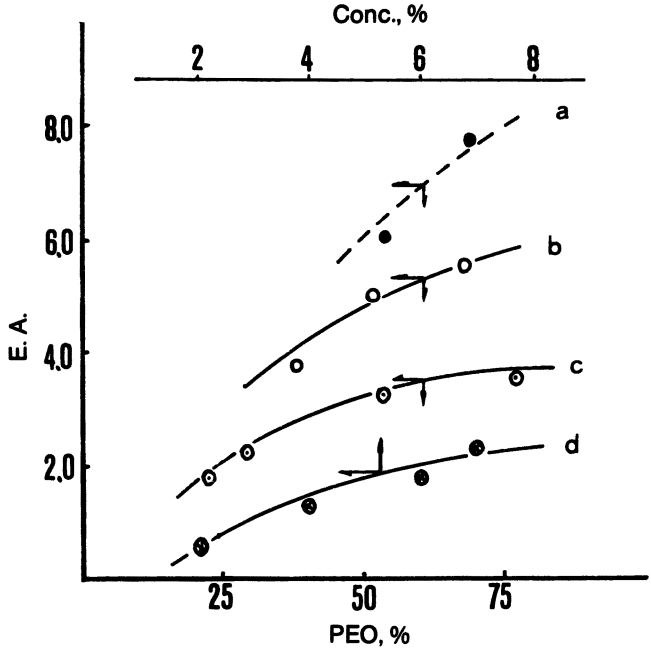

Figure 6. Relationship between the emulsifying ability (E.A.) and PEO content or initial concentration of copolymer: (a) graft copolymer, (b) PEO–PS–PEO, and (c) and (d) PEO–PS.

Table I. Emulsifying Ability of Some Block Copolymers

Block Copolymer	*PEO (wt%)*	M_n ($\times 10^{-4}$)	*E.A.*[a]
PEO–PS–PEO(1)	37.4	2.00	3.9
PEO–PS–PEO(2)	36.4	8.00	1.9
PEO–PS(1)	24.5	2.75	2.3
PS–PEO–PS(1)	24.5	5.84	1.4

[a] Emulsifying ability.

copolymer is wholly attributed to the PEO block (Figure 7) and can be calculated according to the following equation by graphical integration:

$$X_c = \frac{\int_0^\infty S^2 I_c(S)\,dS}{\int_0^\infty S^2 (I_c + I_a)(S)\,dS}$$

where S is 2 sin ϕ/λ, I_c is the diffraction intensity of crystals, and I_a is the diffraction intensity of the amorphous region.

Experimental results shown in Figure 8 indicate that X_c increases with PEO content and decreases in the following order: PEO–PS–PEO > PEO–PS > PS–PEO–PS. Perhaps, in the PS–PEO–PS triblock copolymer, amorphous PS blocks at the ends of PEO block limit the folding of the PEO block. In the PEO–PS–PEO copolymer, however, the PEO blocks situated at the ends of the chain can be folded more freely and easily, and, thus, crystals can be formed more completely.

MELTING TEMPERATURE. In Figure 9, the T_m of the PEO blocks in the block copolymer increases with X_c. When X_c is low, the thermal effect is smaller, and the melting temperature range is wider. Thus, the crystals are probably imperfect and have serious defects. But when X_c is high, the heat of melting seems larger and the transition sharper. Thus, the crystallization of the PEO blocks in the polymer with the higher X_c may be more regular and perfect.

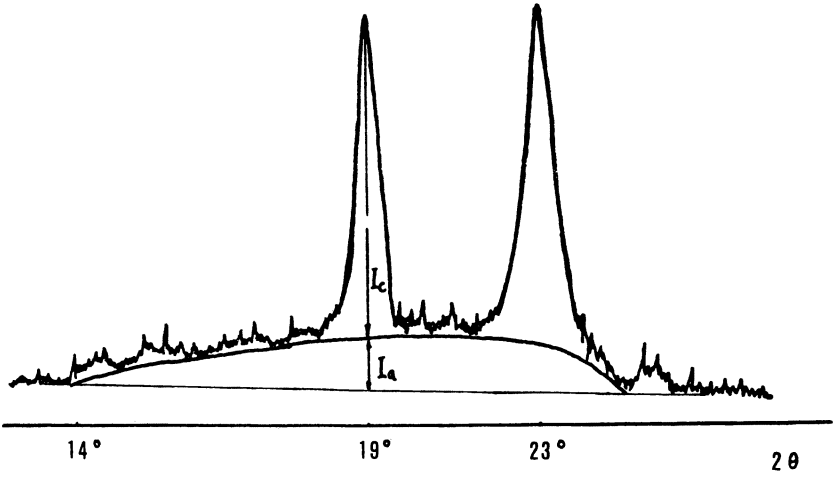

Figure 7. X-ray diffraction diagram of the PS–PEO diblock copolymer.

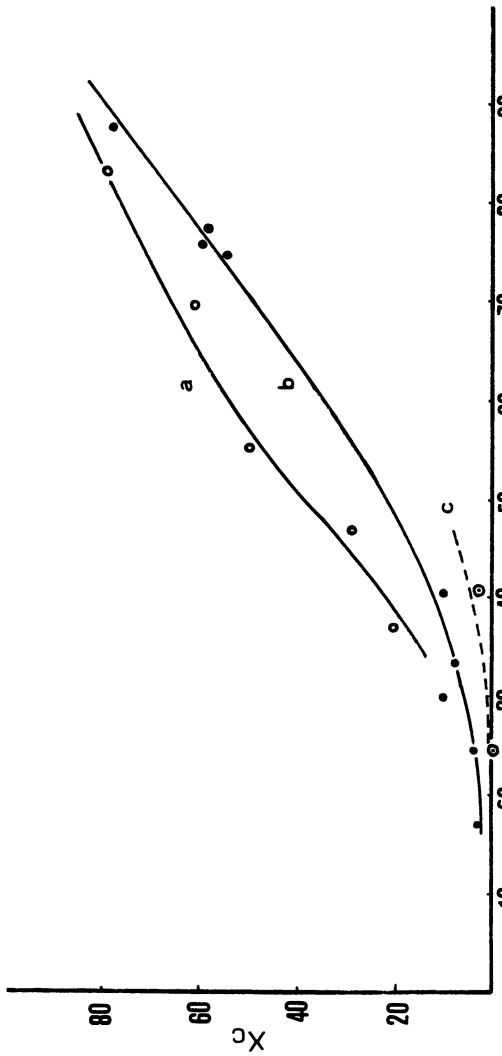

Figure 8. Relationship between PEO content and X_c: (a) PEO–PS–PEO, (b) PEO–PS, and (c) PS–PEO–PS.

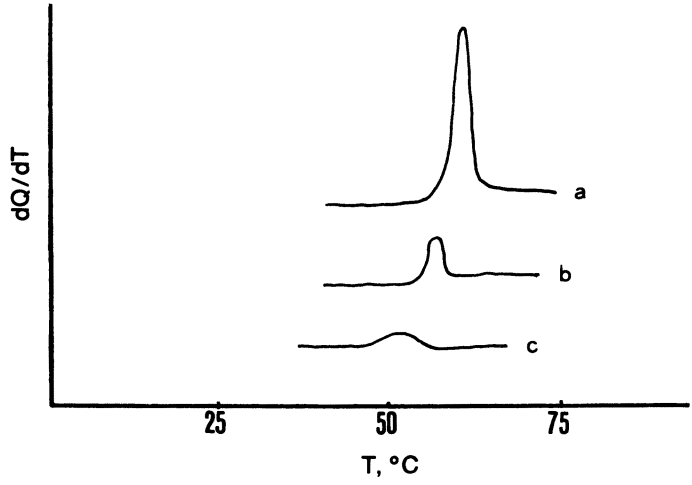

Figure 9. DSC curves of block copolymers with different crystallinity: (a) X_c *= 0.69 and* T_m *= 62 °C, (b)* X_c *= 0.10 and* T_m *= 57 °C, and (c)* X_c *= 0.04 and* T_m *= 52 °C.*

Literature Cited

1. Richards, D. H.; Szwarc, M. *Trans. Faraday Soc.* **1959**, *55*, 1644.
2. Finaz, G. P.; Rempp, P.; Parrod, J. *Bull. Soc. Chim. Fr.* **1962**, 262.
3. Zgonnik, V. N.; Shibaev, L. A.; Nikolaev, N. I. *Kinet. Mech. Polyreactions Int. Symp. Macromol. Chem. Prepr.* **1969**, *4*, 319.
4. Marti, S.; Nervo, J.; Riess, G. *Prog. Colloid Polym. Sci.* **1975**, *58*, 114.
5. O'Malley, J. J.; Crystal, R. G.; Erhardt, P. F. *Macromol. Synth.* **1972**, *4*, 35.
6. Minoura, Y. *Kogyo Kagaku Zasshi* **1966**, *69(3)*, 549.
7. Orhan, E. H.; Yilgor, I.; Baysal, B. M. *Polymer* **1977**, *18*, 286.
8. Seiler, E.; Fahrbach, G.; Gerberling, K.; Stein, P. *Ger. Offen.* 2,301,224, 1974.
9. Lundberg, R. D.; Thame, N. G. *Ger. Offen.* 2,403,934, 1974.
10. Riess, G.; Nervo, J.; Rogez, D. *Polym. Eng. Sci.* **1977**, *17(8)*, 634.
11. Gervais, M.; Gallot, B. *Makromol. Chem.* **1973**, *171*, 157.
12. Gervais, M.; Gallot, B. *Makromol. Chem.* **1973**, *174*, 193.
13. Xie, H. Q.; Sun, W. B. *Polym. Prepr.* **1984**, *25(2)*, 67.

RECEIVED for review November 15, 1984. ACCEPTED February 25, 1985.

10

Interpenetrating Polymer Networks Based on Polybutadiene and Polystyrene

Morphology and Phase Dimensions by Small-Angle Neutron Scattering and Electron Microscopy

A. M. FERNANDEZ[1], G. D. WIGNALL[1,2], and L. H. SPERLING[1,2,3]

[1]Polymer Science and Engineering Program, Materials Research Center No. 32, Lehigh University, Bethlehem, PA 18015
[2]Oak Ridge National Laboratory, Oak Ridge, TN 37830
[3]Department of Chemical Engineering, Materials Research Center No. 32, Lehigh University, Bethlehem, PA 18015

*Poly(*cross-*butadiene)*-inter-*poly(*cross-*styrene) interpenetrating polymer networks (IPNs), semi-IPNs, and chemical blends were prepared in which the second polymer synthesized, polystyrene, was fully deuterated to produce contrast for small-angle neutron scattering (SANS) and permit the dimensions of the individual polymer domains to be evaluated. Correlation lengths of 35–60 Å were found for the IPNs, 50–100 Å for the semi-I IPNs, and 160–80 Å for the semi-II IPNs and the chemical blends; the larger correlation lengths corresponded to the lower level of cross-linking. Equivalent diameters were several hundred angstroms for the IPNs. Specific surface areas ranged from 200 to 20 m^2/g for these same materials, in the range of true colloids. The morphology by transmission electron microscopy (TEM) is highly suggestive of dual phase continuity, especially for the full IPNs. The Debye theory SANS results correspond to the lower range of the TEM diameters. The two techniques have different systematic errors and measure somewhat different aspects of the morphology; therefore, comparisons are useful.*

THE ENGINEERING AND TECHNOLOGICAL USE of multicomponent polymeric materials occurs almost exclusively in the solid state. To efficiently utilize these polymeric materials, a detailed understanding of their morphological structure is required. Small-angle neutron scattering (SANS) instrumentation can be applied to problems related to phase domain size and shape and

0065-2393/86/0211/0153$06.00/0

interfacial areas. This method of analysis takes advantage of the contrast between the protonated (normal) and the deuterated molecules resulting from the differences in the coherent scattering length of deuterium and hydrogen atoms.

Interpenetrating polymer networks (IPNs) are a special kind of multicomponent polymeric material. An IPN may be defined as a combination of two polymers, each in network form, in which at least one was polymerized or cross-linked in the immediate presence of the other (*1–3*). Sequential IPN formation involves the synthesis of network I, a subsequent swelling of monomer II with initiator and cross-linking agent, and polymerization of monomer II in situ. In semi-I IPN materials, the first polymer synthesized is cross-linked, and the second polymer is linear. In semi-II IPN materials, the first polymer synthesized is linear, and the second polymer is cross-linked (*2*). Generally the IPN polymer components are structurally different, and immiscibility results from the low entropy of mixing. However, because of their interlocking chain structure, the extent of phase separation is restricted, and the domain dimensions are substantially smaller than those formed in polymer blends (*1–3*).

The morphology problems of IPNs, especially the sizes and shapes of the phase domains and aspects of dual phase continuity, have been the object of considerable scientific interest during the past decade. Earlier research at Lehigh University focused on IPN morphology via transmission electron microscopic (TEM) techniques. The experimental measurements were in good agreement with predictive equations derived to explain the dependence of the phase domain dimensions of polymer II on the cross-linking density of both polymers (*4–8*). The availability of small-angle scattering techniques such as small-angle light scattering (SALS), small angle X-ray scattering (SAXS), and small-angle neutron scattering (SANS) has yielded significant progress in the understanding of the molecular structure and morphological features of phase-separated polymer blends (*9–14*).

A study of the metamorphosis of the IPN morphology of poly(*cross*-butadiene)-*inter*-poly(*cross*-styrene) (PB–PS) IPNs by SANS and TEM (*5*) showed that the SANS data exhibited a maximum in scattering intensity at the value of the scattering vector, K, equal to 0.01. This value corresponds to a scattering dimension of the order of 700–900 Å. Because the maximum was relatively constant as a function of polystyrene conversion, a model of interconnecting cylinders was evolved. This maximum disappears late in the conversion; thus the IPN has an increasingly irregular structure.

The present work is part of a larger study to measure the phase domain dimensions of IPNs. For this chapter, poly(*cross*-butadiene)-*inter*-poly(*cross*-styrene)[1] IPNs, polybutadiene-*inter*-poly(*cross*-styrene) semi-II

[1] Formerly, this compound name was written polybutadiene–polystyrene. Nomenclature is discussed in Chapter 2 of this volume.

IPNs, and a polybutadiene–polystyrene chemical blend[1] were prepared in which the second polymer synthesized, polystyrene, was fully deuterated to produce contrast for SANS and permit the dimensions of the individual polymer domains to be evaluated. Electron microscopy of osmium tetroxide stained samples yields domain sizes and shapes. The two methods have different systematic errors and measure somewhat different aspects of the morphology; thus, comparisons are useful.

The principles of neutron scattering as applied to the solution of polymer problems were described previously (*9*, *15–17*).

The coherent intensity in a SANS experiment is described by the differential scattering cross section $d\Sigma/d\Omega$ per unit solid angle per unit volume of the sample in units of reciprocal centimeters. The quantity $d\Sigma/d\Omega$ expresses the neutron scattering power of a sample and is the counterpart of the Rayleigh ratio $R(\theta)$ used in light scattering. For polymer blends consisting of deuterated polymer molecules dispersed in a protonated polymer matrix, SANS in the Guinier region arises from the contrast between the deuterated and the protonated species.

An expression was derived for SANS from labeled two-phase polymer blends (*18*, *19*). Thereby, the SANS technique can be used to measure both the conformation of the individual labeled chains within a domain and the dimensions of the individual phase domains. For an incompressible two-phase polymer blend in which one of the phases is composed of a mixture of labeled and unlabeled molecules, the total scattering cross section is (*14*, *18*, *19*)

$$\frac{d\Sigma}{d\Omega}(K, \phi_D) = \phi_D(1 - \phi_D)(a_H - a_D)^2 N_P S_S(K) + \left[a_H(1 - \phi_D) + a_D\phi_D - \frac{a_S V_P}{V_S}\right]^2 \frac{S_T(K)}{V} \quad (1)$$

The system contains two polymer species: P, in which a fraction, ϕ_D, of molecules has been labeled (deuterated), and S, which consists of totally protonated molecules. The quantity a_S is the coherent neutron scattering length of monomer repeat units of the S species; a_H is the coherent neutron scattering length of the protonated monomer repeat units of the P species; a_D is the coherent neutron scattering length of the deuterated monomer repeat units of the P species; N_P is Avogadro's number; S_S is the single-chain

[1] The term "chemical blend" here means one polymer polymerized in the presence of another. Earlier literature denotes these as "graft copolymers," regardless of the actual extent of grafting. The corresponding terms "mechanical blend" and "solution blend" refer to mechanically mixed and solution mixed blends, respectively.

form factor; S_T is the structure form factor; V is the total volume of sample; and V_P and V_S are the monomer repeat unit molar volumes of the P and S species, respectively. The quantity K is equal to $4\pi\lambda^{-1} \sin(\theta/2)$, where λ is the neutron wavelength and θ is the angle of scatter.

Equation 1 yields the phase-separated polymer domain scattering. The quantity $S_T(K)$ is proportional to the total scattering from a blend in which the P species is fully deuterated ($\phi_D = 1$).

The materials studied were IPNs in which the first polymer synthesized was a protonated polybutadiene [$PB(H_6)$] network, S species, and the second polymer synthesized was deuterated polystyrene [$PS(D_8)$].

For a sample in which all the P species molecules have been deuterated ($\phi_D = 1$),

$$\frac{d\Sigma}{d\Omega}(K, \phi_D = 1) = \left(a_D - a_S \frac{V_P}{V_S}\right)^2 \frac{S_T(K)}{V} \tag{2}$$

If the monomer structural units (mers) of polybutadiene and polystyrene are $-C_4H_6-$ and $-C_8D_8-$, respectively, the values of the mer scattering lengths are $a_D = 10.656 \times 10^{-12}$ cm and $a_S = 0.416 \times 10^{-12}$ cm. This cross-section is proportional to the scattered intensity, which depends on the fluctuations in scattering length density in the solid and on the sizes of the regions over which these fluctuations occur. In such a case, the scattering can be described by the theory first introduced by Debye and co-workers as a treatment of the scattering of radiation by an inhomogeneous solid material (*20*, *21*). The inhomogeneities present in a random two-phase material may be characterized by a spatial two-point correlation function, which measures the degree of correlation between two fluctuations as a function of their distance of separation. The correlation function $\gamma(r)$ is given by the equation

$$\gamma(r) \langle \eta^2 \rangle_{AV} = \langle \eta_A \eta_B \rangle_{AV} \tag{3}$$

where η_A and η_B are the local fluctuations in scattering length density at points A and B, which are a distance r apart, and $\langle \eta^2 \rangle_{AV}$ is the mean square deviation over all points. If the product of η_A and η_B depends only on the separation of the scattering elements, the scattering is proportional to $S_T(K)$.

$$S_T(K) = \frac{4\pi V}{\left(a_D - a_S \frac{V_P}{V_S}\right)^2} \langle \eta^2 \rangle_{AV} \int_0^\infty \gamma(r)\, r^2 \frac{\sin Kr}{Kr}\, dr \tag{4}$$

For a two-phase system in which the domains are randomly interdispersed, $\gamma(r)$ may be obtained from a Fourier inversion of the variation of scattered

intensity with angle or by fitting a mathematical expression to the data as proposed by Debye and Bueche (*20*)

$$\gamma(r) = \exp^{-r/a} \tag{5}$$

where a is the correlation distance that defines the size of the heterogeneities. After integration, Equation 4 reduces to

$$S_T(K) = \frac{4\pi V}{\left(a_D - a_S \frac{V_P}{V_S}\right)^2} \langle \eta^2 \rangle_{AV} \frac{2a^3}{(1 + K^2a^2)^2} \tag{6}$$

Substituting Equation 6 for $S_T(K)$ in Equation 2 yields

$$\frac{d\Sigma}{d\Omega}(K,\phi_D = 1) = \frac{8\pi \langle \eta^2 \rangle_{AV} a^3}{(1 + K^2a^2)^2} \tag{7}$$

The intensity of SANS is proportional to the mean square fluctuation of the neutron scattering length density. For a two-phase system this is given by (*9*, *15*, *16*)

$$\langle \eta^2 \rangle_{AV} = (K^*)^2 \phi_P \phi_S \tag{8}$$

where the quantity K^* is the contrast factor

$$K^* = \frac{\Sigma b_D}{V_P} - \frac{\Sigma b_S}{V_S} \tag{9}$$

where $\Sigma b_d/V_P = a_D/V_P$ and $\Sigma b_H/V_S = a_H/V_S$, which are the total scattering lengths for the nuclei in species P and S, divided by their respective molar volumes. These are sometimes called scattering length densities. Thus, Equation 8 can be written as

$$\langle \eta^2 \rangle_{AV} = \left(\frac{a_D}{V_P} - \frac{a_S}{V_S}\right)^2 \phi_P^* \phi_S^* \tag{10}$$

and Equation 7 becomes

$$\frac{d\Sigma}{d\Omega}(K,\phi_D = 1) = \frac{8\pi a^3 \left(\frac{a_D}{V_P} - \frac{a_S}{V_S}\right)^2 \phi_P \phi_S}{(1 + K^2a^2)^2} \tag{11}$$

where ϕ_P is the volume fraction of the polystyrene phase and ϕ_S is the volume fraction of the polybutadiene phase.

A plot of $[d\Sigma/d\Omega(K)]^{-1/2}$ as a function of K^2 should yield a straight line having a slope–intercept ratio proportional to a^2. For dilute dispersions, a may be taken as a measure of the size heterogeneity of the dilute component. Debye (*20*) demonstrated that for random phase structures the ratio of interphase surface area A to the volume V is related to the correlation distance by

$$S_{SP} = \frac{A}{V} = \frac{4\phi_P\phi_S}{2} \tag{12}$$

where S_{SP} is the specific surface area. For a more concentrated heterogeneous system, Porod and Kratky (*22*) treated the correlation distance by introducing the transverse lengths L_P and L_S which are the average lengths of random chords passing through the two phases. These chord lengths are defined (*22*) by

$$L_P = \frac{4\phi_P}{(A/V)} \tag{13}$$

and

$$L_S = \frac{4\phi_S}{(A/V)} \tag{14}$$

Therefore,

$$L_P = \frac{a}{\phi_S} \tag{15}$$

and

$$L_S = \frac{a}{\phi_P} \tag{16}$$

Thus, a is seen to be a harmonic average of the phase dimensions:

$$\frac{1}{a} = \frac{L_S + L_P}{L_S L_P} = \frac{1}{L_P} + \frac{1}{L_S} \tag{17}$$

Because the scattering particles are spherical (volume fraction ϕ_D or ϕ_H), the average diameter is given by

$$D = \frac{3}{2}\frac{a}{(1 - \phi)} \tag{18}$$

The absolute scattering intensity at $K = 0$ is also of interest. From Equation 11,

$$\frac{d\Sigma}{d\Omega}(0) = 8\pi a^3\left[\frac{a_D}{V_P} - \frac{a_S}{V_S}\right]^2 \phi_P\phi_S \tag{19}$$

For the present system,

$$\frac{d\Sigma}{d\Omega}(0) = 8\pi a^3(0.0646 - 0.0041)^2 \times 10^{24}\,\phi_P\phi_S \tag{20}$$

where a is expressed in centimeters. Finally,

$$\frac{d\Sigma}{d\Omega}(0) = 0.092a^3\,\phi_P\phi_S \tag{21}$$

where a is in angstroms and $d\Sigma/d\Omega$ is in units of reciprocal centimeters.

Experimental

Materials and Synthesis. The full IPN and semi-IPN materials were synthesized by thermal polymerization techniques. Poly(*cross*-butadiene) (PB) networks were selected as the elastomeric phase of the materials, polymer I. Linear PB (Diene 35 NFA/AC, Firestone Synthetic Rubber and Latex) was purified by dissolving it in tetrahydrofuran (THF) and precipitating it with methanol; then it was washed several times with methanol and dried. The dried PB was redissolved in THF and mixed with the appropriate amount of dicumyl peroxide (Di-cup, K and K Laboratories) for cross-linking, and the solvent was re-evaporated. The PB matrix was partially cured in a compression molding operation at a temperature of 120 °C and a pressure of 45 psi for 20 min, and then placed in a nitrogen atmosphere chamber for about 4 h at 130 °C. The remaining un-cross-linked PB chains were extracted by refluxing with toluene for 2 days. To form the plastic phase of the materials, polymer II, deuterated styrene monomer (Aldrich Chemical Co.), was deinhibited by a chromatographic column technique using neutral alumina (Fisher Scientific). Styrene monomer solutions were prepared containing 0.4% w/v benzoyl peroxide and 1 mol% of divinylbenzene (DVB) (Polysciences).

To swell the monomer, a known weight of poly(*cross*-butadiene) was immersed in the styrene mixture at room temperature. The swollen polymer then was placed in an airtight container with a saturated styrene atmosphere for approximately 12 h so that a uniform distribution of monomer could be achieved throughout the sample. Next, the styrene was polymerized thermally at 70 °C for a period of 15 h and at 100 °C for 1 h. Finally, the materials were subject to a vacuum drying operation to remove unreacted monomer. For the semi-I IPNs, the DVB component was omitted, which yielded linear polystyrene (23).

In addition, the synthesis of a semi-II IPN and a chemical blend (neither phase cross-linked), both having 10% PB by weight and 90% PS by weight, was carried out to investigate their morphological features. The chemical blend, made without stirring to prevent phase inversion, follows the synthetic pattern developed previously (2).

The semi-II IPN material was prepared by dissolving the linear PB into a styrene monomer, plus initiator and DVB, followed by thermal polymerization similar to the other IPNs. The chemical blend was prepared by dissolving linear PB into a styrene monomer plus initiator, followed by thermal polymerization. At the end of the reaction period, the samples were vacuum dried to remove unreacted monomer.

Throughout this text, the subscript S will represent polybutadiene and the subscript P will represent polystyrene, the protonated and deuterated species, respectively. The samples are designated by letters, as follows: A, semi-I IPN, 0.1% Di-cup; B, semi-I IPN, 0.2% Di-cup; C, full IPN, 0.1% Di-cup; D, full IPN, 0.2% Di-cup; E, semi-II IPN; and F, chemical blend. The Di-cup cross-links the polybutadiene.

Polymer Characterization

Polybutadiene Molecular Weight Characterization. Gel permeation chromatography (GPC) experiments were carried out with a Waters chromatograph Model 440.

Analysis was performed on linear PB as received from the suppliers. The carrier solvent was THF. Instrument calibration was made with narrow molecular weight distribution standard polystyrenes (Waters).

Because the molecular weight determination is referred to the polystyrene calibration, the results should be considered approximate. The average molecular weights are summarized in Table I.

Values of $K = 1.56 \times 10^{-3}$ mL/g and $a = 0.80$ cm were used for $[\eta] = KM^a$ (*see* Reference 24).

Polybutadiene Homopolymer Network Characterization. The parameters usually employed to characterize a tridimensional polymer network are the amount of extractable polymer and the molecular weight between cross-links M_c.

Flory–Rehner theory (25) describes the swelling of a polymer network

$$M_c = \frac{-V_1 d_2 (v_2^{1/3} - v_2/2)}{\ln (1 - v_2) + v_2 + \chi v_2^2} \tag{22}$$

where v_2 is the volume fraction of polymer in the swollen gel, V_1 is the solvent molar volume, d_2 is the polymer density, and χ is the polymer–solvent interaction parameter. For polybutadiene–benzene, $\chi = 0.319$ (*26a*).

Table I. Molecular Characterization of Polybutadiene Polymers by GPC, Solvent Extraction, and Swelling Experiments

Sample	*% Di-cup in PB (w/w)*	$M_n \times 10^{-3}$ *(g/mol)*	$M_w \times 10^{-3}$ *(g/mol)*	M_c *(g/mol)*	V[a]	*% Extractable Materials*
Linear PB	0	103	244	—	—	—
PB network	0.1	—	—	5930	0.17	4
PB network	0.2	—	—	2600	0.23	2

[a] Volume fraction of polymer when fully swollen.

Toluene was used to extract the polybutadiene samples after cross-linking. The amount extractable (i.e., the fraction of polymer not incorporated into the network) is shown in Table I.

Instrumental. SANS MEASUREMENTS. The scattering experiments were performed on two SANS instruments, both at Oak Ridge. The first part of this study was conducted on two full IPNs and two semi-I IPNs. Measurements were made with the 30-M SANS spectrometer at the HFIR reactor by using neutrons of $\lambda = 4.75$ Å and a sample-to-detector distance of 19 m. The second part of this research utilized the 10-M SANS spectrometer at the Oak Ridge Research Reactor, neutrons of $\lambda = 4.75$ Å, and a sample-to-detector distance of 4.65 m. The measurements on both instruments were converted into absolute differential scattering cross sections, in units of reciprocal centimeters, by comparison with well-characterized precalibrated secondary standards (*26b*).

The semi-II IPN material was simultaneously tested on both instruments. Good agreement in the results was found, indicating that the 10-M instrument resolution range was suitable to study the morphology of the materials.

ELECTRON MICROSCOPY. Transmission electron microscopy (TEM) was used to elucidate the IPN morphology. A modification of Kato's (*26c*) osmium tetroxide (OsO_4) staining technique was used to prepare the specimens for the microscope. A Porter-Blum MT-2 ultramicrotome equipped with a diamond knife was used to obtain sections of about 700 Å thickness, at room temperature. The specimens were directly observed in a Philips 300 TEM and photomicrographs were obtained.

Results

Polymer Characterization. Table I shows the molecular characterization data on polybutadiene. The soluble fractions were relatively small (usually a few percent, *see* Table I), and this result indicates that the cross-linking reactions were efficient.

TEM Measurements. The compositions of samples A–F are shown in Table II. In the semi-I IPNs, only the polybutadiene was cross-linked. In the semi-II IPNs, only the polystyrene was cross-linked. In the chemical blend, neither polymer was cross-linked. In Figure 1, IPN and semi-I IPN morphologies of PB–PS materials are compared. Figure 2 shows the morphologies of two additional materials, a semi-II IPN and a chemical blend. In each case, the PB-rich elastomer phase is stained dark with OsO_4, but the PS-rich plastic phase is white.

The electron micrograph of the semi-I IPN (0.1% Di-cup) in Figure 1 shows that the elastomeric phase is more continuous, while the PS phase domains exhibit a bimodal distribution. A further increase in the cross-linking level of the semi-I (0.2% Di-cup) produces a finer morphology with smaller PS domains. The full IPNs have a finer morphology than the semi-I IPNs and give a greater indication of dual phase continuity. As other studies suggest (*5*), these are probably interconnected cylinders. The phase domain size also decreased in a styrene–butadiene rubber (SBR)–PS IPN (*23*) upon going from the semi-I to the full IPNs, and the polymer II phase do-

Published on December 9, 1985 on http://pubs.acs.org | doi: 10.1021/ba-1986-0211.ch010

Table II. Poly(*cross*-butadiene)-*inter*-poly(*cross*-styrene) (D_8) Full IPN, Semi-I and Semi-II IPN, and Chemical Blend Dimensions by SANS and TEM Techniques

Sample Code	*Volume Fractions*		*Correlation Lengths*	*Intercept Lengths, a (Å)*			*Diameters (Å)*	
	ϕ_S	ϕ_P	a (Å)	L_S	L_P	$S_{sp}(m^2/g)$	D *Values*[a]	D *Range*[b]
A	0.193	0.807	106	131	549	58.8	D_S 197	300–2000
							D_P 824	700–1500
B	0.270	0.730	53	73	194	149	D_S 109	150–1200
							D_P 294	350–600
C	0.230	0.770	58	75	252	122	D_S 113	150–1200
							D_P 378	500–1100
D	0.240	0.760	37.5	49	154	196	D_S 74	300–600
							D_P 234	400–800
E	0.116	0.884	161.1	182.2	1388.8	25.5	D_S 273	150–300
							D_P 2080	1000–2250
F	0.116	0.884	182.6	206.6	1574.1	22.5	D_S 310	200–400
							D_P 2360	1200–2500

[a] From SANS, $D_S = (3/2)[a/(1 - \phi_S^*)]$; $D_P = (3/2)[a/1 - \phi_P^*)]$.
[b] From TEM measurements.

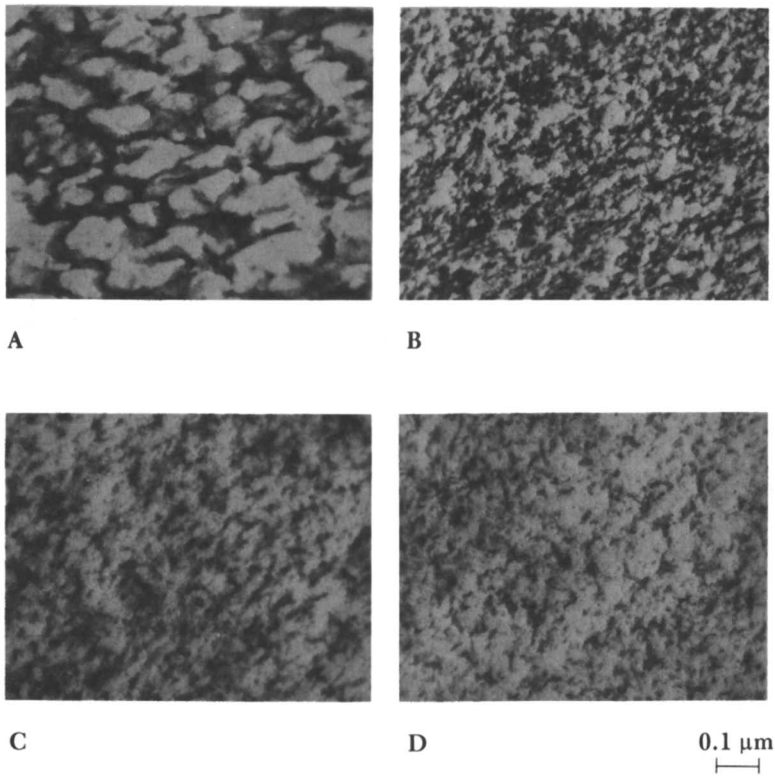

*Figure 1. Poly(*cross-*butadiene)*-inter-*poly(*cross-*styrene) IPN and semi-I IPN morphologies via TEM. Poly(*cross-*butadiene) phase stained with osmium tetroxide. Increased cross-linking decreases domain sizes. Monographs A and B are semi-I IPNs with 0.1 and 0.2% Di-cup, respectively. Monographs C and D are full IPNs with 0.1 and 0.2% Di-cup, respectively.*

mains were further decreased by increasing the cross-linking level of polymer I.

The electron micrograph of the semi-II IPN in Figure 2 shows that the PB phase remains continuous, but the PS phase forms domains of approximately 2300 by 1000 Å. The electron micrograph of the chemical blend shows the PB phase to be continuous, and the discontinuous PS phase forms domains approximately 2500 by 1200 Å, slightly larger than those observed in the semi-II IPN material.

Table II summarizes the dimensions of the multicomponent polymeric materials estimated by the TEM technique. The dimensions are reported in terms of the average diameter of the polybutadiene and polystyrene phase domain sizes *D*.

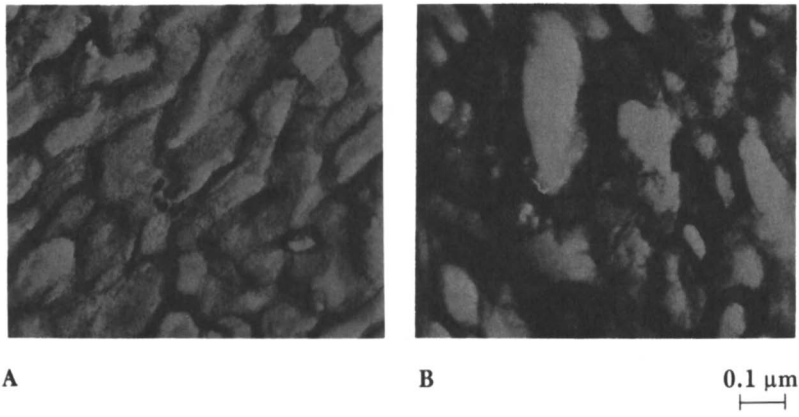

Figure 2. Comparison of semi-II IPN and chemical blend morphologies of polybutadiene and polystyrene combinations: A, semi-II IPN PB–PS(D_8) (1% DVB); and B, chemical blend PB–PS(D_8).

Given the difficulties involved in the estimation of the specific surface areas by electron microscopy, only the one corresponding to sample A was calculated. With the morphology shown in Figure 1, a 3000 × 3000-Å^2 area was selected, and it had 14 domains. A depth of 3000 Å was assumed to contain three domains, for a total of 42 domains in all, or 1.55×10^{15} domains/cm^3. Based on an average area per domain of $\pi D^2 = 3.8 \times 10^{-14}$ m^2, a specific area of about 59 m^2/g can be calculated. This result agrees with the value obtained by SANS (Table II) more closely than might otherwise be expected.

SANS Experiments. The SANS experiments were performed on these same six samples. Figures 3 and 4 show the Debye plots displayed in terms of $d\Sigma/d\Omega(K)^{-1/2}$ versus K^2. The correlation lengths evaluated from the ratio of the slope to the intercept of these plots indicate that the size of the domains ranges from 182.6 to 37.5 Å (*see* Table II). The values of L_H (transverse length for the PB phase), L_D (transverse length for the PS phase), and S_{sp} shown in Table II were calculated by using Equations 17, 18, and 14, respectively.

Figure 5 is a montage of the coherent scattering intensity as a function of K for two semi-I IPNs (samples A and B) and two full IPNs (samples C and D). The waviness is thought to be due to residual regularity in the size of the domains, as discussed elsewhere (5).

In addition to measuring the domain dimensions shown in Table II, the experimental values of $d\Sigma/d\Omega(0)$ for samples A–D were compared with values calculated from Equation 11 and Equations 19–21. In each case, good agreement between the theoretical and the experimental values was

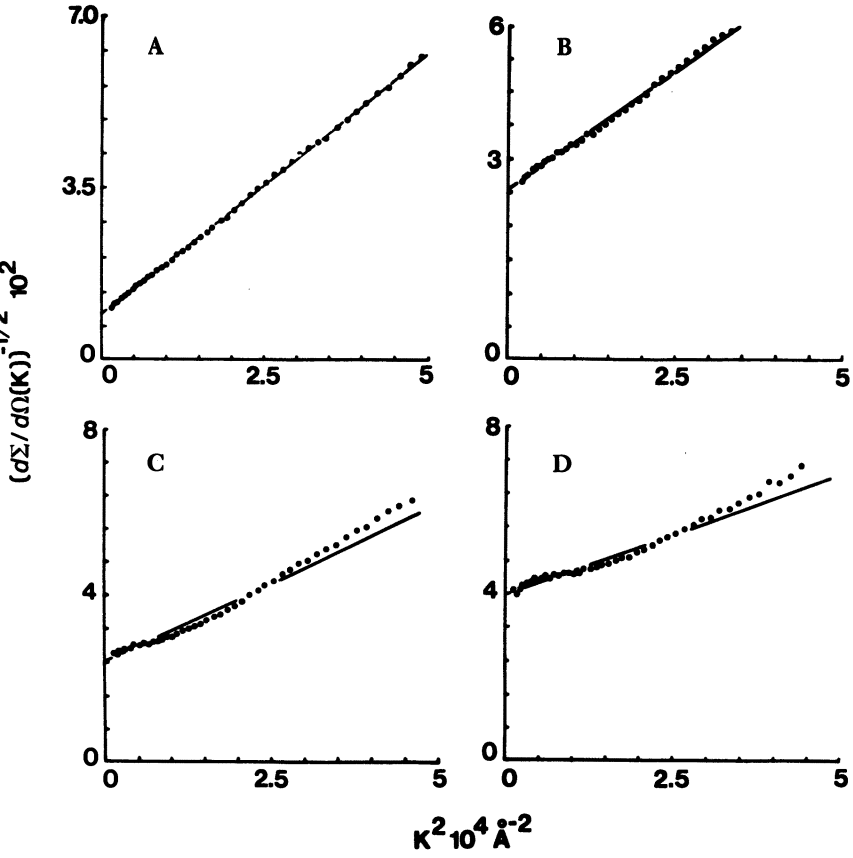

Figure 3. Debye plots (fully deuterated PS) for the evaluation of the correlation length a: *A* (a = *106Å), semi-I IPN PB (0.1% Di-cup)–PS; B* (a = *53Å), semi-I IPN PB (0.2 Di-cup)–PS; C* (a = *58Å), IPN PB (0.1% Di-cup)–PS; and D* (a = *37.5Å), IPN PB (0.2% Di-cup)–PS. Increasing cross-linking levels results in smaller correlation lengths.*

obtained (*see* Table III). This result indicates that the absolute calibration performed was correct and confirms that phase separation was more or less complete.

Discussion

The specific surface areas shown in Table II range from 50 to 200 m^2/g for the semi-IPNs and full IPNs. Increasing the cross-link density of polymer I and/or cross-linking polymer II causes S_{sp} to increase, as might be expected. These values are in the range of true colloids. For example, similar values are obtained from carbon black and silicas used to reinforce elastomers. Because interfacial surface area per se is thought to be important in tough-

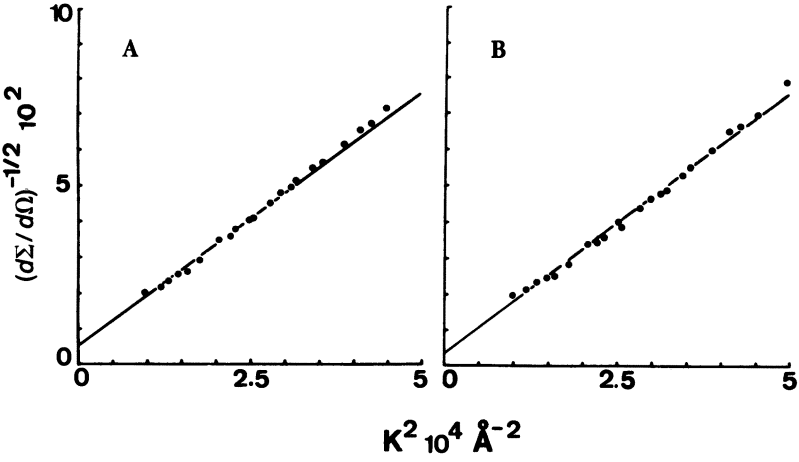

*Figure 4. Polybutadiene-*inter*-poly(*cross*-styrene) semi-II IPN and chemical blend Debye plots (fully deuterated PS): A (a = 161.1 Å), semi-II IPN PB–PS (1% DVB); and B (a = 182.6 Å), chemical blend PB–PS.*

ening (interfacial bonding is also important and present here), these specific surface areas may help explain why poly(*cross*-butadiene)-*inter*-poly(*cross*-styrene) is so tough and impact resistant.

Lipatov et al. (*27*, *28*) determined the specific surface areas of several polyurethane-based IPNs and simultaneous interpenetrating networks (SINs) using small-angle X-ray scattering techniques. They obtained results ranging from 10 to 300 m^2/g, depending on composition, and these results substantially span the present results.

Specific surface areas provide a unique result not readily available from electron microscopy. Chord lengths can be determined by TEM, but S_{sp} also is one of the few values common to both phases and is a direct measure of the interfacial area.

The SANS equivalent diameters (or the sizes of the phase domains) are in the lower range of TEM equivalent diameters. These are really interconnected phases and not isolated spheres. Many experiments with sequential IPNs show that polymers II exhibit some degree of dual phase continuity (*29*). Smaller SANS values probably result from the uneven interfacial surfaces.

Debye plots and morphologies via TEM show that the PS domain size in the semi-II IPN is slightly smaller than in the chemical blend. This result is expected because the presence of cross-links in the second polymer [deuterated $PS(D_8)$] of the semi-II IPN produces smaller PS domains. The originally linear PB becomes partly grafted and cross-linked during styrene polymerization. After extraction for several days in toluene, a highly swellable network remains. The IPNs and semi-IPNs are similarly grafted.

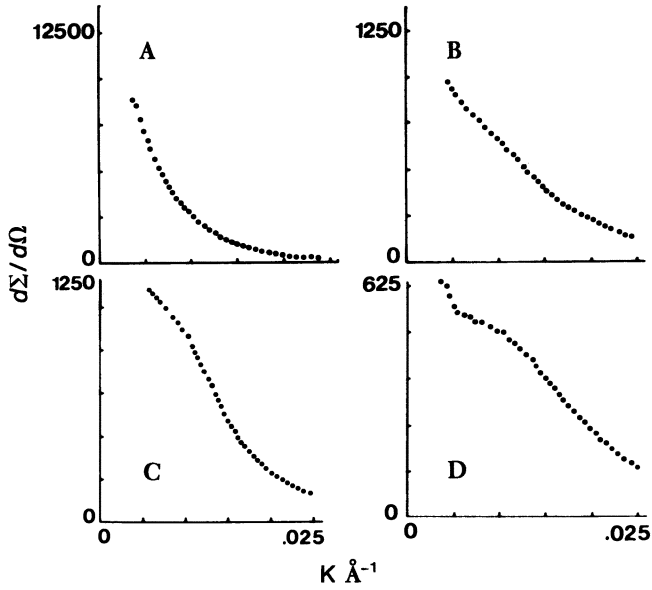

Figure 5. Coherent scattering intensity vs. K for the same compositions shown in Figure 1: A, semi-I IPN (0.1% Di-cup); B, semi-I IPN (0.2% Di-cup); C, full IPN (0.1% Di-cup); and D, full IPN (0.2% Di-cup).

Table III. Comparison of Theoretical and Experimental Scattering Intensities at Zero Angle

	$d\Sigma/d\Omega(0)$ (cm^{-1})	
Sample Code	*Measured*	*Calculated*
A	21600	17200
B	2010	2730
C	3220	3180
D	1160	885

However, in this case the morphology is dominated by the presence of the cross-links.

Debye plots show that increasing cross-linking results in smaller correlation lengths. The two semi-I IPNs (samples A and B), as well as the semi-II IPN and the chemical blend (samples E and F), exhibit a better linearity in the Debye plots. The less linear behavior is shown by the full IPN (0.2% Di-cup) (sample C). The montage of Figure 5 shows that the shapes of the scattered intensity, $d\Sigma/d\Omega$, versus K plots can be related to the morphological features of the materials. For the full IPN (0.2% Di-cup), the lower linearity in the Debye plot goes together with an incipient peak. The ob-

served changes may be related to aspects such as randomness, the onset of continuity in both phases, or a finer morphology for both polymers.

The slight curvature in the Debye plots shown in Figure 3 has been ignored. Before the polymerization of monomer II is complete, however, a well-defined maximum in the scattering intensity is observed (5). The maximum, near $K = 0.01$ (or $K^2 = 1 \times 10^{-4}$), corresponds to a scattering dimension of 700–900 Å. This dimension remained nearly constant in the range of 35–75% polystyrene content, which leads one to interpret it as the diameter of interconnected cylinders. The scattering maximum arises from the cylinder diameters early in the polymerization. No regularity in packing was noted. The results of this work are in general agreement with Reference 5, although the intensity maximum vanishes at the end of the polymerization, probably as a result of increased irregularity in the morphology. Thus, the two studies utilized quite different analyses of the SANS data.

Conclusions

Low cross-linked IPNs and semi-I IPNs present a geometry characterized by dual phase continuity (2,3). The TEM micrographs show that an increase in the cross-linking level of both polymers produces a finer morphology with rather greater regularity. When both polymers are cross-linked, the indications are stronger that two continuous phases are evolved. As the domains become smaller or more irregular, their characterization and measurement, which become more difficult by TEM, become easier when SANS is utilized.

The Debye theory equivalent diameters are from 300 to 800 Å, in the lower range of the equivalent diameters by TEM. Specifically, the Debye treatment measures smaller structures not recorded easily during TEM studies. Interfacial surface areas of 100–200 m^2/g were obtained in the present experiment; these are in the range commonly found for true colloids. The large interfacial areas indicated by S_{sp} are sites of grafting and interfacial bonding, and are clearly important for good mechanical behavior.

SANS can be used to complement TEM results in IPNs and to provide information about interfacial surface areas and chord lengths. Thus, TEM provides a semiquantitative pictorial view of the material, whereas SANS provides a quantitative, albeit statistical, analysis of the system.

The Debye treatment of phase domain dimensions does not impose geometric requirements, but rather assumes a random interdispersion of the phases and a sharp boundary between them. Interconnected, interpenetrating phases come close to meeting this requirement. Therefore, the SANS technique seems to present a special advantage when applied to dual phase continuous IPN materials.

Of more general importance, SANS provides a tool for examining multicomponent polymer materials that do not stain easily, or are too soft to cut, and cannot be studied by TEM. This study provides a basis of comparison: the domain sizes estimated by the Debye theory are likely to be somewhat smaller than those obtained by TEM, but they vary in the same general pattern.

Acknowledgments

The authors acknowledge financial support through the Polymers Program of the National Science Foundation, Grant No. DMR 8106892. The SANS experiments were performed at the National Center for Small-Angle Scattering Research and were funded by NSF Grant No. DMR 7724458 through interagency agreement No. 40-637-77 with DOE.

Literature Cited

1. Klempner, D.; Frisch, K. C., Eds. "Polymer Alloys III"; Plenum: New York, 1983.
2. Sperling, L. H. "Interpenetrating Polymer Networks and Related Materials"; Plenum: New York, 1981.
3. Manson, J. A.; Sperling, L. H. "Polymer Blends and Composites": Plenum: New York, 1976.
4. Huelck, V.; Thomas, D. A.; Sperling, L. H. *Macromolecules* **1972**, *5*, 340, 348.
5. Fernandez, A. M.; Sperling, L. H., unpublished data.
6. Donatelli, A. A.; Sperling, L. H.; Thomas, D. A. *J. Appl. Polym. Sci.* **1977**, *21*, 1189.
7. Michel, J.; Hargest, S. C.; Sperling, L. H. *J. Appl. Polym. Sci.* **1981**, *26*, 743.
8. Yeo, J. K.; Sperling, L. H.; Thomas, D. A. *Polymer* **1983**, *24*, 307.
9. Higgins, J.; Stein, R. S. *J. Appl. Crystallogr.* **1978**, *11*, 346.
10. Chu, B.; Creti, D. M. *J. Phys. Chem.* **1967**, *11*, 346.
11. Caulfield, D.; Yao, Y. F.; Ullman, R. "X-ray and Electron Methods of Analysis"; Plenum: New York, 1968.
12. Blundell, D. J.; Longman, G. W.; Wignall, G. D.; Bowden, M. *Polymer* **1974**, *15*, 33.
13. Khambatta, F. B.; Warner, F.; Russell, T.; Stein, R. S. *J. Polym. Sci. Polym. Phys. Ed.* **1976**, *14*, 1391.
14. Wignall, G. D.; Child, H. R.; Samuels, R. J. *Polymer* **1982**, *23*, 957.
15. Stein, R. S.; Hadziioannou, G. P. In "Polymer Characterization"; Craver, C. D., Ed.; ADVANCES IN CHEMISTRY SERIES No. 203; ACS: Washington, D.C., 1983.
16. Maconnachie, A.; Richards, R. W. *Polymer* **1978**, *19*, 739.
17. Sperling, L. H. *Polym. Eng. Sci.* **1984**, *24*, 1.
18. Jahshan, S. N.; Summerfield, G. C. *J. Polym. Sci. Polym. Phys. Ed.* **1980**, *18*, 1859.
19. Koberstein, J. T. *J. Polym. Sci. Polym. Phys. Ed.* **1982**, *20*, 593.
20. Debye, P.; Bueche, A. M. *J. Appl. Phys.* **1949**, *20*, 518.
21. Debye, P.; Anderson, H. R.; Brumberger, H. *J. Appl. Phys.* **1958**, *28*, 579.
22. Kratky, O. *Pure Appl. Chem.* **1966**, *12*, 483.

23. Donatelli, A. A.; Sperling, L. H.; Thomas, D. A. *Macromolecules* **1976**, *9*, 571.
24. Brandrup, J.; Immergut, E. H., Eds. "Polymer Handbook," 2d ed.; Wiley: New York, 1975.
25. Flory, P. J.; Rehner, J. *J. Chem. Phys.* **1943**, *11*, 512.
26a. Jessup, R. S. *J. Res. Natl. Bur. Stand.* **1958**, *60*, 47.
26b. Hayashi, H.; Flory, P. J.; Wignall, G. D. *Macromolecules* **1983**, *16*, 1328.
26c. Kato, K. *J. Polym. Sci. Part B* **1966**, *4*, 35.
27. Lipatov, Y. S.; Shilov, V. V.; Bogdanovitch, V. A.; Sergeeva, L. M. *J. Polym. Sci. USSR* **1980**, *22*, 1492; *Vysokomol. Soedin.* **1980**, *A22(6)*, 1359.
28. Shilov, V. V.; Lipatov, Y. S.; Karbanova, L. V.; Sergeeva, L. M. *J. Polym. Sci. Polym. Chem. Ed.* **1979**, *17*, 3083.
29. Widmaier, J. M.; Sperling, L. H. *Macromolecules* **1982**, *15*, 625.

RECEIVED for review November 15, 1984. ACCEPTED May 17, 1985.

11

Polyurethane–Polysiloxane Simultaneous Interpenetrating Polymer Networks

J. R. EBDON, D. J. HOURSTON[1], and P. G. KLEIN

Department of Chemistry, University of Lancaster, Lancaster, LA1 4YA, United Kingdom

Room temperature (20 °C) cured simultaneous interpenetrating polymer networks (SINs) based on polyurethanes and polysiloxanes were prepared and were shown to range from coarsely phase separated to entirely miscible materials. Interpenetrating polymer networks (IPNs) based on a polyether urethane and polydimethylsiloxane were found by light microscopy and dynamic mechanical analysis to be highly incompatible, but proton decoupled carbon-13 NMR linewidth measurements showed evidence of some mutual penetration of the respective networks. Systems based on polyether urethanes and polyphenylmethylsiloxane either were found to be phase separated or could, over a limited composition range, be made to show only one narrow glass transition, indicating miscibility.

Interpenetrating Polymer Networks

Although interpenetrating polymer networks (IPNs) are a branch of polyblends, they comprise a rather broad subject area and, consequently, have many diverse aspects. An IPN is formed when a pair of polymeric networks is prepared in which at least one network is synthesized and/or cross-linked in the intimate presence of the other. The ideal, but never realized, situation is one network fully interpenetrating the other to form many physical, but no chemical, cross-links. Such a state occurs when one network is totally compatible with the other. This characteristic is, of course, a rarity for pairs of different polymers, but IPNs can be synthesized in which both networks are the same polymer. Such IPNs are called Millar (*1*) or homo-IPNs. Those systems so far investigated (*2*) show that even they do not correspond to the idealized concept of two fully interpenetrating networks. In reality, a comprehensive degree of phase separation is found in which substantially pure domains of each network coexist. Thus, extensive physical cross-linking is localized at the phase boundaries. Therefore, to optimize interpenetration, the phases should be as small as possible.

[1] Author to whom correspondence should be addressed.

0065–2393/86/0211/0171$06.50/0

When only one of the polymers is cross-linked, the material is called a semi-IPN; in a semi-I IPN, the first formed polymer is cross-linked.

IPNs may be classified according to the method of synthesis. For example, sequential IPNs (*3*) occur when one network is formed before the other. In a simultaneous IPN (SIN) (*4*), both networks are synthesized at the same time and are formed by noninteracting mechanisms. Further discussion of SINs is presented in the next section.

IPNs may also be prepared (*5*) by using emulsion polymerization techniques. The first network is synthesized, and the second monomer and cross-linker are then added, but no further emulsifier is used. The belief is that no new particles are generated; however, core-shell latex particles may, under favorable circumstances, be generated.

An outstanding practical advantage of latex IPNs, as long as the extent of cross-linking is relatively low, is that each particle is an individual IPN that can be molded like a thermoplastic. Siegfried et al. (*6*) have made use of the network-forming mechanisms of the thermoplastic elastomers and ionic polymers to generate so-called thermoplastic IPNs. Such an approach could have substantial processing advantages. Another method of generating IPNs is to mix already formed latexes (*7*). Both of these approaches lead to rather coarse morphologies.

Simultaneous Interpenetrating Networks

One of the attractions of SINs is the possibility of producing systems that are potentially easy to process compared to most other types of IPNs. A system might be prepolymerized close to the gel point and then, while still fluid, be introduced into a mold or processed through a die where polymerization could be completed. Epoxy–acrylic simultaneous systems (*8*) have been much studied. When the gelation of both networks occurred at the same time (*9*), a minimum in the physical properties was observed. Better materials were produced when one of the networks was formed slightly faster than the other.

For the polyurethane-based systems, Frisch and coworkers (*10*, *11*), reported on the influence of the extent of mutual solubility on the resulting morphology of SINs. Sperling et al. (*12–16*) conducted a comprehensive study of SINs based on castor oil. For a comprehensive review of all types of IPNs, *see* Reference 17.

Cross-linking of Polysiloxanes

α,ω-Hydroxy-terminated polysiloxanes can be cross-linked by using a "structurizing" agent, typically an alkoxysilane such as tetraethylorthosilicate (TEOS). The cure proceeds via elimination of ethanol. The main mechanism suggested (*18*) for the condensation of silanol and alkoxy groups (in the absence of a catalyst) is attack by the silanol on the silicon atom of the alkoxysilane.

The cure may be accelerated by the addition of a catalyst, such as tin octonoate or dibutyltin dilaurate. In this system, a complex is formed between the tin catalyst and the alkoxysilane; this complex formation is the rate-determining step (*19*) in the cure. The smaller the substituent attached to the tin atom, the more readily the complex formation with the TEOS occurs. Vulcanization of polyorganylsiloxanes with hydroxyl end groups can also be achieved (*20*) with esters of titanic(IV) acid and aluminum alcoholates.

In addition, there are fundamentally three more processes for cross-linking siloxane polymers. In high-temperature vulcanizing (HTV) systems, polymers with methyl or vinyl groups are cross-linked by using peroxides. The cross-linking of an α,ω-hydroxy polysiloxane with, for example, TEOS is only one of the room temperature vulcanizing (RTV) processes. A newer method involves a metal salt catalyzed reaction between polymers containing silanol groups and polymers containing silicon hydride groups. In low-temperature vulcanizing (LTV) vinyl addition systems, a platinum complex is used to catalyze the addition of silicon hydrides to vinyl-containing silicones. In addition, cross-linking can be initiated by high-energy radiation.

Thermal Transitions in Polysiloxanes

Lee et al. (*21*) studied crystallization and the glass transition of polydimethylsiloxane by differential scanning calorimetry, reporting a glass transition temperature T_g of -123 °C, a cold crystallization process centered at -90 °C, and two melting peaks at -45 and -37 °C. The cold crystallization peak indicated that during fairly rapid cooling a proportion of the polymer remained uncrystallized. This peak disappeared at low cooling rates. The degree of crystallinity was calculated to be approximately 79%. Weir et al. (22) also report a T_g of -123 °C, which was unaffected by the incorporation of filler or by cross-linking. Fischer (*23*) reports a pseudoequilibrium crystallization temperature of -38.5 °C. In a study of the dynamic mechanical behavior of polydimethylsiloxane of molecular weight 200 to 136,000 g/mol, Cowie (*24*) found a major damping peak associated with the T_g that increased in temperature to an asymptotic value of -125 °C when the molecular weight exceeded 5000 g/mol. A sample of 2400 g/mol showed a tan δ maximum at -50 °C, associated with crystallinity. Dynamic mechanical studies by Clark and others (*25*) show values for T_g between -121 and -130 °C and melting temperatures of -49 to -58 °C. An activation energy for the glass transition of 146.4 kJ/mol was reported.

Polmanteer and Hunter (*26*) studied the stiffening temperatures of a number of polysiloxanes, substituting varying amounts of phenylmethylsiloxane units for dimethylsiloxane units. For polydimethylsiloxane, a stiffening temperature of -38 °C was observed. Up to a concentration of 7.5%

phenylmethylsiloxane units, the stiffening temperature decreased, reaching a minimum of −113 °C. Further incorporation of phenylmethylsiloxane units raised the temperature to about −25 °C for the polyphenylmethylsiloxane polymer itself. No crystallization was found for the compositions containing 7.5–15% phenylmethylsiloxane units, and a T_g of −86 °C was reported for polyphenylmethylsiloxane.

Polyurethane–Polysiloxane Copolymers, Blends, and IPNs

The formation of polyurethane–polysiloxane copolymers is described in the literature (*20*, *27–29*). The copolymers cannot be synthesized by the reaction between isocyanate and silanol groups, because the resulting silylurethane linkage is easily hydrolyzed (*30*, *31*). To avoid this problem, several workers (*20*, *31*) have used silicone polymers in which the end groups are protected by primary alcohols, often in the form of dimethylsiloxane–polyoxyalkylene triblock copolymers. Kuznetsova (*32*) prepared coatings by the reaction of $HO(CH_2)_2OCH_2[Si(CH_3)_2O]_nSi(CH_3)_2CH_2O(CH_2)_2OH$ (820 g/mol) with toluene 2,4-diisocyanate (TDI) and trimethylolpropane (TMP). Similarly, Adrianov (*33*) prepared silicon-containing urethane elastomers by using identical components and with the addition of diphenyldihydroxysilane and butane-1,4-diol as chain extenders. The resulting rubbers had better strength and heat resistance than polyester-based urethane elastomers. The materials were claimed to be stable for 25 days in boiling water.

Colquhoun and Rauner (*34*) also found improvement in elongation, flexibility, and abrasion resistance by incorporation of a siloxane–polyoxyalkylene copolymer.

Polyurethane–polysiloxane block copolymers provide antithrombotic coatings for blood-contacting biomedical devices (*35–39*), and other patent claims (*40*, *41*) are for use as selectively permeable membranes. Block copolymers exhibiting surface-active properties have been synthesized by Kotomkin and coworkers (*42*, *43*). Andrianov et al. (*44*) have reported on the thermal degradation of polyurethane–polysiloxane block copolymers. For further work on copolymers *see* References 45–47.

Polyurethane–polysiloxane graft copolymers have been prepared (*48*) by exposing a cross-linked polyurethane sheet to methyltrichlorosilane vapor and by reaction with primary and secondary amine groups in a polydimethylsiloxane (*28*).

Numerous publications (*49–51*) deal with the incorporation of silicones into polyurethanes, either to serve as flow agents or plasticizers, or to improve physical properties such as the flame resistance of polyurethane (PU) foams. Usually, the components are not cross-linked, and the silicone does not enter into chemical reaction with the polyurethane.

Some publications describe (*52*, *53*) polyurethane–polysiloxane blends that lead to the formation of IPNs. Klempner and coworkers (*52*) prepared

partial topologically interpenetrating networks from polyurethane urea and polysiloxanes. The networks were formed by combining equal weights of the two polymers as aqueous emulsions together with their cross-linking agents and stabilizers. The homogeneous mixtures were cast into films. The properties of the resulting materials were not outstanding.

Schurb and Evans (*53*) prepared "joined" IPNs from various diisocyanate prepolymers and an amine-modified polydimethylsiloxane by using a phenol–formaldehyde resin as a cross-linking agent. The reaction was performed in a common solvent, and the solvent was then evaporated and the substrate heated to effect the cure.

Arkles (*54*, *55*) described a process by which a blend of polysiloxane and a polyurethane was converted into a semi-IPN during processing. The polysiloxane network was formed by a platinum-catalyzed vinyl addition. Other publications dealing with polyurethane–polysiloxane blends include applications as imaging materials (*56*), composite foams with adhesive layers (*57*, *58*), and synthetic fabrics (*59*).

Sperling and Sarge (*60*) have investigated some aspects of polydimethylsiloxane–polystyrene and polydimethylsiloxane–poly(methyl methacrylate) IPNs. In addition, several patents (*61–63*) describe epoxy–siloxane systems.

In this study, three cold-curing PU–polysiloxane IPN systems are discussed from the morphological point of view. They were investigated by dynamic mechanical analysis (DMA) and by carbon-13 nuclear magnetic resonance (^{13}C NMR) spectroscopy. Such materials could ultimately lead to an improvement in tear strength over pure polysiloxanes and may be useful in certain biomedical applications.

Experimental

Three systems were investigated (*see* Box). Adiprene L-100 (Du Pont) is an isocyanate-terminated polyether urethane prepolymer (*64*). Silopren C18 (Compounding Ingredients) is an α,ω-hydroxy polydimethylsiloxane. The HPPMS prepolymer was supplied by Dow Corning Corporation. The characterization data for these prepolymers and for PPG are shown in Table I.

For all syntheses, the mole ratio of isocyanate to hydroxyl used in the PU network preparations and the hydroxyl-to-ethoxy ratio in the polysiloxane network

Three PU–Polysiloxane IPN Systems

System A: Adiprene L-100 + TMP → PU
Silopren C18 + TEOS → polydimethylsiloxane (PDMS)
System B: Adiprene L-100 + TMP → PU
α,ω-hydroxy polyphenylmethylsiloxane (HPPMS)
+ TEOS → polyphenylmethylsiloxane (PPMS)
System C: TDI + poly(propylene glycol) (PPG) + TMP → PU
HPPMS + TEOS → PPMS

Table I. Prepolymer Characterization

Prepolymer	$\bar{M}_n$ *(g/mol)*	$\bar{M}_w/\bar{M}_n$
Adiprene L-100	1,900	2.0
Silopren C18	15,000	2.4
HPPMS	620	—
PPG	425	—

NOTE: $\bar{M}_n$ equals the number-average molecular weight; $\bar{M}_w$ equals the weight-average molecular weight.

syntheses were 1 : 1. The required amount of TMP was dissolved in tetrahydrofuran (10% by weight of total constituents). Adiprene L-100, or the PPG plus TDI for system C, and the polysiloxane prepolymer were mechanically blended. TEOS and the TMP solution were then added to this mixture and vigorously mixed with a high-speed mechanical blender for 5 min. The catalyst (dibutyltin dilaurate for both networks in system A, and stannous octanoate for both networks in systems B and C) was then added and carefully blended into the mixture. The mixture was then thoroughly degassed prior to being poured into a Teflon-lined Perspex mold fitted with an aluminum spacer. The mold was then placed in a desiccator at 20 °C and left for 24–48 h for the sheets to cure fully. All sheets were placed under vacuum at 20 °C for at least 1 week prior to testing.

The homogeneous networks were prepared similarly. Their characterization data are shown in Table II. The possible side reactions in systems A, B, and C are believed to be negligible. Silanol and isocyanate groups can react slowly to form the silylurethane linkage that is sensitive to hydrolysis with atmospheric moisture (*30*). No deterioration of the properties of the IPNs was observed on storage in the atmosphere at room temperature, which indicates that this side reaction is negligible. TEOS and TMP only react under highly acidic conditions (*48*), and TEOS will only react with isocyanate groups at elevated temperatures (*49*). All the IPNs were synthesized at room temperature. The silanol group is much more acidic then the methylol group (*50*); consequently, the rate of the silanol–TEOS reaction is relatively fast.

The DMA measurements were made (Polymer Laboratories dynamic mechanical thermal analyzer) at a heating rate of 2 °C/min. The frequency used is quoted in each figure caption.

Table II. Homogeneous Network Characterization Data

System	*Network*	$\delta \times 10^{-3}$[a] $(J/m^3)^{1/2}$	$\bar{M}_c$[b] *(g/mol)*
A	PU	19.4	3,000
	PDMS	14.7	14,600
B	PU	19.4	3,000
	PPMS	18.5	1,000
C	PU	19.5	1,300
	PPMS	18.5	1,000

[a] Solubility parameter determined by swelling measurements.
[b] Average molecular weight between cross-links.

Proton-noise-decoupled ^{13}C NMR spectra (Varian Associates CFT-20 NMR spectrometer) were recorded at 20 MHz and at ambient probe temperature (approximately 40 °C). The materials were cured in an 8-mm tube that was then inserted into a standard 10-mm tube containing D_2O. The resulting sleeve of D_2O provided the internal lock signal. Chemical shifts are quoted relative to TMS at 0 ppm (parts per million) but were referenced initially to the D_2O lock frequency. Relevant instrument operating parameters for the materials, whose results are presented in Table III, were as follows: sweep width, 2000 Hz; pulse width, 19 μs (corresponding to a nuclear tip angle of approximately 80°); and acquisition time, 2 s (with no additional pulse delay). Spectra were sampled by using 8000 data points and were the results, normally, of 2000–3000 accumulations. An optical microscope, (Nikon, model L-Ke) was used for the measurement of domain diameters. The flash on the sheets molded for the DMA experiments was of the right thickness for microscopy.

Results and Discussion

System A. The substantial difference in solubility parameters of the parent networks (Table II) is likely to result in a high level of incompatibility. Therefore, to achieve materials with small phase dimensions, and, hence, a significant level of internetwork penetration, the networks should be cured as rapidly as possible. The rate of cure was limited by the necessity to degas the material before the rise in the viscosity of the system made this impossible.

From optical microscopy, these materials were, by IPN standards, grossly phase separated (*see* Figure 1). At 10% and at 90% by weight of PU, the average phase dimensions were ~ 10 μm, but this value rose to about 80 μm at the midcomposition point.

The IPNs containing 10 and 20% by weight of PU showed an enhanced initial modulus relative to that of the PDMS network. These tensile observations (*68*) are consistent with the gross multiphase morphology observed by light microscopy. At PU contents of 50% and above, this component is continuous, with isolated domains of cross-linked PDMS. At PDMS concentrations of 60% or more, the situation is reversed.

Table III. Line Width Measurements for System A

Composition (wt% PU)	*Line Width, $(\Delta\nu)_{1/2}$ (Hz)*	
	C-1	*C-2*
0	—	—
20	20.1	12.0
40	25.8	17.0
70	32.1	18.9
100	44.0	26.7
Chemical shift (ppm)	72.0	28.2

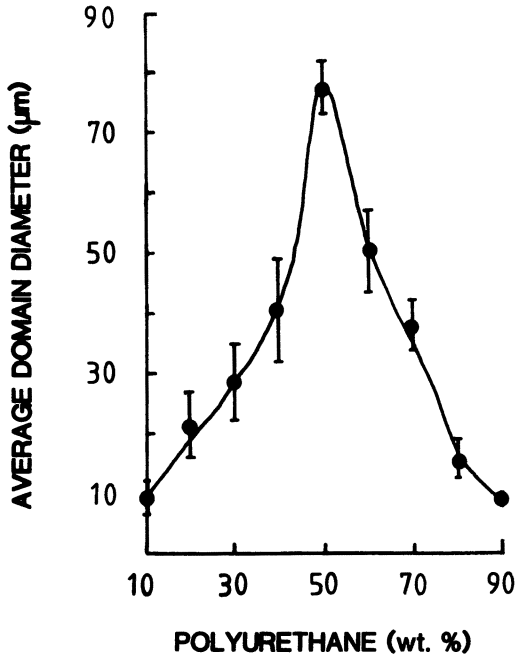

Figure 1. Average domain diameter versus composition for system A IPNs.

Figures 2 and 3 show the tan δ–temperature dispersion, the dynamic storage modulus (E'), and the dynamic loss modulus (E'') versus temperature plots for the polyether urethane homogeneous network. This material has been well characterized (*68*, *69*). The glass transition temperature (T_g) is apparent at − 20 °C in the tan δ–temperature plot. The minor transition at − 108 °C has been ascribed (*69*) to motions of methylene units via a Schatski-type mechanism (*70*). A small transition is also discernible in the E''–temperature plot (Figure 3) at − 68 °C and is probably associated with adsorbed moisture (*69*). For the PDMS network (Figures 4 and 5), three main features are apparent. The transition in tan δ at − 38 °C, corresponding to the catastrophic fall in E', is associated with crystalline melting (*21–23*). The T_g, at − 97 °C, (*21–24*) shows a rather low tan δ maximum value and a corresponding relatively minor drop in E' (approximately a factor of 5). At the crystalline melting point, E' is reduced almost two orders of magnitude. This observation is indicative of a high degree of crystallinity, which has been measured (*31*) by differential scanning calorimetry to be about 74%. A small peak centered in the tan δ–temperature plot at − 68 °C is interpreted as resulting from cold crystallization (*21*).

Figure 6 shows the E''–temperature curves for the IPNs containing 70, 50, 40, and 20% by weight of PU. The 70 and 50% PU IPNs show the

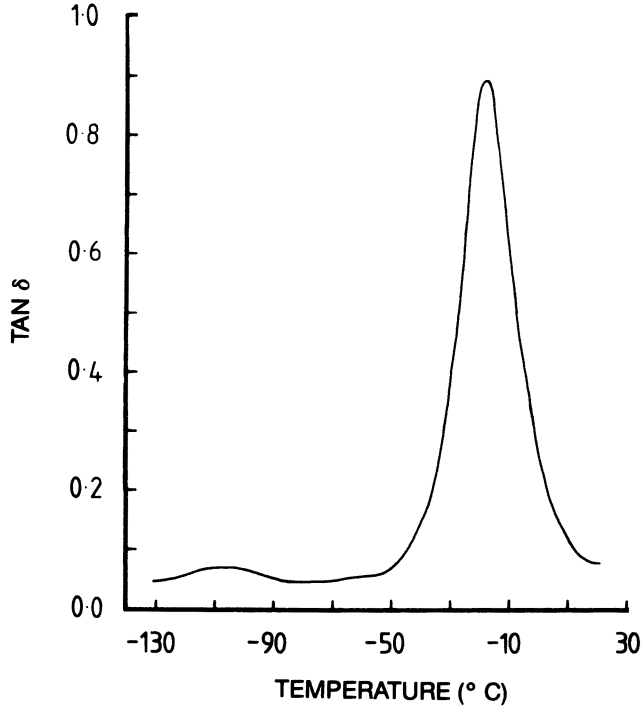

Figure 2. Plot of tan δ versus temperature (10 Hz) for the system A polyurethane network.

features of the PU homogeneous networks, whereas the blends containing 40 and 20% PU have curves similar to that of the pure PDMS network.

These results confirm the high level of incompatibility of this polymer pair; the dispersed phase is almost totally discontinuous. Figure 7 shows the tan δ–temperature behavior close to the compositional midpoint for two of the IPNs. For the 50% IPN, the PU T_g can be seen at − 20 °C, together with the minor transition at − 100 °C. For the 40% PU IPN, the PDMS T_g is apparent, together with the crystalline melting transition at − 38 °C. If the PU network were to any significant extent continuous throughout this latter sample, its T_g would be observable at − 20 °C. However, absolutely no evidence of such a transition is seen, and the contention that the domains are essentially mechanically isolated is supported.

Carbon-13 NMR studies of the cured homogeneous networks and IPNs were undertaken to gain an insight into the degree of interchain mixing at the phase boundaries. For proton-decoupled ^{13}C NMR spectra, the individual peaks can give information about the dynamics of individual carbon atoms in the polymer chain (*71*). For solid, glassy polymers below T_g, the strong carbon–proton dipolar interactions and the chemical shift anisotro-

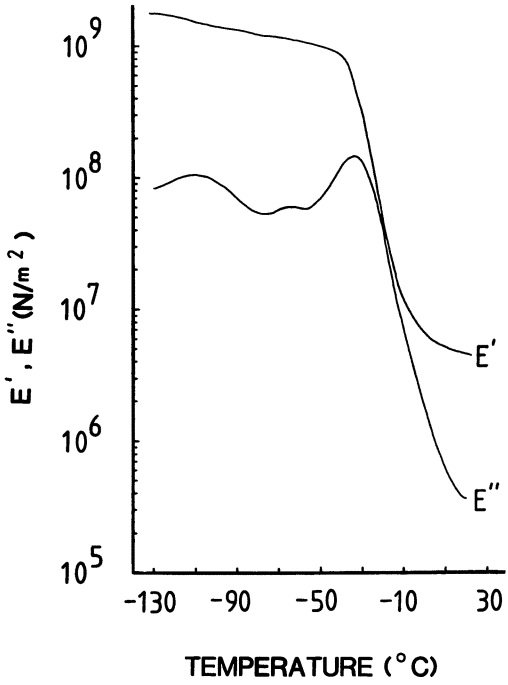

Figure 3. Dynamic storage modulus (E′) and dynamic loss modulus (E″) versus temperature (10 Hz) for the system A polyurethane network.

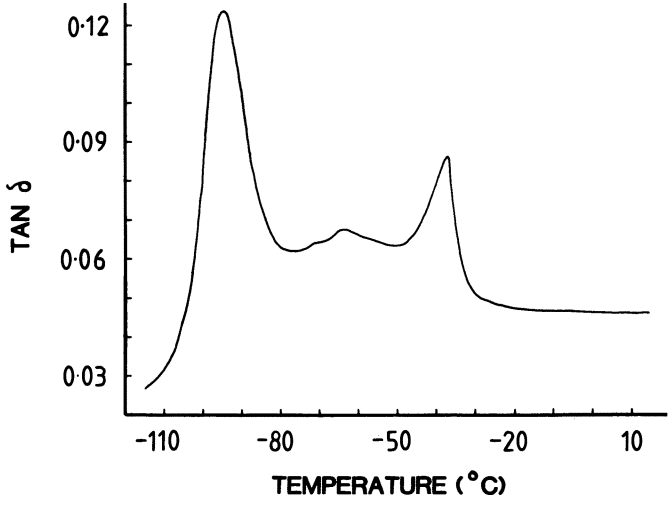

Figure 4. Plot of tan δ versus temperature (10 Hz) for the system A polydimethylsiloxane network.

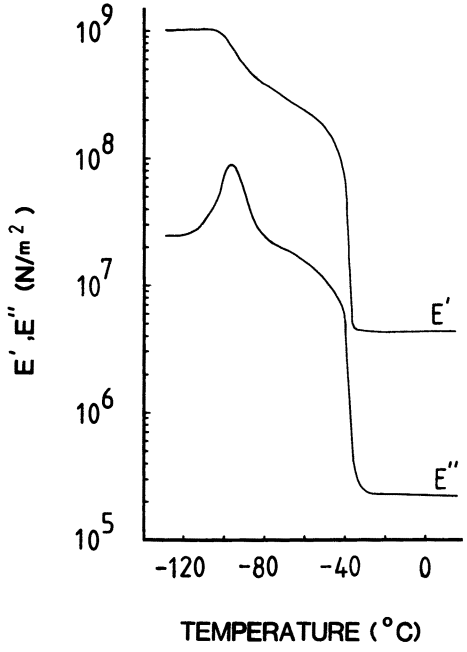

Figure 5. Dynamic storage modulus (E′) and dynamic loss modulus (E″) versus temperature (10 Hz) for the system A polydimethylsiloxane network.

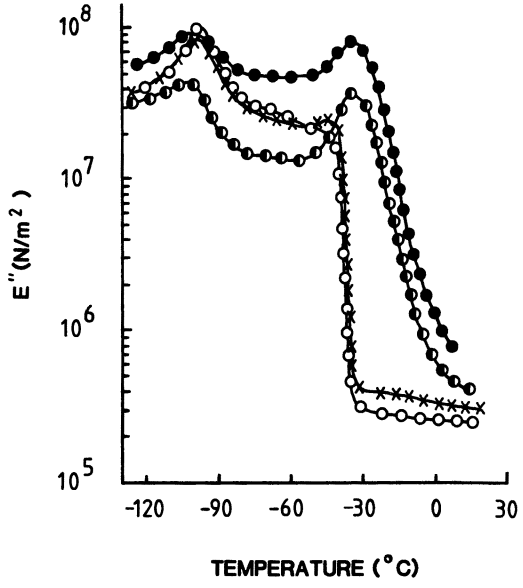

Figure 6. Dynamic loss modulus (E″) versus temperature (10 Hz) for the system A IPNs containing 70 (●), 50 (◐), 40 (×), and 20 (○) wt% polyurethane.

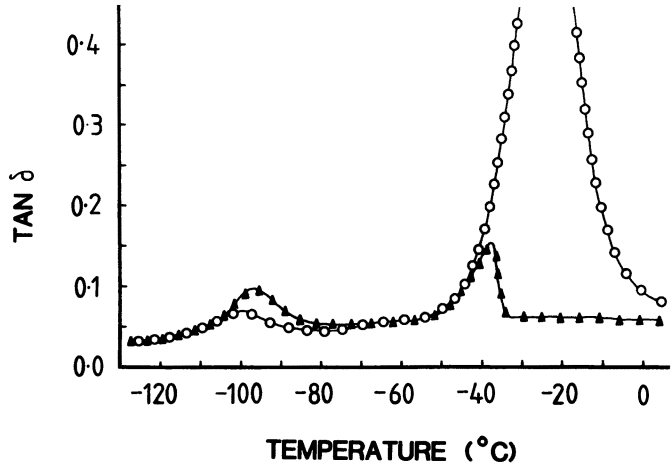

Figure 7. Plots of tan δ versus temperature (10 Hz) for the system A IPNs containing 50 (○) and 40 (▲) wt% polyurethane.

pies lead to very broad lines, typically of several kilohertz width; high resolution spectra can only be obtained on such solids by the use of magic-angle sample spinning and high-power decoupling (*72*).

However, for polymers above T_g, the chain mobility is often sufficient to produce considerable motional narrowing of the peaks, and a reasonably resolved spectrum can often be obtained under the instrumental conditions more usually associated with acquiring solution spectra. For solid polymers, the frequency of segmental motion is generally much lower than that for the motions of small molecules in solution. Thus, the spin–spin relaxation time (T_2) is less than the spin–lattice relaxation time (T_1) and continues to decrease as the isotropic correlation time (τ), describing the segmental motion, becomes longer (*73*). The relationship between the peak width at half height, $(\Delta\nu)_{1/2}$, and T_2 is

$$(\Delta\nu)_{1/2} = \frac{1}{\pi} T_2$$

Consequently, the more rapid the motion of a particular carbon atom in the chain is, the narrower the peak arising from that carbon in the spectrum will be. If a chain segment is associated with rigid domains, the linewidths will be greater than if the chain is in a softer, rubbery environment. In polymer blends and IPNs, the linewidths should give information about the extent of interfacial mixing. For a compatible one-phase blend, chemically identical carbons will have identical relaxation characteristics. For an incompatible blend with some degree of interfacial mixing, the different

mobilities of different regions of the polymer chains will be describable in terms of a distribution of relaxation times (*74*, *75*) among otherwise identical carbons. Thus, a peak in a spectrum of an incompatible blend can be regarded as a superposition of several peaks of varying width. A ^{13}C spectrum of a PU–PDMS IPN consists essentially of three peaks, two from the in-chain methylene ether and methylene carbons of the polyether (C-1 and C-2) (**I**) and one from the methyl carbon of the PDMS (C-3) (**II**).

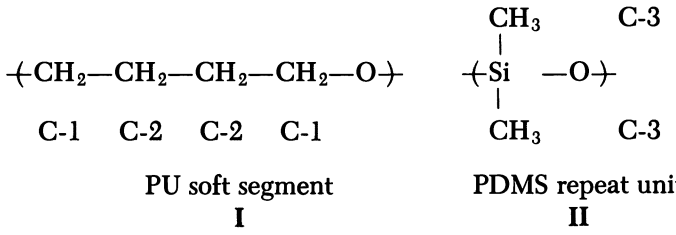

Table III shows the chemical shifts of the carbons and their linewidths for both the solid homogeneous networks and the IPNs. For the PU network, the linewidth for C-2 is consistently narrower than for C-1. This difference has also been observed in ^{13}C NMR studies (*76*) of Hytrel, which contain the same polyether repeat unit. In that system, the difference in linewidths may be due to additional low-frequency modes being available to the central carbons that are not available to the carbons directly bonded to oxygen. Alternatively, the chemical shift anisotropies for the two types of carbon may be different. The peak for C-3 is very narrow, and the linewidth approaches the value obtained in solution. This result is consistent with the flexibility of the siloxane backbone and the fact that the cross-link density is low and the cross-link sites do not restrict reorientation. Both C-1 and C-2 linewidths are narrowed by the addition of PDMS. This result suggests that, at the phase boundaries, polyether chain segments penetrate, to some extent, the polydimethylsiloxane phase and are consequently associated with a more mobile environment. At a 20% PU concentration, the domains are relatively small and have a radius of $\sim$ 10 μm. Furthermore, the PU is the dispersed phase. Thus, the surface area (*SA*)–volume (*V*) ratio of the PU component is relatively high. Consequently, a substantial proportion of the PU chains is in contact with the interface and provides opportunity for mixing. At 40% PU, the domain radius is higher (21 μm). Hence, the *SA*–*V* ratio is correspondingly lower, and a smaller fraction of polyether urethane chains is at the interface. Thus, the C-1 and C-2 peak widths increase, because they now reflect the relatively immobile carbons situated well within the PU domains. At 70% PU, the PU is now the continuous phase, and the contributions to linewidths from carbons at the interface are much less.

The peak width of C-3 is essentially constant at 3–4 Hz over the composition range. Therefore, the local effect of PU chains on the mobility of PDMS chains, probably predominantly methyl group rotation, is very slight

System B. Comparison of the solubility parameters (Table II) would suggest that system B might be more compatible than system A. To accelerate network formation and hence further improve the opportunity for mixing, stannous octanoate replaced dibutyltin dilaurate as catalyst in systems B and C.

Unlike system A, the IPNs were translucent at the compositional extremes but were again opaque in the midrange. However, individual phases were not, this time, discernible with light microscopy.

Figures 8 and 9 show plots of tan δ, E', and E'' versus temperature for the PPMS network. The only event observed is the glass transition at -16 °C.

In Figure 10, the broken lines indicate the T_g values of the homogeneous networks. For all three IPNs, both T_g values are evident at the homogeneous network transition temperatures, and incomplete miscibility but enhanced mechanical coupling between the components when compared with system A is indicated. Carbon-13 NMR spectra (Table IV) again indicate mixing.

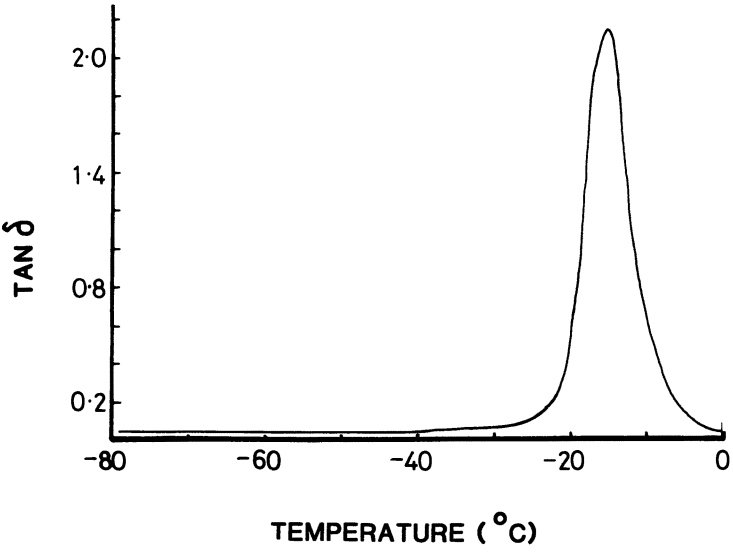

Figure 8. Plot of tan δ versus temperature (0.33 Hz) for the system B polyphenylmethylsiloxane network.

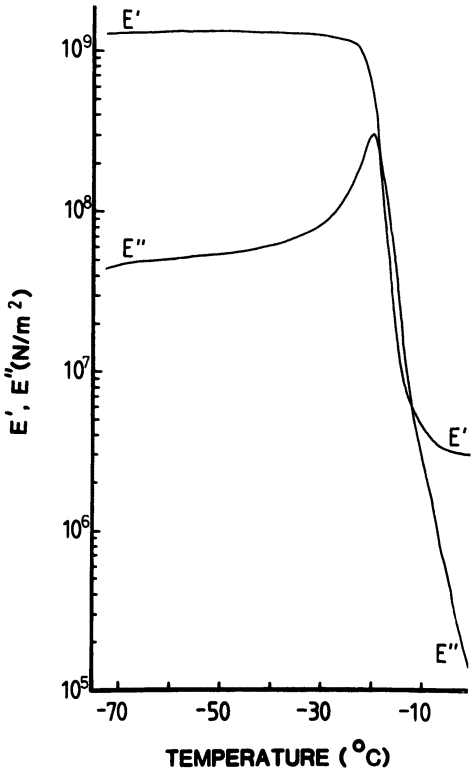

Figure 9. Dynamic storage modulus (E′) and dynamic loss modulus (E″) versus temperature (0.33 Hz) for the system B polyphenylmethylsiloxane network.

System C. To enhance mixing in system C, the value of $\bar{M}_c$ was further reduced by replacing the Adiprene L-100 based PU with the TDI–PPG–TMP system. Figure 11 shows that the T_g for this polymer was 30 °C.

The IPNs containing 50% or more of the PU component have only one T_g (Figure 12). The 30% PU IPN shows phase separation, and the T_g values occur at the temperatures of the constituent networks. Close examination of the tan δ–temperature data for the single T_g IPNs reveals an indication of a very slight shoulder at around the PU T_g value for both the 90% and the 70% PU IPNs. The narrowness of the glass transitions (tan δ–temperature) at half-peak height also indicates a high level of mixing. *See* Table V.

Figure 13 shows T_g plotted versus composition. For miscible polymer blends, examples exist of linear relationships (*77*, *78*) between T_g and composition as well as positive (*79*) and negative (*80*) deviations. For system C, the data may either lie rather poorly on a straight line or have a slightly

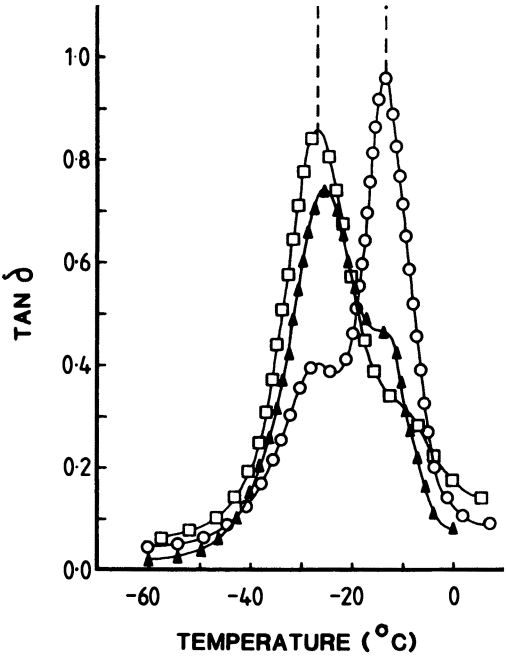

Figure 10. Plots of tan δ versus temperature (0.33 Hz) for the system B IPNs containing 70 (□), 50 (▲), and 30 (○) wt % polyurethane. The broken lines indicate the T_g *values of the individual networks.*

Table IV. Line Width Measurements for System B

Composition (wt % PU)	*Line Width,* $(\Delta\nu)_{1/2}$ *(Hz)*	
	C-1	*C-2*
0	—	—
50	21.6	17.3
70	24.0	16.9
100	44.0	26.7

positive deviation. Positive deviations are associated with strong intermolecular interactions. Exothermic heats of mixing have been measured (*79*) for such systems.

The Gordon–Taylor equation (*81*) may be used to relate the blend T_g to those of the constituents:

$$T_{g\text{blend}} = [W_a T_{ga} + k(1 - W_a) T_{gb}]/[W_a + k(1 - W_a)]$$

where T_{ga} and T_{gb} are the T_g values of the pure components, W_a and W_b are the corresponding weight fractions, and k is the ratio of the thermal

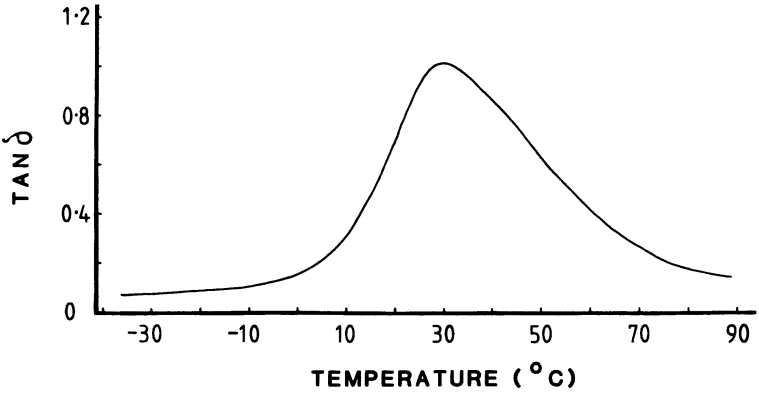

Figure 11. Plot of tan δ versus temperature (0.33 Hz) for the system C polyurethane network.

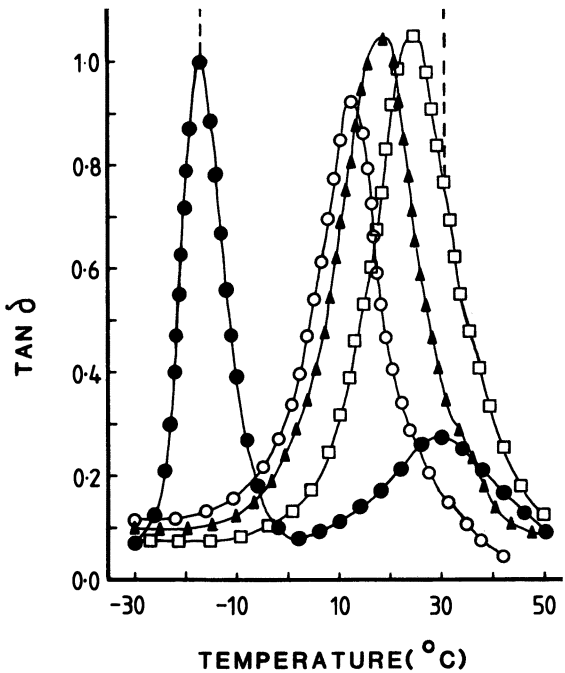

Figure 12. Plots of tan δ versus temperature (0.33 Hz) for the system C IPNs containing 90 (□), 70 (▲), 50 (○), and 30 (●) wt % polyurethane. The broken lines indicate the T_g values of the individual networks.

Table V. Glass Transition Temperature and Half-Peak Widths

Composition (wt % PU)	T_g *(°C)*	*Half-Peak Width (°C)*
100	30	29
90	24	20
70	18	19
50	13	15
0	−16	7

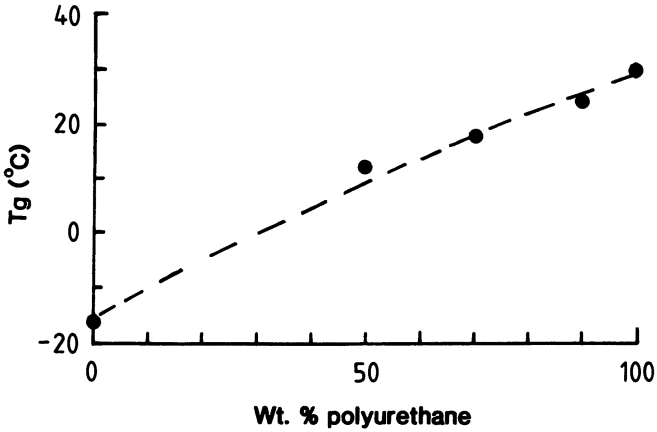

Figure 13. Glass transition temperature (T_g) versus composition for system C. The broken line is the Gordon–Taylor equation with k *equal to 1.2.*

expansion coefficients between the rubber and the glassy states of the component polymers. Certain systems, including poly(methyl methacrylate–poly(vinyl acetate) (*82*) and styrene-*co*-butadiene–polybutadiene (*83*), are miscible and obey the Gordon–Taylor equation. When k is 1.2, a reasonable fit is obtained with the experimental data.

Theories (*84*, *85*) have been developed to relate the modulus of a multiphase system to its composition. Davies (*86*, *87*) proposed the following relationship, which is claimed (*88*) to be suited to systems in which both components are continuous:

$$G^{1/5} = V_a G_a^{1/5} + V_b G_b^{1/5}$$

In this equation, G is the shear modulus of the composite, G_a and G_b are the shear moduli of the components, and V_a and V_b are the volume fractions of the components.

The Davies equation may be regarded as a special application of a general mixing equation presented by Nielsen (*89*), which often successfully predicts certain properties of composites when two continuous phases are present.

$$P^n = V_a P_a^n + V_b P_b^n \quad -1 < n < 1$$

In this equation, P is a physical property such as elastic modulus, and n is some function of the morphology and possibly of the property being measured.

With E' at 0 °C as the property of interest, this equation has been applied to the IPNs exhibiting compatibility. (*See* Figure 14.) In systems where both phase separation and dual phase continuity have been postulated, the Davies equation is obeyed (*90*) or a value of n close to 0.2 has been found (*85*). Clearly, the Davies equation does not fit these experimental data. Therefore, in these apparently compatible systems, the rule of mixtures (n equals 1) is more appropriate. The data fit is much better (curve 1), but the best fit is obtained with n equal to 0.8. If the materials in the incompatible range of compositions are included in the analysis, the Budiansky relation (*91*) is more appropriate.

Conclusions

For system A, in which the component networks have very different solubility parameters, gross phase separation occurred. Only the transition of the continuous component was observed in dynamic mechanical experi-

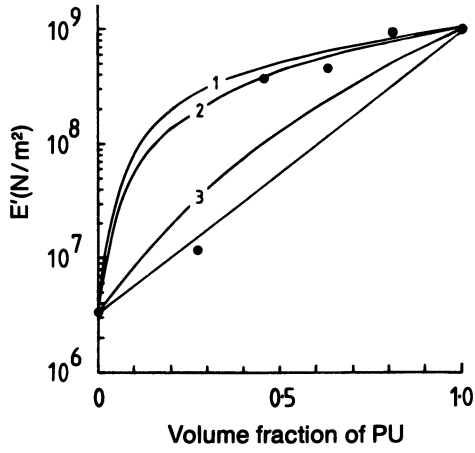

Figure 14. Plots of log E′ *versus composition (0 °C) for system C. Curves 1, 2, and 3 are for* n *equal to 1, 0.8, and 0.2, respectively, in the equation* $E'^n = V_a E_a'^n + V_b E_b'^n$ *(89).*

ments; therefore, mechanical coupling between the IPN constituents was at an exceptionally low level. However, by using ^{13}C NMR linewidth measurements, evidence was found of some network interpenetration at the phase boundaries.

For the PU–PPMS IPNs (systems B and C), the solubility parameters are much closer. In system B, the $\bar{M}_c$ of the polysiloxane network was reduced, and the rate of network formation increased. Materials were formed that were translucent at the compositional extremes, and T_g values of both constituents were now apparent in dynamic mechanical experiments. This enhanced coupling of the components was also detected by NMR.

When, in system C, the $\bar{M}_c$ of the PU component was reduced by using TDI–PPG–TMP, compatibility (only one T_g) was found for the IPNs containing 50% or more of PU.

Nomenclature

T_g	Glass transition temperature, °C; (subscript indicates specific component)
$\bar{M}_n$	Number-average molecular weight, g/mol
$\bar{M}_w$	Weight-average molecular weight, g/mol
$\bar{M}_c$	Average molecular weight between cross-links, g/mol
δ	Solubility parameter, $(J/m^3)^{1/2}$
$\tan \delta$	Loss tangent
E'	Dynamic storage modulus, N/m^2
E''	Dynamic loss modulus, N/m^2
T_1	Spin–lattice relaxation time, s
T_2	Spin–spin relaxation time, s
τ	Isotropic correlation time, s
$(\Delta\nu)_{1/2}$	Peak width at half height
W	Weight fraction (subscript indicates specific component)
k	Ratio of thermal expansion coefficients between rubber and glassy states
V	Volume fraction (subscript indicates specific component)
G	Shear modulus, N/m^2; (subscript indicates specific component)

Literature Cited

1. Millar, J. R. *J. Chem. Soc.* **1960**, *263*, 1311.
2. Siegfried, D. L.; Manson, J. A.; Sperling, L. H. *J. Polym. Sci.* **1978**, *16*, 583.
3. Sperling, L. H.; Friedman, D. W. *J. Polym. Sci.* **1969**, *7*, 425.
4. Sperling, L. H.; Arnts, R. R. *J. Appl. Polym. Sci.* **1971**, *15*, 2317.
5. Sperling, L. H.; Chui, T. W.; Hartman, C.; Thomas, D. A. *Int. J. Polym. Mater.* **1972**, *1*, 331.
6. Siegfried, D. L.; Thomas, D. A.; Sperling, L. H. *J. Appl. Polym. Sci.* **1981**, *26*, 177.
7. Frisch, H. L.; Klempner, D. *Macromol. Rev.* **1970**, *1*, 149.

8. Touhsaent, R. E.; Thomas, D. A.; Sperling, L. H. *J. Polym. Sci.* **1974**, *46C*, 175.
9. Touhsaent, R. E.; Thomas, D. A.; Sperling, L. H. In "Toughness and Brittleness of Plastics"; Deanin, R. D.; Crugnola, A. M., Eds.; ADVANCES IN CHEMISTRY SERIES No. 154, ACS: Washington, D.C., 1976.
10. Kim, S. C.; Klempner, D.; Frisch, K. C.; Frisch, H. L.; Ghiradella, H. *Polym. Eng. Sci.* **1975**, *15*, 339.
11. Kim, S. C.; Klempner, D.; Frisch, K. C.; Radigan, W.; Frisch, H. L. *Macromolecules* **1976**, *9*, 258.
12. Devia N.; Manson, J. A.; Sperling, L. H.; Conde, A. *Polym. Eng. Sci.* **1978**, *18*, 200.
13. Devia, N.; Manson, J. A.; Sperling, L. H.; Conde, A. *Macromolecules* **1979**, *12*, 360.
14. Devia, N.; Manson, J. A.; Sperling, L. H.; Conde, A. *Polym. Eng. Sci.* **1979**, *19*, 869.
15. Devia, N.; Manson, J. A.; Sperling, L. H.; Conde, A. *J. Appl. Polym. Sci.* **1979**, *24*, 569.
16. Devia, N.; Manson, J. A.; Sperling, L. H.; Conde, A. *Polym. Eng. Sci.* **1979**, *19*, 878.
17. Sperling, L. H. "Interpenetrating Polymer Networks and Related Materials"; Plenum: New York, 1981.
18. Novikov, A. S. *Soviet Rubber Technol. Engl. Transl.* **1960**, *12*, 4.
19. van der Weij, F. W. *Macromol. Chem.* **1980**, *181*, 2541.
20. Dolgov, O. N., Voronkov, M. G.; Grinblat, M. P. "International Polymer Science and Technology Monograph," No. 1; Rubber and Plastics Research Association of Great Britain: Shrewsbury, 1977.
21. Lee, C. L.; Johannson, O. K.; Flaningan, O. T.; Hahn, P. *Polym. Prepr. Am. Chem. Soc. Div. Polym. Chem.* **1969**, *10*, 1311.
22. Weir, C.; Lesser, W. H.; Wood, L. A. *Rubber Chem. Technol.* **1951**, *24*, 366.
23. Fischer, D. J. *J. Appl. Polym. Sci.* **1961**, *5*, 436.
24. Cowie, J. M. G. *Polym. Eng. Sci.* **1979**, *19*, 709.
25. Clark, A. J. F.; Shauer, A.; Eisenberg, A., presented at the 179th Natl. Meet. Amer. Chem. Soc., Houston, Tex., March 1980.
26. Polmanteer, K. E.; Hunter, M. J. *J. Appl. Polym. Sci.* **1959**, *1*, 3.
27. Schwartz, A. U.S. Patent 4 002 794, 1977.
28. Schurb, F. A.; Evans, J. L. U.S. Patent 3 997 702, 1976.
29. Kotomki, V. Y.; Lebeder, E. P.; Baburina, V. A.; Yasnikova, T. E.; Kercha, Y. Y. USSR Deposited Doc. SPSTL 13 Khp–D81, 1981, pp. 77–83.
30. Probst, M. W. J. French Patent 1 225 229, 1959.
31. Klein, P. G., Ph.D. Thesis, Univ. of Lancaster, Lancaster, United Kingdom, 1982.
32. Kuznetsova, V. P. *Sint. Fiz. Khim. Polim.* **1971**, *8*, 96.
33. Andrianov, K. A. *Sint. Svoistva. Uretanovykh Elastomerov* **1976**, *19*, 176.
34. Colquhoun, J. A.; Rauner, L. A. British Patent 1 541 637, 1975.
35. Ward, R. S. *Org. Coat. Plast. Chem.* **1980**, *42*, 227.
36. Nippon Zeon Co. Japanese Patent 82 82 347, 1982.
37. Kanegafuchi Chemical Industry Co. Japanese Patent 57 211 359, 1982.
38. Thoratec Laboratories Corp. Netherlands Appl. NL 81 00 975, 1981.
39. Lemm, W.; Buecherd, E. S. *Adv. Biomater.* **1982**, *3*, 459.
40. Nitto Electric Industrial Co. Japanese Patent 57 156 005, 1982.
41. Nitto Electric Industrial Co. Japanese Patent 83 163 403, 1983.
42. Kotomkin, V. Y.; Lebeder, E. P.; Baburina, V. A.; Yakovenko, D. F.; Yakovento, T. V.; Valetdinov, R. K.; Kercha, Y. Y. USSR SU 975 727, 1982.

43. Kotomkin, V. Y.; Baburina, V. A.; Lebedev, V. P.; Kercha, Y. Y. *Sint. Poliuretanov.* **1981**, *86*.
44. Andrianov, K. A.; Pavlova, S. A.; Tolchinskii, Y. I.; Zhuravleva, I. V.; Razmerova, M. V.; Misina, V. P.; Makrova, L. I.; Zhdanov, A. A. *Vysokomol. Soedin. Ser. B.* **1979**, *21*, 540.
45. Keberle, W.; Dieterich, D.; Reischl, A.; Schager, K. German Patent 1 248 287, 1967.
46. Smetankina, N. P. *Sint. Fiz. Khim. Polim.* **1971**, *8*, 34.
47. Andrianov, K. A. *Vysokomol. Soedin. Ser. B.* **1978**, *20*, 758.
48. Hodes, W. U.S. Patent 3 463 622, 1969.
49. Kolycheck, E. G. U.S. Patent 3 932 337, 1976.
50. Shah, K. G. U.S. Patent 3 932 337, 1976.
51. Kishimoto, K.; Imai, T. Japanese Patent 12 896, 1976.
52. Klempner, D.; Frisch, H. L.; Frisch, K. C. *J. Elastoplast.* **1971**, *3*, 2.
53. Schurb, F. A.; Evans, J. L. U.S. Patent 3 957 724, 1976.
54. Arkles, B. C. *Med. Device Diagn. Ind.* **1983**, *5*, 66.
55. Arkles, B. C. *Polym. Mater. Sci. Eng.* **1983**, *49*, 6.
56. Canon, K. K. Japanese Patent 80 143 561, 1980.
57. Shin-Etsu Chemical Industrial Industry Co. Japanese Patent 82 147 568, 1982.
58. Shin-Etsu Chemical Industry Co. Japanese Patent 82 77 558, 1982.
59. Kanebo Ltd. Japanese Patent 82 35 083, 1982.
60. Sperling, L. H.; Sarge, H. D. *J. Appl. Polym. Sci.* **1972**, *16*, 3041.
61. Clark, H. A. U.S. Patent 3 547 842, 1970.
62. Frisch, K. C.; Frisch, H. L.; Klempner, D. German Patent 2 153 987, 1970.
63. Foscante, R. E.; Gysegem, A. P.; Martinich, P. J.; Law, G. H. U.S. Patent 4 250 074, 1981.
64. Hourston, D. J.; Zia, Y. *Polymer* **1979**, *20*, 1497.
65. McLeod, G. D. U.S. Patent 4 086 096, 1978.
66. Blount, D. H. U.S. Patent 4 153 768, 1979.
67. West, R.; Baney, R. H. *J. Amer. Chem. Soc.* **1959**, *81*, 6145.
68. Ebdon, J. R.; Hourston, D. J.; Klein, P. G. *Polymer* **1984**, *25*, 1633.
69. Ferguson, J.; Hourston, D. J.; Meredith, R.; Patsavoudis, D. *Eur. Polym. J.* **1972**, *8*, 369.
70. Schatzki, T. F. *J. Polym. Sci.* **1962**, *57*, 496.
71. Schaefer, J. In "Structural Studies of Macromolecules by Spectroscopic Methods"; Ivin, K. J. Ed.; Wiley-Interscience: New York, 1976.
72. Schaefer, J.; Stejskal, E. O.; Buchdahl, R. *Macromolecules*, **1977**, *10*, 384.
73. Levy, G. C.; Lichter, R. L.; Nelson, G. L. "Carbon-13 Nuclear Magnetic Resonance Spectroscopy"; Wiley-Interscience: New York, 1980; Chap. 8.
74. Schaefer, J.; Sefcik, M. D.; McKay, R. A. *Macromolecules*, **1981**, *14*, 275.
75. Schaefer, J.; Sefcik, M. D.; Stejskal, E. O.; McKay, R. A. *Macromolecules* **1981**, *14*, 188.
76. Jelinski, L. W.; Schilling, F. C.; Bovey, F. A. *Macromolecules*, **1981**, *14*, 581.
77. Kargin, V. A. *J. Polym. Sci.* **1963**, *C4*, 1601.
78. Bartenev, G. M.; Kongarov, G. S. *Rubber Chem. Technol.* **1963**, *36*, 668.
79. Akiyama, S.; Komatsu, J.; Kaneko, R. *Polym. J.* **1975**, *7*, 172.
80. Koleske, J. V.; Lundberg, R. D. *J. Polym. Sci.* **1969**, *7*, 795.
81. Gordon, M.; Taylor, J. S. *J. Appl. Chem.* **1952**, *2*, 493.
82. Ichihara, S.; Komatsu, A.; Hata, T. *Polym. J.* **1971**, *2*, 640.
83. Zlatkevich, L. Y.; Nikolskii, V. G. *Rubber Chem. Technol.* **1973**, *46*, 1210.
84. Nielson, L. E. *J. Compos. Mater.* **1967**, *1*, 100.
85. Hourston, D. J.; Zia, Y. *J. Appl. Polym. Sci.* **1983**, *28*, 3745.

86. Davies, W. E. A. *J. Phys. D.* **1971**, *4*, 1176.
87. Davies, W. E. A. *J. Phys. D.* 1971, *4*, 1325.
88. Nielson, L. E. "Predicting the Properties of Mixtures"; Dekker: New York, 1978; Chap. 4.
89. Nielson, L. E. *J. Appl. Polym. Sci.* **1977**, *21*, 1579.
90. Hourston, D. J.; Zia, Y. *J. Appl. Polym. Sci.* **1983**, *28*, 3849.
91. Budiansky, B. *J. Mech. Phys. Solids* **1965**, *13*, 223.

RECEIVED for review November 15, 1984. ACCEPTED February 26, 1985.

12

Extraction Studies and Morphology of Physical–Chemical Interpenetrating Polymer Networks Based on Block Polymer and Polystyrene

JEAN-MICHEL WIDMAIER and SYLVIE DECROOCQ

Ecole d'Application des Hauts Polymères, Université Louis Pasteur, 4 Rue Boussingault, 67000 Strasbourg, France

Semi-interpenetrating polymer networks based on polystyrene–polyisoprene–polystyrene triblock polymer (physical network) and polystyrene (chemical network) were prepared by anionic polymerization. The chemical network was obtained by copolymerization of "living" polystyrene with divinylbenzene. The main variables were the average functionality of the permanent junction points and the average molecular weight between cross-links. The intent of the present investigation was to get information about the "quality" of the tridimensional structure formed in the second stage of synthesis (i.e., in the presence of another polymer). Therefore, the physical network was destroyed and removed out of the permanent network, and the amount of soluble material was determined as a function of time. The sol-fraction decreases with an increase in the average functionality of the branch points. At the same time, the speed of extraction is increased as the chain length decreases between cross-links. Surprisingly, the network most efficient in retaining the copolymer was the most disturbed as shown by the gel permeation chromatographic (GPC) analysis of the sol-fraction. Transmission electron microscopy of these physical–chemical interpenetrating polymer networks revealed various morphologies that depend upon the cross-link density of the permanent network.

POLYMER BLENDING IS A USEFUL TECHNIQUE to obtain properties not readily achieved in homopolymers. Most of the blends reported to date have been combinations of rubbery and glassy polymers. The mutual incompatibility of those polymers will lead to phase separation, and a variety of morphologies will exist throughout the sample. Properties of the polymer–polymer

0065–2393/86/0211/0195$06.00/0

mixtures depend on the phase morphology and phase interaction as well as composition. Rather than mechanical blends, chemical mixing has been elaborated to control the extent of segregation. Thus, in block or graft polymers, for instance, phase separation is limited to a microscopic scale because of the constraint of two polymers being covalently bonded. Interpenetrating polymer networks (IPNs) differ from other two-phase systems in that the extent of segregation is stabilized by cross-linking (*1*). Various types of IPNs and related materials have been synthesized either sequentially or simultaneously, and their properties have been studied.

Despite very intensive theoretical (*2*) and experimental (*3*) investigations, many questions concerning the microstructure of IPNs are still subject to controversy. As such systems are far from equilibrium, the morphology of IPNs, which affects their ultimate properties, is dependent on the history of the system or on the polymerization conditions. The extent of segregation depends on concurrent factors: the rate of network formation and the rate of interdiffusion of the components. IPNs are extremely complex systems, and the control of these two factors, which are of crucial importance, is very problematical.

In sequential synthesis, for example, the details of network formation in the presence of a preformed network are still incompletely known. The presence of another cross-linked or cross-linkable polymer (polymer I) produces additional complications in the kinetics and mechanisms of the polymerization of the second monomer, and a complicated structure will be obtained. But, thus far, the topology of the network formed in the second place (polymer II) has not been completely determined.

The reason for this lack may be poor investigational methods for tridimensional materials. Attempts to reach the network structure have been made by the use of labile cross-links (*4*). An additional difficulty may be a consequence of the free-radical process usually used in IPN syntheses. The free-radical cross-linking process induces a broad distribution of network chain lengths accompanied by chain scission as a consequence of different reactivity ratios of monomer and cross-linker. The nature of the distribution cannot be determined experimentally, and the empirical average molecular weight between cross-links ($\bar{M}_c$) is an approximation and has a limited significance.

We have tried to overcome these problems by anionic synthesis of physical–chemical IPNs. The anionic technique allows the introduction of cross-links after polymerization and therefore leads to uniform distribution of the cross-links. That end-linking technique, originally used by Rempp et al. (*5*) for the preparation of model networks, allows the choice of the length of the chain between two branch points with low fluctuation in average length. Homopolymer gels obtained (*6*) by that method exhibit satisfactory homogeneity.

A physical–chemical IPN is a combination of one nonpermanently cross-linked polymer with one covalently cross-linked polymer. Some examples (*7*) of physically cross-linked polymers are polystyrene–polybutadiene–polystyrene triblock polymers in which the glassy end blocks act as physical cross-links at room temperature. Semicrystalline polymers like polyethylene or polypropylene can be considered physically cross-linked polymers up to the melting point of the crystallites. In ionomers, too, the ionic groups form domains of noncovalent cross-links. Physical–chemical IPNs are also called pseudo-IPNs (*8*) or semi-IPNs (*1*).

In the IPNs discussed in this chapter, the polymer prepared first, or polymer I, was an ABA poly(styrene–isoprene) triblock polymer (SIS). Polymer II was polystyrene (PS) cross-linked with divinylbenzene (DVB) in the presence of polymer I. The SIS triblock polymer was chosen for two reasons: In a multiphase system, at least one of the phases must be easily recognized. Block polymers from styrene and dienes exhibit organized structures (*9*). Depending on the relative volume fraction of the two block components, three main types of domains have been found: spheres, cylinders, and lamellae. Hence, these identifiable structures will facilitate morphological studies of our samples by transmission electron microscopy (TEM). According to Scott (*10*), who was the first to apply the Flory–Huggins theory of polymer solutions (*11*) to mixtures of polymers, the compatibility of polymer pairs depends on their interaction parameter, which can be adequately estimated from the solubility parameters of the two polymers. Hence, by changing the composition (i.e., the solubility parameter of the block polymer) the state of miscibility between polymer I and polymer II can be varied.

The main variables of our study were as follows: Polymer I—by changing the composition of the triblock polymer, the miscibility between the two networks was modified and ranged from partially compatible to fully incompatible pairs. Polymer II—the change in $\bar{M}_c$ between two successive permanent junction points, thus modifying the constraints of interpenetration, and the change in the average functionality ($\bar{f}$), thus altering the fluctuation of the average position of the cross-links, affect polymer formation. One property that should be dependent on molecular topology is the diffusion of molecules in polymer matrices. We report the results of measurements on the rate of release of polymer I from the polystyrene network. The solvent-extractable part was analyzed, and the equilibrium swelling degree of the remaining network was measured for various cross-link densities. In addition, the morphology of these physical–chemical IPNs was examined by TEM.

Experimental

Polymerization and cross-linking were carried out in a closed apparatus under a slight pressure of dry nitrogen.

Materials. Benzene and tetrahydrofuran (THF) were purified for anionic use. Styrene and isoprene were repeatedly distilled on sodium wire. Divinylbenzene (DVB) was dried, and the inhibitor was removed by a column chromatographic technique using basic alumina. It was then stored over molecular sieves at 0 °C. A monomer composition of 50% DVB, 45% ethylvinylbenzene, and 5% diethylbenzene was reported by the manufacturer. The monofunctional initiator was *n*-butyllithium in solution in hexane and was used as received. The difunctional initiator was the disodium salt of α-methylstyrene tetramer and was prepared (*12*) by the reaction of α-methylstyrene with sodium in THF. Concentrations of the initiators were determined by titration, using the method of Eppley and Dixon (*13*).

Block Polymer Synthesis. Polystyrene–polyisoprene–polystyrene triblock polymers were prepared anionically at 50 °C by a three-step polymerization (*14*). Table I summarizes the results of their characterization by gel permeation chromatography (GPC) of PS precursors combined with compositional analysis by UV spectroscopy. The terminal PS blocks were assumed to be of equal molecular weight. The GPC measurements were made in THF at 25 °C (Waters Associates Model 200 instrument) with a series of six Styragel columns with exclusion limits ranging from 5×10^2 to 10^7 Å. GPC analysis demonstrated the complete absence of both PS and diblock material in all triblock polymers. The weight fraction of styrene blocks was determined in $CHCl_3$ solution from the UV absorption at 262 nm.

IPN Synthesis. Physical–chemical IPNs were obtained by anionic copolymerization of styrene and DVB, according to the method described by Rempp et al. (*5*) for the preparation of model networks. A detailed description is given in a previous publication (*15*). In brief, the SIS block polymer was first dissolved in a benzene–THF mixture. Then a "living" α,ω-dicarbanionic PS precursor was prepared at −35 °C in that solution by using the disodium α-methylstyrene tetramer. After completion of the polymerization, part of the solution was precipitated in methanol, washed, and dried. Its molecular weight was determined by GPC. A small amount of DVB was then added to the reaction medium, and rapid gelation occurred. The "living" gel was left for 12 h and termination of the remaining carbanions was accomplished with methanol to prevent chain-coupling reactions that can occur by exposure of the active chain ends to atmospheric oxygen (*16*). Polymerization was conducted over a range of concentrations from 4 to 15% by volume to avoid syneresis during gelation. The gels were dried under vacuum at 30 °C for several days until the samples were at constant weight.

A series of physical–chemical IPNs with various SIS block polymers was prepared by varying the molecular weight of the precursor (i.e., the molecular weight between cross-links) from 3,000 to 60,000 g/mol. The other variable was the num-

Table I. Molecular Characterization of the SIS Block Polymers

Sample	*Total Molecular Weight (g/mol)*	*Polyisoprene Content (%)*
Homopolystyrene	62,000	0
A	60,000	30
B	63,000	58
C	64,000	72

ber of connected polymer chains. The exact value of the functionality was unknown. However, as in the synthesis of star-shaped macromolecules (*17*), when the amount of DVB used per carbanionic chain-end increases, the size of the nodules of polyvinylbenzene and their average functionality increase as well. PS networks having 4–16 molecules of DVB per living end were prepared.

Solvent Extraction and Analysis. The IPNs were washed continuously with benzene in a Soxhlet apparatus to extract the nonpermanent network and the unattached PS chains. Extractions were performed to permit quantitative comparison between extraction efficiencies in homologous series. Reproductibility was within ± 1%. Aliquots of the benzenic solution were taken from time to time, evaporated to dryness, and weighed. The final sol-fraction was also analyzed by GPC. Once free of extractable constituents, the equilibrium swelling degree of the remaining gel was determined in benzene, according to the procedure described by Weiss et al. (*18*). The accuracy of that method is ~ 5%. TEMs were taken on a high-resolution electron microscope (Philips EM 300). IPN samples were stained by osmium tetroxide by following Kato's procedure (*19*).

Results and Discussion

To promote dual phase continuity, the SIS block polymer and the PS network were combined in a 50:50 ratio. Whatever the cross-link density, no solvent expulsion was observed when the gel was formed. This result was achieved by choice of suitable monomer and THF concentrations (*20*) during synthesis. Whereas pure homopolystyrene networks were transparent, the IPNs were opaque in the swollen state as well as in the dry state. Opaqueness indicates microsynereris, the formation of a dispersion of droplets of solvated block polymer inside the gel. The appearance of turbidity coincides with the gelation time. Cloudiness increases with the diene content of the triblock polymer and with the cross-link density of the PS network.

The extraction data are presented as plots of the weight fraction of soluble material as a function of time. The influence of the molecular weight of the elastic chains is shown in Figure 1. These curves correspond to IPNs with low polyisoprene content (series with polymer A). The amount of extractable polymer tends to an asymptotic value within 10 days of continuous extraction. However, the initial rate of disorption is of primary interest. Polymer I is extracted faster out of the PS network when the molecular weight between cross-links decreases. That behavior is the opposite of previous experimental (*21*) and theoretical (*22*) studies on the diffusion of polymer chains into a network. In these studies, the amount of linear polymer that may enter into a network decreases strongly when the mesh size of the network is decreased. Therefore, increasing amounts of microscopic defects (i.e., dangling chains and loops from incomplete cross-linking) are expected when $\bar{M}_c$ decreases. The efficiency of the linking reaction at both ends, which is usually the highest for the shortest chain lengths, should have drastically dropped because of the hindrance caused by the presence of polymer I.

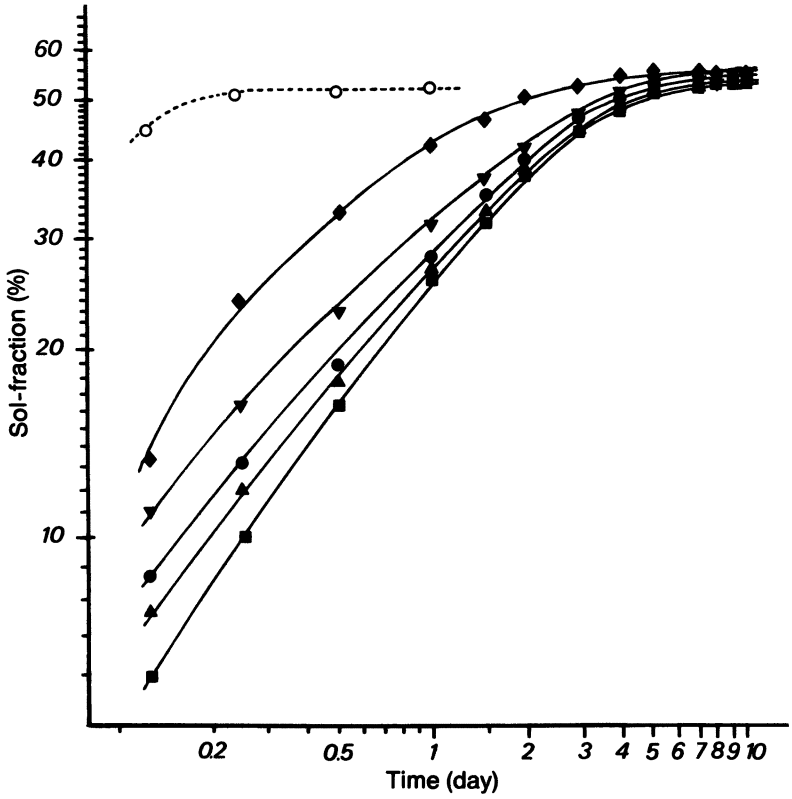

Figure 1. Time dependence of the sol-fraction extracted from physical-chemical IPNs with various $\bar{M}_c$. *A comparison with mechanical blends (------) is included. SIS block polymer A is polymer I. Key* ($\bar{M}_c$): ◆, *4500;* ▼, *9500;* ●, *21,000;* ▲, *35,000; and* ■, *60,000.*

Figure 1 also indicates that polymer I and polymer II must interpenetrate each other to a certain extent as previously suggested by the absence of macrosyneresis. The dotted line, which corresponds to a 1:1 mechanical blend of SIS block polymer and PS network, shows that the soluble part of the blend is almost immediately found in solution, whereas the extraction occurs more slowly when combined in IPN form.

The same dependence of the rate of extraction on the mesh size of the PS network was observed for samples with higher polyisoprene content (B and C as polymer I). The behavior of different IPNs with identical crosslink densities is shown in Figure 2. By increasing the diene content of the triblock polymer, the incompatibility between polymer I and polymer II increases, and network formation is disturbed. Consequently, the extraction curves are shifted to higher values.

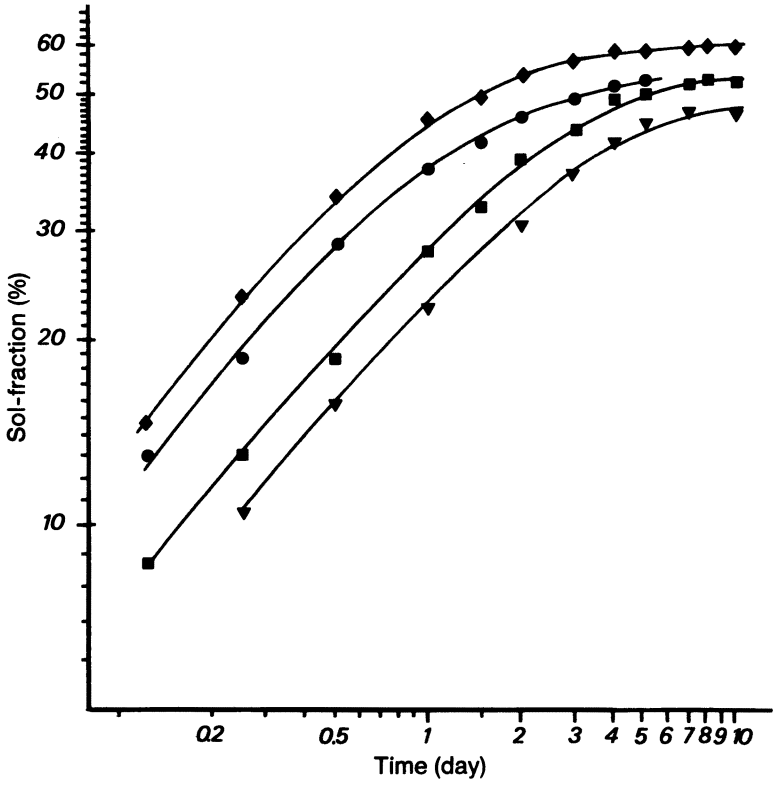

Figure 2. Time dependence of the sol-fraction extracted from physical-chemical IPNs as a function of the diene content (weight percent) of polymer I. Key: ▼ *, 0;* ■*, 30;* ●*, 58; and* ◆*, 72.*

For the previous series, the average functionality of the cross-links was low (4 DVB per living end), and the final amount of extracted material, mainly composed of SIS block polymer, roughly corresponds to the amount of polymer I. The slight difference observed (*see* Figure 2) may be a result of an increase in the amount of PS precursor chains not integrated into the network: 3.8 and 6.5% uncross-linked PS was found for samples with low and high diene content, respectively. However, when the average functionality increases (Figure 3), the amount of polymer that can be extracted significantly decreases. On the other hand, the release efficiency increases from the very beginning of the extraction. The fact that one cannot pass from one curve to the other by a simple shift implies that the kinetics of extraction do not depend on tortuosity and constriction effects only. The relatively large amount of soluble polymer found immediately in the solution does not consist of pure polymer I. Homopolystyrene chains, unable to be cross-linked because of sterical hindrance, are extracted first, and their

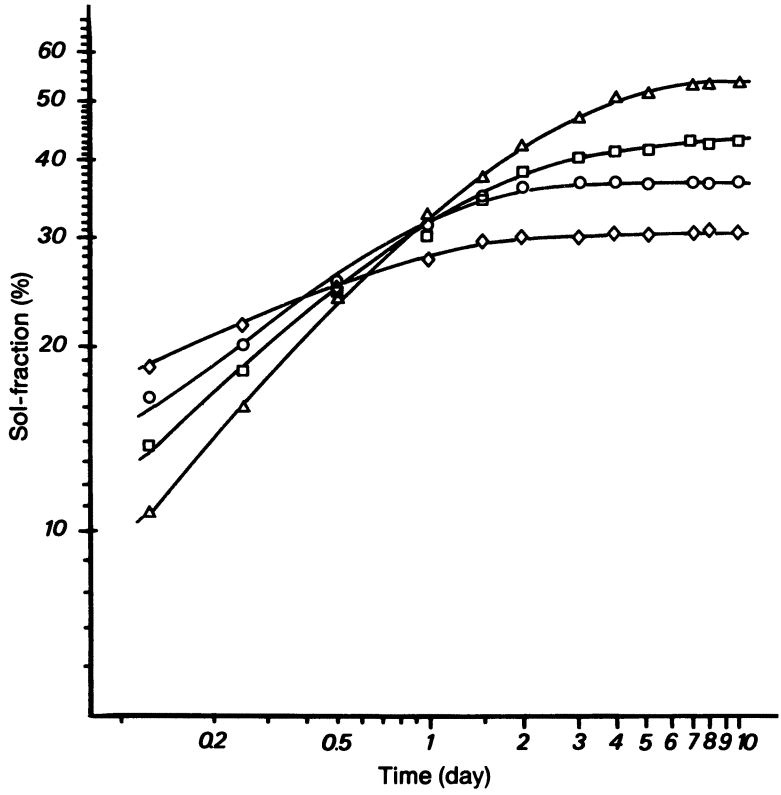

Figure 3. Time dependence of the sol-fraction extracted from physical-chemical IPNs with various functionalities. Key: (molecules of DVB per chain end) △, 4; □, 8; ○, 12; and ◇, 16.

amount reflects the effect of the presence of the triblock polymer during formation of network II. This observation is corroborated by the GPC analysis of the sol-fraction.

Typical chromatograms are displayed in Figure 4. The elution curve of the sample taken before addition of DVB is formed by two peaks corresponding to the SIS block polymer, which is eluted first, and to the network precursor. The polydispersity of the PS remains low (around 1.2) in spite of the presence of the triblock polymer. At low functionality, the extracted material is formed of SIS block polymer, as already mentioned. Free PS precursor chains appear as a shoulder on the GPC curve. The intensity of the peak corresponding to the PS precursor increases as the amount of DVB increases. This increase indicates that more and more chains are not linked at both ends in the course of the reaction and therefore remain soluble (i.e., extractable). Hence, the network formed with a large amount of DVB must be inhomogeneous and of poor "quality". In addition, because of the

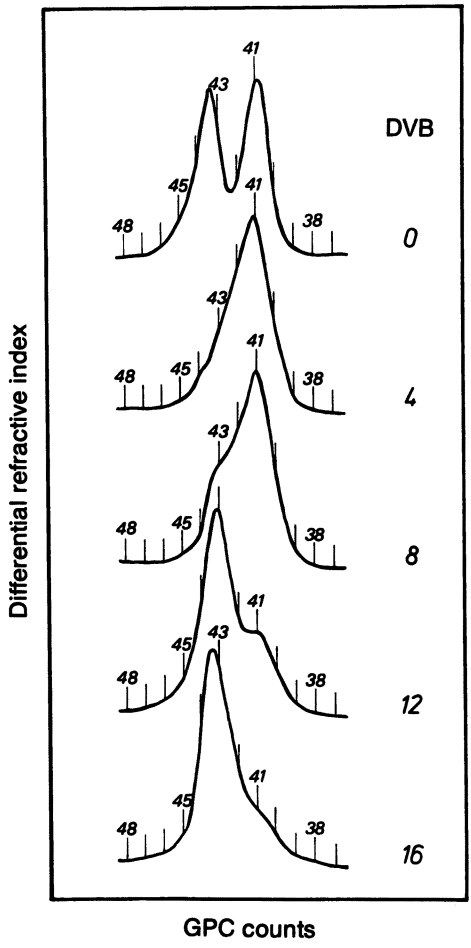

Figure 4. GPC chromatograms of final sol-fractions as a function of functionality (polymer I at 40.9; PS precursor [20,000 g/mol] at 43.4).

high average functionality of the junction points that were formed, the tighter network becomes more efficient in retaining the block polymer. Only 25–30% of the soluble material (*see* Figure 3), mainly uncross-linked PS (*see* Figure 4, bottom), can be extracted compared with the initial 50% SIS block polymer content. That effect is only due to mechanical interlocking of the chains and not to accidental grafting between polymer I and polymer II, which is unlikely in standard anionic synthesis (23).

Another parameter that should reflect the defects of the tridimensional structure is the degree of swelling. Measurements were limited to transluscent gels (4 DVB per living end) completely freed of linear chains. Figure 5 shows the variation of the equilibrium swelling degree by volume

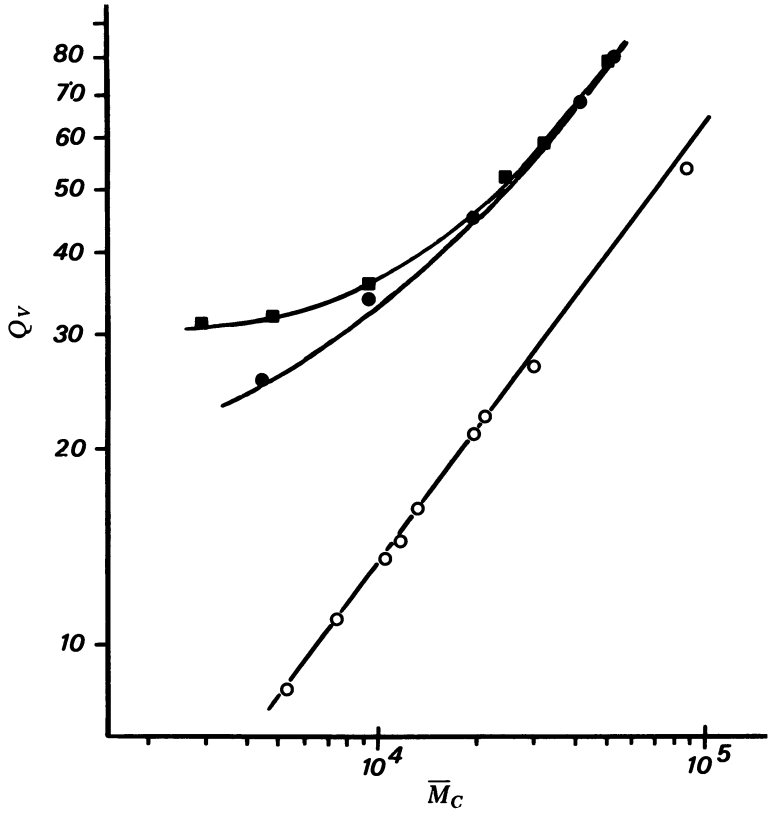

Figure 5. Effect of chain length between cross-links on the equilibrium swelling degree for model PS networks (○) and for remaining PS networks (after extraction) prepared with 4 DVB per living end. Key: ●, SIS block polymer A as polymer I; and ■, SIS block polymer C as polymer I.

(Q_v) of the remaining PS network as a function of $\bar{M}_c$. In the same figure, values of Q_v of model PS networks (*21*) are reported for comparison. The extracted IPN swells significantly more than the pure network. Because of cavitations formed in the sample after polymer I removal that may entrap some liquid during swelling, values of Q_v are not an accurate measure of the network properties. However the important point to emphasize is that Q_v, which should be a linear function of the molecular weight of the elastic chains on a log–log scale (*18*), deviates from a straight line when $\bar{M}_c$ decreases. The level of the deviation is a function of the composition of the SIS block polymer (i.e., the incompatibility factor between polymer I and polymer II). Clearly, networks formed in the presence of a polymer have more defects than ones prepared in pure solvent.

The morphology of several physical–chemical IPNs was investigated by TEM. The presence of polyisoprene as part of the triblock polymer produces contrast between polymer I and polymer II after exposure to osmium tetroxide vapors. The structure of our end-linked IPNs is quite different from similar radical IPNs (*24*) and depends upon the PS cross-link density. The first series of micrographs (Figures 6–8) shows the structure of samples with decreasing $\bar{M}_c$. In Figure 6, the molecular weights of the SIS block polymer and of the PS precursor chains are identical. The black points, which correspond to the polyisoprene phase, are randomly dispersed through the sample. Polymer I and polymer II are, therefore, intimately mixed. When the mesh size of the PS network decreases (Figure 7), the dispersion becomes very irregular, and polymer I, recognizable by its typical morphology, gathers in what seems to be network defects. Figure 8, which corresponds to the IPN with the lowest $\bar{M}_c$, shows isolated large areas of SIS block polymer. The origin of the very sharp segregation between both components must be topological inhomogeneity and gross phase separation during cross-linking.

As may be expected, an identical change in the morphology occurs when the average functionality is increased for a fixed $\bar{M}_c$. Variations in the composition of the SIS block polymer also have an effect upon the final structure (Figure 9). Figure 10 gives an example of the low "quality" of the

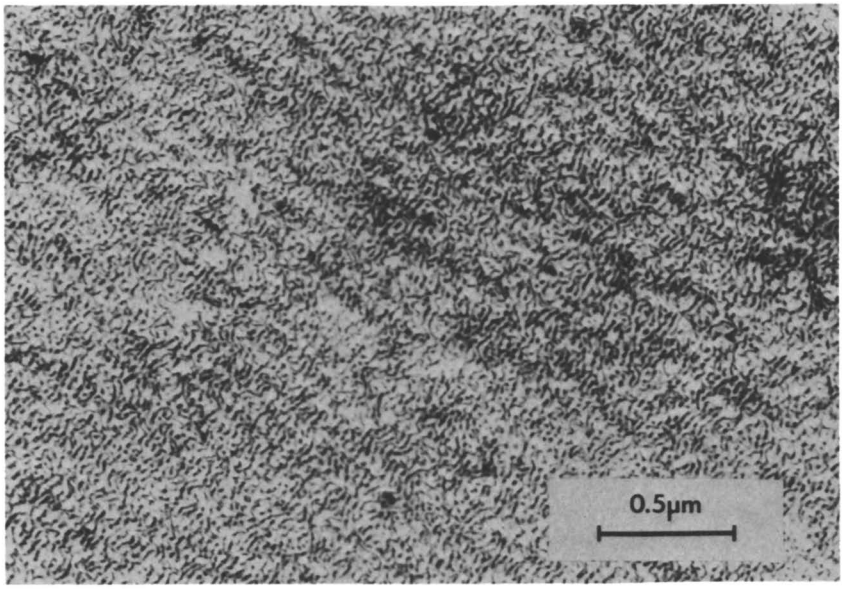

Figure 6. TEM of a physical–chemical IPN. Polymer I is SIS block polymer A, and polymer II $\bar{M}_c$ *is 60,000 g/mol.*

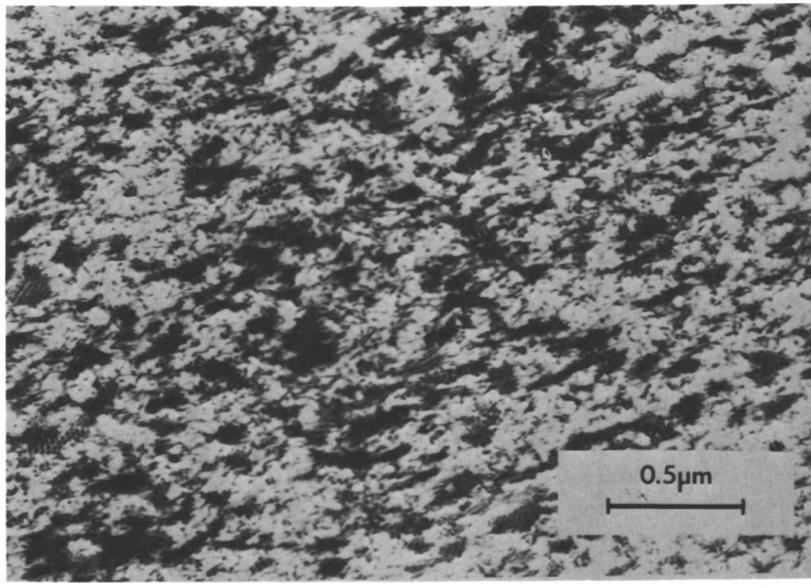

Figure 7. TEM of a physical–chemical IPN. Polymer I is SIS block polymer A, and polymer II $\bar{M}_c$ *is 17,000 g/mol.*

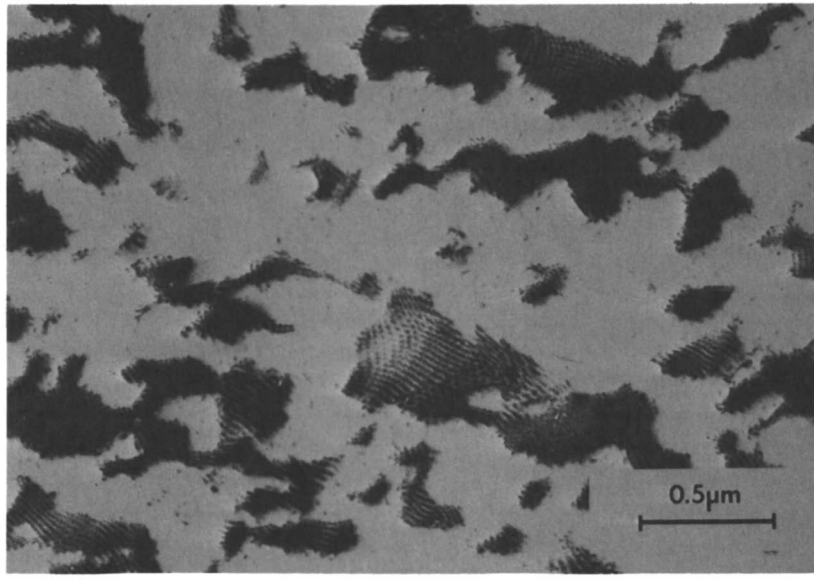

Figure 8. TEM of a physical–chemical IPN. Polymer I is SIS block polymer A, and polymer II $\bar{M}_c$ *is 4500 g/mol.*

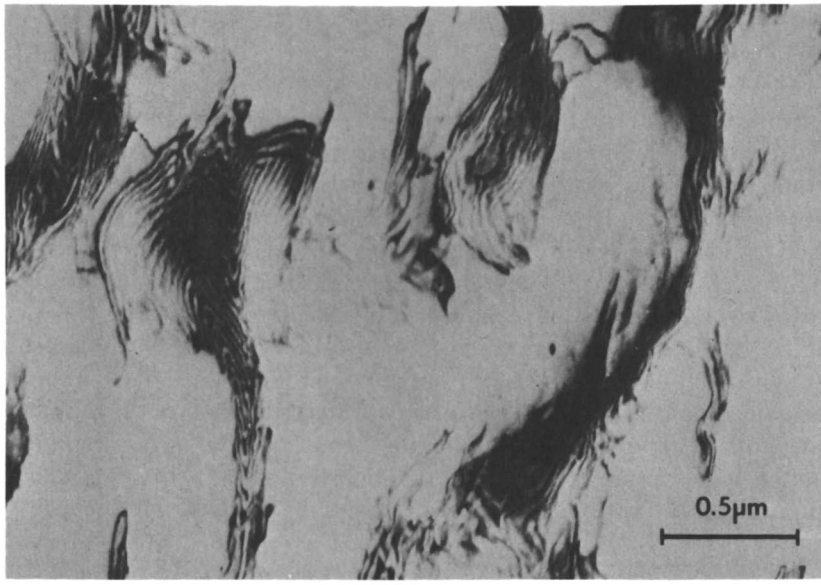

Figure 9. TEM of a physical–chemical IPN. Polymer I is SIS block polymer B, and polymer II $\bar{M}_c$ *is 20,000 g/mol.*

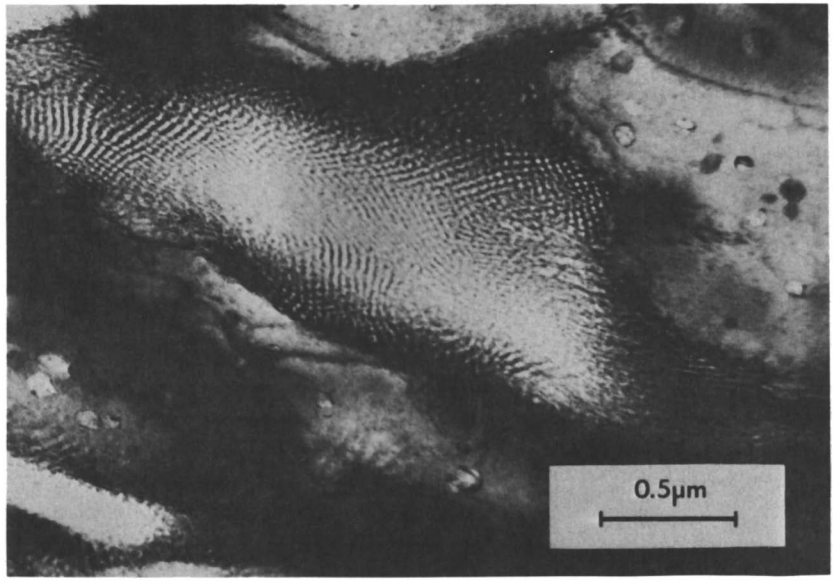

Figure 10. TEM of a physical–chemical IPN. Polymer I is SIS block polymer C, and polymer II $\bar{M}_c$ *is 4800 g/mol. The functionality is 16 DVB per living end.*

tridimensional structure found in the system with a high polyisoprene content in polymer I associated with a densely cross-linked network II.

Conclusion

Contrary to random methods of network preparation involving radicals, the end-linking technique gives more precise samples to investigate. This method was used to synthesize well-characterized physical–chemical IPNs. The formation and, hence, the topology of network II are significantly affected by the presence of polymer I. The tridimensional structure formed in the second stage of the sequential synthesis deviates all the more from an ideal network and must have more and more defects as the cross-link density (i.e., the reciprocal of the molecular weight of the elastic chains associated with the functionality) of the network increases. Variations in the degree of incompatibility of the two components also influence the formation of network II. Therefore, very inhomogeneous material forms at a microscopic level, especially for tightly cross-linked samples. This conclusion is supported by the various morphologies found by electron microscopy.

Nomenclature

$\bar{M}_c$ Average molecular weight between cross-links
$\bar{f}$ Average functionality of the cross-links
Q_v Equilibrium swelling degree by volume

Literature Cited

1. Sperling, L. H. "Interpenetrating Polymer Networks and Related Materials"; Plenum: New York, 1981; Chaps. 1–2.
2. Sperling, L. H.; Widmaier, J. M.; Yeo, J. K.; Michel, J. In "Polymer Alloys III"; Klempner, D. L.; Frisch, K. C., Eds.; Plenum: New York, 1983; p. 191.
3. Huelck, V.; Thomas, D. A.; Sperling, L. H. *Macromolecules* **1972**, *5*, 340.
4. Widmaier, J. M.; Sperling, L. H. *Macromolecules* **1982**, *15*, 625.
5. Weiss, P.; Hild, G.; Herz, J.; Rempp, P. *Makromol. Chem.* **1970**, *135*, 249.
6. Belkebir-Mrani, A.; Beinert, G.; Herz, J.; Mathis, A. *Eur. Polym. J.* **1976**, *12*, 243.
7. Dawkins, J. V. In "Block Copolymers"; Allport, D. C.; Janes, W. H., Eds.; Appl. Sci.: London, 1973; p. 409.
8. Frisch, H. L.; Frisch, K. C.; Klempner, D. *Pure Appl. Chem.* **1981**, *53*, 1557.
9. Molau, G. E. In "Colloidal and Morphological Behavior of Block and Graft Copolymers"; Plenum: New York, 1971.
10. Scott, R. L. *J. Polym. Sci.* **1952**, *9*, 423.
11. Flory, P. J. "Principle of Polymer Chemistry"; Cornell Univ. Press: Ithaca, N.Y., 1962; Chap. 12.
12. Lee, C. L.; Smid, J.; Szwarc, M. *J. Phys. Chem.* **1962**, *66*, 904.
13. Eppley, R. L.; Dixon, J. A. *J. Organomet. Chem.* **1967**, *8*, 176.
14. Fetters, L. J. In "Block and Graft Copolymerization"; Ceresa, R. J., Ed.; Wiley: London, 1972; Vol. 1, p. 99.
15. Widmaier, J. M.; Hubert, J.; Meyer, G. C. *J. Polym. Sci. Polym. Lett. Ed.* **1981**, *19*, 463.
16. Fetters, L. J.; Firer, E. M. *Polymer* **1977**, *18*, 306.

17. Worsfold, D. J.; Zilliox, J. G.; Rempp, P. *Can. J. Chem.* **1969**, *47*, 3379.
18. Weiss, P.; Herz, J.; Rempp, P. *Makromol. Chem.* **1971**, *141*, 145.
19. Kato, K. *J. Polym. Sci. Part B* **1966**, *4*, 35.
20. Bates, F. S.; Cohen, R. E. *Macromolecules* **1981**, *14*, 881.
21. Hild, G.; Froelich, D.; Rempp, P.; Benoit, H. *Makromol. Chem.* **1972**, *151*, 59.
22. Brochard, F.; *J. Phys.* **1981**, *42*, 505.
23. Morton, M.; Fetters, L. J. *Macromol. Rev.* **1967**, *2*, 71.
24. Curtius, A. J.; Covitch, M. J.; Thomas, D. A.; Sperling, L. H. *Polym. Eng. Sci.* **1972**, *12*, 101.

RECEIVED for review November 15, 1984. ACCEPTED June 27, 1985.

13

Two- and Three-Component Interpenetrating Polymer Networks

D. KLEMPNER[1], K. C. FRISCH[1], H. X. XIAO[1], E. CASSIDY[2], and H. L. FRISCH[2]

[1]Polymer Institute, University of Detroit, Detroit, MI 48221
[2]Department of Chemistry, State University of New York at Albany, Albany, NY 12222

Two-component interpenetrating polymer networks (IPNs) with opposite-charge groups (tertiary amine and carboxyl groups) were synthesized from polyurethanes and polymethacrylates, and their properties and morphologies were investigated. The improved molecular mixing in these IPNs, as determined by differential scanning calorimetry (DSC) and scanning electron microscopy (SEM), may be due to the influence of the opposite-charge groups in these systems. A comparison was made between full IPNs, pseudo-IPNs, graft copolymers, and related homopolymers from polyurethanes and epoxies. Increased compatibility in full IPNs and graft copolymers was observed by means of DSC, SEM, and dynamic mechanical spectroscopy. Three-component IPN systems made from polyurethanes, epoxies, and polymethacrylates containing charge groups were synthesized. They included full IPNs, pseudo-IPNs, and graft IPNs. The opposite-charge-containing IPNs exhibited better mechanical properties than the IPNs containing similar charge groups and no charge groups. A single-phase morphology was observed for the full IPNs and graft IPNs with opposite charge groups.

INTERPENETRATING POLYMER NETWORKS (IPNS) (*1–6*) are unique blends of cross-linked polymers containing essentially no covalent bonds, or grafts, between them. True IPNs are also homogeneous mixtures of the component polymers.

IPNs possess several interesting characteristics in comparison to normal polyblends. Formation of IPNs is the only way of intimately combining cross-linked polymers; the resulting mixture exhibits (at worst) only limited phase separation. Normal blending or mixing of polymers results in a multiphase morphology because of the well-known thermodynamic immiscibility of polymers. However, if mixing is accomplished simultane-

0065–2393/86/0211/0211$06.00/0

ously with cross-linking, phase separation may be kinetically controlled by permanent interlocking of entangled chains.

IPNs synthesized to date exhibit varying degrees of phase separation, dependent principally on the miscibility of the polymers. With highly incompatible polymers, the thermodynamic forces leading to phase separation are so powerful that it occurs substantially before the kinetic ramifications can prevent it. In these systems, only small gains in phase mixing occur. In systems in which the polymers are more miscibile, phase separation can be almost completely circumvented. Complete miscibility is not necessary to achieve complete phase mixing, because the permanent entanglements (catenation) can effectively prevent phase separation. With intermediate miscibility, intermediate and complex phase behavior results. Thus, IPNs with dispersed phase domains ranging from a few micrometers (immiscible) to a few tens of nanometers (intermediate) (*4*) and, finally, to those with no resolvable domain structure (complete mixing) (*8–10*) have been reported.

Recent studies on IPNs at the University of Detroit's Polymer Institute have encompassed a variety of areas, including effects of molecular weight of prepolymers and extent of cross-linking on the morphology and properties and the effects of charge groups on intentional grafts, pseudo-IPNs, and three-component IPNs. The polymers studied were polyurethanes, acrylic polymers and copolymers, and epoxies.

Experimental

Preparation. Preparation of all the various IPNs followed the same basic procedure. The urethane prepolymer was mixed with a prepolymer syrup of acrylic (~10–20% conversion) or with an epoxy resin together with chain extenders, cross-linking agents, and catalysts. This combination was then mixed, and sheet specimens were prepared by casting in aluminum molds and curing at 100 °C on a platen press. In some systems, solvents were used to facilitate mixing. The solvents were then removed by allowing the mold to remain open overnight. In ternary IPNs, a calculated amount of polyacrylic syrup and 1% BPO (benzoyl peroxide) were added to a dry disposable plastic beaker. The mixture was stirred at 60 °C until the BPO dissolved. In a second beaker, the PU (polyurethane) prepolymer and epoxy resin were homogeneously mixed at 60 °C. At the same time, a third beaker containing calculated amounts of 1,4-BD (1,4-butanediol), TMP [2,2-bis(hydroxymethyl)-1-butanol], T-12 (dibutyltin dilaurate), Epon D (tertiary amine salt), and TMPTMA [1,1,1-[tris(methacryloyloxy)methyl]propane] was degassed at 60 °C. The contents of all three beakers were homogeneously mixed for 90 s at 60 °C with a high-torque stirrer. To remove trapped air and moisture, a 1-mmHg vacuum was applied for 6 min, and mixtures were placed in aluminum molds and cured in the same manner described for the preparation of PU networks.

Three-component pseudo-IPNs were prepared in the manner described for IPNs except that the PU prepolymer was chain-extended with 1,4-BD to give a NCO:OH value of 1.05. The result was the formation of a linear thermoplastic polyurethane (LUO). In another system, TMPTMA was omitted from the formulation, and a linear polyacrylic structure (LA) was formed. Finally, a pseudo-IPN

containing only one cross-linked polymer (epoxy) was prepared by removing TMP and TMPTMA from the formulation.

Three-component graft-IPNs were prepared in the manner of IPN preparation except that the acrylic prepolymer syrup was replaced by a [(thiocarbonyl)amino]ethyl methacrylate (IEM) monomer that contains a methacrylate and an isocyanate group. Also, more 1,4-BD and TMP were used in the chain-extension and cross-linking of the PU prepolymer, in order to take into account the pendant isocyanate groups of the IEM. Therefore, isocyanate groups of the IEM monomer were allowed to react with the primary hydroxyl groups of 1,4-BD and TMP and graft with the PU prepolymer. This mixture was simultaneously cured with epoxy and 10% Epon D to form the graft IPN.

The urethane prepolymers were prepared by reacting a polyol with excess diisocyanate at 60–80 °C (under dry conditions in nitrogen) until the isocyanate content reached the desired level, as determined by the *n*-butyl-1-butanamine titration method (*7*). All polyols were first dried at 80 °C under vacuum for 16 h.

The acrylic prepolymers were prepared by heating the washed and distilled monomer at 60–80 °C using dibenzoyl peroxide as a catalyst. Cross-linking was accomplished by curing with ethylene glycol dimethacrylate or 2-ethyl-2-(hydroxymethyl)-1,3-propanediol trimethacrylate.

In pseudo-IPNs, the cross-linking agent was omitted from the formulation. Various amounts of different charge-group-containing monomers were employed in these syntheses for two- as well as three-component IPNs in order to deduce the effects of secondary valence forces on the morphology and properties.

Characterization of Polymers. The durometer hardness was measured according to ASTM[1] D-2240 at room temperature with Shore A and Shore D hardness testers. The modulus at 100% elongation (M_{100}), modulus at 300% elongation (M_{300}), ultimate tensile strength (TS), and elongation at break (E) were measured at room temperature on a tensile tester (Instron Model 1130). ASTM D-638 procedure was followed, and a cross-head speed of 2 in./min was used.

The mechanical spectra were run on a dynamic viscoelastomer (Rheovibron Model DDV-II-C) with a temperature scan from 200 to 450 K (not exceeding a scanning rate of 1 deg/min). The storage modulus (E') and loss modulus (E'') were calculated from measurements of the loss angle (tan δ) and were plotted versus temperature. Glass transition temperatures (T_g) were obtained from such plots. In some systems, T_g values were determined via differential scanning calorimetry (DSC) (Perkin-Elmer DSC II) at a scanning rate of 20 °C/min.

Samples were prepared for scanning electron microscopy (SEM) (Phillips Model SEM 505) by freeze-fracturing in liquid nitrogen and applying a gold coating of approximately 200 Å.

Polyurethane-Poly(methyl Methacrylate) IPNs

PU-poly(methyl methacrylate) (PMMA) IPNs were first prepared by Kim et al. (*11–14*) by the simultaneous technique in bulk. Polyester-based urethanes were employed. In the present study, polyether-based urethanes were employed, and the IPNs were prepared from solution. In addition, to further study the effects of interpenetration, the molecular weight of the prepolymer was varied by changing the NCO : OH ratio in the prepolymer. Polyols of various molecular weights (650, 1000, and 2000) (*15*) were also used. Furthermore, charge groups were introduced into the component polymers to achieve higher miscibility between the urethane and the

[1] American Society for Testing and Materials.

acrylic polymers and to deduce the effects on the morphology and physical properties of the IPNs (*16*). The PU was cured with bis(2-chlorsanilinyl)methane (MBCA). The isocyanate was 4,4′-(carbonylamino)diphenylmethane (MDI). IPNs composed of 80 and 90% PU were prepared.

Table I shows the formulation of the various urethane prepolymers. The glass transitions of the IPNs and the component polymers are shown in Tables II and III. The most miscibility is evidenced when prepolymers were based on either a low molecular weight polyol or an increased NCO:OH ratio in the prepolymer. This result may be deduced from the greater T_g shift—to the higher temperature of the low molecular weight prepolymer materials [i.e., closer to T_g(A), the calculated T_g]—as well as the presence of a second T_g in the highest molecular weight prepolymer

Table I. PU Prepolymers of Different NCO% and Molecular Weight of Polyols

Description	*Composition*	*NCO:OH*	*Theoretical NCO%*	*Experimental NCO%*
PU-I	Polymeg 1000[a] + MDI	2.76	8.75	8.63
PU-II	Polymeg 1000[a] + MDI	2.49	7.7	7.62
PU-III	Polymeg 1000[a] + MDI	2.25	6.7	6.61
PU-IV	Polymeg 1000[a] + MDI	2.00	5.6	5.52
PU-V	Polymeg 1000[a] + MDI	1.86	4.95	4.84
PU-VI	Polymeg 650 + MDI	1.62	4.95	4.83
PU-VII	Polymeg 2000 + MDI	2.49	4.95	4.84

[a]Poly(1,4-oxybutylene) glycol
SOURCE: Ref. 15.

Table II. Effect of NCO:OH Ratios in PU Polymers on Glass Transition Temperatures

Composition of Materials	*NCO:OH of PU Prepolymer*	T_g *(D)*[a] *K (by DSC)*	T_g *(A) K (Calc)*
PU-I–PMMA (90:10)	2.76	253	255.4
PU-II–PMMA (90:10)	2.49	249	253.6
PU-III–PMMA (90:10)	2.25	245 (267)	250.9
PU-IV–PMMA (90:10)	2.00	242 (253)	249.1
PU-V–PMMA (90:10)	1.86	238 (260)	246.4
PU-I	2.76	247	—
PU-II	2.49	245	—
PU-III	2.25	245	—
PU-IV	2.00	240	—
PU-V	1.86	237	—
PMMA	—	331	—

NOTE: Glass transition temperatures by DSC.
[a] T_g (D) means that the T_g was determined by DSC.
SOURCE: Ref. 15.

Table III. Effect of Molecular Weight of Polyols in PU on Glass Transition Temperatures

Composition of Materials	*Molecular Weight of Polyol in PU*	T_g *(D) K (by DSC)*	T_g *(A) K (Calc)*
PU-V–PMMA (90:10)	1000	239	246.4
PU-VI–PMMA (90:10)	650	245	251.8
PU-VII–PMMA (90:10)	1904	200 (269)	214.9
PU-V (100%)	1000	237	—
PU-VI (100%)	650	243	—
PU-VII (100%)	1904	202	—
PMMA (100%)	—	331	—

NOTE: Glass transition temperatures by DSC. The numbers in parentheses are the second T_g for the sample.
SOURCE: Ref. 15.

materials (PU-III, PU-IV, PU-V, and PU-VII in Tables II and III). The T_g of the pure PMMS was about 40° lower than normally reported for PMMA because of the use of a telomer at a high initiator concentration. The SEMs agree with this behavior (i.e. the most homogeneous-looking IPNs are those prepared from the lower molecular weight prepolymers. The mechanical properties of these IPNs (Tables IV and V) show that the best strength properties are exhibited by the most miscible IPNs.

Table IV. Effect of NCO:OH Ratio in the PU Prepolymers on Mechanical Properties

Composition of Materials	*NCO:OH Ratio of PU*	*Tensile Strength (psi)*	*100% Modulus (psi)*	*300% Modulus (psi)*	*Elongation (%)*	*Hardness (Shore A)*
PU-I–PMMA (90:10)	2.76	8284	3662	5464	640	96
PU-II–PMMA (90:10)	2.49	7200	3035	4688	610	95
PU-III–PMMA (90:10)	2.25	5447	1967	2864	670	93
PU-IV–PMMA (90:10)	2.00	4938	1527	2177	765	91
PU-V–PMMA (90:10)	1.86	4607	1437	1967	835	88

SOURCE: Ref. 15.

Table V. Effect of Polyol Molecular Weight in the PU on Mechanical Properties

Composition of Materials	*Molecular Weight of Polyol in PU*	*Tensile Strength (psi)*	*100% Modulus (psi)*	*300% Modulus (psi)*	*Elongation (%)*	*Hardness (Shore A)*
PU-V–PMMA (90:10)	1000	4607	1437	1967	885	88
PU-VI–PMMA (90:10)	650	7308	1767	3115	650	92
PU-VII–PMMA (90:10)	1904	3845	1056	1413	1135	85

SOURCE: Ref. 15.

Increased miscibility and mechanical properties with IPNs prepared from low molecular weight prepolymers are undoubtedly due to the increased miscibility of the initial prepolymer mixture (because of the lower molecular weight). In addition, an increase in the NCO:OH ratio in the prepolymer will result in a more highly cross-linked PU–urea, which is also conducive to interpenetration over the range studied (*15*, *16*).

Introduction of charge groups into the polymers also resulted in increased interpenetration, as shown by glass transition behavior (Tables VI and VII) and electron microscopy. Again, increased miscibility resulted in

Table VI. Composition of PUs, Polymethacrylates, and IPNs with Charge Groups

Description	*Materials*	*Composition*
PU	polyurethane	PTMO[a] 1000, MDI, and MBCA, NCO:OH = 2:1, NCO:NH_2 = 1.05
NPU	tertiary amine-containing polyurethane	PTMO 2000, MDI, BHPA[b], and MBCA, NCO:OH = 2:1, NCO:NH_2 = 1.05
PMMA	poly(methyl methacrylate)	prepolymer solution of MMA
P(MMA–MAA)	poly(methyl methacrylate-methacrylic acid)	prepolymer solution of MMA and MAA at different ratios of MMA:MAA (4:1, 6:1, 8:1, and 10:1)
IPN-I	PU–PMMA	PU:PMMA = 80:20
IPN-II	NPU–P(MMA–MAA)	NPU:P(MMA–MAA) = 80:20

[a] PTMO = poly(tetramethylene oxide).
[b] Bis-(2-hydroxypropyl)aniline mixed with PTMO 2000 to achieve an average molecular weight of 1000.
SOURCE: Ref. 16.

Table VII. Effect of Charge Groups on the T_g Values of IPNs by DSC

Composition	*MMA:MAA (mol)*	*–COOH% (mol)*	T_g *(D) K (DSC)*	T_g *(A) K (Calc)*
PU (100%)	—	—	240	—
NPU (100%)	—	—	242	—
PMMA (100%)	—	—	331	—
P(MMA–MAA) (100%)	4:1	20	357	—
P(MMA–MAA) (100%)	6:1	14.3	351	—
P(MMA–MAA) (100%)	8:1	11.3	348	—
P(MMA–MAA) (100%)	10:1	9.0	345	—
IPN-II (80:20)	4:1	20	263	265
IPN-II (80:20)	6:1	14.3	260	263.8
IPN-II (80:20)	8:1	11.3	258	263.2
IPN-II (80:20)	10:1	9.0	254	262.6
IPN-I (80:20)	—	—	242 (253)	249.1

SOURCE: Ref. 16.

enhanced mechanical properties (*see* Tables VIII and IX). The charge groups undoubtedly provide for specific interactions between the component polymers (e.g., ionic bonding) that could reduce the enthalpy of mixing to result in an overall reduction of the free energy of mixing (*16*).

Polyurethane–Epoxy IPNs

PU–epoxy IPNs were first prepared by Frisch et al. (*1*, *14*) by using the simultaneous technique in bulk. In this study, the effects of only cross-linking one polymer (pseudo-IPNs) and intentional grafting between the component polymers were studied. The PUs in this system were chain extended and cross-linked with a 4:1 equivalent ratio of butanediol (BD)–TMP. The epoxy was a glycidyl ether of bisphenol A (Ciba-Geigy Corporation, Araldite GT-7014). It was cured with a boron trichloride–ethanamine Lewis acid complex (Ciba-Geigy Corporation, XU-213). Pseudo-IPNs were prepared by omitting the 2-ethyl-2-(hydroxymethyl)-1,3-propanediol. Grafting was introduced by using less BD and TMP and incorporating dibutyltin dilaurate (0.05%) to catalyze the reaction between the now excess isocyanate and the pendant secondary hydroxyl groups on the epoxy resin.

Table VIII. Effect of Charge Groups on Mechanical Properties of IPNs

Composition	*MMA:MAA (mole)*	*Tensile Strength (psi)*	*100% Modulus (psi)*	*300% Modulus (psi)*	*Elongation (%)*	*Hardness (Shore A)*
PU (100%)	—	4401	1084	1574	910	90
NPU (100%)	—	5533	1589	2457	650	92
IPN-I (80:20)	1:0	5541	1571	2716	557	92
IPN-II (80:20)	4:1	7226	1699	2966	685	91

SOURCE: Ref. 16.

Table IX. Effect of Charge-Group Concentration in Methacrylate Polymers on Mechanical Properties of IPNs

Composition	*MMA:MAA (mole)*	*–COOH[a] (%)*	*Tensile Strength (psi)*	*100% Modulus (psi)*	*300% Modulus (psi)*	*Elongation (%)*	*Hardness (Shore A)*
NPU	—	—	5533	1589	2457	650	92
IPN-II (80:20)	4:1	20	7226	1699	3199	685	91
IPN-II (80:20)	6:1	14.3	6341	2001	3135	633	91
IPN-II (80:20)	8:1	11.1	6419	1850	3076	643	91
IPN-II (80:20)	10:1	9	5925	1900	2966	623	92
IPN-I (80:20)	—	—	5826	1198	2048	720	88

[a] Theoretical calculation from MMA:MAA mole ratios.
SOURCE: Ref. 16.

Table X describes the polymers and IPNs. The morphology of the IPNs varied. The Rheovibron data (Figure 1) showed that the full IPN and the graft had only one T_g, whereas the pseudo-IPN exhibited two T_g peaks. In addition, the peak from the graft IPN was slightly sharper than that of the full IPN, and even greater miscibility was indicated. This result would be expected because covalent bonds between component polymers would be expected to increase miscibility in a manner similar to charge groups. The two T_g peaks of the pseudo-IPN probably reflect the fact that permanent interpenetration of networks was impossible because the PU was linear. However, the PU and epoxy T_g peaks have shifted inward (toward one another) from the T_g peaks of the corresponding homopolymers.

The full IPN exhibited only one T_g. In this system, both polymers were cross-linked networks, which enhanced the possibility for permanent interpenetration. Presumably, the two T_g peaks of the pseudo-IPN shifted to result in a single T_g for the full IPN, and a single-phase morphology was indicated. The position of the T_g of the graft has shifted to a higher temperature from the full IPN T_g because of the introduction of the rigid epoxy structure into the PU backbone.

The electron microscopy again agrees with these results. The pseudo-IPN showed a clear two-phase morphology, with epoxy domains of 50 μm dispersed throughout the PUs. The full IPN showed a microphase dispersion (even smaller domains) of epoxy in the PU matrix, whereas the graft showed no visible phase separation.

The mechanical properties show the same behavior as the acrylic IPNs (i.e., the best strength properties occur with the most homogeneous materials) (Table XI).

Introduction of charge groups into the component polymers resulted in effects similar to that of the acrylic IPNs (i.e., increased miscibility and mechanical properties) (Tables XII and XIII and Figure 2) (*16*).

Table X. Description of Samples

Abbreviation of Sample	*Composition (PU–Epoxy)*	*PU Type*	*Epoxy Type*	*Covalent Bonding Between Networks*
LU[a]	100–0	linear	—	—
PU	100–0	cross-linked	—	—
PE	0–100	—	cross-linked	—
Pseudo-IPN	80–20	linear	cross-linked	no
Full IPN[b]	80–20	cross-linked	cross-linked	no
Graft	80–20	cross-linked	cross-linked	yes

[a] LU is linear polyurethane.

[b] Any covalent chemical bonding between the polyurethane and epoxy networks is occasional and random.

SOURCE: Ref. 17.

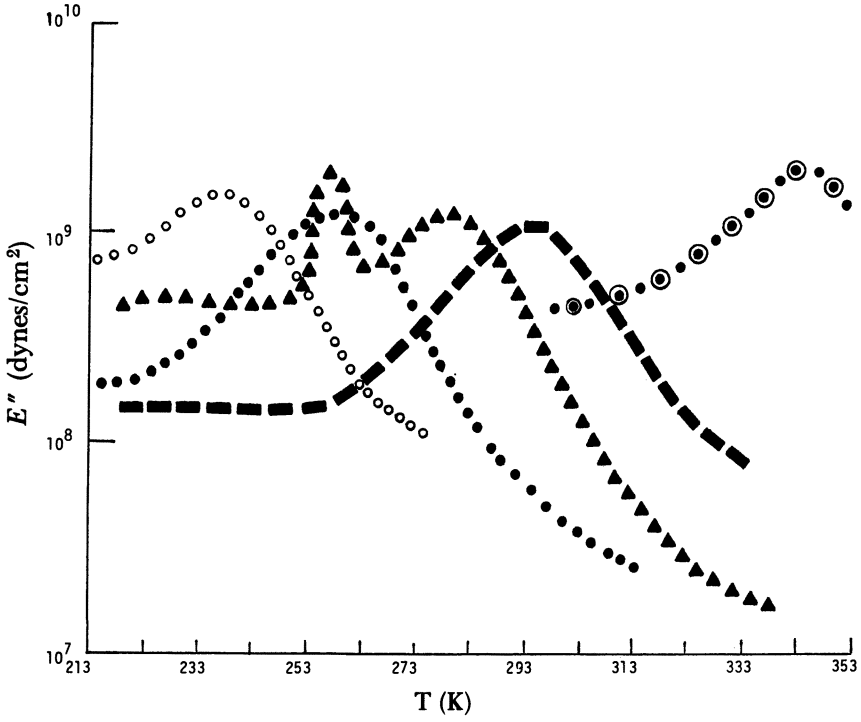

Figure 1. Loss modulus (E″) versus temperature for various homopolymers and polymer alloys (17). Key: ○, linear urethane; ■, graft; •◉•, epoxy; ▲, pseudo-IPN; and ●, full IPN.

Table XI. Mechanical Properties of Samples

Sample	*100% Modulus (psi)*	*300% Modulus (psi)*	*Tensile Strength (psi)*	*Elongation (%)*	*Hardness*		*Physical Appearance*
					Shore A	*Shore D*	
LU	1873	2714	3025	683	69	18	uniform
PU	1895	2853	3429	587	73	20	uniform
PE	—	—	8772	2	98	86	uniform
Pseudo-IPN	2373	—	3491	297	84	37	nonuniform
Full IPN	2492	—	4087	289	85	40	uniform
Graft	2657	—	4304	232	88	46	uniform

NOTE: Polyurethane–epoxy ratio is 80:20.
SOURCE: Ref. 17.

The Type-I IPN (opposite-charge groups) showed a very sharp and distinct T_g, and excellent miscibility was therefore indicated between networks. The Type-II IPN (similar charge) exhibited a broader T_g than the Type-I IPN. Thus, there was less phase mixing and less miscibility in comparison to the Type-I IPN. The Type-III IPN (charge free) showed the

Published on December 9, 1985 on http://pubs.acs.org | doi: 10.1021/ba-1986-0211.ch013

Table XII. Description and Properties of Polyurethanes

Polyurethane Abbreviation	*Polyurethane Type*	*Diols*	*Charge Group Concentration (%)*	*100% Modulus (psi)*	*300% Modulus (psi)*	*Tensile Strength (psi)*	*Elongation (%)*	*Hardness (Shore A)*
LU	I	PRMO 1000	—	1873	2714	3025	683	69
PU	II	PTMO 1000	—	1895	2853	3429	587	73
BrPU	III	PTMO 2000 + DBBD[a]	2.96 (−Br)	1285	1938	3086	555	80
COOHPU	III	PTMO 2000 + BHMOA[b]	1.62 (−COOH)	1304	1965	2987	721	64
N_1PU[c]	III	PTMO 2000 + BNHPA[c]	0.51 (−N(=)−)	1298	1747	3152	850	70
N_2PU[d]	III	PTMO 2000 + NMDEA[d]	0.48 (−N(−)−)	1345	1988	3194	777	68

[a] 2,3-Dibromobutane-1,4-diol.
[b] 9,9,10-Bis(hydroxymethyl)octadecanoic acid.
[c] *N,N'*-Bis(2-hydroxypropyl)aniline.
[d] *N*-Methyldiethanolamine.
SOURCE: Ref. 18.

Published on December 9, 1985 on http://pubs.acs.org | doi: 10.1021/ba-1986-0211.ch013

Table XIII. Descriptions and Properties of IPNs

IPN Abbreviation	*IPN Type*	*Charge Group Concentration (%)*		*100% Modulus (psi)*	*300% Modulus (psi)*	*Tensile Strength (psi)*	*Elongation (%)*	*Hardness*	
		Polyurethane	*Epoxy*					*Shore A*	*Shore D*
BrPU-0510[a]	I	2.37	1.08	3128	—	3901	152	98	61
COOHPU-0510	I	1.30	1.08	3074	—	4257	163	97	55
BrPU-MY-720[b]	I	2.37	1.32	3039	—	4902	156	97	57
COOHPU-MY-720	I	1.30	1.32	3298	—	4683	125	98	72
N_1PU-8049[c]	I	0.41	10.0	1685	2083	3954	472	86	29
N_2PU-8049	I	0.38	10.0	1537	2086	3912	379	90	33
N_2PU-0510	II	0.38	1.08	1939	—	3620	223	96	53
N_2PU-MY-720	II	0.38	1.32	2049	—	3749	209	96	56
PU-EPN 1139[d]	III	—	—	1926	2813	3561	351	92	36
LU-EPN 1139	IV	—	—	1124	2023	3406	389	90	32

[a] Trisglycidyl ether of *p*-aminophenol.
[b] Tetraglycidyl ether of 4,4′-methylene bis(aniline).
[c] Glycidyl ether of tetrabromobisphenol A.
[d] Glycidyl ether of phenolic novolac.
NOTE: Polyurethane-epoxy ratio is 80:20.
SOURCE: Ref. 18.

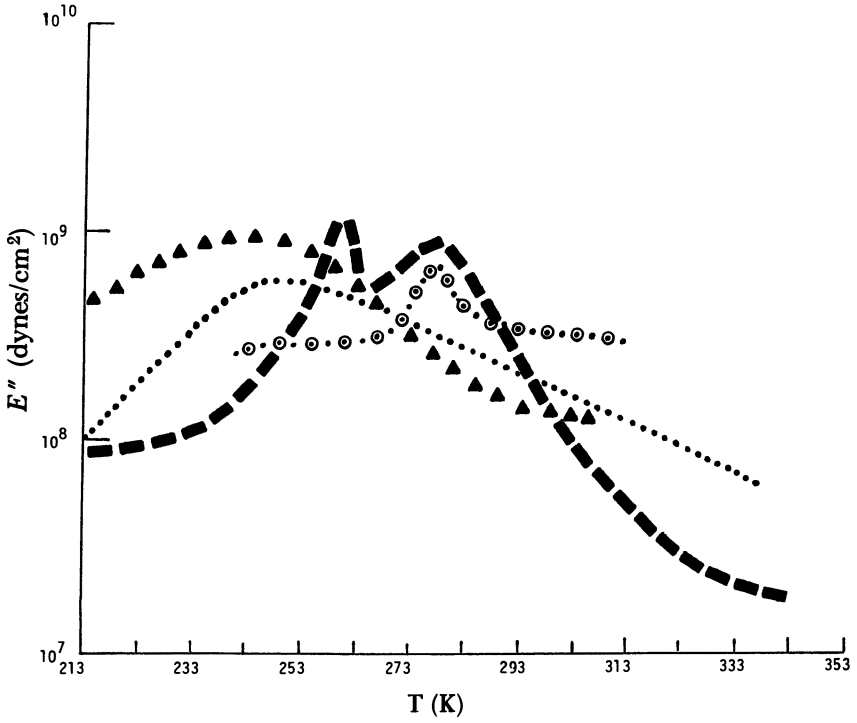

Figure 2. Loss modulus (E") vs. temperature for various IPN types (18). *Key:* •⊙•, *Type-I IPN (BrPU-0510);* ▲, *Type-II IPN (N_2PU-0510);* •••, *Type-III IPN (PU-EPN 1139); and* ■, *Type-IV (LU-EPN 1139).*

broadest single T_g, which indicates the possibility for the existence of phase separation. The Type-IV IPN (pseudo-IPN) exhibited two distinct T_g peaks.

The results of the mechanical spectroscopy were confirmed by SEM. The Type-III IPN showed a microphase dispersion of the epoxy phase in the PU matrix with distinct boundaries between the phases. The Type-II IPN showed slight phase separation with undefined boundaries between the phase domains of the two polymers. Thus, some permanent interpenetration of the networks is suggested. The Type-I IPN exhibited a single-phase morphology with no observable phase separation.

The mechanical properties of these IPNs are listed in Table XIII. The IPNs with opposite-charge groups exhibited better mechanical properties than the other types of IPNs. Because these IPNs (Type I) contained opposite-charge groups in the backbones of the constituent polymers, physical interactions could occur between the PU and epoxy networks. These interactions may cause a decrease in the enthalpy of mixing and thus result in a lowered free energy of mixing for these two polymers. Improved miscibility

can result in an increased degree of phase mixing and a greater possibility for interpenetration or permanent entanglement between the two networks. Thus, enhanced mechanical properties result.

The Type-I IPNs prepared from PUs containing pendant carboxylic acid groups (COOHPU) exhibited better properties than the IPNs containing pendant bromine groups (BrPU). In IPN systems containing the same epoxy (e.g., COOHPU–0510 and BrPU–0510, or COOHPU–MY-720 and BrPU–MY-720), better properties were exhibited by the IPN containing the carboxyl groups. One explanation may be that there is an increased chance for physical interactions to occur between networks containing carboxylic acid groups in the PU and tertiary amine groups in the epoxy. Systems of this type can physically interact more easily than systems containing pendant secondary halides in the PU (BrPU) with tertiary amine groups in the epoxy.

The Type-I IPNs prepared from PUs containing both aromatic tertiary amine groups and aliphatic tertiary amine groups (N_1PU and N_2PU, respectively) with pendant bromine groups in the epoxy (8049) differed very little in mechanical properties. This result may be due to the low probability for physical interactions to occur between the networks in both cases. The epoxy contained bromine groups that were attached to benzene rings, which made them highly unreactive toward any ionic interactions. In this system, any differences in properties were probably due to structural differences between the IPN containing aromatic tertiary amine groups in the PU and the IPN containing aliphatic tertiary amine groups.

The IPN containing no charge groups, as well as the pseudo-IPN, was prepared from a novolac epoxy resin (EPN 1139). The charge-free IPN (PU–EPN 1139) exhibited a higher modulus, ultimate tensile strength, and hardness when compared with the pseudo-IPN (LU–EPN 1139) in which the PU was linear. Because the pseudo-IPN had only one cross-linked polymer, permanent interpenetration of networks could not be formed. The elongation of the pseudo-IPN was higher than that for the full-IPN of similar composition.

Three-Component IPNs

Tables XIV and XV show the compositions of the individual components and the ternary IPN. The mechanical spectra of the Type-III IPNs (opposite charge) are shown in Figure 3. As the concentrations of epoxy and acrylic polymers were increased, T_g (peak in E'' vs. T) shifted to the right (higher temperature) and gradually broadened. The three-component IPN containing 70% PU exhibited the broadest glass transition. Its loss modulus peak contained a small shoulder, and slight phase separation with two or even three T_g peaks superimposed on one another is indicated. When the concentrations of epoxy and acrylic polymers were increased to a combined total greater than 30%, sharp E'' peaks were again observed. We would

Table XIV. Descriptions of Polyurethane, Epoxy, and Acrylic Homopolymers—Three-Component IPNs With or Without Charge Groups (Bromine and Tertiary Amine)

Sample Abbreviation	Sample Type[a]	Composition	Diols (in Polyurethanes)[b]	Charge Group Concentration (%)		
				Polyurethane	Epoxy	Acrylic
CU[a]	i	PU 100%	A + 1.4 BD	—	—	—
NPU	i	PU 100%	A + NMDEA	0.48 (−N−)	—	—
BrPU	i	PU 100%	A + DBBD	2.96 (−Br)	—	—
LBrPU	ii	LU 100%	A + DBBD	2.96 (−Br)	—	—
0510	iii	PE 100%	—	—	5.40 (−N−)	—
BMA[c]	iv	PA 100%	—	—	—	—
DMA[d]	iv	PA 100%	—	—	—	8.92 (−N−)
LDMA[e]	v	LA 100%	—	—	—	8.92 (−N−)

[a] i, Cross-linked polyurethane; ii, linear thermoplastic polyurethane; iii, cross-linked epoxy; iv, cross-linked poly(methacrylate); and v, linear thermoplastic poly(methacrylate).
[b] A is PTMO 2000.
[c] Butyl methacrylate.
[d] Dimethylaminoethyl methacrylate.
[e] Linear poly(dimethylaminoethyl methacrylate).
SOURCE: Ref. 18.

Table XV. Descriptions of Three-Component IPNs With or Without Charge Groups

IPN Abbreviation	IPN Type	Composition (% by wt.) Polyurethane-Epoxy Acrylic	Charge Group Concentration (%)		
			Polyurethane	Epoxy	Acrylic
CU-0510-BMA	I	80–10–10	—	0.54	—
NPU-0510-DMA	II	80–10–10	0.38	0.54	0.89
(BrPU-0510-DMA)	III	90–05–05	2.66	0.27	0.45
(BrPU-0510-DMA)	III	80–10–10	2.37	0.54	0.89
(BrPU-0510-DMA)	III	70–15–15	2.07	0.81	1.34
(BrPU-0510-DMA)	III	60–20–20	1.78	1.08	1.78
(BrPU-0510-DMA)	III	50–25–25	1.48	1.35	2.23
LBrPU-0510-DMA	IV	80–10–10	2.37	0.54	0.89
BrPU-0510-LDMA	IV	80–10–10	2.37	0.54	0.89
LBrPU-0510-LDMA	IV	80–10–10	2.37	0.54	0.89
BrPU-0510-IEM	V	80–10–10	2.37	0.54	—

SOURCE: Ref. 18.

like to suggest that phase inversion occurred near the glass transition of the composition containing 70% PU.

The mechanical spectra of four types of three-component polymer alloys with the composition PU–PE–PA equals 80 : 10 : 10 are shown in Figure 4. The graft IPN exhibited a very sharp peak. Thus, the degree of interpenetration between the BrPU–IEM grafted network and the epoxy network was high, with excellent molecular mixing. In the absence of covalent

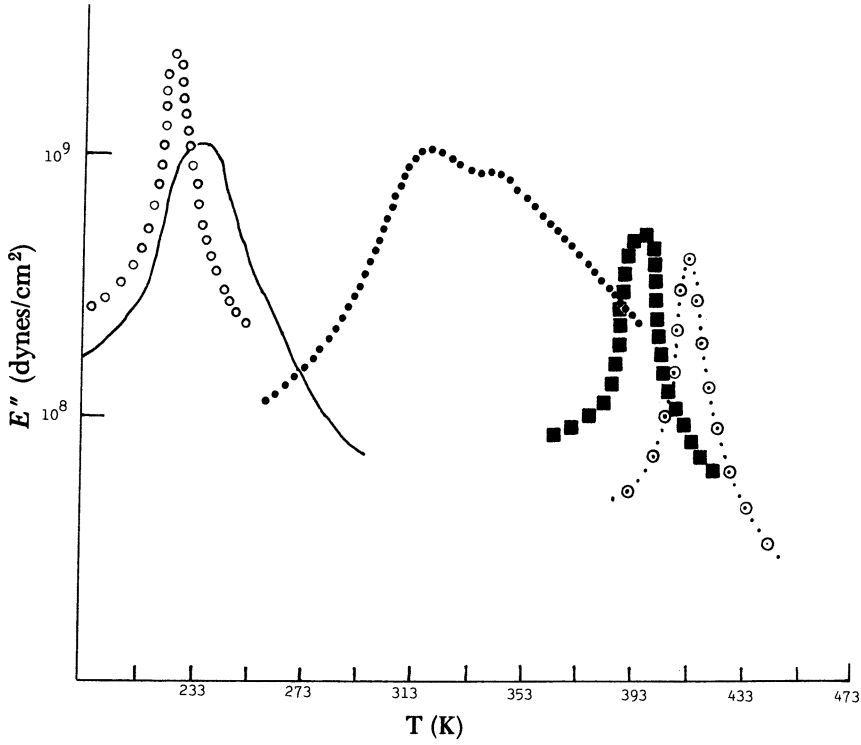

Figure 3. Effect of varied composition of Type-III ternary IPNs (opposite charge) on mechanical spectra (18). Key (percent BrPU): ○, 90; —, 80; ●, 70; ■, 60; and •◉•, 50.

chemical bonding between the PU and methacrylate polymers and a replacement of such bonding with weak physical attractions between opposite charge groups in the constituent networks, the E'' peak was broadened. This broadening may be seen in Figure 4 by comparing the relative breadths of the graft IPN and Type-III glass transitions. Obviously, secondary physical attractions are much weaker than primary covalent bonds, and as a result the degree of molecular mixing was decreased. When these weak physical attractive forces were eliminated in the Type-II IPN (similar charge), the E'' peak observed was even broader, and the molecular mixing was further decreased. Finally, the pseudo-IPN containing linear PU and acrylic polymers exhibited two distinct T_g peaks. However, because the epoxy was cross-linked and entanglement of the linear PU and methacrylate chains with the epoxy network was possible, the two T_g peaks were relatively close to one another (*see* Tables XVI and XVII). The morphological changes observed in the mechanical spectra are accompanied by similar changes in mechanical properties.

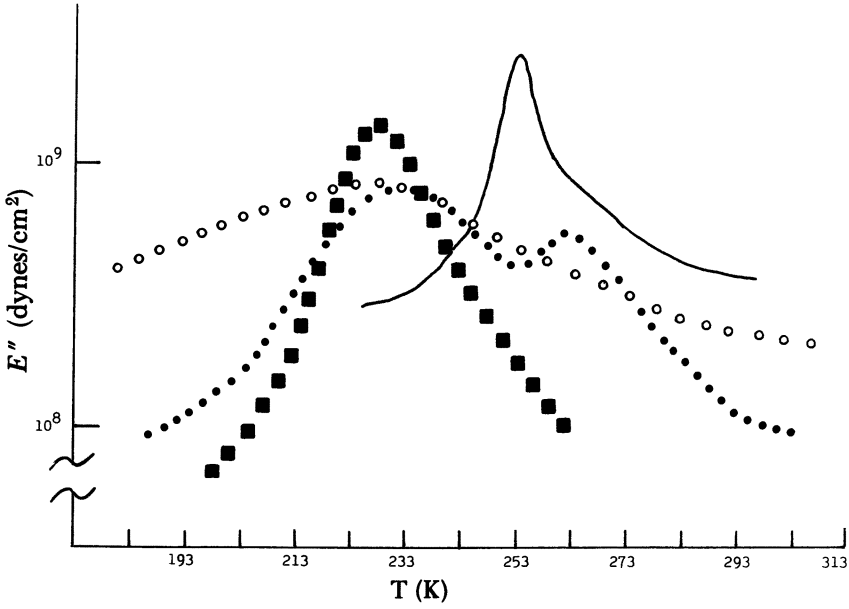

Figure 4. Comparison of the mechanical spectra for four types of ternary IPNs (18). Key: ○, Type-II IPN (similar charge); ■, Type-III IPN (opposite charge); ●, Type-IV pseudo-IPN; and —, Type-V graft IPN.

Table XVI. Glass Transition Temperature of Polyurethane, Epoxy, and Acrylic Homopolymers by Rheovibron

Sample	T_g *(K)*
CU	207
NPU	219
BrPU	216
LBrPU	211
0510	447
BMA	313
DMA	322
LDMA	320

SOURCE: Ref. 18.

The electron microscopy results revealed morphologies consistent with the T_g studies.

The mechanical properties of the PU, epoxy, and acrylic homopolymers are listed in Table XVIII. The cross-linked epoxy (0510) exhibited the highest tensile strength and lowest elongation at break because of high cross-link density and rigid structure.

As shown in Table XIX, the Type-V graft IPN exhibited the best mechanical properties because of covalent chemical bonding between the

Table XVII. Glass Transition Temperatures of Three-Component IPNs by Rheovibron

IPN	*IPN Type*	T_g *(K)*
CU-0510-BMA	I	226
NPU-0510-DMA	II	224
(BrPU-0510-DMA)	III	223
(BrPU-0510-DMA)	III	228
(BrPU-0510-DMA)	III	316
(BrPU-0510-DMA)	III	394
(BrPU-0510-DMA)	III	415
LBrPU-0510-DMA	IV	222
BrPU-0510-LDMA	IV	229
LBrPU-0510-LDMA	IV	231, 264
BrPU-0510-IEM	V	254

SOURCE: Ref. 18.

Table XVIII. Mechanical Properties of Polyurethane, Epoxy, and Acrylic Homopolymers

Sample	*100% Modulus (psi)*	*300% Modulus (psi)*	*Tensile Strength (psi)*	*Elongation (%)*	*Hardness*	
					Shore A	*Shore D*
CU	1046	1853	3004	568	67	17
NPU	1345	1988	3194	777	68	18
BrPU	1285	1938	3086	555	75	24
LBrPU	1149	1721	2984	586	73	21
0510	—	—	8615	2	97	84
BMA	—	—	4848	15	91	59
DMA	—	—	4412	13	90	56
LDMA	—	—	4197	14	89	54

SOURCE: Ref. 18.

Table XIX. Mechanical Properties of Three-Component IPNs

IPN	*IPN Type*	*100% Modulus (psi)*	*300% Modulus (psi)*	*Tensile Strength (psi)*	*Elongation (%)*	*Hardness*	
						Shore A	*Shore D*
CU-0510-BMA	I	2467	—	4459	185	78	28
NPU-0510-DMA	II	3920	—	4628	128	80	30
(BrPU-0510-DMA)	III	1439	3547	3622	325	76	25
(BrPU-0510-DMA)	III	3572	—	4705	145	87	35
(BrPU-0510-DMA)	III	—	—	4878	75	94	46
(BrPU-0510-DMA)	III	—	—	5040	26	97	58
(BrPU-0510-DMA)	III	—	—	5178	15	98	67
LBrPU-0510-DMA	IV	3497	—	3945	175	88	36
BrPU-0510-LDMA	IV	3755	—	4489	142	84	39
LBrPU-0510-LDMA	IV	3011	—	3715	191	79	30
BrPU-0510-IEM	V	3871	—	4795	132	80	33

SOURCE: Ref. 19.

Table XX. Comparison of Experimental and Calculated Ultimate Tensile Strengths of Three-Component IPNs

IPN	IPN Type	Tensile Strength (psi)			Percent Difference[d]
		TS[a]	TS'[b]	ΔTS[c]	
CU-0510-BMA	I	4459	3750	709	19
NPU-0510-DMA	II	4628	3858	770	20
(BrPU-0510-DMA)	III	3622	3429	193	6
(BrPU-0510-DMA)	III	4705	3772	934	25
(BrPU-0510-DMA)	III	4878	4114	764	19
(BrPU-0510-DMA)	III	5040	4457	583	13
(BrPU-0510-DMA)	III	5178	4800	378	8
LBrPU-0510-DMA	IV	3945	3690	255	7
BrPU-0510-LDMA	IV	4489	3750	739	20
LBrPU-0510-LDMA	IV	3715	3668	47	1

[a] Experimental tensile strength.

[b] The calculated ultimate tensile strengths (TS') were obtained from the equation $TS' = X_i TS_i$ where X_i is the weight fraction of the i-th component, and TS_i is the ultimate tensile strength of the i-th component homopolymer.

[c] $\Delta TS = TS - TS'$

[d] $\text{Percent differences} = \frac{\Delta TS}{TS'} \times 100$

Source: Ref. 19.

IEM and BrPU networks. The Type-III IPNs (opposite charge) also exhibited improved properties over the other IPN types. Presumably, weak physical ionic interactions brought about by the charge groups in the constituent networks and grafts between the components enhanced polymer miscibility. This enhancement undoubtedly decreased the degree of phase separation and aided in the formation of IPNs with enhanced properties and more homogeneous morphologies. The Type-II IPN (similar charge) showed improved properties over the Type-I IPN (no charge). The high concentration of tertiary amine groups in the Type-II IPN helped to match the cross-linking rates of the three components, and the chance for interpenetration of the networks was increased. The Type-IV pseudo-IPN prepared from cross-linked PU and epoxy with linear thermoplastic acrylic (BrPU-0510-LDMA) exhibited better properties than the other two pseudo-IPNs. In this system, only the acrylic polymer (10 wt%) was linear, so the BrPU and epoxy networks could still interpenetrate with one another. The lowest mechanical properties were exhibited by the pseudo-IPN containing both linear PU and acrylic polymers (LBrPU-0510-LDMA) because of the absence of a permanent interpenetration of networks. By increasing the concentrations of epoxy and acrylic polymers, higher tensile strength, modulus, and hardness, as well as decreased elongation were observed for the Type-III IPNs. This result was due to an increased rigid structure in the IPNs and a higher cross-link density.

A comparison of experimental and calculated ultimate tensile strengths for the three-component IPNs is shown in Table XX. The calculated tensile strengths were obtained from the linear additivity of the constituent homopolymer tensile strengths based upon weight fraction. In all of the three-component IPN types, ΔT values were positive. Therefore, the IPNs exhibited mechanical properties that were improved over a mere blending of the constituent polymers. For IPNs of the same composition (PU–PE–PA equals 80:10:10) the percent difference was highest for the Type-III IPN (opposite charge) (25%) and lowest for the pseudo-IPN containing the linear PU and acrylic polymers (1%). Obviously, the high degree of interpenetration and good miscibility in the former system led to an experimental tensile strength that was much higher than that calculated.

Literature Cited

1. Lipatov, Y.; and Sergeeva, L. "Vzaimopronikayushchie Polimerovye Setki" (Interpenetrating Polymer Networks); Naukova Dumka: Kiev, 1979 (in Russian).
2. Millar, J. R. *J. Chem. Soc.* **1960**, 1311; Shibayama, K.; Suzuki, Y. *Kobunshi Kagaku* **1966**, *23*, 249; *Kobunshi Kagaku* **1966**, *24*; Shibayama, K.; *Zairyo* **1962**, *12*, 362; Shibayama, K. *Kobunshi Kagaku*, **1962**, *19*, 219; *Kobunshi Kagaku* **1963**, *20*, 221.
3. Frisch, H. L.; Klempner, D.; Frisch, K. C. *J. Polym. Sci. Polym. Lett.* **1969**, *7*, 775; Frisch, H. L.; Klempner, D.; Frisch, K. C. *J. Polym. Sci. Part A2*, **1970**, *8*, 921; Matsuo, M.; Kwei, T. K.; Klempner, D.; Frisch, H. L. *Polym. Eng. Sci.* **1970**, *10*, 327; Klempner, D.; Frisch, H. L. *J. Polym. Sci. Part B* **1970**, *8*, 525.
4. Sperling, L. H.; Friedman, D. W. *J. Polym. Sci. Part A2* **1969**, *7*, 425; Sperling, L. H.; Taylor, D. W.; Kirkpatrick, M. L.; George, H. F.; Bardman, D. R. *J. Appl. Polym. Sci* **1970**, *14*, 73; Sperling, L. H.; George, H. F.; Huelck, V.; Thomas, D. A. *J. Appl. Polym. Sci.* **1970**, *14*, 2815.
5. Frisch, H. L.; Klempner, D. *Adv. Macromol. Chem.* **1979**, *2*, 149.
6. Klempner, D. *Angew. Chem.* **1978**, *17*, 97.
7. David, D. J. "Analytical Chemistry of Polyurethanes"; Wiley: New York, 1969; Vol. 16, p. 138.
8. Frisch, K. C.; Frisch, H. L.; Klempner, D.; Mukherjee, S. K. *J. Appl. Polym. Sci.* **1974**, *18*, 689.
9. Frisch, K. C.; Klempner, D.; Antzak, T.; Frisch, H. L. *J. Appl. Polym. Sci.* **1974**, *18*, 683.
10. Frisch, K. C.; Klempner, D. Migdal, S.; Frisch, H. L.; Ghiradella, H. *Polym. Eng. Sci.* **1975**, *15*, 339.
11. Kim, S. C.; Klempner, D.; Frisch, K. C.; Radigan, W.; Frisch, H. L. *Macromolecules*, **1976**, *9(2)*, 258.
12. Kim, S. C.; Klempner, D.; Frisch, K. C.; Frisch, H. L. *Macromolecules*, **1977**, *10*, 1187.
13. Kim, S. C.; Klempner, D.; Frisch, K. C.; Frisch, H. L. *Macromolecules*, **1976**, *9(21)*, 263.
14. Frisch, H. L.; Frisch, K. C.; Klempner, D.; *Polym. Eng. Sci.* **1974**, *14(a)*, 646.
15. Xiao, H. X.; Frisch, K. C.; Frisch, H. L. *J. Polym. Sci.* **1983**, *21*, 2547.
16. Xiao, H. X.; Frisch, K. C.; Frisch, H. L. *J. Polym. Sci.* **1984**, *22*, 1035.

17. Cassidy, E. F.; Xiao, H. X.; Frisch, K. C.; Frisch, H. L. *J. Polym. Sci.* 1984, *22*, 1839.
18. Cassidy, E. F.; Xiao, H. X.; Frisch, K. C.; Frisch, H. L. *J. Polym. Sci.* 1984, *22*, 1851.
19. Cassidy, E. F.; Xiao, H. X.; Frisch, K. C.; Frisch, H. L. *J. Polym. Sci.* 1984, *22*, 2667.

RECEIVED for review November 15, 1984. ACCEPTED April 30, 1985.

14

Poly(acrylourethane)–Polyepoxide Semi-interpenetrating Networks Formed by Electron-Beam Curing

Compatibility and Mechanical Behavior

ELIAS HAGE[1,3], W. K. WALSH[1], and TAKAYUKI MURAYAMA[2]

[1]School of Textiles, North Carolina State University, Raleigh, NC 27695-8301
[2]Monsanto, Polymer Product Company, Springfield, MA 01151

Semi-interpenetrating networks (semi-IPNs) were prepared by electron beam initiated polymerization of difunctional acrylourethane oligomers in the presence of a linear epoxy. Single glass transitions, by differential scanning calorimetric (DSC) and mechanical spectral analyses, were observed for all blend levels, before and after polymerization, indicating a high degree of compatibility. Glass transition temperatures varied smoothly with blend level in the cured semi-IPNs, but marked deviations were noted in the uncured blends. Crystallization of the oligomer by aging the films before curing effected phase separation that could be fixed by electron curing, and optically clear films with two transitions resulted. Stress–strain measurements on the cured films showed a very sharp maximum in toughness around 50% oligomer. Phase separation forced by precrystallization produced significant toughness increases.

An interpenetrating polymer network (IPN) is formed when a material composed of two cross-linked components is prepared so that at least one of the networks is synthesized and/or cross-linked in the presence of the other. If only one of the components is cross-linked, the material is a semi-IPN. IPNs and semi-IPNs have been the subject of several reviews (*1–4*). The synthesis and properties of semi-IPNs based on polyurethanes and polymethyl acrylate have been reported (5–7).

This chapter reports the mechanical properties of poly(acrylourethane)–polyepoxide IPNs. The network was formed by electron beam (EB) initiated polymerization of an acrylourethane oligomer formed from a

[3]Current address: Departamento de Engenharia de Materialis, Universidade Federal de Sao Carlos, Caixa Posta 676, 13560, Sao Carlos—SP, Brazil

0065-2393/86/0211/0231$07.25/0

poly(ethylene adipate) diol capped with toluene 2,4-diisocyanate and hydroxyethyl acrylate.

Radiation-cured films and coatings using oligomers have been reported (*8–11*). Many advantages result from radiation curing, but cured films are usually deficient in toughness. One reason is that high glass transition temperatures (T_g) are usually associated with high degrees of cross-linking in these films, and films with high extensibility have T_g values too low for maximum toughness. Formation of semi-IPNs offers a possible escape from this restraint. By using a high T_g linear polymer in a low T_g network, it is possible to have T_g increase as cross-linking decreases, while varying the composition of the polyblend. Such a system would not be a conventional radiation-curing process, because of the viscosity limitations imposed by the linear polymer, but would serve to demonstrate the range of properties obtainable if research in synthesis of radiation-curable materials were pursued in areas that are not now common.

According to Harris and coworkers (*12*), the polyepoxide used is compatible with poly(ethylene adipate) (PEA) and a number of other polyesters. In their study, crystallization of the PEA from the blends gave a constant heat of fusion. In addition, the value of the interaction parameter derived from melting point depression was in reasonable agreement with the hypothesis that compatibility was enhanced by hydrogen bonding between the hydroxyl of the polyepoxide and carbonyl of the PEA.

The oligomer used also showed a high degree of compatibility with the polyepoxide and was able to crystallize from the blend. By forming the semi-IPN through EB curing after crystallization and simultaneously melting the oligomers, phase separation that was stabilized by the network could be achieved. When network formation was initiated by gamma radiation, polymerization could be achieved without melting the oligomer, because the much lower radiation intensity allowed the heat of polymerization to be dissipated without a significant temperature increase.

Experimental

An acrylourethane oligomer and a high molecular weight epoxy were used as constituents of the polymer blends. The acrylourethane is a radiation-curable oligomer (Thiokol/Chemical Division). Its simplified formula is shown in Structure I where *A* and *B* represent the hard and soft segments, respectively, and *X* indicates the active sites for the radiation cross-linking. The molecular weight of the oligomer is about 6000; therefore, the calculated value of *n*, in the molecular formula, is about 15. The pure oligomer generally is in a crystallized state at room temperature and has the appearance of a hard wax. When melted and cross-linked through UV photoradiation or high energy electrons, the resulting film behaves like an elastomer.

Compound II[1] is an epoxy resin with a molecular weight of about 200,000 (the Shell Chemical Company, trademark EPONOL 55-L-32). The hydroxyl content is

[1] α-[α-[*p*-(2,3-Epoxypropoxy)phenyl]-*p*-cumenyl]-ω-2,3-epoxypropoxy)poly-[oxy(2-hydroxytrimethylene)oxy-*p*-phenyleneisopropylidene-*p*-phenylene].

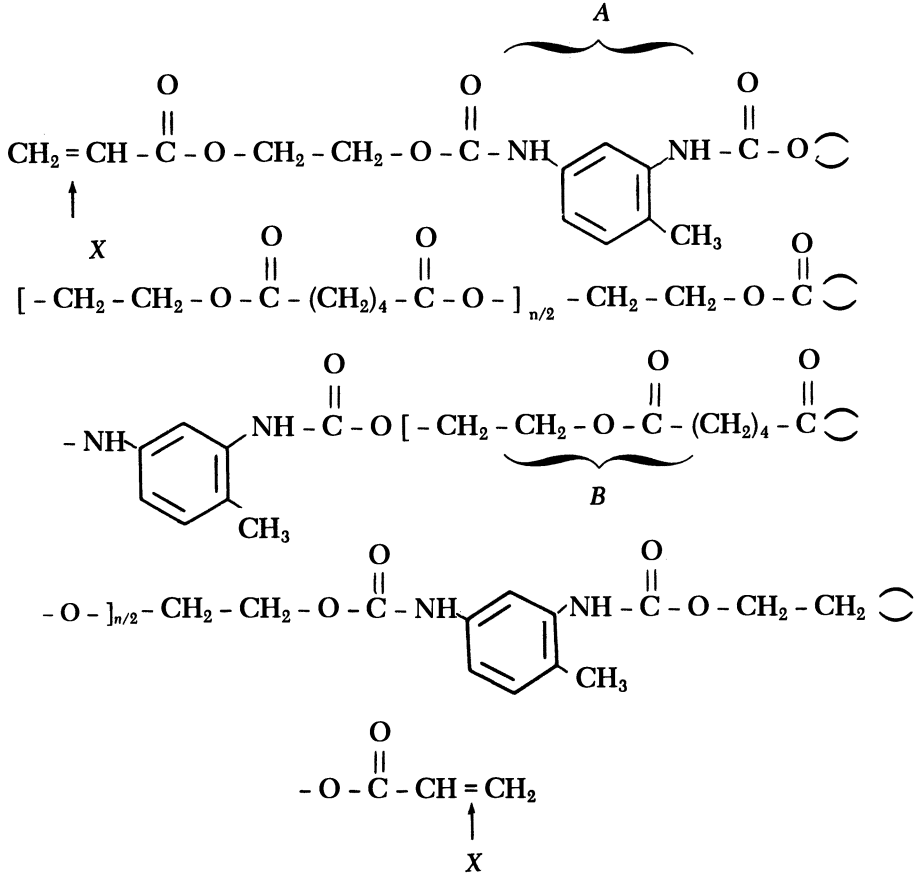

Compound I

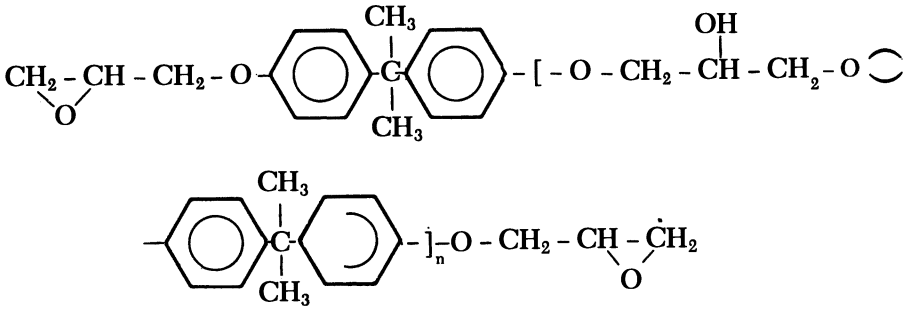

Compound II

0.35 equiv/100 g of resin. Basically, the structure of the epoxy can be defined as a linear poly(hydroxyl ether). Because the epoxy was furnished as a 32-wt% solution in 2-ethoxyethyl acetate (Union Carbide's Cellosolve Acetate), this solvent was used to prepare all of the polymer blends.

Irradiation Equipment. An electron accelerator and a cobalt-60 Gammacell-220 were used as radiation sources to irradiate the polymer blends.

The electron accelerator (the High Voltage Engineering Corporation) has a maximum beam current of 20 mA and is operated at 500,000 V (from an insulated core transformer). This equipment uses a horizontal beam that scans an area 48 in. × 6 in. The samples were hung vertically on a conveyor that carried them in front of the beam twice in each pass through the equipment so that the samples received half of their total dose from each side. All irradiations were carried out in a nitrogen atmosphere. Ziploc polyethylene bags (Dow Chemical Corporation) were used to hold the films. Before irradiation, each bag was flushed with nitrogen gas. The dose rate of the electron accelerator was about 1 Mrad/s.

The gamma radiation source was a Gammacell 220 unit (Atomic Energy of Canada, Ltd.). The radiation field in the Gammacell was produced by a fixed cobalt-60 source in the form of a squirrel cage. The sample chamber could be lowered into the source cage for irradiation and returned to a position outside of the unit for unloading. All irradiation was also carried out in a nitrogen atmosphere, which was continuously flushed during irradiation. The dose rate supplied by the cobalt-60 source was approximately 0.2 Mrad/h.

Preparation of the Blends and Semi-IPNs. Both the acrylourethane oligomer and the epoxy were dissolved in 2-ethoxyethyl acetate. The ratios of epoxy to oligomer (E/O) in the mixtures refer to weight percentage. The mixtures of the constituents were maintained in solution for 30 min with constant agitation to assure homogeneity. Solutions of high concentration of oligomer required some heating to accelerate the oligomer dissolution. Therefore, these solution blends were kept at 50 °C for 10 min under intense agitation. After this period, the solutions were allowed to cool with agitation for an additional 20 min.

Films of acrylourethane oligomer, epoxy, and their mixtures were cast from the 2-ethoxyethyl acetate solution on Mylar film or on a specially coated paper for polyurethane casting (Warren's Transkote VELCIS) at room temperature. A rubber rod covered with thin Mylar film was used as an apparatus to cast the films with a smooth upper surface and an even thickness. The solvent was allowed to evaporate for 24 h in an oven at 45 °C and under a constant stream of air. The resulting films were subjected to further drying in a vacuum for 48 h at 40 °C. The average film thickness after solvent removal was about 25 μm.

After solvent removal, half of the films were allowed to crystallize at 25 °C and the other half were freshly irradiated. These irradiated films are designated as *cured fresh blends.* Some of the aged films were irradiated just after the aging period of 4 weeks. The others were melted, after the aging period, at 50 °C for 3 h before irradiation. The former aged blends are designated as *cured aged blends,* and the latter are *cured melted aged blends.* The rest of the aged films were not irradiated (i.e., were uncured). This set of blends is called *uncured aged blends.* All aged blends were crystallized for 4 weeks unless otherwise noted.

The fresh and aged films were cured by EB in a sealed polyethylene bag filled with nitrogen gas. The double bonds located in the acrylate end groups of the oligomer were the major target for the cross-linking. Therefore, the cross-linking process of the acrylourethane oligomer under the presence of the linear high molecular weight epoxy produced a semi-IPN. Gamma radiation was used to cure only aged blends.

The first tests performed on the films cured by EB were to detect the optimum dose of curing. The tensile breaking strength was used to study the effect of the dose of radiation.

The optimum chosen dose was 10 Mrad because the breaking strength levels off well before this point. All the cured samples used to study the mechanical and thermal behavior were irradiated at 10 Mrad.

Analysis. Optical microscopy was carried out using a polarizing microscope (Nikon) with a hot stage (Mettler FP52) and a camera (Canon Model AE-1). Films were cast on glass slides and covered with a cover plate after solvent removal. Pictures were taken after solvent removal. Sample thickness was 10–12 μm.

Dynamic mechanical properties of the films were measured (Rheovibron Model DDV-11) in dry nitrogen at 110 Hz at a heating rate of 1 °C/min over a temperature range of −75 to +125 °C. Before the test, the cured fresh samples were preheated to 110 °C in the presence of nitrogen for 15 min. This procedure was used to ensure the removal of moisture and the release of stress generated by the film casting.

The tensile properties were determined (Instron, Model TT-B) at ambient conditions. All the calorimetric thermal analyses were performed with a differential scanning calorimeter (Perkin-Elmer Model DSC-II with data station, TADS).

Results and Discussion

T_g measurements were conducted on a wide range of compositions of nonirradiated, freshly prepared epoxy–oligomer blends. The T_g values, taken at the midpoint of the glass transition region, are reported in Table I. A single T_g was observed at each composition, and compatibility was indicated over the full range. Table I also shows the arithmetic mean of the T_g

Table I. Glass Transition Temperatures of Nonirradiated Blends

E/O in the Sample	T_g *(Uncured)* K	T_g *(Fox)* K	T_g *(Average)* K	T_g *(Gordon–Taylor)*[a] K
0/100[b]	246.0 (1.0)	246.00	246.0	246.0
5/95	250.4 (2.3)	249.4	250.6	249.7
10/90	253.8 (1.4)	252.9	255.3	253.6
20/80	260.1 (2.4)	260.2	264.5	261.4
25/75	264.7 (0.1)	264.1	269.2	265.5
30/70	267.8 (1.6)	268.0	273.8	269.7
35/65	273.1 (2.0)	272.1	278.4	273.8
45/55	280.4 (1.6)	280.5	287.7	282.7
50/50	277.3 (0.4)	285.0	292.3	287.2
60/40	276.3 (1.8)	294.3	301.6	296.6
70/30	278.3 (1.5)	304.3	310.9	306.4
80/20	322.4 (2.3)	315.0	320.2	316.6
90/10	325.8 (1.8)	326.4	329.4	327.4
100/0[c]	338.7 (3.6)	338.7	338.7	338.7

NOTE: Figures in parentheses indicate standard deviation in the set of 3 samples.

[a] In this equation, k is 0.8.

[b] T_g of the oligomer.

[c] T_g of the epoxy.

values of the components, T_g (average), and the copolymer T_g, calculated according to the Fox and Gordon–Taylor equations. T_{g1} and T_{g2} are the experimental T_g values for the pure oligomer and epoxy, respectively, and W_1 and W_2 are the weight fractions for the oligomer and the epoxy, respectively.

The experimentally obtained data points can be well fitted to the Fox equation up to 45% of epoxy in the blend, and the Gordon–Taylor relationship is also a good prediction for the data points in the same range of composition when k is equal to 0.8. For compositions above 45% of epoxy, however, a significant deviation is observed from the values calculated from either equation. The sudden drop in the T_g below 70% of epoxy could indicate phase separation. Only a single transition was observed, but there is a broadening (about threefold) of the transitions for the blends containing 50–70% epoxy, as shown in Figure 1. The broadening of the glass transition region can be attributed to incipient separation, which may be responsible for the large deviation from the behavior of the oligomer as a simple plasticizer.

The pure epoxy has stiff chains because of the benzene rings along the chain and strong intermolecular OH–OH bonds. When any small amount of oligomer is added to the epoxy, a plasticizing effect can be predicted

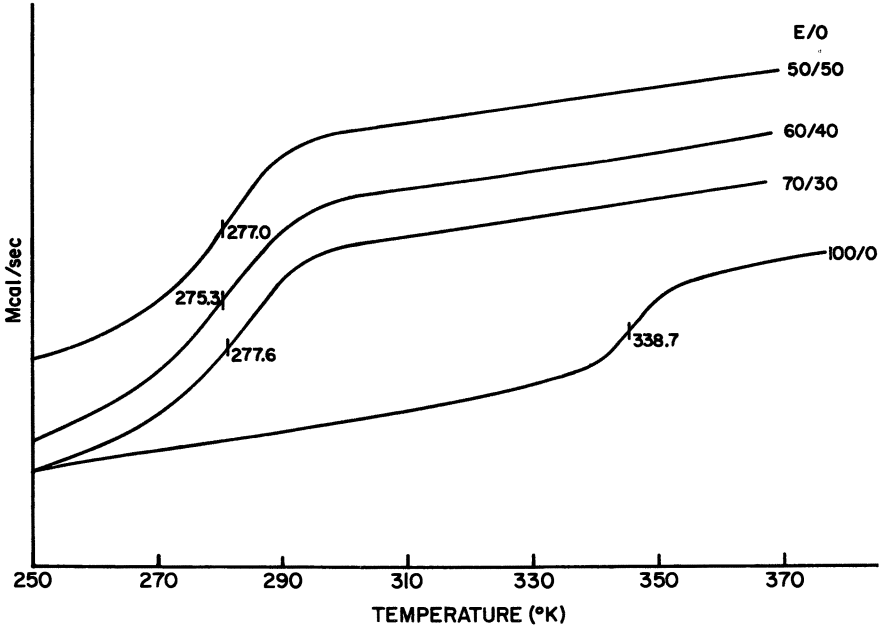

Figure 1. DSC curves for uncured fresh blends at several compositions of epoxy–oligomer.

from the small size of the oligomer molecules and the breaking of the OH–OH bonds provided by the strong interaction between the OH and C=O groups. The interaction between the NH and C=O in the oligomer could be restricted by the large amount of the OH groups at high epoxy content. Further addition of the oligomer to the epoxy could destroy more OH–OH bonds and produce a large number of end acrylate groups, which have tremendous freedom and thereby contribute to the extra free volume. The saturation of the OH groups from the epoxy molecules with the addition of the C=O groups could lead to a significant decrease in the OH–OH strong intermolecular forces. The impossibility of the NH and C=O interactions should give the oligomer molecules higher mobility than the molecules of the pure oligomer. These two latter reasons could account for the abnormality in the T_g at 50–70% epoxy. For instance, the shift in T_g values between the measured T_g and the T_g predicted by the Fox equation at this composition is 26 °C. As the amount of oligomer increases in the blend, the interaction between the NH and C=O groups is facilitated. This specific interaction leads to less freedom for the oligomer molecules. Therefore, the deviation from the Fox equation would disappear at higher concentrations of oligomer. This result can be noticed above 50% of oligomer in the blend. Above this composition, the strong interaction between both components starts to disappear because of the excess of carbonyl groups and end acrylate groups provided by the higher content of oligomer molecules.

The irradiation of the blends with electrons leads to cross-linking through free-radical polymerization of the double bonds located at the oligomer molecular tails. Thus, the mobility is reduced, and the free volume associated with these end groups is removed. The effect of cross-linking on the T_g can be seen in Figure 2. The formation of the semi-IPN leads to a shift of the T_g to higher values compared with the uncross-linked system. The shift in T_g increases as the amount of epoxy is raised, up to 70%. The remarkable shifting in T_g in the range between 50 to 70% of epoxy could be entirely attributed to the cross-linking and resulting loss of mobility in the end groups of the oligomer molecules.

The effect of crystallization on glass transitions of the uncured aged blends can be seen in Figure 3. The crystallization of the oligomer restricts the mobility of the amorphous regions and leads to an increase in the T_g for aged blends, up to about 45% of epoxy. In addition, crystallization removes oligomer from the blend, enriches the amorphous phase in epoxy, and raises the T_g. Above 45% epoxy, the crystallization disappears and does not contribute to any shift in the T_g.

Melting behavior of the crystallized blends is shown in Figure 4 and Table II. The heat of fusion of the 100% oligomer, based on PEA, is about one-half of that observed for pure PEA crystallized under similar conditions (*12*). Additionally, the heat of fusion in the blends (based on oligomer) did not remain constant, but decreased as epoxy was added to the blend. Thus, an inhibition of crystallizational ability was indicated.

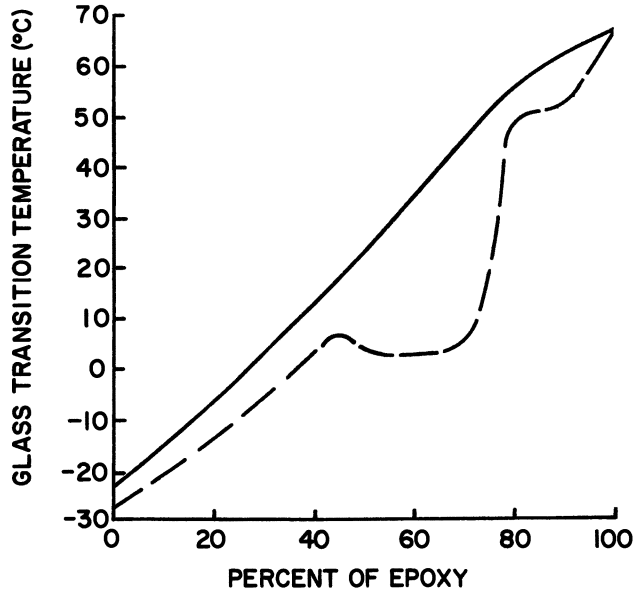

Figure 2. Glass transition temperatures (DSC) of cured (—) and uncured (--) blends as a function of blend composition.

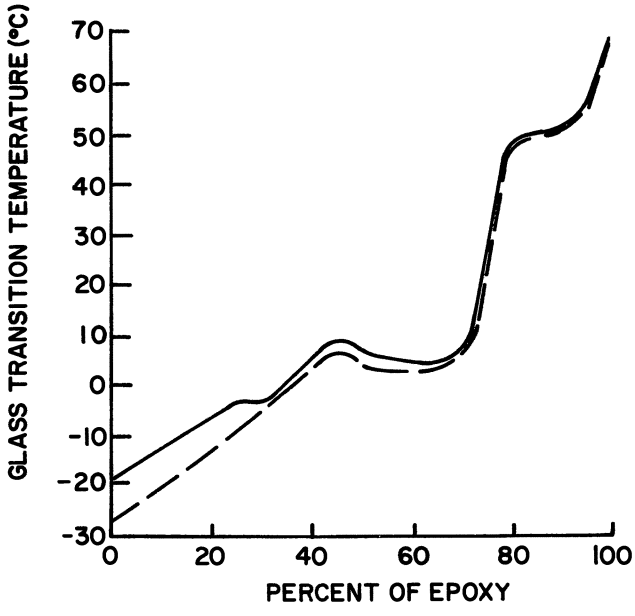

Figure 3. Glass transition temperatures (DSC) of fresh (--) and aged (—) uncured blends.

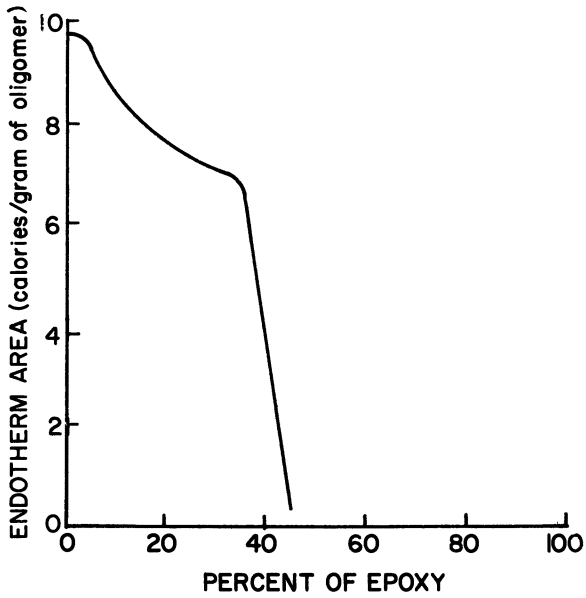

Figure 4. Heats of fusion of uncured, aged blends (DSC).

Melting points (given in Table II) did not decrease upon dilution of the oligomer with epoxy, but increased as epoxy was added. Apparently the epoxy increases the size and degree of perfection of the PEA crystallites. It is significant that in no case does the melting temperature (T_m) exceed that for the pure PEA (*12*). The interference with crystallization by the urethane acrylate end groups on the PEA oligomer is somehow ameliorated by

Table II. Effect of Gamma Irradiation on the Melting Temperatures of Aged Blends at Several Compositions

Composition (% of Epoxy)	T_m (°C)		ΔT_m(°C)[a]
	Nonirradiated	*Irradiated*	
0	35.9 (0.5)	38.2 (0.8)	2.3
5	35.5 (1.0)	—	—
10	36.7 (2.2)	39.7 (1.3)	3.0
20	36.0 (1.2)	50.6 (1.8)	14.6
25	37.5 (1.4)	48.2 (1.5)	10.7
30	38.5 (1.3)	50.4 (1.2)	11.9
35	40.1 (1.2)	48.8 (1.1)	8.7
40	—	45.0 (1.7)	—
45	35.7 (1.)	44.8 (1.0)	9.1

NOTE: Figures in parentheses indicate standard deviation in the set of 3 samples.
[a] ΔT_m equals T_m (irradiated) minus T_m (nonirradiated).

epoxy addition. Network formation by gamma irradiation significantly increases the melting points by lowering the melt entropy (S_m) and, thus, ΔS_m. Heats of fusion were not significantly changed by network formation (for more details, *see* Reference 13). Evidence for alteration of the crystallization of the oligomer by the presence of the epoxy is shown in Figures 5 and 6. Pure oligomer crystallizes with small, highly imperfect spherulites. Addition of epoxy slows the growth and increases the perfection and the interlaminar distances of the spherulites. After 4 weeks, all of the available volume is filled with spherulites. Thus, the noncrystallizable epoxy is held in the interlaminar regions [i.e., Martuscelli's Type-II morphology (*14*)]. Above about 40% epoxy, complete volume filling was not observed, even after 12 weeks of aging. This result gives an approximate indication of the probable epoxy content of the spherulites.

Irradiation increases the film temperature directly by absorption of the electrons and indirectly by the exotherm associated with the polymerization of the double bonds. EB irradiation is so rapid that conditions are nearly adiabatic. In the systems discussed, significant melting of the crystallites in the aged films was obtained with EB curing. Figures 7, 8, and 9 show micrographs of films (before and after curing) containing 10, 30, and 45% epoxy, respectively. All birefringence is removed by the irradiation, but traces of the spherulites can still be seen. These patterns are presumably indicative of separate phases.

The dynamic mechanical properties of the films obtained from the EB-cured fresh and aged blends were determined to detect compatibility and molecular structure differences caused by crystallization before network formation. The most pronounced dispersion in the loss tangent (tan δ) curves indicates the glass transition region. This absorption is usually attributed to the initiation of the micro-Brownian motion of the molecular chains indicating the onset of cooperative diffusional motion of the main chain segments. The phenomenon, accompanied by the drop of the storage modulus (E') is sometimes called the α peak (*15*).

The urethane groups ("hard segments") in the polymerized oligomer are far enough removed in solubility characteristics from the PEA "soft segments" to lead to the prediction of a two-phase system. However, the single α-peak in Figure 10 suggests a one-phase morphology in which the hard and soft segments are well mixed. The broadening of the α dispersion is probably related to the different modes of relaxation of these hard and soft segments.

The effect of aging on the pure oligomer samples is significant, as can be seen in Figure 10. The EB irradiation partially melts the crystallites; however, as implied by the micrographs, the structure of the crystallized oligomer is kept as a memory. The maximum in tan δ for the aged film is shifted to a higher value than the non-aged samples, from around -20 °C for fresh films to $+2$ °C. Also, the aged blends show a shoulder in the tan δ

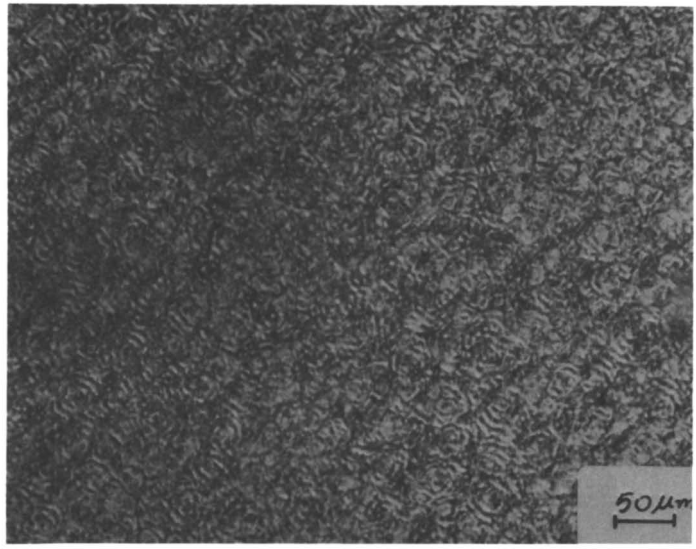

A

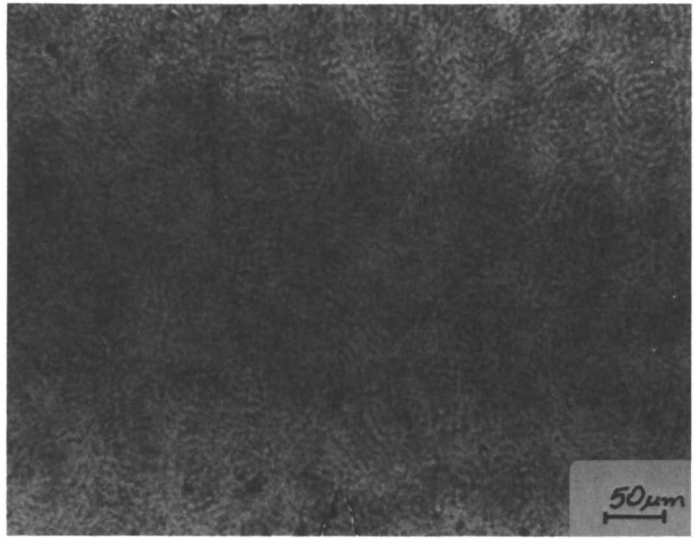

B

Figures 5A and B. Micrographs of unirradiated blends, aged (crystallized) for 2 weeks at 25 °C: A, pure oligomer and B, 10% epoxy.

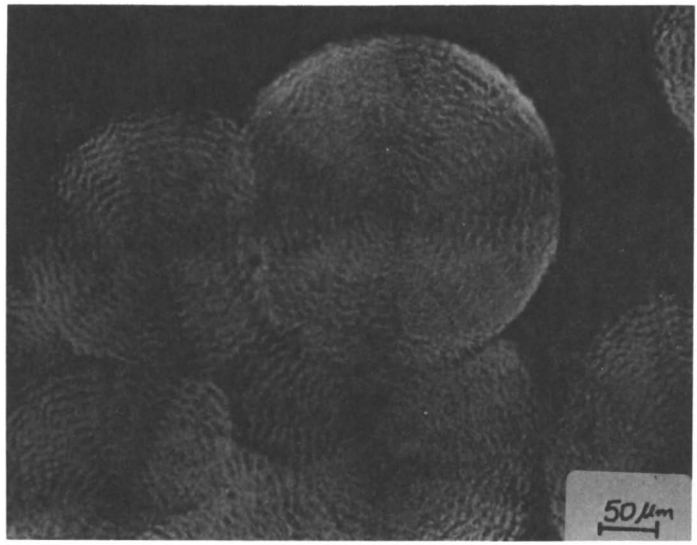

C

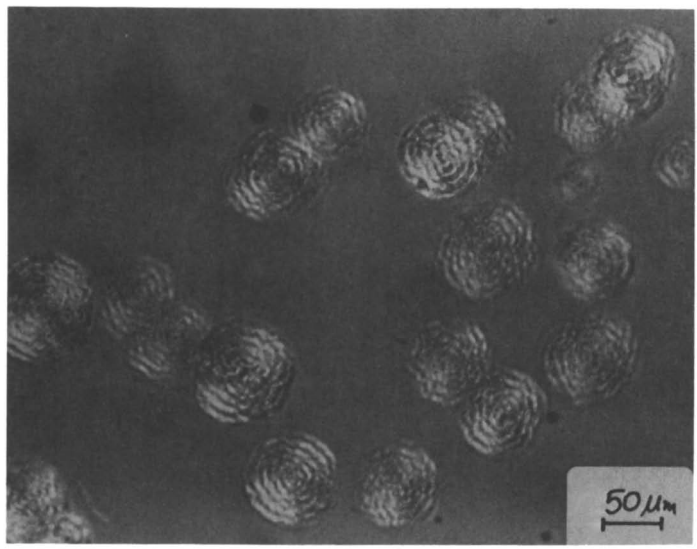

D

Figures 5C and D. Micrographs of unirradiated blends, aged (crystallized) for 2 weeks at 25 °C: C, 20% epoxy and D, 30% epoxy.

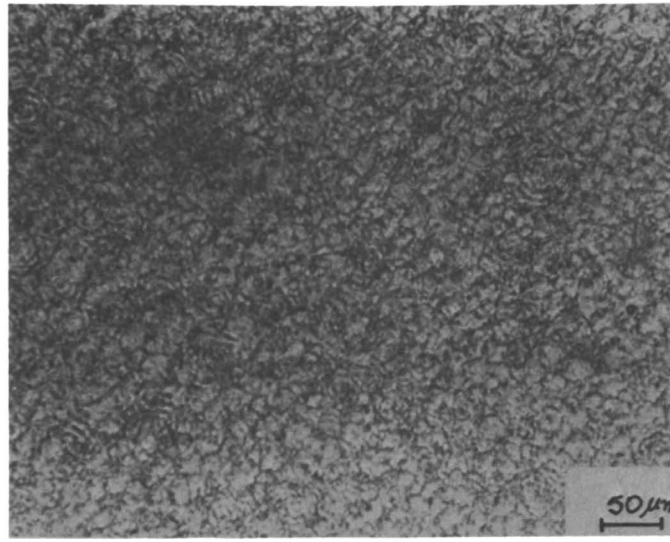

A

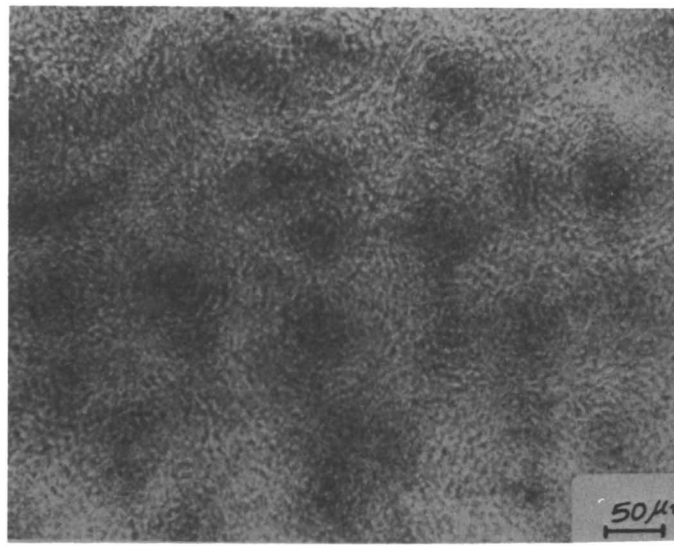

B

Figure 6. Films from Figure 5 after aging 4 weeks: A, pure oligomer and B, 10% epoxy.

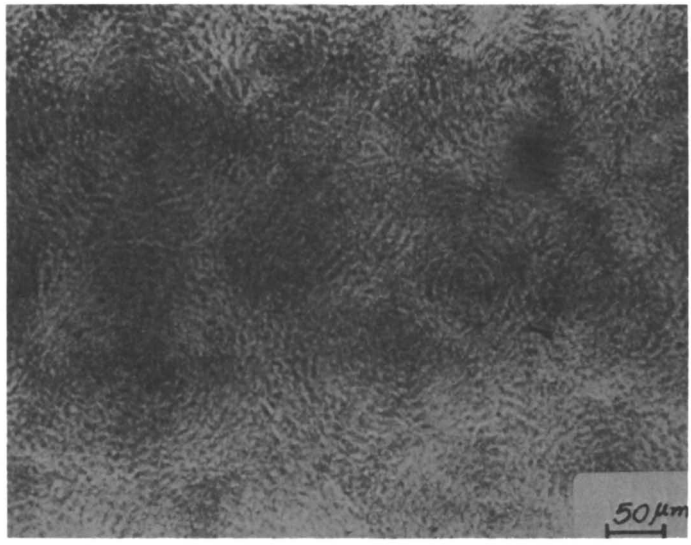

C

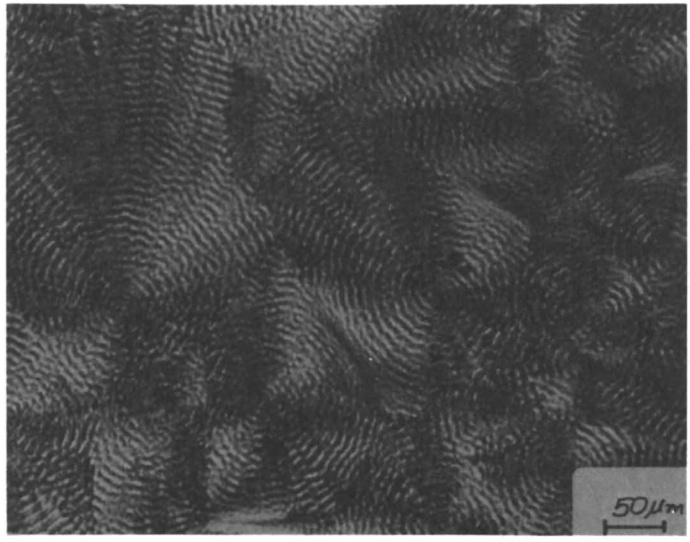

D

Figure 6. Films from Figure 5 after aging 5 weeks: C, 20% epoxy and D, 30% epoxy.

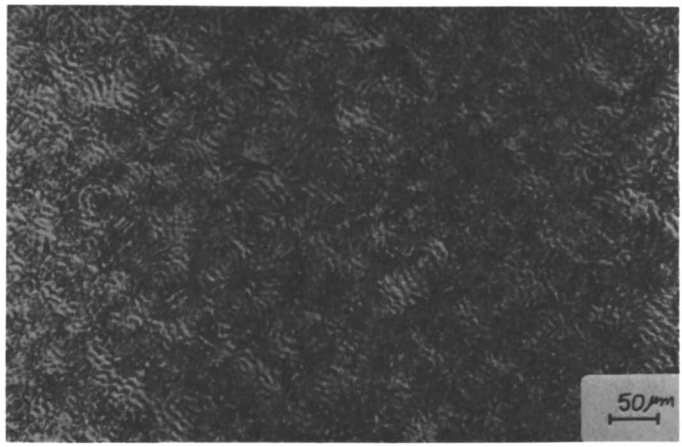

A

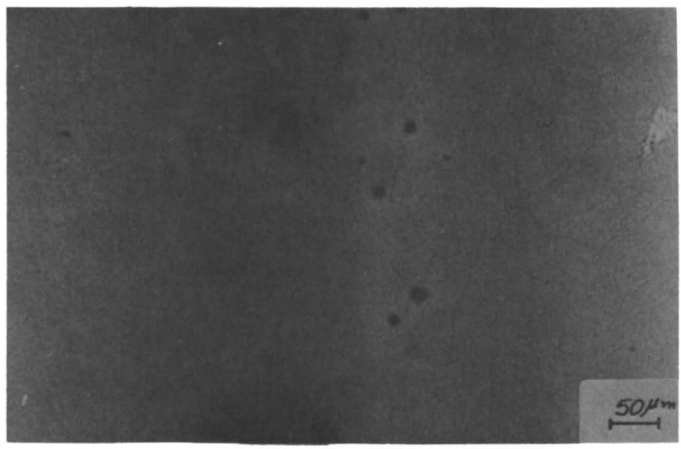

B

Figure 7. Micrographs of an aged 10% epoxy blend before (A) and after (B) EB curing.

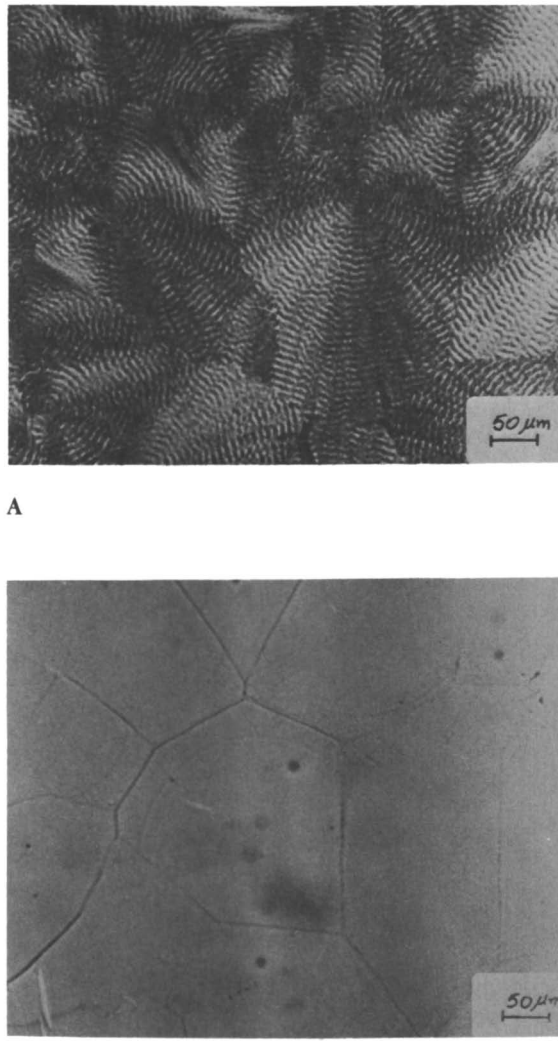

Figure 8. Micrographs of an aged 30% epoxy blend before (A) and after (B) EB curing.

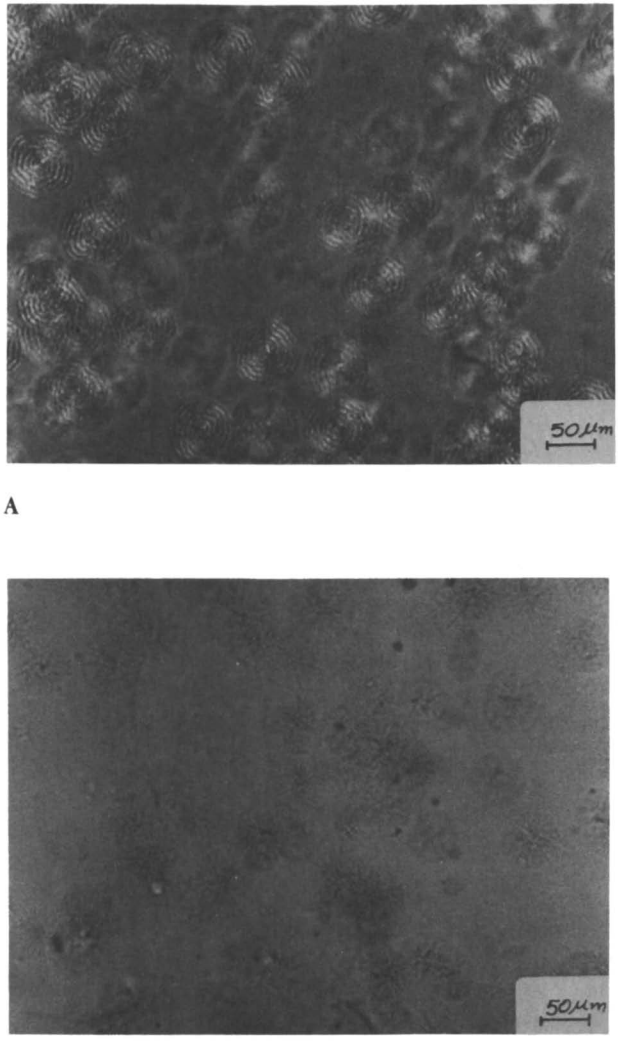

Figure 9. Micrographs of an aged 45 % epoxy blend before (A) and after (B) EB curing.

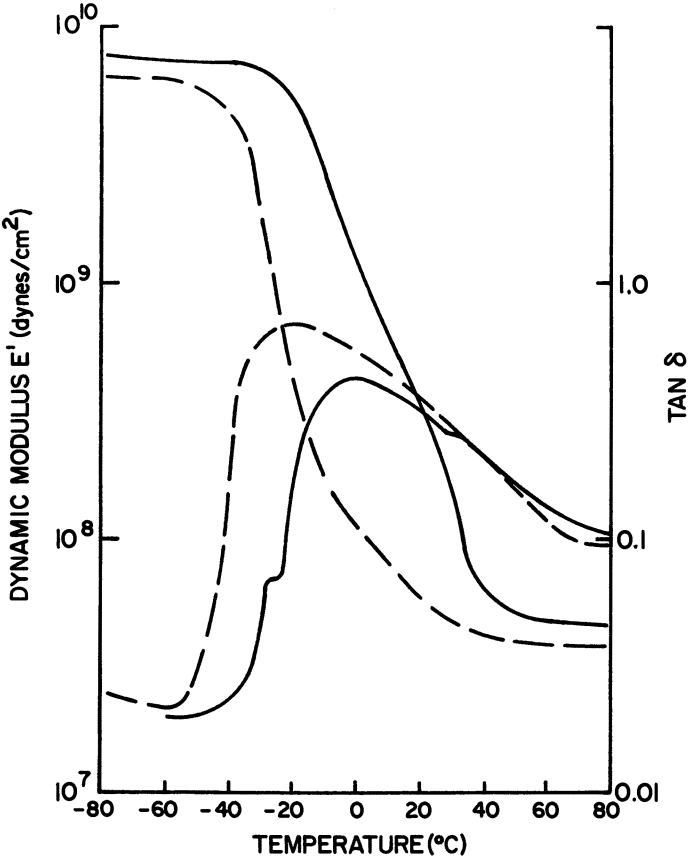

Figure 10. The effect of crystallization on mechanical spectra for EB-cured aged (—) and fresh (--) pure oligomer films.

curve at around − 25 °C. The presence of the shoulder may indicate that the melting during EB irradiation provides a fraction of amorphous polymer that behaves like the fresh samples. This amorphous part has a temperature for the α dispersion in the same range as the EB-cured fresh films. Therefore, the amorphous and partly ordered phases can be distinguished in the α peak. Another shoulder in the tan δ curve is observed at a temperature of about 30 °C. This dispersion is related to the molecular motion within the crystalline phase (*15*) and is called the α_c or a' dispersion. This dispersion is usually located between the α dispersion and the T_m (i.e., 36 °C for the pure crystallized oligomer).

The tan δ_{max} for nonaged films, 0.76, is larger than the value for aged films, 0.425. This difference could be predicted because the chain segments of the amorphous polymer are free from restraint imposed by the crystal-

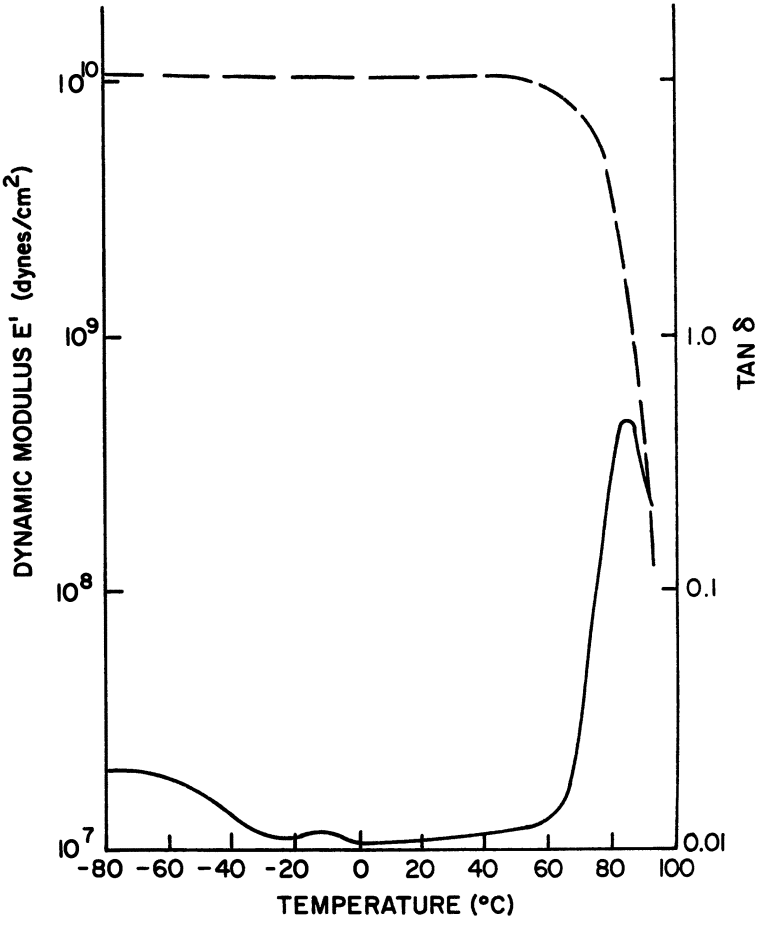

Figure 11. Mechanical spectra for pure epoxy. Key: —, tan δ; and --, E′.

line phase in the glass transition region. This restraint is reflected by the higher modulus E' for aged films in the transition region. Mechanical spectra for pure epoxy are shown in Figure 11. Its properties are not significantly affected by aging or EB curing.

The dynamic mechanical properties of polymer blends are determined primarily by the mutual solubility of the two components. If the two components are compatible and soluble in one another, the dynamic mechanical properties of the blend are nearly the same as those of a random copolymer of the same composition. As a consequence, the loss tangent–temperature curves show only one α peak. If any insolubility between the components is developed, the loss tangent–temperature curve shows two peaks; each peak is characteristic of the T_g of the phase associated with it.

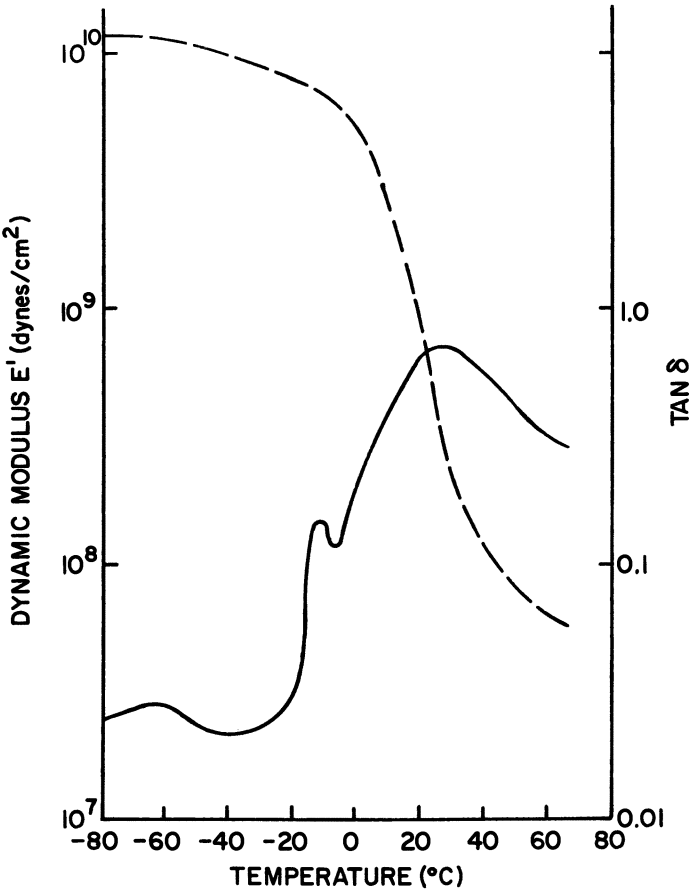

Figure 12. Mechanical spectra for a 25% epoxy blend, aged before EB curing. Key: —, tan δ; and --, E'.

The effects of aging and melting of aged blends are shown in Figures 12–14. Aging produces a low-temperature dispersion that varies from a light shoulder for 20% and 50% of epoxy to an individual peak for 25, 30, and 40% of epoxy. The extra dispersion for aged blends can be attributed to the oligomer-rich phase that was well developed during aging (i.e., crystallization). The melting conditions during EB irradiation are not enough to destroy the two-phase system. The maximum temperature of the extra peak is shifted to higher values as the percentage of epoxy increases in the blend. The temperatures for the maximum dispersion are – 10 °C for 25% of epoxy, 5 °C for 30% of epoxy, and 19 °C for 40% of epoxy. The shift in the temperature of the extra peak is presumably due to the higher concen-

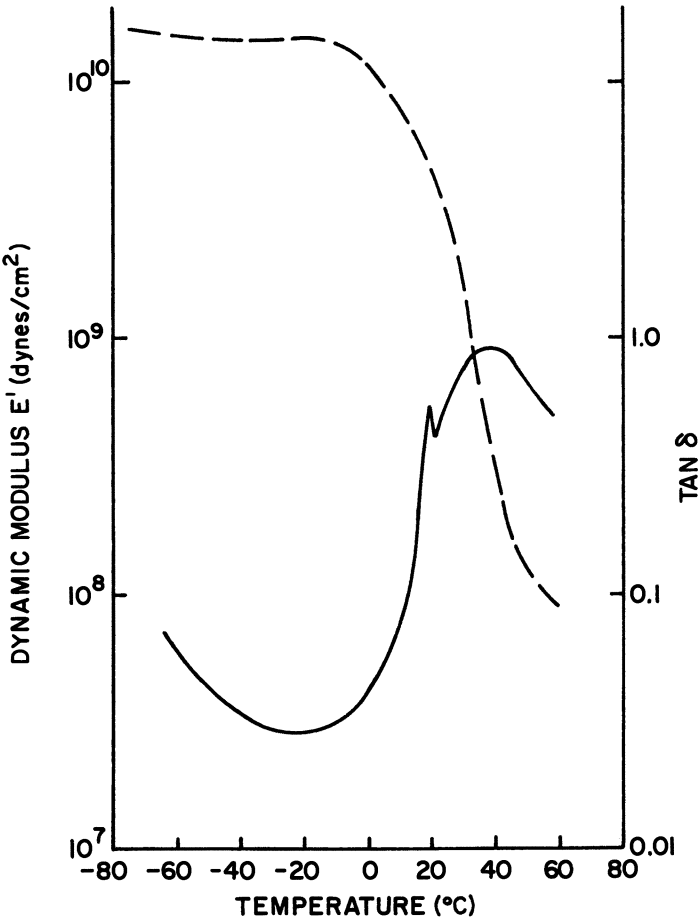

Figure 13. Mechanical spectra for a 40% epoxy blend, aged before curing. Key: —, tan δ; and --, E′.

tration of epoxy molecules in the oligomer-rich phase. Thus, some remixing during irradiation may be indicated.

Melting the aged films (3 h at 50 °C) before EB irradiation caused the low-temperature peaks to disappear for blends with 20, 40, and 50% of epoxy. Again, remixing of the phases is indicated. However, those conditions were not enough to destroy the extra peak for the blend containing 30% epoxy (Figure 14). T_m for this composition, determined by DSC, is about 5 °C above the T_m for the pure crystallized oligomer. This temperature difference could be responsible for the different responses in the kinetics of remixing. In addition to the relative stability of the extra peak, its sharpness is accentuated, and the maximum peak temperature is decreased

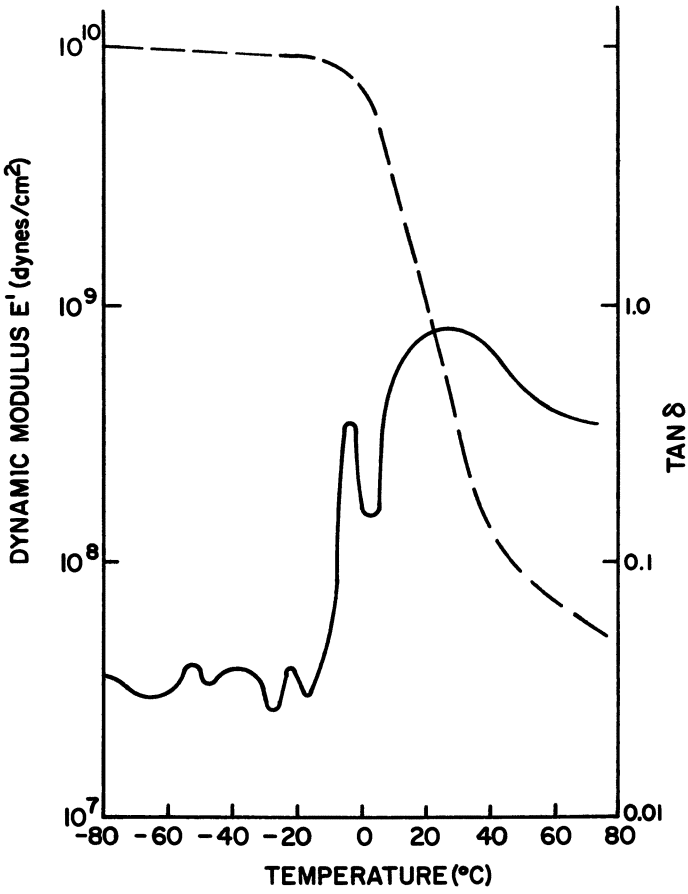

Figure 14. Mechanical spectra for a 20% epoxy blend, aged and remelted before curing. Key: —, tan δ; and --, E′.

by about 5 °C relative to that of the same composition cured without premelting. Therefore, the melting, although not sufficient to cause complete remixing, may eliminate the residual crystallinity that would be left in the oligomer-rich phase if it were irradiated before melting.

The loss tangent–temperature curves for EB-cured fresh (nonaged) blends in the same range of composition are shown in Figure 15 for comparison. No extra peaks or accentuated shoulders can be noticed in those curves, and, therefore, the fresh blends are relatively homogeneous mixtures.

Stress–strain curves and failure envelopes for the cured, fresh semi-IPNs are shown in Figure 16. The plasticization of the epoxy is apparent at high epoxy contents, and a yield develops just below 70% epoxy. In the

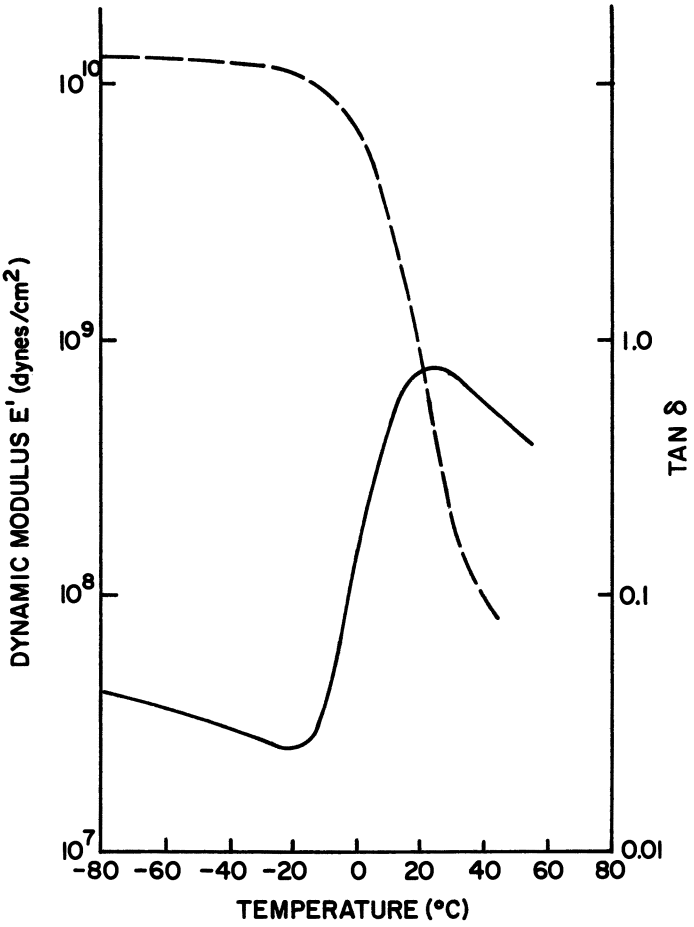

Figure 15. Mechanical spectra for a fresh, EB-cured, 30% epoxy blend.

middle range, the reinforcement of the soft oligomer network by the higher T_g epoxy is most effective. Low levels of epoxy decrease the breaking strength of the network. Stress-induced crystallization of the pure oligomer network, apparent in the stress–strain curve above strains of around 100%, is apparently restricted by the epoxy dilution, and reinforcement does not take place.

Energy to rupture for all the films is shown in Figure 17. The very sharp maximum in toughness at around 50% corresponds to a T_g of 20 °C (DSC). The area where phase separation was forced by precrystallization shows film toughness up to twice the value for those systems cured in the homogeneous condition. In the phase-separated films, the main T_g was increased about 5 °C and the low-temperature peak was at a temperature

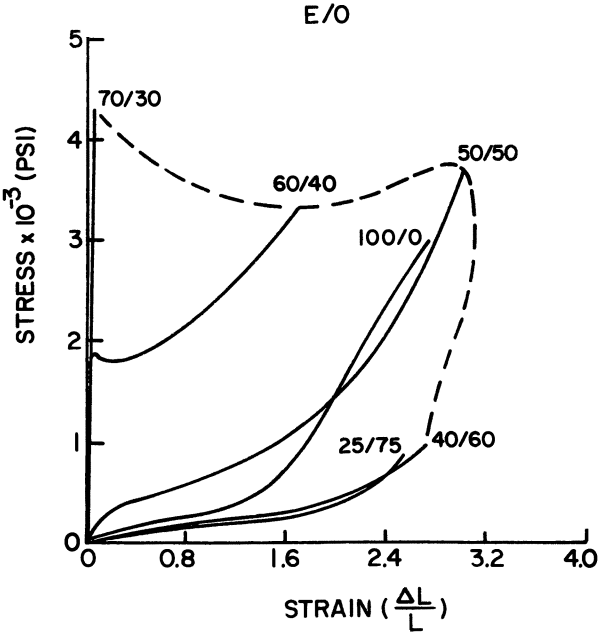

Figure 16. Stress–strain properties and failure envelope for fresh EB-cured blends.

indicative of almost pure oligomer. The removal of oligomer from the matrix would have increased its epoxy fraction (effectively shifting it to the left in Figure 17) and increased its toughness. Holding the aged films above the melt for 3 h apparently did not remove all traces of phase separation.

Summary

It has been shown that an acrylourethane acrylate oligomer based on PEA is compatible with a linear polyhydroxy ether in all proportions, and that semi-IPNs could be formed by polymerizing the end groups of the oligomer with EB or gamma radiation. Anomalously low T_g values were observed in the high-epoxy composition range. These values were presumed to be associated with the mobility in the urethane acrylate end groups, because the anomaly disappeared after IPN formation. Crystallizing the oligomer before IPN formation produced a phase separation that could be stabilized by network formation. Film toughness was twice that of the homogeneous semi-IPN. Melting point depression from epoxy dilution was not observed, and the increase in T_m was associated with a increase in crystalline perfection caused by the epoxy in the blend.

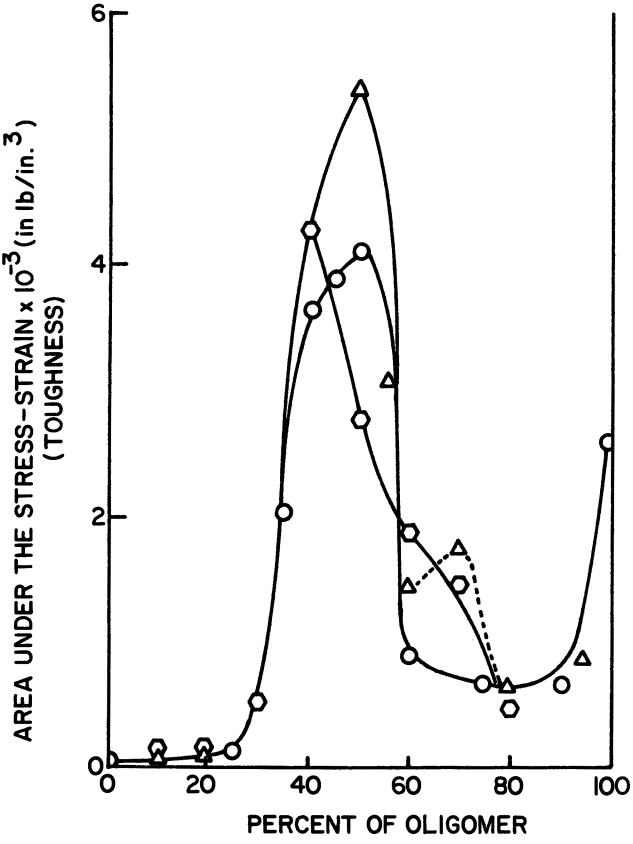

Figure 17. Toughness of EB-cured semi-IPNs. Key: △, aged; ⬡, melted aged; and ○, fresh.

Nomenclature

E/O	Ratio of epoxy to oligomer (percent)
T_g	Glass transition temperature
T_{g1}	Glass transition temperature of the oligomer
T_{g2}	Glass transition temperature of the epoxy
T_m	Melting temperature

Literature Cited

1. Sperling, L. H. "Interpenetrating Polymer Networks and Related Materials"; Plenum: New York, 1981.
2. Thomas, D. A.; Sperling, L. H. In "Polymer Blends"; Paul, D. R.; Newman, S., Eds.; Academic: New York, 1978; Vol. 2.

3. Sperling, L. H. "Polymer Alloys"; Plenum: New York, 1977.
4. Frisch, H. L.; Frisch, K. C.; Klempner, D. *Pure Appl. Chem.*, 1981, *53*, 1557.
5. Hourston, D. J.; Zia, Y. *J. Appl. Polym. Sci.* 1983, *28*, 2139.
6. Hourston, D. J.; Zia, Y. *J. Appl. Polym. Sci.* 1983, *28*, 3745.
7. Hourston, D. J.; Zia, Y. *J. Appl. Polym. Sci.* 1984, *29*, 629.
8. Oraby, W.; Walsh, W. K. *J. Appl. Polym. Sci.* 1979, *23*, 3227.
9. Oraby, W.; Walsh, W. K. *J. Appl. Polym. Sci.* 1979, *23*, 3243.
10. Howard, D. D.; Martin, B. *Radiat. Curing* 1977, *4(2)*, 8.
11. Wadhwa, L. H.; Walsh, W. K. *J. Appl. Polym. Sci.* 1982, *27*, 591.
12. Harris, J. E.; Goh, S. H.; Paul, D. R.; Barlow, J. W. *J. Appl. Polym. Sci.* 1982, *27*, 839.
13. Hage, E., Ph.D. Thesis, North Carolina State Univ., 1983.
14. Martuscelli, E. In "Polymer Blends: Processing, Morphology, and Properties"; Martuscelli, E.; Palumbo, R.; Kryszewki, M., Eds.; Plenum: New York, 1980.
15. Murayama, T. "Dynamic Mechanical Analysis of Polymeric Material"; Elsevier: New York: 1978; p. 64.

RECEIVED for review November 15, 1984. ACCEPTED February 28, 1985.

15

Binary and Ternary Blends of Polybutadiene–Polystyrene Block Copolymers and Homopolymers

Developments in Achieving Toughness Through Control of Particle Morphology

O. S. GEBIZLIOGLU, A. S. ARGON, and R. E. COHEN
Massachusetts Institute of Technology, Cambridge, MA 02139

Crazing as a mechanism of toughening has been investigated in model multiphase polymer blends composed of two polybutadiene–polystyrene (PB–PS) block copolymers with homopolystyrene (PS) and homopolybutadiene (PB). The two block copolymers, each with 23% PB, have different morphologies. Of these blends, one (KRO-1) exhibits a morphology of interconnected rods, whereas the second (KRO-3) has a lamellar morphology. Transmission electron microscopy on ultratomed sections of solution spin-cast films of either KRO-1 or KRO-3 and PS shows broad particle-size distributions of KRO-1 and KRO-3 and a statistical mean-particle radii of 0.4 μm and 0.1 μm, respectively. To improve the craze-initiating efficiencies of particles, low molecular weight polybutadiene (LMWPB) was used to modify the particle morphologies. The efficiency of the modified particle depends on the molecular weight of the added PB, the PB–block copolymer blend ratio, and the block copolymer microstructure. Particle structures with a wide range of elastic compliances are obtained. Tensile tests indicate that toughness depends on the morphology and mechanical properties of the particles.

TOUGHENING OF GLASSY POLYMERS by incorporation of compliant heterogeneities is an important industrial practice. In systems toughened by enhanced dilatational (craze) plasticity, particles with optimum features promote craze initiation within the glassy matrix without permitting the transformation of crazes into cracks or detachment at the particle–matrix interface. The roles of size and internal structure of the particles and the nature of the particle–matrix interface remained ill-understood because of the difficulty of controlling the morphological parameters independently.

0065-2393/86/0211/0259$06.00/0

However, development (*1–6*) in synthesis techniques and in understanding structure–property relationships of block and graft copolymers have led to the preparation of particle–matrix systems with controllable morphologies. Using modern methods of morphology control, we have prepared a variety of particle structures to understand the role of particle structure in craze plasticity and elucidate the basic ingredients of toughening by stable crazing. We will present a brief review of earlier results and summarize some recent developments.

Control of Morphology

After Riess et al. (*7*) and Inoue et al. (*8*) demonstrated that low molecular weight homopolymer components could be solubilized by the corresponding block components in block copolymers, this technique was employed as an effective means of morphological coarsening and for obtaining morphological transformations. By choosing homopolymer molecular weights larger than the molecular weight of the corresponding block in block copolymers, the latter can be emulsified in the homopolymer. A second homopolymer with molecular weight that is smaller than that of the corresponding block component can also be incorporated to affect the morphology. The ternary diagram in Figure 1 gives components and compositions that illustrate the strategy used in the control of morphology in this work.

The right and left sides of the triangle represent blend compositions for K-Resin–polybutadiene (PB) and K-Resin–polystyrene (PS) binaries, re-

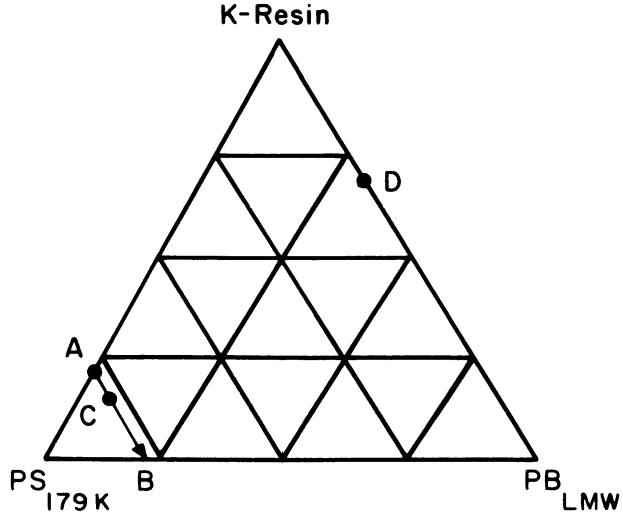

Figure 1. Ternary composition diagram used for the system K-Resin–LMWPB–PS.

spectively. For the particular components used, K-Resin–PS blends are systems of composite particles in a glassy matrix, whereas K-Resin–PB blends give phase-separated materials with various morphologies. On the left side of the triangle, point A represents K-Resin particles at a weight fraction of 0.217 in 268,000 PS. Then, the line A–B depicts ternary blends at a constant particle-weight fraction of 0.217 with various blend ratios of low molecular weight PB (LMWPB) to K-Resin. Along line A–B, PB replaces K-Resin while the amount of PS remains constant.

Experimental

Materials. For binary blends, two commercial PB–PS block copolymers, KRO-1 and KRO-3, were used with a PS of relatively large molecular weight (HH-101). For ternary blends, PBs of narrow molecular weight distribution with various molecular weights were added to binary blends. PBs of molecular weight 6.0 kg/mol (PB6K) and 20 kg/mol (PB20K) were synthesized in this laboratory. PBs of molecular weight 2.5 kg/mol (PB2.5K) and 3.0 kg/mol (PB3K) were obtained from Polysciences, Inc. Table I lists the relevant properties of these components.

Transmission electron microscopy (TEM) shows two radically different microstructures for the block copolymers, KRO-1 and KRO-3. The KRO-1 microstructure consists of randomly wavy and interconnected rods of PB 20 nm in diameter. The KRO-3 films exhibit a morphology of lamellae of PB with a thickness of 20 nm and a large aspect ratio. The PBs used are predominantly the 1,4-addition, as shown by proton NMR spectroscopy.

Methods. FILM PREPARATION. The solutions of K-Resins and PS in toluene were spin-cast to give films with a thickness of 0.5–0.7 mm. For ternary blending, a PB of selected molecular weight was added to the solution that contained K-Resin and PS. The details are described elsewhere (*9*).

TRANSMISSION ELECTRON MICROSCOPY. The microstructures of binary and ternary blends were examined in a transmission electron microscope (Philips 200), which was operated at an accelerating voltage of 80 kV. Prior to microscopy, specimens were stained with a 1% aqueous solution of OsO_4 (*10*).

TENSILE TESTING. All tensile tests were performed on an Instron tensile tester Model 1122. Test details are presented elsewhere (*9*).

Results and Discussion

Basic Blends Investigated. Earlier reports (*5*, *11*) have demonstrated that block copolymers of various microstructures can be emulsified with

Table I. Properties of Materials

Property	*KRO-1*[a]	*KRO-3*[a]	*HH-101*	*PB2.5K*	*PB3K*	*PB6K*	*PB20K*
$\bar{M}_w$	179.0	217.0	268.0	2.5	3.0	6.0	20.0
M_n	132.0	106.0	112.0	~2.5	~3.0	~6.0	~20.0

[a] Weight fraction of PB(K-Resin) is 0.23.

glassy homopolymers and that the resulting particles exhibit the characteristic block copolymer morphologies. The KRO-1 particles with a morphology of interconnected wavy rods have a topologically continuous network of PS. Therefore, the composite particle has relatively greater stiffness. The KRO-3 particles with lamellar morphology have less stiffness. However, neither of these particles is an efficient craze initiator.

For KRO-1–PS blends, addition of LMWPB leads to a transformation in particle morphology from interconnected, wavy rods to concentric shells of PB and PS (*9*). Concomitant with this morphological transformation, the craze yield stress is drastically reduced, and particles become sites of profuse crazing. Although all ternary blends of KRO-1, LMWPB, and PS show substantially reduced craze yield stress, their overall toughness strongly depends on the details of particle structure. The blend with particles of nearly perfect concentric spherical shells exhibits maximum toughness. This feature is illustrated in the plots in Figure 2 for the PB3K–KRO-1–PS system. The role of the PB molecular weight, block copolymer microstructure, and the mechanical properties of the particles in the toughening process will be discussed. Further details appear elsewhere (*9*, *11*, *12*).

Optimum Polybutadiene Molecular Weight in Blends. For solubilization, the molecular weight of PB should be less than that of the corresponding block component. Information on the number and length of the block copolymer arms has not been disclosed for the K-Resins, and their segmental molecular weights are unknown. Therefore, to achieve solubilization, a systematic search over a range of PB molecular weights was undertaken.

The overall weight-average molecular weight of KRO-1 is 179.0 kg/mol, as shown in Table I. For a PB weight fraction of 0.23, the PB and PS segments have overall molecular weights of 41.2 kg/mol and 137.8 kg/mol, respectively. Thus, for the average star-shaped KRO-1 molecule of n arms, the relevant segmental molecular weights of any individual arm will be $41.2/n$ for PB and $137.8/n$ for the PS block. Gel permeation chromatography (GPC) suggests that both KRO-1 and KRO-3 have a distribution of arm numbers (n) and arm lengths. Consequently, for a PB with a narrow molecular-weight distribution, a weight-average molecular weight equal to or smaller than 14,000 should be used for a three-arm-star block copolymer. This assumption is supported by the negative results of the blending trials using PB44K and PB22K (*12*). In those preparations, the particle-volume fraction was kept constant at 0.217 for the same ratio of LMWPB to KRO-1 resin. In a similar trial, PB20K was blended with KRO-1 for two blend ratios, 0.5 and 0.07. As with PB22K and PB44K, the free surface of the cast films contained a sticky layer of centrifugally separated PB20K.

From these results, a substantial reduction in the molecular weight of PB seemed necessary for successful solubilization of the LMWPB into the

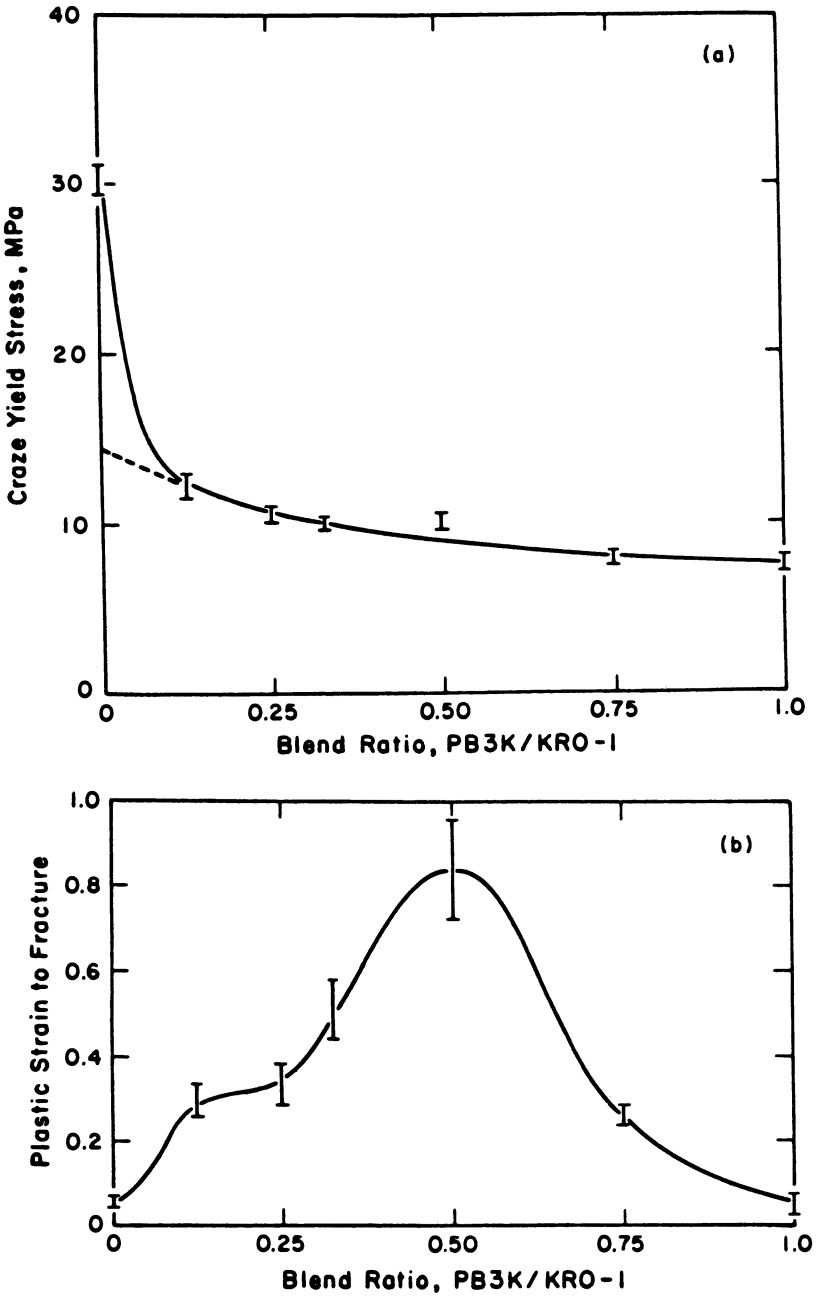

Figure 2. Effect of the increasing blend ratio on mechanical properties: (a) craze yield stress, and (b) plastic strain-to-fracture. (Reproduced from Ref. 11. Copyright 1985 Butterworths Ltd.)

K-Resin morphology. PB6K, PB3K and PB2.5K were separately blended with KRO-1 and PS. Their solubilization leads to a transformation of morphology from distorted rods to concentric shells. Figure 3a shows a micrograph of a PB6K–KRO-1–PS blend with a particle-weight fraction of 0.217 and a PB6K–KRO-1 blend ratio of 0.5. If compared with Figure 3a, the micrograph in Figure 3b shows the structural perfection achievable with PB3K blended into KRO-1. In this figure, the accompanying morphological transformation is clearly visible. Thus, modification with LMWPB gives particles of similar morphology, regardless of the molecular weight of the PB used. However, tensile test results (Figure 4) reveal that the toughening obtainable by particles containing PB3K and PB6K is quite different. For the PB2.5K–KRO-1–PS system, morphology and tensile behavior are similar to those of the PB3K–KRO-1–PS system. Figures 4a and 4b show that incorporation of LMWPB into KRO-1 reduces the craze yield stress from 30 MPa in the binary blend to around 10 MPa. The plastic strain-to-fracture, however, is fourfold larger for the PB3K-modified blend, than for the PB6K–KRO-1–PS blend. Therefore, for the KRO-1–LMWPB–PS system with a particle-weight fraction of 0.217 and a blend ratio of 0.5, a PB

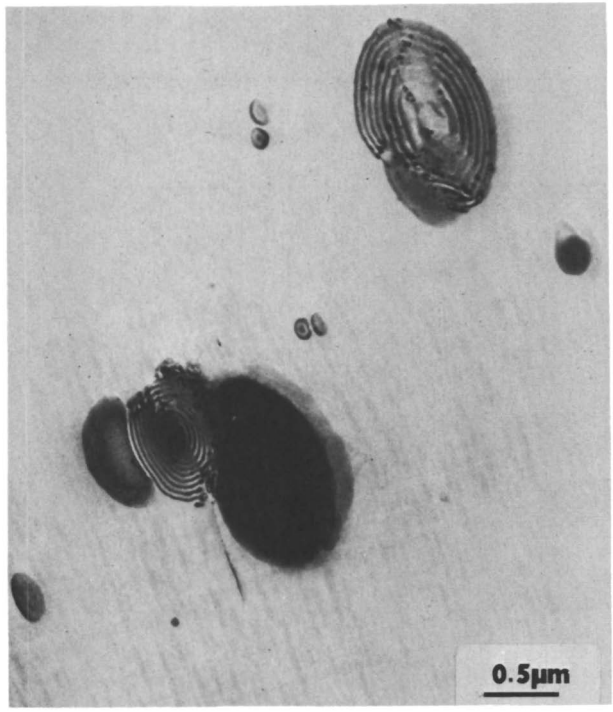

Figure 3a. Transmission electron micrograph of the blend PB6K–KRO-1–PS with a particle-weight fraction of 0.217 and blend ratio of 0.5.

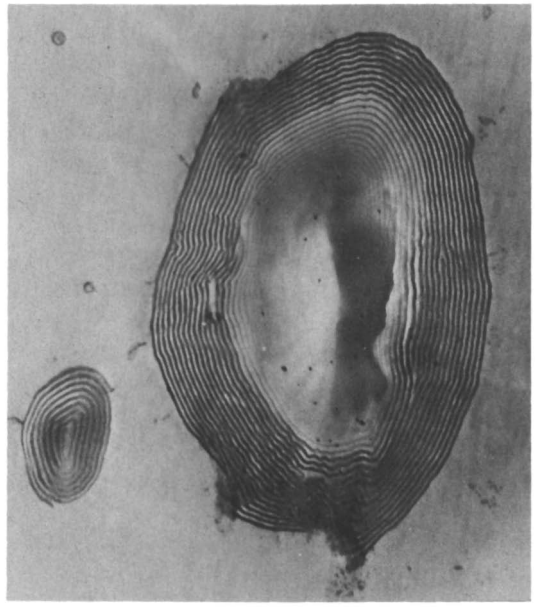

Figure 3b. Transmission electron micrograph of the blend PB3K–KRO-1–PS with a particle-weight fraction of 0.217 and blend ratio of 0.33. (Reproduced from Ref. 12. Copyright 1983 Springer–Verlag.)

molecular weight of 3.0 kg/mol appears to be very close to the optimum molecular weight for maximizing toughness. We have demonstrated (9) that, for PB3K, an optimum blend is one in which most particles have a morphology of concentric spherical shells. Above this blend ratio, particles contain domains of different morphology, and concentric spherical shell regions can coexist with the regions of characteristic KRO-1 morphology and regions of precipitated PB. This result implies that PB3K can only be solubilized up to a limit, which is determined by the chemistry and microstructural features of the block copolymer used. Then, for PB6K, a blend ratio of 0.25 gives a blend whose tensile behavior approaches that of the PB3K–KRO-1–PS blend with a blend ratio of 0.5. This is shown by the tensile test results of Figure 5.

The morphologies examined are nonequilibrium dispersions of particles in the glassy matrix. Under favorable conditions (i.e., slow solvent removal) equilibrium is reached with the complete separation of block copolymer and PS in the centrifugal force field of the spin caster. PB has never been found within the glassy matrix but has always been found associated with the block copolymer domains. Therefore, added PB associates with the block copolymer domains at very early stages of spin casting.

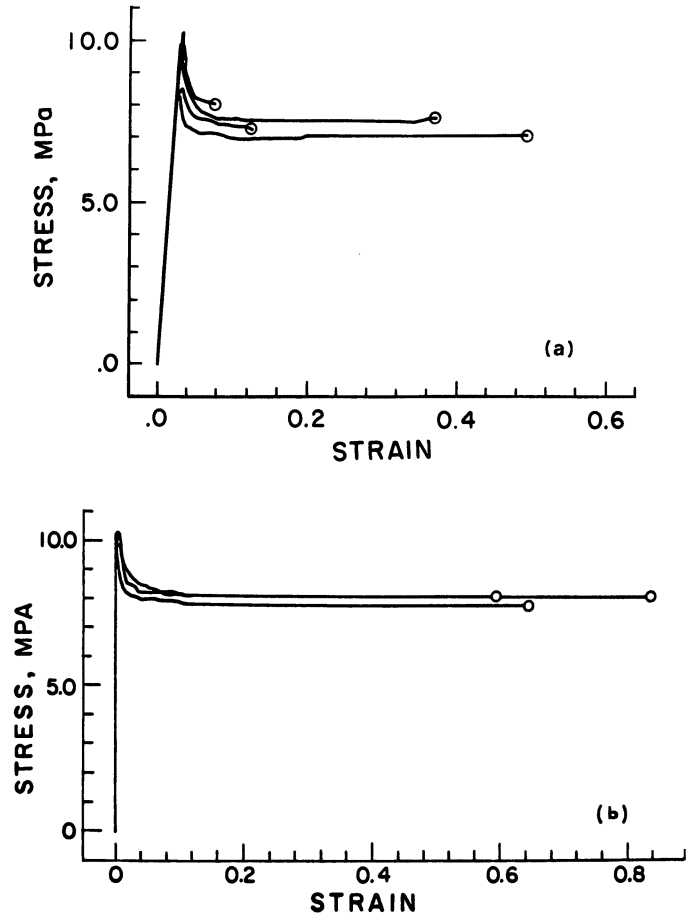

Figure 4. Stress–strain curve for a modified blend with a particle-volume fraction of 0.217 and blend ratio of 0.5: (a) PB6K–KRO-1–PS system; and (b) PB3K–KRO-1–PS system.

The Role of Block Copolymer Microstructure. We have presented evidence that particle structure (constitution and morphology) influences toughness. For a given block copolymer, the molecular weight and blend ratio of the coarsening agent are important parameters of particle internal structure. Next, we discuss the effect of block copolymer microstructure.

To determine the role of block copolymer microstructure, the ternary blend of optimum properties (i.e., KRO-1–PB3K–PS) with a particle-weight fraction of 0.217 and a blend ratio of 0.5 was used as a reference, and a similar blend was prepared with KRO-3 instead of KRO-1. The binary blends of KRO-3 and PS contain particles of characteristic KRO-3 morphology. Therefore, modification of KRO-3 with PB3K does not result

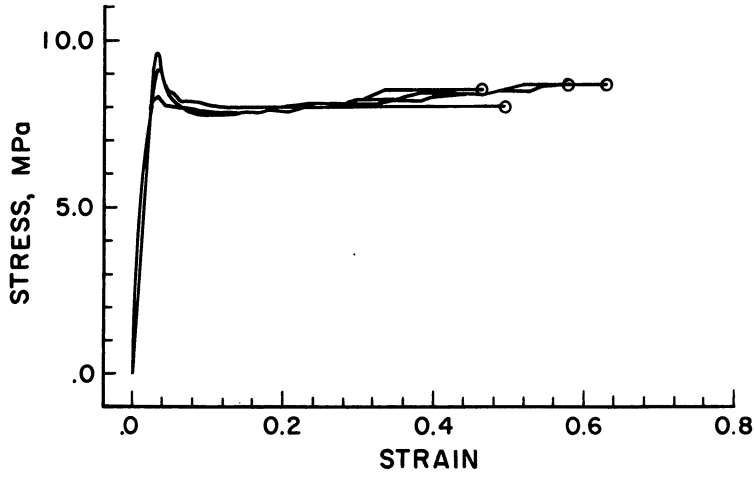

Figure 5. Stress–strain curve for the PB6K-modified blend with a blend ratio of 0.27.

in a morphological transformation. These particles show topological features similar to those of the KRO-1–PB3K–PS blend, and, as shown in Figure 6, they exhibit a tertiary structure of hexagonally packed PS spheres embedded in the PB domains (*13*). Tensile-test results shown in Figure 7 indicate that PB3K modification of KRO-3 gives a dramatic drop in the yield stress. This drop is similar to that observed for the KRO-1–PB3K–PS system. But, in striking contrast with the KRO-1–PB3K–PS blend, plastic strain-to-fracture does not increase appreciably in the KRO-3–PB3K–PS system.

TEM of crazed specimens suggests that crazes are initiated around the modified KRO-3 particles, but they cease to grow within a short distance from the particle boundaries. At this point, any connection between low toughness and the existence of a tertiary structure within the particles is only conjectural. However, TEM results imply that this tertiary microstructure may more readily initiate craze-matter breakdown. Nevertheless, the results presented in this section together with those of preceding sections confirm again that toughness requires profuse initiation and extension of crazes with ready conversion of glassy matrix into craze matter. Also, particle structures vary widely in their toughening characteristics. Two types of particles that are equally effective in craze initiation may impart considerably different levels of toughness. This difference may be due to their different resistance to break down once parts of the particle are incorporated into craze matter.

Morphology and Tensile Behavior of Particles. The properties of the materials from which particles are made may complement the results re-

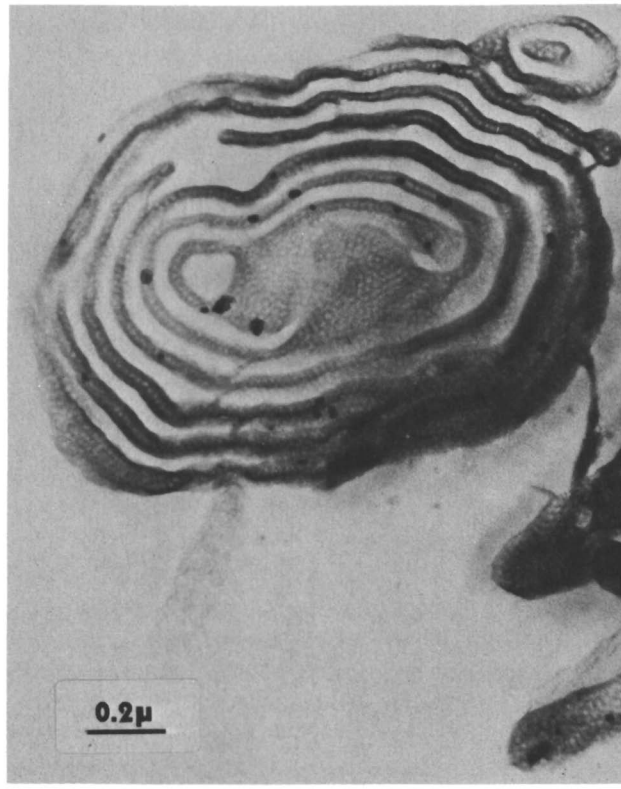

Figure 6. Transmission electron micrograph for the blend of KRO-3–PB3K–PS with a particle-weight fraction of 0.217 and blend ratio of 0.5. (Note the highly ordered tertiary structure inside the PB shells.)

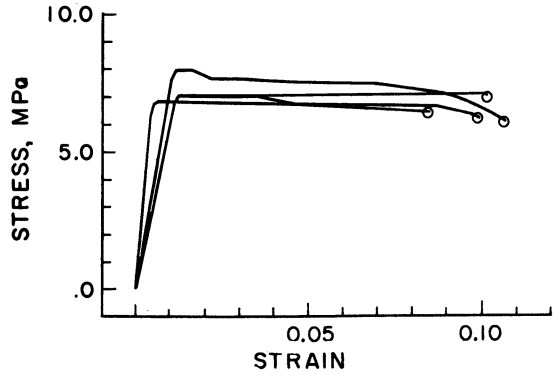

Figure 7. Tensile curves for the KRO-3–PB3K–PS blend with a particle-weight fraction of 0.217 and blend ratio of PB3K–KRO-3 of 0.5.

ported in the preceding sections. In Figure 1, point D on the right side represents the K-Resin–LMWPB blends with weight ratios of 0.5. For both KRO-1 and KRO-3, the blend ratio of 0.5 corresponds to a rubber fraction of 0.49. The micrographs in Figure 8 show that both blends exhibit the characteristic particle morphologies observed in the corresponding ternary blends with PS. For both blends, micrographs indicate the absence of long-range lamellar orientation. This absence is confirmed by the similar tensile behavior observed when the films were tested at two transverse directions.

The tensile tests at the low-strain rate reveal that tensile strengths and strains-to-fracture are low, as shown in Figure 9. Although the moduli are of comparable magnitude, the two blends differ considerably in their tensile strengths and values of fracture strain. Whereas the binary blend of PB3K and KRO-1 exhibits a tensile strength of 1.5 MPa, the strength is less than 1.0 MPa for the PB3K–KRO-3 blend. The PB3K–KRO-1 blend shows a fracture strain which is fourfold larger than that of the PB3K–KRO-3 blend.

The tensile properties of block copolymers KRO-1 and KRO-3 are in sharp contrast with those of their binary blends with PB3K. As presented in Table II (*14*), KRO-1 has lower modulus and strain-to-fracture. Although it breaks at a strain of less than 1%, its binary blend with PB3K shows an extension of nearly 90%. For KRO-3, the trend is reversed.

Again, the connection between the low-fracture strain of PB3K–KRO-3 blend and the existence of a tertiary structure may be subject to the same conjecture presented earlier.

Summary and Conclusions

Toughness of heterogeneous polymers is governed by particle morphology. This morphology is affected by the molecular weights, blend ratios, and chemistry of the component homopolymers and block copolymers.

Through blending studies of KRO-1 and KRO-3 block copolymer resins into high molecular weight PS and further modification achievable with the addition of LMWPB(X)K (X equals 3 or 6), three different particle morphologies were obtained: wavy and randomly interconnected PB rods of the KRO-1 morphology, alternating concentric spherical shells of PB and PS, and concentric spherical shells of PS and PB. The latter system contained occluded microspheres of PS. The total particle-volume fraction was maintained constant (0.217) in all materials examined.

When PB3K was blended into the KRO-1 particles, a morphological transformation from interconnected PB rods to concentric spherical shells was obtained. This transformation systematically increased the thermal misfit stresses in the particles. Increasing thermal stresses and particle compliances produces systematic reductions in craze flow stress and dramatic increases in strain-to-fracture, as long as the PB3K is solubilized into the PB component of the KRO-1 resin. Incorporation of PB(X)K into KRO-3 resin

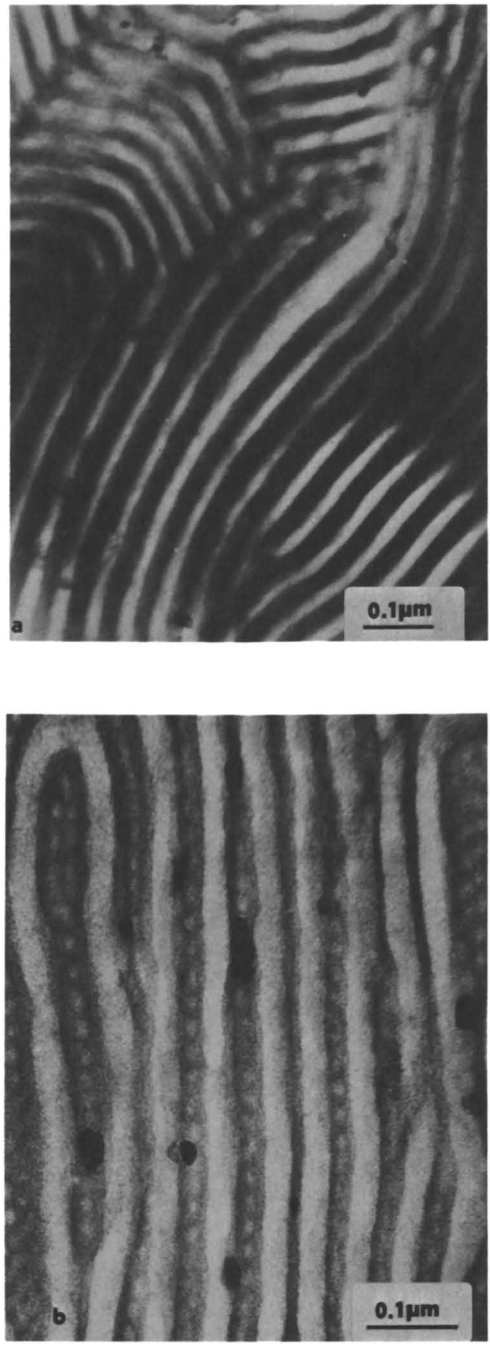

Figure 8. Transmission electron micrograph of the binary blend with a blend ratio of 0.5: (a) PB3K–KRO-1 blend; and (b) PB3K–KRO-3 blend.

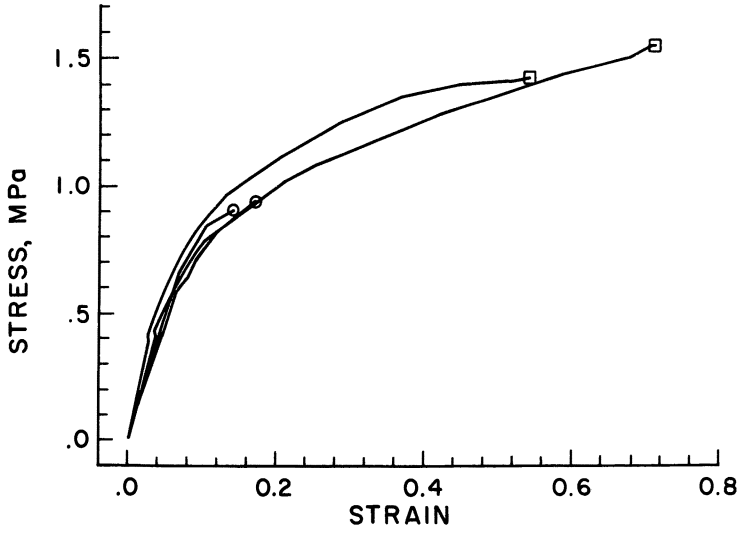

Figure 9. Stress–strain curves for binary blends of K-Resins with PB3K. Key: □, *PB3K–KRO-1, 0.5; and* ○, *PB3K–KRO-3, 0.5.*

Table II. Mechanical Properties of K-Resins at 20 °C

Property	*KRO-1*	*KRO-3*
Yield stress, MPa	20.95	21.00
Modulus, E, MPa	1241.10	1379.00
ϵ_f	0.09	1.10

also produces reductions in craze flow stress, but only moderate increases in strain-to-fracture are achieved.

This trend is paralleled by the tensile strengths and breaking strains of PB3K–KRO-1 and PB3K–KRO-3 binary blends. Thus, PB3K–KRO-1–PS blends exhibit higher craze yield stress (10 MPa) and plastic strain-to-fracture (over 80%) than the craze yield stress (7.5 MPa) and plastic strain-to-fracture (8%) of KRO-3–PB3K–PS blends. The tensile strengths (1.5 MPa for PB3K–KRO-1 blend and 1.0 MPa for PB3K–KRO-3 blend) and breaking strains (70% for PB3K–KRO-1 blend and 18–20% for PB3K–KRO-3 blend) for the binary blends that make up the particles indicate that particles with higher tensile strength and elongation-at-break give tougher composite materials. This important result points out a third ingredient for toughness: the structural integrity of the particles with large stiffness and thermal expansion mismatch.

Acknowledgements

This research has been supported by the National Science Foundation/Materials Research Laboratories under Grant No. DMR 81–19295, through the Center for Materials Science and Engineering at Massachusetts Institute of Technology, and by a post-doctoral fellowship from the Monsanto Polymer Products Company.

Literature Cited

1. Riess, G.; Marti, S.; Refrieger, J. L., Schlienger, M. In "Polymer Alloys"; Klempner, D.; Frisch, K. C., Eds.; Plenum: New York, 1977; p. 327.
2. Riess, G.; Schlienger, M.; Marti, S. *J. Macromol. Sci. Phys.* **1980**, *B17(2)*, 355.
3. Echte, A. *Angew. Makromol. Chem.* **1977**, 58–59, 175.
4. Kruse, R. L. *Polym. Prepr. Am. Chem. Soc. Div. Polym. Chem.* **1977**, *18(1)*, 838.
5. Gebizlioglu, O. S.; Argon, A. S.; Cohen, R. E. *Polym. Prepr. Am. Chem. Soc. Div. Polym. Chem.* **1981**, *22(2)*, 257.
6. Jiang, M.; Huang, X.; Yu, T. *Polymer* **1983**, *24*, 1259.
7. Riess, G.; Kohler, J.; Tournut, C.; Banderet, A. *Rubber Chem. Technol.* **1969**, *42*, 447.
8. Inoue, T.; Soen, T.; Hashimoto, T.; Kawai, H. *Macromolecules* **1970**, *3*, 87.
9. Gebizlioglu, O. S.; Argon, A. S.; Cohen, R. E. *Polymer* **1985**, *26*, 529.
10. Kato, K. *Polym. Eng. Sci.* **1967**, *7*, 38.
11. Gebizlioglu, O. S.; Argon, A. S.; Cohen, R. E. *Polymer* **1985**, *26*, 519.
12. Argon, A. S.; Cohen, R. E.; Gebizlioglu, O. S.; Schwier, C. E. In "Advances in Polymer Science"; Kausch, H. H., Ed.; Springer: Berlin, 1983; p. 275.
13. Gebizlioglu, O. S.; Argon, A. S.; Cohen, R. E. *Polym. Prepr. Am. Chem. Soc. Div. Mater. Sci. Eng.* **1984**, *51*, 630.
14. Fodor, L. M.; Kitchen, A. G.; Biard, C. C. *Polym. Prepr. Am. Chem. Soc. Div. Mater. Sci. Eng.* **1974**, *34(1)*, 130.

RECEIVED for review November 15, 1984. ACCEPTED March 8, 1985.

16

Irreversible Microdeformation in Miscible Polymer Blends

D. L. WILFONG, A. HILTNER, and E. BAER

Department of Macromolecular Science, Case Western Reserve University, Cleveland, OH 44106

The irreversible microdeformation behavior of miscible glassy blends consisting of polystyrene (PS) and poly(2,6-dimethyl-1,4-phenylene oxide) (2MPPO) was studied by simultaneous measurement of craze kinetics and mechanical response. Addition of 2MPPO to PS resulted in an increase in the craze initiation stress, which was due to blend densification, and a subsequent transition from brittle to ductile failure. This transition correlated with an increase in craze density and a decrease in craze length caused by the onset of shear band formation. Ductile deformation was proceeded by highly localized necking, and subsequent stability and growth of the neck was dependent on the previous crazing behavior.

BLENDING OF COMPATIBLE POLYMERS is used for the improvement of thermal, rheological, and mechanical properties and is consequently of considerable commercial interest. One of the most widely known and unusual miscible blend systems consists of polystyrene (PS) and poly(2,6-dimethyl-1,4-phenylene oxide) (2MPPO). These components, which are miscible in all proportions, comprise the matrix material of the engineering thermoplastic known as Noryl (*1*, *2*). The observation of a single glass transition temperature (T_g) located between the T_g values of the respective homopolymers and the linear increase in refractive index with increasing 2MPPO content have been used as criteria for PS–2MPPO blend miscibility (*3–5*). The composition dependence of the blend T_g has been studied extensively by differential scanning calorimetry (DSC), dynamic mechanical methods, dielectric relaxation, probe penetration thermal mechanical analysis, and thermal optical analysis (*3–4*, *6–8*).

Miscibility on the segmental level is implied by the interaction between the phenyl ring of PS and the phenylene ring of 2MPPO as determined from UV and Fourier transform IR (FTIR) spectroscopy (*9*). The dynamic mechanical response of the secondary relaxations also suggests

0065–2393/86/0211/0273$06.00/0

mixing on the segmental level (*10*). The criteria for thermodynamic miscibility is assured through the negative heat of mixing and the positive entropy of mixing. These values were experimentally determined by small-angle neutron scattering (SANS) and microcalorimetry (*11–12*). The negative enthalpy of mixing is attributed to the phenyl–phenylene group coupling.

The PS–2MPPO blends have a negative excess volume of mixing (*13*), that is, the density of the blend compositions is greater than the weighted average of the densities of the component homopolymers. This uncommon synergistic behavior is also reflected in the tensile modulus. The observed moduli (*14*) for the PS–2MPPO blends are greater than expected from a simple rule of mixtures for a two-component system. This correlation between the tensile modulus and the density is a consequence of the strong intermolecular interactions between PS and 2MPPO. Similar synergistic behavior in the yield stress and tensile strength has also been reported (*10*, *15*) for PS–2MPPO blend compositions.

The irreversible deformation processes displayed by PS–2MPPO glassy blends are highly composition dependent. 2MPPO is a ductile polymer that deforms by shear banding, neck formation, and cold drawing. Conversely, PS exhibits extensive crazing upon deformation and subsequently fails at low elongations in a more brittle mode. A very important consequence of blending PS and 2MPPO is that they exhibit a transition from brittle to ductile modes of deformation (*10*, *15–16*). Blends containing low concentrations of 2MPPO craze upon deformation and fail in a brittle manner. However, blends with a high 2MPPO content display shear banding followed by neck formation and cold drawing. Intermediate compositions, in the transition region, show both crazing and shear-banding behavior. Shear-band blunting of craze tips is observed (*16*, *17*) in the transition compositions.

The PS–2MPPO composition in which the brittle-to-ductile or craze-to-shear transition is observed depends on many factors, such as strain rate, test temperature, film thickness, and thermal history (*10*, *15–16*). The mechanism of this transition was examined by Wellinghoff and Baer (*16*) for 3000-Å thick films with electron microscopy. For 10% 2MPPO, well-developed crazes and sharp shear bands are observed in the deformed films. For 20% 2MPPO, a mixed mode of deformation still occurs. The transition is clearly observed at a 30% concentration of 2MPPO: no crazes are visible in the electron micrographs, only diffuse shear bands.

Further examination of this transition is accomplished by using a concurrent optical microscopic–tensile deformation technique. This method (*18*) allows the simultaneous observation of both microdeformation events and mechanical behavior in films of 1-10 μm in thickness. Observations of the films by optical microscopy during conventional tensile tests allow the establishment of the relationship between the irreversible microdeforma-

tion events and mechanical behavior. This technique was first used (*18*, *19*) to elucidate the relationship between the mechanical behavior and craze growth kinetics for PS as a function of molecular weight, strain rate, and thermal history.

As a natural consequence, it is now desirable to examine the transitional behavior displayed by the PS–2MPPO miscible blends by the optical microscopic–tensile deformation method. In this work, the brittle-to-ductile or craze-to-shear band transition was investigated as a function of composition and strain rate, and the optically observed irreversible microdeformation events were correlated with the mechanical behavior.

Experimental

Materials and Film Preparation. The polymers used in this study were narrow-disperse atactic PS (molecular weight of 600,000; M_w/M_n = 1.10; Pressure Chemical Company) and additive-free 2MPPO (molecular weight of 22,000; M_w/M_n = 1.06; General Electric Company). Blends of PS with 20, 40, and 70% by weight 2MPPO were prepared by solution mixing the two homopolymers in chloroform. Thin films were cast from filtered solutions of about 10% by weight 2MPPO–PS onto clean, dust-free glass slides. Film casting and subsequent drying were performed in a covered hood to minimize inclusions of dust in the films. Residual solvent was removed from the films by heating to 5 °C above the T_g of the blend for 4 h. The films were then slowly cooled to room temperature, floated off the glass slides onto distilled water, and, after drying, cut into specimens.

Thermal Analysis. A differential scanning calorimeter (Perkin-Elmer DSC II) was utilized for determining the T_g for both the blended and unblended thin films. The T_g was defined as the midpoint of the heat capacity transition for the sample. A single glass transition that increased with increasing concentration of 2MPPO was observed for all compositions. The T_g values determined at a heating rate of 20 °C/min for PS with 20, 40, 70, and 100% 2MPPO were 109, 126, 140, 176, and 223 °C respectively. A single glass transition has been reported (*1*) for the entire 2MPPO–PS composition range and cited as evidence for miscibility. By combining the Williams–Landel–Ferry (WLF) equation in terms of free volume with the Kelly and Bueche's model for blend T_g values, Prest and Porter (*7*) showed that the composition dependence of the T_g for 2MPPO–PS followed the additivity of free volume. The T_g values determined in this study followed this relationship.

Sample Geometry. Specimens with a gauge height of 20 mm and a width of 3 mm were cut with a specially designed machined razor blade holder (*19*). An interference technique (*20*) using Fourier transform IR (FTIR) spectroscopy was employed to measure film thickness. An oscillating baseline was superimposed upon the thin film spectra, and the distance was measured between wave maxima, which are inversely proportional to film thickness. The average film thickness was between 1 and 10 μm. This sample geometry localized the deformation behavior in the center of the specimen to facilitate observation in the microscope.

Deformation Measurements. Stress and strain (ϵ) measurements were conducted on a standard Instron testing machine and based on the initial cross-sectional area of the film and crosshead displacement. Strain rates ($\dot{\epsilon}$) of 0.1, 0.5,

1.3, 4.0, and 35%/min were used. A 100-power polarizing optical microscope attached to a motor-driven 35-mm camera (Nikon) was used in conjunction with the stress–strain apparatus to simultaneously observe microdeformation processes. Photographs were taken at regular time intervals corresponding to specific strains, and information on the irreversible deformation processes was obtained from the photographs. Craze density (number of crazes per unit area) and craze length (mean length of at least 25 crazes) were evaluated from the photographs as a function of both stress and strain. At least five samples were tested at each strain rate, and the results were averaged.

Results

Simultaneous measurement of stress–strain behavior and irreversible microdeformation processes with the subsequent determination of craze kinetics was performed. The results obtained are presented in the following sections: Mechanical Behavior, Microdeformation Processes, and Craze Kinetics. In the first section, the stress–strain properties of the homopolymers and blends are described. Next, the irreversible microdeformation processes that were observed during the stress–strain measurements are delineated. Finally, the craze kinetics derived from both the stress–strain and irreversible deformation behavior are examined.

Mechanical Behavior. The stress–strain curves for PS, 2MPPO, and the blend compositions, determined at a strain rate of 0.1%/min, are shown in Figure 1. The elastic moduli decreased as the concentrations of 2MPPO in the blend increased and were greater than would be expected if the rule of mixtures were followed. This result is in accord with the results

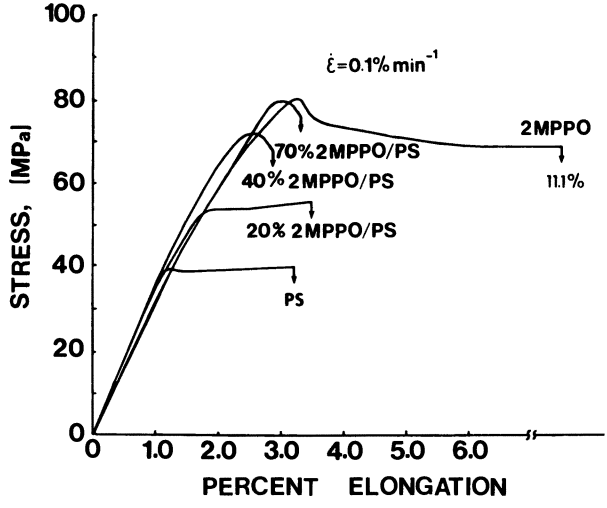

Figure 1. Representative stress–strain curves of PS, 2MPPO, and the blend compositions at a strain rate of 0.1%/min.

obtained by MacKnight and coworkers (*14*). The yield stress increased substantially from 39 MPa for PS to 80 MPa for a blend containing 70% 2MPPO. The yield stress obtained for 2MPPO was approximately the same as for the 70% 2MPPO–PS blend. Both PS and the 20% 2MPPO–PS blend displayed a yield followed by a draw region and fracture at 3% elongation. However, the 40 and 70% 2MPPO–PS blends also fractured at a strain of 3%, but this fracture occurred in the yield instability region. The 2MPPO exhibited a broad yield instability followed by drawing of the film to fracture at 11% elongation.

The mechanical behavior of PS as a function of strain rate is illustrated in Figure 2. PS displayed typical behavior: as the strain rate increased, the strain at fracture decreased, and the yield stress increased. The effect on the mechanical behavior of the addition of 20% 2MPPO to PS is shown in Figure 3. Both the strain at fracture and yield stress exhibited the same type of behavior with strain rate as shown for PS.

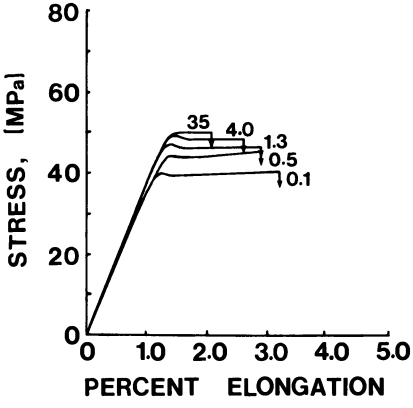

Figure 2. Representative stress–strain curves of PS at strain rates of 0.1, 0.5, 1.3, 4.0, and 35%/min.

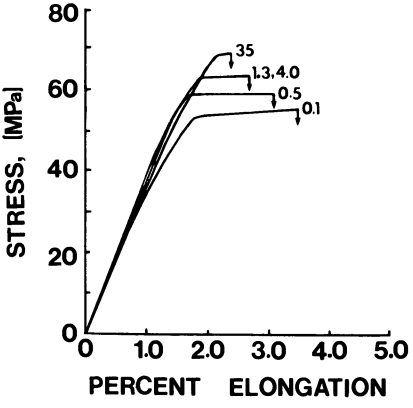

Figure 3. Representative stress–strain curves of the 20% 2MPPO–PS blend at strain rates of 0.1, 0.5, 1.3, 4.0, and 35%/min.

The mechanical behavior of the 40% 2MPPO–PS blend at the various strain rates is shown in Figure 4. Fracture occurred at the yield that was virtually unaffected by strain rate. The stress–strain curves of the 70% 2MPPO–PS blend films in which a highly strain-rate dependent complex fracture behavior was displayed are shown in Figure 5. At low strain rates,

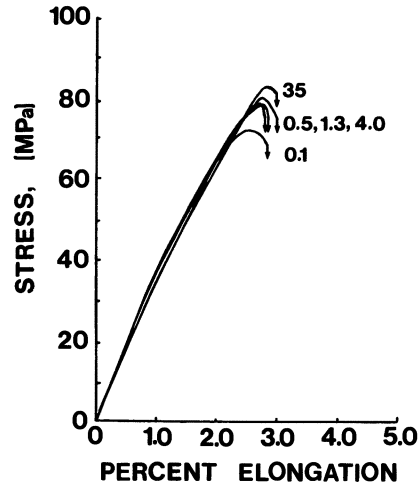

Figure 4. Representative stress–strain curves of the 40% 2MPPO–PS blend at strain rates of 0.1, 0.5, 1.3, 4.0, and 35%/min.

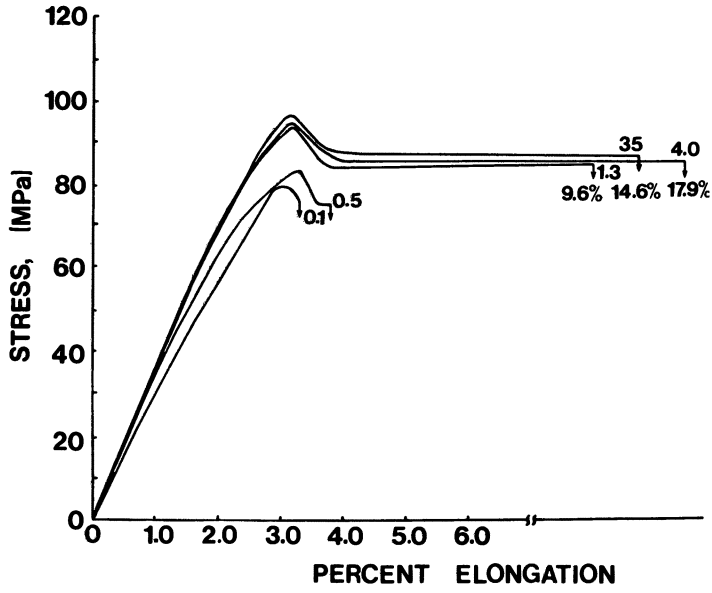

Figure 5. Representative stress–strain curves of the 70% 2MPPO–PS blend at strain rates of 0.1, 0.5, 1.3, 4.0, and 35%/min.

0.1 and 0.5%/min, the films fractured at the yield point. As the strain rate increased, the stress–strain curves displayed a draw region following the yield, and fracture occurred at high strains. The mechanical behavior of the 2MPPO homopolymer as a function of strain rate is shown in Figure 6. The 2MPPO films exhibited a pronounced yield instability and stress drop similar to the 70% 2MPPO–PS blend and showed ductile behavior at all strain rates. The strain at fracture increased with strain rate. All compositions displayed an increase in yield stress with strain rate. A comparison of the shape of the yield region of the 70% 2MPPO–PS blend and 2MPPO with those of PS and the 20% 2MPPO–PS blend shows that the yield instability has broadened and the subsequent stress drop has become much larger.

Microdeformation Processes. The first observable irreversible microdeformation in PS and the 20% 2MPPO–PS blend occurred at the onset of the nonlinear region in the stress–strain curve. At this point, crazes started to nucleate. As the stress and strain continued to increase, more crazes were nucleated, and the existing crazes grew in length. As the stress–strain curve passed through the region of instability, or yield, the crazes continued to grow in length, and their number increased at a much reduced rate. Typical optical micrographs that display the crazing behavior observed for PS and the 20% 2MPPO–PS blend at their respective yield strains are shown in Figure 7. The change in both the number and length of

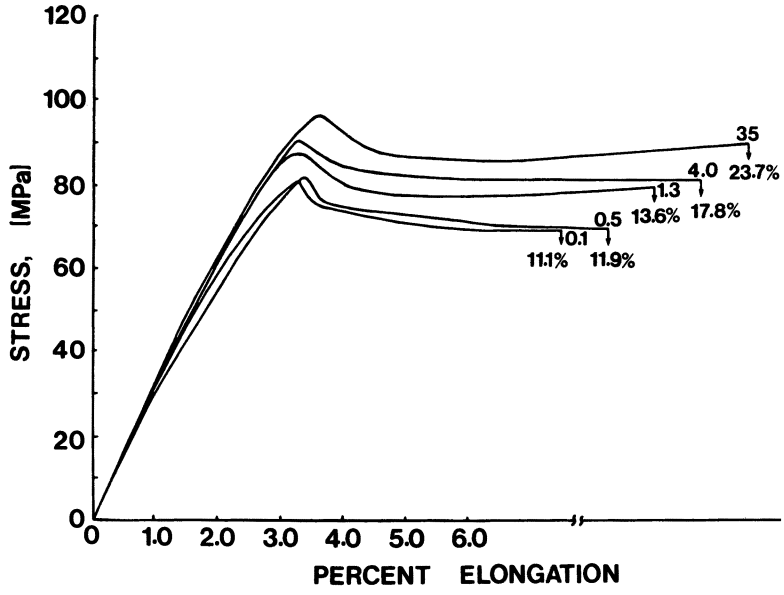

Figure 6. Representative stress–strain curves of 2MPPO at strain rates of 0.1, 0.5, 1.3, 4.0, and 35%/min.

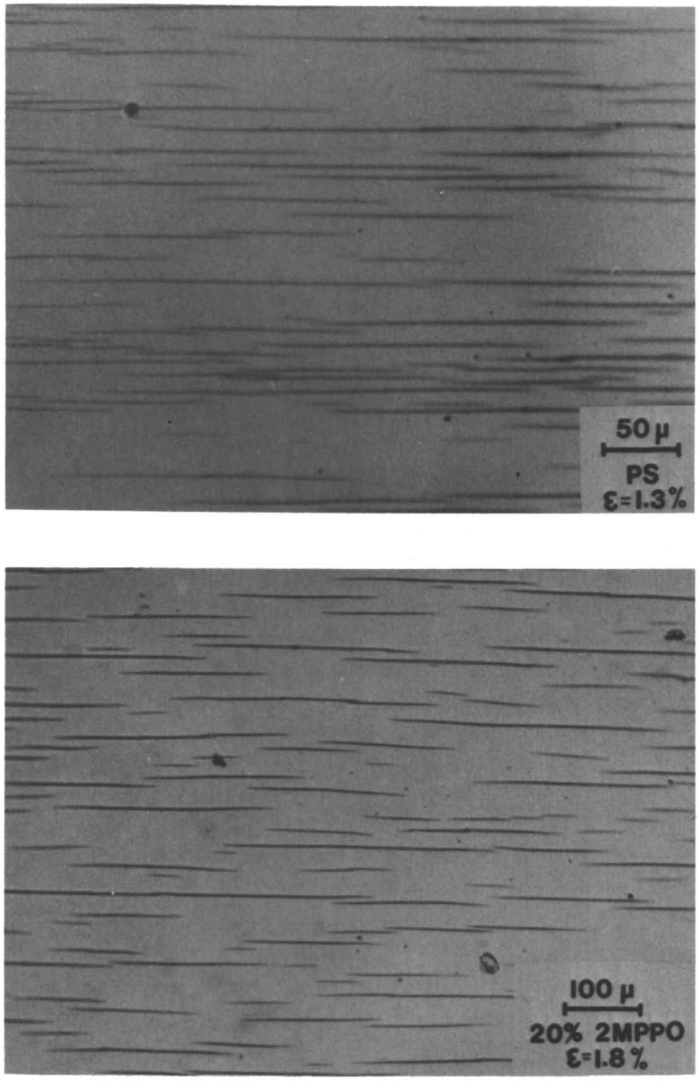

Figure 7. Optical micrographs of crazes in deformed PS (top) and the 20% 2MPPO–PS blend (bottom).

crazes was less pronounced at the draw or work-hardening portion of the stress–strain curve.

The initial mode of microdeformation for the 40% 2MPPO–PS blend was also observed as the nucleation of many small crazes. As the deformation proceeded, crazes were continually nucleated. However, unlike PS and the 20% 2MPPO–PS blend, existing crazes grew only a short distance

(ϵ = 2.1%), as shown in Figure 8a, before they were blunted by shear bands, which could be observed at the tips. An increase in craze nucleation and the subsequent increase in craze density continued until the deformation reached the yield (ϵ = 2.8%) where several areas of localized necks appeared (Figure 8b). These localized necks were unstable and grew only a short distance before fracture ensued (ϵ = 2.9%) (Figure 8c).

The observed microdeformation behavior of 70% 2MPPO–PS blend was very similar to the 40% 2MPPO–PS blend up to the region of instability or yield. That is, many small crazes were nucleated that then grew only a short distance before they were blunted by shear bands while their number continued to increase. At the region of instability, many localized necks formed; the stability and subsequent growth of these localized necks depended on strain rate. At low strain rates, 0.1 and 0.5%/min, the necks were unstable, and fracture occurred at the yield point. At higher strain rates, the specimen formed a stable neck through coalescence of several localized necks (Figures 9a–d) that propagated through the crazed region via a moving shear-band front. Once necking began, no new crazes were initiated, and existing crazes were pulled into the growing neck. These crazes did not continue to grow and appeared slightly deformed as a result of the strain imposed by the neck. The draw ratio, which was determined by comparing the distance between two crazes before necking with their subsequent displacement in the necked region, was about 2.3. The same value of the draw ratio was also obtained for the 40% 2MPPO–PS blend and 2MPPO.

The first observable, irreversible microdeformation events exhibited by 2MPPO films were craze-like structures that were not as sharply defined or as straight as the crazes previously observed. These craze-like structures are the unfibrillated deformation zones reported (*21*) for 2MPPO films. As the deformation of the films continued, the deformation zones were blunted by a continuous network of shear bands. At this point, several necks were formed and observed to coalesce into one stable neck that then propagated by means of a moving shear-band front. Occasionally, new necks would branch in the shear-band direction from the major growing neck. Growth of the neck was unaffected by the deformation zones that were subsequently incorporated by it. The draw ratio increased with strain rate.

Craze Kinetics. Changes in the crazing behavior observed as 2MPPO was added to PS were quantified in terms of craze density and craze length. The effect of composition on the average craze length during deformation is shown in Figure 10. The average length of a craze observed for PS was dramatically reduced by the addition of 20% 2MPPO. Addition of 40% 2MPPO to PS resulted in yet a further reduction in craze length. This trend did not continue, and specimens of the 70% 2MPPO–PS blend

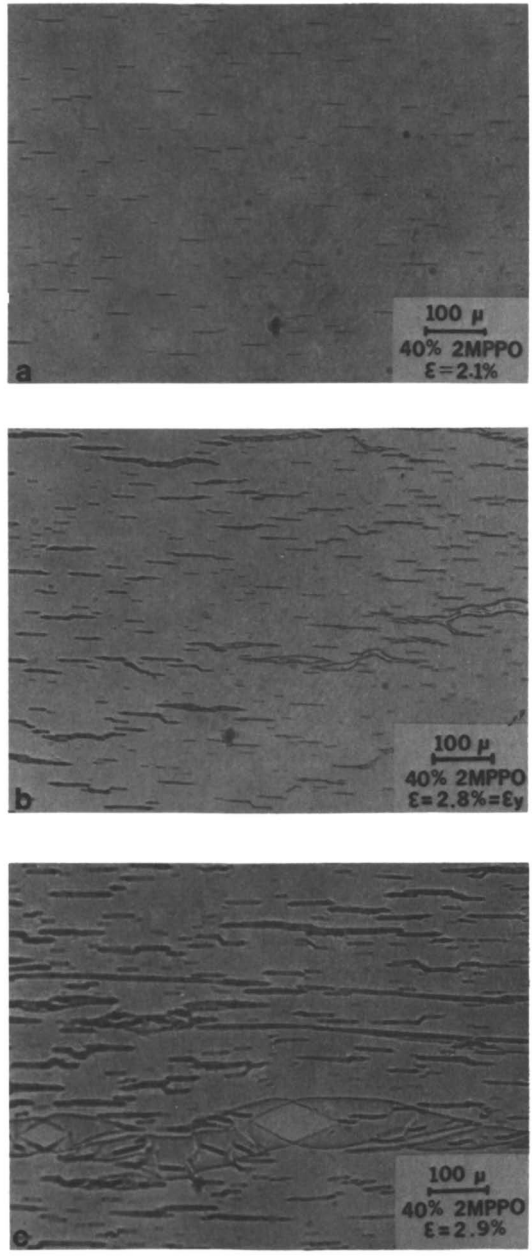

Figures 8a–c. Optical micrographs of the 40% 2MPPO–PS blend during deformation: (a) crazing behavior at $\epsilon = 2.1\%$; (b) formation of localized necked regions at $\epsilon = 2.8\% = \epsilon_y$; and (c) growth of localized necked regions and subsequent failure at $\epsilon = 2.9\%$.

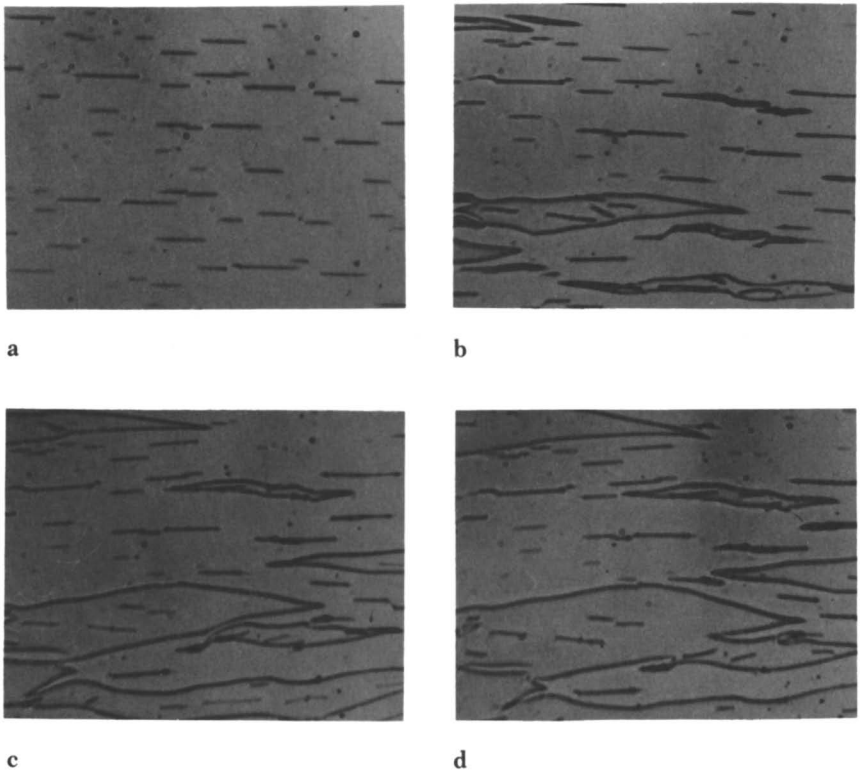

Figures 9a–d. Optical micrographs of stable neck formation through coalescence of several localized necks in 70% 2MPPO–PS deformed films. The value for ϵ is a, 3.1%; b, 3.2%; c, 3.4%; and d, 3.6%.

deformed films showed approximately the same craze length as the 40% 2MPPO–PS blend. Also, the craze length for PS and the 20% 2MPPO–PS blend specimens continued to increase beyond the yield strain, and the craze lengthening process for the 40 and 70% 2MPPO–PS films was arrested before the yield as a result of the localized necking process.

The craze-initiation strain was obtained by extrapolation of the craze-length curves of Figure 10 to zero craze length. The critical strain for craze initiation increased up to the 40% 2MPPO–PS blend and then remained essentially constant. Initial changes in craze length with strain can be estimated from the initial slope of the craze-length curves. The change in craze length per increment of strain for PS was about a fivefold increase over the 40% 2MPPO–PS blend.

The change in craze density during deformation as a function of composition was also measured (Figure 11). An order of magnitude increase in craze density was attained when 20% 2MPPO was blended with PS. The

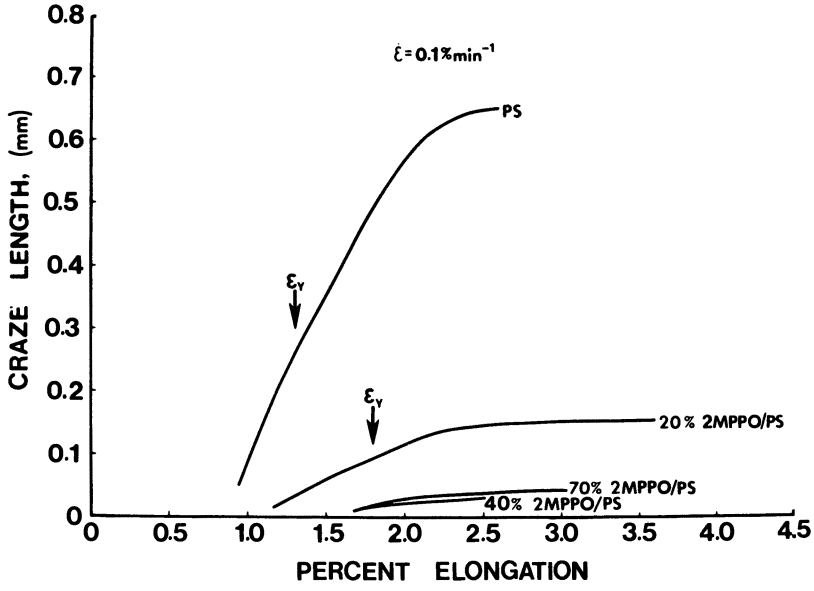

Figure 10. Effect of blend composition on the average craze length during deformation. The arrows mark the strain where yield occurred.

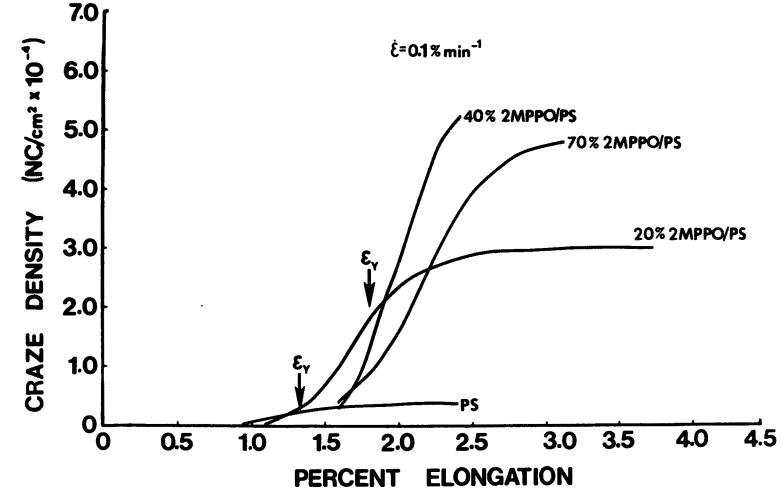

Figure 11. Effect of blend composition on the average craze density during deformation. The arrows mark the strain where yield occurred.

craze density increased beyond the yield for both PS and the 20% 2MPPO–PS blend and leveled off just beyond the yield strain at about 3,500 crazes/cm^2 for PS and 30,000 crazes/cm^2 for the 20% 2MPPO–PS blend. As a result of the previously mentioned necking processes that occurred for both the 40 and 70% 2MPPO–PS blends, no increase in craze density was observed beyond the yield.

The effect of strain rate on craze length and density was examined for PS and the three blend compositions. Increasing the strain rate from 0.1 to 0.5%/min had no significant effect on either craze length or density for PS or for the 20% 2MPPO–PS blend. However, a similar change in strain rate for both the 40 and 70% 2MPPO–PS blend compositions resulted in a twofold increase in craze density and a concurrent decrease in craze length by about one-half. Subsequent increases in strain rate resulted in a continued increase in craze density and the accompanied decrease in craze length. Both the craze-initiation stress and strain increased with strain rate for all compositions examined.

Discussion

Simultaneous observation of the film by optical microscopy during a stress–strain measurement allows for direct correlation between the mechanical behavior and the irreversible microdeformation processes. A typical stress–strain curve that is divided into two deformation regions is shown schematically in Figure 12. Region I is the nonlinear portion of the stress–strain curve where the irreversible microdeformation processes initiate and prop-

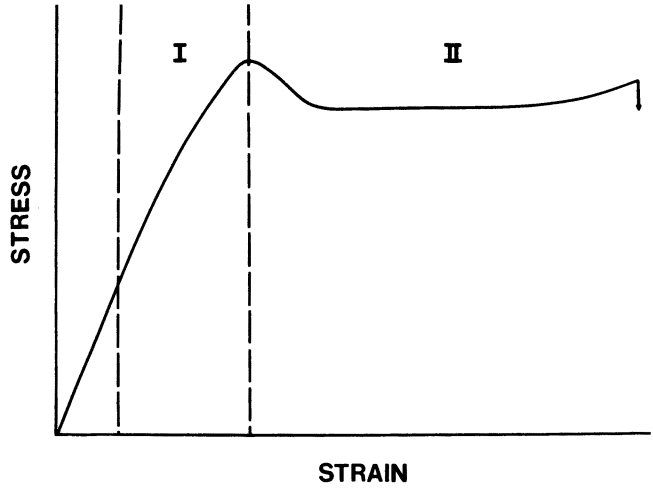

Figure 12. A schematic representation of a typical stress–strain curve divided into two regions. Region I is the portion of nonlinear behavior, and region II consists of the yield, draw, and fracture regimes.

agate. Region II is primarily associated with the yield, draw, and subsequent fracture. Obviously, the behavior of this region evolves from the prior irreversible events associated with region I.

In region I, the critical stress for craze initiation or nucleation was determined from the craze-initiation strain obtained from Figure 10 or 11 and the corresponding stress–strain curve. The behavior displayed by the craze-initiation stress plotted as a function of composition (Figure 13) parallels that reported for the density (*13*, *14*). The large increase in craze-initiation stress with increasing concentration of 2MPPO in the blend can be attributed to the corresponding increase in density that is related to the miscibility of the blend (*13*, *14*). Subsequently, a higher stress is required for cavitational processes associated with craze initiation and growth. Yee and Maxwell (*15*) reported that a consequence of a negative excess volume of mixing for a miscible blend is to raise both the material stiffness and stress to craze. They also suggest that when densification occurs the craze-initiation stress should be greater than expected from a linear combination of the properties of the pure components. Other systems in which densification, either by thermal annealing or pressure, has resulted in an increased craze initiation stress have been reported by Baer and coworkers (*18*, *22–23*).

Once the first crazes were initiated, crazing continued via two competing processes: nucleation of more crazes and growth of crazes already formed. As these competing processes proceeded, the growing crazes approached each other. The interaction of stress fields at the tips of a pair of unaligned crazes first reduced, then finally arrested the lengthening processes (*24*). Consequently, as deformation proceeded the relative rate of nucleation dominated the rate of growth. This competition between the rate of nucleation and the rate of growth was also dependent upon both

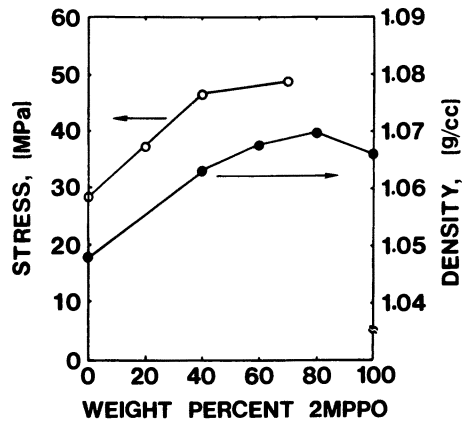

Figure 13. Effect of blend composition on craze-initiation stress and density. (Density values for comparison are taken from ref. 14.)

blend composition and strain rate. As either 2MPPO content or strain rate increased, the relative rate of nucleation increased and, as a result, the crazes were more numerous and smaller as previously shown in Figures 10 and 11.

Before stress field interactions at craze tips could hinder growth of the crazes at the 40 and 70% 2MPPO–PS compositions, a different mechanism for craze-growth abatement intervened. At these compositions, the craze-initiation stress approached the critical stress for shear-band nucleation. Once these crazes formed, they grew only short distances because the stresses at the craze tips, which are greater than the tensile stress, now equaled the critical shear-band initiation stress (*25*). Subsequently, the crazes were blunted by shear bands, and their growth was arrested. Shear-deformation blunting of craze tips has been reported (*16*, *17*, *26*) for several polymeric systems. In these systems, because craze growth was arrested, the rate of nucleation once again dominated the crazing processes.

The yield behavior displayed in region II reflects the nature of the prior irreversible deformation. For PS and the 20% 2MPPO–PS blend, the only irreversible microdeformation process observed when the stress reached a maximum was crazing, and these compositions exhibited craze yielding. In describing craze yielding, Brown (*27*) relates the maximum in stress during tensile experiments to the point at which the strain rate in the craze exceeds that of the specimen, so that the subsequent stress drop is due to the inability of the machine to keep up with the extending specimen.

Following yield, crazing continued until fracture for both PS and the 20% 2MPPO–PS blend. For PS, the craze density leveled off after yield, but craze lengthening continued as the primary energy adsorption mechanism. In the 20% 2MPPO–PS blend, both the craze length and density reached constant values following yield. Thus, the energy adsorption mechanism must subsequently be due to craze widening. Craze widening by drawing material from the bulk surface into the craze has been reported (*22*, *28*). Crack initiation must have occurred in the crazed material for both PS and the 20% 2MPPO–PS blend. The decrease in fracture strain with increasing strain rate as previously shown in Figures 2 and 3 is typical behavior (*22*, *29*) for glassy polymers that deform by crazing.

A transition from craze yielding to shear yielding occurred in the 40% 2MPPO–PS blend in which shear-band blunting of craze growth was first observed. The maximum in the stress–strain curve for the 40 and 70% 2MPPO–PS blends coincided with the onset of localized necking. In this system, as with 100% 2MPPO, the yield was entirely due to shearing processes. The drop in the stress following the yield maximum was due to a decreased cross-sectional area in the propagating micronecked region. The transition from craze yield to shear yield in the 40% 2MPPO–PS blend, which is clearly evident in the microdeformation behavior, does not produce obvious changes in the stress–strain curves.

The transition observed in the 40% 2MPPO–PS blend in the microdeformation behavior correlates with the yield behavior shown in the plot of yield stress versus composition in Figure 14. From 0 to 40% 2MPPO–PS, the yield stress increased in a linear manner, then went through a maximum at about 70% 2MPPO–PS. The observed increase in yield stress beyond the values that would be expected as a result of the weighted averages of the two pure components parallels the synergism reported for the density (*13*, *14*). These synergistic effects are due to the specific intermolecular interactions between the phenyl ring of PS and the phenylene ring of 2MPPO that result in improved glassy-state packing and a negative excess volume of mixing (*9*, *13*). The yield stress increased in the same manner as the craze initiation stress, and a close relationship is suggested between these two processes (*30*). The ratio of craze initiation stress to yield stress was about 0.6–0.7.

The post yield deformation reflects the transition that occurred at the yield from a crazing process to a shearing process. Fracture of the 40% 2MPPO–PS blends occurred at the yield point of the stress–strain curves. Microscopically, the crack initiated at a craze in the thinned micronecked region. Fracture in the necked region as a result of formation of diamond-shaped cavities from either surface crazes or defects has been reported (*31*) for polycarbonate. The 70% 2MPPO–PS films displayed bimodal fracture behavior. At low strain rates, the specimen fractured in the same manner as the 40% 2MPPO–PS blend; and, at higher strain rates, a stable propagating neck was formed. This behavior can be attributed to crack formation from crazes of a critical size. At low strain rates, the crazes were relatively large and served as good sites for crack initiation. As the strain rate

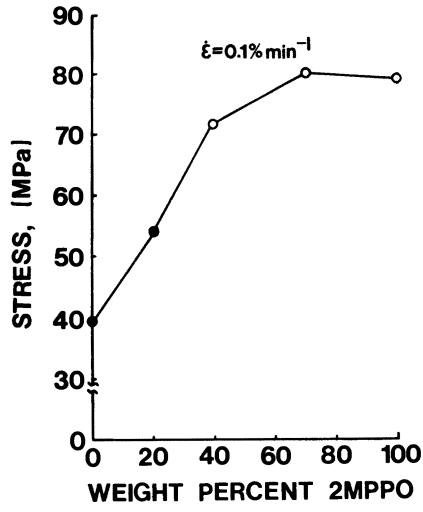

Figure 14. Effect of blend composition on tensile yield stress: ○, shear yield; and ●, craze yield.

increased, the crazes became too small to initiate crack formation. Thus, a stable propagating neck developed. The 2MPPO films always displayed stable neck formation. The increase in fracture strain with strain rate exhibited for 2MPPO was a consequence of the concurrent increase in draw ratio (*24*).

Conclusions

Simultaneous observation of competing irreversible microdeformation processes and mechanical behavior of the 2MPPO–PS miscible blend system was accomplished. A transition from a crazing to a shearing type of irreversible microdeformation was observed that depended on composition.

In region I, blending 2MPPO with PS led to an increase in the critical stress for craze initiation that was attributed to the corresponding increase in density. As the concentration of 2MPPO in the blend increased, crazes became more numerous and shorter. Craze growth was hindered by stress-field interaction at craze tips for PS and the 20% 2MPPO–PS blend and by shear-band blunting of craze tips for the 40 and 70% 2MPPO–PS blends.

In region II, a transition from craze yield to shear yield occurred in the 40% 2MPPO–PS blend as a consequence of shear-band blunting of craze growth. Beyond the yield, deformation proceeded by both craze lengthening and widening for PS and the 20% 2MPPO–PS blend. Localized micronecking was observed for the 40 and 70% 2MPPO–PS blends, and the subsequent stability of the growing neck depended on the crazing behavior of region I.

Nomenclature

T_g Glass transition temperature (°C)
ϵ Strain (%)
$\dot{\epsilon}$ Strain rate (%/min)

Acknowledgment

The authors wish to acknowledge the generous financial support of this research by the National Science Foundation, Polymer Program, Grant No. DMR80–18129.

Literature Cited

1. MacKnight, W. J.; Karasz, F. E.; Fried, J. R. In "Polymer Blends"; Paul, D. R.; Newman, S., Eds.; Academic: New York, 1978; Vol. 1, pp. 185–242.
2. Bair, H. E. *Polym. Eng. Sci.* **1970**, *10*, 247–50.
3. Shultz, A. R.; Beach, B. M. *Macromolecules* **1974**, *7*, 902–9.
4. Stoelting, J.; Karasz, F. E.; MacKnight, W. J. *Polym. Eng. Sci.* **1970**, *10*, 133–38.
5. Jacques, C. H. M.; Hopfenberg, H. B. *Polym. Eng. Sci.* **1974**, *14*, 441–48.
6. MacKnight, W. J.; Stoelting, J.; Karasz, F. E. In "Multicomponent Polymer Systems"; Platzer, N. A. J., Ed.; ADVANCES IN CHEMISTRY SERIES No. 199; ACS: Washington, D.C., 1971; pp. 135–67.

7. Prest, W. M., Jr.; Porter, R. S. *J. Polym. Sci.* **1972**, *10*, 1639–55.
8. Shultz, A. R.; Gendron, B. M. *J. Appl. Polym. Sci.* **1972**, *16*, 461–71.
9. Wellinghoff, S. T.; Koenig, J. L.; Baer, E. *J. Polym. Sci. Polym. Phys. Ed.* **1977**, *15*, 1913–25.
10. Yee, A. F. *Polym. Eng. Sci.* **1977**, *17*, 213–19.
11. Maconnachie, A.; Kambour, R. P.; White, D. M.; Rostami, S.; Walsh, D. J. *Gen. Electr. Tech. Infor. Ser.* **1983**, Report No. 83CRD310, 1–11.
12. Weeks, N. E.; Karasz, F. E.; MacKnight, W. J. *J. Appl. Physics* **1977**, *48*, 4068–71.
13. Hopfenberg, H. B.; Stannett, V. T.; Folk, G. M. *Polym. Eng. Sci.* **1975**, *15*, 261–67.
14. Kleiner, L. W.; Karasz, F. E.; MacKnight, W. J. *Polym. Eng. Sci.* **1979**, *19*, 519–24.
15. Yee, A. F.; Maxwell, M. A. *J. Macromol. Sci. Phys.* **1980**, *B17*, 543–64.
16. Wellinghoff, S. T.; Baer, E. *J. Appl. Polym. Sci.* **1978**, *22*, 2025–45.
17. Donald, A. M.; Kramer, E. J. *J. Mater. Sci.* **1982**, *17*, 1871–79.
18. Moreno, A.; Baer, E. In "Structure–Property Relationships of Polymeric Solids"; Hiltner, A., Ed.; Plenum: New York, 1983; pp. 1–24.
19. Koltisko, B.; Balashin, N.; Hiltner, A.; Baer, E. *ANTEC Soc. Plast. Eng. Conf.* 1983, pp. 440–45.
20. Grasselli, J. G., Ed. "Atlas of Spectral Data and Physical Constants for Organic Compounds"; CRC: Cleveland, 1973; Chap. A19.
21. Donald, A. M.; Kramer, E. J. *Polymer* **1982**, *23*, 1183–88.
22. Trent, J. S.; Palley, I.; Baer, E. *J. Mater. Sci.* **1981**, *16*, 331–40.
23. Matsushige, K.; Radcliffe, S. V.; Baer, E. *J. Mater. Sci.* **1975**, *10*, 833–45.
24. Nielsen, L. E. In "Mechanical Properties of Polymers and Composites"; Dekker: New York, 1974; Chap. 5.
25. Gent, A. N. *J. Mater. Sci.* **1970**, *5*, 925–32.
26. Bucknall, C. B.; Clayton, D.; Keast, W. E. *J. Mater. Sci.* **1972**, *7*, 1443–53.
27. Brown, N. *Phila. Mag.* **1975**, *32*, 1041–50.
28. Lauterwasser, B. D.; Kramer, E. J. *Phila. Mag.* **1979**, *39*, 469–95.
29. Ward, I. M. In "Mechanical Properties of Solid Polymers"; Wiley: New York, 1983; Chap. 11.
30. Haward, R. N.; Murphy, B. M.; White, E. F. T. *J. Polym. Sci. A-2*, **1971**, *9*, 801–14.
31. Morgan, R. J.; O'Neal, J. E. *Polymer* **1979**, *20*, 375–87.

RECEIVED for review November 15, 1984. ACCEPTED March 25, 1985.

17

Fatigue in Rubber-Modified Epoxies and Other Polyblends

J. A. MANSON[1,2,3], R. W. HERTZBERG[1,3], G. M. CONNELLY[1,3], and J. HWANG[1]

[1]Polymer Science and Engineering Program, Lehigh University, Bethlehem, PA 18015
[2]Materials Research Center and Chemistry Department, Lehigh University, Bethlehem, PA 18015
[3]Materials Research Center and Metallurgy and Materials Engineering Department, Lehigh University, Bethlehem, PA 18015

The literature on fatigue in rubber-modified plastics is briefly reviewed, and the fatigue crack propagation (FCP) behavior of a rubber-modified, amine-cured bisphenol-A-type epoxy [glass transition temperature (T_g) equals 94 °C] is described and discussed as a function of test frequency and rubber content [up to 15 parts per hundred parts resin (phr) rubber]. At low frequencies (10–15 Hz), FCP rates at a given value of stress intensity factor range (ΔK) were little affected by the presence of rubber. Stable crack growth could be attained at higher values of ΔK as the rubber content increased. However, at higher frequencies (20–50 Hz), FCP rates increased, and maximum values of ΔK decreased greatly with the controls but much less with the modified resins.

ONE OF THE MOST SIGNIFICANT MILESTONES in the development of engineering plastics has, of course, been the development of polymer blends (*1–5*). The original emphasis was on improving the impact strength of brittle polymers [e.g., polystyrene (PS)] and on the development of improved wire coatings based on poly(vinyl chloride)(PVC)–(acrylonitrile–butadiene) copolymer rubber (NBR) blends. Later work included the improvement of processability or stability and optimization of cost effectiveness. In any study, blending or a related technique is used to economically tailor polymer properties to performance.

Increasing attention has been given to the modification of brittle thermoset resins, such as phenolics and epoxies, by the incorporation of rubbery components to improve toughness. Indeed, even with quite highly cross-linked resins, significant improvements in static toughness can often

0065-2393/86/0211/0291$06.25/0

be achieved. For example, rubber-toughened epoxies now find many applications for both structural and nonstructural purposes (*6*, *7*). Considerable attention has also been given to research on relationships between structure, composition, morphology, and properties (*1*, *4*, *8*, *9*). Evidently a combination of cavitation around the rubber particles with shear yielding in the matrix plays a major role in providing mechanisms for energy dissipation (*1*, *4*, *9–12*); microvoiding and tearing of the rubber particles may also occur (*13–14*).

Although impact strength (as measured, e.g., by Izod or Charpy tests) is often relevant to many applications, repetitive or cyclic loads are certainly common in service. Such loading may involve a range of load spectra, from repeated impacts to cyclic deformations, singly or in combination; the stresses may involve either a single type or a combination. Whatever the details of the load spectrum, weakening due to repetitive or cyclic loading constitutes the phenomenon of fatigue; such loading is often more damaging than static or monotonic loading to the same peak stresses. Fatigue failure may be insidious in its occurrence; it often takes place at peak stresses much less than the yield stress and often involves brittle rather than ductile fracture (*15*, *16*). Although these characteristics are troublesome, the characterization of fatigue behavior has received little attention relative to that accorded other properties such as monotonic tensile and impact strengths. For example, most lists of properties contain no information whatever on fatigue, and the phenomenon has been discussed only recently to any extent in any trade-type compendium of properties and behavior (*17*).

Because of the current trend toward the use of an increasing variety of sophisticated polyblends in engineering applications, consideration of the possible consequences of exposure to fatigue loading is necessary. These consequences may well include unexpected failures that may involve claims of product liability. At the very least, good materials selection and component design require knowledge of this fascinating phenomenon. Although the complexities are great, experiments with well-defined materials and test conditions can provide a useful beginning in the search for fundamental understanding of fatigue in plastics.

The growth of cracks from pre-existent flaws is an important aspect of fatigue. Fabricated articles may contain defects of such a nature that the initiation of a significant flaw capable of growth to a catastrophic size can be assumed to have occurred. Thus, a major program was initiated in these laboratories to study the effects of polymer properties and loading conditions on the kinetics and energetics of fatigue crack propagation (FCP) in a variety of plastics and related multicomponent systems (for a review, *see* Reference 16). Because little information has been published on FCP in neat or rubber-modified epoxy systems, we decided to study the role of composition, state of cure, and test frequency on the rates and micro-

mechanisms of FCP in such systems. For these studies, amine-cured bisphenol-A-based epoxy resins with a low glass transition temperature (T_g) (94 °C, by dynamic mechanical spectroscopy) were selected (*18*). Results obtained (*19*) with resins containing 10 wt% rubber at test frequencies of 10–15 Hz have been published elsewhere; studies (*20*) with higher T_g resins, which are more difficult to test because of high brittleness, are in progress.

The main purpose of this chapter is to describe and discuss FCP behavior of these resins as a function of rubber content and test frequency. To place the research in the context of fatigue more generally, pertinent literature on the fatigue of rubber-modified plastics is also briefly reviewed, and some problems for future research are outlined.

Brief Review on Fatigue in Rubber-Modified Plastics

General Aspects. In classical fatigue tests (*16, 21*) involving so-called *S–N* (stress amplitude versus number of cycles to failure) curves, the number of impulses or cycles (N_f) to failure (however failure is defined) of polished, unnotched specimens is measured at various peak stresses or ranges in stress ($\Delta\sigma$) (Figure 1). Sometimes a limiting value of $\Delta\sigma$ is found below which failure is not observed at any reasonable value of N (e.g., 10^7). On closer examination at a given value of $\Delta\sigma$, one may observe a value of N (N_i) at which cracks begin to form, and a higher value of N (N_f) at which failure occurs. Thus, in general, two *S–N* (or $\Delta\sigma$–*N*) curves exist: one for the initiation of failure and one for the final failure. The difference ($N_f - N_i$) constitutes the number of cycles involved in propagation of the crack initiated previously. If the specimen contains preexistent flaws of significant size. most of the lifetime may be spent in propagation of the flaws.

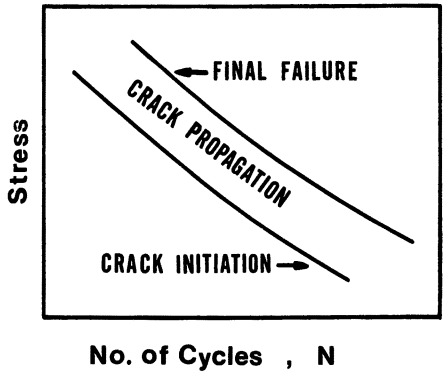

Figure 1. Fatigue response of a polymer showing the relationship between applied stress and number of cycles to failure for both initiation and final failure of fatigue cracks.

Hence, studies are often made of FCP in specimens that are sharply notched. Although such tests are often appropriate, in other systems fatigue crack *initiation* may dominate the lifetime (e.g., in materials containing extremely small flaws and not subjected after synthesis to mechanical damage due to scratching or machining). Initiation phenomena can be important with some rubber-modified plastics. Although we are aware of no published studies of both the initiation and propagation of fatigue cracks in a given epoxy, initiation may well play a major role. In fact, many more cycles are required to initiate stable fatigue crack growth in typical epoxies than to propagate the started crack to failure (*22*).

The failure mechanism may depend on the magnitude of $\Delta\sigma$. At high values of $\Delta\sigma$, hysteretic heating (also favored by high loss compliances and high frequencies) may lead to temperatures high enough to induce failure by softening or even melting (*15*). In contrast, at low values of $\Delta\sigma$, failure may occur by the propagation of a crack in a nominally brittle manner (an insidious process, indeed). Even in the latter system, thermal effects at and beyond the crack tip can modify FCP behavior (*16*, *23*).

The yield stress (σ_y) and tensile modulus (E) are typically reduced by polyblending of a brittle with a rubbery polymer. Also, whereas the ultimate elongation (ϵ_b) in a monotonic tensile test and fracture energy are typically increased in such polyblends, the value of ultimate elongation in cyclic loading may be decreased significantly (*24*, *25*). For reviews, *see* References 16 and 26; the latter reference describes fatigue in toughened styrenic polymers in detail.

Fatigue in Unnotched Specimens. Fatigue in unnotched specimens of several rubber-modified polymers has been studied under constant-load-range cycling. Examples include acrylonitrile–butadiene–styrene terpolymers (ABS) (*15*, *24*, *26–28*), high-impact polystyrene (HIPS) (*15*, *26*, *28–30*), toughened poly(methyl methacrylate) (PMMA) (*31*), and toughened PVC (*32*). HIPS (*25*) and ABS (*25*) have also been examined under constant-strain-range cycling. Unfortunately, comparisons of behavior with respect to matrix materials known to have the same molecular weight (M) as in the blend are not available, though some comparisons (*26*, *33*) with matrix materials of the same general type have been made. Crazing appears to be the dominant deformation mechanism in HIPS, and shear is the dominant mechanism in ABS (*15*, *26*, *29*).

Whereas the fatigue performance of a typical ABS resin has been reported (*33*) to be superior to that of typical PSs, a different result was reported (*26*, *27*, *30*) for HIPS and ABS. With these resins, the overall fatigue life was lower in tension–compression cycling than that of the matrix resins (the latter, however, did not necessarily have the same M as the HIPS). Although an increase in frequency tended to increase fatigue life, the overall performance was still inferior to that of PS. Evidently, both the initia-

tion of crazes and the propagation of cracks from them were facilitated by the presence of the rubber. The lowering of yield stress by the rubber may have been a major factor in facilitating initiation; in fact, after normalization of the applied stress with respect to the yield stress, the modified resin appeared superior (*30*). (*Note* that in unnotched specimens the applied load is experienced by the entire cross section of a specimen.) Also, compressive loading was presumed to have a deleterious effect on the craze fibrils during the propagation stage. Indeed tension–tension loading was sometimes, though not always (*29*, *30*), observed to be less damaging. Even so, the benefits of rubber modification seen in impact strength were not evident in these tests. Deleterious effects of rubber modification have also been reported with some types of toughened PVC tested in tension (*32a*, *32b*) and with rubber-modified polycarbonate (*34*) subjected to impact fatigue. Again, initiation of failure appeared to be facilitated.

Clearly, a high-impact-strength, rubber-toughened polymer cannot be assumed to exhibit superior fatigue performance, especially if compressive loads are experienced. Care must be taken to ensure that service loads will be low enough (probably lower than for typical matrix resins) to avoid unpleasant and costly surprises.

Fatigue in Notched Thermoplastic Specimens. With notched specimens of rubber-modified PVC, Nylon 66, and PS tested at frequencies low enough to minimize extensive hysteretic heating, the incorporation of rubber decreased (*16*, *35–38*) FCP rates at a given stress intensity factor (ΔK). In all systems, comparison was made with respect to unmodified matrices with the same M or cross-linking characteristics as the modified systems. With Nylon 66 and PVC, the decrease in FCP rate varied with the rubber concentration. However, with PVC, doubling the content of the rubber [a methacrylate–butadiene–styrene (MBS) terpolymer] had *relatively* less effect than the incorporation of the lowest concentration used, 6%. Studied of the combined effect of M and rubber content in PVC revealed that a given rubber concentration had a much greater *relative* effect on the lowest-M material. However, the greatest *absolute* resistance to FCP was noted with the highest M and highest rubber content. Indeed, the FCP resistance of this material was somewhat superior to that of a typical polycarbonate (*35*).

In all these systems, impact strengths were also increased. Examination of fatigue fracture surfaces implied major roles of crazing and shear response in HIPS (*39*) and PVC (*40*), respectively. This result also seems to be true with impact testing. The surfaces of toughened Nylon 66 revealed a combination of microcracking and enhanced shear deformation. Interestingly, with both PVC and PS, toughening in FCP was observed at concentrations of rubber less than required for high impact strength (*35*, *38*). This result can be attributed to the effectively lower testing rate in FCP. Thus,

in these systems (PVC and Nylon 66) toughening effects manifested during monotonic loading are paralleled in FCP tests.

Effects of frequency on FCP in thermoplastics are complex. Increasing frequency can result in a decrease in FCP rate at a given ΔK or in a negligible effect. Rubber-modified thermoplastics provide examples of both types of behavior (ABS and MBS–PVC, respectively). Prior to this study, toughened Nylon 66 was the only rubber-modified plastic studied in which an increase in frequency resulted in an *increase* in FCP rates (*16*, *23*). A hypothesis was proposed (*41*) in terms of a competition between hysteretic heating localized at the crack tip and extensive generalized heating in the bulk material ahead of the crack. Hysteretic heating rates in tests between fixed stress limits are proportional to the loss compliance (D'') and $\Delta\sigma$ or the stress intensity factor range (ΔK) (*41*). By combining measurements of D'' with temperature profiles (from IR microscopy) at and beyond the crack tip, the validity of the hypothesis has been confirmed (*23*) for ABS, MBS–PVC, and toughened Nylon 66 (*23*). This point is important, because polyblends may well exhibit high damping and, because of their toughness, may experience high values of $\Delta\sigma$.

However, even though significant hysteresis is typical of each loading cycle in toughened Nylon 66 subjected to impact fatigue using notched specimens, the resistance to fatigue is dramatically superior to that of the unmodified matrix (*42*). In contrast, a deleterious effect (*34*) of rubber on impact fatigue of unnotched PMMA has already been noted.

Fatigue in Notched Thermoset Specimens. Epoxies and other thermoset resins are of particular interest because rubber modification is used (*6*, *7*) extensively to moderate the inherent brittleness of such materials. Indeed, significant increases in, for example, impact strength are often observed. Whereas rubber-modified epoxies do not appear (*1*) to deform in a crazing mode, shear response is evidently possible in spite of the presence of cross-linking. Surprisingly, however, with the rubber-modified epoxies (T_g ~80–90 °C) described previously (*19*), rubber modification resulted in lower FCP rates only with a very brittle formulation that did not give improved impact strengths and resulted in little or no change in FCP rates with a formulation that did improve impact strength. Also, stable crack growth has been difficult to obtain in toughened high T_g epoxies. In FCP tests, the major effect of the rubber was to increase slightly the maximum value of ΔK attainable prior to catastrophic fracture. Stress whitening was evident only in this latter stage, but could not be correlated with features observed on the fracture surface. Extensive hysteretic heating was not observed except during the last few cycles. Fatigue loading may induce failure at the rubber–matrix interface prior to crack advance and thus limit the ability of the rubber to induce energy dissipation in the matrix or to contribute to such dissipation by deformation of itself. In effect, the rubber

domains may not only decrease the modulus per se, but also result in void formation that further weakens the material.

Experimental

The epoxy used was a low molecular weight liquid diglycidyl ether of bisphenol A (DGEBA) (DER 331, Dow Chemical Company). The curing agent (in stoichiometric proportion) was an aliphatic diamine (Jeffamine D-230, Jefferson Chemical Company). The carboxyl-terminated acrylonitrile–butadiene (CTBN) rubbers were used in the form of an epoxy adduct (Kelpoxy 272-100, Spencer Kellogg Division, Textron, Inc.). The CTBN component contained 26% acrylonitrile, and the overall rubber content in the epoxy adduct was 40%. The formulation was adjusted to provide 5, 10, or 15 phr[1] rubber; these concentrations correspond to approximately 3, 7, and 10 wt% of rubber in the total resin. After the desired proportions of prepolymer epoxy and modifier (heated to 62 °C) had been mixed for 2 min with mechanical stirring, the solution was degassed, mixed with the curing agent, and cast between glass plates. The cure cycle was as follows: 24 h at room temperature, 1 h at 66 °C, 2 h at 93 °C, and 4 h at 150 °C, followed by slow cooling to room temperature under ambient conditions. Except for variations in the rubber content and for the use of glass plates, the specimens, designated here as series 3, should be similar to those of series 1 described previously (*19*).

Values of T_g were obtained using a differential scanning calorimeter (Perkin-Elmer model DSC-1B) at a scan rate of 40 °C/min. Because no curing peaks could be detected in the scans, curing was judged to be essentially complete. Dynamic mechanical spectra were obtained at 110 Hz using an Autovibron unit, model DDV-IIIC. Values of T_g were determined from the peaks in the loss factor (tan δ) curves; values of the rubber modulus, E_r, were measured at 120 °C. Tensile properties were obtained with an Instron tester at a crosshead speed of 0.4 mm/s by using specimens machined from the cast sheets. Notched impact strengths were measured by standard techniques (ASTM[2] D256–81) except for the use of a larger notch radius (0.5 mm). Values of plane-strain fracture toughness (opening mode) (K_{Ic}) were determined with using single-edge-notched specimens tested in 3-point bending (ASTM E399–81). Fracture energy (G_{Ic}) was estimated from the relationship G_{Ic} equals $K_{Ic}^2 \times (1 - \nu)/E$, where ν is the Poisson ratio (0.35) and E is the tensile modulus (*4*).

Fatigue tests were made in duplicate under ambient conditions following standard procedures on notched compact tension specimens (6.35 cm × 6.1 cm × 6 mm) (*43*) with an electrohydraulic closed-loop test machine at a sinusoidal frequency of 10, 20, or 50 Hz and a ratio of minimum to maximum load (R) of 0.1. Crack lengths were monitored with a traveling microscope. Crack growth rates per cycle, da/dN, were correlated with ΔK (a measure of driving force at the crack tip); ΔK is given by the ratio $(\Delta P/BW^{1/2}) \cdot f(a/W)$, where ΔP is the range in applied load; B and W are the specimen thickness and width, respectively; and $f(a/W)$ is a geometrical factor (ASTM E399–81). Experience has shown that FCP curves are usually reproducible within ±20%.

With the rubber-modified materials, the FCP curves tended to decrease at high values of ΔK. This curvature was associated with the development of such high compliance that the testing machine could not maintain the programmed loads. In this region of ΔK, shear zones were also seen on the fracture surface. By correcting the computed values of ΔK to reflect the actual (lower) loads experienced, much of the curvature in the plots was removed. Even so, following the

[1] Parts per hundred parts resin.
[2] American Society for Testing and Materials.

crack growth up to final fast fracture or estimating values of a plane-strain fracture toughness was not possible. However, values of a critical toughness parameter (K_c') reflecting the onset of the high-compliance region prior to failure were estimated by dividing ΔK_{max}, the maximum value of ΔK that could be reached, by 0.9 [i.e., by $(1 - r)$, where r equals the ratio of minimum to maximum load].

Although examination of the detailed morphology as a function of rubber content by transmission electron microscopy (TEM) has not been completed, the series 2 resin (15 phr, 10 wt% rubber) was found previously (*44*) to contain rubber particles having a bimodal distribution of sizes with averages of 0.4 and <0.1 μm. Rubber particle sizes at lower rubber contents may be expected to decrease with decreasing rubber content (*44*); the concentration of small particles may decrease as well.

Fracture surfaces were examined at low magnification (50×) with a Zeiss Axiomat microscope in the reflection mode; a scanning electron microscope (SEM) (Etec) was used to obtain micrographs of a few Au–Pd-coated specimens.

Crack-tip temperatures of typical specimens were monitored by means of an IR microscope (Barnes model RM-2B).

Results and Discussion

Dynamic Mechanical Behavior. Dynamic mechanical spectra are presented in Figure 2, and a summary of pertinent experimental and derived data is in Table I. For the sake of convenience, the spectra have been displaced above the spectrum for the control. (Values of E' in the glassy state varied inversely with rubber content, as expected.)

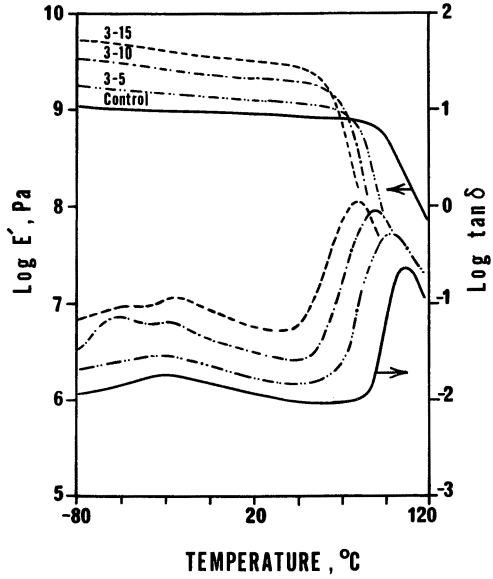

Figure 2. Dynamic mechanical spectra (at 100 Hz) for rubber-modified epoxies (series 3) 3–15, ---; 3–10, - · -; 3–5, - · · ; and control, —. For convenience, the spectra are displaced above the spectrum for the control.

Published on December 9, 1985 on http://pubs.acs.org | doi: 10.1021/ba-1986-0211.ch017

Table I. Dynamic Mechanical Parameters for Control and Rubber-Modified Epoxies

Specimen	*Rubber phr*	ET_g[a] °C	T_{gc}[a] °C	RT_g[a] °C	ET_β[a]	E_r[b] *MPa*	M_c[b]
Control	0	93 (94)[c]	90	—	−(−29)[c]	18.7 (20)[c]	630 (590)[c]
3–5	5	87 —	84	−50[d]	−29	14.5	810 —
3–10	10	79 —	81	−43	−24	10.2	1150 —
3–15	15	75 (82)[c]	79	−48 (−30)[c]	−24 (−19, −30)[c]	9.2 (12)[c]	1180 (920)[c]
CTBN	100	—	—	−30[e]	—	—	—

Note: Measurements at 110 Hz.

[a] ET_g and RT_g are the T_g values of the epoxy and rubber phase, respectively, from the dynamic spectra; ET_β is the temperature of the β transition of the epoxy phase. T_{gc} refers to T_g determined by DSC.

[b] Rubbery modulus measured at 120 °C; M_c, the average molecular weight between cross-links, was estimated by the approximation $E_r \cong G = dRT/M_c$.

[c] From Reference 19.

[d] From data printout; not evident in Figure 2.

[e] Data from torsional braid analysis for CTBN containing 26% acrylonitrile from Reference 44.

Each spectrum shows three transitions: one for the glass transition of the epoxy matrix (ET_g), one for the first secondary (β) relaxation of the epoxy matrix (ET_β), and one for the rubbery component (RT_g). Although not seen as sharply as in torsional braid studies (*26*), the latter peak is superimposed on the broad and slightly asymmetrical β-peak of the epoxy. This peak appears to reach a maximum height near -29 °C for the neat epoxy and near -24 °C for the rubber-modified specimens. (The breadth of the transition precludes a more precise assignment.) The values of ET_g and ET_β are in reasonable agreement with those measured for series 1 and series 2 resins (*19*).

As noted previously (*19*), the T_g for the epoxy phase is depressed by the presence of rubber, presumably a result, in part, of some miscibility with dissolved or finely dispersed rubber. However, the values of RT_g tend to be lower than the T_g of pure CTBN after correction for differences in test frequency used: -15 °C for CTBN containing 26% acrylonitrile (*19*). This difference is undoubtedly due to unrelaxed thermal stresses resulting from differences in the coefficients of expansion on cooling from the curing temperature (*26*, *27*, *31*).

Equation 1 was used to estimate the weight percent of rubber dissolved in the epoxy phase:

$$\frac{1}{T_g} = \frac{W_E}{ET_g} + \frac{(1 - W_E)}{RT_g} \tag{1}$$

where T_g is the observed T_g, W_E is the weight fraction of epoxy, and ET_g and RT_g are the T_g values for pure epoxy and pure rubber, respectively. The values of ET_g and RT_g were corrected (*19*) for the difference in frequency between the torsional braid technique used in the reference and the tests described herein. In this way, values of 4, 9, and 13 v% were predicted for the concentration of rubber in the epoxy matrix for specimens containing 5, 10, and 15 phr rubber, respectively. The value for specimen 3–15 is about 40% greater than reported previously (*19*) for the series 1 epoxy containing 15 phr rubber.

At the same time, variations in cross-link density of the epoxy phase may also contribute to the lowering of ET_g. Thus, nominal values of M_c, the average molecular weight between cross-links, were significantly higher for the modified resins than for the control. Although the presence of dissolved rubber would increase M_c by diluting the cross-linked network, the increase in M_c appears greater than expected if M_c were increased in proportion to the volume fraction of rubber. Also, the value of M_c is significantly higher for specimen 3–15 than for its series 1 counterpart. This deviation may be related to the higher concentration of rubber in the epoxy phase of specimen 3–15; evidently the presence of rubber hinders cross-linking of the matrix.

Unfortunately, estimation of epoxy dissolved in rubber is impossible because of the thermal stress effect previously mentioned.

Static Mechanical Properties. Tensile and impact (*IS*) data are presented in Table II, and, in specimen 3–15, compared with data obtained previously. All the modified resins exhibited a drop in stress after yielding that was noted previously (*19*); such behavior is typical of many rubber-modified polymers (*1*). This behavior was associated with the development of whitening on the fracture surfaces of the modified, but not the control, specimens. As expected, the modified materials exhibited lower E and σ_y but higher ϵ_b and greater areas under the stress–strain curves than the control. With the exception of somewhat lower values of E and σ_y than for series 1 specimens (*19*), the tensile behavior of series 1 and 3 resins was generally similar. As often observed, impact strength was increased by the incorporation of rubber and exhibited a maximum in the range of 5 to 10 phr of rubber. However the value noted for the series 3 control was, for unknown reasons, much lower than for the series 1 control.

Values of K_c' are given in Table III. At frequencies of 30 Hz or less, K_c' was increased in proportion to the rubber content. The magnitude of the increase was less the higher the frequency. This overall trend in K_c' correlates well with the increase in ϵ_b and the decrease in E and σ_y as a function of increasing rubber content. Values of K_{Ic} and G_{Ic} (Table III) also increased with increasing rubber content. Similar improvements in plane-strain fracture toughness have been noted elsewhere for rubber-modified epoxies (*10*, *11*, *45*). For example, the value of G_{Ic} for specimen 3–15 may be compared with a value of 580 J/m^2 reported for a high-T_g epoxy containing the same amount of rubber. However, at a frequency of 50 Hz, K_c' passed through a maximum in the range of 5 to 10 phr rubber as the rubber content was increased. Although this trend is inconsistent with the monotonic variations in tensile properties, it closely parallels the impact behavior.

At constant composition, K_c' decreased with increasing frequency. With specimens containing rubber, the magnitude of the decrease was

Table II. Tensile and Impact Behavior of Control and Rubber-Modified Epoxies of Series 3 Resins

Specimen	*Rubber phr*	σ_y, *MPa*	E, *GPa*	ϵ_b, %	*IS*,[b] *J/m*
Control	0	62 (65)[a]	3.6 (4.5)	10 (15)[a]	25 (64)[a]
3–5	5	57	3.1	15	100 —
3–10	10	53	3.0	16	128 —
3–15	15	45 (52)[a]	2.9 (4.2)	23 (21)[a]	99 (91)[a]

Note: Three and four specimens were used for tensile and impact tests, respectively.
[a] Data for series 1 resins from Reference 19.
[b] Impact strength.

Table III. Fracture Parameter, Fracture Toughness, and Fracture Energy of Neat and Rubber-Modified Epoxies

Specimen	K_c', $MPa \cdot m^{1/2}$ 10 Hz	15 Hz	20 Hz	30 Hz	50 Hz	K_{Ic},[a] $MPa \cdot m^{1/2}$	G_{Ic}[a] J/m^2
Control	1.10	(0.89)[b]	0.81	0.80	0.77	1.04	195
3-5	1.39	—	1.33	—	1.25	1.25	328
3-10	1.52	—	1.37	—	1.27	1.45	456
3-15	2.19	(1.67)[b]	1.39	1.23	0.96	1.65	630

[a] Tests run in triplicate.
[b] From Reference 19, in which K_c' was defined differently.

greater as the rubber content increased. However, the response of the control resin was anomalous; the overall decrease was greater than that observed for samples 3–5 and 3–10. Nevertheless, tests with another control casting gave similar results. Such decreases can be attributed to the associated increase in strain rate or to softening due to hysteretic heating. Because the temperature rises were small (<5 °C), the effect of increased strain rate at higher frequencies is undoubtedly a major factor. Indeed, the fracture toughness of a rubber-modified epoxy decreases markedly with increasing strain rate (or decreasing temperature) in tensile tests (*10*). (The fact that little effect of strain rate was noted with an unmodified resin confirms the conclusion of anomalous behavior in our control resin.) At the same time, an effect of hysteresis cannot be ruled out, because a 5 °C temperature rise in a rubber-modified acrylic resin may result in a significant lowering of yield stress and modulus (*31*).

Effect of Rubber on Fatigue Crack Propagation. The FCP curves for the control and modified resins as a function of rubber content are shown in Figure 3; effects of frequency are discussed in a later section. Although the Paris equation (*46*), $da/dN = A\Delta K^n$ (where A and n reflect material and test parameters) reflects a linear relationship between log da/dN and log ΔK, the response of most systems is somewhat curved.

At a frequency of 10 Hz, the behavior of the series 3 control and specimen 3–15 was generally similar to that of series 1 specimens (*19*), though the curve for specimen 3–15 is shifted slightly to the right. The maximum value of ΔK attained prior to fracture (ΔK_{max}) was ~0.9 MPa · $m^{1/2}$ for the control. This value is between those (*43*) for a 1:1 and a 2:1 4,4′-methylenedianiline (MDA)–Epon 828 resin (~0.6 and 1.0 MPa · $m^{1/2}$, respectively). However, the slope was lower for the latter resins. Thus, as noted with series 1, the FCP response generally resembled that of a nonstoichiometric MDA–Epon 828 resin except for a slightly lower value of ΔK_{max}. The T_g of the series 3 control is about 9 °C lower than for the nonstoichiometric MDA-cured resin (*43*). Such a lowering of T_g is consistent

with a lower cross-link density combined with an inherently more flexible system due to the use of an aliphatic rather than an aromatic curing agent.

In the previous study (*19*), the incorporation of 15 phr rubber in both series 1 and series 2 matrixes (26 and 18% acrylonitrile, respectively) had surprisingly little effect on the FCP rates. The only significant change in FCP behavior of the modified resins from the control was the ability to reach a higher value of ΔK_{max} [corresponding to a higher static fracture toughness (*19*)]. This behavior is in sharp contrast to that typically found in other rubber-modified polymers (*16*, *35–38*) in which rubber greatly increases FCP resistance even if the amount is too small to increase impact strength. Hence, the addition of 15 phr rubber did not significantly improve FCP response except for a trivial increase in fatigue life.

The modified series 3 resins exhibit similar behavior at 10 Hz. However, inspection of the curves in Figure 3a reveals a slight but consistent tendency for the FCP curves to shift towards the right (at high values of ΔK) and to extend to higher values of ΔK as the rubber content is increased. Thus, a small concentration of rubber increases the toughness and ability to resist crack growth, even though the effect on fatigue life is small. (The increase in ΔK_{max} corresponds to an increase of only $\sim 10\%$ in the number of cycles to failure.) At 20 Hz (Figure 3b), a similar trend is noted. In this system, FCP rates at a given ΔK, though similar to those at 10 Hz, are significantly lower than those of the control. However, at 50 Hz (Figure 3c), a major change in behavior is seen. Whereas curves for specimens containing 5 and 10 phr rubber are essentially identical and fall within the envelope for all rubber-modified specimens tested at lower frequencies, the FCP curve for the specimen containing 15 phr rubber is shifted significantly higher. Crack blunting (*16*) may well be the mechanism responsible for the slight effect of rubber concentration on FCP rates at low frequencies, but it must be overcome by some weakening mechanism at 50 Hz, especially at the highest rubber content.

Effect of Frequency on Fatigue Crack Propagation. FCP curves showing the effect of frequency at a given rubber content are shown in Figure 4. Previous studies on this system and on the MDA–Epon 828 resin indicated no significant effect of frequency, at least from 10–15 Hz (*19*). However, with the control and modified specimens containing 15 phr rubber, a pronounced effect of frequency is observed when frequencies are increased above 10 Hz for the control and 30 Hz for specimen 3–15. As seen in Figure 4, FCP rates for these specimens increase significantly at constant ΔK as a function of frequency, especially for the control resin. The effects are also evident in the values for K_c' given in Table III; the lower the K_c', the greater the displacement of FCP curves to higher da/dN values at a given ΔK, or to lower ΔK values at a given da/dN.

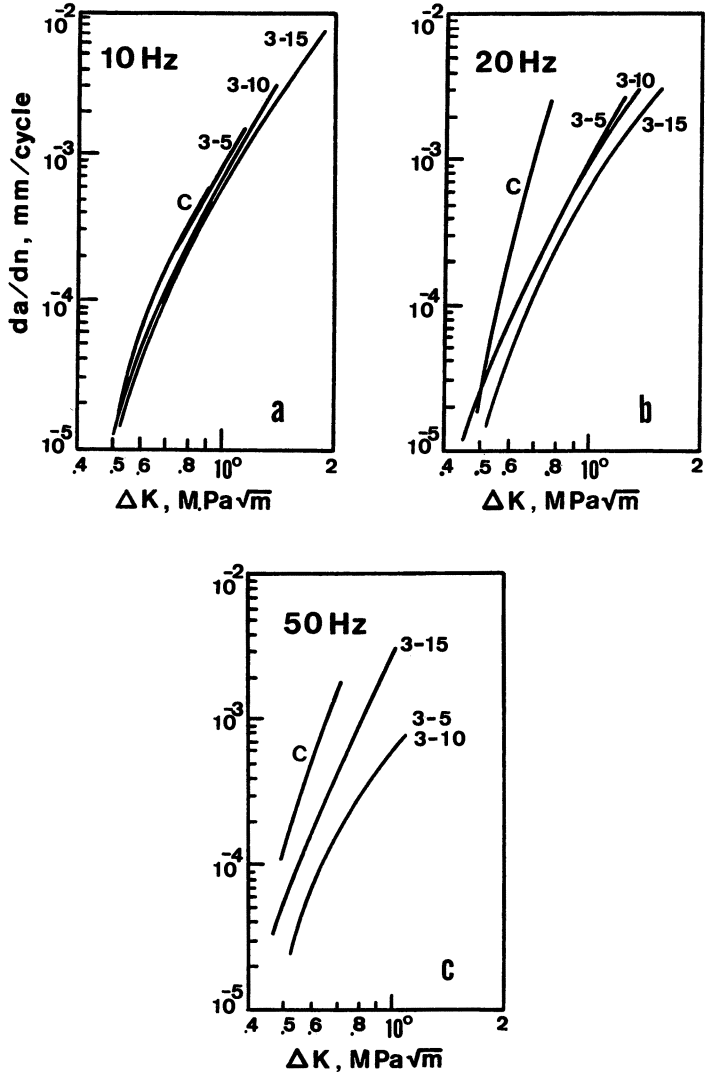

Figure 3. Effect of rubber content on fatigue crack propagation of control (denoted by C) and series 3 rubber-modified epoxies at a given frequency.

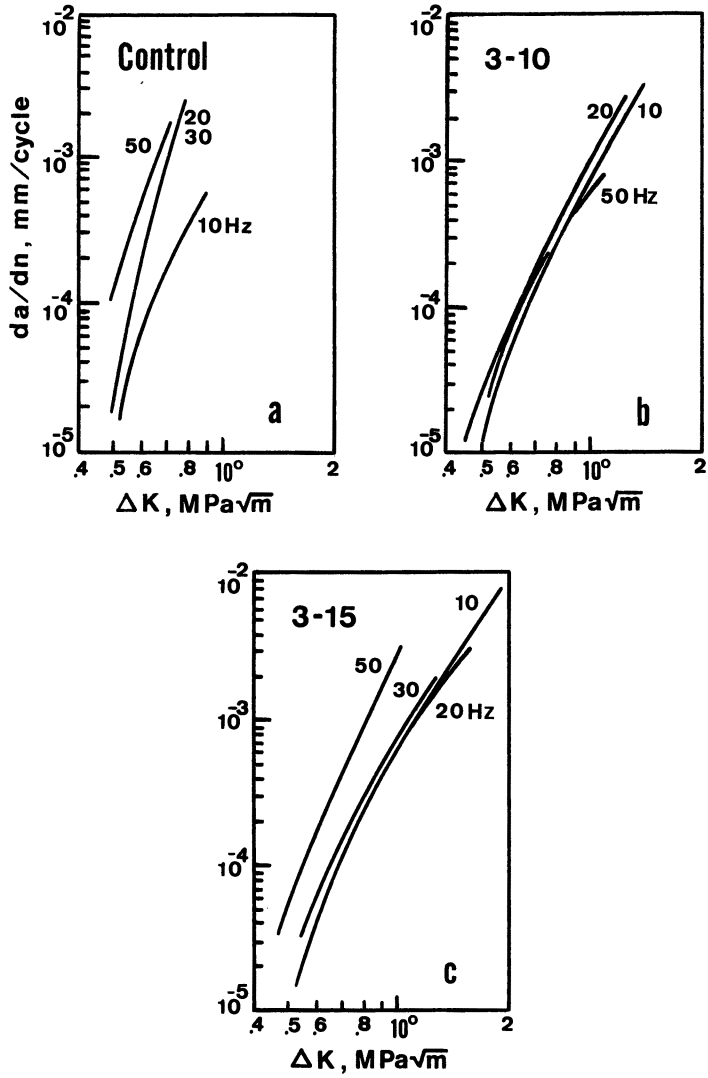

Figure 4. Effect of frequency at constant rubber content on fatigue crack propagation of control and series 3 rubber-modified epoxies. (Curves for 5 phr rubber resemble those for 10 phr.)

This behavior is quite unexpected. Not only is a major effect of frequency unexpected in an epoxy, but the direction of change and the strong sensitivity of the control are surprising. Rubber-toughened Nylon 66 is the only other example known in which an *increase* in frequency *increases* FCP rates at a given ΔK. In all other polymers studied so far (*16*), increased frequency invariably either decreases or has no effect on frequency.

Usually, the effect of frequency on FCP is interpreted (*16*, *23*) in terms of a balance between hysteretic heating localized at a crack tip and heating throughout a large volume ahead of the crack tip. The former is thought to result in beneficial crack blunting, and the latter may result in generalized softening and weakening. Thus, with toughened Nylon 66, extensive heating occurs in the bulk material at high frequencies, with a consequent reduction in resistance to crack propagation. However, with the series 3 resins, only very small temperature rises are observed (<5 °C) throughout most of the fatigue life. The FCP rates at high frequencies are higher than expected at all stages of crack growth, although ΔK is small [the rate of heating $\alpha \Delta K^2$ (*47*)]. With toughened nylon, on the other hand, typical values of ΔK are much higher than those encountered with the modified epoxies. Although even small temperature increases in toughened PMMA result in significant softening in unnotched specimens (*31*), the volume experiencing maximum stresses in notched specimens is small in comparison. (In unnotched specimens, the applied stress is sensed throughout the entire cross section.)

Other effects of increased frequency are a decrease in the integrated time under load for each load excursion and an increase in effective strain rate. However, high-T_g epoxies exhibit no effect of time under load in experiments with different wave forms at a fixed frequency (*16*, *48*) and little effect of temperature and strain rate on fracture toughness (*10*). Moreover, in the latter system, differences in fracture toughness between rubber-toughened and neat resins are minimized at low temperatures and high strain rates. In contrast, with the control and specimen 3–15, differences are minimized at *low* strain rates (low frequencies).

Nevertheless, a possible role of strain rate or time under load cannot be excluded in this system. Because the T_g is relatively low, the viscoelastic response may well be more sensitive to these factors than in higher T_g glasses. The values of K_c' are dependent on frequency (at least at values >10–15 Hz); the higher the frequency, the lower the K_c'. In addition, the relative insensitivity of the modified resins to FCP at low frequencies is easy to understand in terms of the micromechanism for fracture proposed earlier (*19*). At low frequencies in fatigue, the rubber particles may debond prematurely ahead of the crack tip so that any toughening effect is essentially balanced by void formation. Consequently, the overall resistance to crack growth of the matrix is not much improved by rubber particles. Indeed, the size of the damage zone ahead of the crack tip in PMMA varies

inversely with frequency (*49*). If this debonding is present with the frequency-sensitive epoxies, increased FCP rates would be expected. On the other hand, fractographic evidence showed that such debonding was much less common during fast fracture (equivalent to a very high strain rate). Hence, the rubber particles are able to dissipate significant amounts of energy and thereby increase the impact strength. However, the strain rates encountered during fatigue are much lower than those in impact loading, and impact strength, but not fatigue resistance, may be significantly increased by the presence of rubber.

The frequency effects at 50 Hz with 15 phr rubber and with the control are more difficult to understand. With the rubber, the reduction in the damage-zone size suggested to explain the decrease in K_c' at 50 Hz may be a major factor in FCP response. However, although the values of K_c' of the control as a function of frequency correlate with FCP resistance, the behavior relative to that of the modified resins is still anomalous. Thus, the relatively better performance of the modified resins at 20–50 Hz is due to the poorer FCP resistance of the control. Explicit studies of the effect of waveform and strain rate on da/dN, K_c, and the micromechanism of fracture should help elucidate these phenomena.

Fractography. As observed previously for series 1 (15 phr), whitening was observed on the fracture surface on all modified resins prior to fast fracture (*see* Figure 5), and shear zones became evident next to the planar surface at ΔK values close to K_c'. Although these zones did not exhibit the slant-type fracture characteristic of classical shear lips, their occurrence surely reflects a higher component of shear in the stress state at the surface than in the interior. The deformation of epoxies is thought to be dominated by a shear response rather than crazing (*1*).

Another curious feature is the occurrence of discontinuous growth bands (*16*) (*see* Figure 6) on the fracture surface. Whereas each load cycle results in an increment of crack growth in an MDA–Epon 828 epoxy and in a surface marking, this result is not seen with the rubber-modified series 3 resins. Instead, the spacing corresponds to many cycles of loading before the crack jumps to a new position. With polymers that craze, the width of

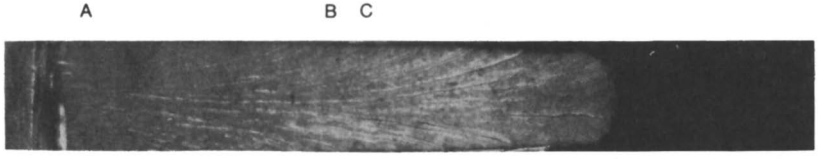

Figure 5. Low-magnification photograph of entire fatigue fracture surface for a rubber-modified epoxy, series 3: A, initial notch; B, onset of shear zone; and C, onset of whitening.

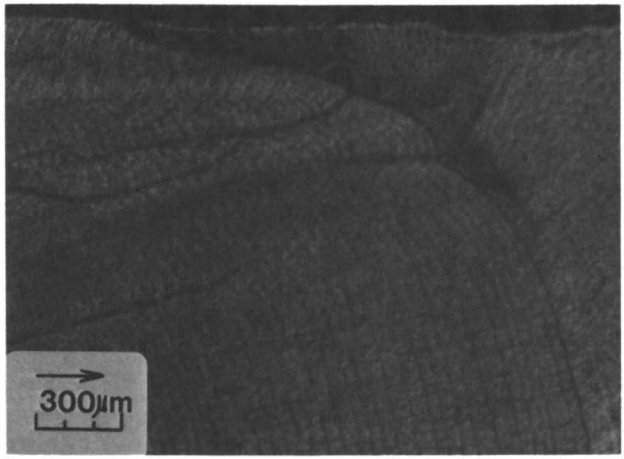

Figure 6. Optical micrograph of series 3 rubber-modified epoxy showing the appearance of discontinuous growth bands and the onset of shear zone on the fatigue fracture surface.

these bands corresponds to a damage zone dimension (r_y) given by the Dugdale equation (*16*):

$$r_y = \frac{\pi}{8}\frac{K^2}{\sigma_y^2} \tag{2}$$

However, Equation 2 does not hold true with the resins studied here. Thus, r_y is proportional to ΔK to a power between 5 and 9. Such large deviations from the power of 2 have been noted only in Nylon 66 (*50*). At present, the micromechanistic aspects of this phenomenon are not understood, although it is tempting to assume a relationship to the voiding mechanism proposed earlier (*19*).

Summary and Recommendation

FCP Behavior. Whereas rubbery phases tend to increase the FCP resistance of several polymeric matrixes, the role of rubber in Nylon 66 and a low-T_g epoxy is complex and not always beneficial. With the latter polymer, the following conclusions may be drawn:

1. At frequencies in the range from 10 to 30 Hz, FCP rates of the rubber-modified epoxy are relatively insensitive to frequency or rubber content over much of the fatigue life (i.e., up to ΔK values of 0.9–1 MPa · $m^{1/2}$) and similar to the FCP rate of the control tested at 10 Hz. However, stable crack growth can be maintained to higher values of ΔK; also, ΔK_{max} varies with rubber content, at least up to 15 phr rubber.

2. The micromechanism of failure in this study may involve cavitation around the rubber particles prior to crack advance so that the inherent static toughness of the modified resin is offset by the creation of voids.

3. As frequency is increased further, the FCP rate of the modified resin containing 15 phr rubber is increased slightly; the rate of increase varies inversely with rubber content. In contrast, the FCP resistance of the controls is dramatically decreased in proportion to the frequency. Thus, the presence of rubber increases the *relative*, but not the *absolute* FCP resistance at frequencies between 20 and 50 Hz.

4. The micromechanism of failure in such cases requires elucidation. Studies of fractography and of the effects of strain rate, dynamic modulus, and integrated time under load should be helpful.

5. Studies in progress with high T_g epoxies will be important because of the lack of correlation between FCP resistance and fracture toughness or impact strength; extension to other thermosets should also be important. Such studies will be relevant to resins that may contain or develop during service significant flaws.

Overall Fatigue Life. Several comments are appropriate:

1. The lack of significant improvement in FCP resistance of a low T_g rubber-modified epoxy at low frequencies and the decrease in FCP resistance at higher frequencies in the epoxy containing 15 phr rubber is disturbing. Even though rubber inclusion lowers FCP rates of the matrix at higher frequencies, the improvement is relative, but not absolute with respect to behavior of the modified resin at lower frequencies.

2. Because of the relative independence of FCP rates on rubber content at low frequencies, the overall fatigue life of unnotched specimens may be lower for the modified resins, which may well require fewer load cycles for initiation than the controls. Speculation about effects at higher frequencies is premature.

3. Better understanding of *both* initiation and propagation of fatigue cracks in rubber-modified polymers of engineering interest is essential for materials selection and design. The high-T_g, brittle resins (e.g., epoxies) are of particular interest. Studies in progress with crack initiation in neat and toughened epoxies should be useful. The effects of loading conditions (for example, tension–tension versus tension–compression loading) and of the environment should be examined. Attention should be given to the relevance to actual service conditions. Studies of this kind will be relevant to resins that may be fabricated without significant flaws and used under conditions that do not involve the fortuitous development of such flaws.

Nomenclature

a Crack length, mm

A Pre-exponential constant in Paris equation

d	Density, g/cm^3
da/dN	Fatigue crack-propagation rate, mm/cycle
E, E', E''	Tensile modulus, storage modulus, and loss modulus, respectively, MPa or GPa
E_r	Tensile modulus in the rubbery state, GPa
ET_g	Glass transition temperature of the epoxy phase, °C
G_{IC}	Strain energy release rate (global fracture energy, measured in the tensile opening mode, plane-strain conditions, J/m^2)
IS	Impact strength, J/m^2
K, ΔK	Stress intensity factor and range in stress intensity factor, respectively, MPa · m$^{1/2}$
ΔK_{max}	Maximum value of K noted before fast fracture, MPa · m$^{1/2}$
K_c'	Quasi-static fracture toughness estimated from ΔK_{max}, MPa · m$^{1/2}$
K_{Ic}	Plane-strain fracture toughness in tensile opening mode, MPa · m$^{1/2}$
M_c	Average molecular weight between cross-links
n	Exponent in Paris equation
N	Number of cycles
N_i, N_P	Number of cycles for initiation and propagation of a crack, respectively
ΔP	Applied load range
r	Ratio of minimum to maximum load
R	Gas constant, 8.31 J/mol/degree
RT_g	Glass transition temperature of rubbery phase, °C
T_g	Glass transition temperature, °C
T_{gE}, T_{gR}	Glass transition temperature of pure epoxy and rubber, respectively, °C
W_E	Weight fraction of epoxy
ϵ_b	Elongation to break, %
σ, $\Delta\sigma$	Stress and range in stress, respectively, MPa
σ_y	Tensile-yield stress, MPa
ν	Poisson's ratio

Acknowledgments

The authors wish to acknowledge partial support by the Polymers Program, National Science Foundation (Grant No. 8106489) and by the Office of Naval Research. We are also indebted to R. S. Drake, C. M. Lizak, and D. R. Egan of the BFGoodrich Company for their advice on the formulation of curing of epoxies.

Literature Cited

1. Bucknall, C. B. "Toughened Plastics"; Appl. Sci.: London, 1977.
2. Manson, J. A.; Sperling, L. H. "Polymer Blends and Composites"; Plenum: New York, 1976; Chap. 3.

3. Paul, D. R.; Newman, S., Eds. "Polymer Blends"; Academic: New York, 1978.
4. Kinloch, A. J.; Young, R. J.; "Fracture Behavior of Polymers"; Appl. Sci.: London, New York, 1983; Chap. 11.
5. Olabisi, O.; Robeson, L. M.; Shaw, M. T. "Polymer–Polymer Miscibility"; Academic: New York, 1979.
6. Drake, R. S.; Siebert, A. R. *Org. Coat. Appl. Sci. Proc.* **1983**, *48*, 491.
7. Drake, R. S.; Siebert, A. R. *SAMPE Q.* **1975**, *6(4)*, 7.
8. Siebert, A. R. In "Rubber Modified Thermoset Resins"; Riew, C. K.; Gillham, J. K., Eds.; ADVANCES IN CHEMISTRY SERIES No. 208; ACS: Washington, D.C., 1984; p. 179.
9. Riew, C. K.; Rowe, E. H.; Siebert, A. R. In "Toughness and Brittleness of Plastics"; Deanin, R. D.; Crugnola, A. M., Eds.; ADVANCES IN CHEMISTRY SERIES No. 154; ACS: Washington, D.C., 1976; p. 326.
10. Hunston, D. L.; Bascom, W. D. In "Rubber Modified Thermoset Resins"; Riew, C. K.; Gillham, J. K., Eds.; ADVANCES IN CHEMISTRY SERIES No. 208; ACS: Washington, D.C., 1984; p. 83.
11. Pearson, R. A.; Yee, A. F. *Polym. Mater. Sci. Eng.* **1983**, *49*, 316.
12. Kinloch, A. J.; Shaw, S. J. *Polym. Mater. Sci. Eng.* **1983**, *49*, 307.
13. Hussain, A. *Polym. Mater. Sci. Eng.* **1983**, *49*, 311.
14. Kunz, S. C.; Sayre, J. A. In "Rubber Modified Thermoset Resins"; Riew, C. K.; Gillham, J. K., Eds.; ADVANCES IN CHEMISTRY SERIES No. 208; ACS: Washington, D.C., 1984; p. 215.
15. Bucknall, C. B.; Stevens, W. W. In "Toughening of Plastics"; Plast. Rubber Inst.: London, 1978; p. 24.
16. Hertzberg, R. W.; Manson, J. A. "Fatigue in Engineering Plastics"; Academic: New York, 1980.
17. Agronoff, J., Ed. "Modern Plastics Encyclopedia"; McGraw-Hill: New York, 1981–84
18. Shah, D. N., M.S. Report, Lehigh Univ., Bethlehem, PA., 1983.
19. Shah, D. N.; Attalla, G.; Manson, J. A.; Connelly, G. M.; Hertzberg, R. W. In "Rubber Modified Thermoset Resins"; Riew, C. K.; Gillham, J. K., Eds.; ADVANCES IN CHEMISTRY SERIES No. 208; ACS: Washington, D.C., 1984; p. 117.
20. Gillham, J. K.; Chan, L. C., in "Rubber Modified Thermoset Resins"; Riew, C. K.; Gillham, J. K., Eds.; ADVANCES IN CHEMISTRY SERIES No. 208; ACS: Washington, D.C., 1984; p. 235.
21. ASTM test D671.
22. Connelly, G. M.; Hwang, J., unpublished research, Lehigh University, 1983.
23. Hahn, M. T.; Hertzberg, R. W.; Lang, R. W.; Manson, J. A.; Michel, J. C.; Ramirez, A.; Rimnac, C. M.; Webler, S. M. In "Deformation, Yield, and Fracture of Polymers"; Plast. Rubber Inst.: London, 1982; p. 19.1.
24. Menges, G.; Weigand, E. *Proc. 21st Annu. Tech. Conf. Soc. Plast. Eng.* **1975**, p. 409.
25. Beardmore, P.; Rabinowitz, S. In "Treatise on Materials Science and Technology"; Arsenault, R. J., Ed.; Academic: New York, 1975; Vol. 6, p. 267.
26. Sauer, J. A.; Chen, C. C. *Adv. Polym. Sci.* **1983**, *52–53*, 169.
27. Sauer, J. A.; Chen, C. C. *Polym. Eng. Sci.* **1984**, *24*, 786.
28. Bartesch, H.; Williams, D. R. G. *J. Appl. Polym. Sci.* **1978**, *22*, 467.
29. Bucknall, C. B.; Marchetti, A. *Polym. Eng. Sci.* **1984**, *24*, 535.
30. Woan, D.-J.; Habibullah, M.; Sauer, J. A. *Polymer* **1981**, *22*, 699.
31. Bucknall, C. B.; Marchetti, A. *J. Appl. Polym. Sci.* **1983**, *28*, 2689.
32a. Murukami, R.; Shin, N.; Kusomoto, N.; Motozato, Y. *Kobunshi Robunshu* **1976**, *33*, 107.

32b. Turkanis, J. M.S. Thesis, Lehigh Univ., 1984.
33. Thorkildsen, R. L. In "Engineering Design for Plastics"; Baer, E., Ed.; Van Nostrand-Reinhold: Princeton, 1964; p. 279.
34. Takemori, M. T.; Morelli, T. A. In "Engineering Design for Plastics"; Plast. Rubber Inst.: London, 1981; Paper 7.
35. Skibo, M. D.; Manson, J. A.; Hertzberg, R. W.; Collins, E. A. In "Durability of Macromolecules Materials"; Eby, R. K., Ed.; ACS SYMPOSIUM SERIES No. 95; ACS: Washington, D.C., 1979; p. 311.
36. Skibo, M. D.; Hertzberg, R. W.; Manson, J. A. In "Deformation, Yield, and Fracture of Polymers"; Plast. Rubber Inst.: London, 1979; p. 4.1.
37. Qureshi, S.; Manson, J. A.; Sperling, L. H. In "Polymer Applications of Renewable Resource Materials"; Carraher, C. E., Jr.; Sperling, L. H., Eds.; Plenum: New York, 1983; p. 249.
38. Hahn, M. T., Ph.D. dissertation, Lehigh Univ., 1983.
39. Manson, J. A.; Hertzberg, R. W. *J. Polym. Sci. Polym. Phys. Ed.* **1973**, *11*, 2483.
40. Rimnac, C. M., unpublished data, Lehigh Univ., 1983.
41. Manson, J. A.; Ramirez, A.; Hertzeberg, R. W. *Polym. Mater. Sci. Eng.* **1984**, *50*, 106.
42. Adams, G. C.; Wu, T. K. In "Fatigue in Polymers"; Plast. Rubber Inst.: London, 1983; Paper 15.
43. Kim, S. L.; Skibo, M. D.; Manson, J. A.; Hertzberg, R. W.; Janiszewski, J. *Polym. Eng. Sci.* **1978**, *18(14)*, 1093.
44. Sohn, J. E.; Emerson, J. A.; Chen, J.-K.; Siegel, A. F.; Koberstein, J. T. *Polym. Mater. Sci. Eng.* **1983**, *49*, 447.
45. Chan, L. C.; Gillham, J. K.; Kinloch, A. J.; Shaw, S. J. In "Rubber Modified Thermoset Resins"; Riew, C. K.; Gillham, J. K., Eds.; ADVANCES IN CHEMISTRY SERIES No. 208; ACS: Washington, D.C., 1984; p. 261.
46. Paris, P. C. *Proc. 10th Sagamore Res. Conf.* **1964**, p. 107.
47. Barenblatt, G. J.; Eutov, V. M., Salganik, R. L. *Proc. Symp. Thermoinelastics Int. Union Theor. Appl. Mech.* East Kilbridge, UK **1968**, p. 33.
48. Skibo, M. D., Ph.D. Dissertation, Lehigh Univ., 1977.
49. Lang, R. W.; Manson, J. A.; Hertzberg, R. W.; Schirrer, R. *Polym. Eng. Sci.* **1984**, *24*, 833.
50. Bretz, P. E., Ph.D. Dissertation, Lehigh Univ., 1980.

RECEIVED for review January 7, 1985. ACCEPTED May 14, 1985.

18

Environmental-Stress Crazing and Cracking of Poly(methyl Methacrylate)–Poly(vinylidene Fluoride) Blends

S. R. MURFF[1], J. W. BARLOW, and D. R. PAUL

Department of Chemical Engineering and Center for Polymer Research, University of Texas, Austin, TX 78712

The tensile properties of miscible blends of poly(methyl methacrylate) (PMMA) and poly(vinylidene fluoride) (PVF_2) were determined in air. These results were interpreted in terms of the plasticization caused by adding PVF_2 to PMMA and the crystallinity of the blends. Strength exhibits a minimum, and elongation at break shows a maximum as a function of blend composition because of the competition between these two effects. The critical strain for the development of crazes or cracks was determined for blends in the presence of seven different liquids by using a Bergen strain jig. For all liquids, this threshold strain or stress increased dramatically as the PVF_2 content of the blend increased.

SCIENTIFIC AND TECHNOLOGICAL INTEREST in polymer blends has been intensifying (*1*, *2*). This increased interest is driven, in part, by the extra dimension blending offers for solving problems. A significant portion of the growing scientific literature in this area was devoted to examining and understanding the phase behavior of such mixtures (*3*) because miscibility is a more common occurrence than originally forecast (*4*). An equally important direction is to learn about the problems that can be solved by this new knowledge base and what the trade-offs are.

This chapter examines the premature physical mechanical failure that many polymers experience when stressed in the presence of certain fluids. This problem is especially serious for amorphous glassy polymers (*5–12*) such as poly(methyl methacrylate) (PMMA). On the other hand, some semicrystalline polymers, such as poly(vinylidene fluoride) (PVF_2), are extremely resistant to chemicals and are generally the materials of choice when this characteristic is critical. Interestingly, these two polymers,

[1] Current address: Catalysts Division, Armak, Pasadena, TX 77507

0065-2393/86/0211/0313$06.00/0

PMMA and PVF_2, when blended form a miscible amorphous phase. These blends may also have a coexisting crystalline phase of PVF_2, depending on composition and thermal history. This blend system has been the object of extensive scientific studies since this fact was first reported in 1971. The question examined here is, how do mixtures of these distinctly different polymers behave mechanically when exposed to hostile liquids?

Sample Preparation and Characterization

The PVF_2 used was supplied by Pennwalt Corporation in the form of pellets and is commercially designated as Kynar 460, which is a general-purpose extrusion and molding grade. The PMMA was Plexiglas V(811)100 molding pellets (Rohm and Haas Company) and has a number average molecular weight ($\bar{M}_n$) of 52,900 and a weight average molecular weight ($\bar{M}_w$) of 130,000.

Blends containing various proportions of PVF_2 and PMMA were fabricated into sheets 0.015 to 0.030 in. thick by the following procedure. Pellets of the two polymers were mixed in the desired proportions and melt blended in a Brabender single-screw extruder by using barrel and die temperatures in the range of 200 to 220 °C. The extrudate was then pelletized. Blend pellets were re-extruded into films approximately 3 in. wide and 0.002 to 0.010 in. thick. These films were too thin for the subsequent test procedures and were rather highly oriented. Consequently, several layers of film were laminated together in a compression mold at 220 °C to produce sheets essentially free of orientation and with the desired thickness. All materials were dried prior to each melt-processing step.

The blends were characterized by differential scanning calorimetry (DSC). Glass transition temperatures (T_g) and melting points agreed very well with previous work (*14*), that is, each blend had a single, composition-dependent T_g as seen in Figure 1. First heats in the DSC gave the crystallinity levels shown in Figure 2. Extruded blends had slightly less crystallinity than compression-molded blends because of the more rapid quenching in this process. Crystallinity goes to zero at about 40% PVF_2.

Mechanical Properties

Mechanical properties were determined for compression-molded sheets by using strips 1 in. wide with a gauge length of 4 in. between the grips of an Instron tensile tester. Crosshead speed was 0.2 in./min for determining the modulus and 2 in./min for determining yield and failure behavior. Crosshead travel and a gauge length of 4 in. were used to compute strain. Figure 3 shows typical stress–strain diagrams. Blends containing 40% or more of PVF_2 exhibited ductile behavior, whereas PMMA and the 20% PVF_2 blend showed typically brittle failure.

Modulus, strength, and percent elongation values were averaged for five to six samples, and the results were plotted versus blend composition

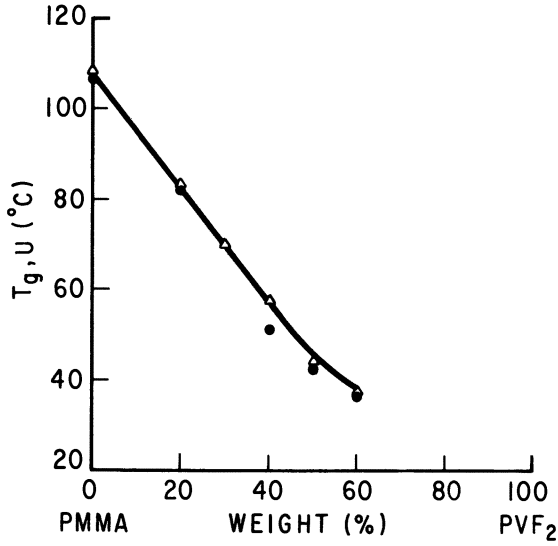

Figure 1. Glass transition behavior of PMMA–PVF_2 blends. Transitions at high PVF_2 contents had very small base line shifts and are not shown. Key: △, previous results (14); and ●, this study.

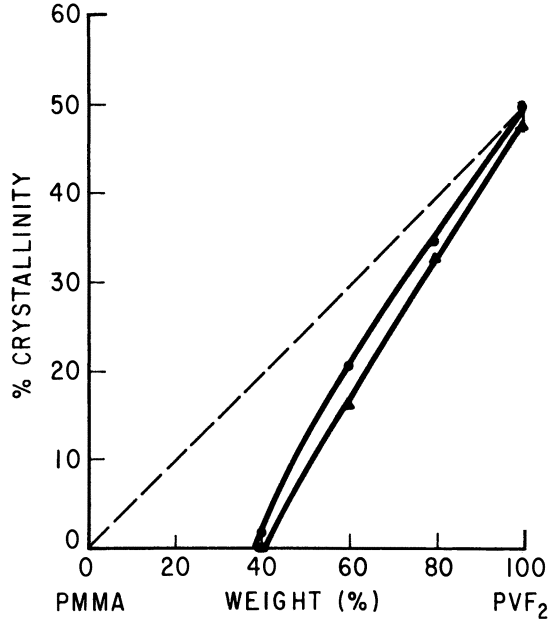

Figure 2. Crystallinity of PMMA–PVF_2 blends. Key: ▲, extruded films; and ●, compression-molded film.

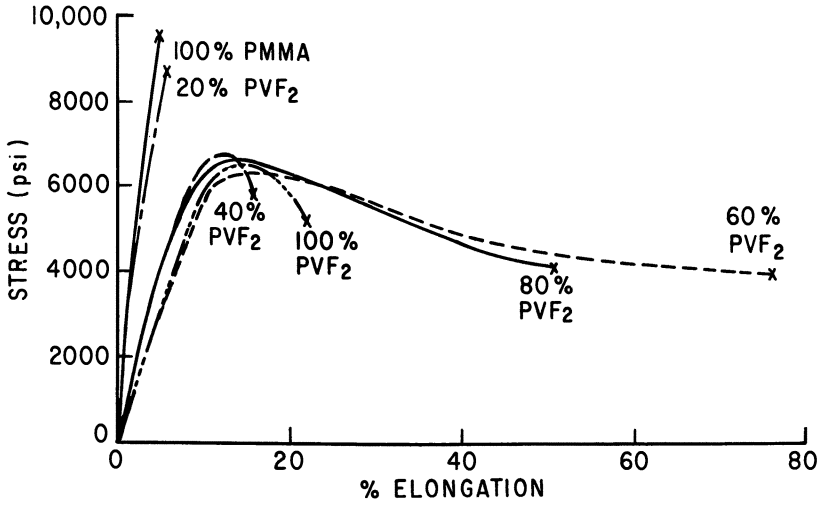

Figure 3. Typical stress–strain diagrams determined in air at room temperature.

(Figures 4–6). The agreement with the results given by Noland et al. (*13*) is quite good where comparisons are possible. Two factors are important to the understanding of the variation of these mechanical properties with blend composition. First, the T_g decreases continuously with PVF_2 content and becomes less than the testing temperature at high PVF_2 contents (*13–16*). Second, these materials are completely amorphous until the PVF_2 content is about 40%, after which crystallinity increases rapidly. Interestingly, the modulus shows no discernible discontinuity at the composition that divides the amorphous material from the semicrystalline materials. However, the competition between the two factors previously mentioned is clearly seen in the yield and failure characteristics given in Figures 5 and 6. Both the yield and the ultimate strengths decrease initially as PVF_2 is added to PMMA. This response is expected when a liquid or rubbery diluent is added to a glassy polymer (i.e., PVF_2 is effectively a plasticizer). However, these properties go through a minimum and then rise on further addition of PVF_2. This response is undoubtedly a result of the strengthening effect caused by the increasing crystallinity occurring in the region of high PVF_2 contents. Conversely, the elongation at break initially increases as PVF_2 is added to PMMA because of plasticization or reduction of T_g. It reaches a maximum value at about 60% PVF_2 and then declines as crystallinity becomes a more dominant factor.

Environmental-Stress Cracking and Crazing

Many polymers, especially glassy ones, develop crazes or possibly cracks when mechanically loaded beyond some threshold stress. This threshold

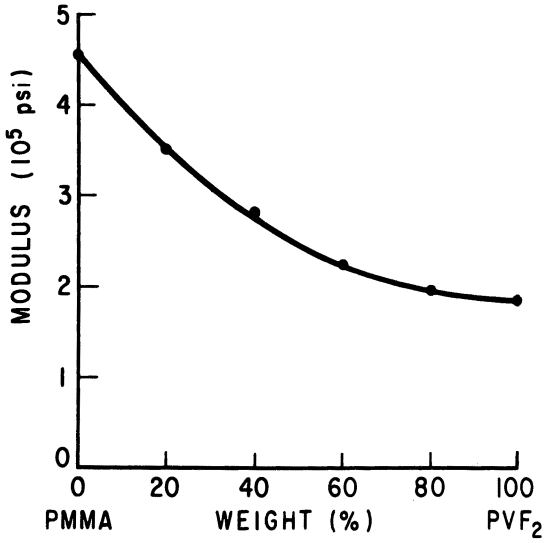

Figure 4. Modulus vs. composition for blends.

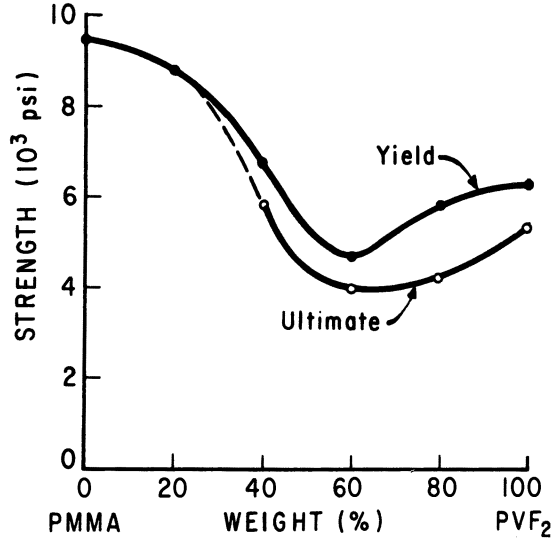

Figure 5. Yield (●) and ultimate (○) strength of blends.

may be considerably lower than the normal yield or failure stress when the sample is exposed to certain fluids (*5–12*). For wholly amorphous, glassy polymers, the reduction of this threshold stress or strain has been directly related (*6–9*, *12*) to the extent particular liquids or vapors swell or are dissolved in the polymer. This threshold, or critical stress, defines an upper

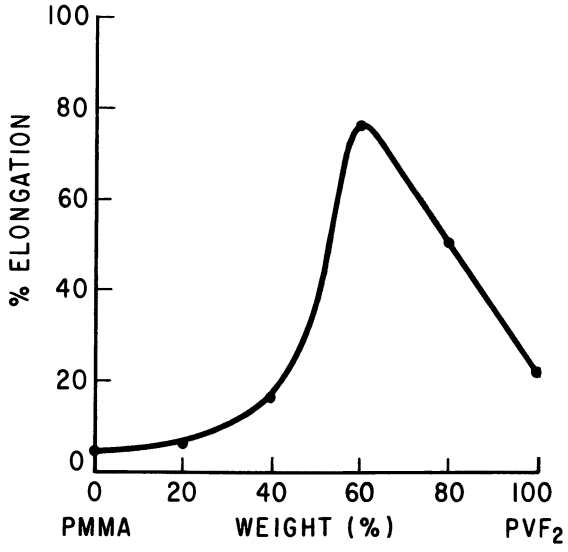

Figure 6. Elongation at break for blends.

limit on the load a polymer can be expected to bear within a certain environment without damage. Several tests have been devised to measure this limit, and one of the most effective is an elliptical-strain jig first described by Bergen (*5*) and used extensively by Kambour (*6–9*, *12*). This technique was the primary one used in this work.

The jigs were machined from aluminum sheet stock 1 in. thick and had the shape of a one-quarter section of an ellipse conforming to the equation

$$\left(\frac{y}{1.5}\right)^2 + \left(\frac{x}{5}\right)^2 = 1$$

where all dimensions are in inches. Sheet specimens 1 in. wide having thicknesses in the range of 0.015 to 0.030 in. and fabricated in the manner described earlier were strapped to the curved surface of the jig. Thus, the specimen experiences a maximum surface strain that varies with its position on the jig surface. The strain at a given position can be calculated from the relationships given by Bergen (5). The clamps prevent cracks in one area from changing the strain in other areas of the sample. The jig with a sample so installed was immersed in the liquid of interest overnight, although apparently all damage to the sample occurred within a few minutes and certainly in less than an hour. After removal from the liquid, the specimen was visually inspected by using a low-power magnifying glass with light from

varying angles of incidence. The distinction between crazing and cracking can be somewhat subjective in difficult samples. Following the usual criteria (*17*), cracking is associated with visible surface rupture. The critical strain below which no cracking or crazing could be seen was determined with an estimated precision of about $\pm 10\%$ based on repeated measurements for each sample and liquid combination.

Table I shows a qualitative summary of the observations for seven different liquids and blends ranging from pure PMMA to pure PVF_2. Each liquid caused severe damage to pure PMMA and had no apparent effect on pure PVF_2. The blends showed various effects between these limits. Figure 7 shows a more quantitative picture by giving the measured critical strain as a function of blend composition for four of these liquids. Except for *N*-methylformamide, the effect of blend composition on the critical strain is quite similar for each liquid. For clarity, data for the other three liquids are not plotted. As a first approximation, the critical-strain values can be multiplied by the tensile moduli measured in air (*see* Figure 4) to give an estimate of the critical or threshold stress. The result is shown in Figure 8. The critical stress is the product of a function that increases with PVF_2 level (critical strain) and a function that decreases with PVF_2 level (modulus). Consequently, the critical stress varies less with blend composition than does the critical strain.

Another more laborious technique for determining the threshold stress for environmental-stress cracking or crazing was used in limited tests for comparison with the results obtained by the Bergen strain jig. In this method, the specimen is loaded to a predetermined stress in an Instron and liquid is applied to an absorbent material clipped to the stressed sample. In the absence of any environmentally active liquid, the sample will presumably support the applied load indefinitely, if it is adequately below the yield stress. However, after applying the appropriate liquid to the wick, the stressed sample breaks catastrophically after a certain time, which is shorter the larger the applied stress. The solid points in Figure 9 define the response for 1-propanol and pure PMMA. As seen in this figure, the time to break becomes very long as the stress level is reduced to a level that defines the threshold stress. The open point in Figure 9 is the critical stress estimated by the Bergen strain-jig approach. The threshold stresses estimated by the two methods agreed very closely.

Summary

The strength and elongation at break of miscible blends of PMMA and PVF_2 are influenced by the T_g–composition relationship, or the plasticizing effect caused by adding PVF_2 to PMMA, and by the development of PVF_2 crystallinity in compositions containing more than about 40% PVF_2. The competition between these two opposing effects causes a minimum in strength and a maximum in elongation at break when these quantities are

Published on December 9, 1985 on http://pubs.acs.org | doi: 10.1021/ba-1986-0211.ch018

Table I. Qualitative Observations on the Influence of Various Liquids on PMMA–PVF_2 Blends Under Stress

Solvent	*100% PMMA*	*20% PVF_2*	*40% PVF_2*	*60% PVF_2*	*80% PVF_2*	*100% PVF_2*
Methanol	cracking and slight dissolution	cracking and swelling	cracking and slight swelling	cracking	no effect	no effect
Ethanol	severe cracking	crazing	crazing	slight crazing	slight crazing	no effect
2-Propanol	severe cracking	cracking and crazing	cracking and crazing	cracking and slight crazing	slight crazing	no effect
1-Propanol	severe cracking	cracking and crazing	cracking and crazing	cracking and crazing	crazing	no effect
2-Butanol	severe cracking	cracking and crazing	cracking and crazing	slight cracking	slight cracking	no effect
n-Methyl-formamide	cracking	cracking and crazing	cracking and crazing	cracking and crazing	very slight cracking	no effect
Toluene	cracking and severe swelling and dissolution	cracking and severe swelling and dissolution	cracking and severe swelling and dissolution	slight cracking and slight swelling	no effect	no effect

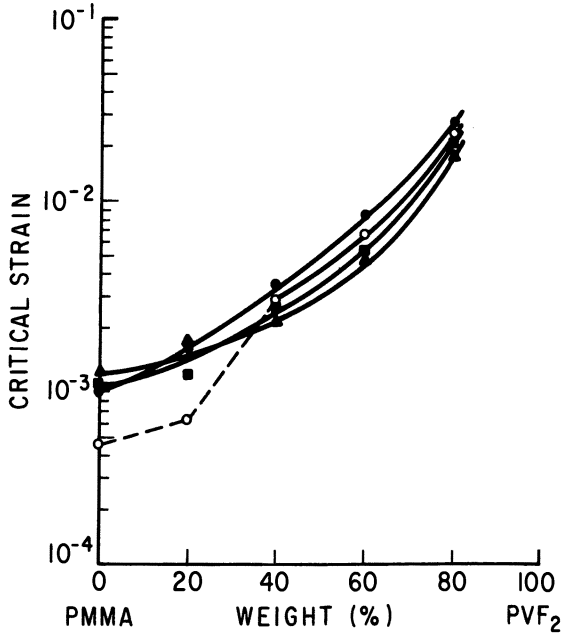

Figure 7. Critical strain determined by Bergen strain jig. Key: ●, 1-propanol; ○, N-methylformamide; ■, ethanol; and ▲, 2-propanol.

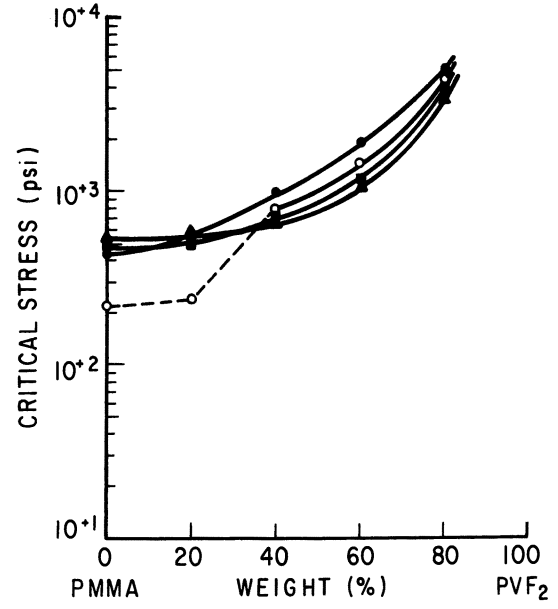

Figure 8. Calculated critical stress. Key: ●, 1-propanol; ○, N-methylformamide; ■, ethanol; and ▲, 2-propanol.

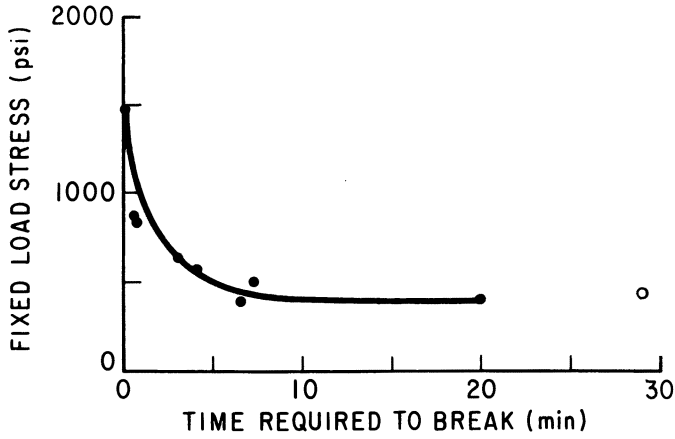

Figure 9. Time to break as a function of tensile stress for PMMA in contact with 1-propanol (●). The open circle is the critical stress estimated with a Bergen strain jig.

plotted versus blend composition. The initial modulus shows a continuous monotonic decline as the PVF_2 content of the blend is increased. No dramatic change occurs at the composition dividing amorphous from semicrystalline mixtures. Interactions between the components that apparently influence the mechanical property relationships for completely amorphous, miscible blends of glassy polymers (*18–20*) are evidently masked by the more influential issues of plasticization and crystallinity in the PMMA–PVF_2 system.

Clearly, addition of PVF_2 to PMMA results in materials that are more resistant to environmental-stress cracking or crazing. This result is indicated by the significant increases in the critical strain and stress obtained by using a Bergen strain jig. Whereas these increases are accelerated as the blends develop crystallinity, significant improvements occur at PVF_2 levels in which crystallinity is absent. Thus, the inherent chemical resistance of PVF_2 is translated into its blends with PMMA by an amount related to the fraction of the blend it occupies.

An interesting way of viewing these results is to superimpose plots of yield strength in air and the critical strength in the presence of a liquid like 1-propanol (*see* Figure 10). The effect of adding PVF_2 to PMMA is to *decrease* the yield strength in air initially (i.e., plasticization), but to *increase* the usable stress when in the presence of hostile liquids. One might speculate that plasticization is also responsible for the latter response to some degree. The dashed continuation of the critical-stress curve in Figure 10 suggests that the stress required for environmentally induced cracking or crazing of pure PVF_2 is higher than its yield stress.

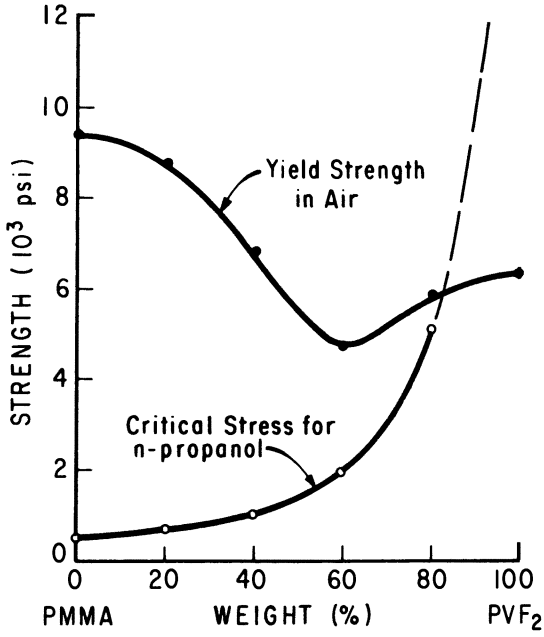

Figure 10. Strength in air compared with critical stress when exposed to 1-propanol.

The results presented illustrate one example of the possibilities for using miscible blends to solve certain problems and the trade-offs involved. With respect to the latter, acrylic plastics like PMMA or its homologue, poly(ethyl methacrylate), are often used when optical clarity is required. This characteristic will obviously be compromised when PVF_2 is blended to the concentration at which crystallinity is developed.

Acknowledgment

This research was supported by the U.S. Army Research Office.

Literature Cited

1. Barlow, J. W.; Paul, D. R. *Annu. Rev. Mater. Sci.* **1981**, *11*, 299.
2. Paul, D. R.; Newman, S., Eds. "Polymer Blends"; Academic: New York, 1978; Vols. 1–2.
3. Olabisi, O.; Robeson, L. M.; Shaw, M. T., "Polymer–Polymer Miscibility"; Academic: New York, 1979.
4. Dobry, A.; Boyer-Kawenoki, F. *J. Polym. Sci.* **1947**, *2*, 90.
5. Bergen, R. L. *SPE J.* **1962**, *18*, 667.
6. Bernier, G. A.; Kambour, R. P. *Macromolecules* **1968**, *1*, 393.
7. Kambour, R. P.; Romagosa, E. E.; Gruner, C. L. *Macromolecules* **1972**, *5*, 335.

8. Kambour, R. P.; Gruner, C. L.; Romagosa, E. E. *Macromolecules* **1974**, *7*, 249.
9. Kambour, R. P.; Gruner, C. L. *J. Polym. Sci. Polym. Phys. Ed.* **1978**, *16*, 703.
10. Haven, R. E.; Sung, N. H. *SPE Tech. Pap.* **1978**, *24*, 406.
11. Bigg, D. M.; Leininger, R. I.; Lee, C. S. *SPE Tech. Pap.* **1981**, *27*, 227.
12. White, S. A.; Weissman, S. R.; Kambour, R. P. *J. Appl. Polym. Sci.* **1982**, *27*, 2675.
13. Noland, J. S.; Hsu, N. N. C.; Saxon, R.; Schmitt, J. M. In "Multicomponent Polymer Systems"; Platzer, N. A. J., Ed.; ADVANCES IN CHEMISTRY SERIES No. 99; ACS: Washington, D.C., 1971; pp. 15–28.
14. Paul, D. R.; Altamirano, J. O. In "Copolymers, Polyblends, and Composites", Platzer, N. A. J., Ed.; ADVANCES IN CHEMISTRY SERIES No. 142; ACS: Washington, D.C., 1975; pp. 371–85.
15. Paul, D. R.; Barlow, J. W.; Bernstein, R. E.; Wahrmund, D. C. *Polym. Eng. Sci.* **1978**, *18*, 1225.
16. Nishi, T.; Wang, T. T. *Macromolecules* **1975**, *8*, 909.
17. Beardmore, P.; Rabinowitz, S. *Crit. Rev. Macromol. Sci.* **1972**, *1*, 1.
18. Kleiner, L. W.; Karasz, F. E.; MacKnight, W. J. *Polym. Eng. Sci.* **1979**, *19*, 519.
19. Olabisi, O.; Farnham, A. G. In "Multiphase Polymers"; Cooper, S. L.; Estes, G. M., Eds.; ADVANCES IN CHEMISTRY SERIES No. 176; ACS: Washington, D.C., 1979; pp. 559–85.
20. Joseph, E. A.; Lorenz, M. D.; Barlow, J. W.; Paul, D. R. *Polymer* **1982**, *23*, 112.

RECEIVED for review November 15, 1984. ACCEPTED February 12, 1985.

19

The Morphology and Mechanical Properties of Ethylene–Propylene Copolymers and Blends

P. PRENTICE, E. PAPAPOSTOLOU, and J. G. WILLIAMS

Department of Mechanical Engineering, Imperial College of Science and Technology, London, England SW7 2BX

The mechanical properties of the group of materials usually referred to as ethylene–propylene block copolymers were found to resemble those of physical blends. According to optical and scanning electron microscopy, an excluded phase exists in these materials that is rubber-like in nature and has dimensions in the range of 0.7 to 5 μm, depending upon the source of supply. Simple extraction experiments demonstrated that the majority of this phase is removable by physical means (i.e., it is not chemically bound to the polypropylene matrix). The loss factor, tan δ, plotted as a function of temperature, resulted in two peaks in both the copolymers and the blends. One peak corresponded to the matrix, and the other peak corresponded to the ethylene-rich phase. From the limited data so far available, we found a correlation between the size of the tan δ peak and the ethylene content.

THE RELATIVELY LOW COST and general availability of polyolefins such as polyethylene (PE) and polypropylene (PP), along with their many and varied properties, have created a broad market for these materials. However, not all the properties of these materials are beneficial, for instance the susceptibility of high-density polyethylene (HDPE) to environmental-stress cracking and the relatively high glass transition temperature (T_g) of PP, which makes it unsuitable for low-temperature applications. Therefore, polyolefin development has concentrated on improving the performance of existing materials. Two areas that have been investigated are the production of physical blends of the homopolymers with various types and amounts of thermoplastic rubbers and the development of copolymers.

Two types of copolymers are available commercially. The first type is random copolymers in which, as their name implies, the comonomer is incorporated into the polymer chain at irregular intervals—this group in-

0065-2393/86/0211/0325$06.00/0

cludes the ethylene–propylene thermoplastic rubbers (EPR). The second group contains the so-called "block" copolymers in which the ethylene comonomer is assumed to be concentrated in distinct regions of the chain. In general, the term *block copolymer* applies to materials in which the various components of the polymer chain are chemically linked. In this chapter, we hope to show that the ethylene-rich regions in commercially available "block" copolymers of ethylene and propylene are not chemically linked to the matrix. Thus, although these materials are copolymers, it may not be technically correct to refer to them as block copolymers. The problem arises because of the considerable uncertainty that exists regarding the true architecture of these materials; most have been assigned structures deduced almost entirely from the synthetic procedure employed. However, the simplest manufacturing process involves the consecutive introduction of two monomers into a reaction vessel, and the existence of residues of the first monomer in the presence of the second leads to a situation in which the relative monomer concentrations are unknown and constantly changing.

The dynamics of a Ziegler–Natta catalyzed reaction are such that the mean lifetime of growing polymer chains at 70 °C is about 10 to 16 min (*1*). After this period of time, they are terminated by a chain-transfer mechanism (*2*). Because, in some processes, the interval between the start of the reaction and the introduction of the second monomer is much greater than this lifetime, many of the initial chains will terminate before encountering the second monomer. For ethylene–propylene copolymers in which propylene is the initial monomer, the addition of ethylene as the comonomer will lead to the initiation of many new chains with an ethylene molecule, because of its smaller size and greater reactivity, while still in an environment rich in propylene. Thus, a large proportion of the ethylene-rich segments will not be chemically linked to the PP preblock. For these reasons, during the transition from one monomer feedstock to another, the resulting product is likely to contain large proportions of an EPR.

The PP and the rubber are mutually incompatible in the melt (*3*), and the rubber forms a dispersed phase when the sample is cooled. Optical (*4*, *5*) and scanning electron microscopy (SEM) provide direct visual evidence of this two-phase morphology.

If the presence of a second, more rubbery, phase is assumed, dynamic mechanical studies should result in the detection of more than one transition in copolymer systems.

Experimental

Materials. Several samples of copolymers from various manufacturers, all commercially available, were examined along with some physical blends. The total ethylene content of these materials ranged from 3 to 14 wt%.

Microscopy. The preparation of specimens and the techniques of optical microscopy are described elsewhere (*4–6*).

For investigation with an SEM (Joel JSM–T200), optically smooth surfaces were prepared from molded plates by using a freshly prepared glass knife. The specimens were then treated with *p*-xylene in an ultrasonic shaker for about 5 min to remove any soluble material from the surface regions. Surfaces treated in this way are superior (*3*) to those prepared by acid etching, and they are indistinguishable from those prepared by solvent etching in a laboratory shaker for 1 to 24 h. The prepared surfaces were subsequently coated with gold by using an Edwards sputter-coating device before viewing in the SEM at an excitation voltage of 15 kV.

Impact Testing. Charpy impact specimens were cut from water-quenched plates molded at 190 °C. Specimen dimensions were 50 × 5.5 mm with a 60° notch of root radius 15 μm introduced by means of a fly cutter. Specimens with different notch depths were tested on a pendulum machine, the principles of which were previously reported by Casiraghi (*7*), at temperatures ranging from −80 to +20 °C.

By using this approach, a fracture-mechanics analysis may be used to determine the strain-energy release rate, or impact fracture toughness, G_c. Such an analysis was originally developed (*8*) for brittle polymers, but was extended (*9*) to more ductile materials. G_c is related to the fracture energy, the specimen and notch dimensions, and the compliance by the equation

$$W = G_c BD\phi + W_k$$

where W is the fracture energy; B and D are the specimen thickness and depth, respectively; and ϕ is the compliance calibration factor (a function of the specimen geometry and notch dimension) that may be obtained from tables (*9*). W_k is the kinetic energy possessed by the specimen as it is thrown forward after fracture. A plot of fracture energy versus $BD\phi$ yields a straight line with a slope of G_c and a positive intercept on the energy axis with the value of W_k.

Specimens for dynamic mechanical testing were thin films that were also compression molded at 190 °C and water quenched. The specimens, approximately 30 mm long and 4 mm wide with a nominal thickness between 0.15 and 0.25 mm, were examined on a direct-reading viscoelastometer (Rheovibron DDV-11) operating at 11 Hz by using a simple tensile stress system.

Results and Discussion

Figure 1 shows a typical copolymer viewed by differential interference contrast (DIC) in an optical microscope and displays the characteristic spherulite structure of polyolefin. Within the bulk of the spherulite, small inclusions are clearly visible that demonstrate the presence of a second phase.

Preliminary experiments (*1*) in these laboratories have demonstrated that this second phase may be extracted, to a greater or lesser extent depending on the origin of the sample, by refluxing in *n*-heptane in a Soxhlet extraction apparatus. The PE content of the extracted sample, determined by IR spectroscopy (*11*), decreases substantially after extraction. The modulus of the extracted rubber may also vary from one copolymer to another, and this variation may have a profound influence on the mechanical properties of the copolymer. This situation is reflected by the electron micrographs of the freshly microtomed surfaces of a polymer blend and two co-

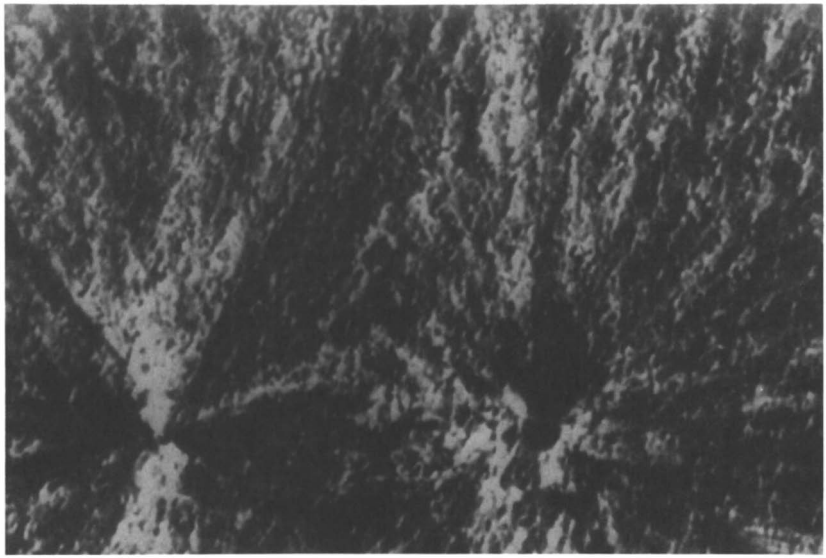

Figure 1. Optical micrograph (viewed in DIC) of a 5-μm section of a copolymer.

polymers after treatment with *p*-xylene in an ultrasonic shaker for 5 min at room temperature. In a ternary blend of PP, EPR, and HDPE (85:10:5) (Figure 2) and in one of the copolymers (Figure 3), the resulting cavities are clean and devoid of any included matter. In another copolymer from a different supplier, however (*see* Figure 4), a significant amount of debris remains even after prolonged exosure to *p*-xylene. This difference between copolymers is evidence that, in the blend and one of the copolymers, the dispersed phase is completely separate and has no chemical linkages to the PP matrix. In the second copolymer, however, a significant amount of true block copolymer acts, in effect, as an emulsifier and cannot be removed from the matrix by simple physical means. The only explanation for the differences between the two copolymer samples appears to relate to the manufacturing methods employed. Very few of the materials examined after extraction displayed the phenomenon of cavity residues. Therefore, most ethylene–propylene copolymers of this type available commercially must exist as simple blends of homopolypropylene and thermoplastic rubber (with the possibility, in some systems, of a third component—linear PE). The rubber component of a ternary blend may completely envelop (3) the HDPE and prevent the latter from cocrystallizing with the PP matrix. The major advantages of a copolymer over a physical blend are a marked improvement in the dispersion of the secondary phase in the copolymers, even after extensive compounding of the blends in a Banbury-type mixer,

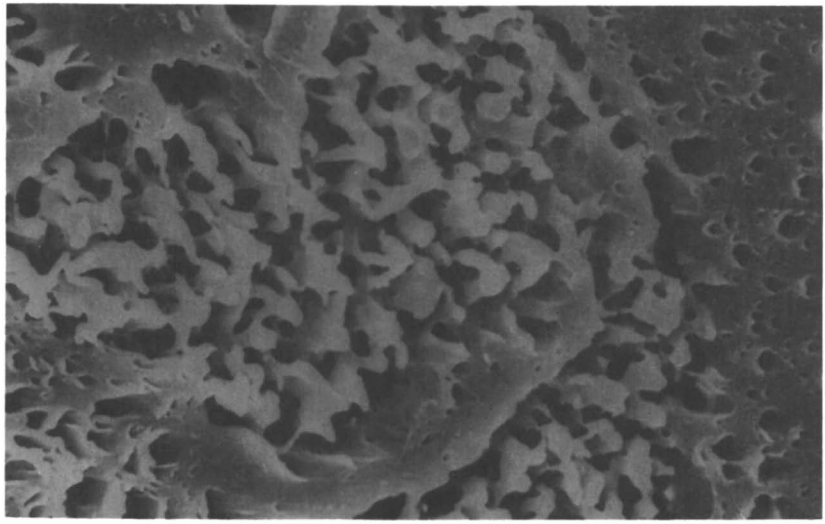

Figure 2. SEM of a microtomed surface of a blend (85% PP, 10% EPR, and 5% HDPE) extracted with p-*xylene.*

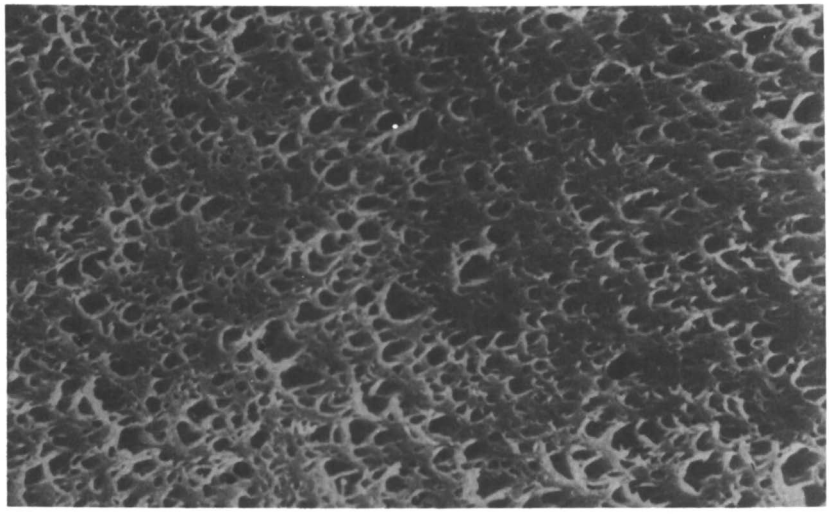

Figure 3. Electron micrograph of an extracted microtomed surface of a copolymer (A).

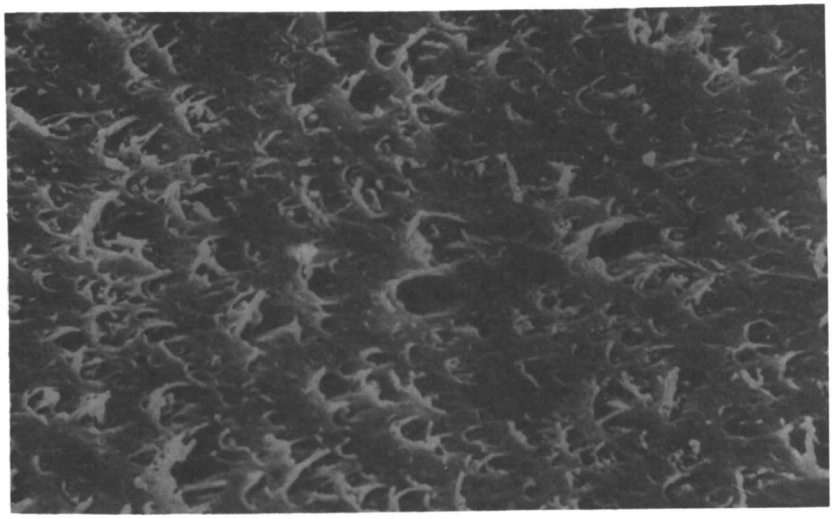

Figure 4. Electron micrograph of an extracted microtomed surface of a second copolymer (B).

and the smaller size of the dispersed phase in many of the copolymers. In their work on blends, Stehling and coworkers (*3*) found that the optimum diameter of the dispersed phase for toughening PP was less than 0.6 μm. The actual size has a marked effect on the impact strength.

The impact and dynamic mechanical data of a selection of copolymers and blends are plotted on the same set of axes in Figures 5a–5d; each plot corresponds to one material. All curves, either for a copolymer or blend, are very similar, and only small variations are apparent in the parameters described. Two major transitions are evident in the temperature range investigated. They are manifested as two peaks in the tan δ versus temperature plot, one at about −40 to −50 °C and another, larger peak at about +10 °C; they also appear as deviations in the in-phase modulus (G') versus temperature plot occurring at about the same temperatures. The main transition at about 10 °C corresponds to the homopolypropylene. The often-quoted (*12*) T_g of PP, a result of main-chain relaxations of the amorphous regions of the solid, is around 5 °C. The corresponding T_g of PE is less well defined, but the increased flexibility of the PE chain compared with PP would be expected to lead to a significantly lower value. One value quoted with some confidence (*12*, *13*) is −20 °C. Transition temperatures are highly rate dependent, and the shift in the value for the T_g of PP, from 5 to about 10 °C, is because of this dependence. Values quoted for T_g are often evaluated on a torsion pendulum at a frequency of 1 Hz, while the data presented here were obtained at 11 Hz on a Rheovibron. Even allowing for this shift, the peak at about −45 °C is unlikely to be due to linear

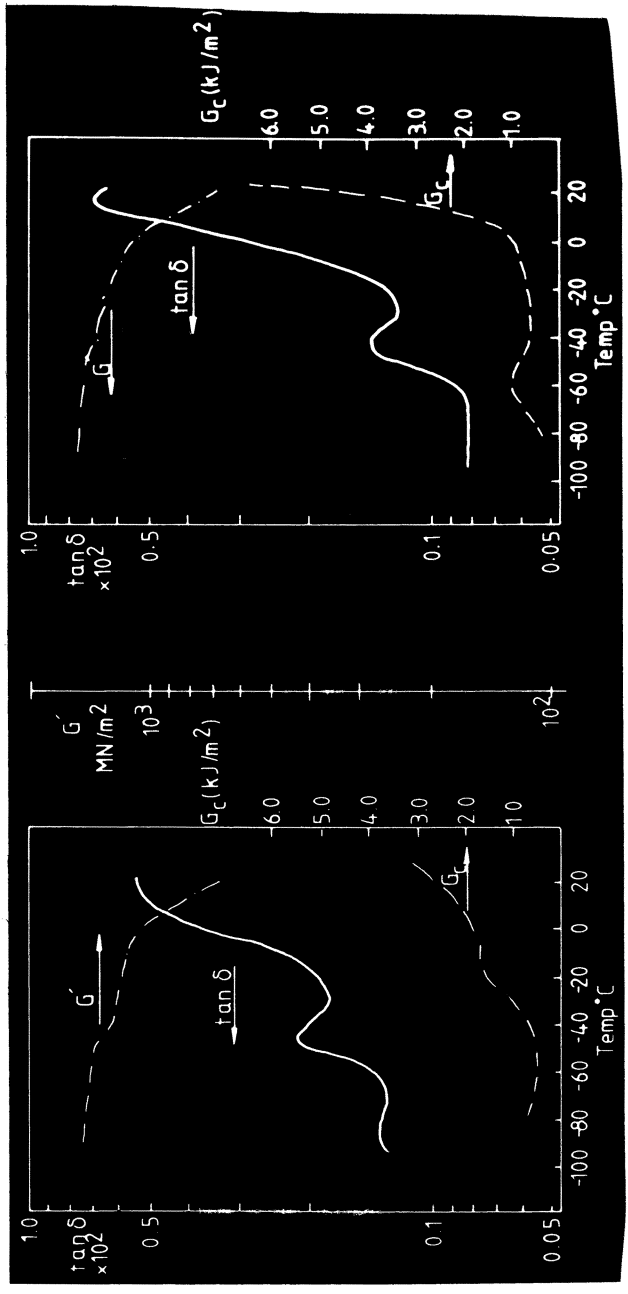

Figures 5a and b. G′, G_c, and tan δ plotted as a function of temperature: a, copolymer C; and b, physical blend.

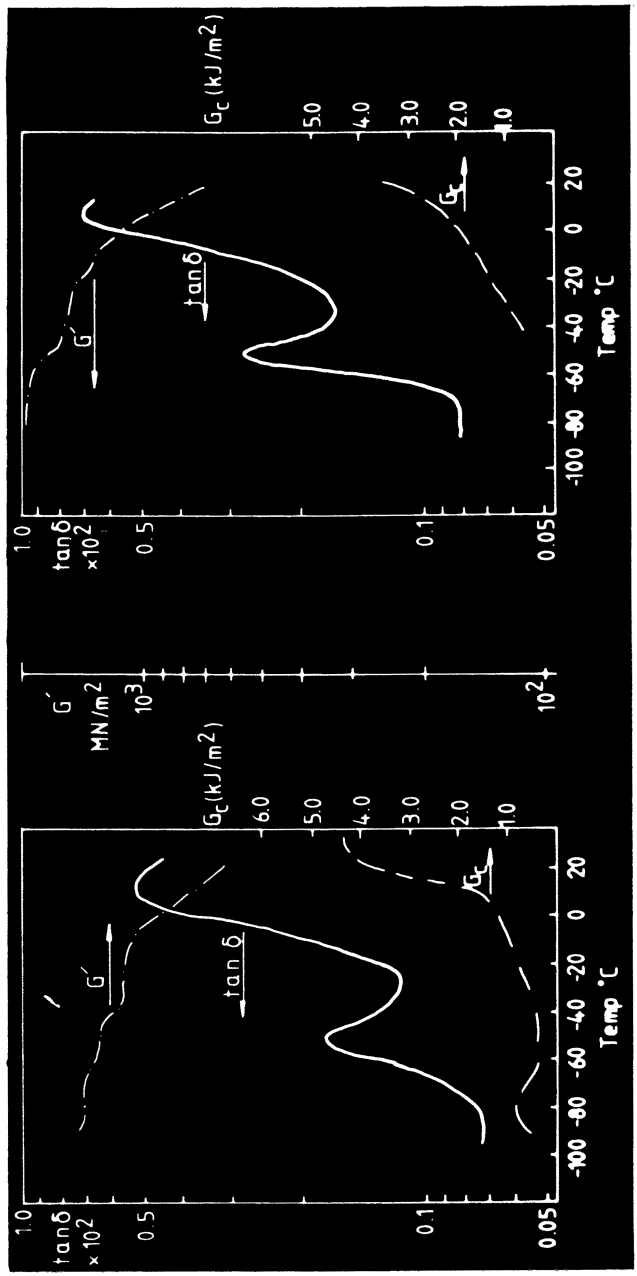

Figures 5c and d. G′, G_c, and tan δ plotted as a function of temperature: c, copolymer B; and d, copolymer D.

PE. More likely, because molecular transitions are also dependent on their local environment, it is due to transitions within the ethylene-rich segments. Indeed, dynamic mechanical testing of a commercial EPR has demonstrated that this material exhibits a single peak in the region of -45 °C.

The impact behavior of these materials, whether a blend or copolymer, was also found to be similar; a rapid decrease in G_c was observed as the temperature decreased and approached the T_g of PP. Below a temperature of about 20 °C, all failures were brittle in nature.

Conclusion

The copolymers of ethylene and propylene manufactured in a two-stage process, previously referred to as block copolymers (in contrast to the low-ethylene random copolymers manufactured in a single stage) exhibit properties very similar to physical blends. The fact that the ethylene-rich regions, which appear as a separate phase, may be removed to a greater or lesser extent depending on the origin of the specimen is evidence that few, if any, chemical linkages exist between the separated phase and the matrix. Some samples do in fact contain some unextractable material that can be seen as a residue in solvent-etched, microtomed surfaces. This debris probably represents an amount of AB-type block copolymer in which A is PP and B is an EPR. The block copolymer will act as an emulsifier and link the excluded phase to the matrix. Therefore, the presence of this component will have a pronounced beneficial effect on the properties of the material as a whole. In summary it appears that most commercial copolymers of ethylene and propylene previously referred to as block copolymers are really composed of two distinct phases with little or no chemical linkage.

Literature Cited

1. Natta, G.; Pasquon, I. *Adv. Catal.* **1959**, *11*, 1.
2. Keii, T. "Kinetics of Ziegler–Natta Polymerization"; Chapman & Hall: London, 1972.
3. Stehling, F. C.; Huff, T.; Speed, C. S.; Wissler, G. *J. Appl. Polym. Sci.* **1981**, *26*, 2693.
4. Prentice, P.; Williams, J. G. *Plast. Rubber Process. Appl.* **1981**, *2*, 27.
5. Prentice, P. *Polymer* **1982**, *23*, 1189.
6. Prentice, P.; Hashemi, S. *J. Mater. Sci.* **1984**, *19*, 518.
7. Casiraghi, T. *Polym Eng. Sci.* **1978**, *18*, 833.
8. Marshall, G. P.; Williams, J. G.; Turner, C. E. *J. Mater. Sci.* **1973**, *8*, 949.
9. Plati, E.; Williams, J. G. *Polymer* **1975**, *16*, 915.
10. Prentice, P.; Williams, J. G., unpublished data.
11. Haslam, J.; Willis, H. A. "Identification and Analysis of Plastics", Illife: London, 1965.
12. Brydson, J. A. "Plastics Materials," 3d ed.; Newnes–Butterworth: London, 1975.
13. Kambour, R. P.; Robertson, R. E. In "Polymer Science;" Jenkins, A. D., Ed.; North–Holland: Amsterdam, 1974.

RECEIVED for review November 15, 1984. ACCEPTED April 15, 1985.

20

A New Silicone Flame-Retardant System for Thermoplastics

R. BRUCE FRYE

Silicone Products Division, General Electric Company, Waterford, NY 12188

The unique polymer blend of a silicone fluid, a silicone resin, and a metal soap effectively provides a flame-retardant system for polypropylene (PP). Optimum flame resistance depends on a good dispersion of the silicones and is optimized with poly(trimethylsilyloxy) silicate and a magnesium soap, magnesium stearate. This system also displays a synergism with decabromodiphenyl oxide but surprisingly is impeded by antimony oxide or high-filler loadings. When well compounded in PP, the silicone system offers the added benefits of impact resistance, processability, mold release, and gloss. In short, the silicone–PP blend has flame retardance and the impact resistance and processability usually associated with PP copolymers.

POLYOLEFINS POSSESS AN ATTRACTIVE BALANCE of chemical, electrical, thermal, and mechanical properties; however, a major limitation is their flammability (*1*). Polypropylene (PP), in particular, requires large quantities of conventional flame retardants (antimony oxide and halogenated compounds) to achieve the UL94 V-1 and V-0 standards. These high additive levels lower the mechanical and electrical properties of the polymer (*2*). In addition, the high levels of halogen can generate corrosive gases, during processing and molding, and corrosive smoke, during burning. Thus, a flame-retardant system is needed that is less corrosive, operates at lower levels (maintaining mechanical properties), is nontoxic, and generates less smoke.

Silicone fluids are widely used in the plastics industry as internal lubricants (processing aids), to reduce wear, and for mold release. Their nonvolatile counterpart, silicone rubber, provides elements of fire retardance for wire and cable insulation. Other attractive properties of silicone rubber are its dielectric strength, thermal stability, and low and noncorrosive smoke evolution (*3*). Could a flame retardant for polyolefins be developed from the relatively inert silicone polymer? The goal of this work was to apply these advantages of silicone to the problem of providing flame-retardancy to PP first, and eventually to other thermoplastics.

0065–2393/86/0211/0337$06.00/0

Experimental

Initial formula optimization was conducted by compounding on a heated two-roll mill at approximately 200 °C, granulating, and compression molding at 195 °C for 10 min. Optimized formulations were compounded on a co-rotating twin-screw extruder (Werner Pfleiderer) at 200 °C, pelletized, dried 3 h at 100 °C when aluminum trihydrate was present, and injection molded. The vertical burn tests were run on 1/8-in. samples according to the UL94 bulletin except that the samples were not preconditioned at 50% relative humidity. The oxygen index (OI) and mechanical properties were measured following the appropriate ASTM[1] test methods.

The base resin for all experiments was a lightly stabilized isotactic PP homopolymer, Hercules Pro-Fax 6523. Magnesium stearate was obtained from Synpro, decabromodiphenyl oxide (DBDPO) came from Great Lakes Chemicals (83R), and aluminum trihydrate was Solem's SB-632 grade.

Discussion

Formula Optimization. Although silicones have been used in the past as flame-retardant agents (*4–13*), none of these formulations is effective enough to achieve a UL94 V-1 or V-0 rating for PP. According to MacLaury and Holub (*7*), a silicone in combination with a metal soap can provide a degree of flame retardance to some thermoplastics including polyethylene (PE) and PP. Continuing this work, we confirmed that practically any high-viscosity silicone polymer in combination with a metal stearate would give the same flame-retardant effect as the gum. Although lower viscosity silicones also show flame retardance in combination with a metal stearate, they permit flaming drips. A rapid screening of various components indicated that the inclusion of a silicone resin seemed to improve flame retardance. A silicone resin is a polymer prepared from multifunctional silanes that provide branched structures. The importance of the resin was verified by running a rotating simplex optimization (*14–17*) and including the resin as one of the seven variables. Further optimization work led to the development of particularly effective silicone flame retardants. Table I lists four optimized formulations for PP.

[1] American Society for Testing and Materials.

Table I. Formulations Using the Silicone Flame Retardant

Compound	*Low-Halogen V-1*[a]	*Nonhalogen V-1*[a]	*V-0*[a]	*5V*[a]
Polypropylene (Pro-Fax 6523)	74.3	78.5	54.3	47.7
Silicone fluid and resin (SFR100, GE)	9.5	10.7	9.2	10.5
Magnesium stearate	4.4	3.6	4.3	4.7
Decabromodiphenyl oxide	6.9	—	11.8	13.5
Talc	5.0	7.2	—	—
Aluminum trihydrate	—	—	20.4	23.3
Oxygen index	27	23	27	27

[a] Values in percent.

Properties. The final properties of the optimized formulations were quite dependent on the degree of compounding. Although most of the optimization experiments were conducted on a heated two-roll mill, an intermeshing co-rotating twin-screw extruder gave the most consistent results. In addition, injection-molded parts were superior to compression-molded ones for mechanical properties, appearance, and flame retardance.

The formulas listed in Table I achieved the primary objective of V-1–V-0 flame retardance with a silicone system. An important side benefit was impact resistance (*see* Table II). The PP homopolymer (Pro-Fax 6523) tested in our laboratory had a Gardner impact resistance (1-in. ring, 5/8-in. dart, 2 1/2 in. × 2 1/2 in. × 1/8 in. injection-molded plate) of approximately 18 in. lbs, and the failure mode was cracking on the unimpacted side. The same homopolymer containing any of the silicone flame-retardant formulations listed in Table I had a Gardner impact resistance of greater than 160 in. lbs (some plates achieved 250 in. lbs), and the mode of failure was a ductile puncture. The improved impact resistance was also present at low temperature, for example, at −40 °C the V-0 plates withstood 25 in. lbs.

The notched Izod impact resistance also increased with the silicone-additive package, from 0.5 for the homopolymer to 1.6 for the silicone system. In addition to flame retardance and impact resistance, the silicone system also provided improved processability, improved mold fill, and gloss.

Table II. Properties of Formulations

Properties	*PP*	*Low Halogen*	*Nonhalogen*	*HAL[a]/ ATH[b,c]*	*HAL[a]/ ATH[b,c]*
UL94	burn	V-1	V-1	V-0	5V
Gardner impact (RT) (in. lbs)	18	160–200	160–200	160–200	160–200
Gardner impact (−40 °C) (in. lbs)	—	—	—	25	—
Density	0.904	1.01	0.97	1.148	1.197
Notched izod	0.5	1.6	—	1.14	
Tensile at yield (psi)	4800	3700	3700	3010	2730
Tensile at break (psi)	2900	—	—	2220	2200
Percent elongation at break	360	290	250	290	195
HDT[d] (264 psi) (°F)	140	130	140	—	130
Flexural modulus (psi)	2.2×10^5	2.2×10^5	2.1×10^5	2.5×10^5	—
Dielectric constant (1 kHz)	—	1.61	—	2.50	2.42
Dielectric strength (V/mil)	650	811	—	775	790
Volume resistivity ($\times 10^{15}$)	—	22.9	—	2.85	1.6
Limiting oxygen index	17	27	23	27	27

[a] Halogen. [b] Aluminum trihydrate. [c] *See* Table I for composition. [d] Heat distortion temperature.

The improved processability is evident in the increase in melt index (ASTM D-1238) from 4 to 10 when the silicone and other components were added (low-halogen V-1 composition). High-temperature gel-phase chromatography showed that the increased melt index was not due to PP degradation; the relative molecular weight did not change. In trichlorobenzene with polystyrene standards, the relative PP weight-average molecular weight was 205,000 before compounding and 209,000 after compounding.

The improved mold fill was demonstrated by using a channel-flow mold. Including the silicone package increased the flow from 8.50 in. to 10.75 in.

Synergism. The synergism between silicone–magnesium stearate and DBDPO was documented by using oxygen index (OI) values. The graph in Figure 1 plots OI versus the flame-retardant additive concentration in Pro-Fax 6523 PP. All of the formulations were compounded on a two-roll mill at < 400 °F and compression molded.

Curves A, B, and F confirm the MacLaury–Holub (7) original findings and extend them to the silicone–resin system. That is, neither the silicone nor the magnesium stearate alone in PP confers any flame retardance. The combination inhibits PP burning.

Curves F, E, and H demonstrate three important points. First, the combination of the silicone and resin with magnesium stearate in PP (i.e., a nonhalogen system) causes a significant rise in OI with concentration; at 25%, this combination attains an OI of 23. Second, DBDPO alone in PP only achieves an OI of 20 at the same 25% concentration. And third, a 1:1 mixture of silicone–magnesium stearate and DBDPO produces a dramatically higher OI (OI equals 31) than either material alone at the same concentration. This effect is synergism. In addition, curve D shows that barium stearate is much less effective than magnesium stearate in this system in PP. Flame retardance in the UL94 test follows approximately the same pattern.

Curves H and G show that DBDPO is more effective in the silicone–magnesium stearate system than the chlorinated cycloaliphatic compound known as Dechlorane Plus (Occidental Chemical Company).

Mechanism. Polyolefins in general burn without char formation. The silicone flame retardant induces a slightly intumescent char in PP, and this solid-phase reaction appears to be a major mode of flame retardance. The brittle char presumably inhibits heat conduction to the plastic and fuel flow to the flame. A stearate-type moiety seems necessary to make the magnesium compatible with the silicone, and this metal soap probably serves as a siloxane rearrangement catalyst at high temperatures promoting silicate char. The MQ resin is a rather unique silicone-soluble form of silicate. MQ resin is the common name for poly(trimethylsilyloxy) silicate. M stands for

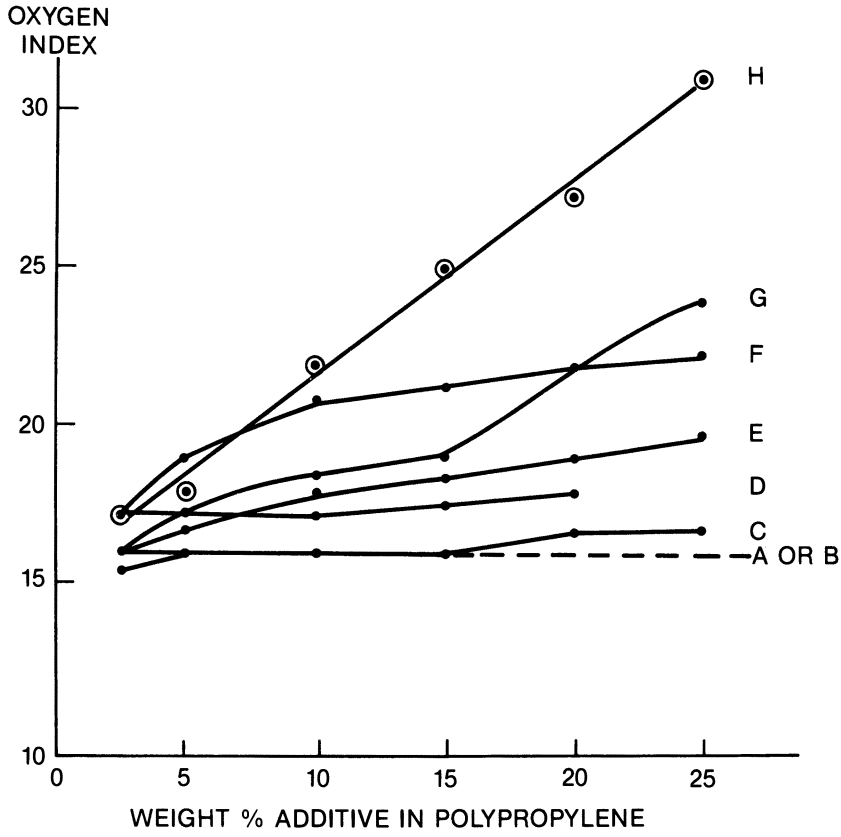

Figure 1. Oxygen index data demonstrate synergistic flame retardance in PP for silicone and magnesium stearate (F), and for silicone, magnesium stearate, and DBDPO. Additives: A, silicone; B, magnesium stearate; C, alicyclic chloride; D, 3:1 silicone-barium stearate; E, DBDPO; F, 3:1 silicone-magnesium stearate; G, 3:1:4 silicone-magnesium stearate-alicyclic chloride; and H, 3:1:4 silicone-magnesium stearate-DBDPO.

a monofunctional silane, and Q represents a tetrafunctional silane (quaternary).

Antimony oxide surprisingly decreases the flame retardance of this system. Mineral fillers also prolong the extinguishing time, perhaps by forming discontinuities in the char.

Conclusions

We have found that the combination of a linear polydimethylsiloxane and a branched silicone resin together with magnesium stearate and other optional components can improve flame retardance in PP and, perhaps, other thermoplastics. Experimental formulations have been developed that can

meet the Underwriters Laboratory UL94 Bulletin criteria. In addition to flame retardance, the silicone package dramatically improves the impact resistance of PP and adds the conventional silicone properties of improved processability, improved moldability, gloss, and good electrical (insulating) properties. The best and most consistent properties require thorough compounding, preferably by using a twin-screw extruder.

Acknowledgments

I wish to thank E. Lovgren, R. Reed, and R. Ronda for compounding, molding, and testing assistance. I am also indebted to A. Torkelson, J. Golba, and M. MacLaury for helpful discussions.

Literature Cited

1. Schwarz, R. J. In "Flame Retardance of Polymeric Materials"; Kuryla, W. C.; Papa, A. J., Eds.; Dekker: New York, 1973; Vols. 1–2.
2. Hayes, W. K.; Lesniewski, J. M. *Plast. Eng.* **1981**, *37*, 25–31.
3. Lipowitz, J. "Flammability, Smoke, Toxicity, and Corrosive Gases of Electric Cable Materials," U.S. Dept. of Commerce, NTIS AD/A-065047, 1978, p. 99.
4. Luce, J. B.; Vaughn, H. A. U.S. Patent 4 235 978, 1980.
5. Betts, J. E.; Holub, F. F. U.S. Patent 4 123 586, 1978.
6. Betts, J. W.; Holub, F. F. U.S. Patent 4 247 446, 1981.
7. MacLaury, M. R.; Holub, F. F. U.S. Patent 4 273 691, 1981.
8. Bialous, C. A.; Luce, J. B.; Mark, V. U.S. Patent 3 971 756, 1976.
9. Japanese Kokai Tokkyo Koho 81 93,207 of Showa Electric Wire and Cable Co., Ltd., 1981.
10. Japanese Kokai Tokkyo Koho 81 20,041 of Showa Electric Wire and Cable Co., Ltd., 1981.
11. Japanese Kokai Tokkyo Koho JP 81 166,246 of Furukawa Electric Co., Ltd., 1981.
12. Moody, A. G.; Pennick, R. J. U.S. Patent 4 265 801, 1981.
13. Weise, C.; Wolfer, D.; Patzke, J. U.S. Patent 4 390 656, 1983.
14. Hendrix, C. *Chemtech* **1980**, *10*, 488.
15. Deming, S. N.; Morgan, S. L. *Anal. Chem.* **1973**, *45*, 178A.
16. Long, D. E. *Anal. Chim. Acta* **1969**, *46*, 193.
17. Leggett, D. J. *J. Chem. Educ.* **1983**, *60*, 707.

RECEIVED for review November 15, 1984. ACCEPTED February 19, 1985.

AUTHOR INDEX

Argon, A. S., 259
Baer, E., 273
Barlow, J. W., 313
Cassidy, E., 211
Cohen, R. E., 259
Coleman, M. M., 77
Connelly, G. M., 291
Cousin, Patrice, 87
Decroocq, Sylvie, 195
Ebdon, J. R., 171
Fernandez, A. M., 153
Fetters, Lewis J., 127
Fried, J. R., 59
Frisch, H. L., 211
Frisch, K. C., 211
Frye, R. Bruce, 337
Gebizlioglu, O. S., 259
Granger, Alice T., 127
Hage, Elias, 231
Hertzberg, R. W., 291
Hiltner, A., 273
Hourston, D. J., 171
Hwang, J., 291
Karasz, F. E., 67
Klein, P. G., 171
Klempner, D., 211
Krause, Sonja, 127
MacKnight, W. J., 67
Manson, J. A., 291
Martynowicz, Lynn M., 111
Moskala, E. J., 77
Murayama, Takayuki, 231
Murff, S. R., 313
Papapostolou, E., 325
Paul, D. R., 3, 313
Prentice, P., 325
Prud'homme, Robert E., 87
Runt, J. P., 77, 111
Sperling, L. H., 21, 153
Su, A. C., 59
Walsh, W. K., 231
Wang, Baoyu, 127
Widmaier, Jean-Michel, 195
Wignall, G. D., 153
Wilfong, D. L., 273
Williams, J. G., 325
Xiao, H. X., 211
Xie, Hongquan, 139
Zhou, Peiguang, 139

SUBJECT INDEX

A

Adhesion, interfacial, blend miscibility, 12
Amorphous phase, miscible blends
  discussion, 7
  effect on crystallization rate, 113
Amorphous polymers, simple, miscible and immiscible blends, modulus behavior, 13
Anionic synthesis, physical-chemical IPNs, 196
Antimony oxide, silicone flame-retardant system for thermoplastics, 341
Association constant
  carbons, NMR studies, polyester-poly(vinyl halide) blends, 98
  solute in a binary solvent, NMR studies, polyester-poly(vinyl halide) blends, 104
Atactic polystyrene (a-PS), radial growth rates of spherulites, 112*f*

B

B-block microstructure, S-B block copolymers, 130
Band broadening, FTIR studies, polyester-poly(vinyl halide) blends, 104
Bimodal distribution, IPNs based on PB-PS, 161
Binary solvent, association constant of a solute, NMR studies, polyester-poly(vinyl halide) blends, 104
Blend(s)
  miscible, background and historical perspective, 6
  possible strength-composition relationships, 15*f*
  random copolymer
    mean field theory, 71
    miscibility, 67–74
Blend melting points, related to polymer-polymer interactions, 117

AUTHOR INDEX

Argon, A. S., 259
Baer, E., 273
Barlow, J. W., 313
Cassidy, E., 211
Cohen, R. E., 259
Coleman, M. M., 77
Connelly, G. M., 291
Cousin, Patrice, 87
Decroocq, Sylvie, 195
Ebdon, J. R., 171
Fernandez, A. M., 153
Fetters, Lewis J., 127
Fried, J. R., 59
Frisch, H. L., 211
Frisch, K. C., 211
Frye, R. Bruce, 337
Gebizlioglu, O. S., 259
Granger, Alice T., 127
Hage, Elias, 231
Hertzberg, R. W., 291
Hiltner, A., 273
Hourston, D. J., 171
Hwang, J., 291
Karasz, F. E., 67
Klein, P. G., 171
Klempner, D., 211
Krause, Sonja, 127
MacKnight, W. J., 67
Manson, J. A., 291
Martynowicz, Lynn M., 111
Moskala, E. J., 77
Murayama, Takayuki, 231
Murff, S. R., 313
Papapostolou, E., 325
Paul, D. R., 3, 313
Prentice, P., 325
Prud'homme, Robert E., 87
Runt, J. P., 77, 111
Sperling, L. H., 21, 153
Su, A. C., 59
Walsh, W. K., 231
Wang, Baoyu, 127
Widmaier, Jean-Michel, 195
Wignall, G. D., 153
Wilfong, D. L., 273
Williams, J. G., 325
Xiao, H. X., 211
Xie, Hongquan, 139
Zhou, Peiguang, 139

SUBJECT INDEX

A

Adhesion, interfacial, blend miscibility, 12
Amorphous phase, miscible blends
  discussion, 7
  effect on crystallization rate, 113
Amorphous polymers, simple, miscible and immiscible blends, modulus behavior, 13
Anionic synthesis, physical-chemical IPNs, 196
Antimony oxide, silicone flame-retardant system for thermoplastics, 341
Association constant
  carbons, NMR studies, polyester-poly(vinyl halide) blends, 98
  solute in a binary solvent, NMR studies, polyester-poly(vinyl halide) blends, 104
Atactic polystyrene (a-PS), radial growth rates of spherulites, 112*f*

B

B-block microstructure, S-B block copolymers, 130
Band broadening, FTIR studies, polyester-poly(vinyl halide) blends, 104
Bimodal distribution, IPNs based on PB-PS, 161
Binary solvent, association constant of a solute, NMR studies, polyester-poly(vinyl halide) blends, 104
Blend(s)
  miscible, background and historical perspective, 6
  possible strength-composition relationships, 15*f*
  random copolymer
    mean field theory, 71
    miscibility, 67–74
Blend melting points, related to polymer-polymer interactions, 117

Blend miscibility, applications of mean field theory, two random copolymers, 71
Blend phase behavior, contemporary view, 6
Block copolymers
AB, synthesis, PS-PEO, 140
ABA synthesis, PS-PEO-PS, 140
BAB synthesis, PEO-PS-PEO, 139
beneficial use in blends, 13
definition, 326
ethylene-propylene, and blends, morphology and mechanical properties, 325–33
nomenclature, 22
PEO-PS, emulsifying and crystalline properties, 139–50
purification and characterization, PS-PEO block copolymers, 142–44
S-B 127–37
tapered, T_g studies, 128
Broadening, band, FTIR studies, polyester-poly(vinyl halide) blends, 104
Brominated polymer, miscibility with polyesters, 88
Brominated solutes, methyl acetate-heptane solvent, NMR, polyester-poly(vinyl halide) blends, 99–101
Butadiene (B) microphase
S-B block copolymers, 127–37
T_g from DSC, 133*t*
Butadiene (B)-S block copolymers, 127–37
2-Butanol, influence on PMMA-PVF_2 blends under stress, 320*t*

C

Carbon(s), association constants, NMR studies, polyester-poly(vinyl halide) blends, 98
Carbon frequency shifts, ^{13}C NMR, PU-polysiloxane SINs, 183
Carbon-13 nuclear magnetic resonance (^{13}C NMR)
cured homogeneous networks and IPNs, PU-polysiloxane, 179
polyester-poly(vinyl halide) blend interactions, 87–108
PU-polysiloxane SINs, 175
Carbonyl band, perturbation, FTIR studies, polyester-poly(vinyl halide) blends, 104
Carbonyl groups, hydrogen bonded, fraction vs. temperature
PVPh blends, 78, 82–85
PVPh-EVA blends, 82, 85*f*
Carbonyl stretching vibration band, polyester-poly(vinyl halide) blends, 90–97
Carboxyl-terminated acrylonitrile-butadiene (CTBN) rubber, fatigue in rubber-modified epoxies, 297
Catalyst
cross-linking of polysiloxane, 173
dibutyltin dilaurate, synthesis of PS-PEO block copolymers, 141
Chain, mechanical interlocking, morphology, PS-SIS-DVB SINs, 203
Chain length, effect, equilibrium swelling degree for model PS networks, 204*f*
Chain mobility, ^{13}C NMR, PU-polysiloxane SINs, 182
Characterization
PB homopolymer network and molecular weight, 160
PS-PEO block copolymers, 142
Chemical blend morphologies, IPNs based on PB-PS, 164*f*
Chemical linkages, ethylene-propylene block copolymers and blends, 333
Chemical shifts, ^{13}C NMR, PU-polysiloxane SINs, 183
Chlorinated polymer, miscibility with polyesters, 88
Chlorinated solutes, methyl acetate-heptane solvent, NMR, polyester-poly(vinyl halide) blends, 97–99
Chlorobrominated solutes, methyl acetate-heptane solvent, NMR, polyester-poly(vinyl halide) blends, 101–3
Chromatography, PMMPO-PS and PMMPO-P4MS blends, 60
Cocontinuous phases, and IPNs, 43
Coherent scattering intensity, IPNs based on PB-PS, 164
Compatibility, background and historical perspective, 4
Compatible polymer blends, crystallization and melting, 111–21
Composition, related to T_g, B microphase, S-B block copolymers, 136
Copolymer blends, random
applications of mean field theory, 71
miscibility, 67–74
Coupling agents between phases, blend miscibility, 12
Crack blunting, effect of frequency on FCP in rubber-modified epoxies, 306
Crack initiation, review, rubber-modified plastics, 293–97
Crazing
and cracking, environmental stress, of PMMA-PVF_2, 313–23
FCP in rubber-modified epoxies, 307
Critical strain, crazing and cracking of PMMA-PVF_2 blends, 321*f*
Critical stress
compared with strength in air, crazing and cracking of PMMA-PVF_2 blends, 323*f*
crazing and cracking of PMMA-PVF_2 blends, 321*f*
Cross-link density of the epoxy phase, variations, effect on T_g of the epoxy matrix, 300

Cross-linking
content related to ultimate elongation of SINs, 32*t*
density, effect on specific surface area, PB-PS IPNs, 165
effect
blend miscibility, 30
PB-PS IPNs, 168
physical, IPNs, 171
polymers, nomenclature, 23
PS-SIS-DVB SINs, 201
polysiloxanes, 172
Crystal thickness term, melting points, miscible polymer blends, 120
Crystalline and emulsifying properties, PS-PEO block copolymers, 139-50
Crystallinity
measurement, PS-PEO block copolymers, 142
PMMA-PVF_2 blends, 315*f*
Crystallite size, changes, miscible polymer blends, 120
Crystallization
finite conditions, miscible blends, 8
polysiloxanes, 173
review of process, miscible blends, 111-17
transitional behavior, miscible blends with one crystallizable component, 7*f*

D

Damping, noise and vibration, IPNs and SINs, 33
Data analysis, PMMPO-PS and PMMPO-P4MS blends, 60
Debye plots, measurement, PB-PS IPNs, 166
Deformation of epoxies, shear response, 307
Dental applications, IPNs, 47
DGEBA—*See* Diglycidyl ether of bisphenol A
Dialysis membranes, IPNs, 35
Diblock copolymer
graft copolymer, phase-inversion points, 146*f*
PEO-PS-PEO, purification and characterization, 142
PS-PEO, synthesis, 141
Dibutyltin dilaurate, catalyst
cross-linking of polysiloxane, 173
synthesis of PS-PEO block copolymers, 141
DIC—*See* Differential interference contrast
Diene content, effect, morphology of physical-chemical IPNs, 200
Differential interference contrast (DIC), ethylene-propylene block copolymers and blends, 327
Differential scanning calorimetry (DSC)
B microphase glass transitions, 133*t*
PEO-PS diblock copolymer and a blend of PS and PEO, 144*f*
Differential scanning calorimetry (DSC)—*Continued*
PVPh-PVAc blends, 79
S-B block copolymers, 130
S-isoprene triblock copolymers, 128
S microphase glass transitions, 133*t*, 134
Diglycidyl ether of bisphenol A (DGEBA), fatigue in rubber-modified epoxies, 297
Dilatometric data, S microphase and PS, S-B block copolymers, 130
Dimethylsiloxane (DMS), T_g studies, S block copolymers, 127
Discontinuous growth bands, FCP in rubber-modified epoxies, 307
Divinylbenzene (DVB), cross-linked with PS in presence of SIS, morphology, 195-208
DMA—*See* Dynamic mechanical analysis
DMS—*See* Dynamic mechanical spectroscopy
Domain(s)
PU-polysiloxane SINs, 177
submicroscopic plastic, reinforced elastomers, 33
Domain characterization, IPNs and SINs via SAXS techniques, 28*t*
Domain diameter vs. composition, PU-polysiloxane SINs, 178*f*
Domain dimensions, IPNs based on PB-PS, 164
Domain growth and formation, IPNs, 35-37
Domain-boundary effect
S-DMS and S-B block copolymers, 134
tapered block copolymers, 128
Drug delivery systems, controlled, IPNs, 44
DSC—*See* Differential scanning calorimetry
Dual phase continuity
IPNs based on PB-PS, 161, 166
morphology of physical-chemical IPNs, 199
requirements, IPNs, 40
sequential IPNs, 24, 25
Dynamic and impact mechanical data, ethylene-propylene block copolymers and blends, 330
Dynamic loss modulus
PU-polysiloxane SINs, 185
vs. temperature, PU-polysiloxane SINs, 180
Dynamic mechanical analysis (DMA), PU-polysiloxane SINs, 175
Dynamic mechanical behavior, FCP in rubber-modified epoxies, 298
Dynamic mechanical data, ethylene-propylene block copolymers and blends, 330
Dynamic mechanical parameters, fatigue in rubber-modified epoxies, 299*t*
Dynamic mechanical spectroscopy (DMS), two-phased nature of IPNs, 22
Dynamic storage modulus
PU-polysiloxane SINs, 185
vs. temperature, PU-polysiloxane SINs, 180

E

Elastomers, reinforced, submicroscopic plastic domains, 33
Electron micrograph, ethylene-propylene block copolymers and blends, 329–30*f*
Elongation at break, PMMA-PVF_2 blends, 318*f*
Emulsifying property
  PS-PEO block copolymers
    discussion, 144
    effect of PEO content, 145
    synthesis and study, 139–50
    test, 142
End-linking technique, synthesis, physical-chemical IPNs, 196
Entropy of mixing, combinatorial, lattice model, polymer blends, 5*f*
Environmental-stress crazing and cracking, PMMA-PVF_2, 313–23
Epoxies, rubber modified, fatigue, review, 291–310
Epoxy phase, variations in cross-link density, effect on T_g of the epoxy matrix, 300
EPR—*See* Ethylene-propylene thermoplastic rubber
Equilibrium melting points, related to polymer-polymer interactions, 118
Ethanol, influence on PMMA-PVF_2 blends under stress, 320*t*
Ethylene-propylene block copolymers and blends, morphology and mechanical properties, 325–33
Ethylene-propylene thermoplastic rubber (EPR), morphology and mechanical properties, 326
Ethylene-type crystallinity, effect on PVPh-EVA miscibility, 79
Ethylene-vinyl acetate (EVA)
  copolymers, FTIR studies of PVPh blends, 77–85
  effect of molecular weight on PVPh blends, 82
EVA—*See* Ethylene-vinyl acetate
Extraction data, morphology of physical-chemical IPNs, 199
Extraction studies and morphology, physical-chemical IPNs based on block polymer and PS, 195–208

F

Failure characteristics, effect of composition, miscible and immiscible blends, 14
Failure mechanism, review, rubber-modified epoxies, 294
Fatigue, in notched thermoplastic specimens, review, rubber-modified epoxies, 295
Fatigue, in notched thermoset specimens, review, rubber-modified epoxies, 296
Fatigue, in rubber-modified epoxies, review, 291–310
Fatigue, in unnotched specimens, review, rubber-modified epoxies, 294
Fatigue crack propagation (FCP)
  effect of frequency, rubber-modified epoxies, 303–7
  effect of rubber, rubber-modified epoxies, 302, 304
  review, rubber-modified plastics, 293–97
  behavior, rubber-modified epoxies and polyblends, 308
Fatigue fracture surface, photograph, rubber-modified epoxy, 307*f*
Fatigue life, overall, rubber-modified epoxies and polyblends, 309
FCP—*See* Fatigue crack propagation
Flame-retardant system, silicone, for thermoplastics, 337–41
Fourier transform IR (FTIR) studies
  ^{13}C-NMR studies, polyester-poly(vinyl halide) blend interactions, 87–108
  PCL-PVC, PCL-PVB, and PCL-PVF blends, 90–97
Fractography, FCP in rubber-modified epoxies, 307
Frequency, effect on FCP
  rubber-modified epoxies, 303–7
  thermoplastics, 296
Frequency shifts
  FTIR studies, polyester-poly(vinyl halide) blends, 104
  IR, related to molecular interactions, 77
FTIR—*See* Fourier transform IR

G

Gel permeation chromatography (GPC)
  curve, PS-SIS-DVB SINs, 202
  PS-PEO block copolymers, 142
  S-B block copolymers, 129
Gelation, IPNs, 30, 36
Glass transition behavior
  B and S microphase, DSC, 133*t*
  PMMA-PVF_2 blends, 315*f*
  polysiloxanes, 173
  related to molecular weight, S block copolymers, 135*f*
  SINs, 31
Glass transition temperature (T_g)
  blends with a homogeneous amorphous phase, 6
  ethylene-propylene block copolymers and blends, 330
  i-PS-a-PS blends, 112
  IPN RIM materials, 39*t*
  PPMS network, 184
  related to molecular weight, microstructure, composition, B microphase, S-B block copolymers, 136
  vs. composition, PU-polysiloxane SINs, 188
GPC—*See* Gel permeation chromatography
Gradient IPNs, and microencapsulation, 44

Graft copolymers
diblock copolymers, phase-inversion points, 146*f*
nomenclature, 23

H

Halogenated molecule–carbon tetrachloride solvent, PCL, NMR, polyester–poly(vinyl halide) blends, 103
Halogenated molecule–heptane solvent, methyl acetate, NMR, polyester–poly(vinyl halide) blends, 101–3
HDPE—*See* High-density polyethylene
Heat of mixing, driving force for miscibility, 6
High-density polyethylene (HDPE), morphology and mechanical properties, 325
High-temperature vulcanization (HTV), cross-linking of polysiloxane, 173
Hoffman–Weeks plots, melting temperatures, miscible polymer blends, 119*f*
Homogeneity
blends, T_g relationship, 6
synthesis, physical-chemical IPNs, 196
Homogeneous IPNs (homo-IPNs), definition, 29
Homogeneous network characterization data, PU–polysiloxane SINs, 176
Homopolymer gels, synthesis, physical-chemical IPNs, 196
Homopolymer–copolymer blends
mean field theory, 70
windows of miscibility, 69
HTV—*See* High-temperature vulcanization
Hydrogen-bonded carbonyl groups, fraction vs. temperature
PVPh blends, 78, 82–85
PVPh–EVA blends, 82, 85*f*
Hydrogen bonding interaction, polyester–poly(vinyl halide) blends, 90–98
Hysteresis, rubber-modified plastic, 296
Hysteretic healing, effect of frequency on FCP in rubber-modified epoxies, 306

I

IEN—*See* Interpenetrating elastomeric network
Immiscible blends
and miscible blends of simple amorphous polymers, modulus behavior, 13
phase morphology, 11
Impact behavior
ethylene–propylene block copolymers and blends, 330, 333
and tensile behavior, fatigue in rubber-modified epoxies, 301*t*
Impact resistance, silicone flame-retardant system for thermoplastics, 338
Incompatibility, background and historical perspective, 4
Inhomogeneities, SANS, PS–PB IPNs, 156
Initiators, preparation, synthesis of PS–PEO block copolymers, 141
Interaction parameter
homopolymer–copolymer blend, 68
PMMPO–PS and PMMPO–P4MS blends, 64
S–DMS, reversed-phase chromatography, 134
segmental interaction, 68
specific retention volumes, PS, PMMPO–PS, P4MS, PMMPO, and PMMPO–P4MS, 62*t*
Interaction strength, differences, polyesters and halogenated polymers, 103
Interfacial adhesion, blend miscibility, 12
Interfacial area, measurement, PB–PS IPNs, 166
Interfacial characterization, sequential IPNs, 28
Interfacial tension, blend miscibility, 12
Interpenetrating elastomeric network (IEN), definition, 22
Interpenetrating polymer networks (IPNs)
based on ion-exchange resins, 34
based on PB–PS, 153–69
cocontinuous phases, 43
commercial materials, 49–51
definition, 22, 154, 171
dental applications, 47
domain growth and formation, 35–37
gradient, and microencapsulation, 44
laboratories, major academic, 52*t*
miscellaneous applications, 45
miscible, negative heats of mixing, 28
morphology, sequential, 24, 26*f*
nomenclature, 23
patent literature, 47
physical-chemical, based on block polymers and PS, extraction studies and morphology, 195–208
physical-chemical, definition, 197
physical cross-linking, 171
recycling of plastics wastes, 37
sequential, dual phase continuity, 25
sequential, two phased, synthesis and properties, 29
SINs
noise and vibration damping, 33
phase separated, mechanical properties, 32
thermoplastic, 41, 48
Interpenetrating polymer network (IPN) constituents, mechanical coupling, 190
Interphase effects, S–B and S–DMS copolymers, 128
Ion-exchange resins, IPNs, 34
IPNs—*See* Interpenetrating polymer networks
IR spectrum, PEO–PS diblock copolymer, 143*f*
Isotactic polystyrene (i-PS), radial growth rates of spherulites, 112*f*

L

Lattice fluid (LF) theory, PMMPO–P4MS and PMMPO–PS blends, 63
Lattice model for combinatorial entropy of mixing, polymer blends, 5*f*
LCST—*See* Lower critical solution temperature
Linking reaction, efficiency, morphology of physical–chemical IPNs, 199
Liquid(s), various, influence on PMMA–PVF_2 blends under stress, 320*t*
Liquid crystalline behavior, PS–PEO block copolymer, 140
Liquid–liquid phase diagram, LCST behavior, 10*f*
Liquid–liquid phase separation, finite, miscible blends, 8
Low-temperature vulcanization (LTV), cross-linking of polysiloxane, 173
Lower critical solution temperature (LCST)
  liquid–liquid phase diagram, 10*f*
  miscible blends, 9
LTV—*See* Low-temperature vulcanization

M

Magic-angle spinning NMR (MASNMR), miscibility of PS and PMMPO, 59
Manufacturing methods, effect on morphology, ethylene–propylene copolymers, 328
MASNMR—*See* Magic-angle spinning NMR
Mean field theory, miscibility in copolymer blends, 67–74
Mechanical behavior, SINs, 32
Mechanical coupling, IPN constituents, 190
Mechanical properties and morphology of ethylene–propylene block copolymers and blends, 325–33
Melting, review of process, miscible blends, 117–21
Melting temperatures
  Hoffman–Weeks plots, miscible polymer blends, 119*f*
  polysiloxanes, 173
  PS–PEO block copolymers, 142, 148
Membranes, dialysis, IPNs, 35
Methanol, influence on PMMA–PVF_2 blends under stress, 320*t*
Methine stretching vibration band, polyester–poly(vinyl halide) blends, 90–97
Methyl acetate–halogenated molecule–heptane solvent, NMR, polyester–poly(vinyl halide) blends, 101–3
Methyl acetate–heptane solvent
  brominated solutes, NMR, polyester–poly(vinyl halide) blends, 99–101
  chlorinated solutes, NMR, polyester–poly(vinyl halide) blends, 97–99
Methyl acetate–heptane solvent—*Continued*
  chlorobrominated solutes, NMR, polyester–poly(vinyl halide) blends, 101–3
Methyl-formamide, influence on PMMA–PVF_2 blends under stress, 320*t*
Microencapsulation, gradient IPNs, 44
Microgel formation, IPNs, 30, 36
Microphase glass transitions
  B and S, DSC, 133*t*
  S–DMS and S–B block copolymers, 127–37
Microscopic defects, morphology of physical–chemical IPNs, 199
Microstructures, related to T_g, B microphase, S–B block copolymers, 136
Miscibility
  background and historical perspective, 4
  behavior, poly(vinyl halide) blends, 88
  copolymer blends, mean field theory, 67–74
  criteria, PMMPO–PS and PMMPO–P4MS blends, 64*t*
  domain, calculated, copolymer blends, 72*f*
  IPNs, negative heats of mixing, 28
  PMMPO–P4MS and PMMPO–PS blends, 63
  PVPh blends, 78
  random copolymer blends, 67–74
  SINs, factors controlling, 31
Miscible blends
  background and historical perspective, 6
  FTIR studies, polyester–poly(vinyl halide) blends, 104
  immiscible blends, simple amorphous polymers, modulus behavior, 13
  one crystallizable component, transitional and crystallization behavior, 7*f*
  PMMA–PVF_2, strength and elongation at break, 319
  T_g, equilibrium melting point and blend composition, 113*f*
Mixing
  ^{13}C-NMR PU–polysiloxane SINs, 184
  degree, PVPh–EVA blends, 81
  enhancement, PU–polysiloxane SINs, 185
  PVF, miscibility with polyesters, 88
Mixing-in-domain effect, tapered block copolymers, 128
Model of sequential IPN morphology, 26*f*
Modulus
  behavior, miscible and immiscible blends of simple amorphous polymers, 13
  PU–polysiloxane SINs, 177, 185
  related to composition, multiphase system, 188
  vs. composition, PMMA–PVF_2 blends, 317*f*
  vs. temperature PU–polysiloxane SINs, 180
Molded systems, thermoplastic IPNs, 42
Molecular weight
  characterization, PB, 160

Molecular weight—*Continued*
effect on blend misciblity, 30
effect on blending, PVPh blends, 82
effect on microphases, S triblock copolymers, 128
related to T_g, B microphase, S-B block copolymers, 136
S-B block copolymers, 130
Morphology
and extraction studies of physical-chemical IPNs based on block polymer and PS, 195–208
IPNs based on PB-PS, 161, 166
and mechanical properties of ethylene-propylene block copolymers and blends, 325–33
problems of IPNs, 154
sequential IPNs, 24, 26*f*
2MPPO—*See* Poly(2,6-dimethyl-1,4-phenylene oxide)
Multiphased systems, PVPh-EVA blends, 84

N

Negative heats of mixing, miscible IPNs, 28
Neutron scattering, principles, applied to IPNs, 155
Nuclear magnetic resonance (NMR) spectroscopy
poly(vinyl halide) blends, 97–104
T_g studies of S-B block copolymers, 129
NMR—*See* Nuclear magnetic resonance
Noise and vibration damping, IPNs and SINs, 33
Nomenclature of polymer blends, blocks, grafts, and IPNs, 22–24
Nonionic surfactant, PS-PEO block copolymer, 140
Notched thermoplastic specimens, fatigue, review, rubber-modified epoxies, 295
Notched thermoset specimens, fatigue, review, rubber-modified epoxies, 296

O

Oxidative degradation, T_g studies of S-B block copolymers, 129

P

Patent literature, IPNs, 47
Percolation theory, IPNs, 36
Perturbation
carbonyl band, FTIR studies, polyester-poly(vinyl halide) blends, 104
FTIR studies, polyester-poly(vinyl halide) blends, 90–97
Phase behavior
blend, contemporary view, 6
related to physical properties, polymer-polymer mixtures, 3–17
Phase continuity diagram, theoretical, 41*f*
Phase domain, development, IPNs, 36
Phase domain dimensions
IPNs, 154
IPNs based on PB-PS, 163
Phase morphology
immiscible blends, 11
IPNs based on PB-PS, 163
Phase(s)
cocontinuous, and IPNs, 43
coupling agents, blend miscibility, 12
PVPh-EVA blends, 81*f*
PVPh-PVAc blends, 79*f*
Phase-inversion point
graft copolymer, 146*f*
PEO-PS diblock copolymer, 145, 146*f*
Phase-separated IPNs and SINs, mechanical properties, 32
Phase separation
degree, 36
ethylene-propylene block copolymers and blends, 333
limitation, block or graft polymers, 196
liquid-liquid type, finite, miscible blends, 8
SINs, 32
Physical-chemical IPNs
based on block polymer and PS, extraction studies and morphology, 195–208
definition, 197
Physical cross-linking, IPNs, 171
Physical properties, related phase behavior, polymer-polymer mixtures, 3–17
Plastic domains, submicroscopic, reinforced elastomers, 33
Plastics wastes, recycling, IPNs, 37
Polyblends, rubber modified, FCP, 291–310
Polybutadiene (PB)
homopolymer network characterization, 160
IPNs with PS, 153–69
molecular weight characterization, 160
Poly(butylene adipate) (PBA), miscibility with poly(vinyl halide)s, 87
Poly(caprolactone) (PCL)
halogenated molecule-CCl_4 solvent, NMR spectroscopy, polyester-poly(vinyl halide) blends, 103
miscibility with poly(vinyl halide)s, 87
Poly(caprolactone) (PCL)-poly(vinyl halide) blends, FTIR spectroscopy, 90–97
Poly(2,6-dimethyl-1,4-phenylene oxide) (PMMPO)
blends, inverse gas chromatography, 59–65
blends with PS and P4MS, miscibility criteria, 64*t*
LF and solubility parameters, 63*t*
specific retention volumes and interaction parameters, 62*t*
Polyester-poly(vinyl halide) blend interactions, FTIR and ^{13}C-NMR studies, 87–108

Polyethylene (PE), morphology and mechanical properties, 325
Poly(hexamethylene sebacate) (PHMS), miscibility with poly(vinyl halide)s, 87
Polymer blends
  compatible, crystallization and melting, 111–21
  nomenclature, 23
Polymer characterization, IPNs based on PB–PS, 161
Polymer–polymer interactions, melting points, miscible polymer blends, 120
Polymer–polymer miscibility, background and historical perspective, 4
Polymer–polymer mixtures, phase behavior related to physical properties, 3–17
Polymerization, synthesis of PS–PEO block copolymers, 141
Poly(α-methyl α-ethyl β-propiolactone) (PMEPL), miscibility with poly(vinyl halide)s, 87
Poly(methyl methacrylate) (PMMA)–PVF_2, environmental-stress crazing and cracking, 313–23
Poly(4-methylstyrene) (P4MS)
  compatibility with PMMPO, 59
  LF and solubility parameters, 63*t*
  specific retention volumes and interaction parameters, 62*t*
Polyolefins, silicone flame-retardant system, 337–41
Polyoxyethylene (PEO)–PS block copolymers, emulsifying and crystalline properties, 139–50
Polypropylene (PP)
  morphology and mechanical properties, 325
  silicone flame-retardant system, 337–41
Polysiloxane(s)
  cross-linking, 172
  thermal transitions, 173
Polysiloxane–PU, SINs, 171–93
Polystyrene (PS)
  atactic (a-PS), radial growth rates of spherulites, 112*f*
  cross-linked with DVB in presence of SIS, morphology, 195–208
  IPNs with PB, 153–69
  isotactic (i-PS), radial growth rates of spherulites, 112*f*
  LF and solubility parameters, 63*t*
  specific retention volumes and interaction parameters, 62*t*
  weight fraction activity coefficients, 62*t*
Poly(styrene–isoprene) (SIS) triblock polymer, morphology, 195–208
Polystyrene (PS)–PEO block copolymers, emulsifying and crystalline properties, 139–50
Polyurethane (PU)–polysiloxane copolymers, blends, and IPNs, formation, discussion, 174
  SINs, 171–193
Poly(valerolactone) (PVL), miscibility with poly(vinyl halide)s, 87
Poly(vinyl acetate) (PVAc)
  effect of molecular weight on PVPh blends, 82
  FTIR studies of PVPh blends, 77–85
Poly(vinyl bromide) (PVB), miscibility with polyesters, 87
Poly(vinyl chloride) (PVC), miscibility with polyesters, 87
Poly(vinyl halide)–polyester blend interactions, FTIR and ^{13}C-NMR studies, 87–108
Poly(vinylidene fluoride) (PVF_2)–PMMA, environmental-stress crazing and cracking, 313–23
Poly(4-vinylphenol) (PVPh) blends
  crystallinity, 315*f*
  effect of molecular weight on blending, 82
  FTIR studies, 77–85
  glass transition behavior, 315*f*
PP—See Polypropylene
Prepolymer characterization, PU–polysiloxane SINs, 176
1-Propanol, influence on PMMA–PVF_2 blends under stress, 320*t*
Property relationships and applications, miscible blends, 13
Purification and characterization of block copolymers, measurement, PS–PEO block copolymers, 142–44
PVF_2—*See* Poly(vinylidene fluoride)
PVPh—*See* Poly(4-vinylphenol)

R

Radial growth rates of spherulites, a-PS and i-PS, 112*f*
Random copolymer blends
  mean field theory, 71
  miscibility, 67–74
Reaction injection molded systems (RIM), SIN based, 38
Recycling of plastics wastes, IPNs, 37
Reinforced elastomers, submicroscopic plastic domains, 33
Repulsion, mutual, miscibility in random copolymers, 67
Resins, IPN-based ion exchange, 34
Reversed-phase chromatography, S-DMS interaction parameter, 134
RIM—*See* Reaction injection molding
Room temperature vulcanization (RTV), cross-linking of polysiloxane, 173
RTV—*See* Room temperature vulcanization
Rubber, effect on FCP, rubber-modified epoxies, 302
Rubber content, effect on FCP, rubber-modified epoxies, 304*f*
Rubber-modified epoxies, fatigue, review, 291–310

S

SALS—*See* Small-angle light scattering
SANS—*See* Small-angle neutron scattering
SAXS—*See* Small-angle X-ray scattering
Scanning electron microscopy (SEM)
  ethylene-propylene block copolymers and blends, 329*f*
  IPN dual phase continuity, 25
Scattering cross section, total, SANS, PB-PS IPNs, 155
Segmental motion, ^{13}C NMR, PU-polysiloxane SINs, 182
SEM—*See* Scanning electron micrograph
Semi-IPNs, extraction and morphology, triblock copolymer and PS, 195
Sequential IPNs
  dual phase continuity, 25
  morphology, 24, 26*f*
  two phased, synthesis and properties, 29
Shifts
  ^{13}C NMR, polyester-poly(vinyl halide) blends, 107*t*
  FTIR, polyester-poly(vinyl halide) blends, 104
Silicone flame-retardant system for thermoplastics, 337–41
Simultaneous interpenetrating polymer networks (SINs)
  definition, 22
  discussion, 30
  IPNs
    noise and vibration damping, 33
    phase separated, mechanical properties, 32
  PU-polysiloxane, 171–193
  RIM systems, 38
  special functional triglyceride oils, 37
  synthetic routes, 34
SINs—*See* Simultaneous interpenetrating polymer networks
Small-angle light scattering (SALS), IPN morphology, 154
Small-angle neutron scattering (SANS)
  IPN morphology, 154
  IPNs based on PB-PS, 153, 164
  miscibility of PS and PMMPO, 59
  PB-PS IPNs, total scattering cross section, 155
  TEM technique, PB-PS(D_8) IPNs and semi-IPN dimensions, 27*t*
Small-angle X-ray scattering (SAXS)
  IPN morphology, 154
  sequential IPNs, 28
  tapered block copolymers, 128
Solubility parameters
  discussion, 184
  SINs, related to phase separation, 189
Special functional triglyceride oils, SINs, 37
Specific retention volumes and interaction parameters, P4MS, PMMPO, PMMPO-P4MS, PMMPO-PS, and PS, 62*t*
Specific surface areas, IPNs based on PB-PS, 165
Spherulites, radial growth rates, a-PS and i-PS, 112*f*
Static mechanical properties, fatigue in rubber-modified epoxies, 301
Sterical hindrance, PS-SIS-DVB SINs, 201
Stiffening temperatures, polysiloxanes, 173
Strength
  in air compared with critical stress, crazing and cracking of PMMA-PVF_2 blends, 323*f*
  yield and ultimate, PMMA-PVF_2 blends, 317*f*
Strength-composition relationships for blends, possible, 15*f*
Stress-strain diagrams, PMMA-PVF_2 blends, 316*f*
Styrene (S), composition, S-B block copolymers, 130
Styrene (S) microphase
  DSC glass transition regions, 134
  S-B and S-DMS systems, discussion, 131–36
Styrene (S)-B block copolymers, 127–37
Styrene (S)-DMS interaction parameter, reversed-phase chromatography, 134
Submicroscopic plastic domains, reinforced elastomers, 33
Surfactant, nonionic, PS-PEO block copolymer, 140
Swelling, degree, morphology, PS-SIS-DVB SINs, 203
Synergism, silicone flame-retardant system for thermoplastics, 339
Synergistic behavior, IPNs, 44
Synthetic routes for making SINs, 34

T

TBA curve, PEO-PS-PEO triblock copolymer, 143*f*
TEM—*See* Transmission electron microscopy
Temperature
  melting, Hoffman-Weeks plots, miscible polymer blends, 119*f*
  related to fraction of hydrogen-bonded carbonyls, PVPh-EVA blends, 85*f*
Tensile and impact behavior, fatigue in rubber-modified epoxies, 301*t*
Tensile stress for PMMA, time to break, 322*f*
Tension, interfacial, blend miscibility, 12
Terminology, interpenetrating polymer network, 43
Ternary blend, PP, EPR, HDPE, morphology, 328
Tetraethylorthosilicate (TEOS), cross-linking of polysiloxanes, 172
T_g—*See* Glass transition temperature
Thermal stress effects, S-B and S-DMS copolymers, 128
Thermal transitions in polysiloxanes, 173
Thermodynamic effects, melting points, miscible polymer blends, 120

Thermoplastic IPNs, discussion, 39–43, 48
Thermoplastic specimens, notched, fatigue, review, rubber-modified epoxies, 295
Thermoplastics, silicone flame-retardant system, 337–41
Thermoset specimens, notched, fatigue, review, rubber-modified epoxies, 296
Time to break as a function of tensile stress for PMMA, 322*f*
Tin octanoate, catalyst, cross-linking of polysiloxane, 173
Toluene, influence on PMMA–PVF_2 blends under stress, 320*t*
Transitional and crystallization behavior, miscible blends with one crystallizable component, 7*f*
Transmission electron microscopy (TEM)
  IPN morphology, 154
  IPNs based on PB–PS, 161
  morphology of several physical–chemical IPNs, 205–208
  SANS techniques, PB–PS(D_8) IPNs and semi-IPN dimensions, 27*t*
  two-phased nature of IPNs, 22
Triblock copolymer
  PEO–PS–PEO
    purification and characterization, 142
    synthesis, 141
  PS–PEO–PS
    purification and characterization, 144
    synthesis, 141
Triglyceride oils, special functional, SINs, 37
Two-phased IPNs, synthesis and properties, 29

U

UCST—*See* Upper critical solution temperature
Upper critical solution temperature (UCST), miscible blends, 8

V

Vibration and noise damping, IPNs and SINs, 33
Vinyl content, related to T_g, B microphase, S–B block copolymers, 136
Volume-temperature measurements, T_g studies of S–B block copolymers, 130

W

Windows of miscibility, homopolymer–copolymer blends, 69

Y

Yield and ultimate strength, PMMA–PVF_2 blends, 317*f*

Copyediting and indexing by Susan Robinson
Production by Meg Marshall
Jacket design by Pamela Lewis
Managing Editor: Janet S. Dodd

Typeset by Action Comp Company, Baltimore, MD
and Hot Type Ltd., Washington, DC
Printed and bound by Maple Press Company, York, PA